

Catherine Suenne de Castro

SYNTHESIS, PHOTOPHYSICAL AND MOLECULAR SIMULATION INVESTIGATIONS ON FLUORESCENT OLIGOMERS AND POLYMERS

Tese de doutoramento em Química, ramo de especialização em Fotoquímica, orientada por Professor Doutor João Sérgio Seixas de Melo e apresentada à Faculdade de Ciências e Tecnologia da Universidade de Coimbra

Setembro 2015



SYNTHESIS, PHOTOPHYSICAL AND MOLECULAR SIMULATION INVESTIGATIONS ON FLUORESCENT OLIGOMERS AND POLYMERS

Catherine Suenne de Castro

Tese de doutoramento em Química, ramo de especialização em Fotoquímica, orientada por Professor Doutor João Sérgio Seixas de Melo e apresentada à Faculdade de Ciências e Tecnologia da Universidade de Coimbra



UNIVERSIDADE DE COIMBRA

Setembro 2015

Acknowledgments

Gostaria de agradecer ao Professor (Prof.) Doutor (Dr.) João Sérgio Seixas de Melo, Prof. Associado (Ass.) com Agregação (Agr.) do Departamento de Química (DQ) da Faculdade de Ciências e Tecnologia (FCT) da Universidade de Coimbra (UC) pela sua orientação científica, apoio e confiança depositada em mim em todo o meu percurso académico.

Ao Prof. Dr. António Luís Vieira de Andrade Maçanita do DQ do Instituto Superior Técnico (IST) por partilhar o seu enorme conhecimento científico e pelas suas palavras animadoras.

Ao Prof. Dr. António Jorge Dias Parola [Prof. Ass. do DQ da Universidade Nova de Lisboa (UNL)] e à Dr. Raquel Gavara pela colaboração e ajuda na síntese dos PNIPAMPy.

Ao Prof. Dr. Carlos Espiño Lodeiro, Prof. Auxiliar do DQ da FCTUNL, à Cristina Núñez e ao resto do grupo por me introduzirem ao mundo dos quimiosensores.

À Dr. Telma Costa pela passagem do testemunho dos PAAMePy e pela contínua disponibilidade sempre que precisava de uns dados de “a 500 anos atrás”.

À Prof. Dr. Isabel Gonçalves, Prof. Ass. do DQ da Universidade de Aveiro (UA) e à Dr. Sandra Gago pela síntese e caracterização desses mesmos polímeros (PAAMePy).

Ao Dr. João Pina por tudo o que me ensinou e continua a ensinar.

Ao Prof. Dr. Alberto António Caria Canelas Pais, Prof. Ass. Com Agg. do DQ da FCTUC, à Dr. Rita Sousa Dias, à Dr. Sandra Cristina da Cruz Nunes e à Doutoranda Tânia Firmino Guerra Guerreiro Cova pela ajuda em toda a parte computacional.

À Prof. Dr. Marta Piñeiro Gomez, Prof. Aux. Do DQ da FCTUC, pela sua prontidão em ajudar nos mais diversos obstáculos geralmente relacionados com purificações.

Ao Prof. Dr. Rui M. Meireles Brito, Prof. Ass. com Agg. do DQ da FCTUC, e ao Mestre Pedro J. F. da Conceição Cruz pela disponibilidade e simpatia na parte de RMN.

Ao Prof. Dr. Jorge Fernando Coelho, Prof. Aux., ao Prof. Dr. Arménio Coimbra Serra, Prof. Aux., e à Doutoranda Joana Mendes do Departamento de Engenharia Química (DEQ) da FCTUC pela ajuda na caracterização dos polímeros PNIPAMPy.

Ao Prof. Dr. Carlos Alberto Lourenço da Serpa Soares pela sua ajuda, paciência e boa disposição sempre que precisava de usar o equipamento de calorimetria fotoacústica ou a fotólise por relâmpago apesar

Acknowledgments

de maior parte do trabalho não ter sido apresentado nesta tese, a sua ajuda foi preciosa no decorrer do meu doutoramento

Ao Prof. Dr. João Carlos dos Santos Silva e Pereira de Lima, Prof. Ass. do DQ da FCTUNL, pela disponibilidade e ajuda na utilização do programa para o uso do Método da Máxima Entropia apresentado na Secção 3.3.

Aos restantes elementos do grupo de Macromoléculas, Colóides e Fotoquímica pela boa disposição e entreaajuda.

Um especial obrigado ao Manuel e à Ana por me aturarem, merecem um lugar no céu. ☺

Aos restantes amigos por estarem sempre presentes quando penso que não tenho para onde me virar.

À minha família que apesar de distante, tem sempre um lugar especial no meu coração.

Ao Departamento de Química da FCTUC, em particular ao Grupo de Macromoléculas, Colóides e Fotoquímica, dirigida no período da tese pelo Prof. Dr. Hugh Douglas Burrows, Professor Catedrático do DQ da FCTUC mas agora Jubilado e Aposentado, pelas condições que me foram disponibilizadas.

À Fundação para a Ciência e Tecnologia (FCT) pela bolsa de Doutoramento (SFRH/BD/75134/2010).

Table of contents

Abstract	xv
Resumo	xvii
Abbreviations and Symbols	xviii
Constants	xxxi
CHAPTER 1	1
Introduction	1
1.1. Relevance of Photochemistry	1
1.2. Unimolecular Photophysical Processes	4
1.2.1. Kinetics of Unimolecular Photophysical Processes	6
1.3. Bimolecular Photophysical Process: Quenching	7
1.3.1. Quenching by Oxygen	8
1.3.2. Excimer and Exciplex	9
1.3.2.1. Intramolecular and Intermolecular Excimers	9
1.3.2.1.1. Conformations of the Excimer	11
1.3.2.1.2. Ground State Dimers (<i>GSD</i>)	12
1.3.2.1.3. Kinetics of Excimer Formation	14
1.3.2.1.4. Thermodynamics of Excimer Formation	16
1.4. Fluorescent Probes	18
1.4.1. Polycyclic Aromatic Hydrocarbons (PAHS)	19
1.4.1.1. Naphthalene	19
1.4.1.2. Pyrene	20
CHAPTER 2	21
Oligomers	21
2.1. Introduction	21
2.1.1. Fluorescence Decay Analysis	25
2.1.1.1. No Model Assumed A Priori	25
2.2. Photophysics of Pyrene-Based Oligomers	28
2.2.1. Dipyrenylalkanes	28

Table of contents

2.2.1.1. Temperature Dependence	28
2.2.1.2. Viscosity Dependence	38
2.2.1.3. Dioxane:water Mixtures	41
2.2.1.4. Summary	48
2.2.1.5. Supplementary Information	48
2.2.2. Dipyrenylacetamides	52
2.2.2.1. Steady-State Behavior	52
2.2.2.2. Time-Resolved Behavior	54
2.2.2.3. Summary	55
2.2.2.4. Supplementary Information	56
CHAPTER 3	59
Polymers	59
3.1. Introduction	59
3.1.1. Polyelectrolytes	60
3.1.2. Solubilisation of Polymers	61
3.1.3. Polymer Conformation	61
3.1.4. Hydrophobically Modified Polymers (HMP)	62
3.1.5. Analysis of the Fluorescence Decays in Polymers	63
3.1.5.1. The Maximum Entropy Method (MEM)	64
3.1.5.2. Blob Model	64
3.2. Poly(acrylic acid) Pyrene Labelled Polymers (PAAMePy)	65
3.2.1. Synthesis	65
3.2.2. Determination of the Probe Content: Degree of Labelling	65
3.2.3. Statistical Characterization of the Pyrene Labelling: Poisson Distribution	71
3.2.1. Dynamics of Short and Long PAAMePy Polymers in Pure Organic Solvents and in Dioxane:Water Mixtures	73
3.2.1.1. Absorption and Steady State (SS) Fluorescence Data	73
3.2.1.1. Time-Resolved Behavior	83
3.2.1.2. Temperature Dependence Behavior	86
3.2.1.3. Summary	93
3.2.1.4. Supporting Information	93
3.2.2. Dynamics of Short and Long PAAMePy Polymers in Aqueous Solutions	93
3.2.2.1. The effect of pH	93
3.2.2.1.1. Absorption Spectra	93

Table of contents

3.2.2.1.2. Steady State Fluorescence	99
3.2.2.1.3. Time-Resolved Fluorescence	106
3.2.2.2. Interaction of PAAMePy Polymers with Neutral and Anionic Surfactants	108
3.2.2.2.1. Introduction	108
3.2.2.2.1.1. Surfactants	108
3.2.2.2.1.2. Interaction Polymer-Surfactant	112
3.2.2.2.2. Results and Discussion	113
3.2.2.2.2.1. Interaction of PAAMePy polymers with an Anionic Surfactant	113
3.2.2.2.2.1.1. Absorption Spectra	113
3.2.2.2.2.1.2. Steady State Fluorescence	114
3.2.2.2.2.2. Interaction of PAAMePy Polymers with a Neutral Surfactant	118
3.2.2.3. Simulations of the PAAMePy Behavior in Water	119
3.2.2.3.1. Introduction	119
3.2.2.3.1.1. Model Systems and Interactions Potential	119
3.2.2.3.1.2. Boundary Conditions	121
3.2.2.3.1.3. Sampling from <i>Ensembles</i>	121
3.2.2.3.1.4. The Metropolis Method	122
3.2.2.3.1.5. Centre of Mass	124
3.2.2.3.1.6. Radius of Gyration	124
3.2.2.3.1.7. Contact Analysis	125
3.2.2.3.2. Results and Discussion	126
3.2.2.3.2.1. System Characterization from Statistical Estimates	126
3.2.2.3.2.2. Simulation	128
3.2.2.3.2.2.1. Effect of Charge/pH	129
3.2.2.3.2.2.3. Molecular Dynamics (MD)	133
3.2.2.3.3. Summary	134
3.2.2.3.4. Supplementary Information	135
3.3. Poly(N-isopropylacrilamide) Pyrene Labelled Polymers	139
3.3.1. Introduction	139
3.3.1.1. Synthesis of Polymers	139
3.3.2. Synthesis of the PNIPAMPy polymers	140
3.3.3. Determination of the Labelling Content	141
3.3.4. Statistical Characterization	141
3.3.1. Results and Discussion	144
3.3.1.1. Absorption and Emission Spectra	144
3.3.1.2. Viscosity Dependence	145

Table of contents

3.3.1.3. Temperature Dependence	147
3.3.1.3.1. Intra vs. Intermolecular Interactions	152
3.3.1.3.2. Monomer That Gives Rise To The Excimer (MAGRE), Isolated Monomers and <i>GSD</i>	152
3.3.1.3.3. Excimer Formation Rate Constant	155
3.3.1.3.4. Excimer Dissociation Rate Constant	155
3.3.1.3.5. Monomer and Excimer Lifetimes	155
3.3.1.3.6. The Blob Model vs. Sum of Exponentials Model	156
3.3.2. Summary	157
3.3.3. Supplementary Information	157
CHAPTER 4	165
Chemosensors	165
4.1. Introduction	165
4.1.1. Chemical Sensors	165
4.1.2. Importance of Fluorescence Probes and Chemosensors	166
4.1.3. Mechanisms of Transduction	166
4.1.3.1. Photoinduced Electron Transfer (PET)	166
4.1.3.2. Excited State Intramolecular Proton Transfer (ESIPT)	167
4.1.4. Competitivity Study	168
4.2. Synthesis	168
4.2.1. Photophysical Characterization of Compound 1	171
4.2.1. Sensorial Ability of Compound 1 Towards H ⁺ , Zn ²⁺ , Cd ²⁺ , Cu ²⁺ , Ni ²⁺ , Pb ²⁺ , Fe ²⁺ , Hg ²⁺ and Al ³⁺ Ions	171
4.2.2. Time-Resolved Data	177
4.2.3. Summary	178
4.2.4. Supporting Information	178
4.2.4.1.1. Crystallography Data	178
4.3. Steady-State and Time-Resolved Investigations on Pyrene-Based Chemosensors	180
4.3.1. Spectrophotometric Studies	180
4.3.2. P and L upon the Addition of Water	183
4.3.3. Time-Resolved Data	186
4.3.4. Interaction of P and L with Metal Cations	188
4.3.5. Time-Resolved Data	193
4.3.6. Conclusions	195

Table of contents

4.3.7. Supporting Information	195
4.4. Photophysical Characterization of Compound 2	198
4.4.1. Sensorial Ability of Compound 2 Towards OH ⁻ , Ag ⁺ , Zn ²⁺ , Cd ²⁺ , Pb ²⁺ , Hg ²⁺ , and Al ³⁺ Ions	200
4.4.2. Summary	202
4.5. Photophysical Studies of a Naphthalene-Based Emissive Probe for Metal Cations	203
4.5.1. Conclusions	208
4.6. Photophysical characterization of L ₁ and L ₂	208
4.6.1. Sensorial Ability of Compound L ₁ and L ₂ Towards Pb ²⁺ , Cu ²⁺ , Ag ⁺ , Zn ²⁺ , Hg ²⁺ and Cd ²⁺ Ions	210
4.6.2. Time-resolved Fluorescence Measurements	217
4.6.1. Multivariate Data Analysis Procedure	220
4.6.1.1. Hierarchical Cluster Analysis	222
4.6.1.2. Principal Component Analysis (PCA)	222
4.6.2. Results and Discussion	224
4.6.3. Summary	228
4.6.4. Supplementary Information	229
CHAPTER 5	233
Coumarins	233
5.1. Introduction	233
5.2. Absorption, Steady State and Time-Resolved Fluorescence	235
5.2.1. 6,7-Dimethoxy-4-Methylcoumarin (67dMet4MC)	235
5.2.2. Scopoletin (7H6MetC)	237
5.2.3. 4-Hydroxy-3-Nitrocoumarin (4H3NC)	242
5.2.4. 4-methylesculetin (67dH4MC)	242
5.2.5. 7-Hydroxy-4-Methyl-8-Nitrocoumarin (7H4M8NC)	248
5.3. Summary	253
5.4. Supplementary Information	253
CHAPTER 6	257
Concluding Remarks	257
CHAPTER 7	259

Table of contents

Methods and Sample Preparation	259
7.1. Compounds	259
7.1.1. Oligomers	259
7.1.2. Coumarins	259
7.1.3. PAAMePy Polymers	259
7.1.3.1. Reagents	259
7.1.3.2. Synthesis	260
7.1.3.3. Physical Measurements	263
7.1.3.4. Monte Carlo	263
7.1.4. PNIPAMPy Polymers	264
7.1.4.1. Preparation of a Polymerizable Pyrene Derivative (1-pyrenylmethyl methacrylate)	264
7.1.4.2. Preparation of Polymers with Different Pyrene Loadings	265
7.1.4.3. Physical Measurements	270
7.1.5. Chemosensors	271
7.1.5.1. L ₁ and L ₂	271
7.1.6. Surfactants	272
7.1.7. Metals	272
7.1.8. Solvents	272
7.1.9. Samples	273
7.1.9.1. Storage	273
7.1.9.2. Preparation of the PAAMePy Polymer Solutions	273
7.1.9.2.1. Organic Solutions	273
7.1.9.2.1. Dioxane:Water (Dx:H ₂ O) mixtures	273
7.1.9.2.1. Water (at different pH values)	274
7.1.9.2.2. With Surfactants (at two pH values)	278
7.1.9.3. Preparation of the Chemosensors Solutions	278
7.1.9.4. Preparation of an Universal Buffer	279
7.1.10. Cleaning Process	280
7.1.10.1. Preparation of Chromosulphuric Acid	280
7.1.10.2. Preparation of EDTA	281
7.2. Techniques	281
7.2.1. pH Measurements	281
7.2.2. Temperature	281
7.2.3. Deoxygenation	281
7.2.4. Binding Constant Determination	282

Table of contents

7.2.5.	UV-Vis Absorption	282
7.2.5.1.	Molar extinction coefficients	284
7.2.5.2.	Spectrophotometric titrations	284
7.2.5.2.1.	P_A Parameter Determination	284
7.2.5.2.2.	pK_a Determination	285
7.2.6.	Fluorescence	287
7.2.6.1.	Steady-State Fluorescence	287
7.2.6.1.1.	Fluorescence Quantum Yield (Φ_F) Determination	289
7.2.6.1.2.	Spectrofluorimetric Titrations	290
7.2.6.1.2.1.	I_E/I_M Determination	290
7.2.6.1.2.2.	I_1/I_3 Determination	291
7.2.6.1.2.3.	P_M-P_E Determination	291
7.2.6.2.	Time-Resolved Fluorescence	292
7.2.6.2.1.	With Nanosecond Time Resolution	295
7.2.6.2.2.	With Picosecond Time Resolution	296
7.2.6.2.3.	Fluorescence Decay Analysis	296
7.2.7.	Phosphorescence	296
7.2.7.1.	Steady-State and Time-resolved Phosphorescence	296
7.3.	Theoretical studies	297
7.3.1.	Molecular Dynamics	297
CHAPTER 8		299
References		299
Appendices		317
APPENDIX A. SOLUTION OF THE BIRKS' KINETIC SCHEME		317
APPENDIX B. SOLUTION OF A KINETIC SCHEME INVOLVING TWO MONOMERS AND ONE EXCIMER	325	
APPENDIX C. SOLUTION OF A KINETIC SCHEME INVOLVING ONE MONOMER AND TWO CONFORMATIONALLY DIFFERENT EXCIMERS [E.G. 1PY(3)1PY]		331
APPENDIX D. MATLAB PROGRAM FOR THE KINETICS INVOLVING ONE MONOMER AND TWO CONFORMATIONALLY DIFFERENT EXCIMERS [E.G. 1PY(3)1PY]		337
APPENDIX E. OCTAVE PROGRAM		341

Table of contents

Abstract

The present work consists on a comprehensive photophysical study of several pyrene based polymers (with acrylic acid and isopropylacrilamide backbones) and oligomers in solution (different solvents, pH and surfactants) and as a function of temperature. Additionally the photophysical behavior in the singlet and triplet excited states of five hydroxy and methoxycoumarins was investigated in organic solvents and water as a function of pH. Several kinetic schemes have been proposed and discussed.

In Chapter 3, two poly(acrylic acid) polymers (PAA), with different molecular weights (2 and 450 kg/mol), randomly hydrophobically modified, in different percentages (a total of 14 polymers), with pyrene were investigated. The study was carried out in different solvent media -methanol, dioxane, dioxane:water mixtures, water (at different pH values) and water:surfactant mixtures- and temperature. These were followed by absorption, steady state and time-resolved fluorescence (in the ns and ps time domain) techniques. As additional tools in the understanding of this complex system, simulations, dynamic modelling and fluorescence data from model compounds, namely, two oligomers linking the two pyrene units by alkylic chain of three [1Py(3)1Py, 1,3-di(1,1'-pyrenyl)propane] and ten [1Py(10)1Py, 1,10-di(1,1'-pyrenyl)decane] atoms of carbon and some dipyrenylacetamides (with different size chains between both pyrene units) were also obtained. The results show that the size of the PAA chain, together with the degree and location of the fluorescent probes strongly influence the photophysical behavior of these compounds. Molecular modelling studies allowed the interpretation of these different behaviours, namely that the excimer formation of polymers modified with pyrene depends primarily on the encounter of the probes at short distances and that the synthetic procedures may be important in the localization of the chromophores.

For the poly(N-isopropylacrylamide), polymers of different chain sizes and labelling degree (L.D.) were synthesized and for one of these polymers the excited state kinetic behavior was obtained from the analysis of the decays assuming the sum of exponential model and further compared with the method of maximum entropy, Chapter 3.

In Chapter 4, different pyrene and naphthalene-based chemosensors were characterized, with the determination of the association constants with metal cations aiming to obtain selectivity towards some of these ions. Moreover, with two of these chemosensors, a Hierarchical cluster analysis of the spectral and photophysical data was used as an additional tool.

Abstract

In Chapter 5, the excited state behaviour of four hydroxycoumarins (7H6MetC, 4H3NC, 67dH4MC and 7H4M8NC) and of the model methoxycoumarin (67dMet4MC), was obtained in water (as a function of pH) and in dioxane:water mixtures.

Resumo

O presente trabalho consiste num estudo fotofísico abrangente de vários polímeros [poli(ácido acrílico) e poli(*N*-isopropilacrilamida)] e oligómeros com pireno em solução (diferentes solventes, pH e agentes tensoactivos) e, em função da temperatura. Adicionalmente, o comportamento fotofísico dos estados excitados singlete e tripleto de cinco hidroxi e metoxicumarinas foi investigado em solventes orgânicos e água em função do pH. Vários esquemas cinéticos foram propostos e discutidos.

No Capítulo 3, dois polímeros de poli(ácido acrílico) (PAA), com pesos moleculares diferentes (2 e 450 kg/mol), aleatoriamente modificado hidrofobicamente, em diferentes percentagens (um total de 14 polímeros), com pireno, foram investigados. O estudo foi efectuado em diferentes meios - metanol, misturas dioxano:água, água (a diferentes valores de pH) e misturas de água:surfactante - e temperatura. Estes foram seguidos por técnicas de absorção, estado estacionário e por fluorescência resolvida no tempo (no domínio temporal dos ns e ps). Como ferramentas adicionais na compreensão deste sistema complexo, simulações, modelação dinâmica e dados de fluorescência de compostos modelo, ou seja, de dois oligómeros que ligam as duas unidades de pireno de cadeia alquílica de três [1Py(3)1Py, 1,3-di(1,1'-pirenil)propano] e dez [1Py(10)1Py, 1,10-di(1,1'-pirenil)decano] átomos de carbono e de alguns bipirenilacetamidas (com cadeias de diferentes tamanho entre as duas unidades de pireno) foram igualmente obtidos. Os resultados mostram que o tamanho da cadeia de PAA, em conjunto com o grau de marcação e localização das sondas fluorescentes influenciam fortemente o comportamento fotofísico destes compostos. Os estudos de modelação molecular permitiram a interpretação destes diferentes comportamentos, nomeadamente que a formação de excímero de polímeros modificados com pireno depende principalmente do encontro das sondas em distâncias curtas e que os métodos de síntese podem ser importantes na localização dos cromóforos.

Para o poli(*N*-isopropilacrilamida), polímeros de cadeias de diferentes tamanhos e graus de marcação foram sintetizados e para um destes polímeros o comportamento cinético do estado excitado foi obtido a partir da análise dos decaimentos assumindo o modelo da soma de exponenciais e comparando-o com o método de entropia máxima, Capítulo 3.

No Capítulo 4, sensores químicos à base de pireno e naftaleno foram caracterizados, com a determinação das constantes de associação com catiões metálicos com o objectivo de obter selectividade para alguns destes iões. Além disso, com dois destes sensores químicos uma análise hierárquica de *clusters* dos dados espectrais e fotofísicos foi usada como ferramenta adicional.

No Capítulo 5, o comportamento do estado excitado de quatro hidroxycumarinas (7H6MetC, 4H3NC, 67dH4MC e 7H4M8NC) e de uma metoxicumarina modelo (67dMet4MC), foi obtido em água (em função do pH) e em misturas dioxano:água.

Abbreviations and Symbols

Acronym	Definition	Acronym	Definition
" α "	Fraction of single labelled chains relative to all labelled chains (intrinsically isolated pyrene units)	$\Delta\lambda_1$	Difference between the wavelength correspondent to the absorption maximum of the transition $S_0 \rightarrow S_1$ from the compound that form excimer relatively to the parent compound
α	Constant of proportionality of the rate constant vs. viscosity' plot	$\Delta\lambda_2$	Difference between the wavelength of maximum intensities of the excitation spectra collected in the excimer and monomer region
α	Swelling coefficient or fractions of free monomers in polymers	$\Delta O.D.$	Variation of optical density
α_0	Equilibrium angle	ΔP_A	Maximum variation in the P_A parameter, see P_A
α_i	Pre-exponential factors in a sum of continuous, smooth functions in the maximum entropy method	$\Delta P_M - P_E$	Maximum variation in the $P_M - P_E$ parameter, see $P_M - P_E$
$\alpha(1-\beta)$	Fractions of GSD	ΔS	Entropy
α, β, γ	Light fractions associated to the excitations of the different existing species a given system	ΔS^*	Excited state entropy
β	$1/k_B T$	ΔU	Change in internal energy
χ	Chi	δV_{nm}	Change in potential between state n and m (before and after motion)
χ^2	Chi-squared value	$\Delta(1/2)$	Width at half maximum of the excimer emission band
Δ	Difference between the curve defining the normal regime and the crossing point of the lines defining the <i>HTL</i> and <i>LTL</i> regimes in a Stevens-Ban plot	δ -pulse	Ultrashort pulse
Δ	Variation/difference	ϵ	Extinction coefficient
ΔH	Enthalpy	ϵ_0	Vacuum permittivity
ΔH^*	Excited state enthalpy	ϵ_λ	Extinction coefficient at a given wavelength
$\Delta I_E/I_M$	Maximum variation in the I_E/I_M parameter, see I_E/I_M	ϵ_r	Relative dielectric permittivity
$\Delta I_1/I_3$	Maximum variation in the I_1/I_3 parameter, see I_1/I_3	$\epsilon_{reference}$	Extinction coefficient of the reference
		ϕ_{Dx}	Volume fraction of dioxane in dx:H ₂ O mixtures

Abbreviations

Acronym	Definition	Acronym	Definition
ϕ_E	Excimer fluorescence quantum yield	$\hat{\mu}_e$	Electronic dipole moment operator
ϕ_F	Fluorescence quantum yield	μL	Microliter (volume unit)
ϕ_F^E	Excimer fluorescence quantum yield	$\hat{\mu}_n$	Nuclear dipole moment operator
ϕ_F^M	Monomer fluorescence quantum yield or fluorescence quantum yield of the specie M	ρ	Density
ϕ_M	Monomer fluorescence quantum yield	ρ_{PAAMePy}	Density of the PAAMePy polymer
ϕ_{QM}	Quantum yield of quenching of the specie/molecule M by the quencher Q	$\rho(\Gamma)$	Density of probability
Γ	Position of a particular point in the phase space	$\rho_{\text{ens.}}(\Gamma)$	Density of probability for the ensemble
η	Viscous flow	σ	Standard deviation
η	Viscosity or shear viscosity	σ	Finite distance at which the inter-particle potential is zero in the LJ potential
λ	Wavelength or concentration of chromophores per gram of polymer (blob model)	τ_A	Anion decay time
$\lambda_{\text{abs.}}$	Absorption wavelength	τ_E	Excimer decay time
$\lambda_{\text{em.}}$	Emission wavelength	τ_{E1}	Assymmetric excimer decay time
$\lambda_{\text{max.}}^{\text{abs.}}$	Absorption maximum wavelength	τ_{E2}	Symmetric excimer decay time
$\lambda_{\text{max.}}^E$	Fluorescence emission wavelength maximum of the excimer	τ_F^E	Excimer fluorescence decay time
$\lambda_{\text{max.}}^{\text{em.}}$	Emission wavelength maximum	τ_F^M	Monomer fluorescence decay time
$\lambda_{\text{exc.}}$	Excitation wavelength	τ_i	i^{th} decay time
λ_i	i^{th} reciprocal lifetime	τ_j	j^{th} decay time
μ	Micro	τ_M	Monomer decay time
μ	Chemical potential	τ_M^0	Parent monomer decay time
$\hat{\mu}$	Dipole moment operator	τ_{M0}	Parent monomer decay time
		τ_N	Neutral specie decay time
		τ_{QM}	Fluorescence lifetime of M quenched by Q
		τ_0	Monomer decay time

Abbreviations

Acronym	Definition	Acronym	Definition
ξ	Random number	1PyCH₂NH₂	1-pyrenylmethylamine
ξ_1	Random number 1	1PyCH₂NH·HCl	1-pyrenylmethylamine hydrochloride
ξ_2	Random number 2	1Py(3)1Py	1,10-Bis-(1-pyrene)propane or 1,1'-dipyrenylpropane
ψ	Wavefunction of the fundamental state	1Py(10)1Py	1,10-Bis-(1-pyrene)decane or 1,1'-dipyrenyldecane
ψ_{es}	Electronic wavefunction	$^1(\text{DA})^*$	Singlet excited dimer of A and D
ψ_v	Nuclear wavefunction	$^1(\text{M}\cdots\text{O}_2)^*$	Oxycomplex of molecule/specie M and O ₂
ψ^*	Wavefunction of the excited state	1,3DCC	1,3-dicyclohexylcarbodiimide
(1- α)	Fraction of excited <i>GSD</i> in a scheme involving two species (monomer and excimer)	2M	2 molecules/species M
(1- α)(1- β)	Fraction of MAGRE monomers	$^3\text{O}_2$	Triplet state of molecular oxygen
^1A	Electron acceptor atom or molecule A in the singlet ground/fundamental state	<i>a</i>	Size of the monomer (blob model)
$^1\text{A}^*$	Electron acceptor atom or molecule A in the singlet excited state	A	Property or solute A, amplitude of a GaussMod function, area of a Gauss function
1CH₃Py	1-methylpyrene	A	Ratio for pre-exponential factors at the monomer emission
^1D	Electron donor atom or molecule D in the singlet ground state	Å	Ångström (length unit)
$^1\text{D}^*$	Electron donor atom or molecule D in the singlet excited state	$\langle A[\Gamma(t)] \rangle_{time}$	Temporal average of A(Γ) in a very long time range
$^1\text{H-NMR}$	Proton nuclear magnetic resonance	AA	Acrylic acid
^1M	Molecule/specie M in the singlet ground state	Abs.	Absorption or absorbance
1MP	1-methylpyrrolidone	A.C.	Autocorrelation functions
$^1\text{M}^*$	Molecule/specie M in the singlet excited state	ADC	Analog-to-digital converter
1Py	1-methylpyrene	<A>_{ens.}	Average of the property A for all the members of the ensemble

Abbreviations

Acronym	Definition	Acronym	Definition
a_i	Pre-exponential factors obtained at a given emission wavelength and associated with the i^{th} decay time	C	Carbon
AIBN	2,2'-Azobisisobutyronitrile	C	Centi (unit prefix)
$a_{i,j}$	Pre-exponential factors obtained at the i^{th} emission wavelength and associated with the j^{th} decay time	c	Speed of light
a_j	Pre-exponential factors obtained at a given emission wavelength and associated with the j^{th} decay time	C₁	Fractional contribution of the 1 st lifetime
A_λ	Absorbance at a given wavelength	C₁₂E₄	Tetraethyleneglycol monododecylether
Al	Aluminium	[C₁₂E₅]	Concentration of C ₁₂ E ₅
$A_{obs.}$	'Macroscopic' property experimentally observable	C₁₂E₅	Pentaethyleneglycol monododecylether
$A_{PAAMePy}$	Absorbance of the PAAMePy polymer	C₂	Fractional contribution of the 2 nd specie
ATB	Automated force field topology builder	Ca.	Around
$\langle A \rangle_{\text{time}}$	Temporal average of A(Γ) in a very long time range	CAC	Critical aggregation concentration
a.u.	Arbitrary units	CACTUS	University of Santiago de Compostela, Spain
BandWN	Bandwidth ratios (calculated using a GaussMod function) of the band of the fluorescence emission spectra ($\lambda_{exc.} = 360$ nm) present at longer wavelengths between the ligand with 100 equivalents of metal and the free ligand	CFD	Constant fraction discriminator
BBFO	Broad Band Fluorine Observation	ch	Channel
BBMS	Bobetic, Barker, Maitland and Smith	CH₂Cl₂	Dichloromethane
		CH₃CN	Acetonitrile
		CHEF	Chelation enhanced fluorescence
		CHEQ	Chelation enhancement of the quenching
		C_i	Fractional contribution of the i^{th} specie
		cm	Centimetre (distance unit)
		CM	Centre of mass
		CMC	Critical micelle concentration
		COOH	Carboxylic group

Abbreviations

Acronym	Definition	Acronym	Definition
CT	Charge transfer	Ens.	<i>Ensemble</i>
CTAB	Cetyl trimethylammonium bromide	E	Excimer
C _v	Heat capacity	E	Energy
Cx	Cyclohexane	E _η	Energy of the viscous flow
CW	Continuous wave	E ₁	Asymmetric excimer
C _{2v}	Point group symmetry of, e. g., acenaphthalene	E ₁ [*]	Asymmetric excimer
<i>d</i>	Distance	E ₂	Symmetric excimer
D	Dimer or Donor	E ₂ [*]	Symmetric excimer
D	Diffusion coefficient	E _a	Activation energy
D2	Deuterium	EDTA	Ethylene Diamine Tetraacetic acid disodium salt dehydrate
D _{2h}	Point group symmetry of, e. g., pyrene	e.g.	That is
D _{6h}	Point group symmetry of, e. g., benzene	E _i	Total energy of the system in the respective microstate
DA	Donor-acceptor complex	Em.	Emission
DAB	Diffusivity of A towards B	Eq.	Equivalent
DAF	Delay after flash	ESIPT	Excited state intramolecular proton transfer
DMF	Dimethylformamide	<i>Et al.</i>	And others
DMSO	Dimethylsulfoxide	Et ₂ O	Diethyl ether
DOSY	Diffusion-ordered spectroscopy	EtOH	Ethanol
<i>d</i> _{Py-Py}	Distance between two consecutive pyrene units (given in N ^o of monomer units)	Exc.	Excitation
DQ	<i>Departamento de Química</i>	E [*]	Excimer
%dx	Dioxane percentage in dx:H ₂ O mixtures	[E [*]](t)	Time-concentration dependence of the excimer
Dx	Dioxane	Exp.	Exponential function
e	Elementary charge or exponential function	F	Fluorescence
		<i>f</i> ₁	Function 1
		<i>f</i> ₂	Function 2

Abbreviations

Acronym	Definition	Acronym	Definition
FA	Fluorescent agents	H₂O	Water
FCT	<i>Faculdade de Ciências e Tecnologias</i>	H₃BO₃	Boric acid
FCTUC	<i>Faculdade de Ciências e Tecnologias da Universidade de Coimbra</i>	<i>i</i>	Index for the microstates of the system
FCTUNL	<i>Faculdade de Ciências e Tecnologias da Universidade Nova de Lisboa</i>	I	Intensity and radiation intensity that leave the sample
FRET	Förster resonance energy transfer	I	Initiator molecule
FTIR	Fourier transform infrared spectroscopy	I₀	Radiation intensity that penetrate the sample and fluorescence intensity for [M]/[L]= 0
g	Gram (mass unit)	I_{0.9-2.4}	Area of the peak between 0.9 and 2.4 ppm
GPC	Gel permeation chromatography	I₁	First vibronic intensity of the fluorescence emission spectra
GSD	Ground State Dimers	I_{11.7-12.6}	Area of the peak between 11.7 and 12.6 ppm
GUI	Graphical user interface	I_{1/I₃}	Ratio between the first and third vibronic intensities of the fluorescence emission spectra
h	Planck Constant	I₃	Third vibronic intensity of the fluorescence emission spectra
H	Enthalpy or height in a function	I_{7.6-8.7}	Area of the peak between 7.6 and 8.7 ppm
HCA	Hierarchical cluster analysis	IBW	Instrumental bandwidth
HOMO	Highest occupied molecular orbital	ICT	Internal charge transfer
HMP	Hydrophobically modified polymers	<i>i.e.</i>	That is
HPLC	High-performance liquid chromatography	I_E	Excimer intensity
HPSEC	High performance size-exclusion chromatography	I_E (t)	Excimer intensity dependence with time
HSAB	Hard and soft (Lewis) acids and bases	I_{E/I_M}	Excimer-to-monomer ratio
HTL	High temperature limit	I_F	Fluorescence intensity
Hz	Hertz (frequency unit)		

Abbreviations

Acronym	Definition	Acronym	Definition
I_{F_0}	Offset for GaussMod and Gauss functions and base for a BiGauss function	k_a^{TR}	Excimer formation rate constants obtained from time-resolved experiments
I_F^M	Fluorescence intensity of specie/molecule M	k_B	Boltzmann constant
$I_F^M(t)$	Fluorescence intensity dependence with time of specie/molecule M	k_{bond}	Bonf force constant
I_M	Monomer intensity	kCounts	Kilocounts
IR	Infrared	k_d	Excimer dissociation rate constant
IRF	Instrumental response function	k_d^0	Intercept of the Arrhenius equation for k_d as a function of temperature
I_{M_0}	Monomer intensity of the parent compound	k_E	Excimer decay rate constant
I_M^0	Monomer intensity of the parent compound	k_E^0	Intercept of the Arrhenius equation for k_E as a function of temperature
I(t)	Fluorescence intensity as a function of time	k_F	Fluorescence rate constant
J	Joule (energy unit)	k_F^M	Radiative decay rate constant of the monomer and of specie/molecule M
K	Kilo (unit prefix)	k_F^E	Radiative decay rate constant of the excimer
K	Kelvin (temperature unit)	kg	Kilogram (mass unit)
K	Kinetic energy	k_i^0	Intercept of the Arrhenius equation for any rate constant as a function of temperature
K_2CO_3	Potassium carbonate	kic	Internal conversion rate constant
k_a	Excimer association rate constant	k_{IC}^M	Internal conversion rate constant of specie/molecule M
k_a	Average excimer formation rate constant in a blob	kisc	Intersystem crossing rate constant
K_a	Acidity constant	k_{ISC}^M	Intersystem crossing rate constant of specie/molecule M
k_a^0	Intercept of the Arrhenius equation for k_a as a function of temperature	kJ	Kilojoule (energy unit)
k_a^{SS}	Excimer formation rate constants obtained from steady state experiments	k_M	Monomer decay rate constant

Abbreviations

Acronym	Definition	Acronym	Definition
k_{NR}	Non radiative rate constant	LUMO	Lowest unoccupied molecular orbital
k_{NR}^E	Non radiative rate constant of the excimer	m	Meter (distance unit)
k_{QM}	Rate constant of quenching of the specie/molecule M by the quencher Q	m	Mass
k_X	Sum of the excimer association and monomer decay rate constants	m	Milli (unit prefix)
k_M^{Ph}	Phosphorescence rate constant of specie/molecule M	m	Mean number of pyrene substituents in polymers
k_M^X	Fluorescence or phosphorescence rate constants	M	Total mass
k_Y	Sum of the excimer dissociation and decay rate constants	M	Monomer, molecule or specie <i>M</i>
<i>l</i>	Path length or length of one bond	M	Transition moment
L	Litre (volume unit)	M_A	Free/isolated monomers
LCST	Low critical solution temperature	M_A[*]	Free/isolated monomers in the excited state
L.D.	Labelling degree	M_{AA}	Acrylic acid molar mass
LED	Light emitting diode	MAGRE	Monomers that gives rise to the excimer
<i>lim</i>	Limit of a function	MALDI	Matrix-assisted laser desorption/ionization
LINCS	Linear constraint solver for molecular simulations	Max.	Maximum
LJ	Lennard-Jones	m_b	Mass of blob
LMCT	Ligand to metal charge transfer	M_B	MAGRE monomers
ln	Natural logarithm function	M_B[*]	MAGRE monomers in the excited state
log	Logarithm function	MC	Monte Carlo
l_p	Persistence length	MCH	Methylcyclohexane
<i>LTL</i>	Low temperature limit	MCPMT	Microchannel plate photomultiplier
		MD	Molecular dynamics
		ME	Maximum entropy
		MEM	Maximum entropy method
		MeOD	Deuterated methanol

Abbreviations

Acronym	Definition	Acronym	Definition
MeOH	Methanol	mole	Amount unit
Method A	This method consist on getting the maximum intensity value at the maximum excimer wavelength and at the maximum monomer band	m_{PAAMePy}	Mass of the PAAMePy polymer
Method B	This method consist in first normalizing both parent compound and compound of interest. Then, the normalized emission of the parent compound is taken as the monomer emission of compound of interest and the area under this spectra leads to the I _M value. The area under the normalized emission spectra of the compound of interest is taken and the monomer band subtracted from it, therefore allowing to obtain the remaining area which is the I _E	m_{Py grafted}	Mass of the pyrene derivative grafted onto the polymer
Method C	In this method the excimer band is fitted with a GaussMod function	M_{Py grafted}	Molecular weight of the Py derivative grafted onto the polymer chain
Method D	In this method the excimer band is fitted with a BiGauss function	m_{Py grafted}	Mass of the pyrene derivative grafted onto the polymer per gram of polymer
M_i	Molecular weight	μs	Microsecond (time unit)
min.	Minimum	M_w	Molecular weight
mL	Millilitre (volume unit)	m_x	Mass of X per gram of polymer
m_i	Mass of particle/atom or molecule <i>i</i>	[M*]	Concentration of the specie/molecule M at time t after excitation
MLCT	Metal to ligand charge transfer	[M*]₀	Concentration of the specie/molecule M at time 0
mm	Millimetre (distance unit)	[M*](t)	Time-concentration dependence of the monomer
M_{mon}	Molecular mass of the monomer (blob model)	<n>	Average of chromophores pr blob (blob model)
M_n	Nominal weight	n	Number of methylene groups in oligomers
		n	Number of particles or bonds
		N	Neutral or specie/molecule N
		N	No
		N	Refraction index
		N	Nano (unit prefix)
		N	Number of particles/atoms or molecules
		N	Possible numbers of pyrene units substituents in polymers

Abbreviations

Acronym	Definition	Acronym	Definition
N	Number of carbons atoms in cyclohexane	ns	Nanosecond (time unit)
N	Moles (amount unit)	Ns/ch	Nanosecond per channel
N	Random number of occurrences	$N_{seg.}$	Total number of segments in which the molecule is split
NA	Not applicable	n_T	Total number of contacts
N_A	Avogadro constant	n_x	Moles of X per gram of polymer
Na₂Cr₂O₇·2H₂O	Sodium dichromate dehydrate	NVT	Canonical <i>ensemble</i>
Na₂SO₄	Sodium sulphate	N^g	Number
n_{AA}	Number of AA segments	O₂	Oxygen molecule
NaCl	Sodium chloride	ORTEP	Oak Ridge Thermal Ellipsoid Plot
$N_{agg.}$	Aggregation number	P	Pico (unit prefix)
NaOH	Sodium hydroxide	P	Pressure
n_c	Number of chains used as basis	p	pico
ND	Not determined or not defined	p	Sum of the moments for all the atoms or molecules involved
N_i	Number of chains with i substituents	p	Probability of a certain occurrence
N_i	Number of blobs in chain i (blob model)	p	Probability distribution for distances
NIPAM	<i>N</i> -isopropylacrylamide	p	Probability of the presence of chains with N pyrene substituents in polymers
NLLS	Non linear least square	P_A	Peak-to-valley absorbance ratio, corresponding in the first vibronic $S_2 \leftarrow S_0$ transition
Nm	Nanometre (distance unit)	PAA	Poly(acrylic acid)
$N_{mon.}$	The same as $N_{seg.}$	PAAMePy	Randomly pyrene labelled poly(acrylic acid)
NMR	Nuclear magnetic resonance	PAH	Polycyclic aromatic hydrocarbon
NP	Not possible to determine	PC	Principal component
n_{PP}	Number of pyrene-pyrene contacts	PCA	Principal component analysis
NPT	Isothermal–isobaric <i>ensemble</i>		
$n_{Py\ grafted}$	Moles of the pyrene grafted on the polymer chain		
$n_{Py\ grafted}$			

Abbreviations

Acronym	Definition	Acronym	Definition
PCT	Photoinduced charge transfer	PNIPAM	Poly(N-isopropylacrylamide)
PD	Photodiode	PNIPAMPy	Randomly pyrene labelled poly(N-isopropylacrylamide)
PDI	Polydispersity index	Prof.	Professor
P_E	Peak-to-valley fluorescence emission intensities ratio, corresponding to the transition (0,0) of the excitation spectrum collected at maximum of the excimer emission.	ps	Picosecond (time unit)
PE	Polyelectrolyte	PS	Polystyrene
PE	Polyethylene	Ps/ch	Picosecond per channel
PEG	Polyethylene glycol	PVC	Polyvinyl chloride
PEO	Polyethylene oxide	Py	Pyrene
PET	Photoinduced electron transfer	q	Sum of the coordinates of all the atoms or molecules
pH	Logarithm of the activity of the hydrogen ion	Q	Quencher
P.I.	Polarity index	q_i	Function of the set of coordinates of each atom or molecule i
PI	Polyion	Q*	Quencher in the excited state
p_i	Moment of each atom or molecule i	r	Position or distance between atoms
$p_{i\alpha}$	Momentum of nucleus i in rotating direction α	R	Ideal gas constant or hydrocarbon chain
pK_a	Logarithmic acid dissociation constant	R²	R-squared
P_M	Peak-to-valley fluorescence emission intensities ratio, corresponding to the transition (0,0) of the excitation spectrum collected at maximum of the monomer emission	r_{CM}	Position of the centre of mass of a body
P_{M-P_E}	Parameter consisting on the difference between P_M and P_E	R_{ee}	End-to-end distance
PMT	Photomultiplier tube	Ref.	Reference
		R_g	Radius of gyration
		$\langle R_g^2 \rangle^{1/2}$	Square root of the average radius of gyration of a chain
		$\langle R_g^2 \rangle_0^{1/2}$	Square root of the average radius of gyration of a non labelled chain
		R_{gyr}	Radius of gyration

Abbreviations

Acronym	Definition	Acronym	Definition
r_i	Position of particle, atom, segment or molecule i	[SDS]	SDS concentration
R_i	Radius of particle i or hard sphere radius of chain segments and simple ions	SI	International System of Units
r_{ij}	Distance between ions or particles i and j	SI	Supporting/Supplementary information
r_{ij}^n	Distance between i and j atoms when in position n	S(k)	Structure factor
r_{ij}^m	Distance between i and j atoms when in position m	sp	Kind of hybridization: 2s orbital mixed with one of three p orbitals
r_j	Vector distance or position of particle, atom or molecule j	SPC	Single photon counting
r_k	Position of particle, atom or molecule k	SS	Steady State
RMSD	Root-mean-square deviations	T	Temperature
RPM	Revolutions per minute (unit of rotation frequency)	T	Transmittance
r_{sph}	Radius of the spherical cell	TAC	Time to amplitude converter
RX	Structure with an hydrocarbon R and a polar group X	TCSPC	Time-correlated single photon counting
R•	Radical specie	TEA	Triethylamine
s	Second (time unit)	THF	Tetrahydrofuran
s	Spin	T_λ	Transmittance at a given λ
S	Entropy	TMS	Tetramethylsilane
S	Shanon-Jaynes entropy function	T_1	1 st triplet excited state
S ₀	Ground state	T_n	n^{th} triplet excited state
S ₁	1 st singlet excited state	$t_{obs.}$	Long finite time
S ₂	2 nd singlet excited state	TR	Time-resolved
SB	Stevens-Ban	T*	Transition temperature
S _n	n^{th} singlet excited state	TV	Television
SDS	Sodium dodecyl sulphate	U	Total potential energy
		$U_{ang.}$	Angular potential energy
		U_{bond}	Bonded potential energy
		UC	<i>Universidade de Coimbra</i>

Abbreviations

Acronym	Definition	Acronym	Definition
u_{ij}	Electrostatic potential plus hard sphere repulsion		
UNL	<i>Universidade Nova de Lisboa</i>	X	Molecular weight of the ungrafted polymer (for PAAMePy) and of the total polymer (for PNIPAMPy) in kg/mol
U_{nonbond}	Non bonded potential energy	X	AA or Py grafted
UV	Ultraviolet	X	Polar (or ionic) group
ν	Frequency or constant taking the value of 0.5 for θ -solvents and 0.6 for good solvents (blob model)	X	Fractions of MAGRE monomers, $(1-\alpha)(1-\beta)$
V	Volume or potential energy	x_{dx}	Mole fraction of dioxane in dx:H ₂ O mixtures
V_b	Volume of blob	x_i	Fraction of chain i in the sample (blob model)
ν_c	Center of the xx' axis (in frequency)	x_{uv}	Degree of labelling determined by UV spectroscopy
V_{dx}	Volume of dioxane	y	Number of repetition of monomer y in polymers
V_{H_2O}	Volume of water	Y	Yes
Vis.	Visible	Y	Labeling degree of the polymers
V_{nm}	Potential between state n and m (before and after motion)	Y	Fraction of GSD, $\alpha(1-\beta)$
$V_{PAAMePy}$	Volume of the PAAMePy polymer solution	z_i	Charge of ion i
V:v	Volume/volume	Z_i	Valence of particle i
Vs.	Versus	z_j	Charge-charge interaction potential
ν^{zz}	Charge-charge interaction potential	$Z_{mon.}$	The same as $Z_{seg.}$
w	Width	Zn	Zinc
w_1	Width of the left side of a Bigauss function	Zn-Al	Zinc-Aluminium
w_2	Width of the right side of a Bigauss function	Z_{NVT}	Partition function of the canonical distribution function
Wl	Halogen	$Z_{seg.}$	Segment charge of the polyion
x	Number of repetition of monomer x in polymers or degree of labeling	*	Excited state

Constants

Symbol	Denomination	Value	SI Units
\AA	Ångström	1×10^{-10} m	
μ	micro	1×10^{-6}	
π	Pi	3.14159265	
c	Speed of light	2.998×10^8	m/s
c	centi	1×10^{-2}	
h	Planck constant	6.626×10^{-34}	$\text{m}^2 \cdot \text{kg} / \text{s}$
k	kilo	1000	
k_B	Boltzmann constant	1.381×10^{-23}	$\text{J} \cdot \text{K}^{-1}$
n	nano	1×10^{-9}	
N	mole	6.022×10^{23} particles	mol
N_A	Avogadro constant	6.022×10^{23}	mol^{-1}
p	pico	1×10^{-12}	
R	Gas constant	8.314	$\text{J} \cdot \text{K}^{-1} \cdot \text{mol}^{-1}$

Chapter 1

Introduction

1.1. Relevance of Photochemistry

Photochemistry is the field of chemistry that studies the interaction of electromagnetic radiation with matter. The importance of studying such interaction is visible in our everyday life (Figure 1.1). Amongst other examples, plants do photosynthesis (converting energy coming from light into chemical energy), the mechanism of vision is associated to the cis-trans photoisomerization of retinal, the fireflies glow (bioluminescence) to attract mates (producing light through a chemical reaction), some mushrooms glow to spread spores, some fishes (as some jellyfish, the cookiecutter shark and the anglerfish), some kinds of squids and some coral glow to attract, eat and/or to defend themselves, and the humans produce vitamin D (important to the correct functioning of the body) by exposure to sunlight.

Moreover, several useful apparatus, equipment and accessories were developed with large application in the industry, science, technology and health. For example, photoinitiated polymerization and photopolymerization are used in photography,¹ fluorescent agents (FAs) are used in laundry to make clothes look whither² and in money bills for the detection of counterfeit money, exciplex-based lasers are used to make eye surgery, chemiluminescence is used in glow sticks by military, solar energy is used to provide electric energy (in photovoltaic panels), light emitting diodes (LED) are used in televisions, X-rays are used for diagnoses and phosphorescent compounds are used in exit signs and in decorative ornaments.

The electromagnetic radiation is a form of energy that combines both wave- and particle-like properties. In the wave model, the electromagnetic radiation is characterized by a wavelength, λ , a frequency, ν , and a velocity, c . The three quantities are related by Equation 1.1. The value of c is constant (2.998×10^8 m/s in vacuum) whereas λ (and consequently ν) may cover a wide range of values. The SI units for λ and ν are the meter (m) and hertz (Hz), respectively.

Introduction

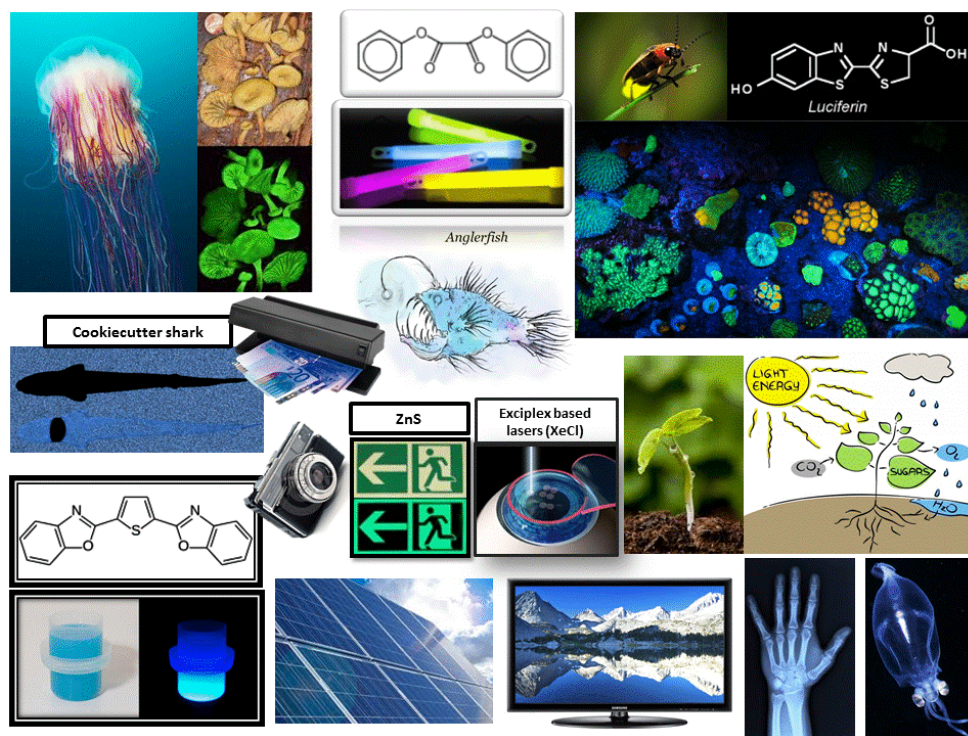


Figure 1.1. Collage illustrating the relevance of photochemistry. From left to right and top to bottom. Semenov, Alexander. [Photograph; Underwater Experiments: Astounding Photographs of Jellyfish]³ from Stevani, Cassius V. [Photographs; Bioluminescent mushroom specie *Neonothopanus gardneri*]⁴, [Photograph; Glow sticks],⁵ [Photograph; Firefly]⁶, [Photograph; Bioluminescence of a coral]⁷, [Photographs; Bioluminescence of a cookie cutter shark viewed from below]⁸, [Photograph; UV Black Fluorescent Tube Currency Detector Machine EURO],⁹ from Ross, Ben. [Illustration; Anglerfish],¹⁰ [Photograph; Camera]¹¹, [Photograph; Phosphorescent exit sign]¹², [Illustration; Refractive surgery and Exciplex laser]¹³, [Photograph; Plant]¹⁴, [Illustration; Photosynthesis]¹⁵, [Photograph; Laundry detergent under day and UV lights]¹⁶, [Photograph; Solar panels],¹⁷ [Photograph; LED TV]¹⁸, [Photograph; left hand X ray]¹⁹ and [Photograph; bioluminescence of a googly-eyed glass squid].²⁰

$$c = \lambda\nu$$

Equation 1.1

In the quantum model, a beam of radiation is regarded as a stream of photons, or *quanta*. A photon has a specific energy, E in joules (J), related to the frequency of the radiation ν by Equation 1.2.

$$E = h\nu$$

Equation 1.2

Where h is the Planck's constant (6.63×10^{-34} J.s).

The spectrum of electromagnetic radiation includes not only the radiation the human eye can detect (thus known as visible radiation or simply "light") but also radio waves, microwaves, infrared, ultraviolet, X-rays and γ -rays (see Figure 1.2).

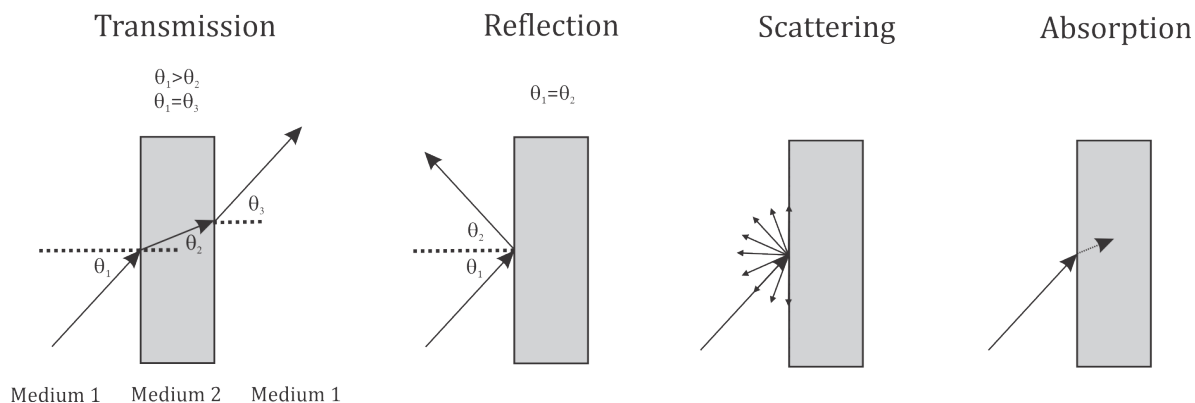


Figure 1.3. Summary of possible paths of an incident electromagnetic wave in a material. Adapted from ref. ²⁹.

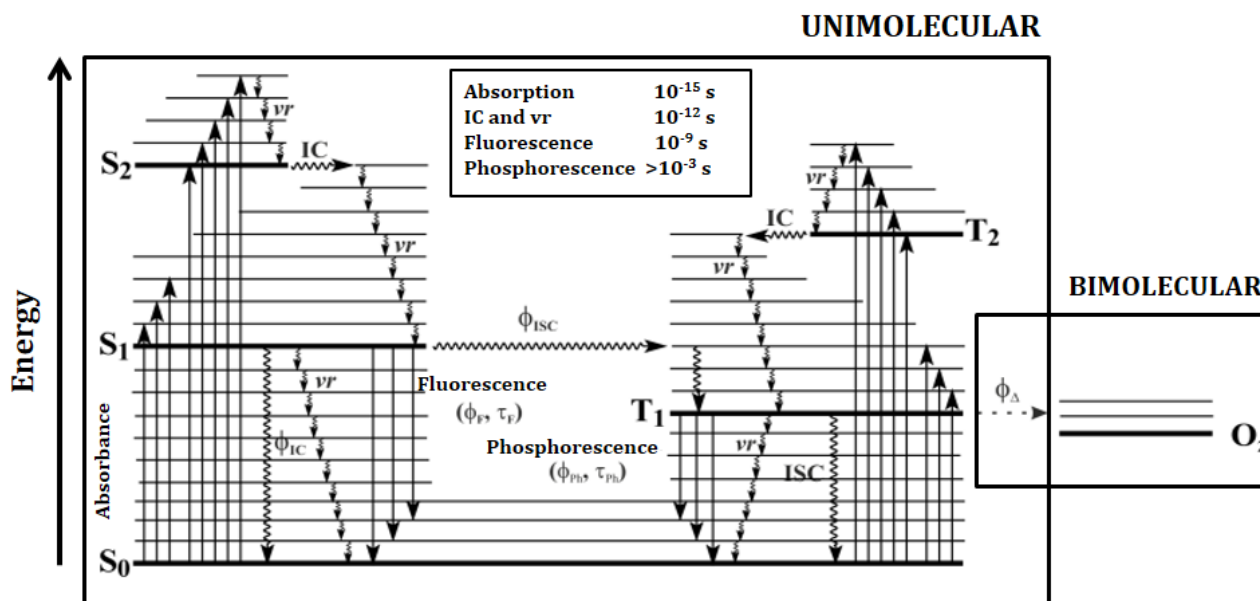
1.2. Unimolecular Photophysical Processes

The interaction that will be discussed here will be only assuming the absorption of a single photon and no interaction with other molecules (unimolecular processes).

If a molecule in its lower energy state (ground state) is exposed to (UV-Vis) radiation having an energy that matches a possible electronic transition within the molecule, some of the light energy will be absorbed as the electron is promoted to a higher energy orbital, i.e., in the excited state (this excitation can also happen by heat or a chemical reaction but in this work only excitation by radiation will be discussed).³⁰ This excited state is unstable and the molecule returns to the ground state. This “coming back” may be accompanied by the emission of radiation (fluorescence or phosphorescence), release of heat (internal conversion or intersystem crossing), a photochemical reaction (degradation) or by a combination of these processes. Fluorescence differs from phosphorescence because the first involves two states with the same spin multiplicity, i.e., between the singlet lowest energy state (S_1) and the ground state (S_0) whereas phosphorescence involves two states of different spin multiplicity (such as $T_1 \rightarrow S_0$). The internal conversion is a non-radiative process that occurs between two states with the same spin multiplicity while the intersystem crossing involves two states of different spin multiplicity. These processes are usually demonstrated by the Jablonski-Pérrin diagram, see Figure 1.4.

The electronic transition from a ground state to an electronically excited state by the absorption of a quantum of light. The necessary condition is that the photon energy (Equation 1.2) matches the energy gap between the ground and excited state, Planck’s law. The energy, for low-energy states of common organic and inorganic molecules, corresponds to light in the UV, visible and near infrared regions.

The absorbance (A) at each wavelength is given by the Beer-Lambert law (Equation 1.3).

Figure 1.4. Jablonski-Pérrin Diagram. Adapted from ref.³¹

$$A_{\lambda} = \log\left(\frac{I_0}{I}\right)_{\lambda} = -\log T_{\lambda} = \varepsilon_{\lambda} c l \quad \text{Equation 1.3}$$

Where I_0 and I are the radiation intensities that penetrates and leaves the sample, respectively, T is the transmittance of the sample at a given wavelength (λ), ε is the extinction coefficient at that wavelength (in $M^{-1}.cm^{-1}$), c is the concentration of the sample (in M) and l is the path length of the solution in cm.

In a very simplified way, Beer's law states that the absorbance is directly proportional to the solution concentration with a proportionality constant ε . However, this law is no longer valid in a high concentration regime.

Ultraviolet and visible radiation interacts with matter which causes electronic transitions (promotion of electrons from the ground state to a high energy state). The ultraviolet region falls in the range between 190-380 nm while the visible region falls between 380-750 nm. The electronic transitions that are possible are $n - \pi^*$, $\pi - \pi^*$, $n - \sigma^*$, $\pi - \sigma^*$, $\sigma - \pi^*$ and $\sigma - \sigma^*$.

As a rule, energetically favoured electron promotion will be from the highest occupied molecular orbital (HOMO) to the lowest unoccupied molecular orbital (LUMO).

The region where a coloured compound absorbs (a chromophore) can be provided by the colour wheel since when a white light passes through or is reflected by a coloured substance, a characteristic portion of the mixed wavelengths is absorbed. The remaining light will then assume the complementary colour to the wavelength(s) absorbed.

For example, if a compound is red it must absorb at the complementary colour (the diametrically opposite colour), i.e., green (between ~490 and 560 nm). See example in the left panel of the Figure 1.5.

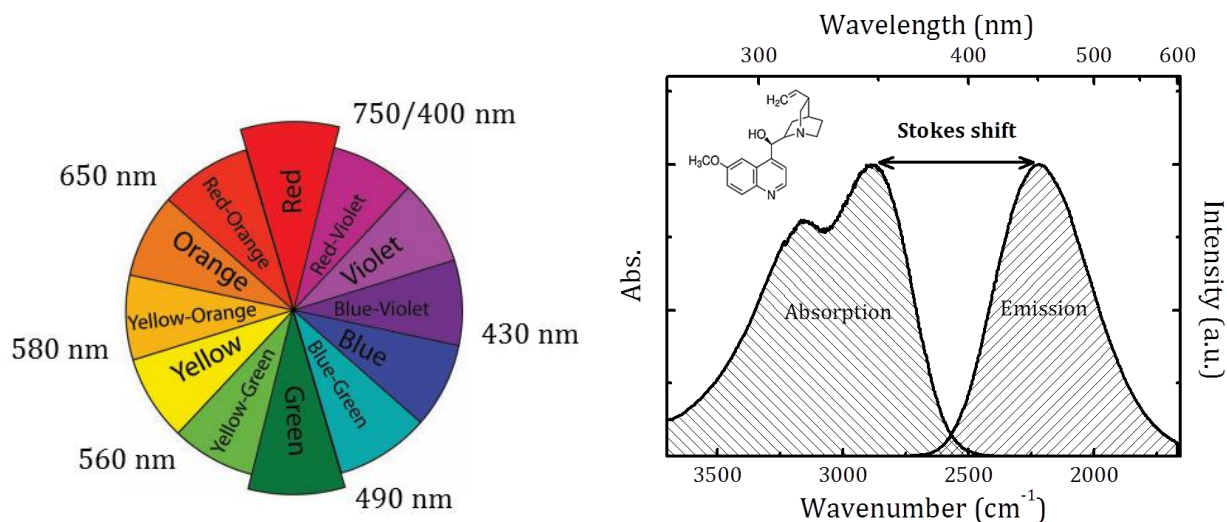


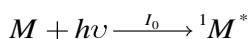
Figure 1.5. From left to right. Illustration of the colour wheel adapted from [Image; Complementary Colours]³² and absorption and fluorescence emission spectra ($\lambda_{\text{exc}} = 348 \text{ nm}$) of quinine sulphate in acidic water. Note: Quinine sulphate is only soluble in acidic medium.

Some terms are used when describing shifts in absorption.³³ The bathochromic (or red) shift is the shift of the absorption spectrum towards longer wavelengths whereas the hypsochromic (or blue) shift is the shift of the absorption spectrum towards smaller wavelengths. A hyperchromic shift is an increase in the absorption intensity and a hypochromic shift is a decrease in the absorption intensity.

In case of fluorescence emission and due to energy dissipation during the excited-state lifetime, the energy of the emitted photon is lower and, therefore, of longer wavelength, than the photon that excite the sample, i.e., the absorbed photon. This difference of energy is defined as the Stokes shift, see right panel of Figure 1.5.

1.2.1. Kinetics of Unimolecular Photophysical Processes

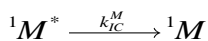
The unimolecular photophysical process that involve the singlet excited state of a specie M can be schematized by Scheme 1.1 to Scheme 1.4.



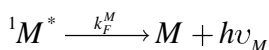
Scheme 1.1



Scheme 1.2



Scheme 1.3



Scheme 1.4

The fluorescence intensity dependence with time $[I_F^M t]$, resulting from the excitation with a ultrashort (or δ -) pulse, is given by Equation 1.4.

$$I_F^M t = k_F^M [M^*] = k_F^M [M^*]_0 e^{-t/\tau_M} \quad \text{Equation 1.4}$$

Where $[M^*]$ and $[M^*]_0$ are the concentrations of the excited species at time t after excitation and at time zero, respectively, and τ_M is the fluorescence lifetime given by Equation 1.5.

$$\tau_M = \frac{1}{k_F^M + k_{ISC}^M + k_{IC}^M + k_{NR}^M} \quad \text{Equation 1.5}$$

In steady state conditions, for example, the fluorescence quantum yield is given by the ratio between the number of emitted photons and the number of absorbed photons, which is given by Equation 1.6.

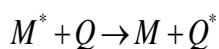
$$\phi_M = \frac{1}{[M^*]_0} \int_0^\infty I_F^M t = \frac{k_F^M}{k_M} \quad \text{Equation 1.6}$$

Where k_M correspond to the sum of all the rate constants of the deactivation process involved.

Besides the unimolecular processes shown in Figure 1.4, there are other that are characterized by involving the excited species and another (equal or different) species (bimolecular process). The next Section one of these processes (quenching) will be explained shortly.

1.3. Bimolecular Photophysical Process: Quenching

Due to the fact that a molecule in the excited state (M^*) is highly reactive, it can deactivate due to the interaction with other molecules. One of these deactivation processes is quenching and can occur when the lifetime of the excited state is long enough to allow the encounter between the molecule and the quencher Q. The quenching process can be described by



With a rate constant k_{QM} . If this rate constant is not time-dependent, then the lifetime is given by Equation 1.7 and the quantum yield by Equation 1.8.

$$\tau_{QM} = \frac{1}{k_M + k_{QM}[Q]} \quad \text{Equation 1.7}$$

$$\phi_{QM} = \frac{k_M^X}{k_M + k_{QM}[Q]} \quad \text{Equation 1.8}$$

Where k_M^X stands for the fluorescence or phosphorescence rate constants (k_M^F and k_M^{Ph} , respectively).

Considering Equation 1.7 and Equation 1.8 one can obtain Equation 1.9.

$$\frac{\tau_M}{\tau_{QM}} = \frac{\phi_M}{\phi_{QM}} = 1 + k_{QM}\tau_M [Q] \quad \text{Equation 1.9}$$

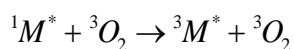
From Equation 1.9 it can be seen that the quenching will be more important the longer the lifetime of the emissive species.

The main photophysical processes responsible for quenching are collision with a heavy atom (e.g., I⁻) or a paramagnetic species (e.g. O₂), excimer and exciplex formation, electron, proton and energy transfer.³⁴

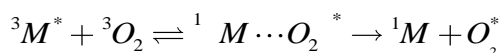
1.3.1. Quenching by Oxygen

The interaction of oxygen (which ground state electronic configuration is a triplet) with a fluorophore in the (singlet or triplet) excited state involves the formation of oxycomplexes between the excited molecule and the oxygen in the ground state.

For the quenching of the singlet, the process most probable, in solvents of small viscosity, is mirrored by an increase of the intersystem crossing describe by the process



The quenching of the triplet states involves the formation of oxycomplexes of different multiplicities (singlet, triplet and quintet).



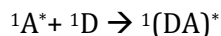
This process is extremely important for the phosphorescence quenching since the lifetimes can go to the second time range. For this reason, phosphorescence emission is measured generally at low temperatures (e.g. 77 K, with liquid nitrogen) in order to minimize quenching. The oxygen concentration in several solvents at standard atmosphere pressure and temperature can be found in ref³⁵.

Molecular oxygen is a very efficient quencher, such that for sensitive and reproducible in most solutions it is necessary to remove the oxygen either by carrying out a number (up to 5) of freeze-pump-thaw cycles (cooling in liquid nitrogen, evacuating to remove any gas, sealing from the atmosphere and thawing to release dissolved gases) or by purging an inert gas (e.g. nitrogen) through the solution with subsequent sealing of the cuvette.³⁶ The latter will be discussed with more detail in Section 7.2.3.

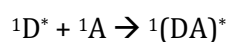
In both methods, some precautions must be taken. In the freeze-pump-thaw method, care should be taken for the cell not to break while when bubbling nitrogen into the solution is necessary to check if there is no evaporation of the solvent and consequent increase of the solution concentration. Moreover the freeze-pump-thaw is avoided when delicate structures (e.g. proteins) are involved since they can be altered or destroyed.³⁷

1.3.2. Excimer and Exciplex

As previously mentioned, another possibility to have quenching can occur by the formation of an excited state dimer. The term *excited dimer* is employed to designate an electronically excited complex of an atom or molecule with another atom or molecule. This excited state complex is stabilized by charge-transfer interactions between the electron donor (D) and electron acceptor (A) atom or molecule, but is generally not stable in the ground state.³⁸⁻⁴⁰ These dimers usually result from the collision between an electronically excited A or D, with D or A in its ground state.



or



If D and A are identical molecules, the dimer is named excimer (from the junction of *excited state dimer*), but, if D and A are not the same, it is an exciplex (from the junction of *excited state complex*), it is also known as *heteroexcimer*, although it is less commonly used.

Excimers can occur with atoms (helium, xenon, neon, argon, *etc.*) and with aromatic molecules (benzene, naphthalene, anthracene, pyrene, *etc.*).⁴⁰ Excimers from aromatic molecules have been observed in fluid solutions, pure liquids, vapours and crystals when the crystal structure allows a close overlap of the molecular planes. The stoichiometry of the formed complex is usually 1:1, but 2:1 exciplexes have also been reported.⁴⁰

An additional concept, introduced by Birks, is that of mixed dimers,³⁸⁻⁴⁰ consisting of exciplex formation between a pair of different, but very similar molecules, e.g., the exciplex formed between an aromatic hydrocarbon and an alkyl derivate of this same aromatic hydrocarbon. In this case, the perturbation of the electronic levels by the alkyl chain is very small. Two distinct situations can occur in the case of mixed dimers, depending on whether the fluorescence emission intensity of the mixed dimer is higher or lower than the sum of the excimer emission intensities of the two pure compounds.⁴¹ The first situation occurs in a mixture of e.g., pyrene and 1-methylpyrene, where the resultant excimer emission is twice the sum of the excimers formed by pure pyrene and 1-methylpyrene solutions. The opposite occurs in a mixture of pyrene and benzo[a]phenanthrene (chrysene) and has been explained by the formation of non-fluorescent mixed-dimers.³⁸

1.3.2.1. Intramolecular and Intermolecular Excimers

Intramolecular and intermolecular excited dimer (Figure 1.6 and Figure 1.7) are distinguished by the type of interaction that leads to the formation of the dimer and consequently will affect some parameters.

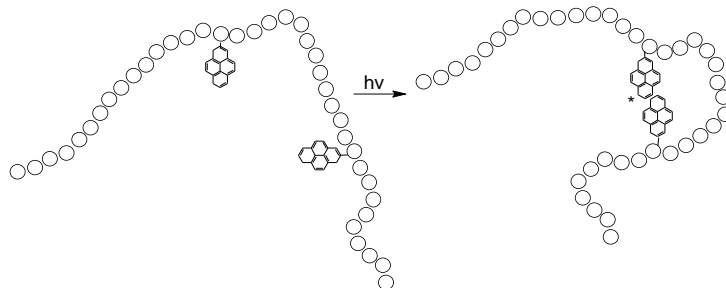


Figure 1.6. Illustration of the process of intramolecular excimer formation.

As can be seen in Figure 1.7, the formation of an intramolecular excimer follows, as stated above, interaction between two monomers, one in the other in the ground state and other in the excited state. When it comes to intermolecular excimer, as the name implies, results in interaction between two (or more) chromophores units from different (polymer or oligomer) chains.

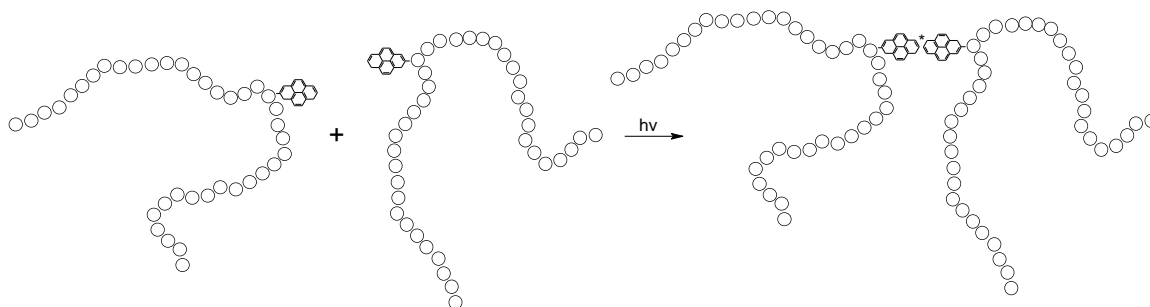


Figure 1.7. Illustration of the process of intermolecular excimer formation.

These dimers are only obtained when the concentration is quite high (1×10^{-2} - 1×10^{-3} M), but as in this work the solutions were prepared with an absorbance at 335 nm between 0.1 and 0.2 (i.e., with concentration is approximately 1×10^{-6} M) then, it is correct to assume that there is only intramolecular excimer formation. This can be further visualized by the I_E/I_M (Section 7.2.6.1.2.1 in Chapter 7) ratio as a function of the concentration. See example in Figure 3.57 in Chapter 3.

It is also known that the rate constant for formation of excimer (k_a) depend on the concentration of the monomer can be said to a process intermolecular ($k_a[M]$) and in the opposite case, the procedure is to be intramolecular.

The presence of dimers (excited -intra or inter- or ground state dimers) are usually first noticed by the observation of a broad and structureless band which is shifted *ca.* 5000-6000 cm^{-1} to lower frequencies relative to the monomer fluorescence.

The first reported excimer dated from 1954, when Förster and Kasper observed that, although the absorption spectrum of pyrene remained unchanged at high concentrations, the emission spectrum displayed an additional band at longer wavelengths. In this case, the dimer formed was an *intermolecular excimer*.

1.3.2.1.1. Conformations of the Excimer

Theoretical studies performed on dimers of benzene, naphthalene and anthracene showed to have 3, 4 and 4 different excimer configurations with different relative orientations and distances, respectively: one sandwich-like, and one parallel displaced and two T-shaped (except for benzene that only possess one) configurations.^{42,43} The parallel-displaced conformation was found to be the most stable, due to the higher interpenetration of the electron clouds and consequent stabilization of the electrostatic interaction. In the case of naphthalene and anthracene, the conformers with the lowest energy showed crossed and parallel-displaced configurations.^{42,43} The T-shaped conformation is not a minimum since it transforms promptly into a crossed structure. However, two higher energy T-shaped minima were found (see Figure 1.8). Additionally the displacement between the aromatic molecules, in a parallel-displaced fashion, decreases with the increase in the number of benzene rings of the aromatic hydrocarbon molecules.⁴³

Excimers with crossed and parallel-displaced conformations are frequently obtained when the fluorophore is linked to an alkyl chain, see Section 2.1.⁴⁴⁻⁴⁷

These conformational different excimers, which have been found on several aromatic hydrocarbons, such as carbazole,⁴⁸ pyrene,⁴⁴⁻⁴⁷ and perylene,^{49,50} emit in the same wavelength range, but show different decay times, which make them distinguishable from time-resolved (TR) fluorescence measurements.

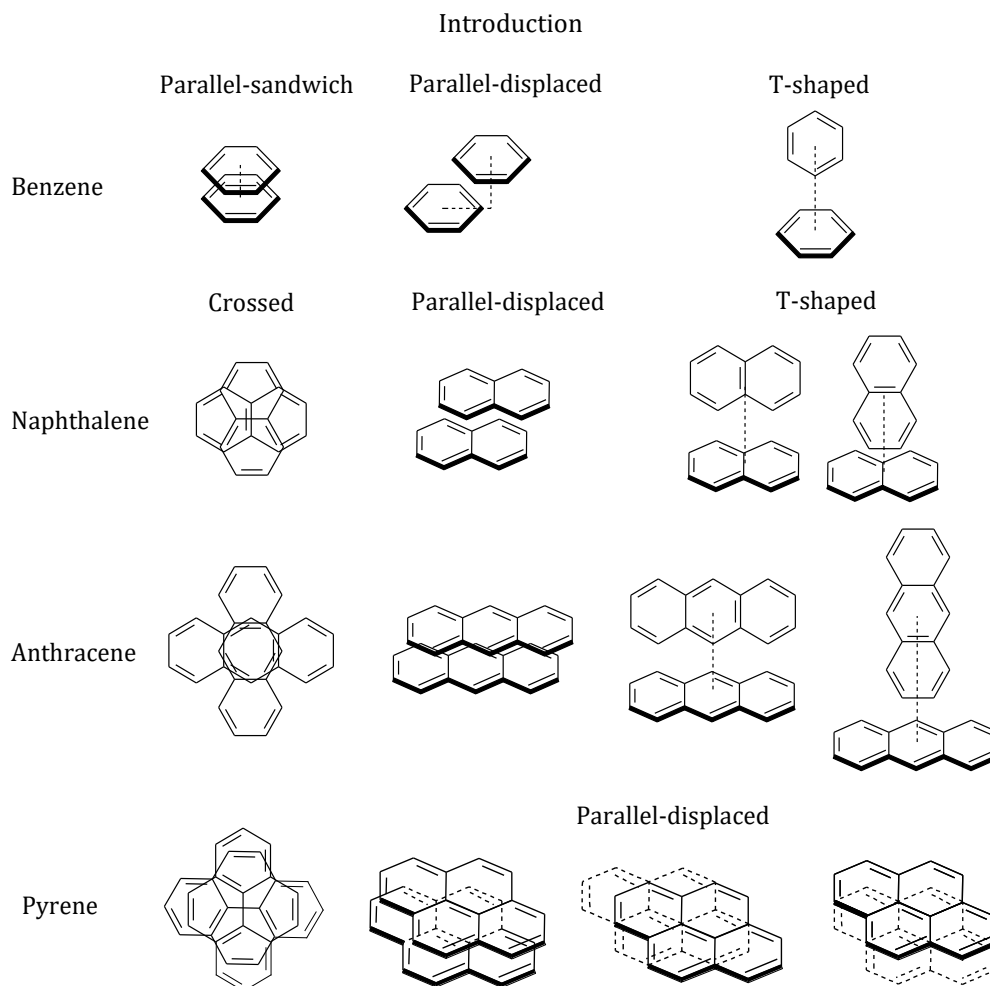


Figure 1.8. Configuration of benzene, naphthalene, anthracene and pyrene dimers.^{51,52}

1.3.2.1.2. Ground State Dimers (*GSD*)

A ground state dimer is observed, not due the diffusive encounter between two species but, instead, due to the direct excitation of dimers that are pre-associated in the ground state.

Ground state dimers (*GSD*) of aromatic molecules are commonly observed when the chromophores are found labelled into a polymer chain, when absorbed on silicas, aluminas, clays or zeolites;⁵³⁻⁵⁸ or when forming complexes with cyclodextrins,^{59,60} calixarenes,⁶¹ or metal ions⁶² or even when in bad solvents (e.g. PAA labelled with pyrene in water).⁶³⁻⁶⁵ These excimers are formed through a static mechanism (in contrast with the dynamic excimer formation which implies the diffusive encounter between two molecules). The *GSD* is characterized by the existence of a minimum in the ground state potential energy curve.

The presence of a *GSD* can be qualitatively detected from the absorption, emission and excitation spectra. The existence of *GSD* is mirrored by a broadening and red-shift of the absorption spectra when compared to the equivalent spectra in the absence of ground state dimer, i.e., the spectra of the monomer. The relative degree of the band broadening is also followed by a parameter: the peak-to-valley ratio of the S_0 - S_2 absorption band (P_A ratio, see Section 7.2.5.2.1 in Chapter 7); a higher ground

state dimer contribution induces a lower P_A value. Values of $P_A = 3$ for pyrene labelled polymers are generally considered to be indicative of the absence of *GSD*.⁶⁶ The red-shift of the absorption spectra can be measured from the $\Delta\lambda_1$ parameter (see Chapter 7), which again may be related with the preferential absorption from *GSD* on the red-edge of the spectra. Accordingly, the increase in the wavelength of excitation also results in an increase of the I_E/I_M ratio.

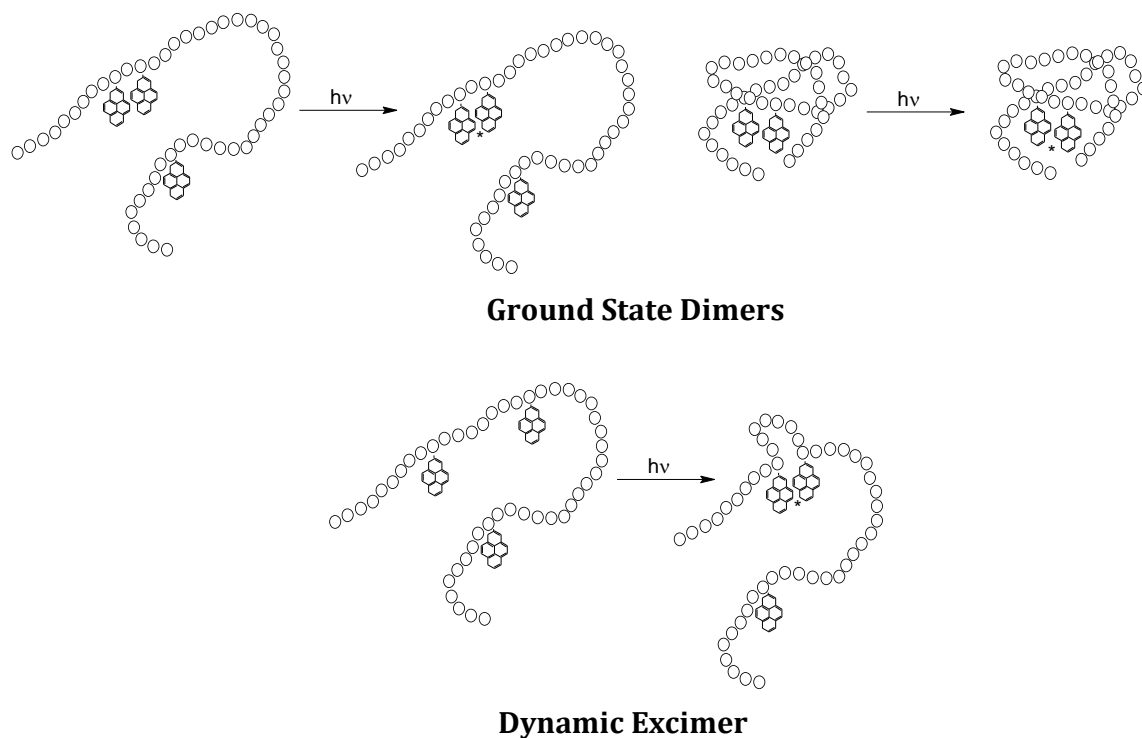


Figure 1.9. *From top to bottom.* Illustration of the process of *GSD* (from consecutive or not pyrene units, from left to right) and dynamic excimer formation.

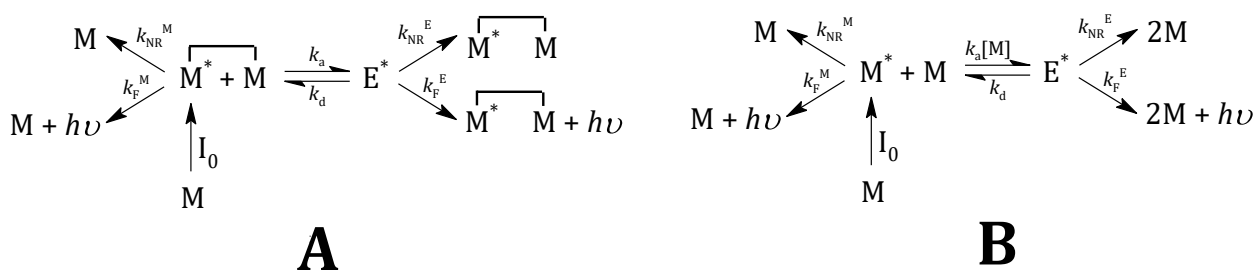
In the absence of *GSD*, the excitation spectra, collected at the monomer and excimer emission wavelengths, should totally overlap. The presence of *GSD* is mirrored by the occurrence of (i) a shift between the maxima of the excitation spectra ($\Delta\lambda_2 > 0$) and (ii) a difference between the peak-to-valley ratios, obtained at the monomer (P_M) and excimer (P_E) emission wavelengths, $P_M - P_E$ (see Section 7.2.6.1.2.3 in Chapter 7). Differences between the excitation spectra collected in the monomer and excimer regions are strongly enhanced when pyrene is located in constrained environments such as encapsulated into cyclodextrin⁶⁰ cavities or incorporated into Zn–Al layered double hydroxides.⁵⁵

Anthracene and perylene also show changes in their photophysical properties at high concentrations.⁶⁷ With these compounds, a new vibronically resolved band appears at the absorption spectrum which is the mirror image of the excimer-like emission band, strongly supporting the idea of dimer formation.

Finally, the presence of *GSD* is seen from the departure from zero of the sum of the pre-exponential factors at the excimer emission wavelength ($a_{2,1}+a_{2,2}$). This is often observed with randomly labelled polymers where low and highly labelled regions coexist within the same polymer chain. In the case where excimer formation mainly occurs through the direct excitation of *GSD*, no rise-time (in a nanosecond time domain) is observed at the excimer emission wavelength. In the case of coexistence of dynamic and static excimer formation, the equations derived from Birks' kinetic scheme for the pre-exponential factors are no longer valid and a model which now depends on the fraction $(1-\alpha)$ of excited *GSD*, must be considered. In this case $a_{2,1}+a_{2,2}= 1-\alpha$.^{63,68}

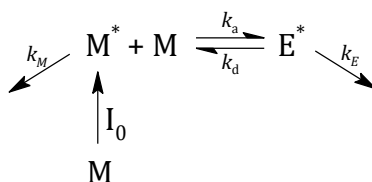
1.3.2.1.3. Kinetics of Excimer Formation

The kinetic for the excimer formation can be schematized for one specie *M* of concentration [*M*] by Scheme 1.5.



Scheme 1.5. Kinetic scheme for (A) intra- and (B) intermolecular excimer formation.

The non-radiative rate constants (k_{NR}) and the fluorescence rate constants will be included in an only constant, for example, for the excimer $k_E = k_F^E + k_{NR}^E$. And the ground state species recovered from the fluorescence emission (below the arrow with k_F rate constants) will be omitted from now on for simplification (Scheme 1.6). Besides and since only intramolecular excimer formation will be discussed, the lines linking the monomers in Scheme 1.5A will be omitted as well for simplification.



Scheme 1.6. Simplified kinetic scheme for excimer formation. Birks kinetic scheme.

In the Scheme 1.5, *M* is the ground state monomer and *M** and *E** are the excited state monomer and excimer, respectively. For the excimer, the * is redundant since this specie does not exist in the ground

state. k_a and k_d are the association and dissociation rate constants of excimer formation whereas k_M and k_E are monomer and excimer fluorescence decay rates ($1/\tau_M$ and $1/\tau_E$, respectively). The time evolution of the monomer and excimer intensities can be obtained by the Equation 1.10 and Equation 1.11, respectively.⁴⁴

$$\frac{d[M^*]}{dt} = -\underbrace{\left(k_a + \frac{1}{\tau_M}\right)}_{k_X} [M^*] + k_d [E^*] \quad \text{Equation 1.10}$$

$$\frac{d[E^*]}{dt} = k_a [M^*] - \underbrace{\left(k_d + \frac{1}{\tau_E}\right)}_{k_Y} [E^*] \quad \text{Equation 1.11}$$

The time-concentration dependence equations of the monomer and excimer are given by Equation 1.12 and Equation 1.13.⁴⁴

$$[M^*]_t = a_{11}e^{-\lambda_1 t} + a_{12}e^{-\lambda_2 t} = \frac{I_M t}{k_F^M} \quad \text{Equation 1.12}$$

$$[E^*]_t = a_{21}e^{-\lambda_1 t} + a_{22}e^{-\lambda_2 t} = \frac{I_E t}{k_F^E} \quad \text{Equation 1.13}$$

Where a_{1i} and a_{2i} are the pre-exponential factors associated with the decay times τ_i ($i=1, 2$) at the monomer and excimer emission wavelengths, respectively. $k_F^M = \phi_M/\tau_M$ and $k_F^E = \phi_E/\tau_E$ are the monomer and excimer radiative rate constants, which express the efficiency of excimer and monomer fluorescence, respectively, and ϕ_M and ϕ_E are the fluorescence quantum yields for the monomer and excimer species.

The eigenvalues λ_1 and λ_2 are obtained by the resolution of the second order determinant of the coefficient matrix of Equation 1.10 and Equation 1.11, Equation 1.14.

$$\begin{vmatrix} -k_X + \lambda & k_d \\ k_a & -k_Y + \lambda \end{vmatrix} = 0 \quad \text{Equation 1.14}$$

Equation 1.14 gives rise to the quadratic equation (Equation 1.15)

$$\lambda^2 - (k_X + k_Y)\lambda + k_X k_Y - k_a k_d = 0 \quad \text{Equation 1.15}$$

The solutions of the quadratic equation are given by Equation 1.28.

$$\lambda_{1,2} = \frac{k_X + k_Y \pm \sqrt{k_Y - k_X}^2 + 4k_a k_d}{2} \quad \text{Equation 1.16}$$

From these equations (Equation 1.10 to Equation 1.16), the association and dissociation rate constants in Scheme 1.5 can be determined (Equation 1.17 to Equation 1.19).

$$k_a = \frac{\lambda_1 + A\lambda_1}{A+1} - \frac{1}{\tau_M} \quad \text{Equation 1.17}$$

$$k_d = \lambda_1 + \lambda_2 - k_X - \frac{1}{\tau_E} \quad \text{Equation 1.18}$$

$$k_E = k_Y - k_d \quad \text{Equation 1.19}$$

Where $A = a_{12}/a_{11}$. The equations and formulas relating the rate constants to the decay times and pre-exponential factors can be found in Appendix A. The excimer to monomer (I_E/I_M) ratio, obtained from the steady state fluorescence emission spectrum is related to the efficiency of excimer formation and with the k_a and k_d rate constants, by the Equation 1.20.

$$\frac{I_E}{I_M} = \frac{k_F^E}{k_F^M} \frac{k_a [M^*]}{k_d + 1/\tau_E} \quad \text{Equation 1.20}$$

1.3.2.1.4. Thermodynamics of Excimer Formation

The temperature fluorescence emission spectra allow the determination of thermodynamic parameters: the enthalpy (ΔH) (from the high temperature limit - *HTL*) and the activation energy (from the low temperature limit - *LTL*) of excimer formation (E_a). For that, a plot $\ln(I_E/I_M)$ as a function of the reciprocal of the temperature ($1/T$) should be obtained. The curve obtained has usually a bell shape and is known as the Steven-Ban plot. From the slope of the *LTL*, the activation energy of the excimer formation is obtained from the Equation 1.27 and the slope of the *HTL* gives us the enthalpy binding energy of the excimer by Equation 1.28. From the activation energy and enthalpy, the dissociation energy (E_d) can be further obtained, Equation 1.28. The transition temperature (T^*) is given by the x value of the crossing point of both *HTL* and *LTL* linear fittings of the curve while the difference between the y value of this crossing point and the value of the $\ln(I_E/I_M)$ of the Stevens-Ban (SB) curve is defined as δ . This value is $\ln 2$ for a pure dynamic process. Indeed, this value can be used to determine if the *LTL* and *HTL* are well defined, or if Birks kinetics is in fact the ideal model to describe excimer formation in the investigated system.⁶⁹

For the photostationary fluorescence dependence with temperature, Equation 1.20 can be rewritten, Equation 1.21.

$$\frac{I_E}{I_M} = \frac{k_F^E}{k_F^M} \frac{k_a}{k_d + k_E} \quad \text{Equation 1.21}$$

$$\frac{I_M^0}{I_M} - 1 = \frac{k_a \tau_M}{k_d + k_E} \quad \text{Equation 1.22}$$

In general, when the temperature is increased, the excimer dissociation rate constant, k_d , increases faster than k_E , giving rise to a limit where $k_d \gg k_E$ (*HTL*) and leading to a simplification of the Equation 1.21 and Equation 1.22 to Equation 1.23 and Equation 1.24.⁶⁹

$$\left(\frac{I_E}{I_M} \right)_{HTL} = \frac{k_F^E k_a}{k_F^M k_d} \quad \text{Equation 1.23}$$

$$\left(\frac{I_M^0}{I_M} - 1 \right)_{HTL} = \frac{\tau_M k_a}{\tau_E k_d} \quad \text{Equation 1.24}$$

This means that, within this limit, the k_a/k_d ratio is the equilibrium constant for excimer formation. The opposite consideration, i.e., $k_d \ll k_E$ (*LTL*) leads to the simplification of the Equation 1.21 and Equation 1.22 to the Equation 1.25 and Equation 1.26.^{69,70}

$$\left(\frac{I_E}{I_M} \right)_{LTL} = \frac{k_F^E k_a}{k_F^M k_E} \quad \text{Equation 1.25}$$

$$\left(\frac{I_M^0}{I_M} - 1 \right)_{LTL} = k_a \tau_M \quad \text{Equation 1.26}$$

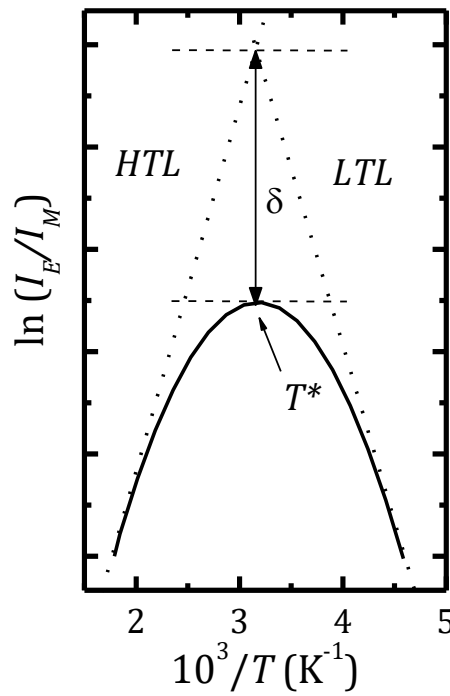


Figure 1.10. Schematic representation of the Stevens-Ban plots. Generic bell-shaped curve showing the *HTL* and *LTL* regions; the difference (δ) between the curve defining the normal regime and the crossing point of the lines defining the *HTL* and *LTL* regimes, T^* (transition temperature between the two regimes), are clearly identified.⁵¹

The resulting Arrhenius-type plots of $\ln(I_E/I_M)$ versus the reciprocal of temperature, yield two straight lines, the slope of which define, in the *LTL*, the activation energy for excimer formation (E_a) and, in the *HTL*, the enthalpy of formation (ΔH), or the binding energy, for the excimer complex, Equation 1.27 and Equation 1.28, respectively (Figure 1.10).

$$\left(\frac{d \ln \left(\frac{I_E}{I_M} \right)}{\frac{1}{T}} \right)_{LTL} = -\frac{E_a}{R} \quad \text{Equation 1.27}$$

$$\left(\frac{d \ln \left(\frac{I_E}{I_M} \right)}{\frac{1}{T}} \right)_{HTL} = -\frac{\Delta H}{R} = -\frac{(E_a - E_d)}{R} \quad \text{Equation 1.28}$$

At room temperature, a system can be either in the *LTL* or in the *HTL* region, depending on the chromophores and on the solvent. The intersection between the two temperature limits corresponds to the situation where $k_d = k_E$ and to the temperature where the maximum efficiency of excimer formation is reached.

For a reversible reaction, the equilibrium constant can be measured at a variety of temperatures. The equilibrium constant of excimer formation in this case is given by the k_a/k_d ratio. By plotting the $\ln(k_a/k_d)$ as a function of the reciprocal of the temperature (van't Hoff plot), both enthalpy and entropy can be obtained by the slope and intercept in the yy' axis, respectively.

$$\ln \frac{k_a}{k_d} = -\frac{\Delta H}{RT} + \frac{\Delta S}{R} \quad \text{Equation 1.29}$$

$$\ln k_i = \ln k_i^0 - \frac{E_a}{RT} \quad \text{Equation 1.30}$$

Where k_i can be any of the rate constants (k_a or k_d). Equation 1.30 is known as the Arrhenius equation.

1.4. Fluorescent Probes

Probes are molecules that exhibit characteristics that depend on the spectroscopic properties of the medium. The appearance of new bands, spectral shift of the wavelength of absorption and/or emission and changes in the fluorescence intensity provide an indication of the environment where the probe is located.

From a photochemical point of view, probes can be either phosphorescent or/and fluorescent. However, the majority are focussed on fluorescent probes. Besides, it can be added to the system to be studied (extrinsic) or being already part of the system under study (intrinsic).

A good probe needs to have some particular characteristics. It is therefore necessary that there is little overlap between the emission spectra and absorption in order to avoid self-absorption. Furthermore, its spectrum should contain some characteristic that is dependent on the polarity of the solvent (as I_1/I_3 in Pyrene, see Section 7.2.6.1.2.2 in Chapter 7). It should induce variations in the relative intensity of

emission bands, the peak wavelength of fluorescence or the fluorescence quantum yield. A good probe has long lifetimes in the singlet state, may form exciplex or excimer with monomer and excimer/exciplex bands well separated. In addition to the probes herein studied and the studies mentioned above there are many applications of pyrene molecular probes in studies related to nucleic acids, proteins, cell membranes and ions. Their primary application is to detect and measure the concentration of these molecules, to determine the flexibility of membranes, *etc.*⁷¹ In addition, a large number of molecular probes have been used for the experimental determination of the polarity of the solvents or on pyrene microenvironments in proteins and membranes.⁷²⁻⁷⁴

1.4.1. Polycyclic Aromatic Hydrocarbons (PAHS)

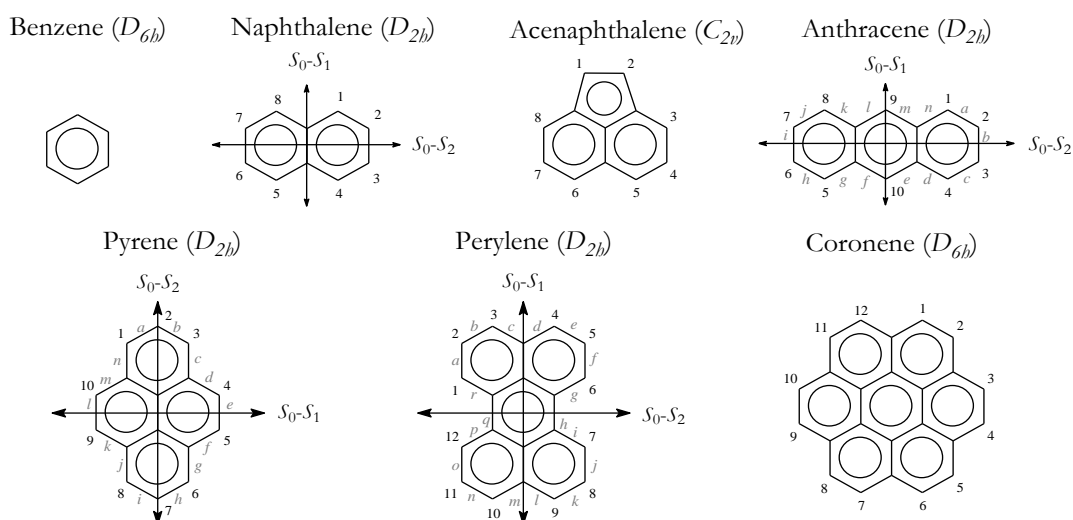


Figure 1.11. Name, structure, symmetry group, numbering and absorption ($S_0 \rightarrow S_1$ and $S_0 \rightarrow S_2$) transition moments of selected PAHs.³⁴

From this extensive list of PAHs (Figure 1.11), two will be highlighted, naphthalene and pyrene once they are referred often in this work.

1.4.1.1. Naphthalene

Naphthalene was discovered in the early 1820s and described as a white solid with a pungent odour. John Kidd proposed the name *Naphthaline* as it had been derived from a kind of naphtha (a broad term encompassing any volatile, flammable liquid hydrocarbon mixture, including coal tar).⁷⁵ Naphthalene's chemical formula was determined by Michael Faraday in 1826. The structure of two fused benzene rings was proposed by Emil Erlenmeyer in 1866,⁷⁶ and confirmed by Carl Gräbe three years later. It is best known as the main ingredient of small balls of chemical pesticide and deodorant (mothballs) used to protect clothing from mold or moth larvae.

Aside from coal tar (and, consequently as a component of pollution), trace amounts of naphthalene are produced by magnolias and certain types of deer, as well as the Formosan subterranean termite and some fungus (namely, *Muscodor albus* and *Muscodor vitigenus*). Besides it was found in meteorites.⁷⁷

The quantum yield of naphthalene in cyclohexane is 0.23.⁷⁸

1.4.1.2. Pyrene

Pyrene has firstly been discovered by the French chemist Auguste Laurent in 1837 by extraction from coal tar (as Naphthalene) but the correct chemical formula has been determined later by Gräbe 1871 and the structure by Bamberger and Philip in 1887.⁷⁹⁻⁸¹ Since its discovery pyrene has predominantly attracted attention for its outstanding photophysical properties, which is why pyrene is called “the fruit fly of photochemists”.⁸² Pyrene is a nonpolar polyaromatic hydrocarbon with low solubility in water (6×10^{-7} M) and it is undoubtedly the probe the most publicized and used due to its particular characteristics. Solubility tables of pyrene in several solvent or mixtures of solvents can be found in reference ⁸³.

The isolated pyrene chromophore has a resolved absorption and emission spectra ($\phi_F = 0.65$).⁸⁴ For concentrations inferior or equal to 1×10^{-5} M, the emission spectrum consists of a single band vibrationally resolved corresponding to the monomer emission with a maximum at approximately 375 nm. For higher concentrations, the absorption spectra remain unchanged while the fluorescence emission spectrum is modified, that is, the bandwidth of the monomer becomes less intense and appears another band to longer wavelengths without vibronic resolution (approximately 470 nm), which corresponds to emission band the intermolecular excimer of pyrene.

Other features that make it attractive as a fluorescent probe its sensitivity to the micropolarity and microviscosity of the microenvironment where it is found. The microviscosity of the medium is related to the ratio I_E/I_M . Considering that the excimer formation process controlled by diffusion, an increase in the ratio I_E/I_M implies a decrease in viscosity of the medium where the probe is located.

Pyrene is used to probe protein conformation and conformational changes^{85,86}, to determine the critical micelle concentration (CMC) of a surfactant, as chemosensor, termosensor, etc.

Chapter 2

Oligomers

2.1. Introduction

The word oligomer derives from the agglutination of the Greek *oligo-* (few) and *-mer* (parts). As the origin of the word suggests, an oligomer is a molecule in which one or more type of simple chemical units (known as monomers) are repeated in a small and finite number in contrast to a polymer [*poly-* (many) + *-mer*] that, at least in principle, consists on a nearly unlimited number of monomers. Dimers, trimers, and tetramers are, for instance, oligomers respectively composed of two, three and four monomers. The physical properties of an oligomer strongly depend on the type and number of units.⁸⁷

The oligomers can have natural origin (e.g. peptides) or synthetic as 1,1'-dipyrenylalkanes (Figure 2.1). In our work these oligomers have one or two fluorophoric units present.

These oligomers can be used to study the influence of several factors, such as chain length, pressure, solvent and temperature on the intramolecular excimer formation process.^{44,45,47,68,88} Intramolecular excimer formation in molecules where chromophoric units are linked to the extremities of a connecting chain, has been extensively studied, using pyrenyl,^{44,47,62,89-91} naphthyl⁹² and phenyl^{68,92} groups, among others. The main chain can be either a hydrocarbon,^{44,45,89,91,93} a fluorocarbon⁹⁴ or an oligosilane⁹⁵ chain. Bichromophoric compounds such as the oligomers can be used as models to elucidate the complex behaviour found in polymers, namely in randomly labelled polymers, and used to draw conclusions about the relative orientations of the chromophores.

The two dipyrenylalkanes studied here only differ from each other by the number of carbon units separating the two pyrene chromophores. 1Py(3)1Py (1,1'-dipyrenylpropane) is an oligomer having a propane (three -CH₂) whereas 1Py(10)1Py (1,1'-dipyrenyldecane) has a decane (ten of those units) between the two pyrene molecules (Figure 2.1). These oligomers have been used as fluorescent probes in several biological studies in rats while studying the causes of diseases such as diabetes and Alzheimer.^{71,96,97}

Oligomers

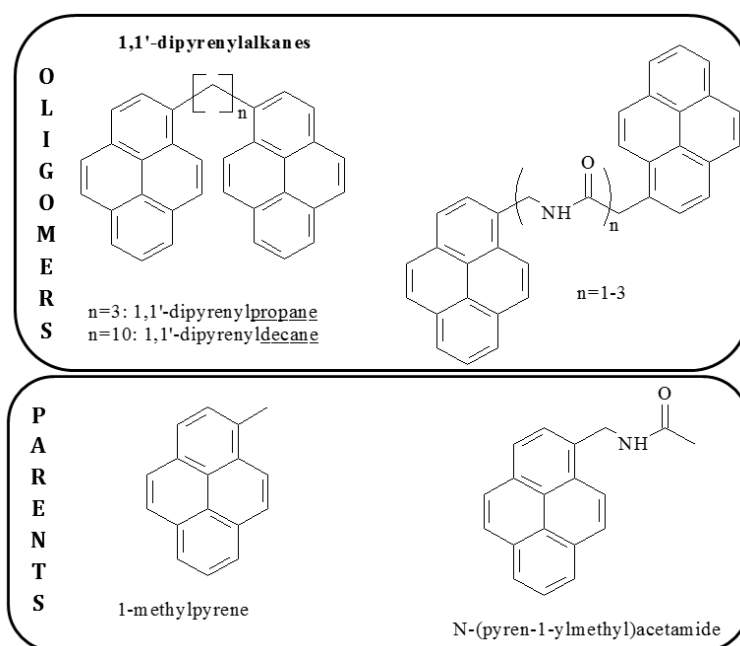


Figure 2.1. Structure of some relevant oligomers investigated in this thesis.

Hirayama was the first to report intramolecular excimer formation in a series of 1, n -diphenylalkanes, with $n=1-6$.⁹⁸ Since, excimer emission was only observed for 1,3-diphenylpropane, the $n=3$ rule, also known as Hirayama's rule, was coined. This shows that intramolecular excimer formation is maximized when maximum π -overlap is attained, which occurs when the chromophores are connected by a three-carbon alkane chain.⁹⁸ When $n=3$ the strain energy of the propyl chain, in the excimer conformation required for π -overlap is minimized as is the ring strain energy of cycloalkanes, more specifically, the three methylene carbons plus the two attaching carbons in the aromatic rings plus a sixth "ghost" carbon accounting for the ca. 3.4 \AA distance between aromatic rings, i.e., 6 carbons, is equivalent to cyclohexane (Figure 2.2). This rule was also found to be valid with 1, n -di(N-carbazolyl)alkanes.⁹⁹ Zachariasse *et al.* performed exhaustive studies on the chain length effect in a series of 1, n -di(1-pyrenyl)alkanes⁴⁶ and 1, n -bis(1-pyrenylcarboxy)alkanes⁸⁹ ($n=1-16, 22$ and 32). With 1, n -di(1-pyrenyl)alkanes, although a maximum excimer emission was achieved for $n=3$, in agreement with Hirayama's rule, excimer emission was detected in all studied compounds, with the exception of $n=7$.⁴⁶ When n ranges between 3 and 7, an oscillating decrease of (intramolecular) excimer formation, pairing that of alkanes cyclization rate, was observed.⁴⁶ From $n=7-12$, an increment of the excimer emission followed by a further gradual decrease with the increase in chain length was obtained. In the case of the 1, n -bis(1-pyrenylcarboxy)alkanes,⁸⁹ the maximum was now attained at $n=5$ and it gradually decreased with increasing the chain length⁸⁹ while in the case of 1, n -di(1-pyrenylmethoxy)carbonyl alkanes [1PyCH₂OCO(CH₂) _{n} OCOCH₂1Py], the maximum efficiency occurred at $n=1$.¹⁰⁰

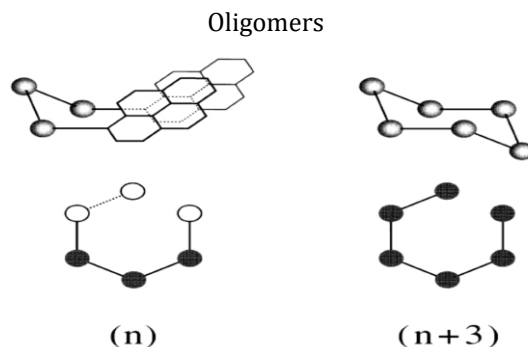


Figure 2.2. The number (n) of the methylene groups in 1Py(3)1Py [or 1PC(3)1PC], as compared with that (N) of the carbon atoms in cyclohexane: $N = n + 3$. In the former case, three “phantom” atoms (open sphere) are drawn, see text. From ref. ^{46,89}

The position at which the pyrene chromophore is linked (position 1 or 2) to the chain was also found to be of major importance. For instance, the geometry of the formed excimer strongly depends on the substitution position. This effect was investigated with particular relevance for the 1,3-dipyrenylpropane.^{44,45} When pyrene is linked to the alkyl chain through the position 2, [2Py(3)2Py], bi-exponential decays are obtained at both monomer and excimer emission wavelengths.⁴⁴ When the link is made through the position 1, [1Py(3)1Py], tri-exponential decays were obtained, i.e., an additional species is coupled to the other two, was found in the system, which corresponds to the emission of an additional excimer with a different geometry (see Figure 2.3).^{44,46} This latter excimer (with the shorter decay time, $\tau_{E1} = 62.5$ ns in MCH) presents a decay time similar to that found for the intermolecular pyrene excimer.⁴⁶ Accordingly, the shortest-lived excimer (more stable, E_1) displays a twisted sandwich geometry while the longer lived ($\tau_{E2} = 117.5$ ns in MCH) (less stable, E_2) has a parallel sandwich-like conformation (see Figure 2.3).⁴⁴⁻⁴⁶

Because only one excimer-like conformation can exist when the pyrene chromophores are linked to the chain through the position 2 (parallel sandwich, Figure 2.3), double-exponential decays are predicted as experimentally observed. When pyrene is linked through the position 1 in one extremity of the alkyl chain and through the position 2 at the other extremity [1Py(3)2Py], only excimer E_1 is observed.⁴⁵

The chain length is also a ruling factor with a strong impact on the relative orientation of the chromophores. When the chromophores are separated by short chains, the restrictions imposed by the chain are higher than those with long chains. This was observed in the case of 1,n-di(1-pyrenyl)alkanes, when the fluorescence decays at the excimer emission wavelength for $n = 3$ and $n > 12$ were compared.¹⁰¹ For $n = 3$, the fluorescence decays were found to be tri-exponentials and attributed to one monomer and two conformational different excimers. This means that due to the restrictions of the hydrocarbon chain, the excimer with a less stable conformation is also formed and prevented to directly relax to the more stable one without dissociation.¹⁰¹ When $n > 12$, only the decay times attributed to the monomer and to the more stable excimer emission were observed.¹⁰¹ Due to the higher conformational flexibility all relative orientations are, in principle, possible and the two pyrene groups orient themselves in order to adopt the more stable conformation. On the other hand, even for small connecting chains, the

flexibility of the linker is of extreme importance. In the limit of null flexibility, 1,4-di(1-pyrenyl)butadiyne¹⁰² [C(sp)] has shown negligible π - π stacking, i.e., intramolecular excimer formation is absent. This oligomer behaves as a single molecular entity with extended resonance between the two pyrene units and the connecting chain. Consequently, it also shows completely different photophysical properties from the pyrene probe itself: small Stokes shift, short fluorescence lifetime values ($\tau = 1.2 \pm 0.1$ ns), higher ϕ_F values (~ 0.95) and insensitivity to solvent polarity and presence of oxygen.¹⁰²

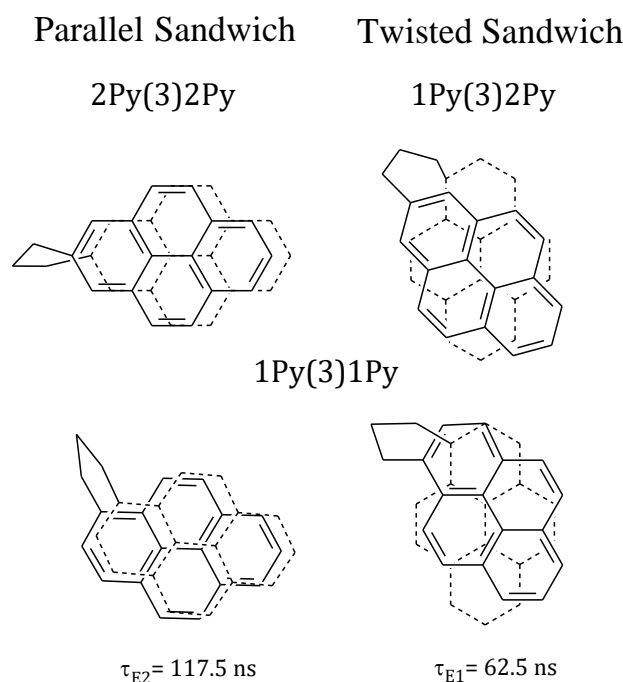


Figure 2.3. Schematic representation of the excimer conformations of 2Py(3)2Py, 1Py(3)2Py and 1Py(3)1Py oligomers.⁵¹

Solvent viscosity is another factor influencing both inter- and intramolecular excimer formation in compounds with flexible linking chains. For a pure diffusion-controlled process, the association rate constant (k_a) is reciprocally proportional to the solvent viscosity, $k_a \sim \eta^{-1}$ (Debye–Smoluchowski equation), i.e., k_a increases with the decrease of (solvent) viscosity. With intramolecular excimer formation, the solvent viscosity is still important but it shares the control of k_a with the energy barriers for chain rotation and diffusion and no longer follows the Debye–Smoluchowski behaviour. Instead, $k_a \sim \eta^{-\alpha}$, with $\alpha < 1$ decreasing with the increase of rotational energy barriers.^{31,103} The impact of the viscosity of the solvent on the intramolecular excimer formation process increases with the chain length.⁸⁹

When the number of these basic units (monomers) exceeds a given value the molecule is no longer an oligomer. This value is set by the variation of the properties of the molecule itself. Thus, if the increase

in the number of units causes significant changes in its properties, the molecule is no longer an oligomer, becoming a polymer.¹⁰⁴

2.1.1. Fluorescence Decay Analysis

In the next section the approach of analysing and interpreting the fluorescence decays used in the present thesis will be briefly described.

2.1.1.1. No Model Assumed A Priori

The analysis of the experimentally obtained fluorescence decays is commonly done using empirical functions to fit the decay profiles, in which no specific model is assumed. Moreover, because excited species usually decay exponentially, the method of fitting with discrete exponentials is the most widely used method to fit decays and it is known as the classical method of analysis. It consists on fitting the fluorescence decays with a sum of exponentials (Equation 2.1, where $I(t)$ is the fluorescence intensity as a function of time, n is the number of exponential terms, a_i the pre-exponential factors which represents the contribution of each exponential term at $t=0$, and τ_i are the associated fluorescence decay times), from which the fluorescence lifetimes (τ_E and τ_M for PAAMePy in Section 3.2 and PNIPAMPy in Section 3.3, τ_A and τ_N for hydroxycoumarins in Chapter 5, for example) and the pre-exponential factors can be obtained.

$$I(t) = \sum_{i=1}^n a_i e^{-t/\tau_i} \quad \text{Equation 2.1}$$

The fractional contribution (C_i) of each species (when in presence of a bi- or higher order decay) is given, for each emission wavelength, by Equation 2.2.¹⁰⁵

$$C_{i,\lambda_{em}} (\%) = \frac{a_i \tau_i}{\sum_{j=1}^n a_j \tau_j} \times 100 \quad \text{Equation 2.2}$$

Generally, all decay analysis are made with the minimum number of species. For that reason, the analyses begins by fitting with a single exponential (see top panel of Figure 2.4).

Upon analysis with one exponential, the quality of the fitting is evaluated from the chi square value, weighted residuals and autocorrelation functions. If the fitting is not acceptable, another exponential must be added. In the case of Figure 2.4, three were the minimum exponential terms needed to correctly fit the decay, meaning, at least in principle, that three species are present in the excited state.

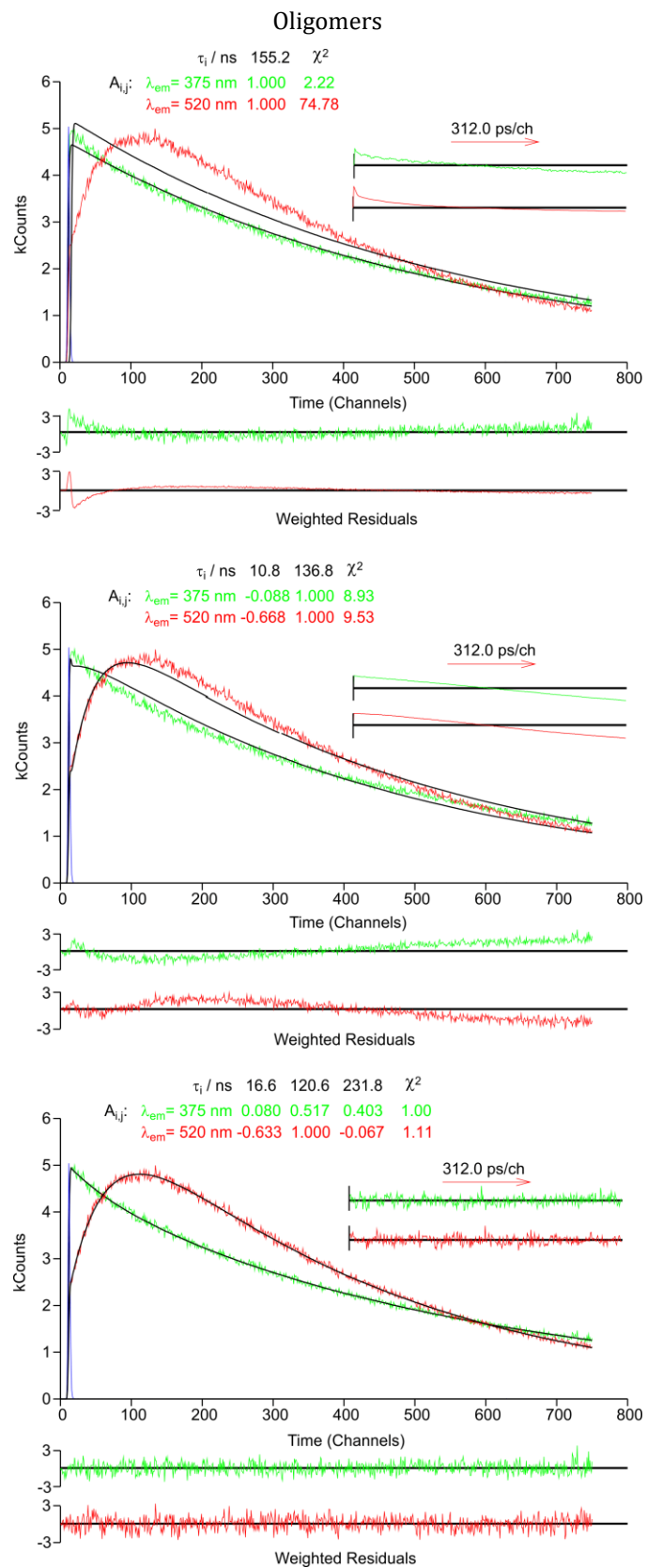


Figure 2.4. From top to bottom. Global fluorescence decay analysis with one, two and three exponentials for a pyrene labelled poly(N-isopropylacrylamide) (PNIPAMPy) in DMF at T= 293K. The instrument profile curve, decay times (τ_i), pre-exponential factors (A_{ij}), χ^2 values, weighted residuals, and autocorrelation functions (A.C.) are shown as the insets. Green and red graphs correspond to the decay collected at $\lambda_{em} = 375$ and 520 nm, respectively.

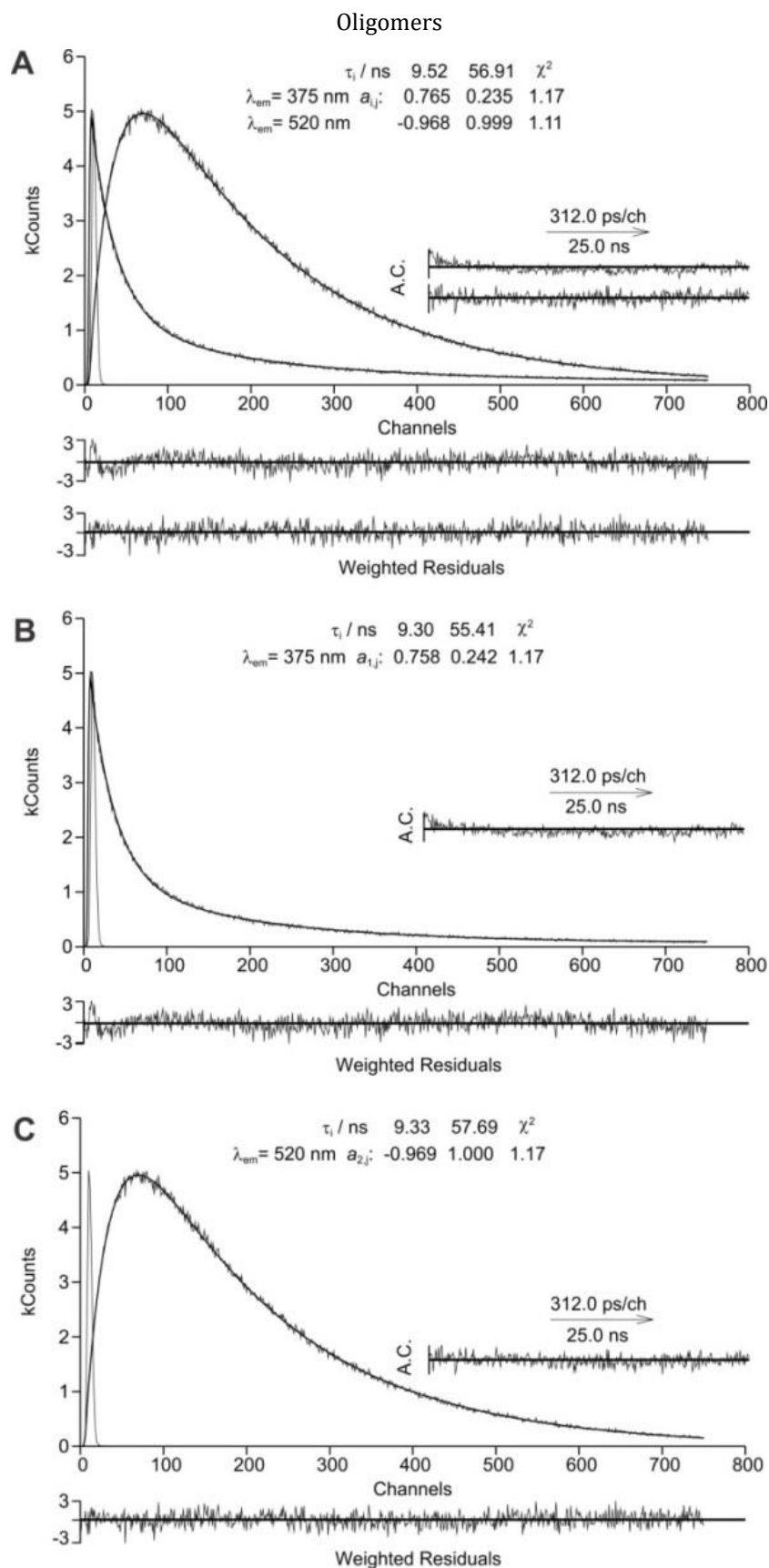


Figure 2.5. (A) Global fits and individual fits of fluorescence decays at (B) the monomer ($\lambda_{em} = 375$ nm) and (C) the excimer ($\lambda_{em} = 520$ nm) of 1,10-di(1,1'-pyrenyl)decane [1Py(10)1Py]] in heptane at 303 K.

Furthermore, individual (independent), and global analysis of the fluorescence decays can be obtained and compared. In the former case the decays, obtained at different emission wavelengths, are fitted

independently (Figure 2.5B and C), whereas in the latter, two (or more) decays are measured at different emission wavelengths and simultaneously fitted with identical decay times, see Figure 2.5A.

In general, the global analysis of the decays offers more reliable results and a higher accuracy of the recovered parameters than individual analysis, essentially due to the larger number of counts (the global analysis of e.g., three decays with 10 kCounts at the peak is roughly equivalent to a decay with 30 effective kCounts), but also because a given decay component maybe poorly defined at one or more wavelengths and better defined at others. Within this context it is worthwhile to mention that many reports found in literature on the minimum number of counts at the peak that are required for a correct definition of decay times and pre-exponential coefficients in multi-exponential decays should be considered with caution.⁵¹

A convincing experimental proof of that has been given by Zachariasse and Striker,¹⁰³ where triple-exponential fluorescence decays measured with different number of counts at the peak (from 500–30 000 counts) provided equally trustful values for decays times and pre-exponential factors. More often, when too long measurement times are needed to increase the number of counts, the results may worsen.³¹

2.2. Photophysics of Pyrene-Based Oligomers

2.2.1. Dipyrenylalkanes

2.2.1.1. Temperature Dependence

Figure 2.6 shows the normalized fluorescence emission spectra of 1Py(10)1Py and 1Py(3)1Py oligomers (panels A and B, respectively) together with a parent compound (1-methylpyrene) in heptane at room temperature (293 K).

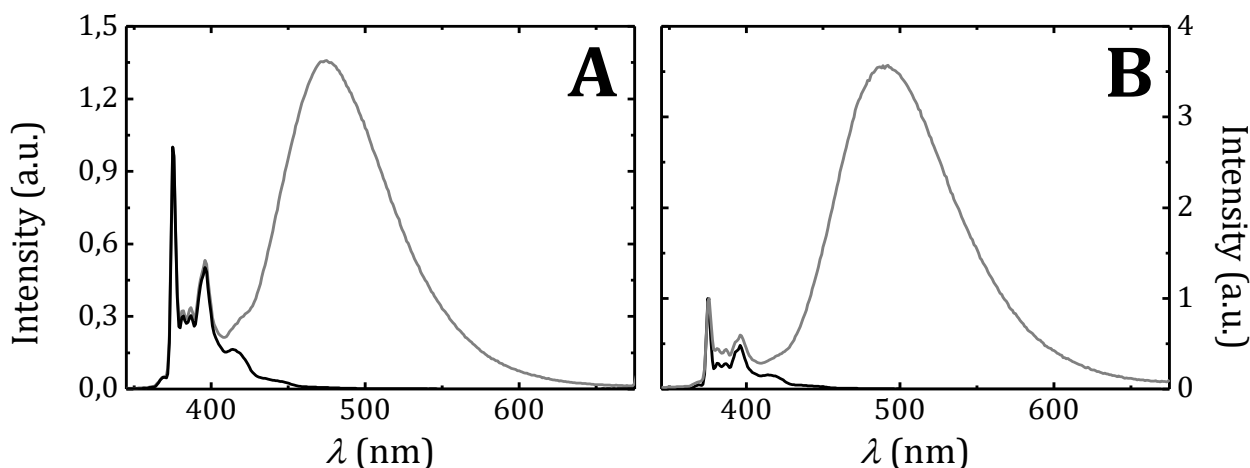


Figure 2.6. Normalized (at λ_M) fluorescence emission spectra ($\lambda_{exc.} = 339$ nm) of (A) 1Py(10)1Py and (B) 1Py(3)1Py (grey lines) with 1-methylpyrene (black line) in heptane at 20 °C.

Although not easily visible from the observation of Figure 2.6, it can be seen that the excimer emission band for 1Py(3)1Py (~ 492 nm) is red-shifted and that I_E/I_M is ~ 12 times higher compared with 1Py(10)1Py ($\lambda_{\max}^E \sim 475$ nm).

The normalized spectra showing the full vibronic overlap, give further support to the validity of 1-methylpyrene as an adequate model compound, especially for the 1Py(10)1Py oligomer although one could expect the opposite since the alkyl chain length of 1Py(3)1Py (in comparison to the parent compound) is more similar. However this parent compound was often used as model for both oligomers.^{46,106}

Figure 2.7 shows the fluorescence spectra of 1-methylpyrene (panel A) and of the 1Py(10)1Py oligomer in heptane (panel B) as a function of temperature ranging between -10 and 90 °C.

From Figure 2.7 panels C and D it can be seen that the maximum excimer emission shifts to lower wavelength values with the increase of temperature, whereas the monomer emission shifts to longer wavelengths. The last is also observed with the monomer emission of the parent compound (panel A).

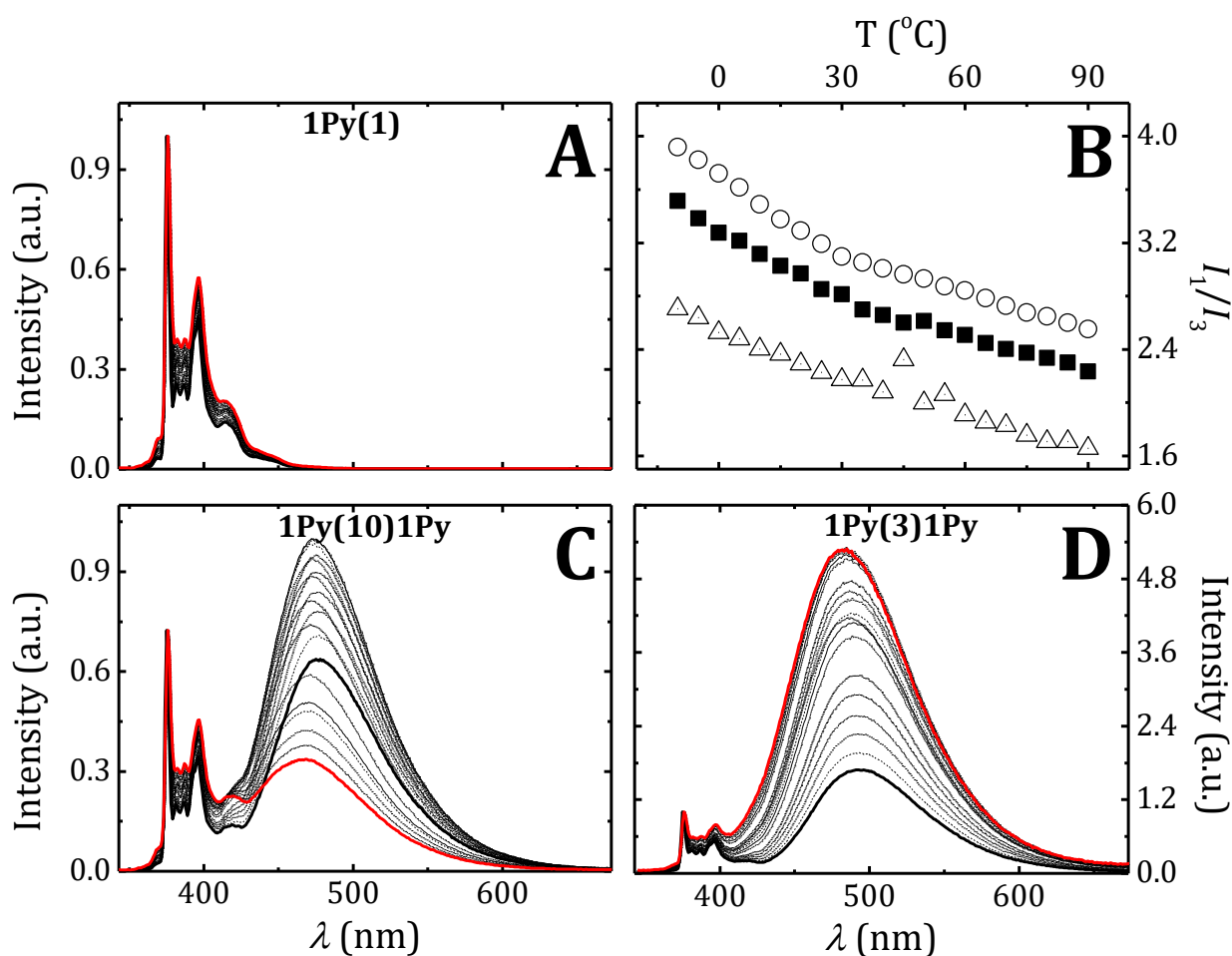


Figure 2.7. Fluorescence emission spectra ($\lambda_{\text{exc.}} = 339$ nm) of (A) 1-methylpyrene, (C) 1Py(10)1Py and (D) 1Py(3)1Py in heptane normalized at the λ_M . The bold red and black lines stand for $T = 90^\circ\text{C}$ and $T = -10^\circ\text{C}$, respectively. (B) I_1/I_3 as a function of the temperature for ○ 1CH₃Py, ■ 1Py(10)1Py and △ 1Py(3)1Py.

Figure 2.8 shows the fluorescence excitation spectra of both 1Py(10)1Py (panels A and B) and 1Py(3)1Py (panels C and D) oligomers and 1-methylpyrene (1CH₃Py, panel E) collected at the monomer emission wavelength (375 nm, panels A, C and E, respectively) and at the excimer emission wavelength as well (520 nm, panels B and D). In panel F, the P_E values taken from the excitation spectra (collected at the excimer emission band) are shown.

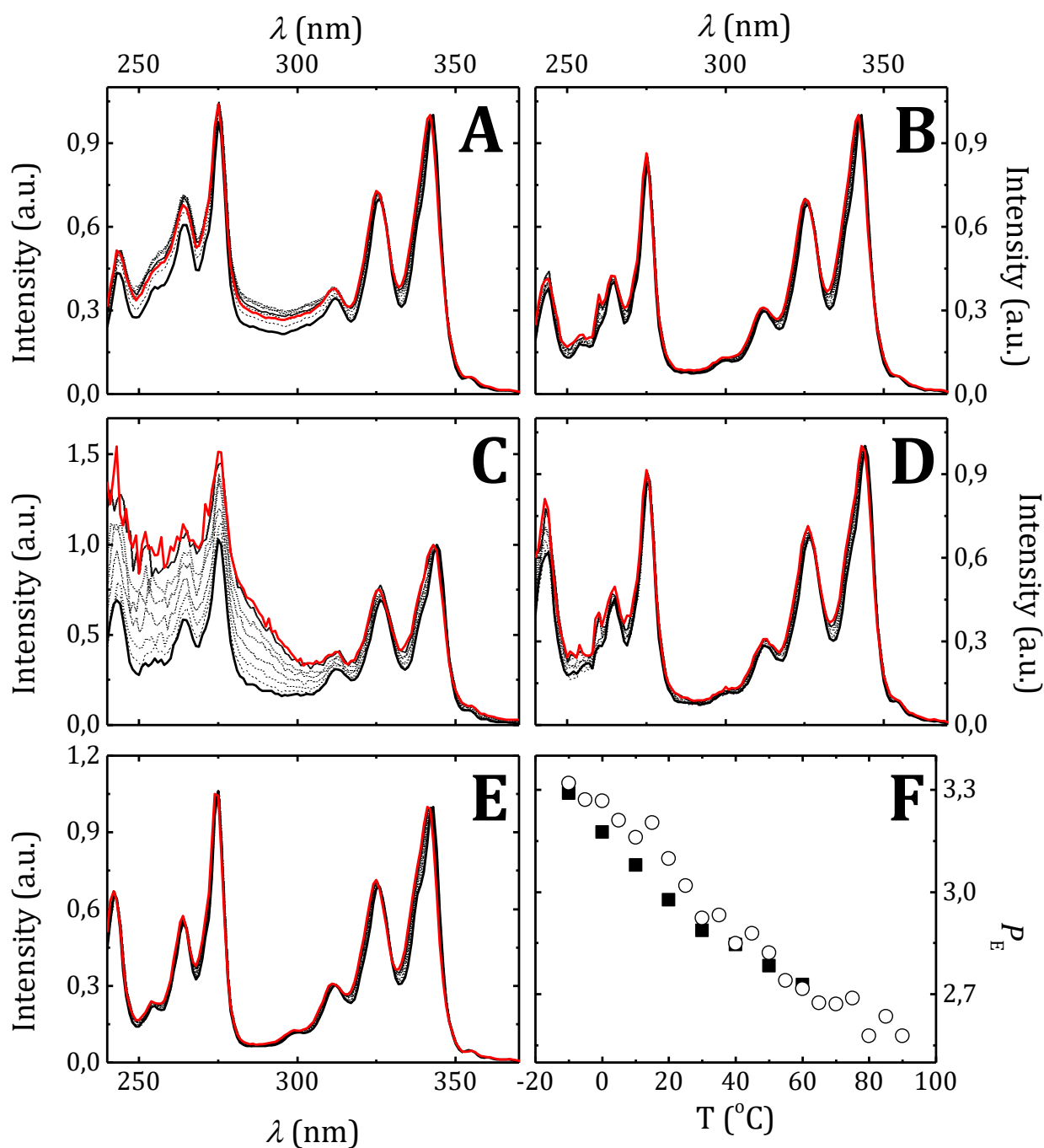


Figure 2.8. (A and B) 1Py(10)1Py, (C and D) 1Py(3)1Py and (E) 1CH₃Py in heptane. Normalized (at 335 nm) fluorescence excitation spectra with at (A, C and E) $\lambda_{em} = 375$ nm and (B and D) 520 nm. (F) P_E as a function of temperature for 1Py(10)1Py (■) and 1Py(3)1Py (○) in heptane. The bold **black** and **red** lines correspond, respectively, to the spectra at -10 and 60 °C.

From Figure 2.8F, note that P_E (see Section 7.2.6.1.2.3 in Chapter 7) is practically identical for both oligomers which was expected since the excimers from both oligomers should be formed by the dynamic via. It is also interesting to note that P_E is practically identical for both oligomers which should not be the case considering that 1Py(10)1Py present only one excimer and 1Py(3)1Py, two.

Another interesting feature observable from Figure 2.8, is that the excitation spectra shift to lower wavelengths while increasing temperature.

Oligomers

The Stevens-Ban curve (see Section 1.3.2.1.4) obtained by using the data of the fluorescence emission spectra (SS) as a function of the temperature of both 1Py(10)1Py and parent 1-methylpyrene (Figure 2.7 panel C and A, respectively) in heptane are depicted in Figure 2.9 where four different methods of obtaining the excimer to monomer (I_E/I_M) ratio were used.

Method A consisted on getting the maximum intensity value at the maximum excimer wavelength (466-477 nm) and at the maximum monomer band (375-376 nm). Method B consisted in first normalizing both parent compound (in this case, 1-methylpyrene in the same solvent and temperature) and 1Py(10)1Py oligomer for all temperatures. Then, the normalized emission of the parent compound is taken as the monomer emission of 1Py(10)1Py and the area under this spectra leads to the I_M value. The area under the normalized emission spectra of 1Py(10)1Py oligomer is taken and the monomer band subtracted from it, therefore allowing to obtain the remaining area which is the I_E . In the method C and D, the use of parent compound was not needed, and the excimer band was fitted with a function [GaussMod and BiGauss, respectively (see equations in Section 7.2.6.1.2.1)]. The area under this fitting was then obtained and subtracted from the overall emission as in method B. The parameter used to define the best method for obtaining the I_E/I_M ratio was defined by the agreement between the SS and TR data.

From the observation of both Stevens-ban plot [$\ln(I_M^0/I_M - 1)$] and $\ln I_E/I_M$ vs the reciprocal of temperature, Figure 2.9A and Figure 2.9B to F, respectively], two observations should be taken into consideration: 1) the best method to obtain I_E/I_M is clearly the method D (due to the match between SS and TR data) for the 1Py(10)1Py oligomer and 2) the high temperature range (left part of the plot) is well defined in contrast with the *LTL* region which is poorly defined for the 1Py(10)1Py oligomer.

The TR data presented in Figure 2.9 was obtained first by obtaining the fluorescence decays of both 1Py(10)1Py and 1CH₃Py at all temperatures. In the case of 1CH₃Py this was found to be always monoexponential in all conditions used in the present thesis (i.e., as a function of viscosity, fraction of dioxane in dx:H₂O mixtures and as a function of temperatures).

In heptane the global analysis of the decays for 1Py(10)1Py were found to need three exponential terms. The third term having a residual exponential value was considered to be due to a small impurity of the solvent and/or compound. However a biexponential decay for 1Py(10)1Py in DMF was latter obtained which indicates that, most probably, the impurity come from the solvent.

In Figure 2.9 panel B, κ_F^E/κ_F^M (Equation 1.21 from Section 1.3.2.1.4) [1Py(10)1Py] was set as 1. In the remaining panels, the κ_F^E/κ_F^M was chosen in order to make the best match, at the highest temperature, between the I_E/I_M from time-resolved (TR) data and the one from the steady state. Then it is assumed that this ratio is basically temperature independent.

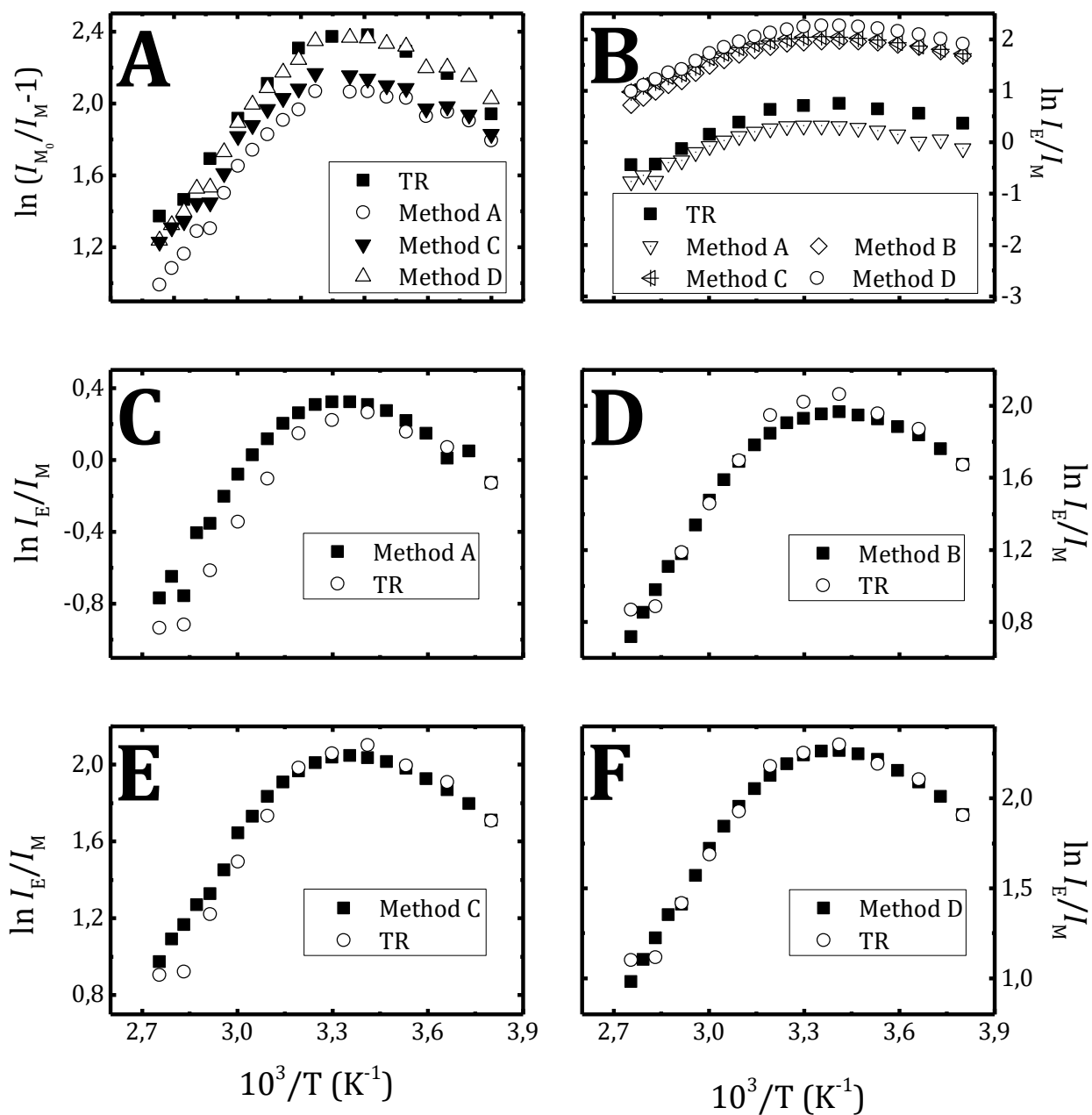


Figure 2.9. 1Py(10)1Py in heptane. (A) $\ln(I_{M0}/I_{M-1})$, (B to F) $\ln(I_E/I_M)$ obtained by different methods with (B) $k_F^E/k_F^M=1$, (C to F) k_F^E/k_F^M adjusted to match the value from SS at -10°C , $\lambda_{exc}=339\text{ nm}$. Methods A to D, are identified in the text.

In Figure 2.10, the global biexponential analysis of the fluorescence decays of 1Py(10)1Py in DMF at room temperature can be observed.

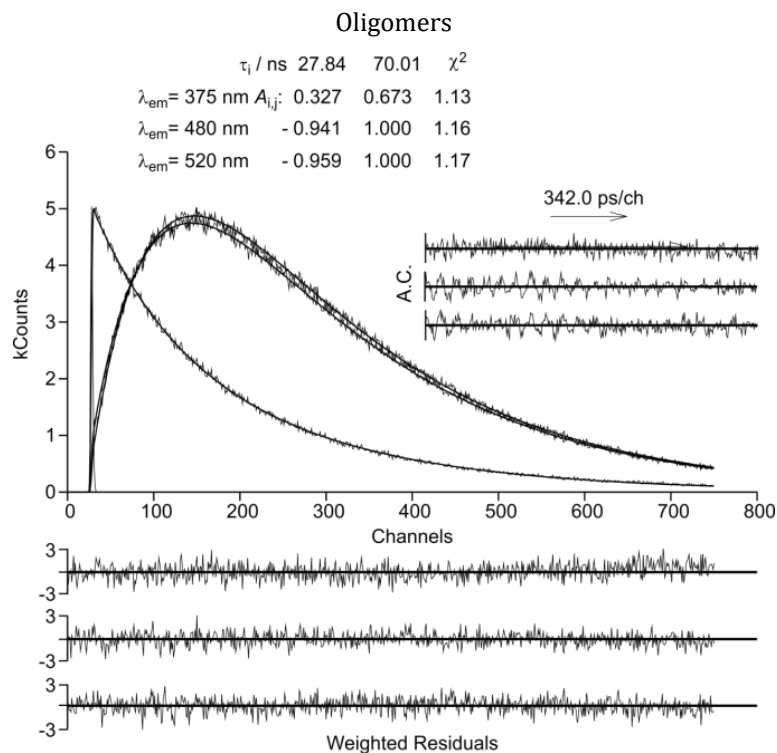


Figure 2.10. Global analysis of the fluorescence decays of 1Py(10)1Py in DMF at T= 293 K, at 375, 480 and 520 nm. The excitation pulse (339 nm) is depicted. The instrument profile curve, decay times (τ_i), pre-exponential factors ($A_{i,j}$), chi-squared values (χ^2), weighted residuals, autocorrelations functions (A.C.) are shown as insets.

From Figure 2.11, k_a and k_d are the rate constants which have the strongest temperature dependence.⁶⁹

Moreover, the temperature dependence behavior of 1Py(10)1Py clearly shows that excimer-to-monomer reversibility is present at room temperature. Indeed the plot of the ratio A ($=A_{1,2}/A_{1,1}$) decreases with the increase in temperature (Figure 2.11 panel C) and the log of the rate constants (obtained from the Birks Kinetic formalism)¹⁰⁷ show an Arrhenius dependence with E_a and E_d values of 12.0 and 36.1 kJ.mol⁻¹, respectively.

The τ_E and τ_M values for 1Py(16)1Py in heptane at 25 °C of 61 and 262 ns, respectively are higher than the one obtained for 1Py(10)1Py in the same solvent¹⁰⁸ The association rate constant for excimer formation (k_a) for 1Py(10)1Py in MCH, reported previously,⁴⁶ has a value of ~ 0.05 ns⁻¹ at 25 °C⁴⁶ which is in between the values obtained in this work from TR and SS data in heptane.

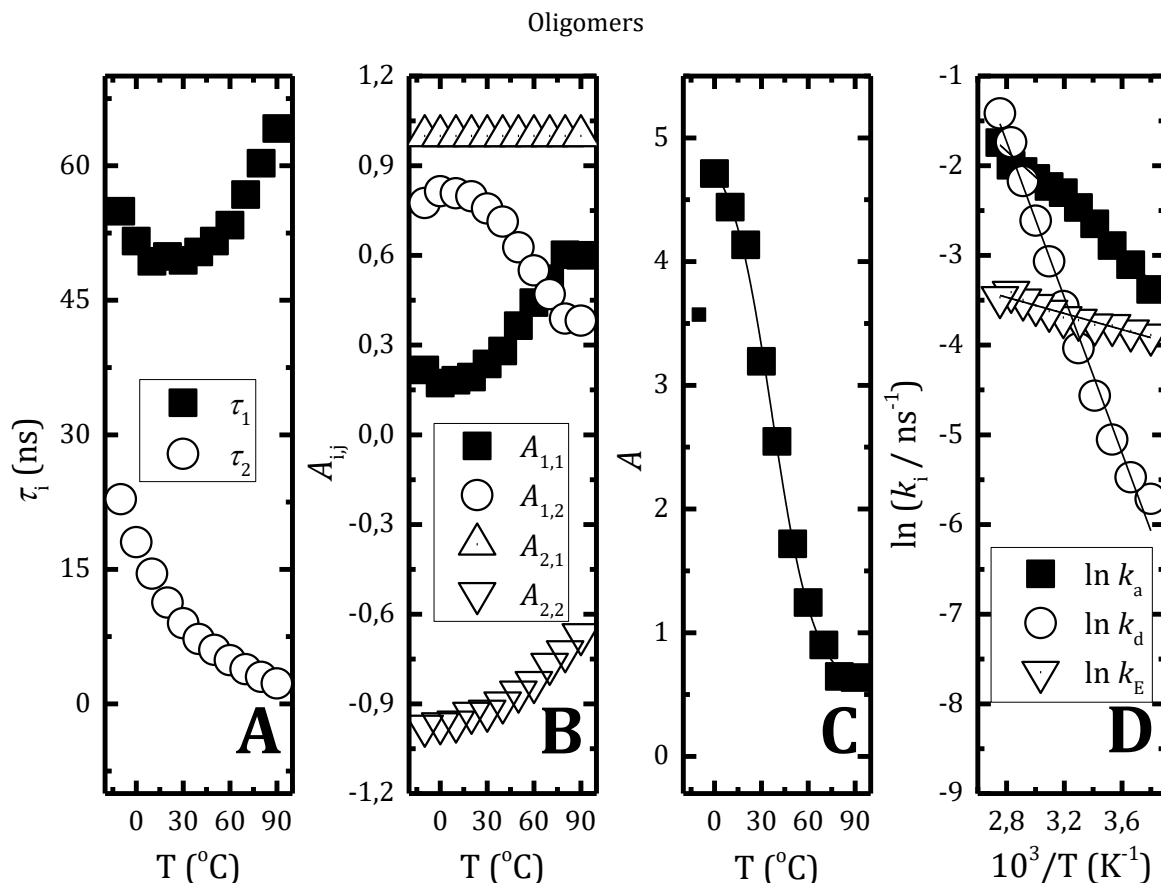


Figure 2.11. Dependence of (A) decay times, (B) pre-exponential factors collected at the monomer ($A_{1,i}$) and excimer ($A_{2,i}$) emissions wavelengths, (C) pre-exponential ratio (A) as a function of the temperature and (D) plots of natural logarithm of k_a , k_d and k_E as a function of the absolute reciprocal temperature of the 1Py(10)1Py oligomer in heptane.

In Table 2.1, the values plotted in Figure 2.11 are gathered and shows the comparison between the association rate constants, k_a , obtained from TR and the steady-state data using Equation 1.26.

Table 2.1. Monomer and excimer fluorescence lifetime (τ_M and τ_E , respectively), $I_M^0/I_M - 1$ and rate constants of excimer formation (k_a) from both steady state (k_a^{SS}) and time-resolved (k_a^{TR}) experiments. Excimer dissociation (k_d) and decay rate constants (k_E) for 1Py(10)1Py in heptane for the temperature range investigated.

Temperature Limit	T (°C)	τ_M (ns)	τ_E (ns)	$\frac{I_M^0}{I_M} - 1$	k_a^{TR} (ns ⁻¹)	k_a^{SS} (ns ⁻¹)	k_d (ns ⁻¹)	k_E (ns ⁻¹)
LTL	-10	237 ^a	48.7	6.08	0.034	0.026	0.003	0.021
	0	232 ^a	46.5	6.59	0.045	0.028	0.004	0.022
	10	227 ^a	43.8	6.65	0.056	0.029	0.006	0.023
	20	222	43.5	7.23	0.071	0.033	0.010	0.023
	20 ^b	158	45.5	ND	0.015		0.007	0.022
	30	218	41.3	6.87	0.086		0.018	0.024
T*	40	214	40.2	6.10	0.101	NA	0.028	0.025
HTL	50	211	37.4	5.19	0.108		0.047	0.027

Oligomers							
60	207	35.0	4.26	0.118	0.073	0.029	
70	204 ^a	33.0		0.134	0.114	0.030	
80	201 ^a	30.3	<i>ND</i>	0.135	0.176	0.033	
90	198 ^a	32.1		0.172	0.243	0.031	

NA – not applicable, *ND* – not determined, ^a values extrapolated, see Figure 2.20 in SI. ^b in DMF.

For 1Py(3)1Py a plateau is reached, and therefore the transition temperature between the *HTL* and *LTL* is not possible to define (Figure 2.12). However, as done with the 1Py(10)1Py, it was assumed that T^* can be given by the $\ln(I_E/I_M)$'s value where the natural logarithm of the excimer-to-monomer ratio is the highest.

In order to obtain additional information on the 1Py(3)1Py oligomer, TR measurements were made. All the fluorescence decays were properly fitted with three exponential terms.

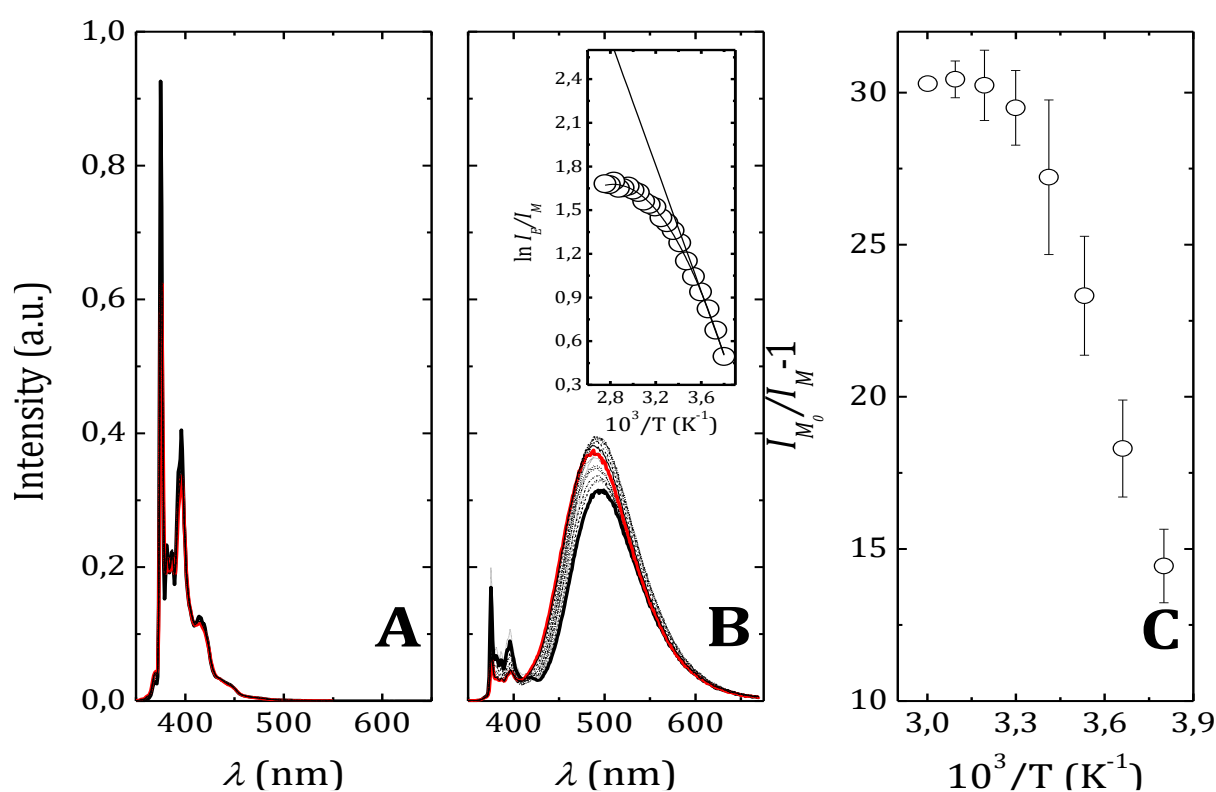


Figure 2.12. Fluorescence spectra of (A) 1-methylpyrene and of (B) 1Py(3)1Py in heptane (*inset*: plot of $\ln(I_E/I_M)$ vs. $10^3/T$) and (C) $I_{M0}/I_M - 1$ vs. $10^3/T$, $\lambda_{\text{exc.}} = 337$ nm. The bold red and black lines stand for $T = 60^\circ\text{C}$ and $T = -10^\circ\text{C}$, respectively.

Since the temperature dependence on the 1Py(3)1Py oligomer in heptane was already published in ref. ¹⁰⁸, the values obtained in this work were only compared with 1Py(10)1Py in Table 2.2. In Table 2.2 some relevant parameters, taken from the TR and steady state experiments as a function of temperature, are presented.

Table 2.2. Relevant parameters [transition temperature (T^*) between HTL and LTL regimes, difference (δ) between the curve defining the normal regime and the line defining the HTL regime at the crossing point, T^* , where $k_d = \tau_E$, enthalpy of excimer formation (ΔH), activation, dissociation and excimer decay energies (E_a and E_d) and entropy (ΔS)] obtained from the Arrhenius Plots of $\ln(I_E/I_M)$ as a function of the temperature reciprocal ($1/T$) for 1Py(10)1Py and 1Py(16)1Py¹⁰⁸ oligomers in heptane.

Parameters	Units	Method						
		1Py(3)1Py ¹⁰⁸	1Py(10)1Py				1Py(16)1Py ¹⁰⁸	
		TR	SS				TR	TR
		A	B	C	D			
T^*	(°C)		27.4 (34.5)	21.7 (33.7)	25.5 (33.2)	21.8 (30.9)	17.8 ^c	
δ			0.67 (0.21)	0.60 (0.28)	0.41 (0.23)	0.51 (0.26)	0.70 ^c	
$-\Delta H^a$	(kJ.mol ⁻¹)	15.2 23.7	21.2	23.8	20.8	23.2	24.1 ^c 17.3 ^d	40.3
E_a	(kJ.mol ⁻¹)	18.4 ^e 19.3 ^e	10.3 ^b	9.5 ^b	10.8 ^b	9.8 ^b	12.0 ^e	11.8
E_d	(kJ.mol ⁻¹)	33.6 ^e 43.0 ^e	31.5 ^b	33.3 ^b	31.6 ^b	33.0 ^b	36.1 ^e	52.1
k_F^E/k_F^M		2.1	0.62	3.73	3.87	4.70		
ΔS^{od}	(J.mol ⁻¹)	-14 -55					-68.2	-109
k_a^{0e}	(ns ⁻¹)	100 270					9.1	15.0
k_d^{0e}	(ps ⁻¹)	0.56 190		NA			0.3 ^f	
k_E^{0e}	(ns ⁻¹)						0.1	
E_E^e	(kJ.mol ⁻¹)						3.7	

^{a, b} Apparent enthalpy variation, activation and dissociation energies associated with excimer formation obtained from the HTL (ΔH) and LTL (E_a) region of the Stevens Ban plot, see Section 1.3.2.1.4. ^c Obtained from the Stevens ban curve produced with the TR data. ^d Obtained from the van't Hoff plot, see Section 1.3.2.1.4. ^e Obtained from the Arrhenius plot, Method A: intensities ratios, method B: deconvoluted bands, method C: GaussMod, method D: BiGauss, T^* and δ was considered to be given by the maximum value of $\ln I_E/I_M$ and by making the subtraction of the value given the linear fitting of $\ln(I_E/I_M)$ and $\ln(I_E/I_M)$ obtained at this temperature, respectively. ^f in μs^{-1} . NA - not applicable. ND - not defined. The values in parenthesis were obtained considering a reduced number of points (~ 3) in the LTL region.

The value found for ΔS and E_a (-68.2 J.mol⁻¹ and 12.0 kJ.mol⁻¹) in heptane is similar to the one reported in ref.¹⁰⁸ for 1Py(16)1Py in the same solvent with a value of -109 J.mol⁻¹ and 11.8 KJ.mol⁻¹, respectively.

The E_a value is higher than the activation energy value for the viscous flow in heptane [$E_\eta(\text{Heptane})= 9.5 \text{ kJ/mol}$]¹⁰³, consistent with an additional barrier associated to the chain.

Analyses of the data (see Table 2.2) shows that the excimer to monomer ratio should not be taken from the absolute fluorescence intensity at the monomer and excimer band. For the 1Py(10)1Py oligomer, all data seem to indicate that the best way to determine this parameter is by using method B (Figure 2.9). Beside, since the SS and TR Stevens-Ban curves are coincident, this allows concluding that the decay analysis and the kinetic scheme used are correct. One important point to address in this discussion is the excimer to monomer reversibility, since this has consequences in the monomer-excimer kinetics in polymeric systems with pyrene, where frequently this process is neglected. From Table 2.2, it is clear that the reversibility process is present at all temperatures. Furthermore, this is reflected by the fact that the fluorescence decay collected at the monomer region is never single exponential, see Figure 2.10 for 1Py(10)1Py in DMF. Independent analysis of the monomer decay is shown in Figure 2.22 in SI. Moreover, the values obtained with the 1Py(10)1Py oligomer (associated to the excimer decay) that appear in the monomer decay associated with this reversibility process are also present in polymer systems with pyrene.

From Table 3.6, the δ value for 1Py(10)1Py varies between 0.41 and 0.67 depending on the method used to determine the excimer-to-monomer ratio, which is slightly lower than the typically found, $\ln 2$ (= 0.693), when the process is totally dynamic. It can therefore be considered that the *LTL* is not properly defined for 1Py(10)1Py, which can be easily explained by observing the Stevens-Ban plot (Figure 2.9, see Section 1.3.2.1.4). Besides, if only the three lowest points of the Stevens-Ban plot in the *LTL* are considered, the δ (and T) values varies between 0.21 and 0.28 (30.9 and 34.5) which lacks sense (values in brackets in Table 2.2).

2.2.1.2. Viscosity Dependence

The decay times and pre-exponential factors obtained for 1Py(10)1Py in the alkane series (of different viscosity) are presented in Figure 2.13. All the analysis were triexponential due to the small impurity, see previous section. From these data and solving the Birks' kinetic scheme, the excimer formation rate constant k_a values could be obtained.

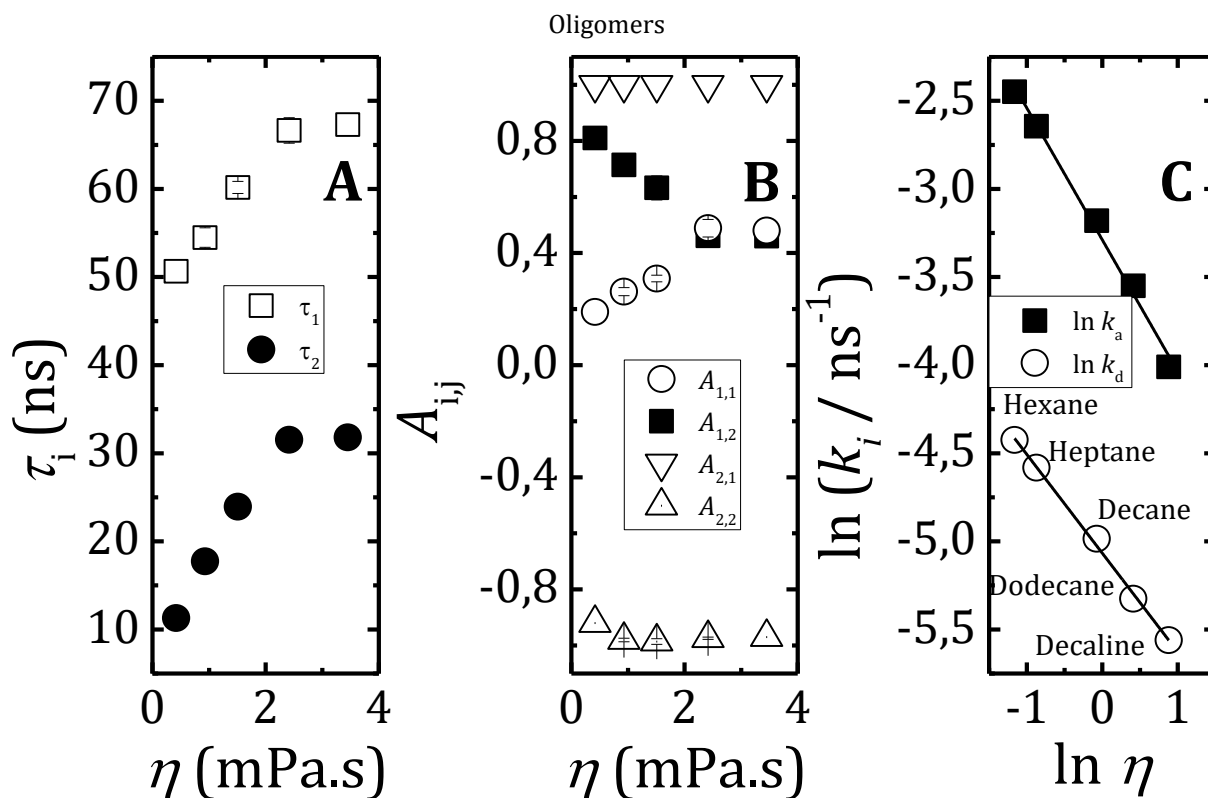


Figure 2.13. Dependence of (A) decay times, (B) pre-exponential factors collected at the monomer ($A_{1,i}$) and excimer ($A_{2,i}$) emissions wavelengths and (C) plots of natural logarithm of k_a and k_d of the 1Py(10)1Py oligomer in alkane solvents as a function of the viscosity at T= 293 K.

The fluorescence lifetime of 1-methylpyrene (τ_M^0) was measured in solvents of different viscosity. The natural logarithm of τ_M^0 as a function of the natural logarithm of the viscosity (log-log plots) gave origin to a linear trend. The equation of this linear trend was then used to estimate the values of τ_M^0 in other solvents, see Figure 2.20 in the Supplementary information. These lifetimes were then used to determine the rate constants of 1Py(10)1Py as a function of the viscosity.

The log-log plot of k_a vs. solvent viscosity is linear with a slope equal to 0.75, showing that Debye-Smoluchowski relationship does not apply.¹⁰⁹ The value obtained ($\alpha = 0.75$) is significantly lower than that expected for a purely diffusion-controlled process, where $\alpha = 1$. Similar departures from a pure diffusion-control of end-to-end chain cyclization (in order to achieve the excimer conformation) have been reported previously¹⁰³ like for the end-labelled pyrene polyethylene polymers ($\alpha = 0.52$).¹¹⁰ The departure from $\alpha = 1$ mirrors the multi-barrier crossing dynamics of intramolecular excimer formation involving several bond rotations in the presence of the solvent frictional forces acting on the chain.¹⁰³

The lifetimes obtained for 1Py(10)1Py in hexadecane are similar to those obtained from Vasilescu *et al.*¹¹¹

The global analysis of the fluorescence decays of the 1Py(3)1Py oligomer, collected at the monomer (375 nm) and excimer emission wavelengths (480 and 520 nm), gave rise (again as a function of the

viscosity) to fluorescence decays which could be properly fitted only with tri-exponential decay laws; see Figure 2.14.

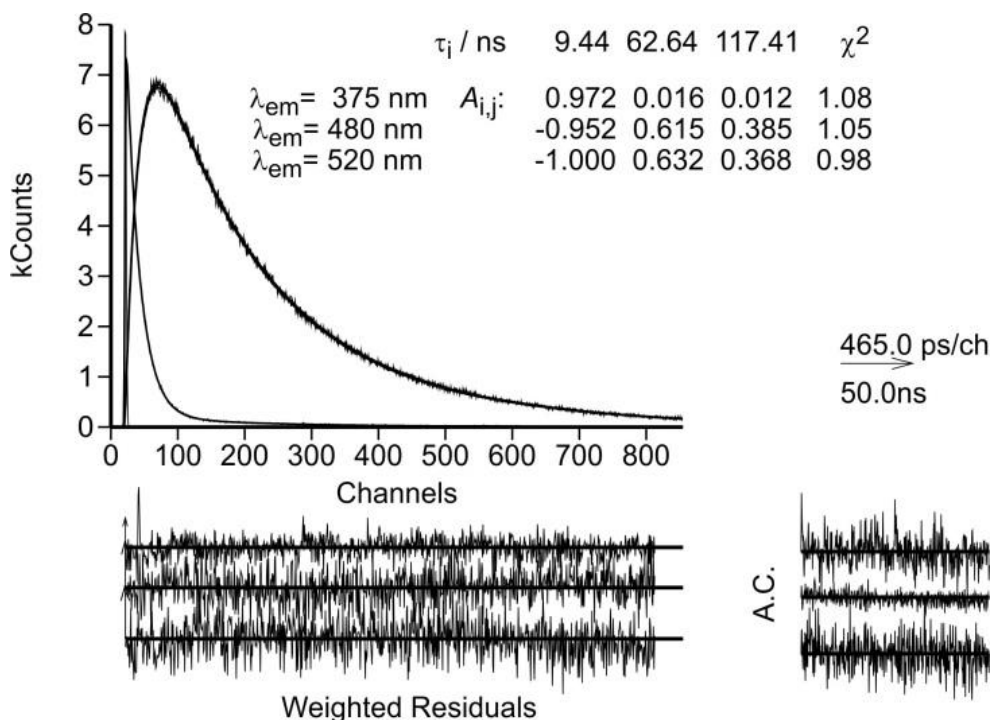


Figure 2.14. Fluorescence decays of the 1Py(3)1Py oligomer in MCH at different emission wavelengths and $T = 293$ K. For a better visualization of the quality of the fits the weighted residuals, autocorrelations functions (A.C.) and chi-squared values (χ^2) are shown as insets.

The three exponential terms were assigned to the monomer ($\tau_3 = 9.5$ ns) and to two excimers with an asymmetric ($\tau_2 = 62.5$ ns) and symmetric ($\tau_1 = 117.5$ ns) geometries.^{44,112,113} The observation of two excimers with 1Py(3)1Py, corresponding to the two possible relative conformations of the two pyrene rings, results from the impossibility of interconversion between the two conformations without excimer dissociation, introduced by the very short propane chain. This does not occur with longer connecting chains ($n > 7$) because the chain is sufficiently flexible to allow slipping of the two pyrene units to form the most stable excimer.^{44,113} In these cases only one excimer is observed as with 1Py(10)1Py. For 1Py(3)1Py, the kinetic scheme is, consequently, more complex than that found for the 1Py(10)1Py oligomer. At the excimer emission wavelengths the sum of the pre-exponential factors cancels out (Figure 2.14), which discards the possibility of excimer formation through the direct excitation of pre-associated dimers.

Since the viscosity dependence on the 1Py(3)1Py oligomer was already published in ref.¹⁰⁸, the values obtained in this work were only compared in Table 2.3.

Oligomers

Table 2.3. Rate constants of excimer formation (k_a), dissociation (k_d) and decay (k_E) obtained for 1Py(3)1Py in different solvents at 20 °C. The viscosity of the solvents at this temperature (η)¹¹⁴ are also presented.

Solvent	η (mPa.s)	$k_a(1)$ (ns⁻¹)	$k_a(2)$ (ns⁻¹)	$k_d(1)$ (ns⁻¹)	$k_d(2)$ (ns⁻¹)	$k_E(1)$ (ns⁻¹)	$k_E(2)$ (ns⁻¹)
Pentane ¹⁰⁸	0.235 ³⁵	~0.075	~0.132	~0.0003	~0.007	~0.006	~0.012
Hexane ¹⁰⁸	0.3126 ³⁵	~0.066	~0.115	~0.0006	~0.004	~0.006	0.012
Heptane	0.4181 ³⁵	0.053 ^b	0.098 ^b	0.0006 ^b	0.004 ^b	0.006 ^b	0.013 ^b
THF ¹⁰⁸	0.575	~0.024	~0.054	~0.0004	~0.004	~0.006	~0.015
Toluene ¹⁰⁸	0.5859 ³⁵	~0.108	~0.066	~0.0004	~0.004	~0.007	~0.015
MCH	0.734 ³⁵	0.059	0.039	0.002	0.005	0.008	0.013
Decane ^a	0.9284 ³⁵	~0.032	~0.066	~0.0003	~0.002	~0.006	~0.012
Dodecane ^a	1.508 ³⁵	~0.024	~0.057	~0.0002	~0.001	~0.006	~0.010
Hexadecane ^a	3.454 ¹¹⁵	~0.018	~0.043	~0.0002	~0.001	~0.007	~0.010

^a Estimated from ref. ¹⁰⁸, ^b Data from ref. ¹¹⁶.

2.2.1.3. Dioxane:water Mixtures

Figure 2.15 and Figure 2.16 show the absorption and fluorescence emission spectra of 1Py(10)1Py and 1Py(3)1Py, respectively, in dioxane:water mixtures together with the $\lambda_{\max}^{abs.}$, P_A , I_E/I_M and I_1/I_3 values as a function of the dioxane content.

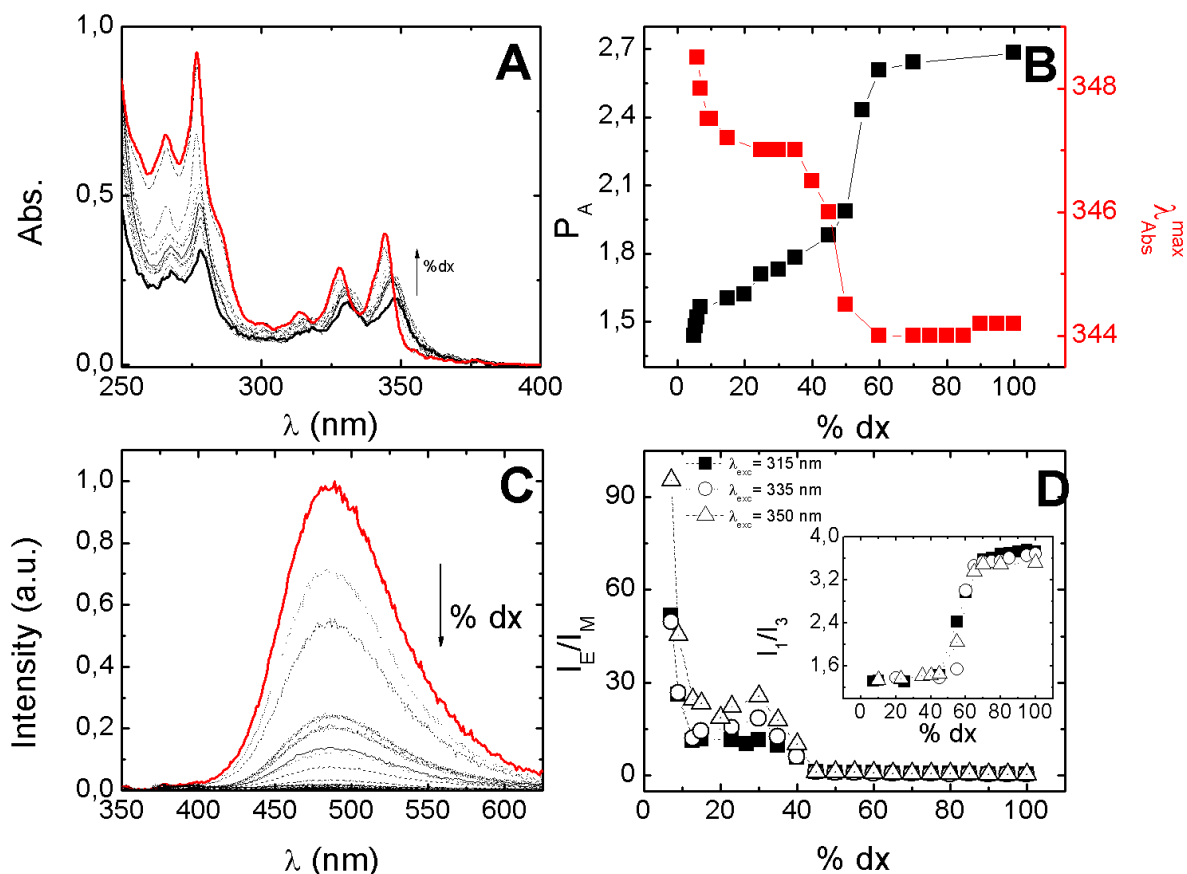


Figure 2.15. (A) Absorption spectra (B) P_A and λ_{\max}^{Abs} as a function of the dioxane content, (C) fluorescence emission spectra with $\lambda_{exc} = 315$ nm, (D) I_E/I_M as a function of the dioxane content and inset of (D) I_1/I_3 as a function of the dioxane content with $\lambda_{exc} = 315, 335$ and 350 nm of 1Py(10)1Py in different fractions of dx:H₂O at 298 K.

A comparison between Figure 2.15 and Figure 2.16 for 1Py(10)1Py and 1Py(3)1Py, respectively, reveals that for higher water content in the dioxane water mixtures the I_E/I_M is higher, for a factor of one order of magnitude. This is not observed in the low water content mixtures and suggests that for higher water content aggregation is likely to occur which is more favourable to occur, due to the larger alkyl chain, in 1Py(10)1Py.

The plots A from Figure 2.15 and Figure 2.16 clearly show that, upon going from a solvent mixture with higher content of dioxane, leads to an absorption band of the monomer, which is a clear sign of the better nature of this solvent to the probe. The question is if the gradual shift of the absorption band with the water increment indicates aggregation of the oligomer or of the presence of *GSD*. Time resolved data for high concentration of water in the mixture for both oligomers (data not shown) show that aggregation is likely to be present, as seen by a strong contribution of a short subpicosecond scattering component.

Oligomers

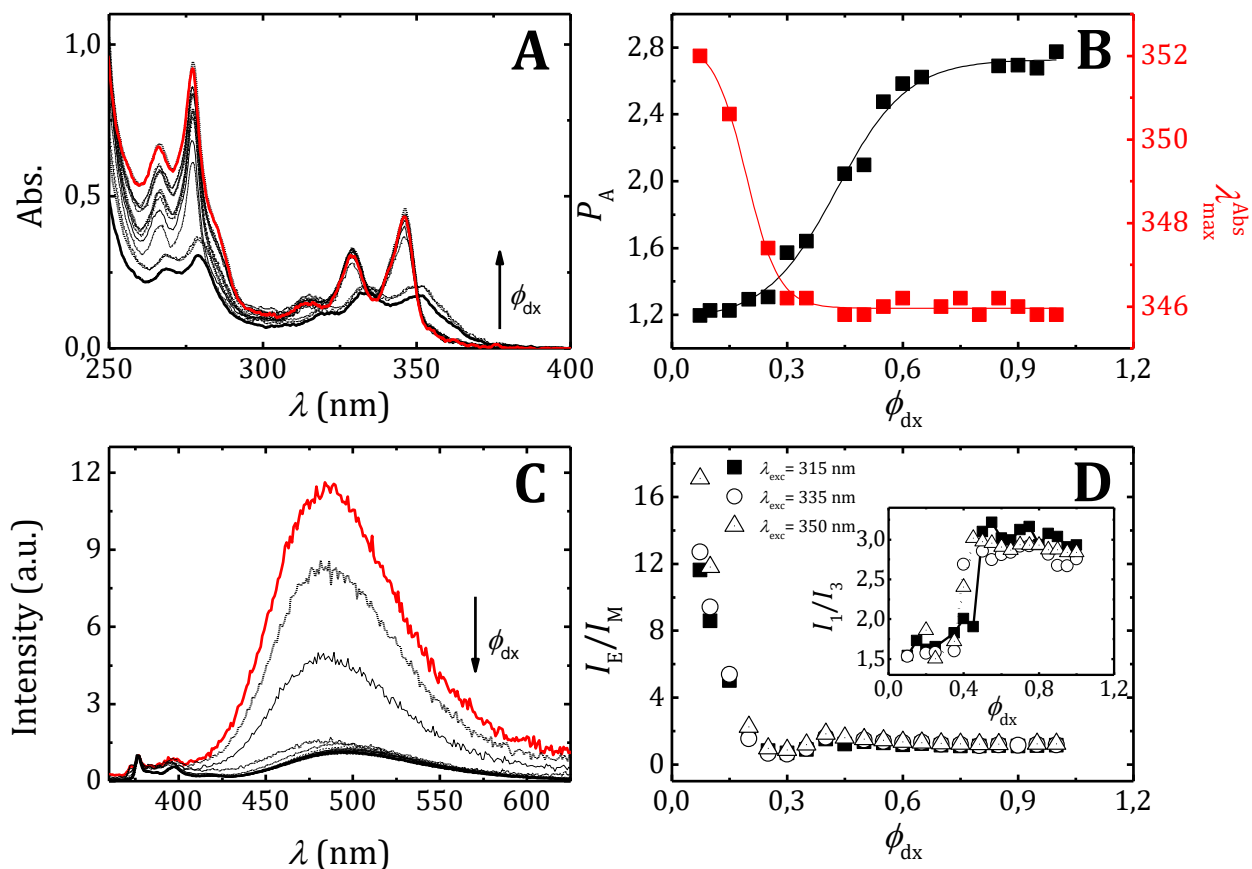


Figure 2.16. (A) Absorption spectra (B) P_A and λ_{\max}^{Abs} as a function of the dioxane content, (C) fluorescence emission spectra with $\lambda_{exc.} = 315$ nm, (D) I_E/I_M and inset of (D) I_1/I_3 as a function of the dioxane volume fraction with $\lambda_{exc.} = 315, 335$ and 350 nm of 1Py(3)1Py in different fractions of dx:H₂O at 298 K.

Moreover, as illustrated in Figure 2.17, the fluorescence excitation spectra of 1Py(3)1Py in dx:H₂O mixtures with H₂O ≤ 55% are identical when collected in the monomer and excimer region, whereas in the case of dx:H₂O (with H₂O > 55%) the spectra is different for the different emission wavelengths, strongly suggesting aggregation of the oligomers in these Dx:H₂O mixtures.

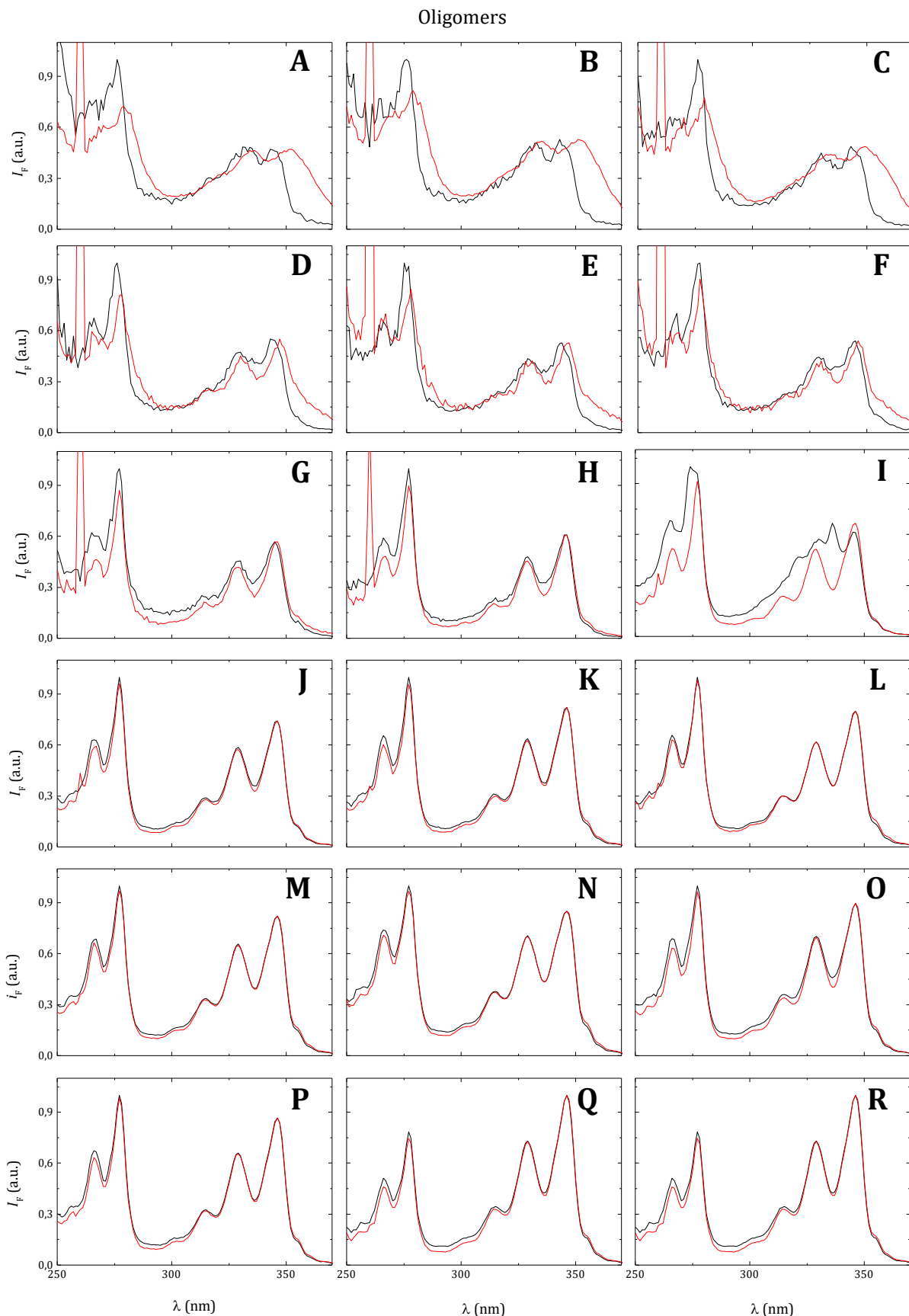


Figure 2.17. Fluorescence excitation spectra of 1Py(3)1Py in dioxane:water mixtures. Black and red lines for $\lambda_{em} = 375$ and 520 nm, respectively. (A) 7.3, (B) 10, (C) 15, (D) 20, (E) 25, (F) 30, (G) 35, (H) 40, (I) 45, (J) 55, (K) 60, (L) 65, (M) 70, (N) 75, (O) 80, (P) 85, (Q) 90 and (R) 95% Dx.

From Figure 2.17 it is observed that up to 45% in dioxane (in dx:H₂O mixtures), the excitation spectra obtained for different emission wavelengths (375 and 520 nm), have different shapes and maxima. For dioxane percentages between 20% and 40%, there is a widening of the excimer band compared to the monomer band. At 50%, the normalized excitation spectra have the same shape and maxima wavelengths. These observations have shown that, as had been done before, just from a 50% dioxane fraction is that we have 1Py(3)1Py completely dissolved, despite the error associated with these determinations. For lower proportions of dioxane in dioxane: water mixture it indicates the presence of preformed dimers of 25% to 40% and lower percentages of aggregates. However, in view of easy precipitation of solutions one can ensure that there are only non-aggregated up to 25%, will be studying aggregates possibly even higher percentages. But if that is really watching dimers are pre-formed, it can be concluded that it is higher for lower rates in dioxane (i.e., high percentages of water). The decrease $\Delta\lambda_1$ and $\Delta\lambda_2$ confirm the reduction of preformed dimers with increasing dioxane solution. This is also true in the absorption spectra (harvested at the same day) that can be seen clearly two types of absorption spectra, one corresponding to the spectra up to 45% in dioxane (with wider band and red shift) and other which belongs to the absorption spectra of the solutions with higher percentages in dioxane. For 1Py(10)1Py in dioxane:water mixtures with high content of dioxane (higher or equal to 60%), the global (simultaneous) analysis of the fluorescence decays, at the monomer (375 nm) and excimer (520 nm) emission wavelengths, leads to a bi-exponential decay law. A negative pre-exponential factor, at the excimer emission wavelength, is always observed (Figure 2.10).

In dx:H₂O mixtures, ranging from 60 to 100 % in dioxane, the decay time values increase and the sum of the pre-exponential factors at 520 nm ($A_{2,1} + A_{2,2}$) cancels out, showing that excimer formation proceeds from a dynamic route and the kinetic formalism can therefore be described by the Birks' kinetic scheme.³⁸ The rate constants for excimer decay, association, and dissociation were obtained using this kinetic formalism considering 1-methylpyrene as model compound.¹¹²

The fluorescence lifetime of 1-methylpyrene (τ_M^0) was measured in different dioxane:water mixtures. The plot of τ_M^0 as a function of the volume fraction of dioxane displays a Gaussian-type curve. The equation of this trend was then used to estimate the values of τ_M^0 in other mixtures, see Figure 2.21B in SI. These lifetimes were used (as the τ_M^0 values) in the analysis of Scheme 1.6 in Chapter 1, for the determination of the rate constants of 1Py(10)1Py as a function of x_{dx} .

Figure 2.18 shows the dependence of the decay times, pre-exponential factors and rate constants of 1Py(10)1Py as a function of the dioxane volume fraction in dioxane:water mixtures.

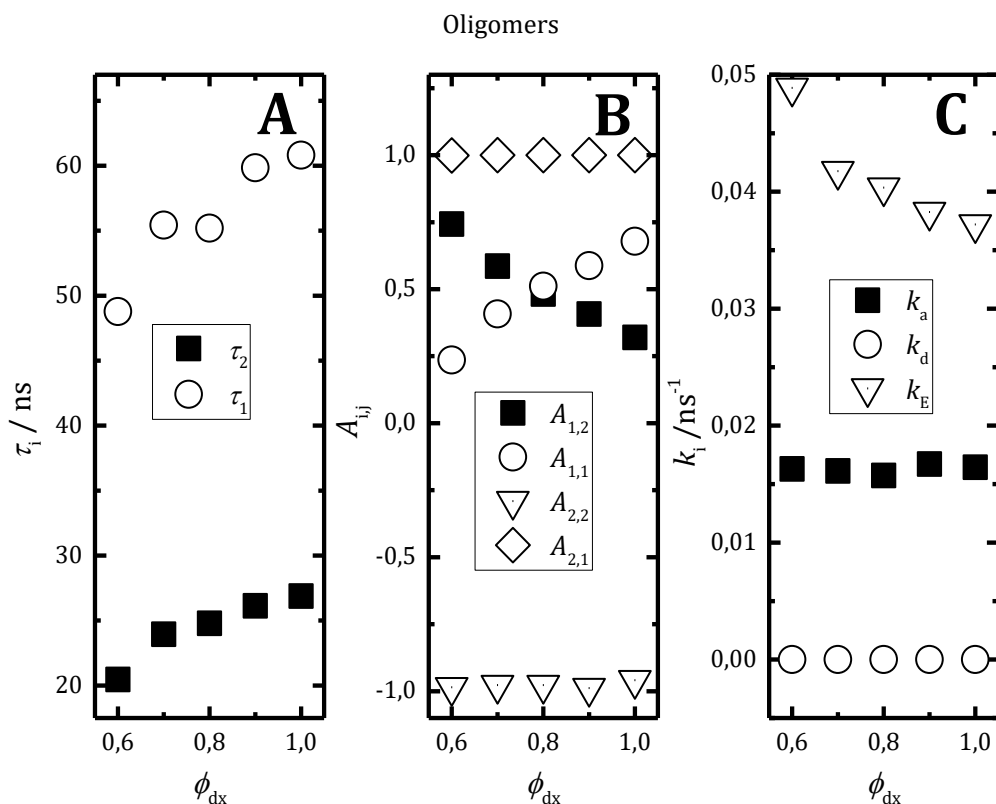


Figure 2.18. Dependence of (A) decay times, (B) pre-exponential factors collected at the monomer ($A_{1,i}$) and excimer ($A_{2,j}$) emissions wavelengths and (C) rate constants of excimer formation (k_a), dissociation (k_d), and decay (k_E) of the 1Py(10)1Py oligomer in dioxane:water mixtures.

In Figure 2.19, the dependence on ϕ_{dx} of the experimental decay times and pre-exponential factors obtained from the global analysis of the fluorescence decays of 1Py(3)1Py in dx:H₂O mixtures are shown. In contrast to that found for 1Py(10)1Py, the decay times and the pre-exponential factors remain constant with (the increase in) the dioxane content of the mixture. Another important observation is that the relative contribution from two different excimers is, as seen by the dependence of the pre-exponential factors at 520 nm, constant with ϕ_{dx} .

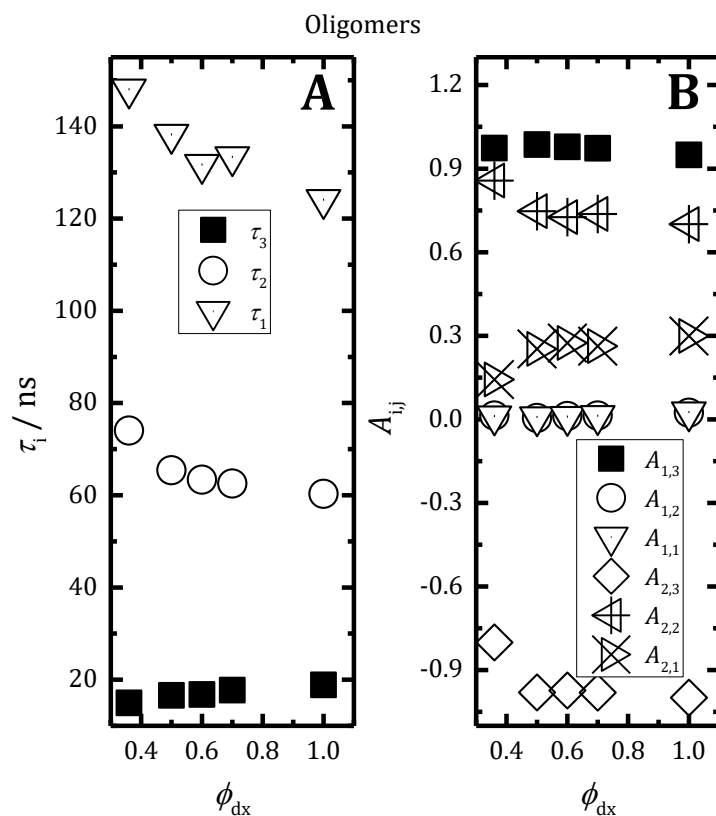


Figure 2.19. Dependence of the (A) decay times (τ_i) and (B) pre-exponential factors obtained from the fluorescence decays collected at the monomer (375 nm, $A_{1,i}$) and excimer (520 nm, $A_{3,i}$) emission wavelengths on the dioxane content, for the 1Py(3)1Py oligomer in dioxane:water mixtures. The $A_{1,2}$ values are very close to the $A_{1,3}$ values.

In conclusion, because in the alkane solvents k_a does substantially increase with the (decrease in) the solvent viscosity, in the case of 1Py(10)1Py in Dx:H₂O the observed constant values suggest that in these mixtures, the solvent viscosity plays a minor role in the excimer formation process (k_a).

For 1Py(3)1Py in dioxane:water mixtures with high content [although lower than for 1Py(10)1Py] of dioxane (higher or equal to 36%), the global (simultaneous) analysis of the fluorescence decays, at the monomer (375 nm) and excimer (520 nm) emission wavelengths, leads to a tri-exponential decay law. A negative pre-exponential factor, at the excimer emission wavelength, is always observed (Figure 2.10).

In dx:H₂O mixtures, from 36 to 100 % dioxane, the decay time values increase and the sum of the pre-exponential factors at 520 nm ($A_{2,1} + A_{2,2}$) cancels out, showing that excimer formation occurs uniquely from a dynamic route and the kinetic formalism can therefore be described by the Birks' kinetic scheme.³⁸ The rate constants of excimer decay, association, and dissociation were obtained using this kinetic formalism considering 1-methylpyrene as the model compound.¹¹²

Oligomers

Table 2.4. Rate constants of excimer formation (k_a), dissociation (k_d) and decay (k_E) obtained for 1Py(3)1Py in different Solvents at 20 °C. The viscosity of the solvents at this temperature (η)¹¹⁴ are also presented.

Solvent	η (mPa.s)	$k_a(1)$ (ns ⁻¹)	$k_a(2)$ (ns ⁻¹)	$k_d(1)$ (ns ⁻¹)	$k_d(2)$ (ns ⁻¹)	$k_E(1)$ (ns ⁻¹)	$k_E(2)$ (ns ⁻¹)
60 % dx	2.22 ^a	0.054	0.009	0.0015	0.0020	0.005	0.035
80 % dx	1.938 ^a	0.033	0.010	0.0009	0.0019	0.008	0.015
90 % dx	1.581 ^a	0.034	0.012	0.001	0.0022	0.007	0.014
100 % dx	1.308 ¹¹⁴	0.036	0.012	0.001	0.0022	0.008	0.015

^a obtained from Figure 2.21A in SI.

2.2.1.4. Summary

The photophysical characterization of the oligomers 1Py(3)1Py and 1Py(10)1Py was obtained in organic solvents (with different viscosities), in dioxane:H₂O mixtures, and as a function of temperature (in heptane). Different methods for the determination of the I_E/I_M ratio, obtained for 1Py(10)1Py in heptane as a function of the temperature were discussed and compared with the data obtained from the fluorescence decays. The Method D, which consist on fitting the excimer band with a GaussMod function (see Section 7.2.6.1.2.1 in Chapter 7), have shown to give a better fit of the excimer band and therefore of the I_E/I_M ratio. Two conformationally different excimers were found with the 1Py(3)1Py oligomer, whilst with 1Py(10)1Py only one, the more stable excimer, was found. Application of the Birks' kinetic scheme allowed the determination of the excimer association rate constant (k_a). In pure organic solvents the decrease of the viscosity led to a decrease in k_a . Preliminary results on flash photolysis experiments were presented for both oligomers and pyrene in concentrations that undergo intermolecular excimer in MCH and dioxane.

2.2.1.5. Supplementary Information

The log-log graph of the monomer lifetime of 1-methylpyrene in a series of alkane solvents is shown in Figure 2.20.

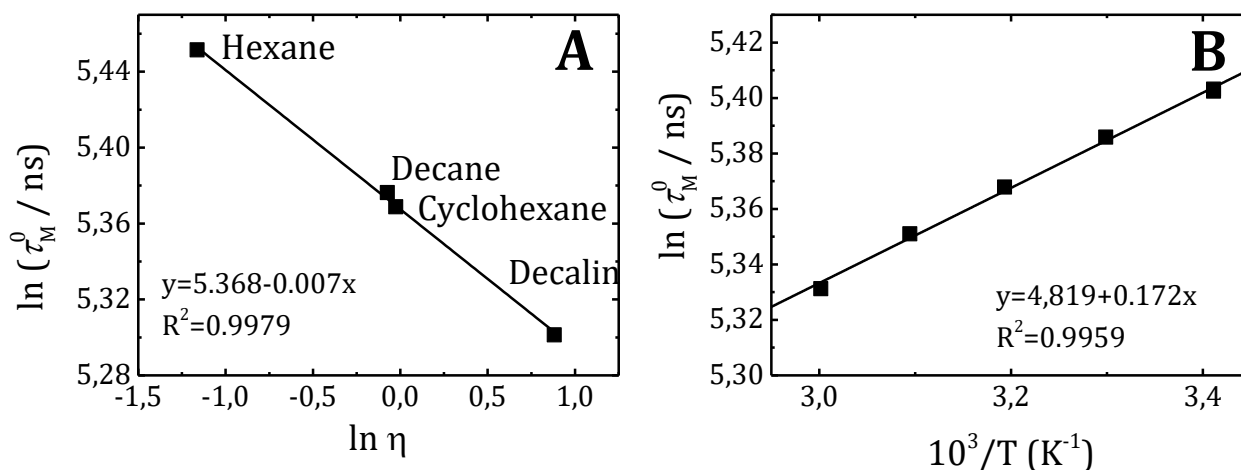


Figure 2.20 (A) $\ln \tau_M^0$ vs $\ln \eta$ of 1-methylpyrene [parent compound used for 1Py(10)1Py and 1Py(3)1Py] in a series of (alkane) solvents and (B) $\ln k_M$ as a function of the absolute reciprocal temperature for 1-methylpyrene in heptane.

The viscosity of the dioxane:water mixtures presented in Figure 2.21A were taken from ref.¹¹⁴ whereas in panel B, the fluorescence lifetimes of deoxygenated solution of 1CH₃Py in different fractions of dioxane (in dx:H₂O mixtures) are displayed.

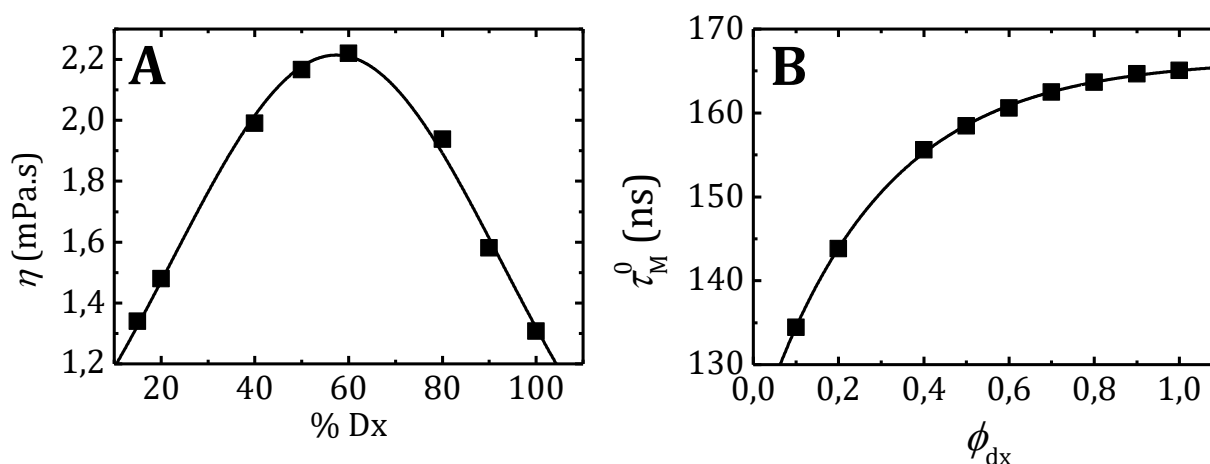


Figure 2.21. (A) Viscosity as a function of the dx content in a mixture of dx:H₂O at 293 K¹¹⁴ adjusted with the following Gaussian function $\eta \text{ (Pa.s)} = 4.99 \times 10^{-4} + \left[0.15 / \left(70.14 \times \sqrt{\pi/2} \right) \right] \times \exp \left[-2 \times \left((\% \text{Dx} - 57.37) / 70.14 \right)^2 \right]$ and (B) fluorescence lifetime of 1-methylpyrene in different d:water mixtures fitted with the following equation $\tau_M^0 = 166.41 - 6255.06 / [1 + \exp((\phi_{dx} + 1.40) / 0.28)]$.

In Figure 2.22 the independent monoexponential analysis of the fluorescence decay of 1Py(10)1Py collected in the monomer emission wavelength shows to not be properly fitted with one exponential and the value obtained for the monoexponential analysis indicates that, in these conditions, there is

excimer reversibility. The global analysis (with the excimer emission decay) of this compound can be seen in Figure 2.10.

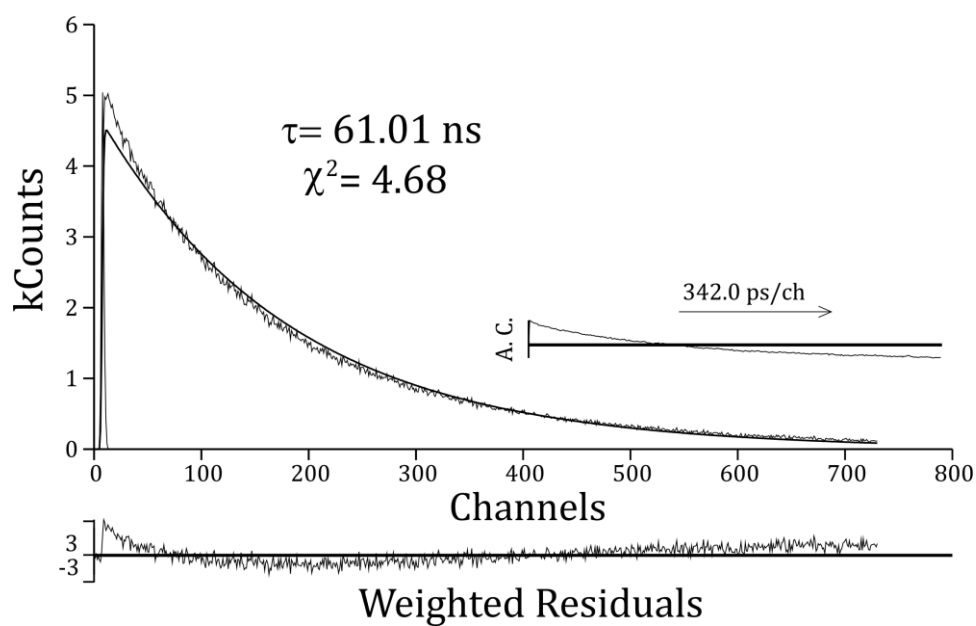


Figure 2.22. Individual monoexponential fit of the fluorescence decay collected at the monomer ($\lambda_{\text{em.}} = 375 \text{ nm}$) of 1,10-di(1,1'-pyrenyl)decane [1Py(10)1Py]] in DMF at 293 K.

In Table 2.5 and Table 2.6Table 2.4, all the steady state and TR data (presented in Section 2.2.1) are presented for 1Py(10)1Py, respectively.

Oligomers

Table 2.5. Relevant parameters obtained from the steady state (SS) [$\lambda_{\max}^{abs.}$, P_A , λ_{\max}^M , λ_{\max}^E , I_1/I_3 , I_E/I_M , $\Delta\lambda_2$ and P_M-P_E] for the 1Py(10)1Py oligomer in different solvents and mixture of solvents at 293 K unless noted. The viscosities of the solvents (η) are also presented.

Solvent	η (mPa.s)	$\lambda_{\max}^{abs.}$ (nm)	P_A	λ_{\max}^M (nm)	λ_{\max}^E (nm)			I_1/I_3			I_E/I_M			$\Delta\lambda_2$ (nm)	P_M-P_E
					$\lambda_{exc=}$	$\lambda_{exc=}$	$\lambda_{exc=}$	$\lambda_{exc=}$	$\lambda_{exc=}$	$\lambda_{exc=}$	$\lambda_{exc=}$	$\lambda_{exc=}$	$\lambda_{exc=}$		
					315 nm	335 nm	350 nm	315 nm	335 nm	350 nm	315 nm	335 nm	350 nm		
Hexane	0.3126 ³⁵	342.4	3.95	376 ^{b-d}	476	476	478	3.04	2.87	2.54	1.66	1.72	2.17	0.10	
Heptane	0.4181 ³⁵	343	3.20	375 ^e		475 ^e			2.87 ^e		1.28 ^{e,f}			0	-0.14
MeOH	0.5929 ³⁵							3.18	3.38	2.59	1.68	1.63	2.06		
Decane	0.9284 ³⁵	343.4	3.45	376 ^{b-d}	475	476	479	3.01	2.91	2.55	1.02	1.06	1.23	0.06	
Dioxane	1.3075 ^a	344.2	2.68					3.60	3.35	3.33	0.33	0.33	0.37		
90% Dx	1.581 ^a	344.2	2.55					3.69	3.50	3.38	0.37	0.40	0.43		
80% Dx	1.938 ^a	344.0	2.60					3.60	3.50	3.43	0.46	0.49	0.54		
70% Dx	2.107 ^a	344.0	2.64					3.62	3.53	3.31	0.56	0.58	0.64		
60% Dx	2.22 ^a	344.0	1.97					2.42	3.37	3.25	0.74	0.74	0.82		
Decalin	2.415(3) ¹¹⁷	344.2	3.77	376 ^{b-d}	481	478	483	3.07	2.89	2.76	0.53	0.56	0.61	0.05	

^a Obtained from Figure 2.21A in SI. ^{b, c, d} and ^e Obtained with $\lambda_{exc} = 315, 335, 350$ and 339 nm. ^f The maxima intensities were taken.

Oligomers

Table 2.6. Decay times (τ) and pre-exponential factors obtained from the fluorescence decays collected at the monomer (375 nm, $A_{1,i}$) and excimer (520 nm, $A_{2,j}$) emission wavelengths and chi-squared values (χ^2) recovered from the fitting for the 1Py(10)1Py in different solvents and mixture of solvents at 293 K unless noted. The viscosities of the solvents (η) are also presented.

Solvent	η (mPa.s)	τ_2 (ns)	τ_1 (ns)	τ_M (ns)	$A_{1,2}$	$A_{1,1}$	$A_{2,2}$	$A_{2,1}$	χ^2	
									M	E
Hexane	0.3126 ³⁵	9.5	54.5	233 ^b	0.81	0.16	-0.91	1		
Heptane	0.4181 ³⁵	11.3	50.6	229 ^c	0.81	0.18	-0.94	1		
MeOH	0.5929 ³⁵	8.2	44.2	223 ^c	0.87	0.09	-0.92	1		
MCH	0.734 ³⁵	17.7	55.3	219 ^c	0.73	0.24	-0.95	1		
DMF	0.924 ³⁵	27.8	70.0	216 ^c	0.33	0.67	-0.96	1		
Decane	0.9284 ³⁵	17.7	54.4	216 ^b	0.72	0.26	-0.98	1		
Dx	1.3075 ¹¹⁴	28.0	70.0	210 ^c	0.32	0.68	-0.98	1		
Dodecane	1.508 ³⁵	23.9	60.2	208 ^c	0.67	0.27	-0.99	1		
90% Dx	1.581 ^a	26.1	60.0	207 ^c	0.42	0.57	-0.99	1		
80% Dx	1.938 ^a	25.0	55.1	204 ^c	0.49	0.49	-0.98	1		
70% Dx	2.107 ^a	22.7	57.1	203 ^c	0.60	0.40	-0.98	1		
60% Dx	2.22 ^a	20.7	48.5	202 ^c	0.76	0.22	-0.98	1		
Decalin	2.415(3) ¹¹⁷	31.5	66.6	201 ^b	0.41	0.56	-0.98	1		
Hexadecane	3.451 ¹¹⁵	31.8	67.3	196 ^c	0.48	0.46	-0.97	1		

^a obtained from Figure 2.21A in SI. ^b Lifetime of 1CH₃Py in the respective solvent. ^c Obtained by the equation obtained from Figure 2.20A.

2.2.2. Dipyrenylacetamides

In order to study oligomers which could more closely resemble the PAAMePy polymers (see Chapter 3) another group of pyrene oligomers was investigated in DMF.

2.2.2.1. Steady-State Behavior

The absorption spectra of the oligomers in DMF are depicted in Figure 2.23. The λ_{\max}^A and P_A do not follow any trend with the chain length (data not shown). However these values for the oligomer with only one pyrene unit are considerably different (smaller λ_{\max}^A and higher P_A).

Oligomers

Table 2.7. Relevant data [excimer emission band maximum λ_{\max}^E , width at half maximum of the excimer emission band $\Delta(1/2)$, excimer-to-monomer fluorescence intensities ratio] from the fluorescence spectra of the $1\text{Py}(\text{CH}_2\text{NHC}=\text{O})_n\text{CH}_2\text{-1Py}$ in DMF at 20°C.

$1\text{Py}(\text{CH}_2\text{NHC}=\text{O})_n\text{CH}_2\text{-1Py}$	Nº of atoms	λ_{\max}^E (nm)	$\Delta(1/2)$ (nm)	I_E/I_M
1	4	431	79	0.19
2	7	468	82	0.63
3	10	473	83	0.84

The emission spectra of all the oligomers in all the solvents used display a structured monomer emission band. The oligomers with two pyrene units possess, in addition, the characteristic structureless band of the (intramolecular) excimer. Monomer and excimer bands are well separated in exception for the oligomer with $n=1$.

All the oligomers undergo intramolecular excimer formation in a variety of solvents except for the parent compound (with only one pyrene unit). In Figure 2.23 the fluorescence spectra of the four compounds (three bipiryrenyl and the parent compound) in DMF at 20 °C are presented.

The excimer-to-monomer fluorescence intensities ratio (I_E/I_M) (which is an approximation to the excimer-to-monomer fluorescence quantum yield) increased linearly with the increase in the chain length, Figure 2.23.

Unfortunately, the absence of more compounds with smaller n , does not allow to verify if these compounds follow Hirayama rule, see Section 2.1 (since with $n=1$, there are already 4 atoms linking the pyrene units).⁸⁹ The λ_{\max}^E and the width at half-maximum of the excimer emission band are listed in Table 2.7. With increasing the chain length both parameter gradually increases.

Note that even though the smaller molecule with possibility to form intramolecular excimer ($n=1$) is not that small since both pyrene units are separated by a chain constituted by four atoms. Although, some rigidity may be given by the carbonyl group, the possibility of the chain to bend and form the more stable excimer is to be expected.

Oligomers

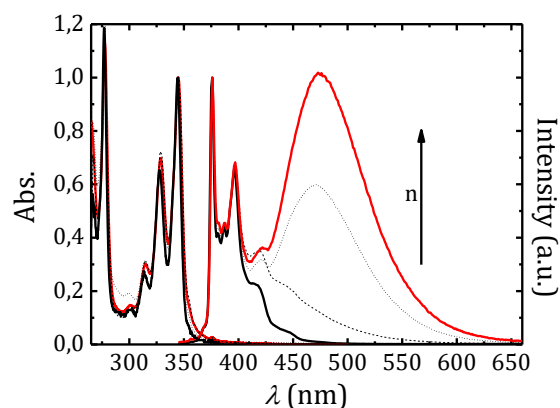


Figure 2.23. Absorption and fluorescence emission spectra of $1\text{PyCH}_2\text{NHC}=\text{OCH}_3$ and of $1\text{Py}(\text{CH}_2\text{NHC}=\text{O})_n\text{CH}_2-1\text{Py}$ for $n=1, 2$ and 3 in DMF at 293 K with $\lambda_{\text{exc.}}=339\text{ nm}$.

Considering the analysis (both independent and global) made of the fluorescence decays of all the bi-chromophoric oligomers, it is reasonable to consider that they follow the Birks' kinetic scheme (see more detail in Appendix A).⁸⁹

In Figure 2.23 the absorption and fluorescence emission spectra of two oligomers (parent and with $n=1$) in cyclohexane are depicted. In contrast to the observed in Figure 2.23, in Cx is the turn of the monomer emission band to be masked.

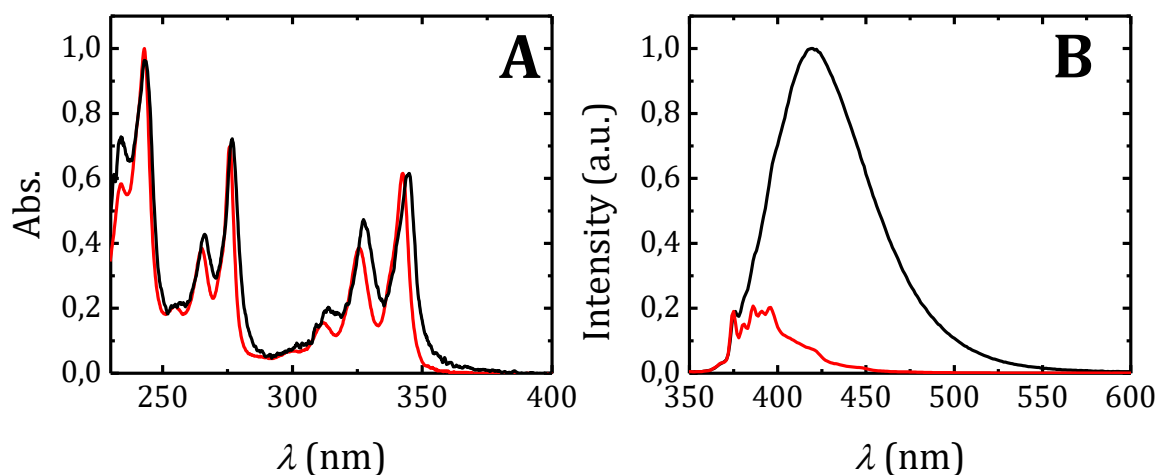


Figure 2.24. (A) Absorption and (B) Fluorescence emission spectra of $1\text{PyCH}_2\text{NHC}=\text{OCH}_3$ (red line) and of $1\text{Py}(\text{CH}_2\text{NHC}=\text{O})_n\text{CH}_2-1\text{Py}$ for $n=1$ in Cx at 293 K with $\lambda_{\text{exc.}}=315\text{ nm}$.

2.2.2.2. Time-Resolved Behavior

All the fluorescence decays were found to fit with a biexponential with the exception of $n=1$ in dioxane which can be explained by the presence of a residual amount of water, see Table 2.10 in SI. The Birks'

kinetic scheme was further considered to obtain the rate constants for excimer formation, dissociation and decay with these compounds, see Table 2.8.

Table 2.8. Rate constants of excimer formation, dissociation and decay (k_a , k_d and k_E), monomer and excimer fluorescence decay times (τ_M and τ_E) in different solvents at 20 °C. The viscosities of the solvents (η) are also presented.

Compound	Solvent	η (mPa.s)	k_a (ns ⁻¹)	k_d (ns ⁻¹)	k_M (ns ⁻¹)	k_E (ns ⁻¹)	τ_E (ns)	τ_M (ns)
1PyCH ₂ NHC=OCH ₃	MeOH	0.5929 ³⁵	NA			NA		233.8
1PyCH ₂ NHC=OCH ₃			NA			NA		
1Py(CH ₂ NHC=O)CH ₂ -1Py	DMF	0.924 ³⁵						222.7
1Py(CH ₂ NHC=O) ₂ CH ₂ -1Py			0.030	0.014		0.030	33.8	
1Py(CH ₂ NHC=O) ₃ CH ₂ -1Py			0.049	0.019		0.022	46.5	
1PyCH ₂ NHC=OCH ₃	Cx	0.975 ³⁵	NA		0.004	NA		
1Py(CH ₂ NHC=O)CH ₂ -1Py								
1PyCH ₂ C=ONH ₂			NA			NA		
1PyCH ₂ NHC=OCH ₃	Dx	1.3075 ¹¹⁴						229.4
1Py(CH ₂ NHC=O)CH ₂ -1Py			0.048	0.023		0.021	46.6	
1Py(CH ₂ NHC=O) ₂ CH ₂ -1Py			0.019	0.016		0.038	26.0	

NA – not applicable.

The steady state and time-resolved data of 1PyCH₂NHC=OCH₃ in MeOH as a function of the temperature was also obtained. This compound was found as an adequate model compound for PAAMePy, see Section 3.2.1.2.

2.2.2.3. Summary

The photophysical characterization of the dipyrenylacetamides was obtained in DMF, Cx, MeOH and Dx. An increase of I_E/I_M ratio with the increase of the chain length (between the two pyrene units) was observed with the presence of only one excimer for all the oligomers. The Birks' kinetic scheme was found to be adequate to the observed kinetic behavior and allowed the determination of all the rate constants involved.

2.2.2.4. Supplementary Information

In Table 2.9 all the parameters taken from SS were gathered.

Table 2.9. Relevant parameters obtained from the steady state (SS) [λ_{\max}^{abs} , P_A , λ_1 , λ_{\max}^E , I_1/I_3 , I_E/I_M , $\Delta\lambda_2$ and $P_M \cdot P_E$] for 1PyCH₂C=ONH₂, 1PyCH₂NHC=OCH₃ and 1Py(CH₂NHC=O)_nCH₂-1Py (n= 1,2 and 3) in different solvents. The viscosities of the solvents (η) are also presented.

Compound	Solvent	η (mPa.s)	λ_{\max}^{abs} (nm)	P_A	λ_1 (nm)	λ_{\max}^E , ^a (nm)	I_1/I_3				I_E/I_M				$\Delta\lambda_2$	$P_M \cdot P_E$	
							λ_{exc} (nm)				λ_{exc} (nm)						
							315	335	339	350	315	335	339	350			
1PyCH ₂ NHC=OCH ₃	MeOH	0.5929 ³⁵	341	3.67	374	NA	1.74 ^c	ND				NA					
1PyCH ₂ NHC=OCH ₃			344.3±0.1	3.35	376		2.21	2.24	2.27	2.17							
1Py(CH ₂ NHC=O)CH ₂ -1Py	DMF	0.924 ³⁵	345.6	2.64	376	431	2.26	2.18	2.23	2.12	0.17	0.18	0.17	0.19	0	0.60	
1Py(CH ₂ NHC=O) ₂ CH ₂ -1Py			344.8	2.86	376	468	2.23	2.24	2.31	2.21	0.63	0.61	0.61	0.63	1	0.05	
1Py(CH ₂ NHC=O) ₃ CH ₂ -1Py			345.1	2.65	376	473	2.13	2.05	2.19	1.87	0.77	0.79	1.02	0.84	0	0.01	
1PyCH ₂ NHC=OCH ₃	Cx	0.975 ³⁵	342	3.62	375	NA	1.07	0.94	0.93	0.94	NA						
1Py(CH ₂ NHC=O)CH ₂ -1Py			343.5	1.73	376	420	NP				0.19	0.19	ND	0.18	0 ^d	-0.04	
Py			336	3.55	372		1.57	1.57	1.56	1.34							
1PyCH ₂ C=ONH ₂			344	2.84	376	NA	2.15	2.03	2.08	1.92	NA						
1PyCH ₂ NHC=OCH ₃	Dx	1.3075 ¹¹⁴	343.5	2.98	375		1.87	1.86	1.81	1.78							
1Py(CH ₂ NHC=O)CH ₂ -1Py			344.5	2.80	376	426 ^b	1.63	1.54		1.34	0.55	0.58		0.68	0	0.61	
Py(CH ₂ NHC=O) ₂ CH ₂ -1Py			344	2.88	376	472	1.77	1.70	1.65	1.58	0.56	0.60	0.63	0.62	0	0.08	
1Py(CH ₂ NHC=O) ₃ CH ₂ -1Py			344.0	2.80	375 ^b	472	1.71	1.63	1.77	1.32	0.91	0.94	1.15	1.11	0	0.12	

^a taken from the emission spectra with λ_{exc} = 339 nm, if not otherwise noted. ^{b, c} taken from the emission spectra with λ_{exc} = 335 and 343 nm, respectively. ^d The excitation spectra in the excimer region was collected at λ_{em} = 480 nm. NA - not applicable. ND - not determined. NP - not possible to determine, Figure 2.24.

Oligomers

Table 2.10. Decay times (τ_i) and pre-exponential factors obtained from the fluorescence decays collected at the monomer (375 nm, $A_{1,i}$) and excimer (520 nm, $A_{2,i}$) emission wavelengths for 1PyCH₂C=ONH₂, 1PyCH₂NHC=OCH₃ and 1Py(CH₂NHC=O)_nCH₂-1Py (n= 1,2 and 3) in different solvents at 20 °C. The viscosities of the solvents (η) are also presented.

Compound	Solvent	η (mPa.s)	τ_3 (ns)	τ_2 (ns)	τ_1 (ns)	τ_0 (ns)	$A_{1,3}$	$A_{1,2}$	$A_{1,1}$	$A_{1,0}$	$A_{2,3}$	$A_{2,2}$	$A_{2,1}$	$A_{2,0}$	χ^2	
															<i>M</i>	<i>E</i>
1PyCH ₂ NHC=OCH ₃	MeOH	0.5929 ³⁵				233.8 ±0.7									1.11 1.12	
1PyCH ₂ NHC=OCH ₃				NA		222.7 ±0.5		NA	1			NA			1.04 1.19	NA
1Py(CH ₂ NHC=O)CH ₂ -1Py	DMF	0.924 ³⁵				(42.4)										
1Py(CH ₂ NHC=O) ₂ CH ₂ -1Py			16.5	55.6		NA	0.391	0.608			-0.906	1			1.14	1.07
1Py(CH ₂ NHC=O) ₃ CH ₂ -1Py			12.9	63.1			0.604	0.393			-0.897	1			1.11	1.01
1PyCH ₂ NHC=OCH ₃				NA		316.4		NA	1				NA		1.02	NA
1Py(CH ₂ NHC=O)CH ₂ -1Py	Cx	0.975 ³⁵	10.7	59.1		320.0	0.878	0.117		0.006	-0.973	1		-0.004	1.25	
1PyCH ₂ C=ONH ₂						200.4									1.04	
1PyCH ₂ NHC=OCH ₃				NA		229.4									0.97	NA
1Py(CH ₂ NHC=O)CH ₂ -1Py	Dx	1.3075 ¹¹⁴	2.8	49.7	116.6		0.140	0.077	0.783		-0.449	0.409	0.591		0.94	1.01
1Py(CH ₂ NHC=O) ₂ CH ₂ -1Py			16.2	63.9			0.165	0.835			-0.915	1			1.23	1.28
1Py(CH ₂ NHC=O) ₃ CH ₂ -1Py			12.1	67.2		*	0.554	0.444		0.002	-0.910	1		-0.002	1.18	1.18

The fluorescence decay time in brackets was determined in the presence of oxygen. NA – not applicable

Chapter 3

Polymers

3.1. Introduction

As mentioned earlier, a polymer is a macromolecule formed by the repetition of a large number of monomers, typically covalently bonded, in which the degree of polymerization (number of repeating units) and the type of monomeric units determines the type of macromolecule.

These macromolecules can have natural (e.g., proteins and polysaccharides) or synthetic origins [e.g., polyethylene and poly(acrylic acid)]. Figure 3.1 illustrates some natural and synthetic polymers and their presence in the nature and industry, respectively.

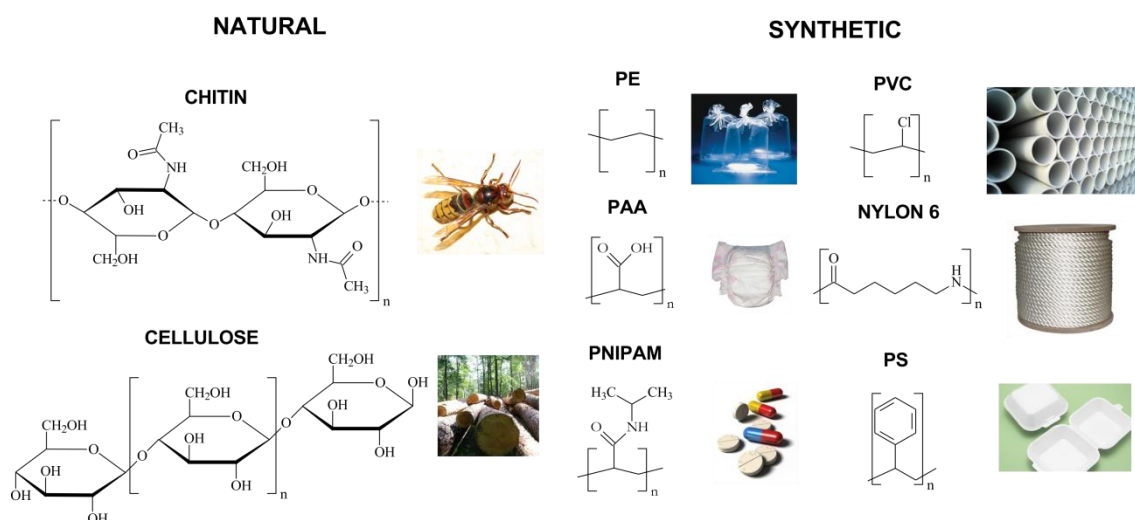


Figure 3.1. Structures of some (natural and synthetic) polymers: chitin [Photograph; bee], cellulose [Photograph; wood], polyethylene (PE) [Photograph; PE bags],¹¹⁸ poly(acrylic acid) (PAA) [Photograph; diapers],¹¹⁹ poly(*N*-isopropylacrylamide) (PNIPAM) [Photograph; medicine],^{120,121} polystyrene (PS) [Photograph; PS fast food container], polyvinyl chloride (PVC) [Photograph; PVC tubes for canalization]¹²² and nylon 6 [poly(hexano-6-lactam)] [Photograph; rope].

Synthetic polymers can be classified according to their structure, composition, thermal, mechanical properties and particular characteristics (e.g. polarity) of its monomeric units. Polymers can be linear, branched or cross-linked. In terms of composition, the polymers can be divided into homopolymers and

Polymers

heteropolymers (also known as copolymers). The first consists of the repetition in succession of the same monomer (such as poly(acrylic acid) with the acrylic acid as monomer), while the second is derived from different monomers, see Figure 3.2.

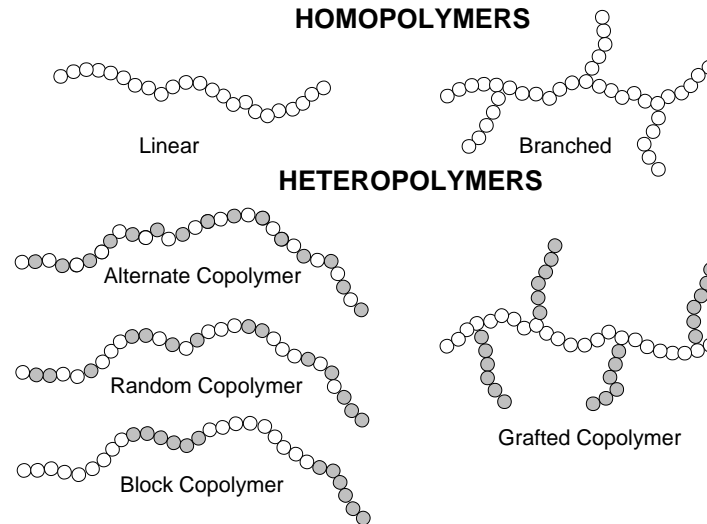


Figure 3.2. Schematic structures of homo- and heteropolymers.⁵¹

In this latter case, monomer units can be found in a regular or non-regular way, for example, they form blocks or be randomly distributed, see Figure 3.2.

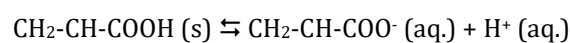
Polymers, according to their polarity, can further be classified into four different classes: (i) non-polar, (ii) polar but water insoluble, (iii) water-soluble and (iv) ionisable polymers or polyelectrolytes.

3.1.1. Polyelectrolytes

An electrolyte is a substance that ionizes when dissolved in suitable ionizing solvents such as water

For example, when table salt (sodium chloride), NaCl, is placed in water, the salt (a solid) dissolves into its component ions (Na⁺ and Cl⁻)

Electrolyte solutions can also result from the dissolution of some biological [e.g., DNA, polypeptides] and synthetic polymers [e.g., polystyrene sulphonate, poly(acrylic acid)], termed polyelectrolytes, whose repeating units bear an electrolyte group. For example, when PAA is placed in water, the solid dissolves into its component ions, according to the dissociation reaction



In this case, the polyelectrolyte PAA is also a polyacid since it contains acid groups.

As happens with electrolytes, the polyelectrolytes can be termed strong and weak depending on whether a high proportion of the solute dissociates to form free ions or most of the solute does not dissociate. For example, PAA is a weak polyelectrolyte.

The degree of ionization (or dissociation, α) is related the amount of solute dissociated into ions per mole. With very strong acids and bases, this value will be close to 1. Less powerful acids and bases will have smaller degree of dissociation.

Moreover, the interactions of polyelectrolytes with other colloid structures show a wide variety of applications in fields as different as medicine, water treatment, paints or food industries.

3.1.2. Solubilisation of Polymers

The dissolution of non-polymeric materials is different from polymers because they dissolve instantaneously while the polymers do not. In fact, a polymer solution is often left some time with agitation and temperature to allow dissolution.

Generally, when an uncrosslinked, amorphous, glassy polymer is in contact with a compatible solvent, the solvent will diffuse into the polymer and a gel-like swollen layer is formed; with time, the polymer dissolves.¹²³

As observed in this work (discussed with more details in Section 7.1.9.2) to an increased polymer molecular weight there is a concomitant decrease in the dissolution rate.¹²⁴

3.1.3. Polymer Conformation

The conformation of a polymer chain in solution may strongly depend on the solvent. One of the reasons for conformational differences is the thermodynamic “quality” of the solvent. When a polymer is in a solution where the solvent has a greater attraction for segments of the polymer than the polymer segments have for each other, the chain length is extended (Figure 3.3). In contrast, contraction will occur when a polymer is in a solvent in which the solvent-polymer attraction is less than the polymer-polymer attraction. Solvents for a particular polymer have been denoted as “good” if the chain extension is promoted and “poor” if the chain extension is contracted. Good solvents dissolve a larger amount of polymer; if the solvent is too poor, the polymer will not dissolve.^{125,126}

Nevertheless, the configuration of the polymer chain depends not only on the segment-solvent interactions, but also on the polymerization degree and the rigidity between segments. According to this, a high number of intermediate conformations are also possible and their probability is determined by the Boltzmann’s law.¹²⁷ The configuration of a polymer is often described in terms of the persistence length parameter, l_p ,^{127,128} see Equation 3.1.

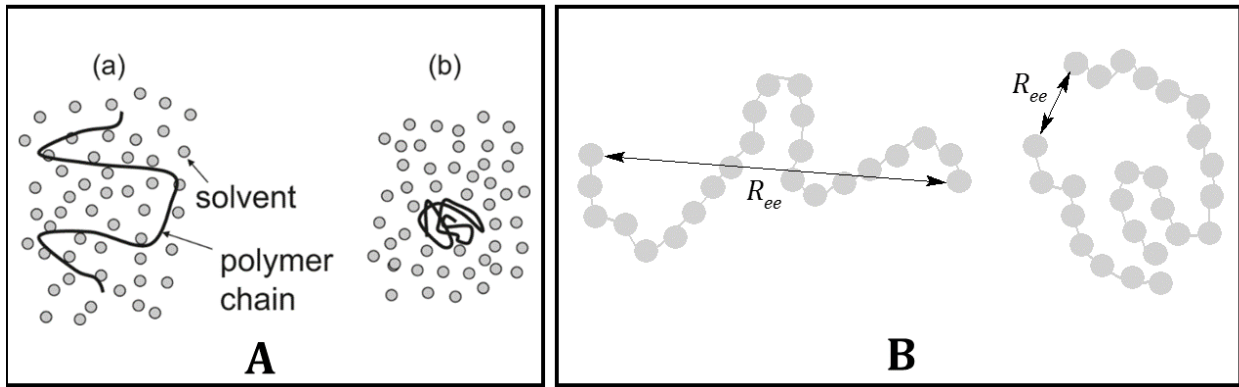


Figure 3.3. (A) The effects of solvent quality on the conformation of a polymer molecule in solution, (a) extended and (b) contracted from ref.¹²⁹ and (B) Illustration of the end-to-end distance.

$$l_p \approx \frac{R_{ee}^2}{2nl} \quad \text{Equation 3.1}$$

In Equation 3.1, R_{ee} is the mean value (of values taken over time) of the end-to-end distance (separation between the two ends of the chain, see Figure 3.3B) and the product nl is the chain length (for n bonds of length l). Thus, the l_p parameter measures the stiffness of the polymer chain. When l_p is high, i.e., when $R_{ee}^2 \ll nl$ [Figure 3.3A(b)], the polymer assumes a very stiff conformation; but in the opposite case, when $R_{ee}^2 \gg nl$ [Figure 3.3A(a)], a flexible chain conformation is adopted.¹²⁷

Besides, the type of interactions found in a polymer can be of intra or intermolecular origin. This depends on the type of polymer and its concentration in solution (diluted, semi-diluted and concentrated regime).

3.1.4. Hydrophobically Modified Polymers (HMP)

Fluorescently labelled polymers are nowadays of extreme relevance in the characterization of polymer dynamics, protein folding, as molecular rulers, chemosensors, *etc.*^{51,130} The randomly and hydrophobically modified PAA and PNIPAM polymers investigated in these thesis are, respectively, randomly grafted and random copolymers. In the first case, a poly(acrylic acid) was grafted with pyrene and in the second two monomers were prepared to produce the copolymer. With both of them generating the random introduction of pyrene. Pyrene modified polymers can be seen as useful probes in aqueous environment because, although pyrene has low solubility in water, the acrylic acid groups allow the solubilisation (also because the polymers have less than 10% of pyrene) of these hydrophobic probe.

Fluorescence techniques offer the advantage that the dynamics of a polymer in solution can be followed at a molecular level. This usually demands the covalent attachment of a fluorescent probe with lifetimes in the ns-time range in order to follow the polymer dynamics. For this purpose, time-resolved fluorescence spectroscopy constitutes a technique of excellence.

Poly(*N*-isopropyl)acrylamide (PNIPAM) has been widely investigated due to its applications in optical/electronic devices, biomedical systems, responsive surfaces, and chemosensors.

In order to understand the dynamics of these polymers at a molecular level a new PNIPAM polymer tagged with pyrene (Py) was synthesised. The particular characteristics of pyrene (long lifetime, formation of excimer(s), vibronic ratio of I_1/I_3 dependent on the polarity of the media¹³¹) making a probe of election to study the dynamics of such polymers. Nevertheless when incorporated in polymers the kinetics of excimer formation leads to complexity with the presence of free pyrene units, ground-state dimers, more than one excimer conformation, *etc.* This has led to different interpretation of its kinetics.

In general two approaches or models have been used to interpret the kinetic of polymers labelled with pyrene/naphthalene: the so-called blob model (which implies a prior analysis with sums of 4-5 exponentials and the inexistence of excimer-to-monomer reversibility) and the discrete sums of exponentials, where the decays are collected at different wavelengths, globally analysed and allow a direct attribution of the exponential terms with the species present. Examples of polymers labelled with pyrene are the poly(acrylic acid) (PAA), polyethyleneglicol (PEG), polyoxyethylene (PEO) and poly(*N*-isopropylacrylamide), PNIPAM.

In the context of these two general models, different types of pyrene labelled PNIPAM derivatives have been studied; interesting examples of these are the amphiphilic asymmetric comb polymer with pendant pyrene groups and poly(*N*-isopropylacrylamide) side chains which was studied in THF and water¹³², or a pyrene (end- and randomly-) labelled PNIPAM polymers studied as a function of the viscosity. In this case, the properties of one (of each) polymer (with similar Py content) were compared. The fluorescence decays were then interpreted using a modified Birks' kinetic scheme and the blob model for the end- and randomly labelled polymers, respectively.¹³³

Besides, Duan *et al.* examined the effects of the molecular weight of the polymer and the concentration of β -cyclodextrin on the *LCST* (lower critical solution temperature) of a (single) pyrene labelled poly(*N*-isopropylacrylamide).¹³⁴ Other studies with (un)modified PNIPAM were made by using pyrene as an extrinsic probe.^{135,136}

3.1.5. Analysis of the Fluorescence Decays in Polymers

As mentioned, all the decays presented in this work were analysed making no model assumption a priori and with a discrete sum of exponential functions, see Section 2.1.1.1. However, along the years, different methods have been used, especially in the investigation of randomly labelled polymers such as those in this thesis. For this reason, some of the models, will be shortly described.

3.1.5.1. The Maximum Entropy Method (MEM)

Another method (beside the discrete sum of exponentials referred in Section 2.1.1.1) can be used in order to analyse the fluorescence decays. The difference is that the fluorescence decay curve is given by a sum of continuous, smooth functions.¹³⁷

$$I(t) = \sum_{i=1}^N \alpha_i \exp(-t/\tau_i) \quad \text{Equation 3.2}$$

The optimum distribution is the one which fits the data correctly ($\chi^2 \sim 1$) and maximizes the value of Shanon-Jaynes entropy function S , as defined in Equation 3.3.

$$S = -\sum p_i \log p_i \quad \text{Equation 3.3}$$

Where $p_i = \alpha_i / \sum \alpha_i$. If the χ^2 is satisfied for many distributions then the maximum entropy (ME) criterion selects the distribution that contains the minimum number of peaks in the distribution and with the maximum width for each peak.¹³⁸

3.1.5.2. Blob Model

The blob model consists in dividing the polymer chain into a sequential set of spheres (called “blobs”) of identical sizes. Each blob has the same volume V_b and contains the same mass of polymer m_b . To consider that processes within each blob are independent of the neighbouring blobs, the blob size is defined in such a way that it becomes smaller as the number of Py groups attached to the polymer chain increases. This model can be used directly via <http://fluodecay.uwaterloo.ca/scriptlist/>.

The blob volume is related to the mass of polymer contained within the blob through the expression given by Equation 3.4.¹³⁹

$$V_b = a^3 \left(\frac{m_b}{M_{mon}} \right)^{3\nu} \quad \text{Equation 3.4}$$

In Equation 3.4 a represents the size of the monomer, m_b the mass of the polymer inside the blob, M_{mon} being its molecular mass and with ν taking the values of 0.5 in a θ -solvent or 0.6 in a good solvent (see Section 3.1.3) for the polymer.¹³⁹

Upon exposure to light, a fraction of the chromophores M are excited. The probability of having two or more M^* in a single blob is negligible.

It is assumed that the processes described in Scheme 1.5 occur fast enough for the distribution of pyrene groups in each blob holds. Using this model, the time dependence of the concentration of the excited chromophore (M^*) in a polymer was given by Equation 3.5¹³⁹

$$I_M(t) = \exp\left\{-\frac{t}{\tau_M} - \langle n \rangle [1 - \exp(-k_a t)]\right\} \quad \text{Equation 3.5}$$

Where $\langle n \rangle$ is the average number of chromophores per blob. As can be seen from Equation 3.5, the fitting of the fluorescence decay of the monomer using this model provides both τ_M , $\langle n \rangle$ and k_a , which is the average excimer formation rate constant in a blob containing M^* and one ground-state M .

With $\langle n \rangle$ and the concentration of chromophores per gram of polymer (λ , obtained by UV spectroscopy using a parent, see Section 3.2.2), m_b can be calculated.

$$\lambda = \frac{\sum x_i N_i \langle n \rangle}{M_n} = \frac{\sum x_i N_i \langle n \rangle}{\sum x_i N_i m_b} = \frac{\langle n \rangle}{m_b} \quad \text{Equation 3.6}$$

Where x_i is the fraction of chains i in the sample and N_i the number of blobs in a chain i .

3.2. Poly(acrylic acid) Pyrene Labelled Polymers (PAAMePy)

3.2.1. Synthesis

The synthesis procedure of hydrophobic modification of the poly(acrylic acid) (PAA) polymers with 1-pyrenylmethylamine hydrochloride is described in ref. ⁶⁵ for PAAMePy(2)52, PAAMePy(2)77, PAAMePy(450)53 and PAAMePy(450)87, in ref. ⁶⁴ for PAAMePy(450)11 and PAAMePy(450)517 and in ref. ¹⁴⁰ for PAAMePy(150)55 and PAAMePy(150)230 polymers.

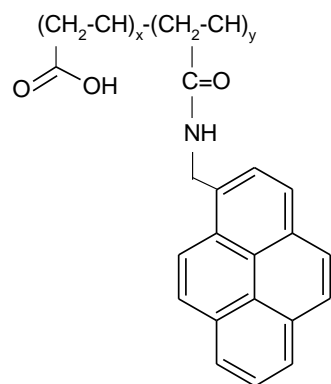
Similar procedures were repeated using the appropriate molecular weight and mass of PAA, H_3BO_3 , 1-pyrenylmethylamine and reflux time for the synthesis of PAAMePy(2)12, PAAMePy(2)18, PAAMePy(2)24, PAAMePy(2)41, PAAMePy(2)132, PAAMePy(2)133, PAAMePy(450)10 and PAAMePy(450)77, see Section 7.1.3.2.

The probed poly(acrylic acid) polymers were synthesized by Prof. Isabel Gonçalves and Dr. Sandra Gago except for the PAAMePy(150) that were kindly provided by Dr. Karin Schillén.

3.2.2. Determination of the Probe Content: Degree of Labelling

The pyrene (Py) labelling content of the PAAMePy polymers were determined by UV spectroscopy by comparison with the parent compound 1-pyrenylmethylamine ($\epsilon = 37\,070 \text{ M}^{-1}\text{cm}^{-1}$ in methanol)⁶⁴ and by ¹H-NMR, Equation 3.7 and Equation 3.10, respectively.

Polymers



PAA: 2 kg/mol

x= 0.925
y= 0.075 PAAMePy(2)12

x= 0.947
y= 0.053 PAAMePy(2)18

x= 0.960
y= 0.040 PAAMePy(2)24

x= 0.976
y= 0.025 PAAMePy(2)41

x= 0.981
y= 0.019 PAAMePy(2)52

x= 0.988
y= 0.013 PAAMePy(2)77

x= 0.992
y= 0.008 PAAMePy(2)132

x= 0.993
y= 0.007 PAAMePy(2)133

PAA: 150 kg/mol

x= 0.980
y= 0.020 PAAMePy(150)55

x= 0.911
y= 0.089 PAAMePy(450)10

x= 0.917
y= 0.083 PAAMePy(450)11

x= 0.982
y= 0.012 PAAMePy(450)53

x= 0.996
y= 0.004 PAAMePy(150)230

x= 0.987
y= 0.013 PAAMePy(450)77

x= 0.989
y= 0.011 PAAMePy(450)87

x= 0.998
y= 0.002 PAAMePy(450)517

PAA: 450 kg/mol

Scheme 3.1. Relative compositions (PAA versus pyrene unimer units) of the polymers used and their corresponding acronyms.

Polymers

$$\begin{aligned}
 x_{UV} &= \frac{n_{AA}}{n_{Py \text{ grafted}}} = \frac{n'_{AA}}{n'_{Py \text{ grafted}}} = \frac{m'_{AA}}{m_{PAAMePy}} = \frac{M_{AA}}{C_{Py \text{ grafted}} \times V_{PAAMePy}} = \frac{1 - m'_{Py \text{ grafted}}}{m_{PAAMePy}} = \frac{1 - (n'_{Py \text{ grafted}} \times M_{Py \text{ grafted}})}{m_{PAAMePy}} \\
 &= \frac{1 - \left(\frac{n_{Py \text{ grafted}} \times M_{Py \text{ grafted}}}{m_{PAAMePy}} \right)}{\frac{M_{AA}}{A_{PAAMePy} \times V_{PAAMePy} \times \epsilon_{reference} \times m_{PAAMePy}}} = \frac{1 - \left(\frac{n_{Py \text{ grafted}} \times M_{Py \text{ grafted}}}{m_{PAAMePy}} \right)}{\frac{M_{AA}}{A_{PAAMePy} \times V_{PAAMePy} \times \epsilon_{reference} \times m_{PAAMePy}}} = \\
 &= \frac{1 - \left(\frac{C_{Py \text{ grafted}} \times V_{PAAMePy} \times M_{Py \text{ grafted}}}{m_{PAAMePy}} \right)}{\frac{M_{AA}}{A_{PAAMePy} \times V_{PAAMePy} \times \epsilon_{reference} \times m_{PAAMePy}}} = \frac{1 - \left(\frac{\frac{A_{PAAMePy} \times V_{PAAMePy} \times M_{Py \text{ grafted}}}{\epsilon_{reference}}}{m_{PAAMePy}} \right)}{\frac{M_{AA}}{A_{PAAMePy} \times V_{PAAMePy} \times \epsilon_{reference} \times m_{PAAMePy}}} = \\
 &= \frac{1 - \left(\frac{A_{PAAMePy} \times V_{PAAMePy} \times M_{Py \text{ grafted}}}{\epsilon_{reference} \times m_{PAAMePy}} \right)}{\frac{M_{AA}}{A_{PAAMePy} \times V_{PAAMePy} \times \epsilon_{reference} \times m_{PAAMePy}}} = \frac{\left[1 - \left(\frac{A_{PAAMePy} \times V_{PAAMePy} \times M_{Py \text{ grafted}}}{\epsilon_{reference} \times m_{PAAMePy}} \right) \right] \times \epsilon_{reference} \times m_{PAAMePy}}{M_{AA} \times A_{PAAMePy} \times V_{PAAMePy}} = \\
 &= \frac{\left[1 - \left(\frac{A_{PAAMePy} \times M_{Py \text{ grafted}}}{\epsilon_{reference} \times \rho_{PAAMePy}} \right) \right] \times \epsilon_{reference} \times \rho_{PAAMePy}}{M_{AA} \times A_{PAAMePy}}
 \end{aligned}$$

Equation 3.7

$$m'_X = \frac{m_X}{1g_{PAAMePy}}$$

Equation 3.8

$$n'_X = \frac{n_X}{1g_{PAAMePy}}$$

Equation 3.9

In Equation 3.8 and Equation 3.9, x can be either the acrylic acid (AA) monomer or the pyrene derivative (Py grafted).

In Figure 3.4, the proton NMR spectra for the smallest of the unlabelled polymers [PAA(2)], the pyrene derivative used to graft all polymers, and samples SNG89, 91 and 92 in MeOD,¹⁴¹ respectively are demonstrated.

Polymers

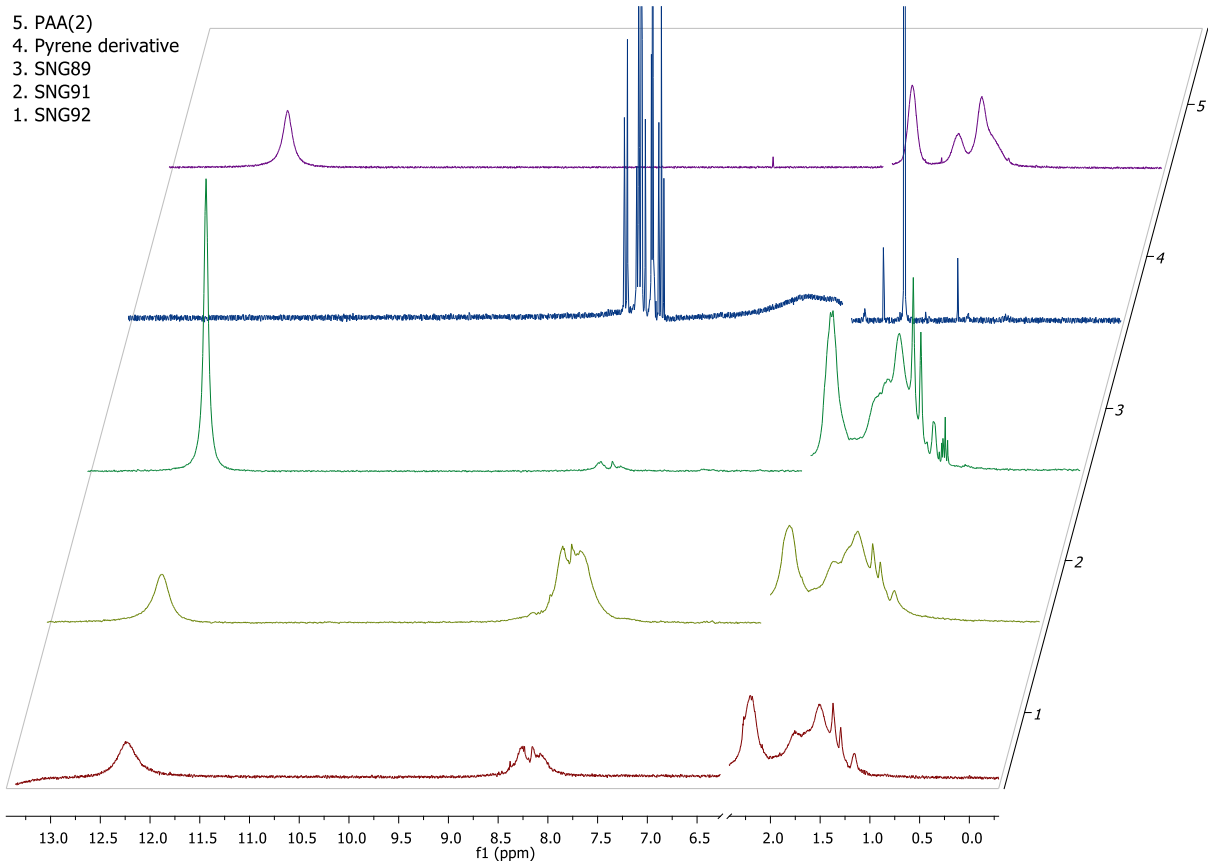


Figure 3.4. ^1H -NMR spectra of 1. SNG92 (red), 2. SNG91 (pale green), 3. SNG89 (dark green), 4. Pyrene derivative (blue) and 5. PAA(2) (violet) in deuterated DMSO.

In the case of PAAMePy the proton in red from the unlabelled monomer [i.e. $-\text{CH}_2\text{CH}(\text{COOH})-$, $M_w = 72 \text{ kg/mol}$] appears between 11.7 to 12.6 ppm, the ones from the main chain of both monomers [i.e. the blue protons of $-\text{CH}_2\text{CH}(\text{COOH})-$ and $\text{CH}_2\text{CH}(\text{C}=\text{ONHCH}_2\text{Py})-$] appears between 0.9 and 2.4 ppm and the ones from the pyrene unit in the labelled monomer [i.e., $-\text{CH}_2\text{CH}(\text{C}=\text{ONHCH}_2\text{Py})-$, $M_w = 285 \text{ kg/mol}$] appear between 7.6 and 8.7 ppm. For instance, for the PAAMePy(2)12 polymer the integration at the higher ppm value is 1, while at the $\sim 8 \text{ ppm}$ is 2.41. Since these should have, respectively, an integration of 1 and 9 if 50% of the polymer was labelled and since they have respectively 1 and 9 protons, the labelling content in % mol can be obtained, Equation 3.10. However, the more accurate way is to use the relation between the proton of the main chain of both monomers ($x+y$) and comparing it to the pyrene unit itself, Equation 3.10.

Polymers

$$\begin{aligned}
 & \text{Theoretical values} \\
 & (1:1, \text{ i.e. } 50\%) \\
 & I_{0.9-2.4} \rightarrow 3 \rightarrow x + y \Leftrightarrow \begin{cases} I_{7.6-8.7} = 9I_{11.7-12.6} \\ x + y = 100\% \end{cases} \Leftrightarrow \begin{cases} \frac{y}{x} = \frac{I_{7.6-8.7}}{I_{11.7-12.6}} = 9 \\ x = 100 - y \end{cases} \Leftrightarrow \\
 & I_{7.6-8.7} \rightarrow 9 \rightarrow y \\
 & I_{11.7-12.6} \rightarrow 1 \rightarrow x \\
 & \begin{cases} \frac{y}{100-y} = \frac{I_{7.6-8.7}}{9I_{11.7-12.6}} \\ \dots \\ \frac{y}{100-y+y} = \frac{I_{7.6-8.7}}{3I_{0.9-2.4}} \end{cases} \Leftrightarrow \begin{cases} \frac{9yI_{11.7-12.6}}{100-y} = I_{7.6-8.7} \\ \dots \\ y = \frac{100I_{7.6-8.7}}{3I_{0.9-2.4}} \end{cases} \Leftrightarrow \begin{cases} 9yI_{11.7-12.6} = I_{7.6-8.7}(100-y) \\ \dots \\ \dots \end{cases} \Leftrightarrow \\
 & \begin{cases} 9yI_{11.7-12.6} = 100I_{7.6-8.7} - I_{7.6-8.7}y \\ \dots \\ \dots \end{cases} \Leftrightarrow \begin{cases} (9I_{11.7-12.6} + I_{7.6-8.7})y = 100I_{7.6-8.7} \\ \dots \\ \dots \end{cases} \Leftrightarrow \\
 & \begin{cases} y = \frac{100I_{7.6-8.7}}{9I_{11.7-12.6} + I_{7.6-8.7}} \\ x = 100 - y \\ y = \frac{100I_{7.6-8.7}}{3I_{0.9-2.4}} \end{cases}
 \end{aligned}$$

Equation 3.10

Where x and y are the %mol of the monomers without $[-\text{CH}_2\text{CHC}(=\text{O})(\text{OH})_x-]$ and with pyrene groups $[-\text{CH}_2\text{CH}(=\text{O})(\text{NHCH}_2\text{Py})_y-]$ from Scheme 3.1, respectively.

The molecular weight (M_w) of a solute (A) (in kg/kmol) can be calculated from its diffusivity (D) using the Polson correlation, see Equation 3.11.¹⁴²

$$M_w(A) = \sqrt[3]{\frac{9.40 \times 10^{-15} \times T}{\eta \times D_{AB}}} \quad \text{Equation 3.11}$$

Where T is the absolute temperature (K), η is the viscosity of the solvent (in kg/m.s) and D_{AB} is the diffusivity of A towards B (solvent) (in m²/s).

The coefficient of diffusion (D) was obtained by diffusion NMR experiment (see details in Section 7.1.4.3) for the PAAMePy(2)12 polymer at 25°C in MeOD ($\eta = 5.45 \times 10^{-4}$ kg/m.s), the value obtained was 3.33×10^{-6} cm²/s (3.33×10^{-10} m²/s). Substituting all the other parameters, a M_w of 2545.65 g/mol was obtained.

Since the monomers with and without pyrene (Scheme 3.1) have a molecular weight of 72.06 and 285.34 g/mol, respectively, and since the grafting was made with a polymer of 2000 g/mol (which correspond of a polymer constituted by 28 monomers). Equation 3.12 can be used in order to estimate the number of pyrene units.

$$\begin{cases} x + y = 28 \\ 72.06x + 285.34y = 2545.31 \end{cases} \Leftrightarrow \begin{cases} x = 25.53 \\ y = 2.47 \end{cases} \quad \text{Equation 3.12}$$

The value of pyrene units calculated ($y = 2.47$) is quite similar to the mean value of pyrene units per polymer chain by spectrophotometry (2.31, see Table 3.2) thus demonstrating that using the Poisson distribution is suitable for this application. Besides, calculus of the labelling content (x/y) gives a value

of ~10 which is very close to the one obtained by spectrophotometry (12). However, the determination of the labelling content by spectrophotometry (compared by diffusion NMR) is not that time consuming and small amounts of polymers are needed. However, simple proton NMR of the polymers can estimate the pyrene labelling of the polymers and since this should be always done after synthesis, the UV determination will not be made for the PNIPAMPy polymers (Section 3.3).

In Table 3.1, the polymers names attributed, the integration of the NMR peaks for the different addressed protons, the %mol of pyrene units and the labelling degree (L.D.) is presented.

Table 3.1. Sample code of the polymers, name of the polymers (based on the L.D.), % mol of labelled monomers with pyrene (%mol Py) and L.D. by ¹H-NMR and UV-Vis spectrophotometry.

Sample code	Polymers	¹ H-NMR					UV-Vis		
		I _{py}	I _{COOH}	I _{0.9-2.4}	% mol Py ^{a,b}	% mol Py ^{a,c}	L.D. ^c	% mol Py ^d	L.D.
SNG91	PAAMePy(2)12	2.73	1.00	6.04	23.27	15.07	6.64	8.03	12.46
SNG89	PAAMePy(2)18	1.00	1.02	5.80	9.82	5.74	17.42	5.57	17.94
SNG77c	PAAMePy(2)24								24.29
SNG90	PAAMePy(2)41								39.82
	PAAMePy(2)132							0.76	131.55
SNG92	PAAMePy(2)133	0.12	1.00	3.99	1.32	1.00	100	0.75	132.73
	PAAMePy(150)55 ⁶³				ND	2.05	48.78	1.82	54.94
	PAAMePy(150)230 ⁶³					0.44	227.27	0.43	232.56
	PAAMePy(450)10							9.5	10.56
SNG96	PAAMePy(450)11 ⁶⁴	1.00	<i>e</i>	3.55	NP	9.4	10.64	9.1	11.10
SNG95	PAAMePy(450)77							1.28	77.84
SNG97	PAAMePy(450)517							0.19	517.60

^a calculated by using Equation 3.10. ^b using the COOH proton. ^c using the proton of the carbon directly connected to the COOH and the consecutive one. ^d obtained by the L.D. (1/L.D.×100). NP - not possible to determine. ND - not determined. ^e Not detected.

The acronyms of the polymers (2nd column of Table 3.1) were based on the molecular weight of the ungrafted PAA polymer and on the Py content of the polymers. The polymers investigated in this work are denoted as PAAMePy(X)Y where Y (10, 11, 12, 18, 24, 41, 52, 53, 77, 87, 132, 133 or 517) correspond to the number of PAA monomer units per Py chromophore, i.e. the L.D., (determined by UV spectroscopy) while X in parenthesis (2, 150 or 450) stands for the molecular weight of the ungrafted polymers in kg.mol⁻¹, see Scheme 3.1.

3.2.3. Statistical Characterization of the Pyrene Labelling: Poisson Distribution

The Poisson distribution was designed, as its name implies, by Siméon Denis Poisson, a French mathematician (1781–1840). This distribution is only applicable when the average number of occurrences of an event is the result of a large collection of situations in which the event can occur and whose probability of occurrence is very small, this is why it is not applicable for PAAMePy(450)10 and PAAMePy(450)11 that have a high value of average pyrene units and thus, a higher probability of occurrences (625 and 568, respectively). According to the Poisson distribution, if the average number of random events per interval is equal to m , the probability p of N occurrences in the range is given by Equation 3.13.

The Poisson distribution is very important to resolve problems that arise on relatively rare event count and mutually independent in an interval of time, length, area or volume.¹⁴³

The Poisson distribution allow to obtain the probability of the presence of chains with N pyrene substituents for an average number of pyrene substituents m ,⁶⁵ see Equation 3.13.

$$p_N(\%) = m^N \exp(-m) / N! \times 100 \quad \text{Equation 3.13}$$

In Equation 3.13 p_N is the fraction of chains containing N Py units and m the mean number of Py units per chain. The average number of Py per chain is given by a simple relation. For instance, if one consider PAAMePy(2)12 that have 12 AA monomer for 1 Py monomer, than 28 monomers [which correspond to the case of this polymer since it has $M_w = 2$ kg/mol, $M_w(\text{PAA})/M_w(\text{AA}) = 2000/72 = 28$] have m pyrene units per chain, with m being in this case 2.315. In the case of the PAAMePy(450)10 and PAAMePy(450)11 polymers, a normal distribution was used, see Equation 3.14.

$$p_N(\%) = \frac{1}{\sigma\sqrt{2\pi}} e^{-\frac{(i-m)^2}{2\sigma^2}} \times 100 = \frac{1}{\sqrt{m}\sqrt{2\pi}} e^{-\frac{(i-m)^2}{2\sqrt{m}^2}} \times 100 = \frac{1}{\sqrt{2\pi m}} e^{-\frac{(i-m)^2}{2m}} \times 100 \quad \text{Equation 3.14}$$

With σ being the standard deviation.

The fraction of single-labelled chains relative to all labelled chains (" α ") (i.e., intrinsically isolated pyrene units) is given by Equation 3.15.

$$" \alpha " = \frac{N_1}{\sum_{i>1}^n N_i} \quad \text{Equation 3.15}$$

In Equation 3.15, N_1 is fraction of chains containing 1 Py unit.

Using the experimentally calculated degree of labelling (number of pyrene unit per acrylic acid unit) and considering a Poisson distribution, the probability of having i pyrene units per chain was obtained for both the short and long PAA chains. The data is summarized in Table 3.2 and can be seen in Figure 3.5.

Polymers

Table 3.2. Mean value of pyrene units per polymer chain m , theoretical fractions of unlabelled N_0 , single labelled N_1 , double labelled N_2 , and multi-labelled ($N>2$) chains, and fraction of single labelled chains relative to all labelled chains (" α ", intrinsically isolated pyrene units) using a Poisson Distribution.

	PAAMePy(2)Y								PAAMePy(150)Y		PAAMePy(450)Y					
Y	12	18	24	41	52	77	132	133	55	230	10^a	11^a	53	77	87	517
m	2.315	1.543	1.167	0.678	0.534	0.361	0.210	0.209	37.88	9.058	625.0	568.2	117.9	81.2	71.8	12.1
N= 0	0.099	0.214	0.311	0.508	0.586	0.697	0.810	0.812	0	0	0	0	0	0	0	0
N= 1	0.229	0.330	0.363	0.344	0.313	0.251	0.171	0.169	0	0.001	0	0	0	0	0	0
N= 2	0.265	0.254	0.212	0.117	0.084	0.045	0.018	0.018	0	0.005	0	0	0	0	0	0
N> 2	0.408	0.202	0.113	0.031	0.017	0.006	0.001	0.001	1	0.994	1	1	1	1	1	1
"α"	0.254	0.419	0.528	0.699	0.757	0.830	0.898	0.899	0	0.001	0	0	0	0	0	0

^a A normal distribution was used in this case, see Equation 3.14.

For the PAAMePy(2) polymers the highest probability of labelling is with 0, 1 or 2 pyrene units. For high molecular weight polymers, the PAAMePy(450)53 polymer have the highest probability associated to 12 pyrene units.

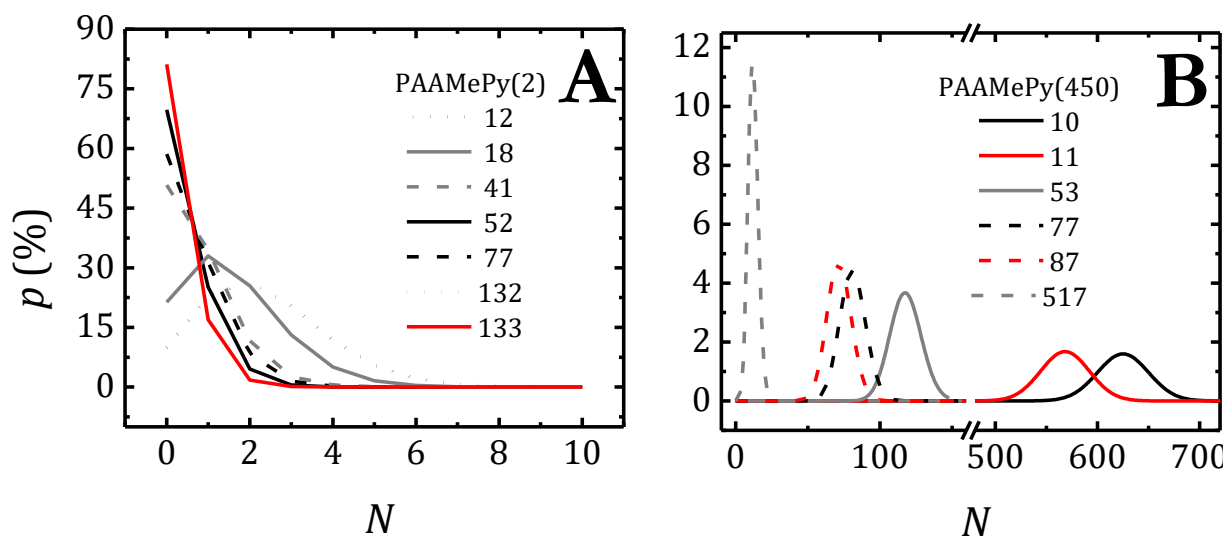


Figure 3.5. Probability of finding a PAA chain with a given number of N pyrene groups per chain, for the (A) short, 28 AA units [the analogous of PAAMePy(2)] and (B) long, 6250 AA units [the analogous of PAAMePy(450)] chain polymers, assuming a Poisson distribution. For PAAMePy(450)10 and PAAMePy(450)11, a normal distribution was used.

Figure 3.19 in the supplementary information shows the probability of finding N pyrene units per chain for the PAAMePy(150) polymers.

3.2.1. Dynamics of Short and Long PAAMePy Polymers in Pure Organic Solvents and in Dioxane:Water Mixtures

3.2.1.1. Absorption and Steady State (SS) Fluorescence Data

Figure 3.6 and Figure 3.7 show the absorption spectra of all the polymers in dioxane and in a mixture of dioxane:water with the dioxane volume fraction $\left[\phi_{dx} = V_{dx} / (V_{dx} + V_{H_2O}) \right]$ of 0.1 (the pH of the water used to prepare all the dx:H₂O mixtures was ~ 5). The absorption spectra for PAAMePy(2)52 and PAAMePy(450)87 as a function of the dioxane content can be found in ref. ¹⁴⁴ and the ones for PAAMePy(450)11 and PAAMePy(450)517 in ref. ⁶⁴.

Due to the high hydrophobicity of pyrene, there is a natural tendency for aggregation of this probe in water, leading to a high degree of *GSD* formation. Dioxane is, instead, a much better solvent for the pyrene probe thus facilitating the disruption of aggregates and the promotion of excimer formation through a dynamic route and consequently a decrease on the *GSD* formation.

Polymers

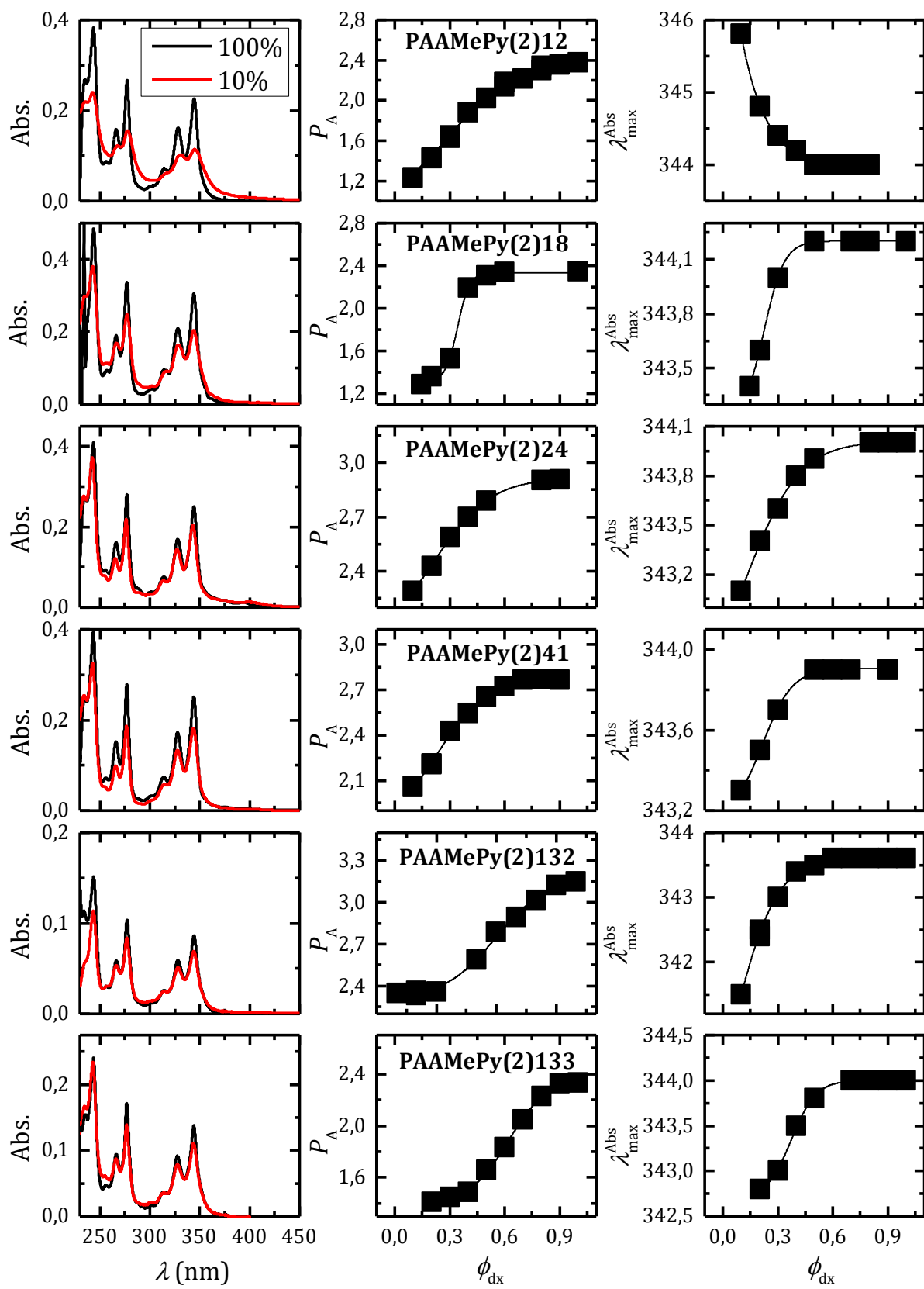


Figure 3.6. From left to right. Absorption spectra for PAAMePy(2) polymers in dioxane:water mixtures as a function of the volume fraction (ϕ_{dx}). Dependence of the P_A ratio and wavelength maxima (λ_{max}^{abs}) with ϕ_{dx} .

The P_A ratio parameter increases with the volume fraction of dioxane for all polymers, which can be explained by the decrease in the GSD since dioxane is a good solvent for this polymer and there is for all, except PAAMePy(2)12, a shift to shorter wavelengths. The unusual behaviour of PAAMePy(2)12 can be explained by the absorption of a new band at longer wavelengths that is merged with the other bands.

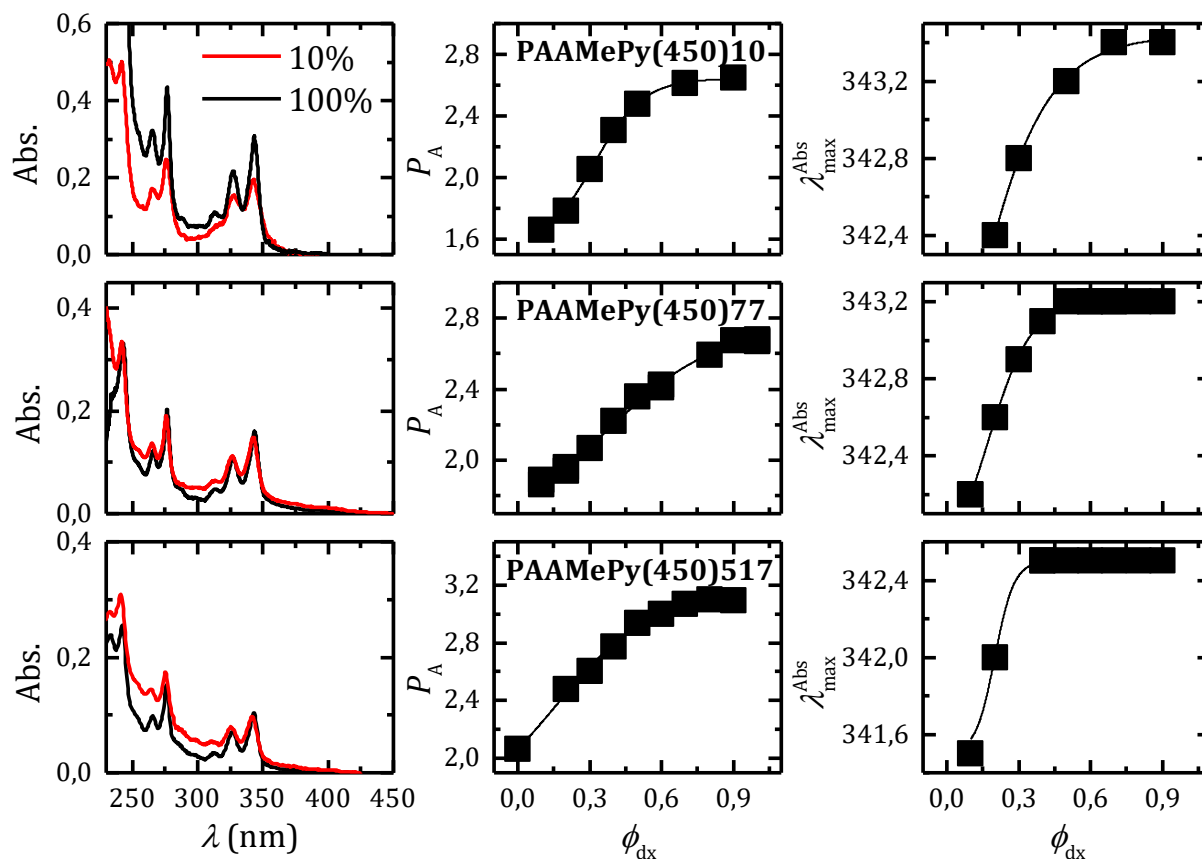


Figure 3.7. From left to right. Absorption spectra for PAAMePy(450) polymers in dioxane:water mixtures as a function of the volume fraction (ϕ_{dx}). Dependence of the P_A ratio and wavelength maxima ($\lambda_{max}^{abs.}$) with ϕ_{dx} .

Figure 3.8 and Figure 3.9 show the fluorescence emission spectra of all polymers in dioxane and in a dioxane:water mixture with $\phi_{dx}= 0.1$ together with the trend of I_E/I_M and I_1/I_3 ratios as a function of the dioxane volume fraction, for PAAMePy(2) and PAAMePy(450) polymers, respectively. The fluorescence emission spectra for PAAMePy(2)52, PAAMePy(2)77, PAAMePy(450)53 and PAAMePy(450)87 can be found in ref. ¹⁴⁴ and for PAAMePy(450)11 and PAAMePy(450)517 in ref. ⁶⁴. In this work, the intensities ratios were taken according to the Method B, i.e., using the normalized fluorescence emission spectra of a parent compound and calculating both areas, excimer (total area-area of the parent monomer) and monomer (parent monomer).

Polymers

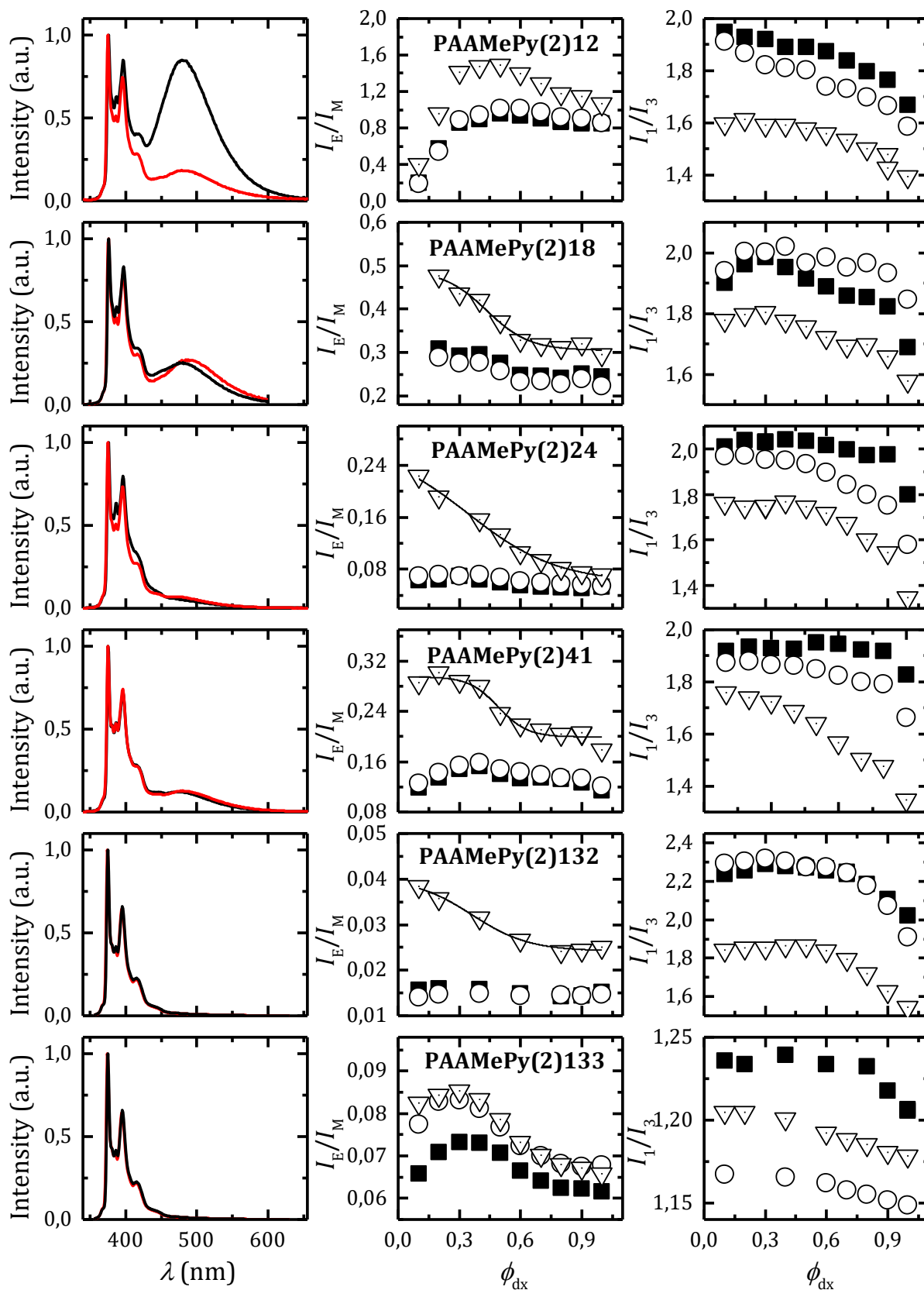


Figure 3.8. From left to right. Fluorescence emission spectra ($\lambda_{exc.} = 350$ nm) for the PAAMePy(2) polymers in dioxane:water mixtures as a function of the volume fraction (ϕ_{dx}) and dependence of the I_E/I_M and I_1/I_3 ratio with ϕ_{dx} . Black and red lines correspond to the 100% and 10% D_x:H₂O, respectively. In the right panels, ■, ○ and ▽ correspond to the data for $\lambda_{exc.} = 315, 335$ and 350 nm.

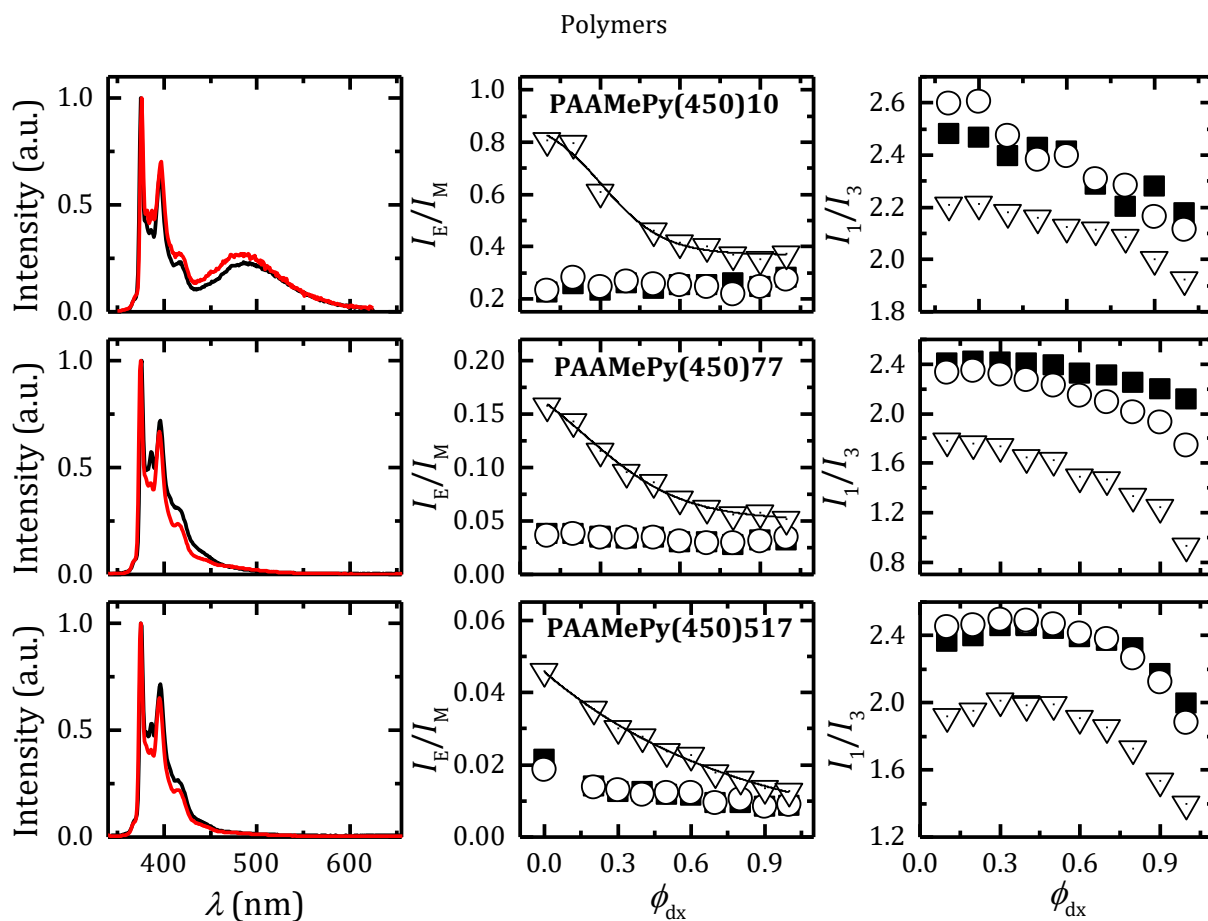


Figure 3.9. From left to right. Emission spectra ($\lambda_{exc} = 350$ nm) for the PAAMePy(450) polymers in dioxane:water mixtures as a function of the volume fraction (ϕ_{dx}) and dependence of the I_E/I_M and I_1/I_3 ratio with ϕ_{dx} . Black and red lines correspond to the 100% and 10% Dx:H₂O, respectively. In the right panels, ■, ○ and ▽ correspond to the data for $\lambda_{exc} = 315, 335$ and 350 nm.

Table 3.3 show the variation of all the parameters taken from Figure 3.6 to Figure 3.9 and from Figure 3.12 and Figure 3.13 for all the polymers from the pure dioxane solution to the dioxane:water mixture with $\phi_{dx} = 0.1$.

The I_E/I_M ratio is higher with $\lambda_{exc} = 350$ nm when compared to the other two excitation wavelength (315 and 335 nm), see left panels of Figure 3.8 and Figure 3.9. This means that, although less dominantly than in water, *GSD* are present in dioxane.

Table 3.3. Variation in the P_A ratio, $\lambda_{max}^{abs.}$, $P_M - P_E$ difference, I_E/I_M and I_1/I_3 ratios for the dioxane:water mixtures investigated (ΔP_A , $\Delta \lambda_{max}^{abs.}$, $\Delta P_M - P_E$, $\Delta I_E/I_M$ and $\Delta I_1/I_3$, respectively).

Polymer	ΔP_A	$\Delta \lambda_{max}^{abs.}$ (nm)	$\Delta P_M - P_E$	$\Delta I_E/I_M^a$	$\Delta I_1/I_3^a$
PAAMePy(2)12	1.14	1.8	0.62	0.67	0.22
PAAMePy(2)18	1.06	0.8	0.34	0.18	0.23

Polymers					
Polymer	ΔP_A	$\Delta\lambda_{\max}^{abs.}$ (nm)	$\Delta P_M - P_E$	$\Delta I_E/I_M^a$	$\Delta I_1/I_3^a$
PAAMePy(2)24	0.61	0.9	0.22	0.15	0.42
PAAMePy(2)41	0.71	0.6	0.39	0.12	0.41
PAAMePy(2)52			~0.70	0.16	
PAAMePy(2)77		ND	ND	0.07	ND
PAAMePy(2)132	0.82	2.1	0.23	0.01	0.32
PAAMePy(2)133	0.92	1.2	0.26	0.02	0.03
PAAMePy(450)10	0.99	1.0	0.68	0.45	0.29
PAAMePy(450)11 ⁶⁴	~0.45	ND	0.40	~0.05	
PAAMePy(450)53		ND	~0.80	1.36	ND
PAAMePy(450)77	0.82	1.0	0.18	0.11	0.85
PAAMePy(450)87 ⁶⁵		ND		0.48	ND
PAAMePy(450)517	1.04	1.0	0.31	0.03	0.61

^a With $\lambda_{exc} = 350$ nm. ND – not determined.

From these plots, it is worth noting that both the short chain [PAAMePy(2)] and long chain polymers [PAAMePy(450)] the I_E/I_M ratio increases with the increase on the label content. These results clearly show the expected behaviour for these polymers since PAAMePy(2)12 is, from the short PAA chain polymers, the one with higher content of pyrene units so for that, the higher excimer fluorescence intensity relatively to the monomer. For larger polymers it is also observed that the I_E/I_M ratio is greater for PAAMePy(450)10 than for other (less labelled) polymers. Also noticeable is the fact that the I_E/I_M ratios being, for the smallest polymers, approximately four-fold higher than the higher molecular weight polymers. On the other hand, it appears that the I_E/I_M ratio is dependent on the excitation wavelength which gives strong support to the fact that there is an association (although low) in the ground state. However, this difference is almost negligible in the less marked polymers, giving an indication that there is a lower incidence of these preformed dimers. This finding is in line with the probability of having two pyrene units in close proximity in the ground state being higher with polymers whose degree of labelling is also higher.

In Figure 3.10, the values for PAAMePy(2)52, PAAMePy(2)77 and PAAMePy(450)87 report to values previously published.¹⁴⁴ What is observed is that for the PAAMePy(450)87, the I_E/I_M ratio is much higher than for PAAMePy(450)77. It would be expected that these two polymers having approximately the same degree of labelling the behaviour would be the same. One reason for this different behaviour may have to do with the fact that pyrene units may be more localized (closer to one another) in

PAAMePy(450)87 and more dispersed (more distant) in PAAMePy(450)77. However, steady state (SS) fluorescence data in water do not appear to indicate this, since it is observed a decrease I_E/I_M with pH (i.e., with the expansion of the chain) for PAAMePy(450)87 and an increase of this ratio for PAAMePy(450)77 (see Section 3.2.2.1.2), indicating that pyrene units must be close to each other. What may be happening is that the conformation of PAAMePy(450)87 favour the formation of dynamic and static excimer. But it is probably due to taking the ratio by another method (see differences in values in Section 2.2.1.1 for example).

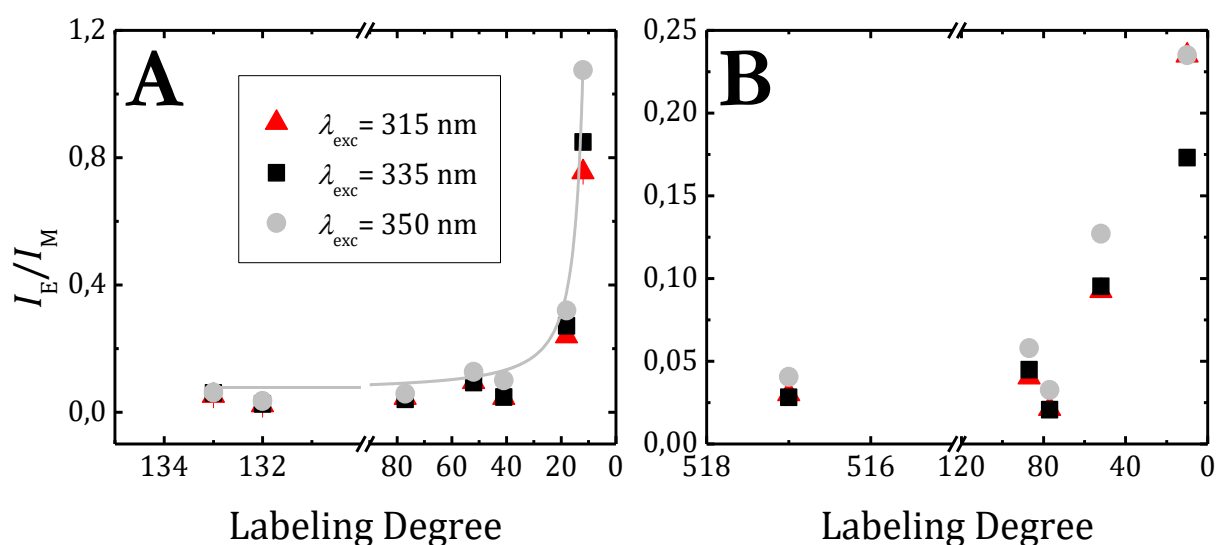


Figure 3.10. Excimer-to-monomer intensity ratios (I_E/I_M) as a function of the labelling degree (L.D.) for (A) PAAMePy(2) and (B) PAAMePy(450) in dioxane. Taken by the intensities at the maximum of each band. The curve of panel A is a guideline for the eye [$I_E/I_M = 0.062 \times \exp(29.481/(L.D.-1.761))$].

In addition to these observations, it has been found that sometimes, the resolution in the monomer band was lost and that almost always was accompanied by an excimer band “merged” to the monomer, i.e., a monomer band slightly wide and with a maximum excimer fluorescence intensity slightly lower wavelength than the ordinary (see Figure 3.11A). Moreover, the loss of band resolution monomer seemed to be indirectly proportional to the excimer fluorescence intensity. The monomer band of PAAMePy typically has 4 vibronic bands (see Figure 3.11B), but the appearance of only two or three (wider) was repeatedly found. This can also be an indication of the presence of dimer even in good solvents such as dioxane. However, this behaviour was noticed more frequently in aqueous solutions (see Section 3.2.2).

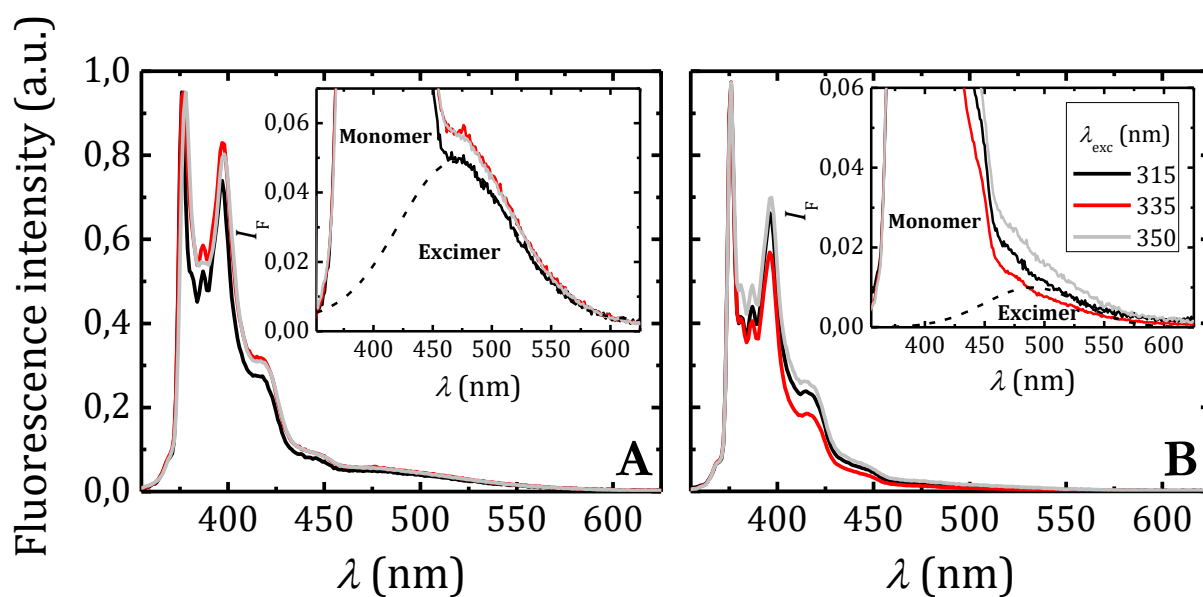


Figure 3.11. Fluorescence emission spectra ($\lambda_{\text{exc.}} = 315, 335$ and 350 nm) in dioxane for (A) PAAMePy(2)133 and (B) PAAMePy(450)517. Insets: zooms in the region of the excimer band of the respective spectra.

Figure 3.12 and Figure 3.13 show the normalized excitation spectra (~ 335 nm) for all the polymers in dioxane and dioxane:water (1:10) and the $P_M - P_E$ difference as a function of the dioxane fraction volume for the PAAMePy(2) and PAAMePy(450), respectively. The fluorescence excitation spectra (and $P_M - P_E$ as a function of the dioxane content in dx:H₂O mixtures) of PAAMePy(450)11 can be seen in ref. ⁶⁴ while for PAAMePy(2)52 and PAAMePy(450)53 polymers in ref. ¹⁴⁴.

Polymers

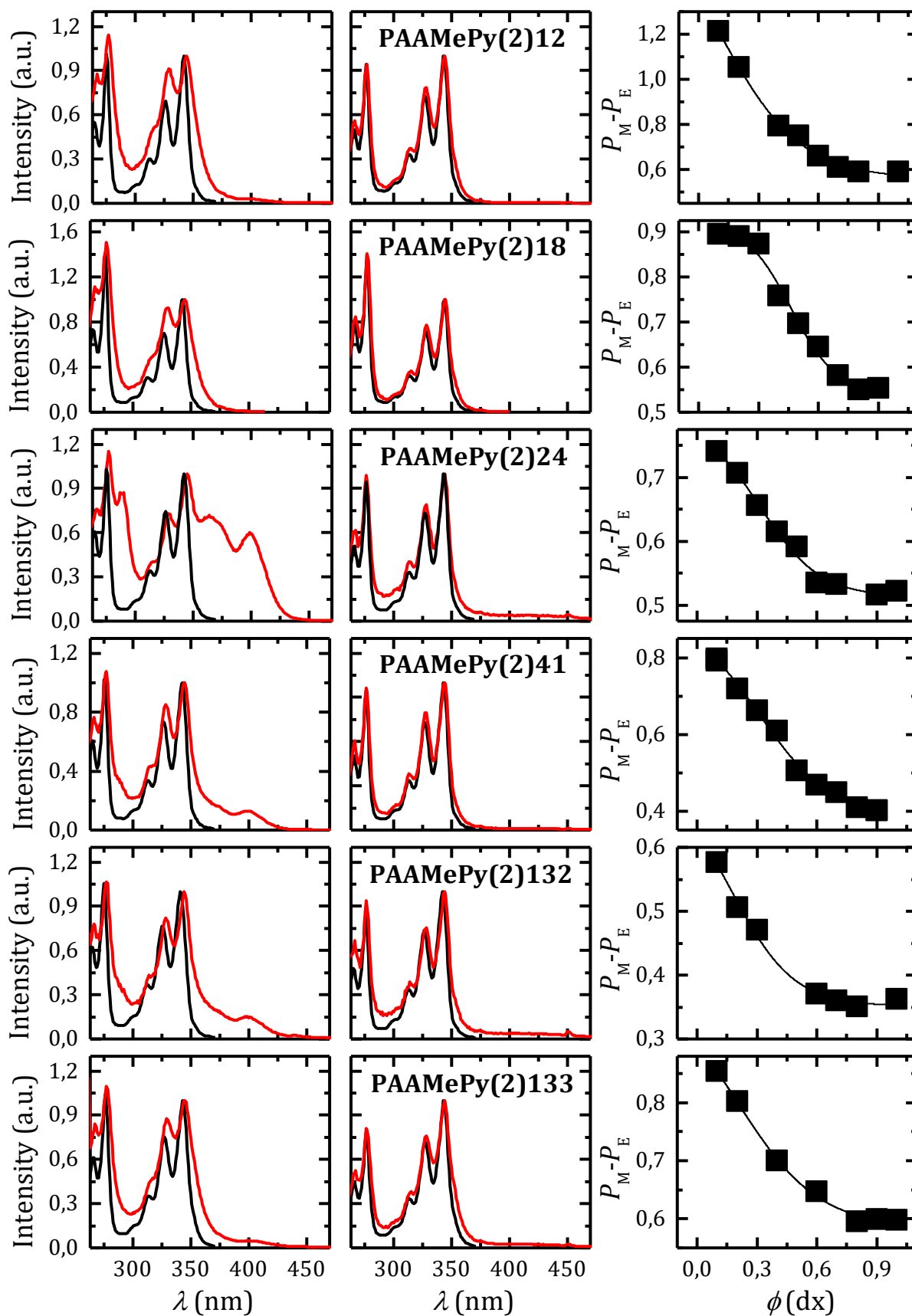


Figure 3.12. Normalized (at ~ 335 nm) excitation spectra collected at the monomer (black line, 375 nm) and excimer (red line, 520 nm) regions in a dioxane:water (1:10) (v:v) mixture and in dioxane (left and middle panels, respectively) for the PAAMePy(2) polymers in dioxane:water mixtures. The $P_M - P_E$ dependence on the volume fraction of dioxane in water is also presented in the right panels.

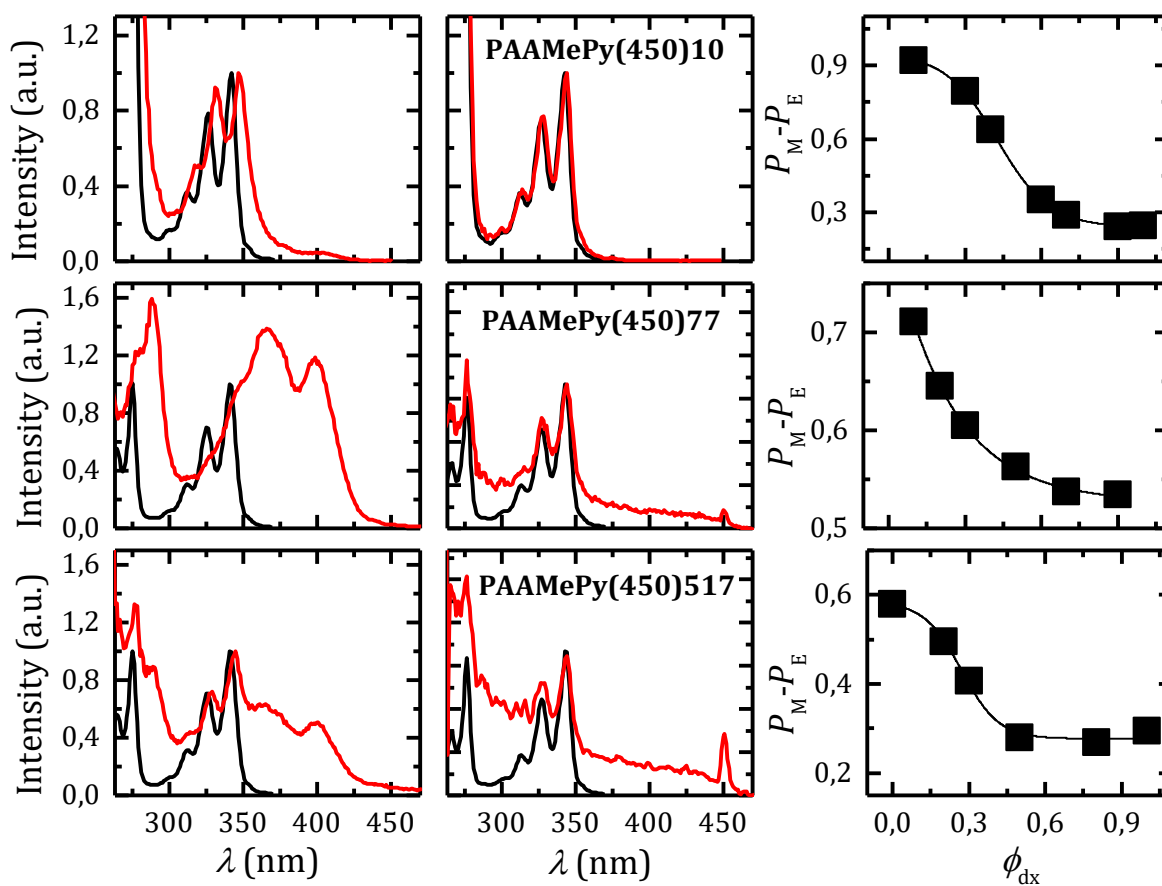


Figure 3.13. Normalized (at ~ 335 nm) excitation spectra collected at the monomer (black line, 375 nm) and excimer (red line, 520 nm) regions in a dioxane:water (1:10) (v:v) mixture and in dioxane (left and middle panels, respectively) for the PAAMePy(450) polymers in dioxane:water mixtures. The P_M-P_E dependence on the volume fraction of dioxane in water is also presented in the right panels.

Figure 3.14 show the excitation spectra ($\lambda_{em}= 520$ nm) for PAAMePy(450)77 and PAAMePy(450)517 polymers for all the fractions of dioxane:water investigated.

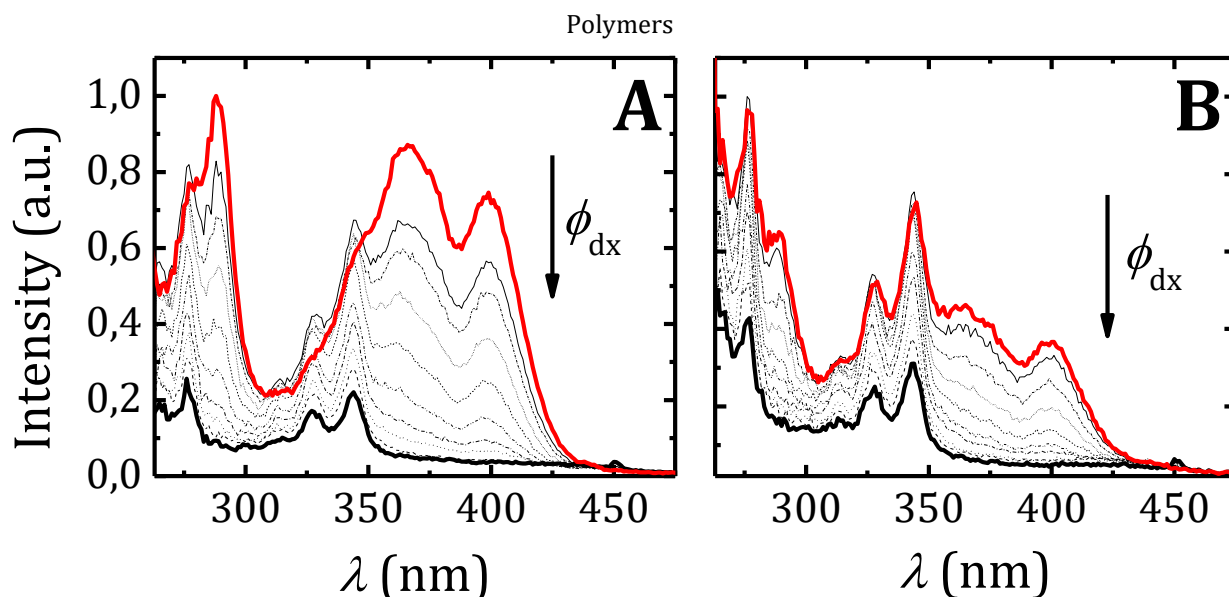
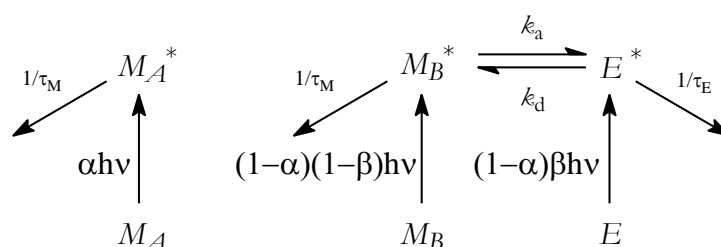


Figure 3.14. Excitation spectra collected at the excimer region ($\lambda_{em}= 520$ nm) for (A) PAAMePy(450)77 and (B) PAAMePy(450)517 polymers in dioxane:water mixtures.

3.2.1.1. Time-Resolved Behavior

All the decays of the PAAMePy(2)52 dioxane:water solutions show to be properly fitted with three exponentials, data not shown.

With both SS and time-resolved (TR) data in mind, the kinetic scheme proposed previously for good solvents was used,⁶⁵ see Scheme 3.2.



Scheme 3.2. Kinetic scheme proposed for PAAMePy(2)52 polymers in dioxane:water mixtures.

In Figure 3.15 the fluorescence lifetimes and the pre-exponential factors taken from the fluorescence TR measurements obtained for the PAAMePy(2)52 polymer as a function of the volume fraction of dioxane are presented.

Using the equations deduced from Scheme 3.2 (see Appendix B), the rate constants were obtained as a function of the dioxane volume fraction in dx:H₂O mixtures (Figure 3.15).

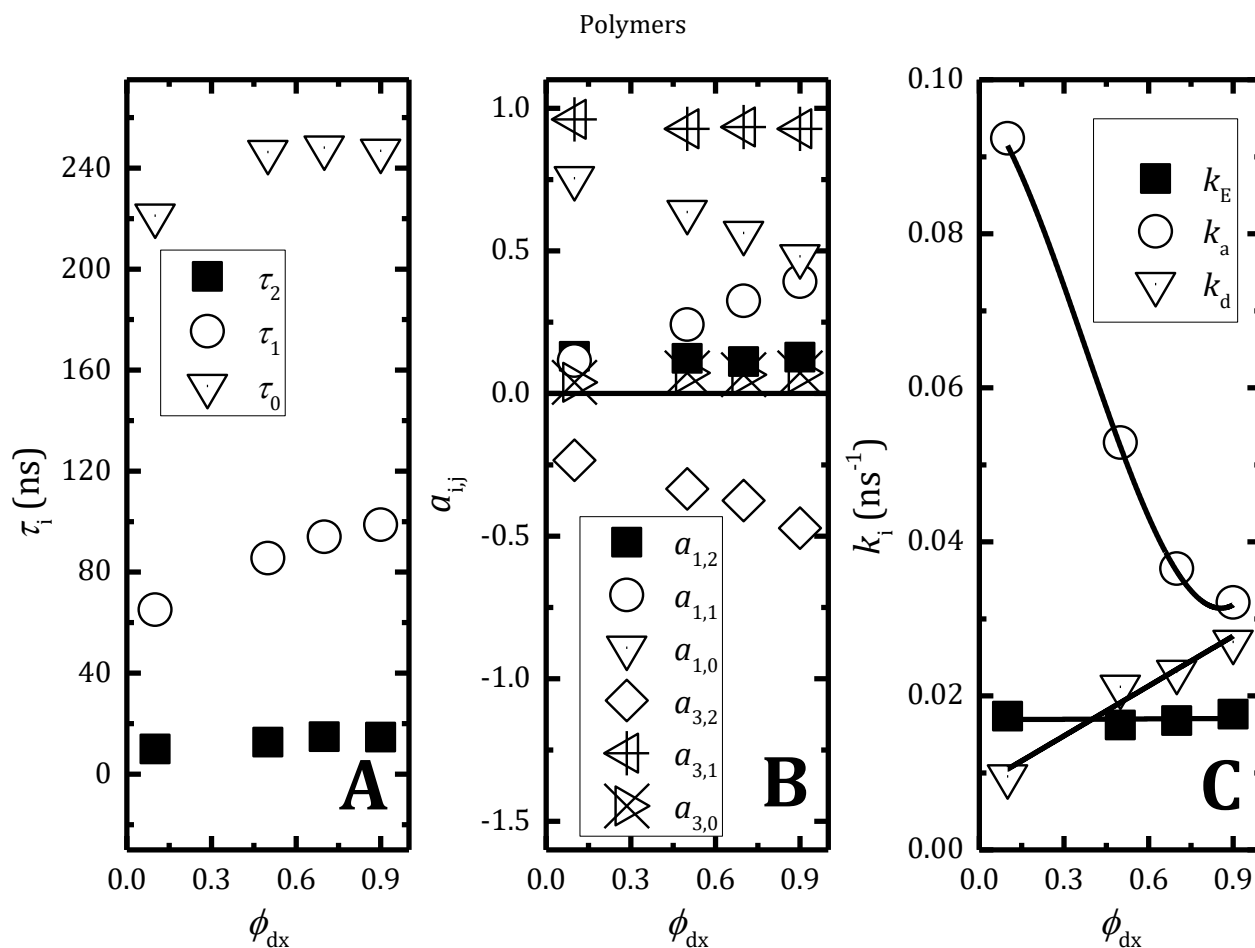


Figure 3.15. Dependence of (A) decay times, (B) pre-exponential factors collected at the monomer ($A_{1,j}$) and excimer ($A_{2,j}$) emissions wavelengths and (C) plots of the rate constants of the PAAMePy(2)52 polymer in dx:H₂O mixtures as a function of the fraction of dioxane at 298 K. Cubic polynomial fitting of k_a and linear fittings of k_d and k_E .

The trends of Figure 3.15 suggest that, as the quality of the solvent mixture increases (with the higher content of dioxane), the mean end-to-end distance, (between the pyrene groups) increases, leading to a decrease in k_a , that surpasses the expected increase due to the lowering of the solvent viscosity. The increase of k_d gives this same indication of the increased stability of extended vs. cyclic chain conformations in the better (dioxane) solvent.⁸⁹

The k_E values remain constant (~ 0.0233 ns⁻¹) corresponding to a τ_E value of ~ 43 ns, a value that is usually found in these systems.^{44,63,65,69}

In order to verify the foregoing interpretation we have analysed the solvent viscosity effect on the k_a of 1Py(10)1Py in well-behaved solvents (alkanes), see Section 2.2.1.2.

In Table 3.4 the rate constants for excimer formation, dissociation and decay, the fractions of each species and the excimer and monomer decay times are gathered for all the PAAMePy polymers in pure dioxane and methanol.

Polymers

Table 3.4. Rate constants of excimer formation, k_a , dissociation, k_d , and decay, k_E , fractions of isolated monomers, α , *MAGRE* monomers, $(1-\alpha)(1-\beta)$, and *GSD*, $\beta(1-\alpha)$, monomer and excimer decay times (τ_M and τ_E) in different solvents at 20°C.

Polymer Solvent	k_a (ns ⁻¹)	k_d (ns ⁻¹)	k_E (ns ⁻¹)	τ_E (ns)	τ_M (ns)	β	α	$(1-\alpha)(1-\beta)$	$\beta(1-\alpha)$
PAAMePy(2)12									
Dioxane	0.051	0.015	0.018	55	201	0.49	0.18	0.42	0.40
Methanol	0.121	0.017	0.016	62	218	0.73	0.40	0.16	0.44
PAAMePy(2)18									
Dioxane	0.037	0.024	0.017	60	190	0.36	0.35	0.42	0.24
Methanol	0.070	0.016	0.016	61	239	0.62	0.64	0.14	0.23
PAAMePy(2)24									
Dioxane	0.037	0.011	0.013	76	191	0.52	0.87	0.06	0.07
Methanol	0.042	0.012	0.014	72	242	0.52	0.91	0.04	0.05
PAAMePy(2)41									
Dioxane	0.030	0.028	0.018	55	224	0.24	0.69	0.23	0.07
Methanol	0.075	0.014	0.015	66	287	0.68	0.83	0.06	0.11
PAAMePy(2)52¹⁴⁴									
Dioxane	0.022	0.029	0.015	66	223	0.13	0.55	0.06	0.39
Methanol	0.031	0.010	0.014	70	270	0.30	0.62	0.11	0.27
PAAMePy(2)77¹⁴⁴									
Dioxane	0.017	0.029	0.018	57	240	0.11	0.61	0.04	0.35
Methanol	0.027	0.017	0.015	66	291	0.23	0.66	0.08	0.26
PAAMePy(2)132									
Dioxane									
Methanol	0.009	0.014	0.017	58	276	0.29	0.81	0.13	0.06
PAAMePy(2)133									
Dioxane	0.023	0.007	0.013	76	226	0.84	0.43	0.09	0.48
Methanol	0.025	0.022	0.016	61	274	0.49	0.59	0.21	0.20
PAAMePy(150)55¹⁴⁴									
Dioxane	0.015	0.014	0.012	83	246	0.44	0.07	0.52	0.41
Methanol	0.025	0.016	0.012	81	254	0.51	0.05	0.47	0.48
PAAMePy(150)230⁶³									
Dioxane	0.009	0.013	0.015	67		0.34	0.19	0.28	
Methanol	0.013	0.013	0.016	63		0.58	0.04	0.56	
PAAMePy(450)10									
Dioxane	0.026	0.024	0.016	64	174	0.55	0.63	0.17	0.20
Methanol	0.038	0.015	0.019	54	255	0.83	0.54	0.08	0.38

Polymers									
Polymer	k_a	k_d	k_E	τ_E	τ_M	β	α	$(1-\alpha)(1-\beta)$	$\beta(1-\alpha)$
Solvent	(ns ⁻¹)	(ns ⁻¹)	(ns ⁻¹)	(ns)	(ns)				
PAAMePy(450)53¹⁴⁴									
Dioxane	0.014	0.018	0.017	57	234	0.11	0.01	0.11	0.88
Methanol	0.025	0.016	0.018	56	228	0.16	0.14	0.14	0.72
PAAMePy(450)77									
Dioxane	0.003	0.008	0.022	45	197	0.13	0.54	0.40	0.06
Methanol	0.062	0.019	0.019	53	177	0.69	0.59	0.13	0.28

As can be seen from Table 3.4 the k_a values increase with the degree of labelling. This result is clear for the short chain sizes polymers, except with the PAAMePy(2)24 and PAAMePy(2)133 polymers. With the higher molecular weight polymers the same behaviour was observed except for PAAMePy(450)77. Moreover, the PAAMePy(450)77 has the lowest k_a value in dioxane and the highest k_a value in methanol, within the high molecular weight polymers, PAAMePy(450). Also with respect to rate constant values, it is noted that they show always higher values in methanol than in dioxane. This is due to the viscosity of the methanol is lower than that of dioxane causing the barrier associated with the intrinsic viscosity of the solvent that has to be overcome in the first solvent is less facilitating thereby the excimer formation. The values for k_d in dioxane in the short chain polymers do not seem to depend on the degree of labelling, ranging from $2.1-2.9 \times 10^7 \text{ s}^{-1}$ with the exception of the value presented by PAAMePy(2)133 polymer. However, in methanol there is a higher variation of k_d which increases with degree of labelling. Regarding the τ_E values, they too can be considered constant for the long chain polymers ranging between 45 and 64 ns. In addition, the *GSD* contribution increases with the degree of labelling due to the fact that pyrene units form more form *GSD* than dynamic excimers. PAAMePy(2)133 seems to be the only polymer that do not follow this behaviour.

3.2.1.2. Temperature Dependence Behavior

Figure 3.16 (panels A and B) shows the fluorescence spectra of 1-pyrenylmethylacetamide and of the PAAMePy(2)52 polymer in methanol as a function of temperature from -10 C and 60 C, respectively.

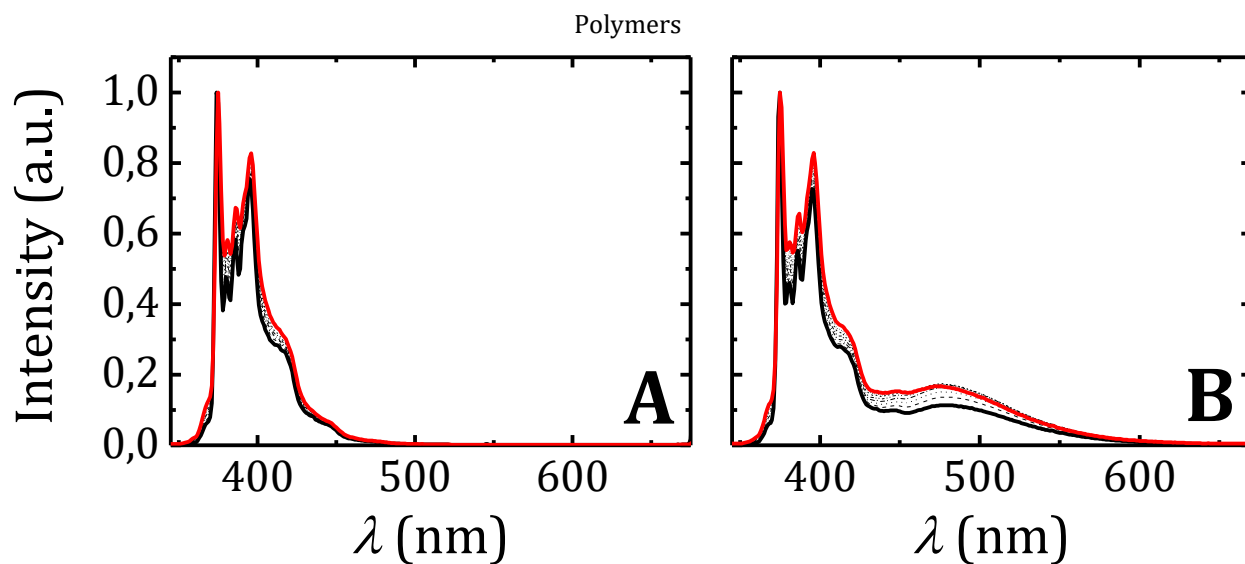


Figure 3.16. Fluorescence emission spectra ($\lambda_{exc}=339$ nm) of (A) parent compound (1-pyrenylmethylacetamide) and (B) PAAMePy(2)52 in methanol normalized at the λ_M . In the fluorescence spectra the bold red and black lines stand for $T=60$ °C and $T=-10$ °C, respectively.

From Figure 3.16B it can be seen that the excimer emission maximum shifts to lower wavelengths with the increase of temperature whereas the monomer emission shifts to longer wavelengths. The latter was also observed to the monomer emission of the parent compound (panel A).

Figure 3.17 depicts the Stevens-Ban plot of the PAAMePy (2)52 in methanol using different methods to obtain the I_E/I_M ratio. In this case, neither one of the two regimes seems to be properly defined.

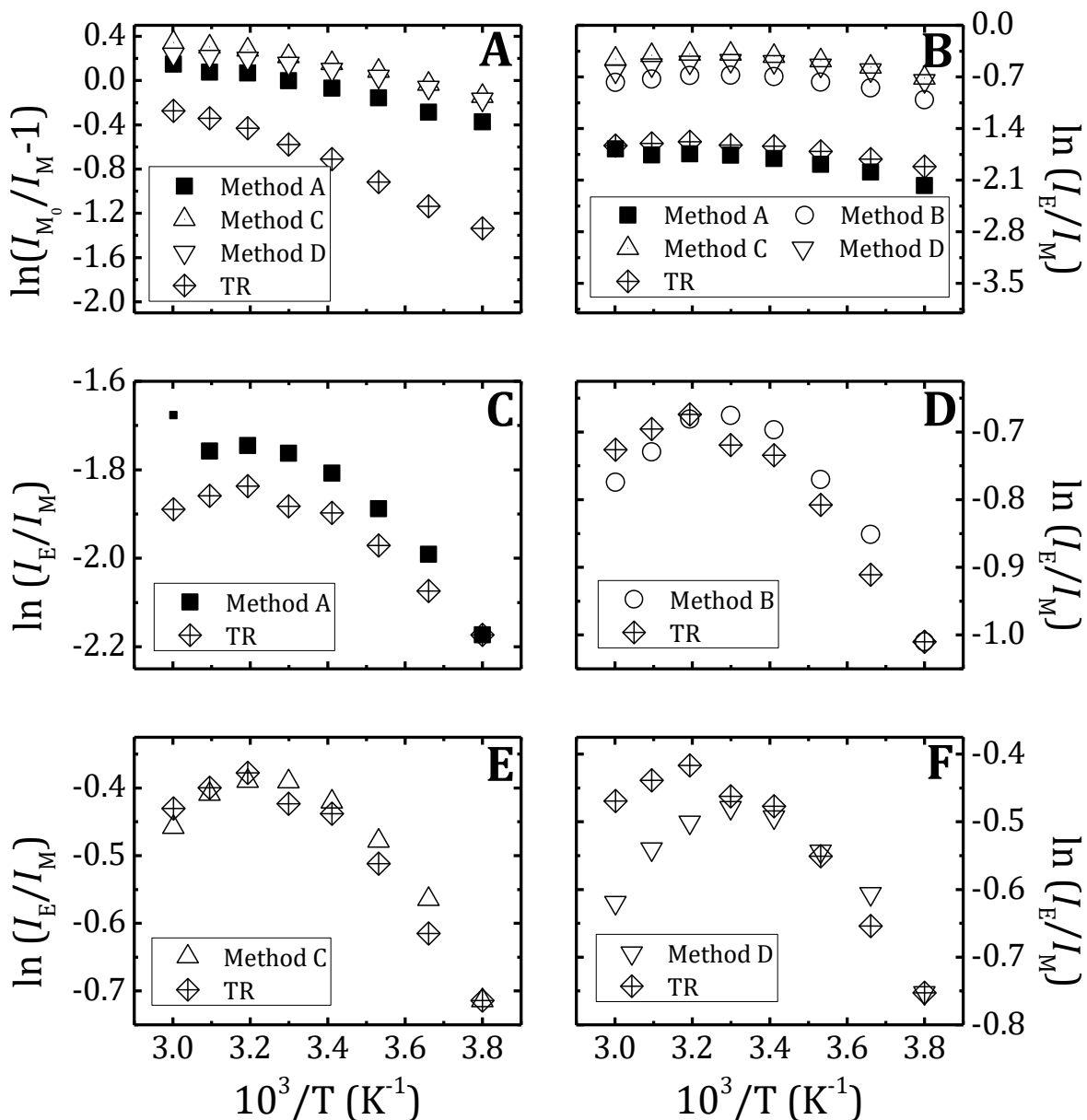


Figure 3.17. PAAMePy(2)52 in methanol. (A) $\ln(I_{M_0}/I_{M-1})$, (B to F) $\ln(I_E/I_M)$ obtained by different methods with (B) $k_F^E/k_F^M = 1$, (C to F) k_F^E/k_F^M adjusted to match the value from SS at -10°C , $\lambda_{exc} = 339 \text{ nm}$. Methods A to D, are, respectively, intensities ratios, deconvoluted bands, GaussMod and BiGauss.

By comparison of all panels in Figure 3.17, the best approach to obtain the correct I_E/I_M ratio seems to be Method C for the PAAMePy(2)52 polymers as a function of the temperature.

In Figure 3.18, the fluorescence decay times, pre-exponential factors, the ratio for pre-exponential factors at the monomer emission, A , ($=A_{1,2}/A_{1,1}$) and the rate constants as a function of the temperature are depicted.

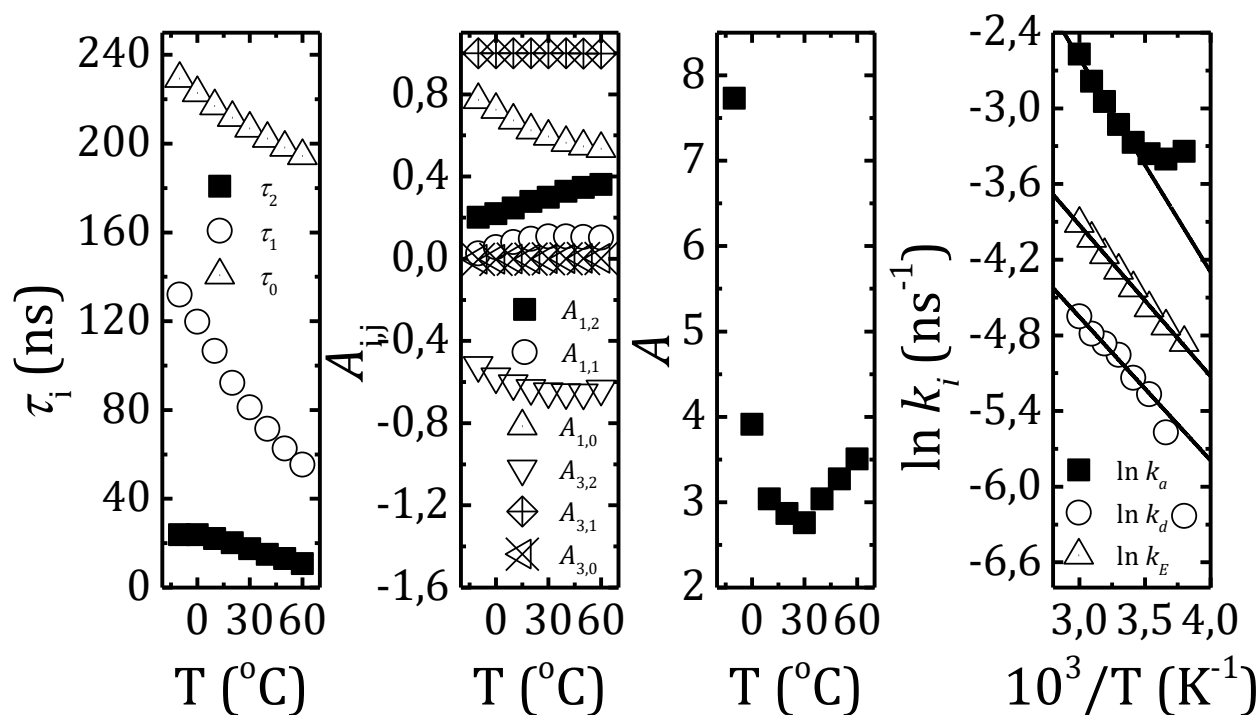


Figure 3.18. From left to right. Dependence of decay times, pre-exponential factors collected at the monomer ($A_{1,i}$) and excimer ($A_{3,j}$) emissions wavelengths, pre-exponential ratio A as a function of the temperature and plots of natural logarithm of k_a , k_d and k_E as a function of the absolute reciprocal temperature of the PAAMePy(2)52 polymer in methanol.

From Figure 3.18, one can observe that the rate constants show an Arrhenius behaviour with temperature between 10 and 60°C.

Table 3.5 gather the excimer and monomer decay times (τ_E and τ_M) and the rate constants for excimer formation (k_a), dissociation (k_d) and decay (k_E) together with the fractions of each specie (X and Y) involved.

Table 3.5. Monomer and excimer decay times (τ_M , τ_E), rate constants of excimer formation (k_a) obtained from the Time-Resolved (k_a^{TR}) and the Steady State (SS, k_a^{SS}) approach Dissociation and excimer decay rate constants (k_d and k_E , respectively) and fractions of MAGRE and GSD ($X = (1-\alpha)(1-\beta)$ and $Y = (1-\alpha)\beta$, respectively) for PAAMePy(2)52 in methanol at different temperatures.

Temperature Limit Range	T (°C)	τ_M (ns)	τ_E (ns)	k_a^{TR} (ns ⁻¹)	k_d (ns ⁻¹)	k_E (ns ⁻¹)	α	X	Y
	0	223	112	0.033	0.004	0.009	0.725	0.165	0.110
LTL	10	217	98	0.035	0.005	0.010	0.673	0.209	0.118
	20	212	84	0.038	0.006	0.012	0.625	0.247	0.128

Polymers

Temperature Limit Range	T (°C)	τ_M (ns)	τ_E (ns)	k_a^{TR} (ns ⁻¹)	k_d (ns ⁻¹)	k_E (ns ⁻¹)	α	X	Y
	30	207	73	0.044	0.007	0.014	0.595	0.273	0.132
	40	202	64	0.053	0.008	0.016	0.564	0.293	0.143
	50	198	56	0.062	0.008	0.018	0.547	0.303	0.150
	60	195	50	0.076	0.010	0.020	0.536	0.301	0.163

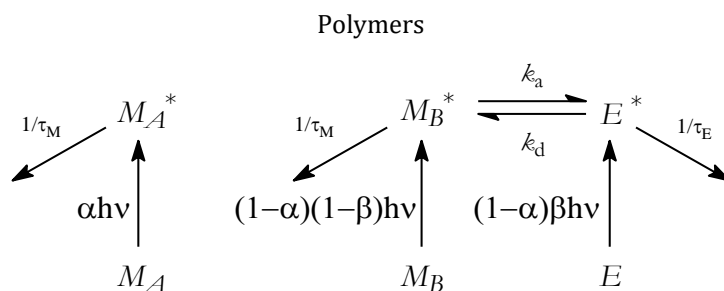
From Table 3.5, it can be observed that the k_a value is temperature-dependent, increasing with the temperature (from 3.3×10^7 to 7.6×10^7 s⁻¹), $\eta_{MeOH} = 0.5929$ mPa.s at 20°C.³⁵

At 20°C, the k_a value is of 3.8×10^7 s⁻¹ which is in agreement with the value found for intramolecular excimer formation for 1Py(10)1Py in methylcyclohexane ($\sim 4.8 \times 10^7$ at 25°C)⁴⁶ ($\eta_{MCH} = 0.670$ cP).³⁵

The values found for the dissociation rate constant k_d (from 0.4×10^7 to 1.0×10^7 s⁻¹) are not so different from those obtained for the reciprocal excimer lifetime k_E (from 0.9×10^7 to 2.0×10^7 s⁻¹), which indicate competition between these two deactivation pathways.

Intra vs. intermolecular interactions. The k_a , k_d and, in special, k_E ($1/\tau_E$) values obtained are not the typically found for intermolecular interactions so the existence of intermolecular interactions is very improbable for the conditions used. This was also confirmed by the non-variation of the I_E/I_M ratio with the concentration of the polymer, see SI.

MAGRE [(1- β)(1- α)], isolated monomers (α) and GSD [$\beta(1-\alpha)$]. In methanol, the fraction of isolated monomers α is relatively high with a value (between 0.536 and 0.725) and similar to the theoretical mole fractions (0.76) of single-labelled chains relative to all labelled chains, i.e., intrinsically isolated monomers (Table 3.2). If the isolated monomers would come only from chains with monolabelled polymers, the fraction of isolated monomers should not change with temperature. This way, the explanation we give for this (small) variation is that some of the isolated monomers at least $\sim 25\%$ (0.189) is due to chains that are not monolabelled but that, at this temperature, are in a conformation that does not allow the pyrene units to be close together in order to form excimer. With the increase of the temperature the chain is more flexible and now is able to form excimer. The 0.536 is, this way, the value that is the closest of the fraction of monolabelled chains. This means that, although only one monomer lifetime is obtained, the experimental value must be an average of different (similar) values from each kind of free monomer, see Scheme 3.3.



Scheme 3.3. Kinetic scheme for a system involving two monomers and one excimer.

Since the fluorescence spectrum of PAAMePy(2)52 in methanol is similar to that of 1Py(10)1Py in heptane, the maxima of the excimer emission bands are both around 480 nm, and both possess only one excimer, 1Py(10)1Py was used as a parent compound.

In Table 3.6 some relevant parameters taken from the variation of the temperature from both SS and TR are shown for 1Py(10)1Py and PAAMePy(2)52 in heptane and methanol, respectively.

Table 3.6. Relevant parameters [transition temperature (T^*) between HTL and LTL regimes, difference (δ) between the curve defining the normal regime and the line defining the HTL regime at the crossing point, T^* , where $k_d = \tau_E$, enthalpy of excimer formation (ΔH), activation, dissociation and excimer decay energies (E_a and E_d) and entropy (ΔS)] obtained from the Arrhenius Plots of $\ln(I_E/I_M)$ as a function of the temperature reciprocal ($1/T$) for 1Py(10)1Py in and PAAMePy(2)52 in heptane and methanol, respectively.

Technique	Parameters	Units	Values							
			1Py(10)1Py				PAAMePy(2)52			
			Method							
A	B	C	D	A	B	C	D			
SS	T^*	(°C)	27.4 (34.5)	21.7 (33.7)	25.5 (33.2)	21.8 (30.9)	40.4	31.6	34.4	30.5
	δ		0.67 (0.21)	0.60 (0.28)	0.41 (0.23)	0.51 (0.26)	0.24	0.14	0.17	0.11
	$-\Delta H^a$	(kJ.mol ⁻¹)	21.2	23.8	20.8	23.2	ND			
	E_a^b	(kJ.mol ⁻¹)	ND				8.86	7.46	7.32	6.51
	k_F^E/k_F^M		0.62	3.73	3.87	4.70	0.77	2.47	3.32	3.20
TR	T^{*c}	(°C)					39.1			
	δ^c						0.10			
	$-\Delta H^o$	(kJ.mol ⁻¹)					7.1 ^{d,g}			
	ΔS^{od}	(J.mol ⁻¹)					38.5 ^g			
	k_a^{0e}	(ns ⁻¹)					6.3 (6.9)			
	E_a^e	(kJ.mol ⁻¹)	12.0				5.98 ^c 12.4 (12.2) ^{h,i}			

Polymers				
	k_d^{0e}	(ns ⁻¹)	0.3	0.3 ⁱ
	E_d	(kJ.mol ⁻¹)	36.1	9.5 ⁱ
	k_E^{0e}	(ns ⁻¹)	0.1	0.7
	E_E^e	(kJ.mol ⁻¹)	3.7	10.0

^{a, b} Apparent enthalpy variation, activation energies of k_a associated with excimer formation obtained from the HTL (ΔH) and LTL (E_a) region of the Stevens Ban plot, see Section 1.3.2.1.4. ^c Obtained from the Stevens ban curve produced with the TR data. ^d Obtained from the van't Hoff plot, see Section 1.3.2.1.4. ^e Obtained from the Arrhenius plot, see Section 1.3.2.1.4. ^f in μs^{-1} . ^g Using the data between 30 and 60 °C. ^h Taken from $1/\tau_2-1/\tau_M$. ⁱ Using the data between 10 and 60 °C Method A: intensities ratios, method B: deconvoluted bands, method C: GaussMod, method D: BiGauss, T^* and δ was considered to be given by the maximum value of $\ln I_E/I_M$ and by making the subtraction of the value given the linear fitting of $\ln (I_E/I_M)$ and $\ln (I_E/I_M)$ obtained at this temperature, respectively. ND – not defined.

In the case of PAAMePy(2)52, the best method to fit the excimer band and therefore to interpret them, was the GaussMod (method C) function, as previously discussed. Moreover, and since the solvent is also different, it is the *HTL* that becomes poorly defined, and for this reason only an apparent E_a could be obtained.

When the temperature dependence (Arrhenius behavior) can be well defined, as it is the case, the slope of the *LTL* will be $-(E_a-E_e)/R$.⁶⁹

Activation energies obtained from the Stevens-Ban of both the SS and TR approaches present, within the experimental error, identical values of ~ 7 kJ/mol for PAAMePy(2)52 (Table 3.6). This value is lower than the activation energy value for viscous flow and methanol, $E_\eta(\text{MeOH})= 9.9$ kJ/mol.¹⁴⁵

Summarizing:

(i) The free monomer displays the longer decay time (282 ns), the *MAGRE* monomer the shorter decay time (20 ns) and the excimer the other decay time (96 ns). This attribution is made unequivocally from the comparison with the data obtained for 1Py(10)1Py oligomer with decay times 11, 50 and 222 ns, respectively.

(ii) Again, as in methanol, the ~ 96 ns species must be identified to the excimer decay (major components at 480 nm). Moreover, if these components (in the monomer decay) would be associated to different quenching degrees of the excited pyrene (different monomers being quenched with different rates) there would be no reason for these decay times to be exactly identical at the excimer emission wavelengths. Furthermore, for the PAAMePy(2)52, neglecting the excimer-to-monomer reversibility process should not be done at any temperatures (from 0 to 60°C) since it leads to an incorrect interpretation of the photophysical processes occurring in these polymers; while in the case of the oligomers it can be considered to be valid for temperatures below 10 °C but not at room temperature.

3.2.1.3. Summary

The kinetics of a PAA polymer labelled with pyrene (consisting essentially of single and double labelled PAA chains) was investigated in methanol (as a function of temperature) and in dioxane:water mixtures. In both solvents, the kinetic scheme proposed involved only three species: *MAGRE*, *GSD* and free monomer as previously observed, although some doubt were found in the case of the dioxane:water mixtures. The kinetics of this pyrene labelled polymer was further compared with the study of pyrene oligomers such as 1Py(10)1Py, Chapter 3. For the PAAMePy polymers, it is shown that the excimer-to-monomer reversibility process (seen as an additional component in the monomer emission decay) is present in all systems at all temperatures.

3.2.1.4. Supporting Information

The probability of finding N pyrene units per chain is given by Figure 3.19 for the PAAMePy(150) polymers.

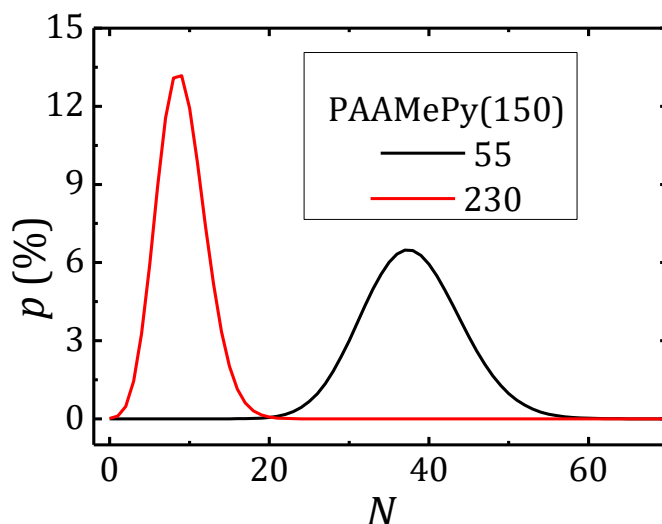


Figure 3.19. Probability (p) of finding a PAA chain with a given number of N pyrene groups per chain, for the 2083 AA units [the analogous of PAAMePy(150)] polymers, assuming a Poisson distribution.

3.2.2. Dynamics of Short and Long PAAMePy Polymers in Aqueous Solutions

3.2.2.1. The effect of pH

3.2.2.1.1. Absorption Spectra

The absorption spectra of all the PAAMePy polymers here investigated are depicted in Figure 3.20 and Figure 3.21. The absorption spectra together with the P_A and $\lambda_{\max}^{abs.}$ variation as a function of the pH for the PAAMePy(2)52, PAAMePy(2)77, PAAMePy(450)53 and PAAMePy(450)87 polymers can be found in ref. ^{65,144} and for the PAAMePy(150)55 and PAAMePy(150)230 polymers in ref. ⁶³. The PAAMePy polymers show the characteristic pyrene resolved spectra with the sole exception of the more labelled

of the smallest polymers [PAAMePy(2)12 and PAAMePy(2)18], which may indicate a high level of ground-state association contribution beneath the monomer absorption. Furthermore, it can be observed that there is no significant shift in the spectra of the polymers relative to the spectra of the model compound 1-pyrenylmethylacetamide, with maxima at ~341-347 nm (polymers) versus ~341-342 nm (1-pyrenylmethylacetamide) in water.

From the dependence of the absorption spectra (Figure 3.21) of the PAAMePy polymers with the pH, two parameters can be extracted: the $\lambda_{\max}^{\text{abs.}}$ and the P_A ratio (see definition in Section 7.2.5.2.1). The dependence of these parameters with the pH gives a clear indication that the absorption spectra result from the sum of two absorbing species: pyrene monomers and *GSD*.

For all the investigated polymers [except the PAAMePy(2)132 and PAAMePy(450)77 polymers], a blue shift of the $\lambda_{\max}^{\text{abs.}}$ with increasing pH is observed, compatible with a decrease in the polarizability of the environment, i.e., exposure to water. On the other hand, the P_A ratios decrease with the pH with the sole exception of PAAMePy(450)10. This was already reported¹⁴⁴ but at the time the assumption was that all the PAAMePy(450) behaved that way. However, this is not the case for PAAMePy(450)77 and PAAMePy(450)517.

From the direct observation of the spectra of the different polymers in water, it can be easily seen that the spectra of PAAMePy(2)12 is broader when compared to the other polymers and PAAMePy(2)18 presents an additional band at longer wavelengths. Moreover, all the polymers have P_A values decreasing and $\lambda_{\max}^{\text{abs.}}$ values increasing with the pH, with the sole exception of PAAMePy(2)132 and PAAMePy(450)10. These observations can be further summarized for the PAAMePy polymers which establishes a division in three groups:

- 1) Increasing P_A and decreasing $\lambda_{\max}^{\text{abs.}}$ as a function of the pH: 12, 18, 24, 41, 133, 77 and 517;
- 2) Decreasing P_A and decreasing $\lambda_{\max}^{\text{abs.}}$ as a function of the pH: 10;
- 3) Increasing P_A and $\lambda_{\max}^{\text{abs.}}$ as a function of the pH: 132.

The first group can be further subdivided in two others if we consider the size of the polymer:

- 1) 12, 18, 24, 41 and 133;
- 2) 77 and 517.

Which leads to an additional division considering the differences on the absorption spectra:

- 1) 12;
- 2) 18;
- 3) 24, 41 and 133.

Polymers

For all the investigated polymers, except for PAAMePy(2)132 and PAAMePy(450)10, a blue-shift of the $\lambda_{\text{max}}^{\text{Abs}}$ with pH is observed (right hand panel of Figure 3.20 and Figure 3.21), compatible with a decrease of the polarizability of the environment, i.e., exposure to water. On the other hand, the P_A ratios decrease with the pH with the sole exception of PAAMePy(450)10. This was already reported¹⁴⁴ but at the time the assumption was that all the PAAMePy(450) presented the same behavior. However, this is not the case for PAAMePy(450)77 and PAAMePy(450)517 polymers.

Polymers

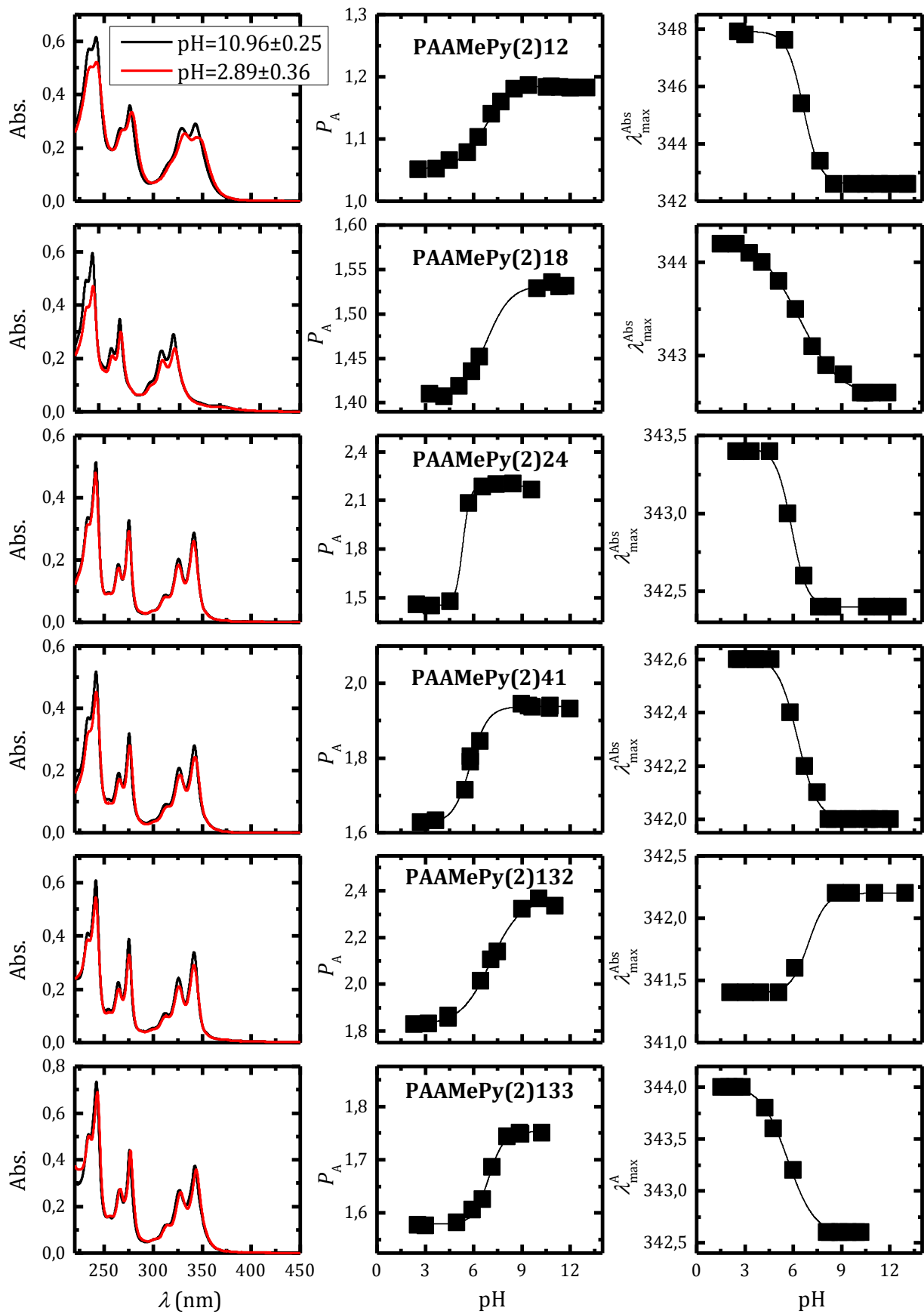


Figure 3.20. From left to right. Absorption spectra for PAAMePy(2) polymers in water as a function of the pH. Dependence of the P_A ratio and wavelength maxima, $\lambda_{\text{max}}^{\text{abs.}}$, with pH.

For pH values above 10, both λ_{\max}^{Abs} and P_A values are kept constant for all the polymers, and the same is valid for the λ_{\max}^{Abs} values which from this same pH value present a constant value of 342-343 nm, thus indicating a similar polarizability. The degree of pyrene labelling has a comparatively smaller effect on the λ_{\max}^{Abs} (seen at pH~10, 0.5-0.6 shift for all polymers).

Again and for all polymers the P_A values are lower than 3, which constitutes qualitative evidence for the presence of *GSD* over the whole pH studied range.¹⁴⁶

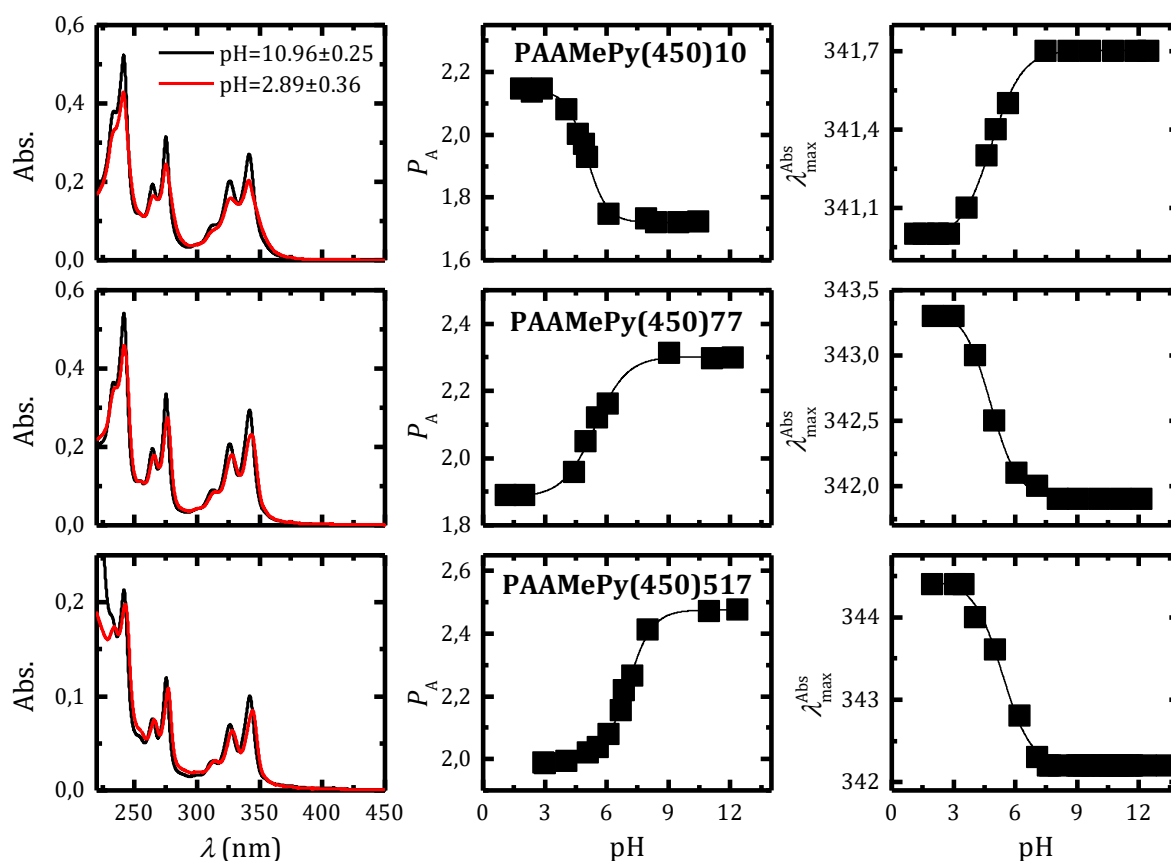


Figure 3.21. From left to right. Absorption spectra for PAAMePy(450) polymers in water as a function of the pH. Dependence of the P_A ratio and wavelength maxima, $\lambda_{\max}^{abs.}$, with pH.

Deprotonation of the carboxylic acids of the PAA chain is known to induce a change from a coiled to an extended conformation (due to electrostatic repulsions), leading to less excimer formation (essentially due to less *GSD* contribution).

The plot of P_A and $\lambda_{\max}^{abs.}$ (Figure 3.21) and P_M , P_E (figure not shown) and P_M-P_E (Figure 3.23) dependencies with pH, shows a clear inflexion from which the pK_a could be estimated.

Polymers

Both the dependence of the P_A and $\lambda_{\max}^{abs.}$ with the pH were fitted to a sigmoidal Boltzmann-like equation according to Equation 7.4.

The obtained results are presented in Table 3.7 (P_A and $\lambda_{\max}^{abs.}$) and Table 3.8, (P_M - P_E) respectively. Considering that the data obtained from fluorescence methods are much more sensitive, the values of the apparent pK_a obtained in Table 3.8 constitute more reliable values. From the P_M - P_E values in Table 3.8, the apparent pK_a values were found between 4.3 and 5.6.

Table 3.7. Values of pK_a for the different polymers [PAAMePy(2) and PAAMePy(450)] obtained by fitting the data in Figure 3.20 and Figure 3.21 [P_A and $\lambda_{\max}^{abs.}$ vs. pH] with Equation 7.4 and variation in the P_A ratio and $\lambda_{\max}^{abs.}$ for the pH range investigated (ΔP_A and $\Delta \lambda_{\max}^{abs.}$, respectively).

Polymer	pK_a		ΔP_A	$\Delta \lambda_{\max}^{abs.}$
	from P_A	from $\lambda_{\max}^{abs.}$		
PAAMePy(2)12	6.71±0.11	6.61±0.05	0.14	5.3
PAAMePy(2)18	6.80±0.10	6.37±0.09	0.13	0.6
PAAMePy(2)24	5.32±0.07	5.89±0.05	0.75	1.0
PAAMePy(2)41	5.80±0.06	6.27±0.05	0.32	0.6
PAAMePy(2)52⁶⁵	6.67±0.13	5.92±0.18	~0.40	~1.7
PAAMePy(2)77⁶⁵	5.23±0.14	5.67±0.19	~0.30	~1.5
PAAMePy(2)132	7.06±0.10	6.94±0.25	0.54	0.8
PAAMePy(2)133	6.94±0.05	5.66±0.07	0.17	1.4
PAAMePy(450)10	5.02±0.04	4.84±0.04	0.43	0.7
PAAMePy(450)53⁶⁵	5.80±0.05	4.82±0.54	~0.25	~3.0
PAAMePy(450)77	5.43±0.08	4.80±0.06	0.42	1.4
PAAMePy(450)87⁶⁵	5.80±0.05	4.82±0.54	~0.30	~3.0
PAAMePy(450)517	7.02±0.05	5.37±0.06	0.49	2.2

The pH of the PAA strongly depends on its degree of ionization. Consequently this has implications on the apparent pK_a values (as seen from the inflexion in P_A , $\lambda_{\max}^{abs.}$, P_M , P_E and P_M - P_E). Taking the equation from the ref.¹⁴⁴ $pH = 6.17 - 2 \log \left(\frac{1-\alpha}{\alpha} \right)$ one can estimate dissociation degree for each pH and vice-versa.

At 25°C, the pK_a for acrylic acid is 4.25 (4-4.5) and for PAA is *ca.* 4.7. From the overall data of Table 3.7, it seems clear that the introduction of pyrene increases the apparent pK_a of the modified PAA polymer.

3.2.2.1.2. Steady State Fluorescence

The fluorescence excitation spectra (Figure 3.22 and Figure 3.23) collected in the monomer and excimer emission regions are both different and pH dependent. This leads to differences in the P_M and P_E values. For all the PAAMePy polymers here shown, the variation of the P_M - P_E difference is clearly pH dependent with a significant change when the pK_a is reached. The fluorescence excitation spectra of PAAMePy(2)52, PAAMePy(2)77, PAAMePy(150)55, PAAMePy(150)230, PAAMePy(450)53 and PAAMePy(450)87 polymers together with the P_M - P_E variation as a function of the pH can be seen in ref. 63,65,144.

Polymers

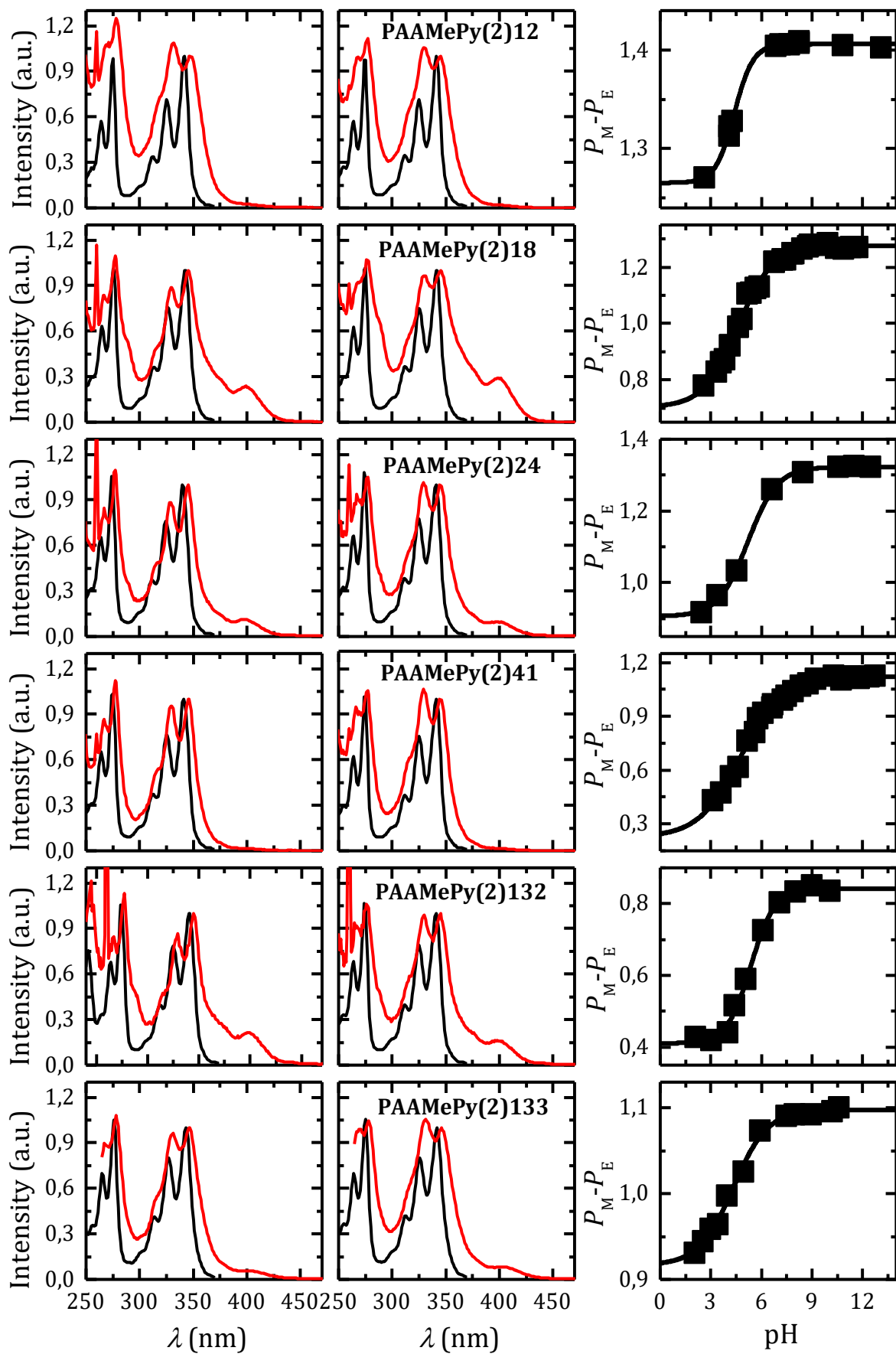


Figure 3.22. From left to right. Fluorescence excitation spectra for the PAAMePy(2) polymers obtained at acidic ($\text{pH} = 3.38 \pm 0.33$) and alkaline ($\text{pH} = 11.56 \pm 0.33$) pH values with $\lambda_{em} = 375$ (black line) and 520 nm (red line) at 20 °C and variation of the $P_M - P_E$ difference with pH.

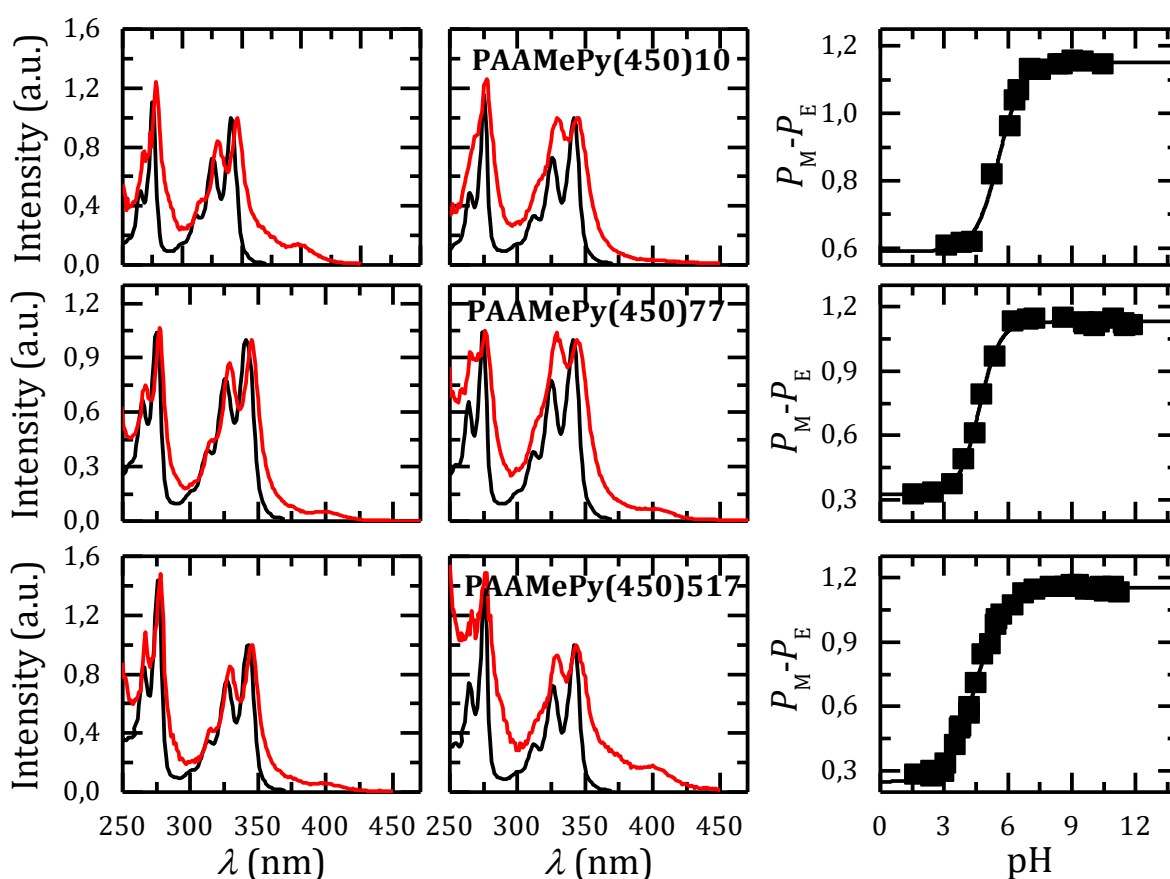


Figure 3.23. From left to right. Fluorescence excitation spectra for the PAAMePy(450) polymers obtained at acidic ($\text{pH} = 3.38 \pm 0.33$) and alkaline ($\text{pH} = 11.56 \pm 0.33$) pH values with $\lambda_{\text{em}} = 375$ (black line) and 520 nm (red line) at 20 °C and variation of the $P_M - P_E$ difference with pH.

The excitation spectra collected at the excimer region is different at acidic and basic pH values. By increasing the pH, the differences between the bands of the excitation spectrum collected in the monomer and the excimer regions, become more evident. On the other hand, the increase in $P_M - P_E$ difference as a function of the pH values is a clear (qualitative) indication of the increase of *GSD*. Comparing both PAAMePy(450)77 and PAAMePy(2)77 it can be suggested that the presence of *GSD* is affected essentially to the size of the polymer chain, the longer the chain, higher the contribution of *GSD*, see Table 3.8.

In Table 3.8 the $\text{p}K_a$ values obtained by the P_M , P_E and $P_M - P_E$ graphs as a function of the pH are gathered together with the total variation of $P_M - P_E$ ($\Delta P_M - P_E$) and I_E/I_M ($\Delta I_E/I_M$) for the pH range investigated.

Polymers

Table 3.8. Values of pK_a for the different polymers obtained by fitting the data in Figure 3.22 and Figure 3.23 ($P_M - P_E$), P_M and P_E vs. pH with Equation 7.4 and variation in the $P_M - P_E$ difference and I_E/I_M ratio (Figure 3.24) for the pH range investigated ($\Delta P_M - P_E$ and $\Delta I_E/I_M$, respectively).

Polymer	pK_a			$\Delta P_M - P_E$	pH*	$\Delta I_E/I_M^c$
	from P_M	from P_E	from $P_M - P_E$			
PAAMePy(2)12		ND	4.38±0.05	0.14	6.0	1.92
PAAMePy(2)18	4.98±0.20	5.21±0.15	4.61±0.09	0.51	8.5	0.50
PAAMePy(2)24	ND	5.49±0.13	5.20±0.10	0.41	8.5	0.06
PAAMePy(2)41	5.62±0.09	5.04±0.15	4.76±0.20	0.70	10.0	0.38
PAAMePy(2)52 ^a			4.97±0.15	0.30	6.0	0.19
PAAMePy(2)77 ^a		ND	4.52±0.06	0.29	7.0	0.12
PAAMePy(2)132	5.21±0.20	5.41±0.14	5.37±0.09	0.43	8.0	0.04
PAAMePy(2)133			4.32±0.17	0.49	7.5	0.04
PAAMePy(150)55 ^b		ND	NA	0.09	NA	0.78
PAAMePy(450)10	5.17±0.45	4.93±0.26	5.58±0.06	0.55	8.0	0.23
PAAMePy(450)53 ^a		ND	NA	0.10	NA	2.28
PAAMePy(450)77	4.50±0.15	4.50±0.29	4.66±0.04	0.82	6.5	0.05
PAAMePy(450)87 ^a			ND			0.58
PAAMePy(450)517	4.47±0.10	4.50±0.18	4.48±0.03	0.89	7.0	0.03

^{a, b} calculated from the values of ref. ⁶⁵ and ¹⁴⁴, respectively ^c Value with $\lambda_{exc} = 350$ nm. pH* is the pH in which the variance between the values of the fitting of $P_M - P_E$ varies less than 0.001% from one pH to another (of difference of 0.5 with each other). ND – not determined, NA – not applicable, the $P_M - P_E$ trend could not be fitted with a Boltzmann-like equation.

The fluorescence emission spectra are presented in Figure 3.24 together with the I_E/I_M ratio as a function of the pH values. These plots are also found in ref. ^{63,65,144} for the PAAMePy(2)52, PAAMePy(2)77, PAAMePy(150)55, PAAMePy(150)230, PAAMePy(450)53 and PAAMePy(450)87 polymers.

In dilute aqueous solutions the fluorescence emission spectra of the PAAMePy polymers show the characteristic vibronically resolved monomer (with maxima ~375 nm) and the structureless excimer (with maxima centred at ~480 nm) bands (Figure 3.24). Moreover, for the polymer it can be seen that the excitation in the red edge of the absorption ($\lambda_{exc} = 350$ nm) leads to an increase in the intensity of the excimer band compared to the spectra at $\lambda_{exc} = 315$ nm.

In Figure 3.24 and Figure 3.25, the fluorescence emission spectra of the PAAMePy polymers at acidic and basic pH values and the I_E/I_M ratio as a function of pH are shown.

Polymers

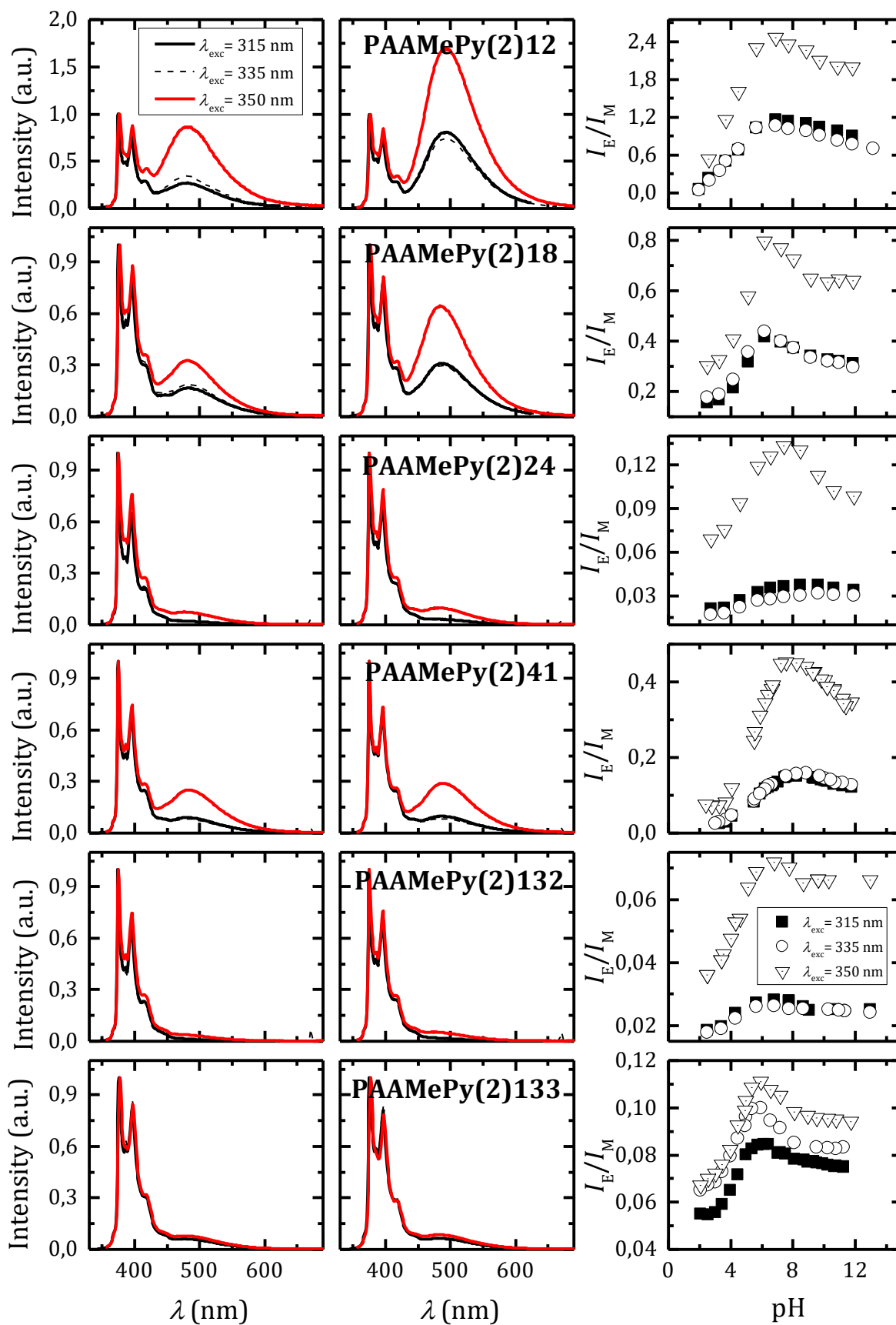


Figure 3.24. From left to right. Fluorescence emission spectra at acidic ($\text{pH} = 3.23 \pm 0.26$) and basic ($\text{pH} = 11.52 \pm 0.38$) pH values and excimer-to-monomer (I_E/I_M) ratio as a function of pH with different excitation wavelengths for the PAAMePy(2) polymers. I_E/I_M ratios were taken with Method A, see Section 7.2.6.1.2.1.

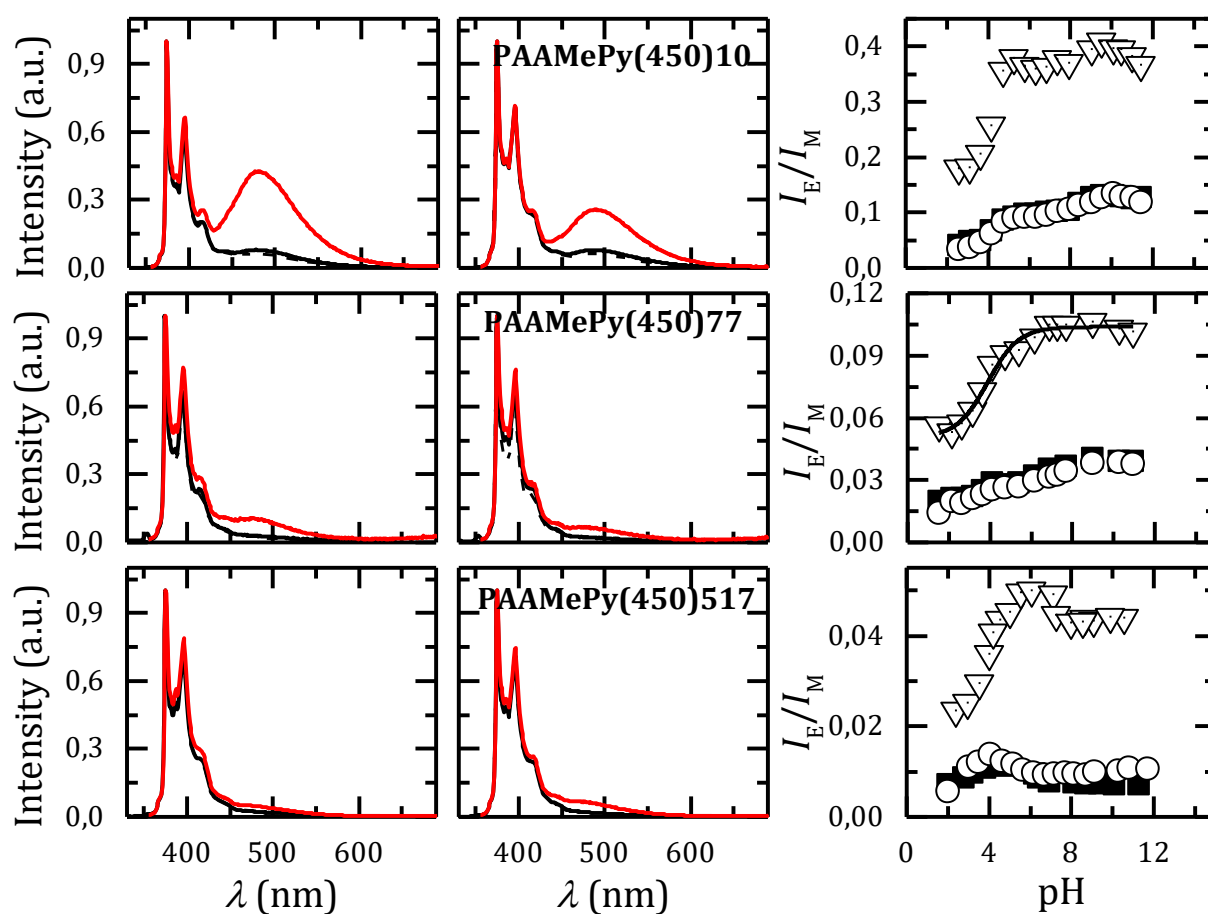


Figure 3.25. From left to right. Fluorescence emission spectra at acidic ($\text{pH} = 3.23 \pm 0.26$) and basic ($\text{pH} = 11.52 \pm 0.38$) pH values and excimer-to-monomer (I_E/I_M) ratio as a function of pH with different excitation wavelengths for the PAAMePy(450) polymers. I_E/I_M ratios were taken with Method A, see Section 7.2.6.1.2.1.

For all the polymers an initial increase of the I_E/I_M ratio at $\text{pH} \sim 5-8$ is observed, followed by a decrease upon this pH value. Having discarded the possibility of existence of intermolecular interactions by a careful preparation of the solutions (see Chapter 7), the increase I_E/I_M can only be associated to an increase in the *GSD* contribution since the increase in the pH would lead to the PAA chain elongation (due to an increase on the electrostatic repulsions) thus leading to a decrease in excimer contribution. Thus, the increase of *GSD* for higher pH (also seen by the P_M-P_E difference as a function of the pH) values should be the result of a change in the conformation of the polymer and/or of the proximity of pyrene groups, the two leading to a higher probability of dimer associations and/or excimer formation. Despite this initial increase, there is always a slight decrease of the excimer-to-monomer intensity ratio at high pH values. This seems to indicate that, despite the conformation favouring the formation of *GSD*, from a given pH value the expansion of the PAA chain prevails leading to a decrease in I_E/I_M ratio. This formation *GSD* is also supported by the fact that the excimer fluorescence intensity increases with the excitation wavelength.

The opposite trends of I_E/I_M seen in ref. ⁶⁵ for the short PAAMePy [PAAMePy(2)] and the longer PAAMePy polymers [PAAMePy(150) and PAAMePy(450)] was not observed with the currently investigated polymers. Indeed, all the investigated polymers present a behaviour that is similar to that found for the short PAAMePy(2) polymers, PAAMePy(2)52 and PAAMePy(2)77. It is important to stress that PAAMePy(450)53 has far higher solubility than PAAMePy(450)77 or even PAAMePy(450)517 that are less labelled. This can be associated to the fact that the pyrene labelling onto the polymer can be made with pyrene in close proximity or far apart. This seems to indicate that the synthesis procedure for PAAMePy(450)77 and PAAMePy(450)517 favoured a more neighbouring pyrene labelling rather than a more distributed along the chain pyrene distribution. This could happen, for instance, if the polymer chain is not stretched at the moment of the labelling.

Data in Figure 3.26 has been previously published ^{65,144}, however the apparent ΔH values were not obtained.

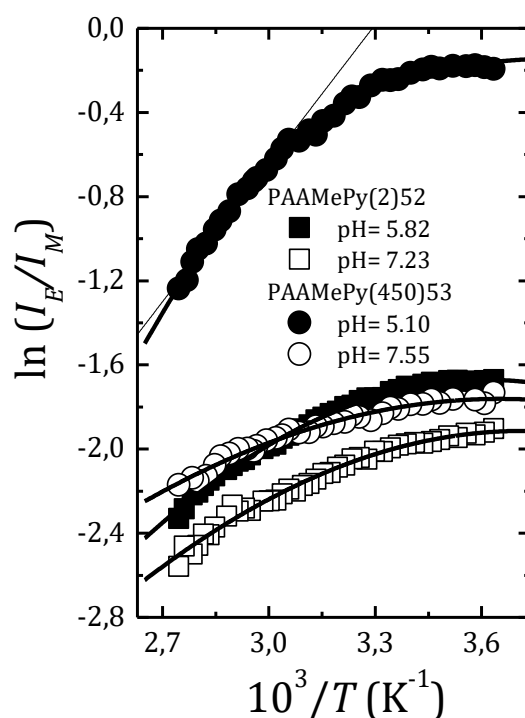


Figure 3.26. Plots of $\ln(I_E/I_M)$ vs. $1/T$ obtained at different pH values for the PAAMePy(2)52 and PAAMePy(450)53 polymers. ^{65,144} I_E/I_M ratios were taken with Method B, see Section 7.2.6.1.2.1.

From the *HTL* regime of Figure 3.26, the excimer enthalpy formation obtained was found to be $-7.6 \text{ kJ}\cdot\text{mol}^{-1}$ and $-6.8 \text{ kJ}\cdot\text{mol}^{-1}$ for PAAMePy(2)52 at pH= 5.82 and 7.23 and $-18.3 \text{ kJ}\cdot\text{mol}^{-1}$ and $-6.5 \text{ kJ}\cdot\text{mol}^{-1}$ for PAAMePy(450)53 at pH= 5.10 and 6.5, respectively. The value obtained at acidic pH (for PAAMePy(2)52 in water) is very similar to the one seen for PAAMePy(2)52 in methanol (-17.6), Table 3.6.

3.2.2.1.3. Time-Resolved Fluorescence

Time-resolved (TR) data provides additional and relevant information to the understanding of the PAAMePy dynamics since it allows to obtain quantitative information on, amongst others, the level of ground-state dimers and isolated monomers in addition to the rate constants associated to the monomer deactivation and excimer formation and deactivation. Due to the complexity of such systems, the use of parent compounds, together with TR data of these polymers in (good: for the hydrophobic pyrene probe) organic solvents with (increasing content of) water is useful. The fact that the water is not a good solvent for the probe can lead to aggregation, precipitation, *etc.*, and should be considered in the data analyses and interpretation.

In Figure 3.27, the free independent analyses of the decays are presented. Panel A shows a bi-exponential fit of the decay at the monomer emission together with the typical decay time values obtained for a quenched monomer, MAGRE (~17 ns) and a free (unquenched) monomer (218 ns).

The independent analysis made for the decays in the excimer region, shows that obtained with a sum of three exponentials the decays are correctly fitted. However, if we restrict the analysis to the beginning of the decay (which, may be seen as obtaining and analysing the decay with a smaller time/channel ratio, in this case, 116 ps/ch), the analysis now leads to two decay times, see Figure 3.27C: the *MAGRE* monomer that gives rise to the excimer (for that, a quenched monomer and with an associated rise-time) with a decay time of ~20 ns which is similar to that obtained for the quenched monomer in the monomer emission (17 ns) and a second decay time, attributed to the excimer decay. The fact that, both free monomer and excimer decay components are not present when the independent analysis of, respectively, the excimer and monomer decays is made, is a consequence of the fact that they contribute little, at these emission wavelengths leading to almost negligible pre-exponential factors values. However, when global analysis is made, these components are needed to properly fit the decays.

When global analysis of the decays is made, the pre-exponential value at $\lambda_{em} = 375$ nm associated to the excimer decay time is, since no excimer emission is observed at this emission wavelength, associated to the excimer-to-monomer reversibility process; nevertheless it is worth noting that at this temperature the PAAMePy(2)52 polymer is found in the *HTL* limit.¹⁴⁴ In this region, it was seen a shift for lower wavelengths of the excimer emission in MeOH (see Figure 3.16B). Moreover, and as a result of the global analysis of the decays, the pre-exponential found in the excimer region and associated to the free monomer is likely to be the result of a residual emission of the monomer at 520 nm.

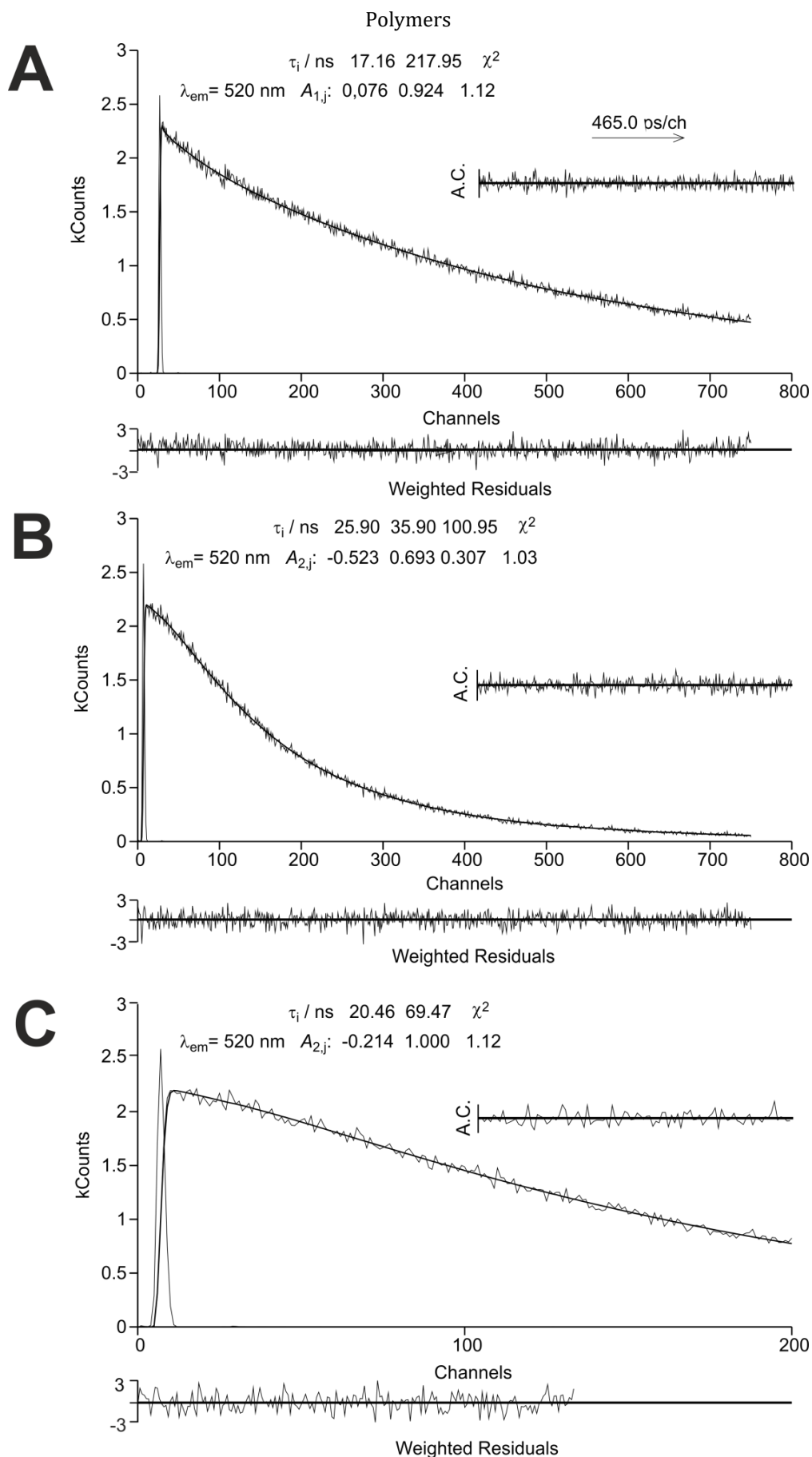


Figure 3.27. Independent analysis of the fluorescence decays of PAAMePy(2)52 in water (pH= 1.74, T= 20 °C), at (A) 375 nm (B and C) 520 nm. The instrument profile curve, weighted residuals and autocorrelations (A.C.) functions are also shown. In (B) and (C) panels, the fluorescence decay analysis were made with all the channels (751) and only for 200 channels, respectively.

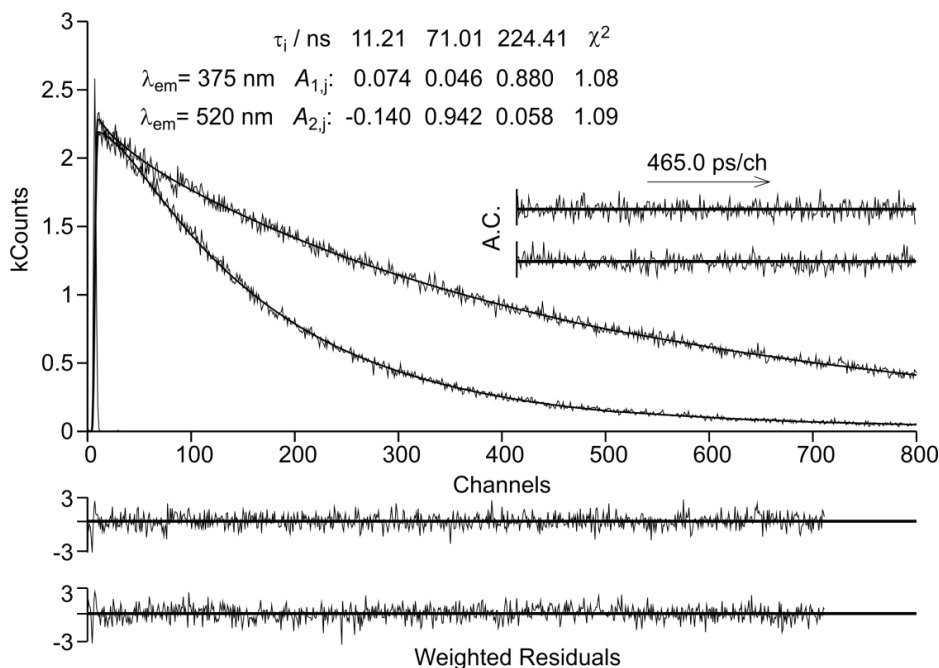


Figure 3.28. Global analysis of the fluorescence decays of PAAMePy(2)52 (pH= 1.74, T= 20 °C), at 375 and 520 nm emission wavelengths analysed with fits of three exponentials. The instrument profile, weighted residuals and autocorrelations (A.C.) functions are also shown.

Indeed two additional facts attest this fact: (i) the monochromator slits used (of 3 mm) leading to a bandpass of ~ 6 -8 nm and (ii) the long emission of the monomer as attested by the emission from the parent compound 1-pyrenylmethylacetamide in water at this pH and temperature (data not shown).

From the data there is evidence is that only three species are present in water. This is further supported by the decays of PAAMePy(2)52 in dioxane:water mixtures (see Chapter 5): *MAGRE*, isolated (free) monomers, and (one) excimer. This contrasts with previous findings where in water the decays were only properly fitted with sums of four exponentials which would contemplate two forms of pyrene excimers: parallel (sandwich-like) and non-parallel oriented.^{65,144} However, it is similar to the found for PAAMePy(150)55 and PAAMePy(150)230 polymers in water.⁶³

3.2.2.2. Interaction of PAAMePy Polymers with Neutral and Anionic Surfactants

3.2.2.2.1. Introduction

3.2.2.2.1.1. Surfactants

Surfactants are widely used in the everyday life in oils for automobiles, in oil exploration, in pharmaceuticals, household products such as shampoos, hair softeners, hair conditioners, detergents and cosmetic products, milk, butter, *etc.*

Surfactants are also often employed to modify the reaction medium allowing the solubilisation of species of low solubility or promoting a new medium that can modify the reaction rate of solubilisation.

The initial problems associated with the use of surfactants in several different products were associated to the use of non-biodegradable compounds, which afforded serious problems of pollution to the environment. To address these drawbacks, new biodegradable surfactants called "green products" have been developed.

A typical surfactant has the structure RX where R is a hydrocarbon chain ranging from 8 to 18 carbon atoms (usually linear) and the head where X is a polar group (or ionic). Depending on X , surfactants can be classified according to their lyophilic chain which may be non-ionic, ionic (anionic or cationic) and zwitterionic.

The surfactant molecules associate themselves spontaneously in aqueous solution from a certain concentration (CMC) to form micelles. Micelles are large molecular aggregates that have two distinct structural regions: the lyophilic and lyophobic (hydrophobic and hydrophilic in the case of water being the solvent).

The presence of a hydrophobic and hydrophilic portion of these molecules confers amphiphilic character, which is responsible for its peculiar features in solution. Under these conditions and due to the low solubility of its hydrophobic moiety in water, the surfactant molecules tend to be located at the air-water interface. Thus, one obtains a marked reduction in the surface tension, to the extent that some molecules of water are replaced by the surfactant molecules. When the concentration reaches the CMC , there is now a dynamic equilibrium between monomers and micelles (Figure 3.29) in which the hydrocarbon chains are close together and the polar groups are oriented to be in contact with water. Micelles have typically a diameter of 3 to 6 nm, corresponding to a 30 to 200 monomers.

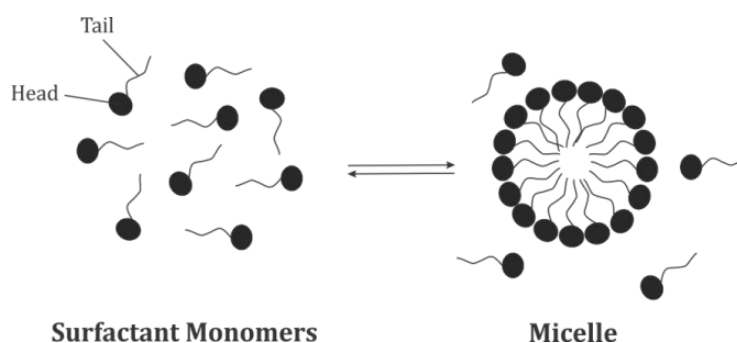



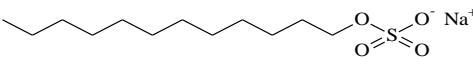

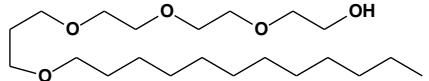

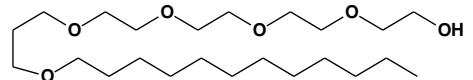

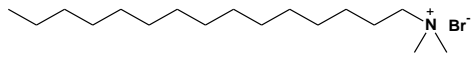
Figure 3.29. Illustration formation process of a micelle.[Illustration, Formation of a micelle]¹⁴⁷

The CMC of the surfactant depends on the structure (size of the hydrocarbon chain) and experimental conditions (ionic strength, counter-ions, temperature, *etc.*). Micelles are thermodynamically stable but could be destroyed by dilution with water when the surfactant concentration is below the CMC . The

aggregation number (N_{agg}) gives a description of the number of molecules present in a micelle once the *CMC* has been reached. Beyond the *CMC*, other properties need to be taken into account: the Krafft point and the cloud point. The Krafft point corresponds to the temperature at which all three phases - crystalline micellar monomer - exist in equilibrium. The cloud point is the temperature at which the salt is no longer completely soluble resulting in a cloudy solution containing a precipitate. Some of the values found for the surfactants used in this thesis are presented in Table 3.9.

Polymers

Table 3.9. Properties (M_w , CMC , $N_{agg.}$, micelle type, cloud point, Krafft point and structure) of several surfactants. The CMC values presented here were determined at 293 K.

Surfactant	Abbreviation	N ^o of carbons	Class	M_w (g/mol)	CMC (mM)	$N_{agg.}$	Micelle type	Cloud point (°C)	Krafft point (°C)	Structure	Ref.
Sodium Dodecyl Sulphate	SDS	12	Anionic	288.37	7-10	62	Spheric 	>100	8		148,149
Tetraethylene Glycol Monododecyl ether	C ₁₂ E ₄	12	Non ionic	363	0.046	905	Reverse 	5.0	NA		149,150
Pentaethylene Glycol Monododecyl ether	C ₁₂ E ₅	12	Non ionic	406	0.065	855	Cylindrical 	26.5	NA		149-151
Cetrimonium Bromide	CTAB	19	Cationic	364.45	1	170	Spheric 	*	~25		148,152

NA – not applicable. * Not found.

The beginning of the formation of aggregates occurs in a small range of concentrations and can be detected by the sudden variation produced in certain physico-chemical properties of the solution depending on the concentration of the surfactant, such as surface tension, osmotic pressure, conductivity (only for ionic surfactant) and the photophysical parameters associated to a probe (such as the ratio of its two vibronic modes (I_1/I_3) and the intensity ratio of excimer to monomer (I_E/I_M), for Pyrene, see example in Figure 3.30).

Thus, with the correct choice of the fluorescent probe, it is possible to determine some important parameters of the system as the CAC of polymer/surfactant and the CMC of surfactant/surfactant systems,¹⁵³⁻¹⁵⁶ the microenvironment of the probe,¹⁵⁷ aggregate structure¹⁵⁷ and size and to make a distinction between intra- and intermolecular associations.

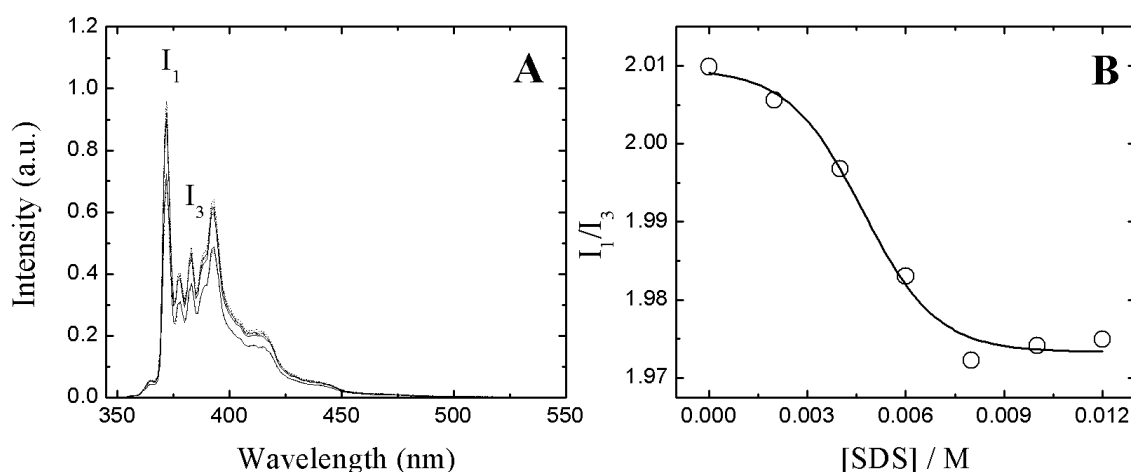


Figure 3.30. Representation of the detection of the CMC of SDS by the I_1/I_3 ratio of pyrene. (A) Fluorescence emission spectra of pyrene in acetonitrile with different concentration of SDS, at $\lambda_{exc}= 335$ nm. (B) I_1/I_3 ratio as a function of [SDS]. The line is obtained using a Boltzmann-like fitting.

Due to the hydrophobic nature of pyrene, its attachment to a water-soluble polymer converts this into a “hydrophobically modified” (amphiphilic) polymer.¹⁵⁸

3.2.2.2.1.2. Interaction Polymer-Surfactant

The presence of polymer solution favours the association of surfactant molecules. The concentration for which this type of interaction starts is defined as the critical concentration of association/aggregation (CAC) and it is usually lower than the CMC by a factor of 10 to 1000.¹⁵⁹ This value depends on the nature of the polymer and surfactant.

The type of polymer-surfactant interaction varies depending on the type of polymer: if homopolymer, if hydrophobically modified polymer (HMP), *etc.* In the case of the homopolymer, the association follows the model of the pearl necklace.¹²⁷ That is, the surfactant molecules form small spherical micellar

aggregates along the polymer chain. These aggregates have the same dimensions as they would have if we were in the presence of the pure surfactant (absence of polymer).

In the case of HMP, hydrophobic grafts are preferred areas of aggregation in water, thereby strengthening the interaction established. Thus, the surfactant molecules interact cooperatively with the hydrophobic groups of the polymers. This interaction causes drastic variations in the viscosity of the solution in respect of HMP in the absence of surfactant or in the presence of surfactant concentration but which does not allow such interaction. This viscosity increase is limited, however, to a narrow range of concentrations of surfactant. The progressive increase in the surfactant concentration leads to a decrease in the number of hydrophobic polymer chains per micelle.

3.2.2.2.2. Results and Discussion

3.2.2.2.2.1. Interaction of PAAMePy polymers with an Anionic Surfactant

3.2.2.2.2.1.1. Absorption Spectra

Figure 3.31 shows the variation of the absorption spectra for PAAMePy(2)132 and PAAMePy(2)133 polymers (top and bottom panels, respectively) with the SDS (with the SDS ranging from 0 to 1.4×10^{-3} M), at pH~9.5.

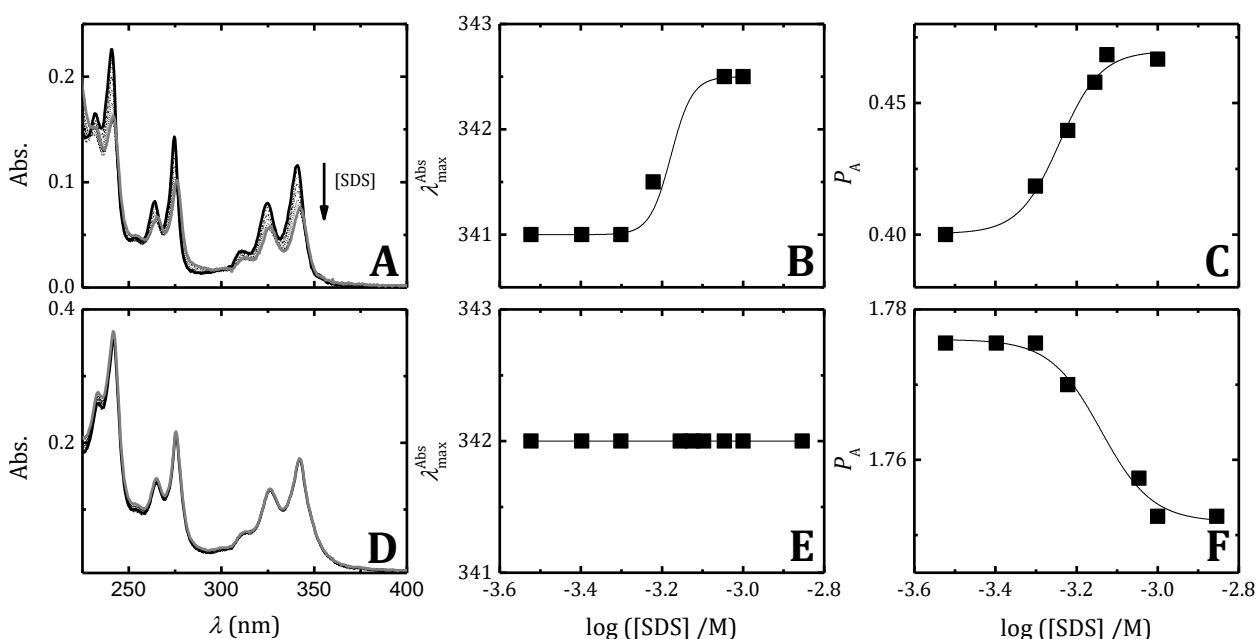


Figure 3.31. From top to bottom. PAAMePy(2)132 and PAAMePy(2)133 in aqueous solutions at pH~ 9.5. (A and D) Absorption spectra in the presence of SDS. Dependence of (B and E) λ_{\max}^{abs} with Boltzmann-like fit in B and (C and F) P_A with the SDS concentration at 20 °C.

Addition of this anionic surfactant does not induce significant changes in the absorption spectra: a red shift of 3 nm is seen in the absorption spectra of PAAMePy(2)132 while the spectra of PAAMePy(2)133

remained practically unchanged. The P_A parameter showed to increase and decrease with the addition of SDS for PAAMePy(2)132 and 133, respectively. Overall these preliminary results do not allow further conclusions.

3.2.2.2.2.1.2. Steady State Fluorescence

The emission spectra of PAAMePy(2)132 and 133 at pH~5.7 and 9.5 in the presence of SDS are displayed in Figure 3.32 and Figure 3.34, respectively. In the two cases, the addition of SDS to the solution leads to an increase in the excimer emission band intensity with a concomitant decrease of the monomer emission band intensity although much more evident for the PAAMePy(2)132 polymer (top panels). The I_E/I_M ratio can be used to directly observe changes in the pyrene labelled poly(acrylic acid) chain conformation and consequently on the level of interaction with SDS.

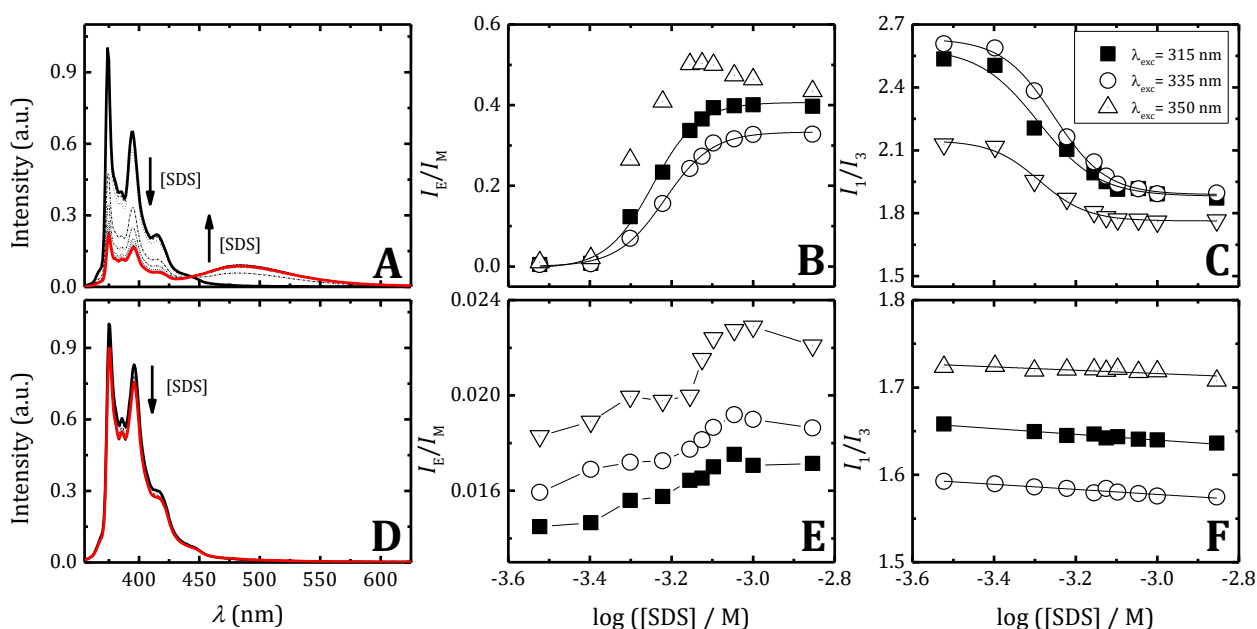


Figure 3.32. From top to bottom. PAAMePy(2)132 and PAAMePy(2)133 in aqueous solutions at pH~ 5.7. (A and D) Emission spectra $\lambda_{exc} = 315$ nm in the presence of SDS. (B and E) Variation of I_E/I_M with Boltzmann fits in B and (C and F) I_1/I_3 ratios with the SDS concentration at 20 °C.

In Figure 3.33 the excitation spectra of PAAMePy(2)132 and PAAMePy(2)133 in aqueous solutions at pH~ 5.7 are showed.

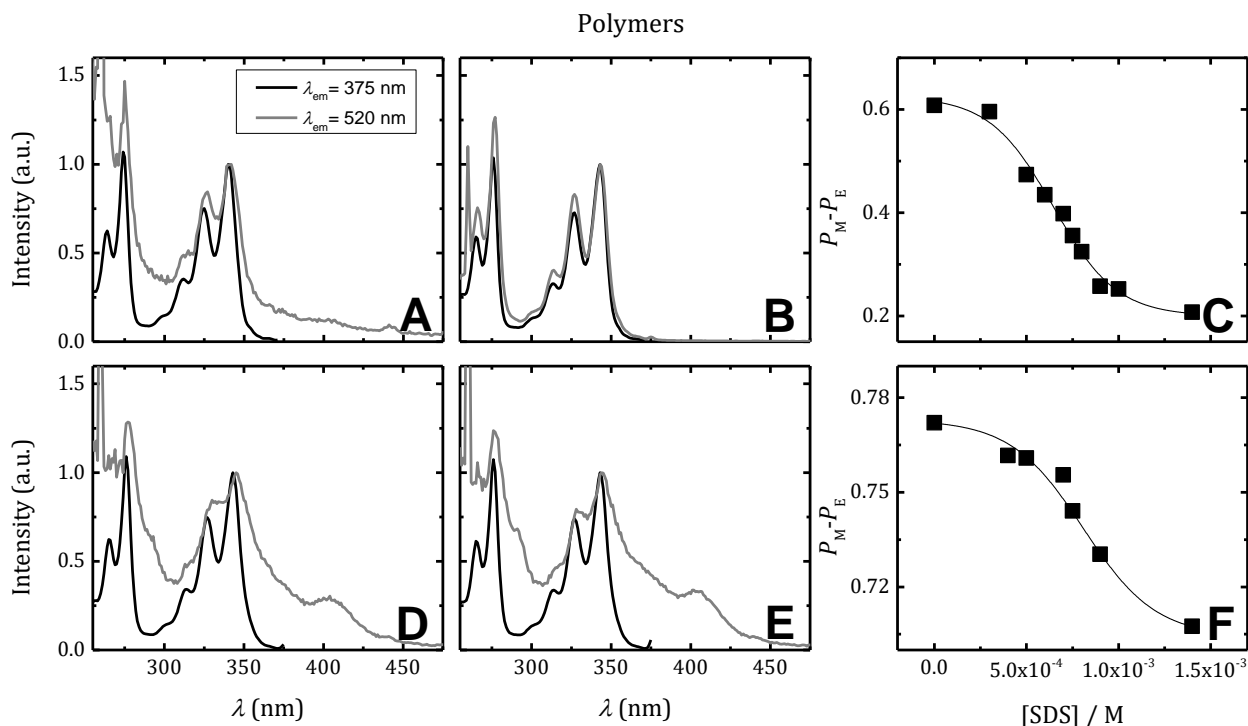


Figure 3.33. From top to bottom. PAAMePy(2)132 and PAAMePy(2)133 in aqueous solutions at pH~ 5.7. Fluorescence excitation spectra of PAAMePy with (A and D) [SDS]= 0 M, (B and E) [SDS]= 1.4×10^{-3} M and (C and F) variation of the $P_M - P_E$ difference with the SDS concentration at 20 °C.

The $\Delta I_E / I_M$, $\Delta I_1 / I_3$ (Figure 3.32) and $\Delta P_M - P_E$ (Figure 3.33, see Section 7.2.5.2.1) are much higher for PAAMePy(2)132.

From these observations it can be concluded that the interaction between the polymers and the surfactant is present, with the formation of micelles around the pyrene groups. The concentration at which the surfactant begins to associate strongly, and therefore begins to induce conformational changes in the poly(acrylic acid) chain, can be seen by the plots C and F of the Figure 3.33, but the first derivative gives a better idea of these values.¹⁶⁰ The value obtained was $5-6 \times 10^{-4}$ M at this pH. However at pH~9.5, the value was 8×10^{-4} M which corresponds to the *CMC* of SDS.

Polymers

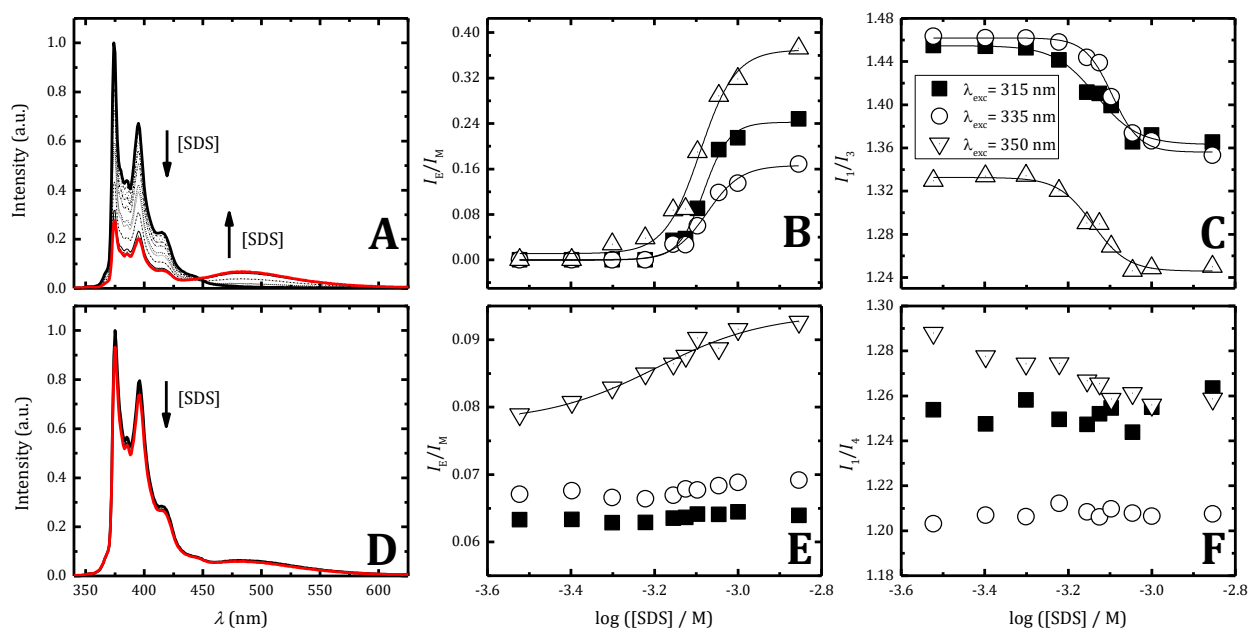


Figure 3.34. From top to bottom. PAAMePy(2)132 and PAAMePy(2)133 in aqueous solutions at pH~ 9.5. (A and D) Emission spectra $\lambda_{exc}= 315$ nm in the presence of SDS. (B and E) Variation of I_E/I_M with Boltzmann fits and (C and F) I_1/I_3 ratios (Boltzmann fits in C) with the SDS concentration at 20°C.

From Figure 3.35 it is clear that for the PAAMePy(2)132 polymer the addition of SDS leads to a decrease on the level of the ground-state dimer contribution as clearly seen when Figures A and B are compared. Indeed, the match of the excitation spectra with $\lambda_{em.} = 375$ and 520 nm indicates (in a qualitative manner) that the excimer contribution from direct excitation of pre-associated pyrene units has decreased. In addition and from Figure 3.34A it is clear that the excimer contribution (band at longer wavelengths) has increased upon addition of SDS. Moreover, the fact that, from the PAAMePy(2)133 polymer (a polymer with an identical degree of labelling), the absorption spectra displays minor changes (Figure 3.31), is indicative that the random labelling of the PAA polymers with pyrene introduces different (more or less densely) labelled probe regions.

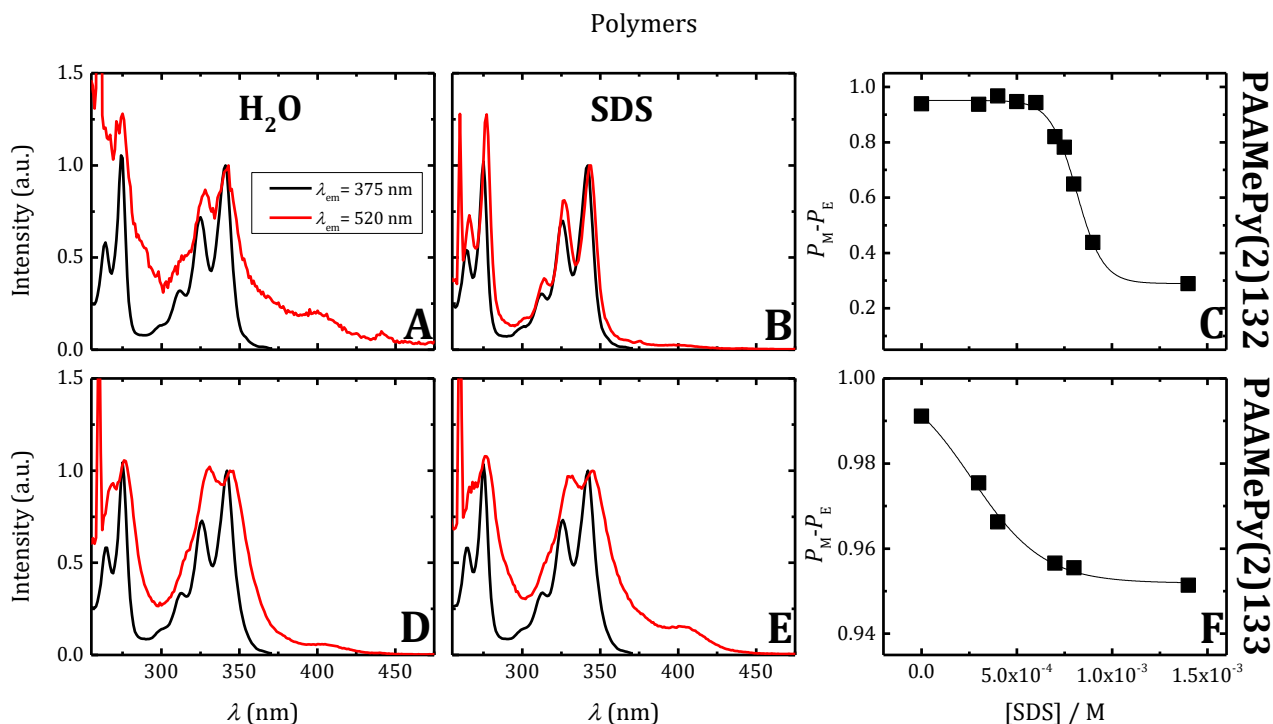


Figure 3.35. From top to bottom. PAAMePy(2)132 and PAAMePy(2)133 in aqueous solutions at pH~ 9.5. Fluorescence excitation spectra of PAAMePy with (A and D) [SDS]= 0 M, (B and E) [SDS]= 1.4×10^{-3} M and (C and F) variation of the $P_M - P_E$ difference with the SDS concentration at 20°C.

The value of critical micellar concentration at pH~5.7 is slightly higher than the value for which the inflexion of I_E/I_M is observed. However, considering the interaction of the polymer with the surfactant, the concentration of critical aggregation value is not identical to the *CMC* of the surfactant. When comparing the plots of I_E/I_M vs log [SDS] it can be seen that the inflection point is reached at lower (acidic) pH values. However, the I_E/I_M vs log [SDS] plots display the same trend which indicates that with increasing pH and increasing concentration of SDS, the general behaviour of the polymer is identical. However, at acidic pH values, the conformation of the polymer facilitates the formation of micelles, see Figure 3.36.

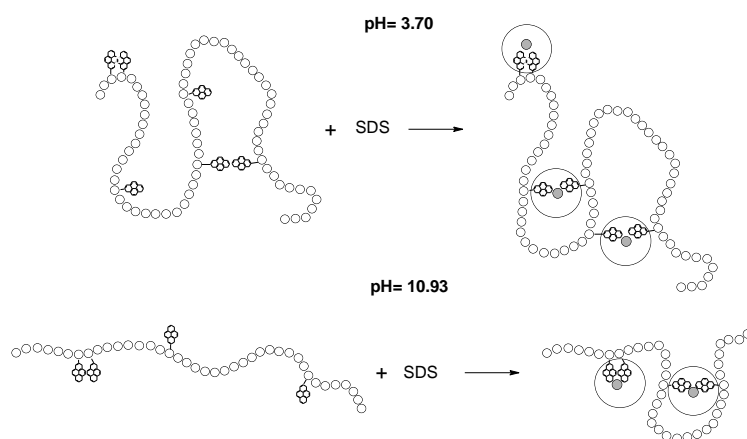


Figure 3.36. Figure illustrating the possible behaviour of the PAAMePy(2)132 and PAAMePy(2)133 polymers before and after the addition of surfactant at acidic and basic pH (top to bottom). Note that the figure is exaggerated for easy understanding of the text.

3.2.2.2.2. Interaction of PAAMePy Polymers with a Neutral Surfactant

The concentration at which the $C_{12}E_5$ surfactant begins to interact with the polymer is significantly lower (4×10^{-5} M) relative to the SDS, which is visible through the inflection of the plot I_E/I_M vs $\log [C_{12}E_5]$. Taking all this into account it is logical to conclude that, when the *CAC* is achieved, i.e. to $[C_{12}E_5] = 4 \times 10^{-5}$ M, the polymer interacts more strongly with this neutral surfactant. The decrease in the ratio I_E/I_M as the surfactant concentration increases is likely due to the creation of areas (cylindrical micelles) that tend to isolate the pyrene units as the surfactant concentration increases. It was not possible to study the interaction of the polymers with a cationic surfactant since for higher concentrations of CTAB, the solutions of PAAMePy(2)132 become turbid and precipitated.

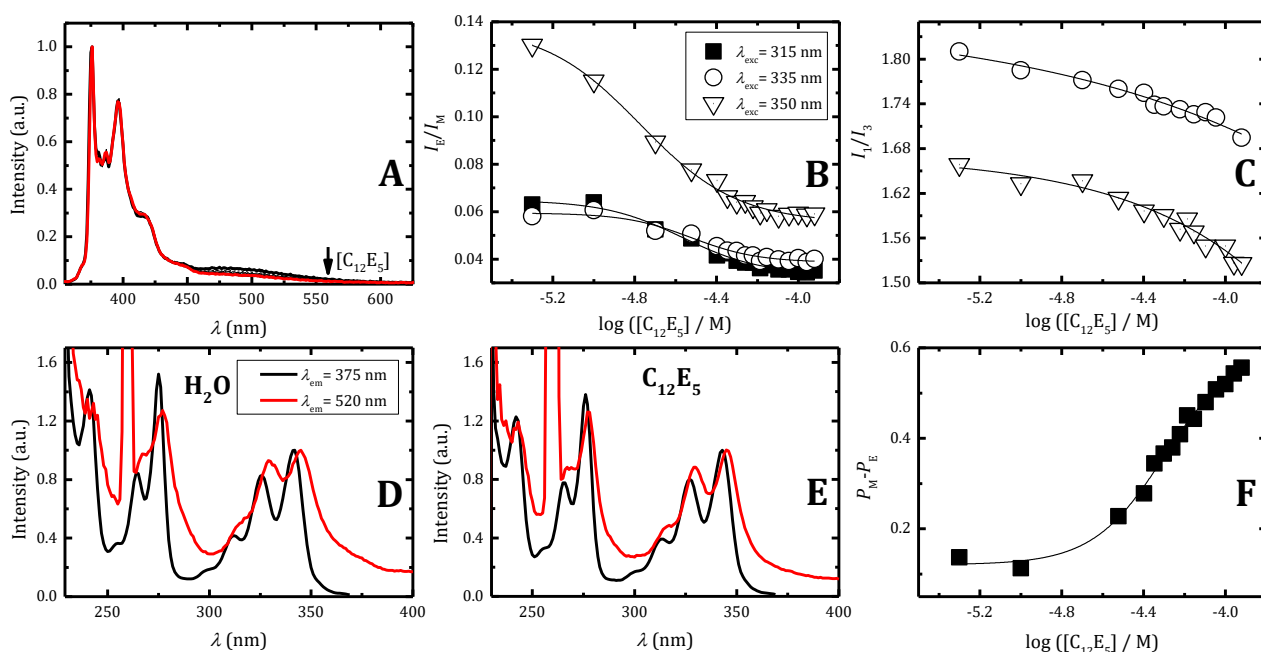


Figure 3.37. (A) Fluorescence emission spectra $\lambda_{exc} = 315$ nm of PAAMePy(2)132 in water at pH= 12, at 20 °C, in the presence of $C_{12}E_5$, (B) variation of I_E/I_M and (C) I_1/I_3 ratios with Boltzmann fits as a function of the concentration of $C_{12}E_5$ for three excitation wavelengths: 315, 335 and 350 nm. Fluorescence excitation spectra with (D) $[C_{12}E_5] = 0$ M and (E) with $[C_{12}E_5] = 1.2 \times 10^{-4}$ M and (F) variation of the $P_M - P_E$ difference with the $C_{12}E_5$ concentration.

From the bottom panels of Figure 3.37 it is clear that for the PAAMePy(2)132 polymer the addition of $C_{12}E_5$ leads to an increase on the level of the ground-state dimer contribution as clearly seen by the increase in the $P_M - P_E$ parameter with the increase on the $C_{12}E_5$ concentration. In addition and from Figure 3.37A it is clear that the excimer contribution (band at longer wavelengths) has decreased upon addition of $C_{12}E_5$.

3.2.2.3. Simulations of the PAAMePy Behavior in Water

3.2.2.3.1. Introduction

In addition to the statistical data obtained in p. 71, we used an additional tool in order to obtain more information about this very complex system. The computer simulation appears in order to try to imitate a real system or model a hypothetical situation to obtain more information about them or predict and explain some results. The simulation can be considered then an additional theoretical tool in the understanding of a complex system. The basis of the simulation can be found in the foundations of statistical mechanics.

3.2.2.3.1.1. Model Systems and Interactions Potential

Statistical mechanics deals with systems with many degrees of freedom. A typical problem in statistical mechanics is to compute the "average" of macroscopic observables of a system for an assumed known Hamiltonian.¹⁶¹

The microscopic state of a system can be defined in terms of positions and moments of a set of particles, atoms and molecules. With the Born-Oppenheimer approximation it is possible to express the Hamiltonian of a system as a function of the nuclear variables, considering that an average for the (fast) motion of electrons is used. Making the additional approximation that a classical description is adequate, the Hamiltonian of the system of N atoms is given by the sum of the kinetic and potential energy functions of the set of coordinates q_i and of the moment p_i of each atom i . Adopting condensed notation as in Equation 3.16 and Equation 3.17.

$$q = (q_1, q_2, \dots, q_N) \quad \text{Equation 3.16}$$

$$p = (p_1, p_2, \dots, p_N) \quad \text{Equation 3.17}$$

We have Equation 3.18.

$$H(q, p) = K(p) + V(q) \quad \text{Equation 3.18}$$

Usually, the kinetic energy (K) has the form given by Equation 3.19 where $p_{i\alpha}$ is the momentum of nucleus i in rotating direction α .

$$K = \sum_{i=1}^n \sum_{\alpha} \frac{p_{i\alpha}^2}{2m_i} \quad \text{Equation 3.19}$$

And the potential energy V (for atomic systems and as approximation for molecular systems) is given by Equation 3.20.

$$V = \sum_i v_1(r_i) + \sum_i \sum_{j>i} v_2(r_i, r_j) + \left[\sum_i \sum_{j>i} \sum_{k>j>i} v_3(r_i, r_j, r_k) + \dots \right] \quad \text{Equation 3.20}$$

The last terms (in square brackets) are rarely included in simulation since the calculation of these sums involves a high computational cost. Happily, the approximation of the pair (1st and 2nd term) describe remarkably well the properties of liquids since the average effects of the terms in parenthesis can be partially included in the “effective” potential pair (v_2^{eff}). Equation 3.20 can be rewritten in a simplified way, Equation 3.21.

$$V \approx \sum_i v_1(r_i) + \sum_i \sum_{j>i} v_2^{eff}(r_{ij}) \quad \text{Equation 3.21}$$

Equation 3.21 describes reasonably the properties of the system if ϵ and σ are properly chosen.¹⁶²

The Lennard-Jones (LJ) potential illustrated together with the BBMS (Bobetic, Barker, Maitland and Smith) potential in Figure 3.38 is given by Equation 3.22.

$$v^{LJ}(r) = 4\epsilon \left[\left(\frac{\sigma}{r} \right)^{12} - \left(\frac{\sigma}{r} \right)^6 \right] \quad \text{Equation 3.22}$$

Where ϵ is the depth of the potential well, σ is the finite distance at which the inter-particle potential is zero and r is the distance between the particles.

This potential is frequently used in simulations in order to substitute the 2nd term in Equation 3.21.

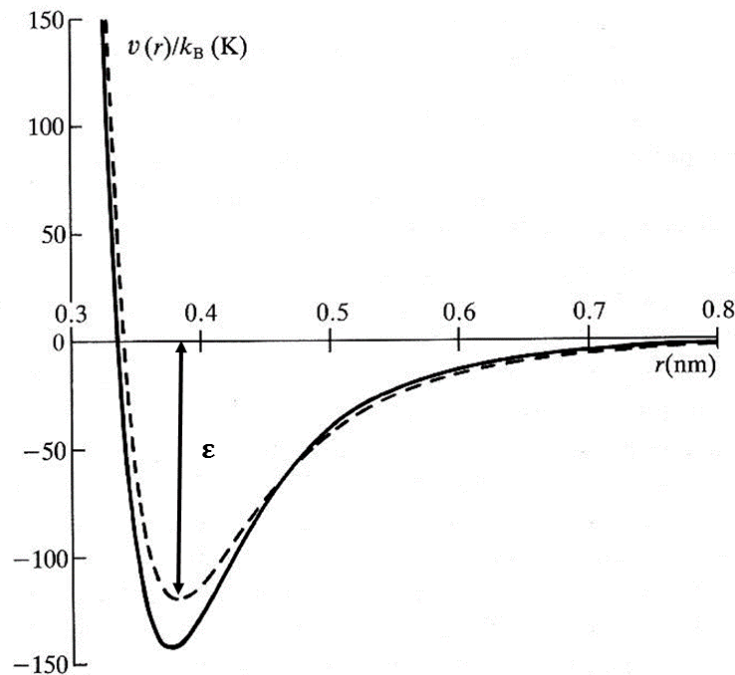


Figure 3.38. BBMS potential of argon (solid line). Effective Lennard-Jones potential used in simulation for liquid argon (dashed line). Adapted from ref. ¹⁶².

As can be seen in Figure 3.38, the LJ potential has a long attraction tail with $-1/r^6$, a valley with a depth of ϵ , and a growingly repulsive wall for distances smaller to $r \sim \sigma$. For ions this potential is not sufficient to represent the long range interactions. A simple approximation for these cases consist in adding a charge-charge interaction potential (v^{zz} , Equation 3.23) to Equation 3.21.

$$v^{zz}(r_{ij}) = \frac{z_i z_j}{4\pi\epsilon_0 r_{ij}} \quad \text{Equation 3.23}$$

Where z_i and z_j are the charges of the ions i and j , respectively, r_{ij} is the distance between the particles i and j and ϵ_0 is the vacuum permittivity.¹⁶²

3.2.2.3.1.2. Boundary Conditions

In numerical simulation it is impossible and unnecessary to simulate the whole universe. Usually a region of interest is chosen, this region has a certain border with the surrounding environment for the simulation to be conducted, the boundary conditions. These boundary conditions can be of various types thereby designated according to their characteristics (regular, spherical, *etc.*).

3.2.2.3.1.3. Sampling from Ensembles

For simplicity, it will be considered a macroscopic system of one component since the extension to a multi-component system is simple. The thermodynamic state of such system is usually defined by a small set of parameters (such as number of particles N , temperature T and pressure P), an ensemble. Other thermodynamic properties (density ρ , chemical potential μ , heat capacity C_v , *etc.*) can be derived by knowing the state and the fundamental equations of thermodynamics. Even quantities as the diffusion coefficient D , the shear viscosity η and the structure factor $S(k)$ are state functions: although they clearly say something about the microscopic structure and system dynamics, its values are completely dictated by few variables (e.g., NPT) which characterize the thermodynamic state and not by the atomic positions and many times that define the instantaneous mechanical state. Even quantities such as diffusion coefficient D , shear viscosity η , and the structure factor $S(k)$ are state functions: although they contain information about the microscopic structure and system dynamic, their value are completely dictated by the few variables (for example, NPT) that characterize the thermodynamic state and not by the many atomic positions and moments that define the instantaneous mechanic state. These positions and moments can be thought of as coordinates in a multidimensional space: phase space. For a system of N atoms, this space has dimensions $6N$. Let's use the Γ abbreviation for a particular point in the phase space and assume that one can write the instantaneous value of a given property A (for example, the potential energy) as a function $A(\Gamma)$. The system involves time so that Γ varies and hence a (Γ) as well.

The abbreviation Γ will be used now for a particular point of the space phase and it will be assumed that the instantaneous value of a property A can be written (potential energy, for example) as function $A(\Gamma)$. The system involves time in a way that Γ changes and, therefore, $A(\Gamma)$ also. It is reasonable to assume

that the ‘macroscopic’ property experimentally observable $A_{obs.}$ is, in reality, the temporal average of $A(\Gamma)$ in a very long time range $\langle A[\Gamma(t)] \rangle_{time}$, Equation 3.24.

$$A_{obs.} = \langle A \rangle_{time} = \langle A[\Gamma(t)] \rangle_{time} = \lim_{t_{obs.} \rightarrow \infty} \frac{1}{t_{obs.}} \int_0^{t_{obs.}} A[\Gamma(t)] dt \quad \text{Equation 3.24}$$

The equations that rule this temporal evolution, the Newton motions equations in a classical system, consists on a system of ordinary differentials equations: to solve them in a computer, with the desired accuracy, is possible for 1000 particles, but not for a true macroscopic number (for example, 10^{23}). On the other hand, it cannot be expected to be possible to extend the integration of Equation 3.24 to an infinite time, however it can be satisfactory to do the average over a long finite time, t_{obs} which is exactly what is done in simulations of molecular dynamics.

The temporal average (given by Equation 3.24) can be substituted by an average for all the members of the *ensemble* $\langle A \rangle_{ens.}$, ‘frozen’ in a given time, Equation 3.25.

$$A_{obs.} = \langle A \rangle_{ens.} = \langle A | \rho_{ens.} \rangle = \sum_{\Gamma} A(\Gamma) \rho_{ens.}(\Gamma) \quad \text{Equation 3.25}$$

In order to do that, some kind of motion equation is invented, i.e., a way to generate from one point of the state $\Gamma(\tau)$, one point of successive state $\Gamma(\tau+1)$ and the average is determined. But in order to use these equations, some conditions have to be followed:

- (i) The density of probability for the *ensemble* $\rho_{ens.}(\Gamma)$ should not vary as the system evolves;
- (ii) Any ‘reasonable’ initial distribution $\rho(\Gamma)$ should tend to the stationary solution;
- (iii) The ergocity [i.e., that has the same behavior averaged over time as averaged over the space of all the system's states (phase space)] must be maintained.

If these conditions are fulfilled, then it is possible to generate, from an initial state, the succession of points of the state that, at long term are given in accordance to the density of probability desired $\rho_{ens.}(\Gamma)$. In these circumstances, the average of the *ensemble* will be equal to a sort of ‘temporal average’.

$$A_{obs.} = \langle A \rangle_{ens.} = \frac{1}{\tau_{obs.}} \sum_{\tau=1}^{\tau_{obs.}} A[\Gamma(t)] \quad \text{Equation 3.26}$$

In Equation 3.26, τ is the calculation index about the state succession or generated trials τ_{obs} where τ_{obs} would be a high finite number in simulation. It is this way that Monte Carlo simulations are made.

3.2.2.3.1.4. The Metropolis Method

For example, the change in potential energy is calculated by computing the energy of the atom i with all other atoms before and after the motion.

$$\delta V_{nm} = \left(\sum_{j=1}^N v(r_{ij}^n) - \sum_{j=1}^N v(r_{ij}^m) \right) \quad \text{Equation 3.27}$$

In Equation 3.27, the sum over all atoms do not consider the atom i . if the new position (r_i^n , Figure 3.39A) have a lower energy, i.e., if the motion has $\delta V_{nm} \leq 0$, then the probability of the state n is lower than of state m and the new configuration is accepted. On the contrary, if the motion has $\delta V_{nm} > 0$, then it is accepted but with a probability of ρ_n/ρ_m . This ratio can be expressed as the Boltzmann factor $[\exp(-E/kT)]$ in the energy difference, Equation 3.28.

$$\frac{\rho_n}{\rho_m} = \frac{Z_{NVT}^{-1} \exp(-\beta V_n)}{Z_{NVT}^{-1} \exp(-\beta V_m)} = \frac{\exp(-\beta V_n) - \exp(\beta V_{nm})}{\exp(-\beta V_n)} = \exp(\beta V_{nm}) \quad \text{Equation 3.28}$$

Where $Z_{NVT} \left[\sum_i \exp(-\beta E_i) \right]$ is the partition function of the canonical distribution function with i being the index for the microstates of the system, β is defined as $1/k_B T$ and E_i is the total energy of the system in the respective microstate. To accept the motion with probability $\exp(-\beta V_{nm})$, a random number ξ is generated uniformly in (0,1). The random number is then compared with $\exp(-\beta V_{nm})$. If it is inferior to $\exp(-\beta V_{nm})$, the motion is accepted. The procedure is illustrated in Figure 3.39B.

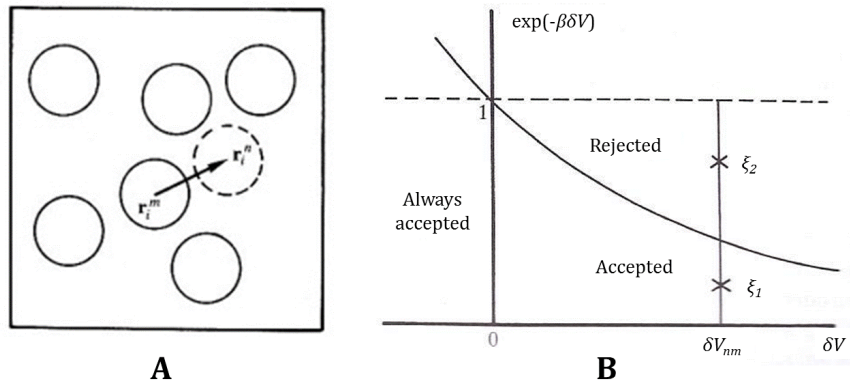


Figure 3.39. (A) The state n is generated from the state m by the movement of the atom i from position r_i^m to r_i^n . (B) Acceptance of the motions with $\delta V_m > 0$ in the Monte Carlo simulations. Adapted from ref. 162.

During the calculation, suppose that a particular motion $\delta V_m > 0$ is tried. If at this point a random number ξ_1 is chosen, the motion is accepted while if ξ_2 is chosen, the motion is rejected. During the calculation, the result is that the energy variation δV_m are accepted with probability $\exp(-\beta V_{nm})$.

If the motion has an energy $\delta V_m > 0$, than it is rejected, i.e., the system stay in the m state. In this case, the atom is retained in its old position and its old configuration is reconsidered as a new position of the chain. This procedure can be summarized noting that any motion is accepted (with $\delta V_m > 0$ or $\delta V_m \leq 0$) with probability $\min[1, \exp(-\beta V_{nm})]$ or $\min[1, \exp(-\Delta U/k_B T)]$.

The new positions can be generated by moving differently the polymer chain, for instance, a single segment (only one monomer moves) or an entire chain (translation) can move. The polymer can also move as a snake (slithering move, see Figure 3.40).



Figure 3.40. Slithering move from ref. ¹⁶³.

These simulations can withdraw various data as the radii of gyration (R_g) and contact analyses. These concepts and the centre of mass (CM) will be discussed in the next section once they are important to the discussion of the results.

3.2.2.3.1.5. Centre of Mass

In classical mechanics, the CM of a body is the point where one can consider that the entire body mass is concentrated. The centre of mass does not necessarily coincide with the centroid (Figure 3.41), it does not even need to be inside the body. For n particles, each with position r_i and mass m_i , the CM is given by Equation 3.29.

$$CM = \frac{1}{M} \sum m_i r_i = \frac{1}{\sum m_i} \sum m_i r_i \quad \text{Equation 3.29}$$

3.2.2.3.1.6. Radius of Gyration

The radius of gyration is given by the average of the distances between the centre of mass and all extreme points (of the molecule, in this case) as can be seen in Figure 3.41, and reflects the extension of the polymer.

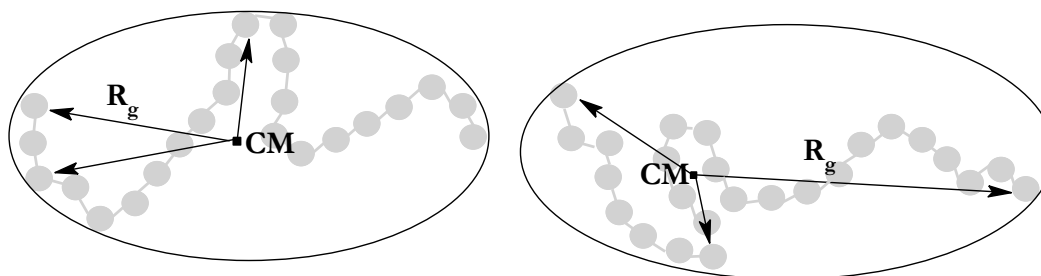


Figure 3.41. Identification of the CM and schematic illustration of the radius of gyration (R_g).

$$\langle R_g^2 \rangle^{1/2} = \left\langle \frac{\sum_{i=1}^N |r_i - r_{CM}|^2}{N_{seg}} \right\rangle^{1/2} \quad \text{Equation 3.30}$$

The square root of the average radius of gyration is, however, usually taken, Equation 3.30.

In Equation 3.30, r_i and r_{CM} are the positions of the segment i and the centre of mass of the molecule, respectively. The N_{seg} is the total number of segments in which the molecule is split. This property can also be configurationally determined by experimental techniques such as light scattering once it depends on particle size directly. The brackets correspond to the average over all possible conformations.

The swelling coefficient, α , is defined as the ratio of the root mean-square radius of gyration, $\langle R_g^2 \rangle^{1/2}$, of a chain and that of the corresponding chain, $\langle R_g^2 \rangle_0^{1/2}$, without substituents, Equation 3.31.

$$\alpha = \frac{\langle R_g^2 \rangle^{1/2}}{\langle R_g^2 \rangle_0^{1/2}} \quad \text{Equation 3.31}$$

3.2.2.3.1.7. Contact Analysis

Contact analysis is the process that provides the detailed information of the regions of contact of two bodies. It is considered, generally, that two particles come into contact when the distance between the centres of both particles in question is less than 8 Å. In this work, multiple figures with the probability distribution of two pyrene units being in touch will be illustrated (see Section 3.2.2.3.2.2.1).

A simple coarse-grained model has been adopted to describe the structure of pyrene-substituted polyions in solution, at various pH values, confined in a spherical volume. A polyelectrolyte (PE) is composed of a polyion (PI) and simple counter ions. A PI consists of a sequence of charged hard spheres (segments) connected by harmonic bonds with the chain flexibility regulated by angular force terms. The solvent enters the model only through its relative permittivity. All interactions are taken as pairwise additive. The total potential energy U of a system can be expressed as a sum of three contributions according to Equation 3.32.

$$U = U_{nonbond} + U_{bond} + U_{ang} \quad \text{Equation 3.32}$$

The nonbonded potential energy, $U_{nonbond}$, is given by Equation 3.33 whereas U_{bond} and U_{ang} are given by Equation 3.35 and Equation 3.36, respectively.

$$U_{nonbond} = \sum_{i<j} u_{ij}(r_{ij}) \quad \text{Equation 3.33}$$

$$u_{ij}(r_{ij}) = \begin{cases} \infty, & r_{ij} < R_i + R_j \\ \frac{Z_i Z_j e^2}{4\pi\epsilon_0\epsilon_r} \frac{1}{r_{ij}}, & r_{ij} \geq R_i + R_j \end{cases} \quad \text{Equation 3.34}$$

In Equation 3.33, the sum extends over the PI segments and simple ions with u_{ij} representing the electrostatic potential plus hard-sphere repulsion according to Equation 3.34.

In Equation 3.34, Z_i and Z_j are, respectively, the valence of particle i and j , R_i and R_j are, respectively, the radius of particle i and j , r_{ij} the distance between particles i and j , e the elementary charge, ϵ_0 the permittivity of vacuum, and ϵ_r the relative permittivity of the solvent. The bond potential energy of the chains, U_{bond} , is given by Equation 3.35.

$$U_{bond} = \sum_{i=1}^{N_{seg}-1} \frac{k_{bond}}{2} (r_{i,i+1} - r_0)^2 \quad \text{Equation 3.35}$$

In Equation 3.35, N_{seg} is the number of segments in which the molecule is split. Furthermore, $r_{i,i+1}$ is the distance between two connected segments, $k_{bond} = 0.4 \text{ N.m}^{-1}$ the bond force constant, and $r_0 = 5.0 \text{ \AA}$ the equilibrium separation of a bond. The angular potential energy of the chains, U_{ang} , is given by Equation 3.36.

$$U_{ang} = \sum_{i=2}^{N_{seg}-1} \frac{k_{ang}}{2} (\alpha_i - \alpha_0)^2 \quad \text{Equation 3.36}$$

In Equation 3.36, α_i is the angle formed by the vectors $r_{i+1} - r_i$ and $r_{i-1} - r_i$, $k_{ang} = 1.7 \times 10^{-24} \text{ J.deg}^{-2}$ the angular force constant, and $\alpha_0 = 180^\circ$ the equilibrium angle.

To simulate excimer formation, attractive Lennard-Jones potential was imposed between two chosen segments according to Equation 3.22 with $\sigma = 5 \text{ \AA}$ and $\epsilon = 30 \text{ kJ.mol}^{-1}$.¹⁶⁴ For simplicity, the same hard-sphere radius $R_i = 2 \text{ \AA}$ has been used for the chain segments and simple ions. The polyion and its counter ions are enclosed in a spherical cell (r_{sph}) with a radius of 400 \AA and 1200 \AA for 28 and 200 segments, respectively. Throughout, $T = 298 \text{ K}$ and $\epsilon_r = 78.4$ ¹⁶⁵ have been used.

3.2.2.3.2. Results and Discussion

3.2.2.3.2.1. System Characterization from Statistical Estimates

For each m (see Equation 3.13) value and for each set of chains with an average of n_{AA} segments (the distance $d = n_{AA}$), it is possible to generate the probability distribution for distances (p), which corresponds to the probability of finding two substituents at each distance, expressed in terms of number of segments. For this, we have used a basis of $n_c = 1 \times 10^5$ chains for which p is given by Equation 3.37.

$$p(\%) = N_i n_c \times 100$$

Equation 3.37

N_i represents the number of chains with i substituents. In each value of i , n_c chains with length d are generated, with the substituents randomly positioned (see Appendix E). The selected values of i are in the range 2: n_{AA} , for chains with $n_{AA} \leq 30$, and $i = m \pm 2m^{1/2}$, for $n_{AA} > 30$, this corresponding to an interval centred in m with an amplitude of $4m^{1/2}$ with m being the mean number of Py units per chain. Finally, all distances between consecutive substituents are determined, and averaged.

The probability of finding two pyrene groups at a distance d , measured in terms of segments, was further investigated for chains of arbitrary labelling, and is represented in Figure 3.42 for the short and long chain PAA polymers [PAAMePy(2) and PAAMePy(450), respectively].

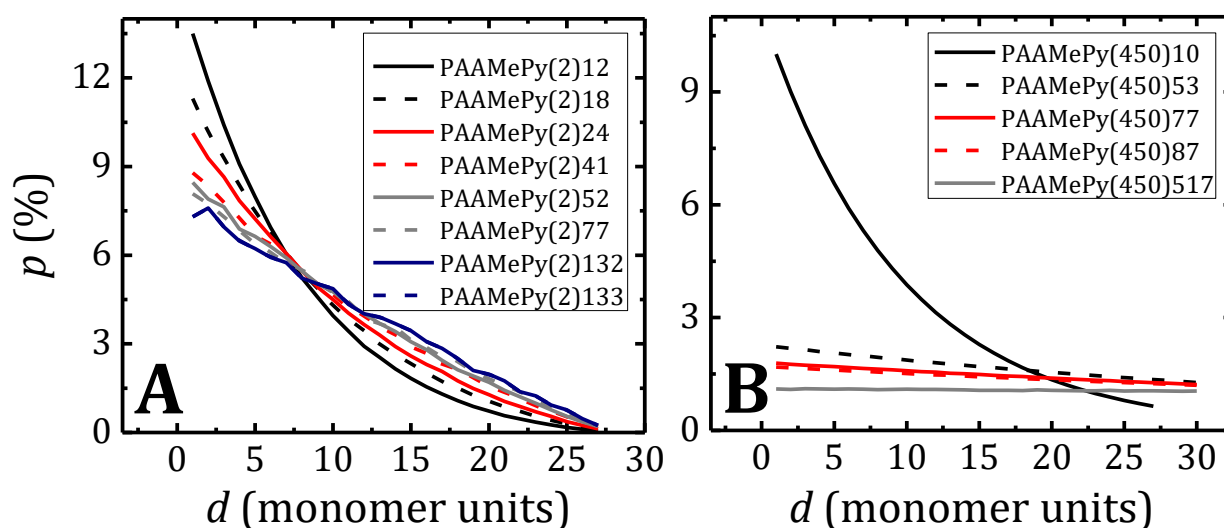


Figure 3.42. Probability (p) of finding two sequential pyrene groups at a distance d in the (A) short, 28 AA units [the analogous of PAAMePy(2)] and (B) long, 6250 AA units [the analogous of PAAMePy(450)] chain polymers.

From Figure 3.42, it can be seen that the probability of finding two pyrene groups at short distances is higher than at longer distances. The explanation for these results is related with the fact of having more cases for shorter distances. For example, in the case of PAAMePy(2) polymers which consists in a polymer with 28 monomeric units, it is only possible to have one polymer configuration with pyrene groups, i.e. with 26 monomer units of distance. In the contrary, there are 26 possible different ways of having them at one monomer unit of distance. Note also, that for the PAAMePy(450)517 polymer the decrease in probability with distance is much less marked than in the other 3 cases [especially, PAAMePy(450)10]. In other words, the relative probability for larger distances is higher, as could be expected for a less marked, longer chain. Comparing PAAMePy(2)77 and PAAMePy(450)77, one can see that the probability of having the pyrene units at shorter distances for the shortest polymer is higher than for the longest.

3.2.2.3.2.2. Simulation

Considering the results from the previous section, which indicate a higher probability of shorter distances, pyrene groups were placed at a distance of 4 monomer units in the simulation studies. Note that the probability of finding two pyrene segments at 0, 1, 2, 3 and 4 monomer units of distance is similar. Besides, it is unlikely that, in the actual systems, two large units (such as the pyrene chromophores) find themselves in contiguous positions. Also, this distance facilitates the inspection of the results as the charge of the chain increases. This distance was further used in the MC studies to impose the location of the pyrene probes in different regions of the PAA skeleton, and assess the influence of the different positions of a potentially interacting pair. For example in the case of the PAA(2) polymer, with a chain consisting of 28 monomer units, this was made with positions 1 and 6 (1-6), 2-7, 3-8, 5-10, 7-12 and 12-17. The direct study of systems corresponding to the longer 6250 monomer units chains [PAAMePy(450)] was not conducted, because of the high computational cost. However, to simulate a long polymer skeleton, a chain composed by 200 monomer units (with two “pyrene” units) was studied. In this last case, a chain with 200 monomer units, the pyrene positions considered were 1-6, 1-100, 1-200, 48-53 and 98-103.

In this work, we have considered systems containing one polyion with an attractive potential between two segments, and its counter ions. We have varied (i) the number of segments of the polyion ($N_{\text{seg}} = 28$ and 200), (ii) the charge of the segment of the polyion (Z_{seg}), simulating variations in the pH, (iii) the position of the two pyrene units along the chains, denoted according to i - j where i and j are the index of the substituted segments. Typically, the segment charges vary between 0 and 1, but values as high as 1.5 was assessed. Pyrene beads were placed in different positions, including: (1) one in one end, the other at increasing distances and (2) at a specific, relatively short distance, along the chain.

The interpretation of the MC results is largely based on the contact analysis. For each configuration, the segments of the chain at a distance inferior to 3.5 Å (the known value of pyrene dimer distances, see Section 1.3.2.1.1), considered in contact, are counted, and those corresponding to Py-Py segments identified. These values are accumulated for the whole simulation, and, in what follows, n_{total} corresponds to the total number of contacts, irrespective of the type of segments involved, while $n_{\text{Py-Py}}$ is the value of the Py-Py contacts.

The analysis of the effect of positioning had a two purposes: (i) assess the contribution made in each situation, and (ii) try and suggest a prevalent positioning from the overall results. If the synthetic route, in experimental terms, promotes the prevalence of a certain region it is likely that a parallel with the simulation results for the same region can be established.

In the next section, the results of the simulations of the short polymer chain (28 monomers) and long polymer chain (200 monomers) both with 2 pyrene units are showed. The simulation for the number of monomers corresponding to the large polymer of 450 kg/mol (6250 monomers) was not made, as previously explained, simply because the computational cost would be very high. However, even the

most probed long chain polymer has approximately the same ratio of pyrene/monomer units of the one used in the MC simulation allowing this way to understand the influence of any variable. These results allow easily verifying the effect of the increase in the polymer chain and, for each of them, the result of increased charge.

3.2.2.3.2.2.1. Effect of Charge/pH

Figure 3.43 and Figure 3.44 represent the evolution of the term α (related to the radius of gyration, see Equation 3.31 in Section 3.2.2.3.1.6) as the segment charge (Z_{seg}) is increased, for pyrene units at different positions. Figure 3.43A present this variation for the different short polymers with a distance of 4 monomers between the pyrene units, panel B however present it for four different polymers with an increasing monomer distance (4, 6, 12 and 26) always with one of the pyrene units in one end of the polymer chain.

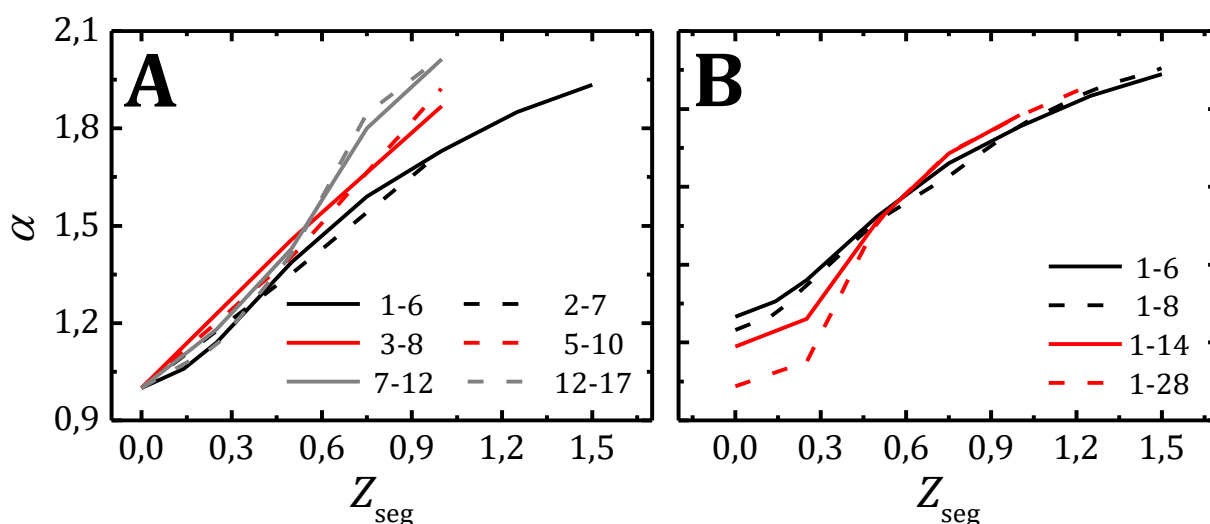


Figure 3.43. Variation of the swelling coefficient (α) for a short “polymers”, 28 segments [the analogous of PAAMePy(2)] with Z_{seg} for “pyrene” groups at positions (A) 1-6, 2-7, 3-8, 5-10, 7-12, 12-17 and (B) 1-6, 1-8, 1-14 and 1-28.

In every case demonstrated in Figure 3.43, it is seen that the value increases with segment charge, irrespectively of the chain being long or short and irrespectively of the labelling distance or relative positions. This is the expected behaviour, determined both by inter-segment repulsion and counter ion release. It is also seen that there is some tendency for a lower radius of gyration if the substituents are placed further apart, but this effect becomes negligible as the charge of the chain increases especially for the highest distances between pyrene units (Figure 3.43B).

In Figure 3.44B, two sets of data (Figure 3.43A and Figure 3.44A) were normalized between 0 and 1 in order to make a valid comparison between short and long polymers.

From Figure 3.44B, it is possible to see that, with the same segment charge, the longest polymer has higher (normalized) values of α . In other words, this means that the longest polymer is more affected by the charge, i.e., should have a smaller pK_a . This is, in fact, verified in the experimental data (Table 3.7 in Section 3.2.2.1.1) with the PAAMePy(2) and PAAMePy(450) polymers with pK_a values between 5.66 and 6.94 and 4.80 and 5.37, respectively.

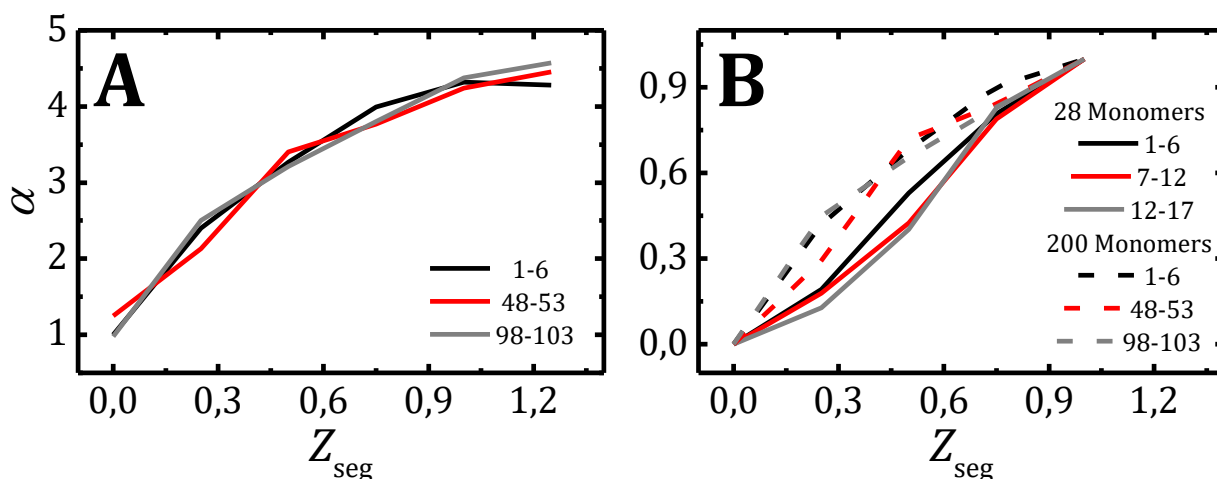


Figure 3.44. (A) Variation of α for a long “polymers”, 200 segments with Z_{seg} for “pyrene” groups at positions 1-6, 48-53, 98-103 and (B) normalization (between 0 and 1) of α for a short and long “polymers”, with the same pyrene relative positions and chain location.

Figure 3.45 shows the number of contacts between pyrene units (i.e., dimer formation) for pyrene at two different positions (1-6 and 7-12) increasing the charge for the shortest polymer (28 monomers) and the snapshot of the conformation of the polymers at these charges.

When the pH values increase (z_{mon}), the chain is extended and the probability to form ground state dimer stop existing at $z_{mon} = 1.5$ and 1 for the pyrene units at the positions 1-6 and 7-12, respectively. The presence of the pyrene units in one end of the polymer appears to favour the contact between pyrene units and seems to show (most evident for $z_{mon} = 0.5$) that the flexibility of the chain is greater at the ends than in the rest of the chain which is therefore an explanation for the need to further increase z_{mon} to reduce the probability of pyrene–pyrene contacts. When looking at the experimental data (Table 3.7), it is possible to have an indication of the positions of the pyrene units along the chain. For instance, the most labelled polymers with 2 and 450 kg/mol [PAAMePy(2)18, 24 and 41 and PAAMePy(450)10] seems to not show any significant variations in the P_M-P_E values (which indicate the absence of dimers, Section 1.3.2.1.2) with the pH for higher values of pH [except for PAAMePy(2)12] compared with the less labelled polymers [PAAMePy(2)52, 77, 132 and 133 and PAAMePy(450)77 and 517]. This data seems to indicate that for these polymers (most labelled), the pyrene units are located nearer to one of the extremity of the labelled chain [with exception for PAAMePy(2)12]. This make sense since if one

Polymers

consider that the labelling is random, the probability of a pyrene unit being at one determined position (as the extremity of the polymer) is higher the greater is the labelling content. For the PAAMePy(450) this seems to not that relevant since the pH values in which the P_M-P_E is stabilized is around the same ($\sim 6.5-8.0$). The fact that P_M-P_E is not zero at the highest pH in the experimental data is due to dynamic contribution of dimers (excimer formation).

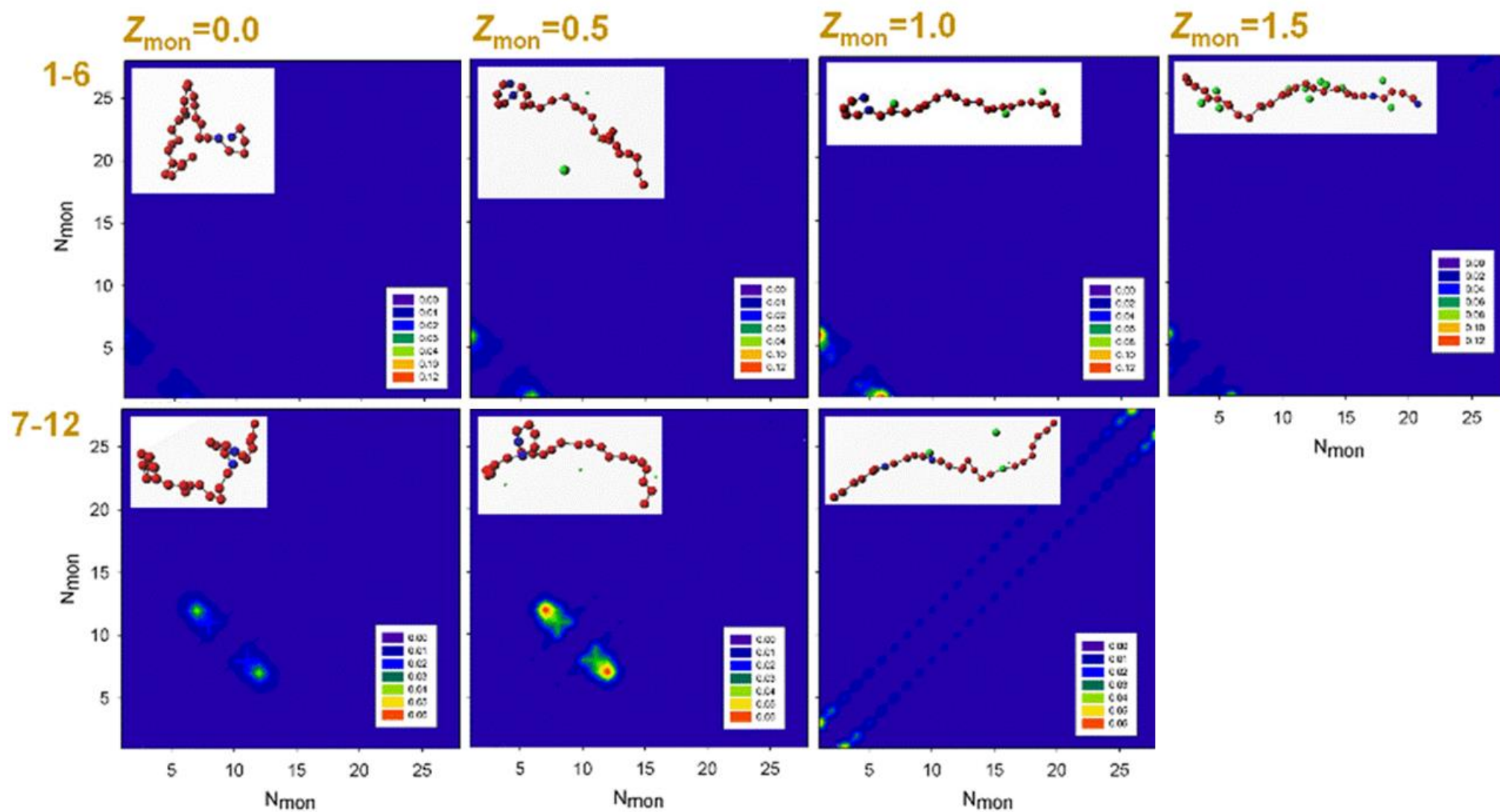


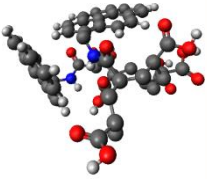
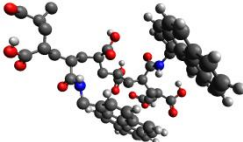
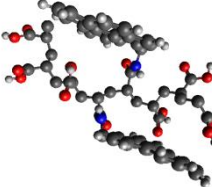

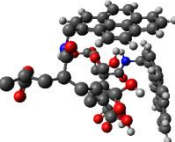
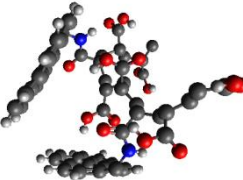
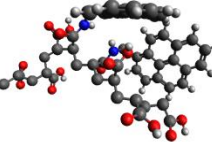

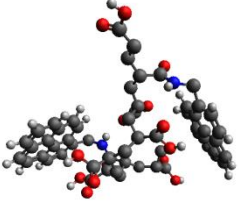
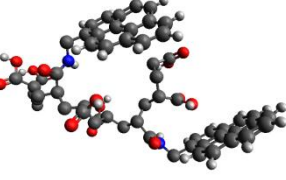
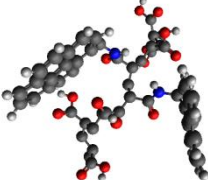
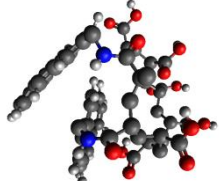
Figure 3.45. Bidimensional graphic of probability of contacts for a polymer with 28 monomers with pyrene units at positions 1 and 6 (top panel) and 7 and 12 (bottom panel) with increasing charge.

3.2.2.3.2.3. Molecular Dynamics (MD)

Four systems (oligomers with 8 monomers) with pyrene units in different positions were considered, with pyrene units at positions 2 and 7, 3 and 6, 4 and 5 and 7 and 8 in water at 298 K. These oligomers have the same structural properties of the PAAMePy but since the computational cost would be enormous, only oligomers were studied. More details can be found in Chapter 7, Section 7.3.1.

The three most probable occurrences for each type of conformations for these oligomers is included in the Table 3.10, the remaining (less probable) occurrence can be found in Table 3.11 in the Supplementary information (Section 3.2.2.3.4).

Table 3.10. Overview of the three most probable conformations sampled during the last 60 ns of the production run at 298 K for PAAMePy oligomers with the pyrene units in positions 2-7, 3-6, 4-5 and 7-8 in aqueous solution. p , R_{ee} , d_{py-py} and l_p are presented as well.

Nº	2-7	3-6	4-5	7-8
1	 $p = 78.21\%$, $R_{ee} = 12.4 \text{ \AA}$ $d_{py-py} = 6.5 \text{ \AA}$, $l_p = 2.9$	 $p = 79.38\%$, $R_{ee} = 13.9 \text{ \AA}$ $d_{py-py} = 7.9 \text{ \AA}$, $l_p = 3.7$	 $p = 61.15\%$, $R_{ee} = 14.7 \text{ \AA}$ $d_{py-py} = 9.3 \text{ \AA}$, $l_p = 4.1$	 $p = 59.43\%$, $R_{ee} = 13.1 \text{ \AA}$ $d_{py-py} = 6.2 \text{ \AA}$, $l_p = 3.3$
2	 $p = 19.29\%$ $R_{ee} = 14.7 \text{ \AA}$ $d_{py-py} = 6.9 \text{ \AA}$, $l_p = 4.1$	 $p = 12.3\%$, $R_{ee} = 13.8 \text{ \AA}$ $d_{py-py} = 9.4 \text{ \AA}$, $l_p = 3.6$	 $p = 15.03\%$, $R_{ee} = 15.4 \text{ \AA}$ $d_{py-py} = 7.9 \text{ \AA}$, $l_p = 4.5$	 $p = 16.46\%$, $R_{ee} = 14.3 \text{ \AA}$ $d_{py-py} = 9.5 \text{ \AA}$, $l_p = 3.9$
3	 $p = 1.45\%$ $R_{ee} = 11.3 \text{ \AA}$ $d_{py-py} = 11.8 \text{ \AA}$, $l_p = 2.4$	 $p = 3.6\%$, $R_{ee} = 12.8 \text{ \AA}$ $d_{py-py} = 10.1 \text{ \AA}$, $l_p = 3.1$	 $p = 11.38\%$, $R_{ee} = 12.1 \text{ \AA}$ $d_{py-py} = 9.5 \text{ \AA}$, $l_p = 2.8$	 $p = 8.38\%$, $R_{ee} = 9.3 \text{ \AA}$ $d_{py-py} = 5.2 \text{ \AA}$, $l_p = 1.7$

From Table 3.10, one can see that none of the most probable configuration have dimer, either because the distance is too high, either because the pyrene units are not parallel or both. The end-to-end distance (Section 3.1.3, R_{ee}) and the pyrene-pyrene distances (d_{Py-Py}) are illustrated in Figure 3.46.

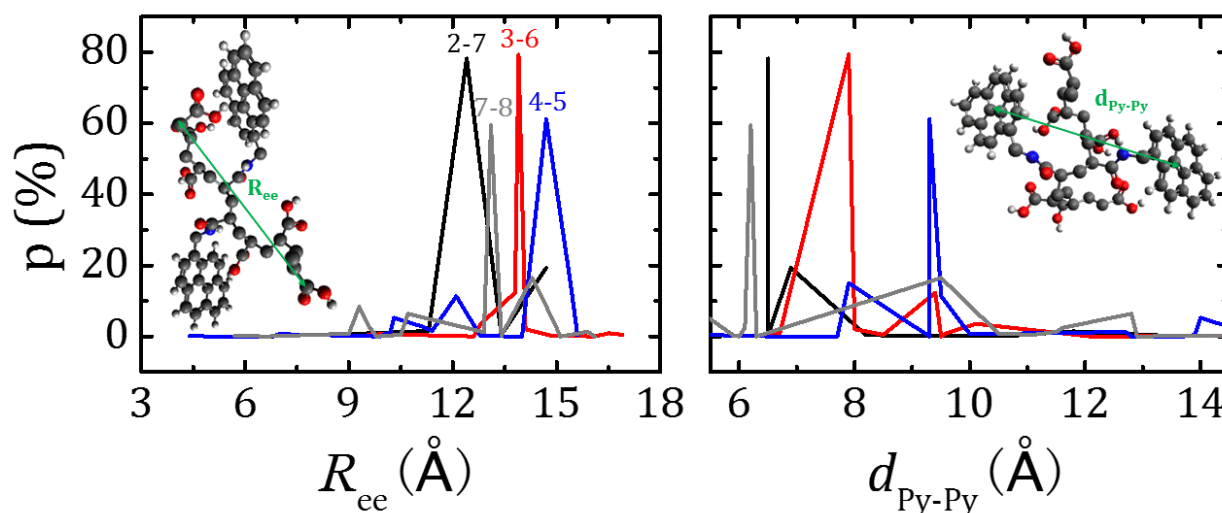


Figure 3.46. From left to right. Distribution of the end-to-end distance (R_{ee}) and the distance between the two pyrene units (d_{Py-Py}). The points considered in each case to define the relevant distances are indicated in the representation included in the plots.

From the inspection of Figure 3.46A, one can observe that all the configurations are quite stiff ($R_{ee}^2 \ll nl$, Section 3.1.3) with exception for the polymer with pyrene units in positions 4 and 5, where two configurations are flexible with a total of occurrence probability of 0.16% (see Table 3.11 in Supplementary Information).

From the observation of Figure 3.46B, one can verify that the only structure that allow the formation of *GSD* is the one with pyrene units closed to each other in the end of the chain (7-8), since only in this case the pyrene units have been found in distances below 5.5 Å. Beside the distance, the pyrene units should be coplanar. The inspection of the configurations for the pyrene units at these distances showed that the occurrence of *GSD* for this oligomer is only ~1% (see Table 3.11 in Supplementary Information).

3.2.2.3.3. Summary

The kinetics of a PAA polymer labelled with pyrene was investigated in water as a function of the pH and with the addition of anionic and neutral surfactants. For PAAMePy(2)52, the kinetic scheme is identical to the one found for these polymers in good solvents, with three species although it was discussed elsewhere in certain circumstances it can have four species. The kinetics of this pyrene labelled polymer was further compared with the study of some pyrene oligomers, e.g. 1Py(10)1Py, Chapter 3. For the PAAMePy polymers, it is shown that the excimer-to-monomer reversibility (seen as

an additional component in the monomer emission decay) is present and cannot be discarded in the analysis of the kinetics of these polymers.

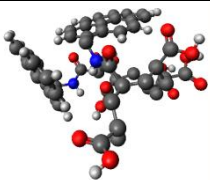
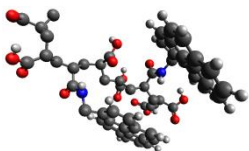
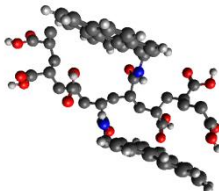
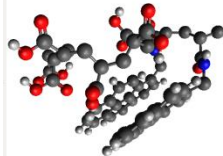
From the joint observation of molecular simulation and photophysical data, one can conclude that:

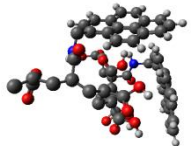
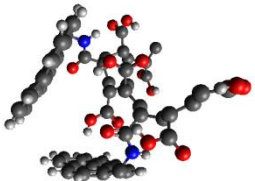
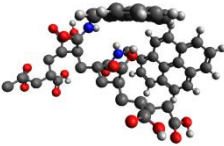
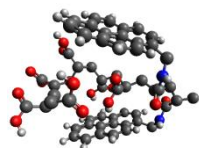
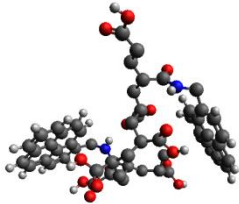
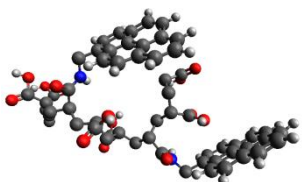
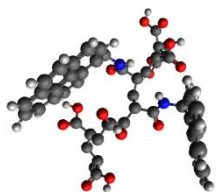
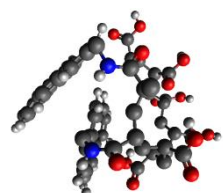
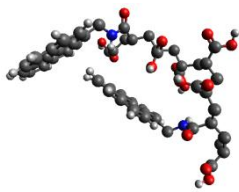
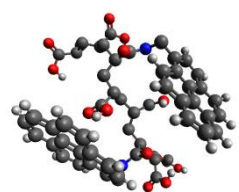
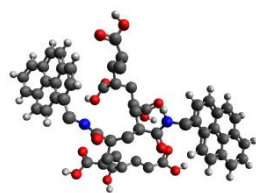
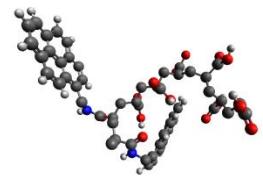
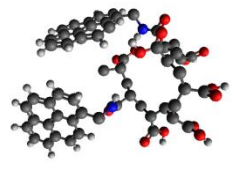
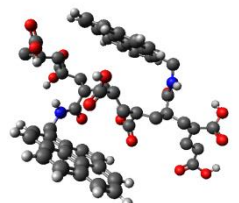
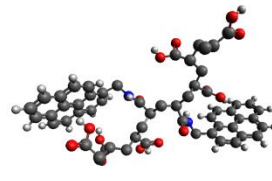
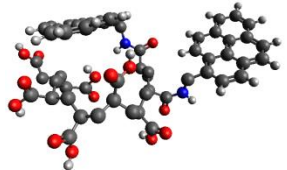
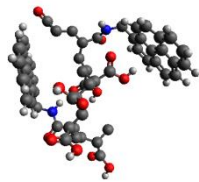
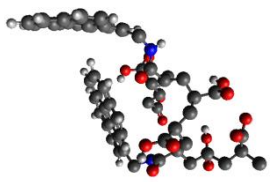
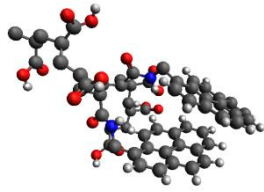
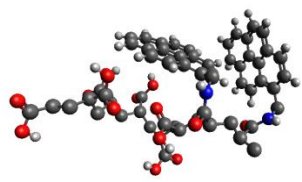
- The probability to find the pyrene units at shorter distances is higher although less important for the PAAMePy(450) polymers;
- The expansion of the chain increase with the charge for all polymers, especially for relatively small charge values when the two pyrene units are at higher distances;
- The polymers with the longer chains are more affected by the charge, i.e., display lower pK_a values;
- The flexibility of the chain in the ends is higher (Monte Carlo), the flexibility of the chain with the pyrene groups in the middle of the oligomer chain (4-5) is higher than with 7-8 (dynamics);
- The presence of GSD is only seen with the pyrene groups both at one extremity of the oligomer chain (7-8), with a probability of occurrence of $\sim 1\%$.
- GSD stop existing at higher charge values when the pyrene groups are both located at one extremity of the chain;
- Pyrene groups are in close proximity and at one extremities of the polymer chain are more likely to interact and be responsible by excimer formation through the formation of GSD.

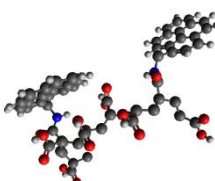
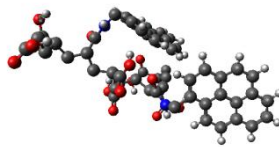
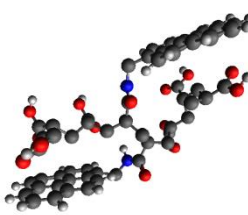
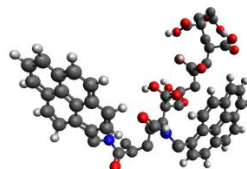
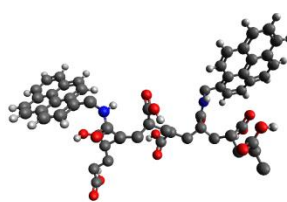
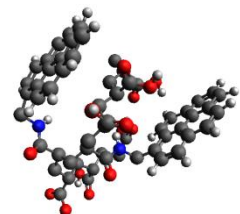
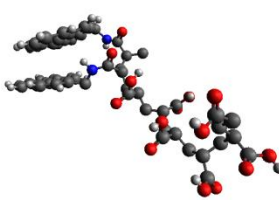
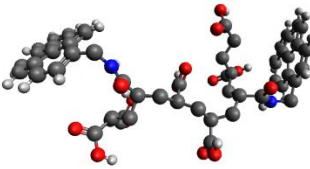
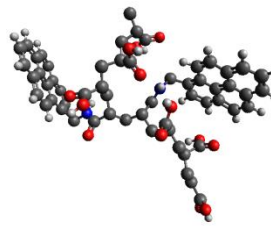
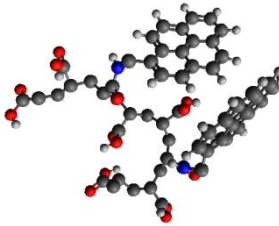
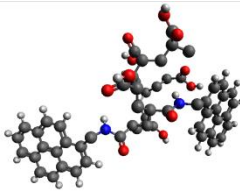
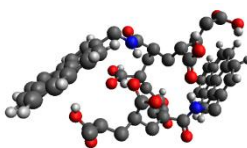
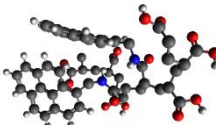
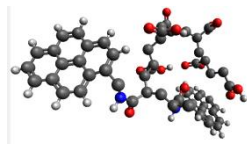
3.2.2.3.4. Supplementary Information


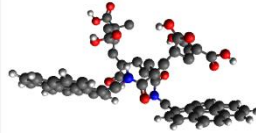
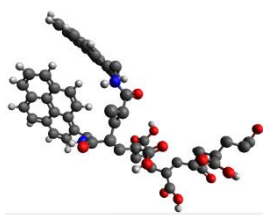
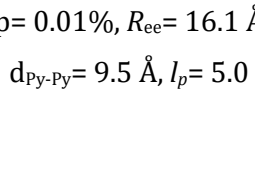
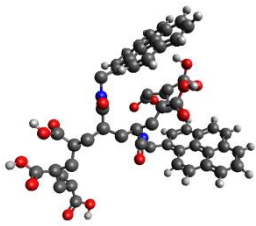
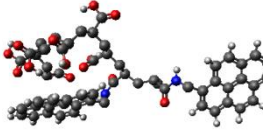
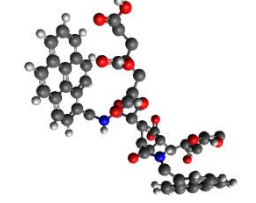
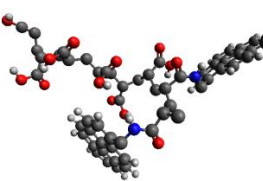
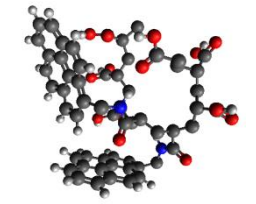
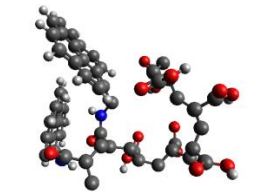
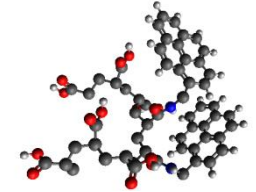
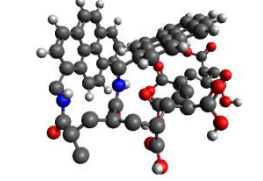
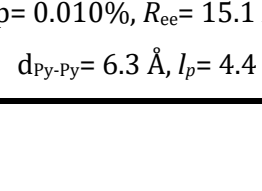
All the possible conformations [with respective occurrence probability (p), R_{ee} , d_{Py-Py} and l_p] are presented in Table 3.11.

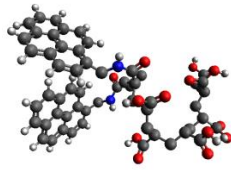
Table 3.11. Overview of the conformations sampled during the last 60 ns of the production run at 298 K for PAAMePy oligomers with the pyrene units in positions 2-7, 3-6, 4-5 and 7-8 in aqueous solution. p , R_{ee} , d_{Py-Py} and l_p are presented as well.

N°	2-7	3-6	4-5	7-8
1	 $p= 78.21\%$, $R_{ee}= 12.4 \text{ \AA}$ $d_{Py-Py}= 6.5 \text{ \AA}$, $l_p= 2.9$	 $p= 79.38\%$, $R_{ee}= 13.9 \text{ \AA}$ $d_{Py-Py}= 7.9 \text{ \AA}$, $l_p= 3.7$	 $p= 61.15\%$, $R_{ee}= 14.7 \text{ \AA}$ $d_{Py-Py}= 9.3 \text{ \AA}$, $l_p= 4.1$	 $p= 59.43\%$, $R_{ee}= 13.1 \text{ \AA}$ $d_{Py-Py}= 6.2 \text{ \AA}$, $l_p= 3.3$

Nº	2-7	3-6	4-5	7-8
2	 <p>p= 19.29% R_{ee}= 14.7 Å d_{py-py}= 6.9 Å, l_p= 4.1</p>	 <p>p= 12.3%, R_{ee}= 13.8 Å d_{py-py}= 9.4 Å, l_p= 3.6</p>	 <p>p= 15.03%, R_{ee}= 15.4 Å d_{py-py}= 7.9 Å, l_p= 4.5</p>	 <p>p= 16.46%, R_{ee}= 14.3 Å d_{py-py}= 9.5 Å, l_p= 3.9</p>
3	 <p>p= 1.45% R_{ee}= 11.3 Å d_{py-py}= 11.8 Å, l_p= 2.4</p>	 <p>p= 3.6%, R_{ee}= 12.8 Å d_{py-py}= 10.1 Å, l_p= 3.1</p>	 <p>p= 11.38%, R_{ee}= 12.1 Å d_{py-py}= 9.5 Å, l_p= 2.8</p>	 <p>p= 8.38%, R_{ee}= 9.3 Å d_{py-py}= 5.2 Å, l_p= 1.7</p>
4	 <p>p= 0.51% R_{ee}= 13.4 Å d_{py-py}= 6.5 Å, l_p= 3.4</p>	 <p>p= 2.09%, R_{ee}= 14.1 Å d_{py-py}= 8.0 Å, l_p= 3.8</p>	 <p>p= 5.25%, R_{ee}= 10.3 Å d_{py-py}= 14.0 Å, l_p= 2.0</p>	 <p>p= 6.39%, R_{ee}= 10.7 Å d_{py-py}= 12.8 Å, l_p= 2.2</p>
5	 <p>p= 0.39% R_{ee}= 8.2 Å d_{py-py}= 8.2 Å, l_p= 1.3</p>	 <p>p= 0.92%, R_{ee}= 16.5 Å d_{py-py}= 9.6 Å, l_p= 5.3</p>	 <p>p= 2.82%, R_{ee}= 11.1 Å d_{py-py}= 16.0 Å, l_p= 2.4</p>	 <p>p= 2.44%, R_{ee}= 9.6 Å d_{py-py}= 11.6 Å, l_p= 1.8</p>
6	 <p>p= 0.09%</p>	 <p>p= 0.70%, R_{ee}= 9.9 Å</p>	 	 <p>p= 2.4%, R_{ee}= 15.0 Å</p>

Nº	2-7	3-6	4-5	7-8
7	$R_{ee} = 11.3 \text{ \AA}$ $d_{py-py} = 10.6 \text{ \AA}$ $l_p = 2.4$	$d_{py-py} = 6.7 \text{ \AA}$, $l_p = 1.9$	$p = 1.58\%$, $R_{ee} = 11.4 \text{ \AA}$ $d_{py-py} = 4.1 \text{ \AA}$, $l_p = 2.5$	$d_{py-py} = 6.1 \text{ \AA}$, $l_p = 4.3$
	 <p>$p = 0.07\%$ $R_{ee} = 11.3 \text{ \AA}$ $d_{py-py} = 13.6 \text{ \AA}$ $l_p = 2.4$</p>	 <p>$p = 0.49\%$, $R_{ee} = 16.9 \text{ \AA}$ $d_{py-py} = 8.5 \text{ \AA}$, $l_p = 5.5$</p>	 <p>$p = 1.27\%$, $R_{ee} = 10.2 \text{ \AA}$ $d_{py-py} = 12.7 \text{ \AA}$, $l_p = 2.0$</p>	 <p>$p = 1.34\%$, $R_{ee} = 15.9 \text{ \AA}$ $d_{py-py} = 11.5 \text{ \AA}$, $l_p = 4.8$</p>
8		 <p>$p = 0.34\%$, $R_{ee} = 14.8 \text{ \AA}$ $d_{py-py} = 16.7 \text{ \AA}$, $l_p = 4.2$</p>	 <p>$p = 0.70\%$, $R_{ee} = 7.0 \text{ \AA}$ $d_{py-py} = 10.0 \text{ \AA}$, $l_p = 0.9$</p>	 <p>$p = 1.22\%$, $R_{ee} = 12.9 \text{ \AA}$ $d_{py-py} = 5.1 \text{ \AA}$, $l_p = 3.2$</p>
	9		 <p>$p = 0.08\%$, $R_{ee} = 12.4 \text{ \AA}$ $d_{py-py} = 17.2 \text{ \AA}$, $l_p = 2.9$</p>	 <p>$p = 0.41\%$, $R_{ee} = 15.6 \text{ \AA}$ $d_{py-py} = 13.9 \text{ \AA}$, $l_p = 4.7$</p>
10			 <p>$p = 0.07\%$, $R_{ee} = 9.2 \text{ \AA}$ $d_{py-py} = 6.1 \text{ \AA}$, $l_p = 1.6$</p>	 <p>$p = 0.15\%$, $R_{ee} = 4.4 \text{ \AA}$ $d_{py-py} = 15.0 \text{ \AA}$, $l_p = 0.4$</p> <p>(f)</p>
	11			 <p>$p = 0.26\%$, $R_{ee} = 5.7 \text{ \AA}$</p>

Nº	2-7	3-6	4-5	7-8
12		<p>$p = 0.02\%$, $R_{ee} = 12.6 \text{ \AA}$ $d_{\text{Py-Py}} = 12.1 \text{ \AA}$, $l_p = 3.0$</p> 	<p>$p = 0.11\%$, $R_{ee} = 12.8 \text{ \AA}$ $d_{\text{Py-Py}} = 6.0 \text{ \AA}$, $l_p = 3.1$</p> 	<p>$d_{\text{Py-Py}} = 14.2 \text{ \AA}$, $l_p = 0.6$</p> 
		<p>$p = 0.01\%$, $R_{ee} = 16.1 \text{ \AA}$ $d_{\text{Py-Py}} = 9.5 \text{ \AA}$, $l_p = 5.0$</p> 	<p>$p = 0.08\%$, $R_{ee} = 5.8 \text{ \AA}$ $d_{\text{Py-Py}} = 12.8 \text{ \AA}$, $l_p = 0.6$</p> 	<p>$p = 0.25\%$, $R_{ee} = 13.4 \text{ \AA}$ $d_{\text{Py-Py}} = 5.9 \text{ \AA}$, $l_p = 3.4$</p> 
13			<p>$p = 0.04\%$, $R_{ee} = 9.9 \text{ \AA}$ $d_{\text{Py-Py}} = 9.3 \text{ \AA}$, $l_p = 1.9$</p> 	<p>$p = 0.07\%$, $R_{ee} = 9.6 \text{ \AA}$ $d_{\text{Py-Py}} = 14.6 \text{ \AA}$, $l_p = 1.8$</p> 
			<p>$p = 0.02\%$, $R_{ee} = 14.0 \text{ \AA}$ $d_{\text{Py-Py}} = 13.7 \text{ \AA}$, $l_p = 3.8$</p> 	<p>$p = 0.033\%$, $R_{ee} = 16.1 \text{ \AA}$ $d_{\text{Py-Py}} = 12.9 \text{ \AA}$, $l_p = 5.0$</p> 
14			<p>$p = 0.01\%$, $R_{ee} = 5.1 \text{ \AA}$ $d_{\text{Py-Py}} = 7.7 \text{ \AA}$, $l_p = 0.5$</p> <p>(f)</p> 	<p>$p = 0.030\%$, $R_{ee} = 9.8 \text{ \AA}$ $d_{\text{Py-Py}} = 6.3 \text{ \AA}$, $l_p = 1.8$</p> 
				<p>$p = 0.010\%$, $R_{ee} = 15.1 \text{ \AA}$ $d_{\text{Py-Py}} = 6.3 \text{ \AA}$, $l_p = 4.4$</p> 
15				
16				

Nº	2-7	3-6	4-5	7-8
17			$p = 0.003\%$, $R_{ee} = 6.8 \text{ \AA}$ $d_{py-py} = 6.8 \text{ \AA}, l_p = 0.9$	 $p = 0.003\%$, $R_{ee} = 6.6 \text{ \AA}$ $d_{py-py} = 6.0 \text{ \AA}, l_p = 0.8$

3.3. Poly(N-isopropylacrilamide) Pyrene Labelled Polymers

3.3.1. Introduction

3.3.1.1. Synthesis of Polymers

There are several mechanisms for polymer synthesis but according to the scope of the present thesis, emphasis will be given to free radical polymerization.

A free radical polymerization is one type of chain polymerization. This kind of polymerization has three common features:

- (i) Initiation: a reactive species is generated and attacks the first monomer molecule.
- (ii) Propagation: a large number of further monomers are sequentially added to give the long polymer chain, still retaining the reactive end groups.
- (iii) Termination: the reactive end groups are deactivated.

In the case of radical polymerization the reactive species is a free radical.

A free radical $R\cdot$ is a species containing a spare unpaired electron. It is highly reactive and undergoes reactions to extract an electron from another substrate to produce a full complement of electrons.

Monomers for addition polymerization normally contains double bonds and are of the general formula $CH_2=CR_1R_2$.

Generally, this kind of polymerization requires an initiator. Activation is needed (termed 'initiation' for polymers) and is produced by splitting an initiator molecule I (as 2,2'-Azobisisobutyronitrile, AIBN) homolytically, usually by thermal degradation, allowing the odd-electron species to react with the monomers M by opening the double bonds. In general terms this can be written as seen in Scheme 3.4 to Scheme 3.8.



Deactivation of the growth process is called termination and occurs when two of these radical species ($R\bullet$ or $RM_x\bullet$) combine to produce a 'dead' polymer (RM_x-M_xR) as follows (Scheme 3.9) or when an inhibitor (as hydroquinone) is added.



Free radical polymerization is known to be inhibited in the presence of oxygen, which itself is a diradical. However, the synthesis is made with a flux of nitrogen and the use of AIBN produces nitrogen as the reaction product guarantying, this way, an inert atmosphere.

The synthetic procedures usually lead to a distribution of different polymer lengths, which means that the synthetic polymers possess some degree of polydispersivity. The polydispersivity is given by the heterogeneity or polydispersivity index (PDI) which can be calculated from the weighted (or weight) molecular weight (M_w) and the nominal (or number average) molecular weight (M_n), see Equation 3.38 to Equation 3.40.

$$M_n = \frac{\sum N_i M_i}{\sum N_i} \quad \text{Equation 3.38}$$

$$M_w = \frac{\sum N_i M_i^2}{\sum N_i M_i} \quad \text{Equation 3.39}$$

$$PDI = \frac{M_w}{M_n} \quad \text{Equation 3.40}$$

With N_i being the number of polymer chains with M_i molecular weight. Polymers with PDI lower than 1.1 are considered rather monodisperse.

3.3.2. Synthesis of the PNIPAMPy polymers

The pyrene probed NIPAM polymers (PNIPAMPy) were synthesized with the kind support from Prof. Jorge Parola and Raquel Gavara (Universidade Nova de Lisboa), see Section 7.1.4 for more details. See structures in Figure 3.47.

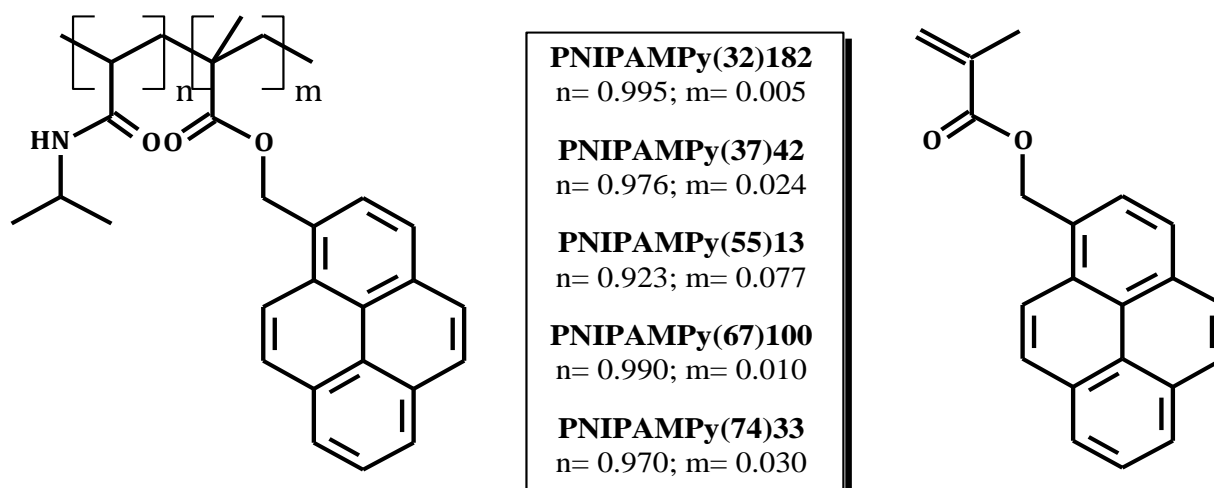


Figure 3.47. Structure of the PNIPAMPy polymers and the parent compound used.

3.3.3. Determination of the Labelling Content

In the case of the PNIPAMPy polymers, the determination of the labelling content was made only by $^1\text{H-NMR}$. In these polymers, the proton bonded to the only ternary carbon of PNIPAM appears at ~ 4 ppm and the ones from the pyrene unit between 7.8 and 8.4 ppm. For instance, for the polymer 16 the integration at the highest ppm is 0.05 while at the smallest is 1. Since there are 9 protons in the pyrene units and only 1 in the other case, a three simple rule is enough to discover the labelling content in %mol as done with the PAAMePy polymers, see Equation 3.41.

Theoretical values

$$\begin{aligned}
 & (1:1, \text{ i.e. } 50\%) \\
 & I_{7.8-8.4} \rightarrow 9 \rightarrow y \\
 & I_{3.5-4.5} \rightarrow 1 \rightarrow x \\
 & \Leftrightarrow \begin{cases} I_{7.8-8.4} = 9I_{3.5-4.5} \\ x + y = 100\% \end{cases} \Leftrightarrow \begin{cases} \frac{y}{x} = \frac{I_{7.8-8.4}}{I_{3.5-4.5}} = 9 \\ x = 100 - y \end{cases} \Leftrightarrow \\
 & \Leftrightarrow \begin{cases} \frac{y}{100-y} = \frac{I_{7.8-8.4}}{9I_{3.5-4.5}} \\ \dots \end{cases} \Leftrightarrow \begin{cases} \frac{9yI_{3.5-4.5}}{100-y} = I_{7.8-8.4} \\ \dots \end{cases} \Leftrightarrow \begin{cases} 9yI_{3.5-4.5} = I_{7.8-8.4}(100-y) \\ \dots \end{cases} \Leftrightarrow \\
 & \Leftrightarrow \begin{cases} 9yI_{3.5-4.5} = 100I_{7.8-8.4} - I_{7.8-8.4}y \\ \dots \end{cases} \Leftrightarrow \begin{cases} (9I_{3.5-4.5} + I_{7.8-8.4})y = 100I_{7.8-8.4} \\ \dots \end{cases} \Leftrightarrow \begin{cases} y = \frac{100I_{7.8-8.4}}{9I_{3.5-4.5} + I_{7.8-8.4}} \\ x = 100 - y \end{cases}
 \end{aligned}$$

Equation 3.41

3.3.4. Statistical Characterization

The probability of finding N pyrene units per chain is given by Figure 3.48 for the PNIPAMPy polymers.

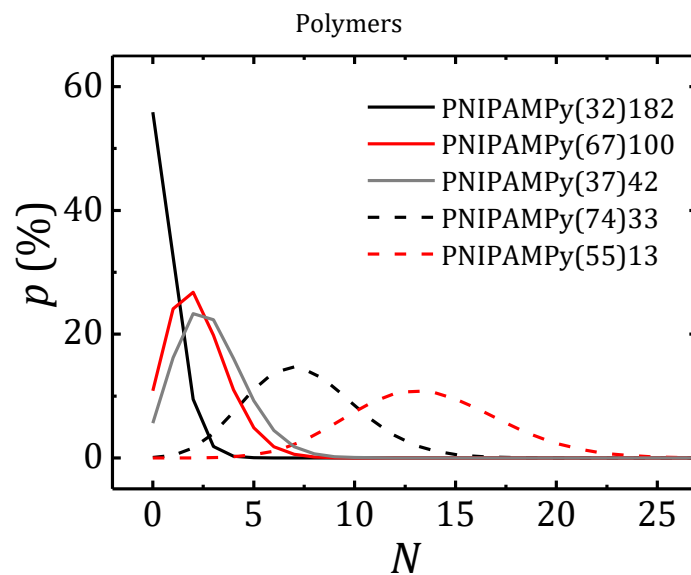


Figure 3.48. Probability of finding a PNIPAM chain with a given number of N pyrene groups per chain assuming a Poisson distribution.

In Table 3.12, the statistical information obtained assuming a Poisson distribution is gathered.

Polymers

Table 3.12. Molecular weight (M_w) of the pyrene labelled PNIPAM polymers (determined by gel permeation chromatography - GPC), polydispersity index (PDI), mean value of pyrene units per polymer chain m , theoretical fractions of unlabelled (with $N= 0$), single labelled (with $N= 1$), double labelled (with $N= 2$), and multi-labelled (with $N> 2$) chains, and fraction of single labelled chains relative to all labelled chains (" α ", intrinsically isolated pyrene units) using a Poisson Distribution.

	PNIPAMPy(32)182	PNIPAMPy(37)42	PNIPAMPy(55)13	PNIPAMPy(67)100	PNIPAMPy(74)33
M_w	31.8	74.2	55.0	66.7	36.6
PDI	6.09	3.35	3.65	3.24	6.00
m	0.58	2.88	13.57	2.22	7.46
$N= 0$	0.559	0.001	0.000	0.109	0.056
$N= 1$	0.325	0.004	0.000	0.241	0.162
$N= 2$	0.095	0.016	0.000	0.268	0.233
$N> 2$	0.021	0.549	1.000	0.357	0.979
"α"	0.737	0.172	0.000	0.270	0.004

From the Poisson distribution for the PNIPAMPy(32)182 it can be seen that 56% of the polymer chains are non-labelled, 32.5% are single labelled, 9.5% are double labelled. Looking only at the labelled chains, 74% of the labelled polymer chains are single labelled, 22% of chains have two pyrene units and only 4.8% have more than two pyrene units.

3.3.1. Results and Discussion

3.3.1.1. Absorption and Emission Spectra

The absorption spectra of the PNIPAMPy(32)182 polymer in DMF solutions is shown in Figure 3.49A. Amongst other parameters, the peak-to-valley ratio (P_A), relative to the first vibronic $S_2 \leftarrow S_0$ transition of the absorption spectrum, gives information regarding the level of *GSD*; usually P_A values ≥ 3 correspond to the situation where *GSD* are absent.^{51,66} With the PNIPAMPy(32)182 the obtained value is 2.68, indicative of the presence of *GSD*. From the comparison of the excitation spectra collected at the monomer ($\lambda_{em} = 375$ nm) and excimer ($\lambda_{em} = 520$ nm) emission wavelengths (Figure 3.49B) the presence of ground state association in PNIPAMPy(32)182 is also evident. Usually, the changes in the excitation spectra are mirrored by the differences in the peak-to-valley ratio relative to the (0,1) transition observed in the monomer (P_M) and excimer (P_E) excitation spectra ($P_M - P_E$), and also by the shift in the maximum wavelength of the two spectra ($\Delta\lambda_2$).^{64,166} The $P_M - P_E$ difference also allow identifying the presence of *GSD* since $P_M \neq P_E$, $P_M - P_E = 0.14$ for PAAMePy(32)182 in DMF. The I_E/I_M ratio, obtained with three different excitation wavelengths, shows that excitation at longer wavelengths results in a slightly higher I_E/I_M ratio (Figure 3.49). This is again compatible with the light absorption for *GSD* at longer wavelengths, as was previously observed for PAAMePy polymers.^{51,65} However, as will be shown below the degree of ground-state dimers is low and the excimer formation is essentially made through a dynamic via.

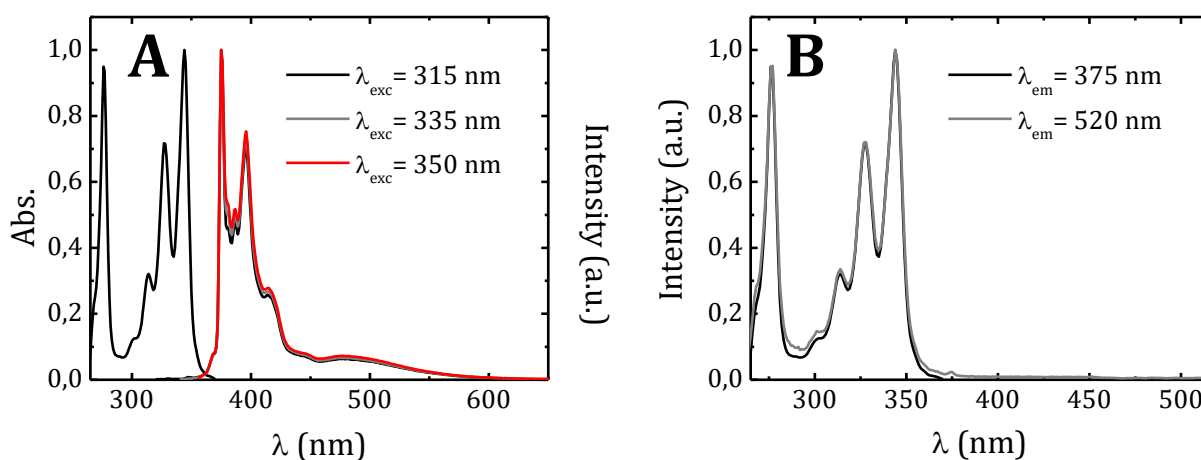


Figure 3.49. Normalized (A) absorption and fluorescence emission spectra obtained at $\lambda_{exc} = 315, 335$ and 350 nm and normalized (B) fluorescence excitation spectra of PNIPAMPy(32)182 in DMF, collected at the monomer (375 nm) and excimer (520 nm) emission wavelengths, at 293 K.

The fluorescence emission spectra of PNIPAMPy(32)182 displays the characteristic monomer (with maxima at ~ 375 nm) and excimer (with maxima at ~ 480 nm) pyrene emission bands (Figure 3.49A). Two clear observations can be made concerning the dependence of these spectra on the excitation wavelength. First, excitation at $\lambda_{\text{exc}} = 350$ nm slightly enhances the excimer emission band when compared with excitation at 335 nm (and 315 nm) (Figure 3.49A), indicating that the long wavelength emission band is only partially promoted by direct excitation of the dimer (or *GSD*), and that the contribution from excimers formed from a dynamic process is dominant. This will be further discussed, with quantitative data, in the time-resolved (TR) data discussion section.

Some preliminary results of another [PNIPAMPy(55)13] polymer (with different degree of labelling and chain size) in CH_2Cl_2 is showed in Figure 3.50.

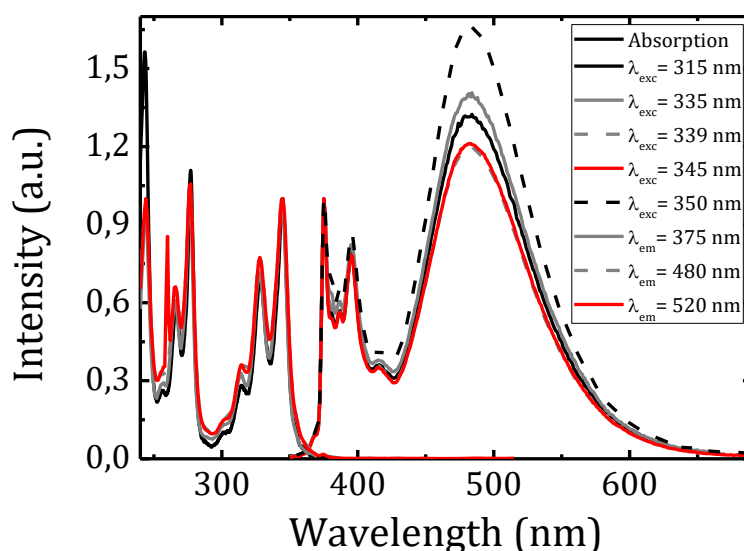


Figure 3.50. Normalized (A) absorption, fluorescence emission spectra obtained at $\lambda_{\text{exc}} = 315, 335, 339, 345$ and 350 nm and fluorescence excitation spectra of PNIPAMPy(55)13 in dichloromethane, collected at the monomer (375 nm) and excimer (480 and 520 nm) emission wavelengths, at 293 K.

3.3.1.2. Viscosity Dependence

The decay times and pre-exponential factors obtained for PNIPAMPy(32)182 in solvents of different viscosity are presented in Figure 3.51.

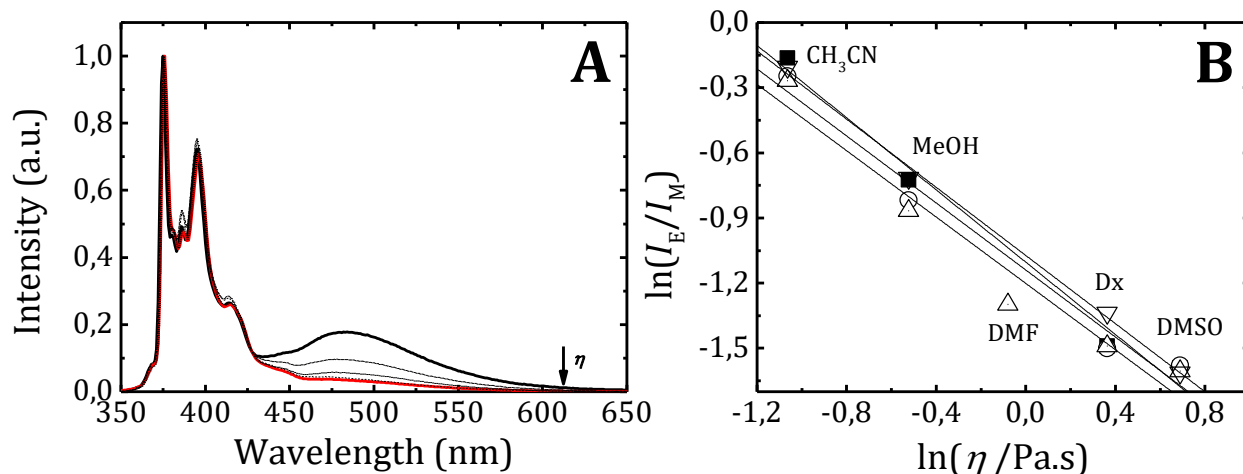


Figure 3.51. (A) Emission spectra and (B) Log-log plot of I_E/I_M ($\lambda_{exc}=339$ nm) versus the viscosity (η) for PNIPAMPy(32)182 at 293 K. I_E/I_M was taken using the Method D, see Section 7.2.6.1.2.1 of Chapter 7. The data in panel B was fitted with the following equation: $\ln(I_E/I_M) = -1.07(\pm 0.05) - 0.83(\pm 0.03) \times \ln(\eta)$.

The above considerations, based on absorption and fluorescence data are strongly limiting of a comprehensive interpretation of the system and therefore further quantitative information is needed which is obtained from TR data. All the decays of PNIPAMPy(32)182 were found to be tri-exponential (Figure 3.52A).

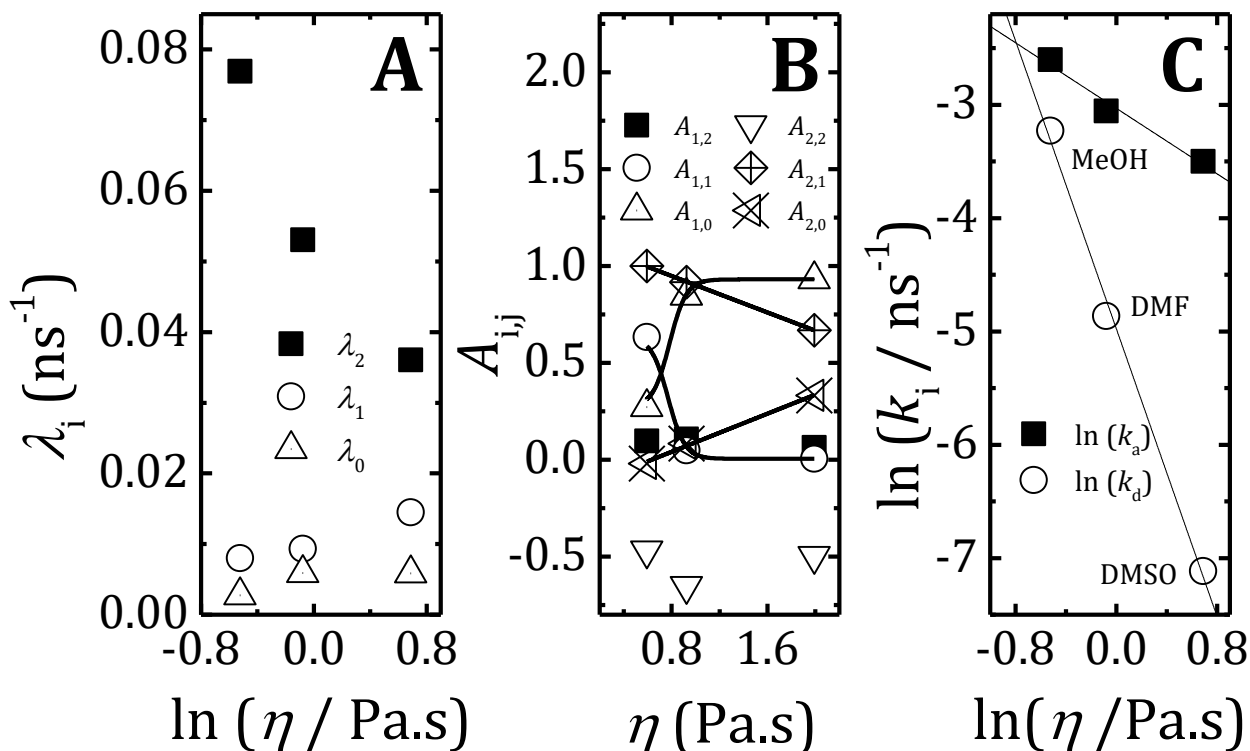


Figure 3.52. Dependence of (A) decay times, (B) pre-exponential factors collected at the monomer ($A_{1,j}$) and excimer ($A_{2,j}$) emissions wavelengths (480 nm, except in DMSO - there it was used at 520 nm, i.e., $A_{3,j}$) and (C) plots of natural logarithm of k_a and k_d of the PNIPAMPy(32)182 polymer in different solvents as a function of the viscosity at $T=293$ K.

The log-log plot of k_a (and k_d) vs. solvent viscosity is linear, with slope equal to 0.72, showing that the Debye–Smoluchowski relationship does not apply. In the kinetics of excimer formation in these polymers, the value obtained ($\alpha=0.72$) is significantly lower than the expected for a purely diffusion-controlled process, where $\alpha=1$. Similar departures from a pure diffusion-control of end-to-end chain cyclization (in order to achieve the excimer conformation) have been reported previously.¹⁰³

The departure from $\alpha=1$ mirrors the multi-barrier crossing dynamics of intramolecular excimer formation involving several bond rotations in the presence of the solvent frictional forces acting on the chain.¹⁰³ A similar value to that obtained with PNIPAMPy(32)182 ($\alpha=0.68$) was obtained for 1Py(10)1Py ($\alpha=0.75$), a polyethylene polymer end-labelled with pyrene ($\alpha=0.52$).^{110,132}

A similar situation ($\alpha<1$) was also observed in a number of other excited state processes, as the intramolecular excimer formation with dipyrenylcarboxypentane ($\alpha=0.78$).⁸⁹ In all these reactions, an additional intrinsic rotational energy barrier of the bond or the chain was present.

3.3.1.3. Temperature Dependence

Figure 3.53 shows the fluorescence decays at three different temperatures. The fluorescence decays are best fitted with sums of three exponential terms. The global analysis of the decays shows, at 20°C (Figure 3.53B), the presence of *MAGRE* and isolated monomers, together with the excimer decay time. The *MAGRE* monomers display a decay time of 17 ns (appearing as a decay at 375 nm and as a rise-time at the 520 nm) whereas the isolated monomers show the longer lifetime 165 ns; finally the 113 ns decay time is associated to the excimer decay. Moreover, the presence of *GSD* is again visible since the sum of the pre-exponential factors at the excimer emission (520 nm, in this case), $A_{2,1}$ and $A_{2,2}$, does not cancel out. At the monomer emission (375 nm) the excimer decay (113 ns) is also present, which may be caused by two major reasons (1) excimer to monomer reversibility is present, k_d in Scheme 3.2 is different than 0 or (2) it may result from monomers being quenched by neighbouring pyrene units, giving rise to a distribution of excimer formation rate constants. However, the fact that the same decay time is present at 520 nm goes in clear favour of (1).

All the above is compatible with the kinetic Scheme 3.2 where M_A stands for the free monomer, M_B the *MAGRE* monomers and E the excimer, i.e., a kinetic scheme with 2 monomers and 1 excimer (Scheme 3.2).⁶⁵ Scheme 3.2 can be analytically solved by relating the pre-exponential factors and the decay times with the rate constants [excimer formation (k_a), excimer reversibility (k_d), excimer decay (k_E) and monomer decay (k_M), see Appendix B]. It also considers the fraction of isolated monomers (α) and of excited monomers giving rise to excimer [$(1-\alpha)(1-\beta)$] and pre-associated excimers [$\beta(1-\alpha)$].

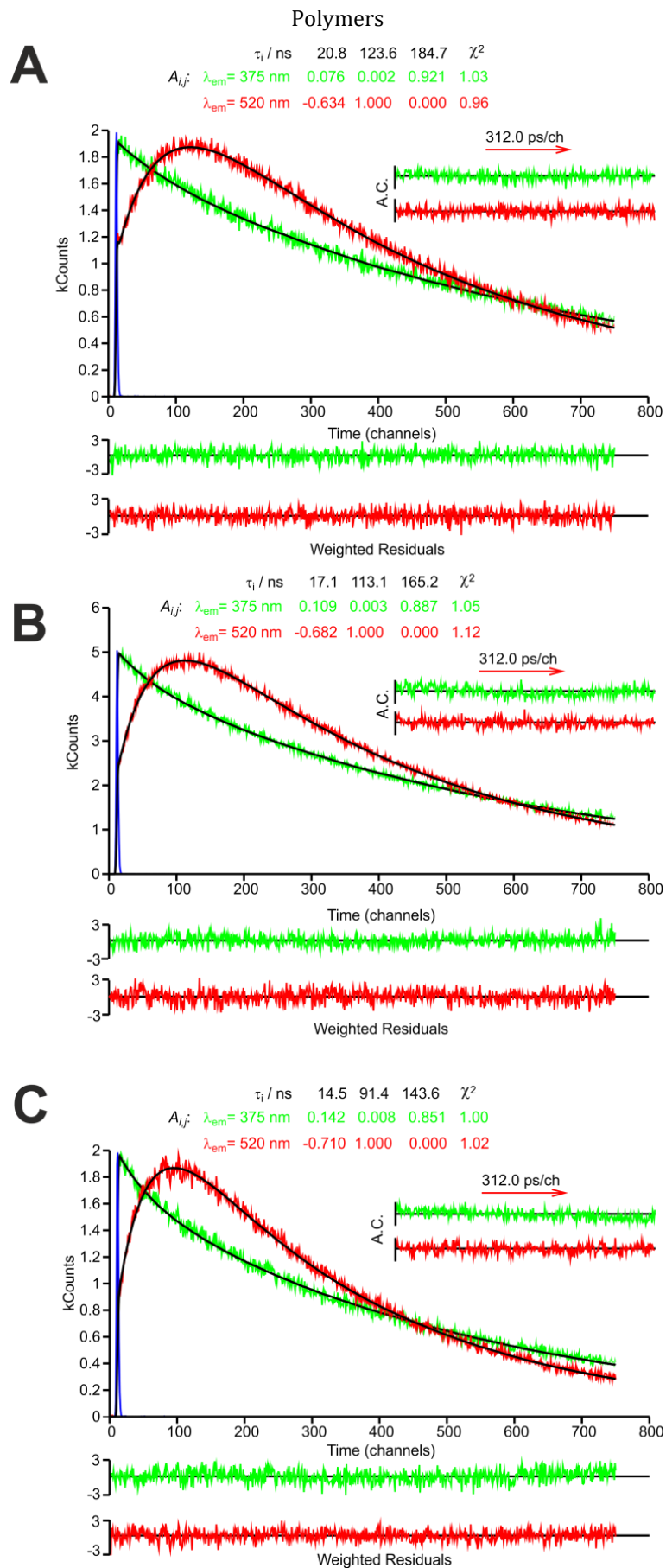


Figure 3.53. Global analysis of the fluorescence decays for the PNIPAMPy(32)182 polymer in DMF at (A) $T = 0^\circ\text{C}$, (B) 20°C and (C) 45°C with excitation at 339 nm and emission at 375 and 520 nm. The instrument profile curve is also shown. For a better judgment of the quality of the fits shown as insets are the weighted residuals and the A.C. functions.

Figure 3.53 shows the decay time and pre-exponential coefficient dependence with the temperature. It can be observed that the longest decay time ($\tau_M = \tau_0$) is found with values ranging between 144 and 185 ns. The two other decay times, τ_1 and τ_2 , display values varying respectively from and 15-21 and 91-124 ns.

The maximum entropy method (MEM) was applied to the analysis of the monomer decay of PNIPAMPy(32)182 in DMF at 80 °C, and showed in Figure 3.54.

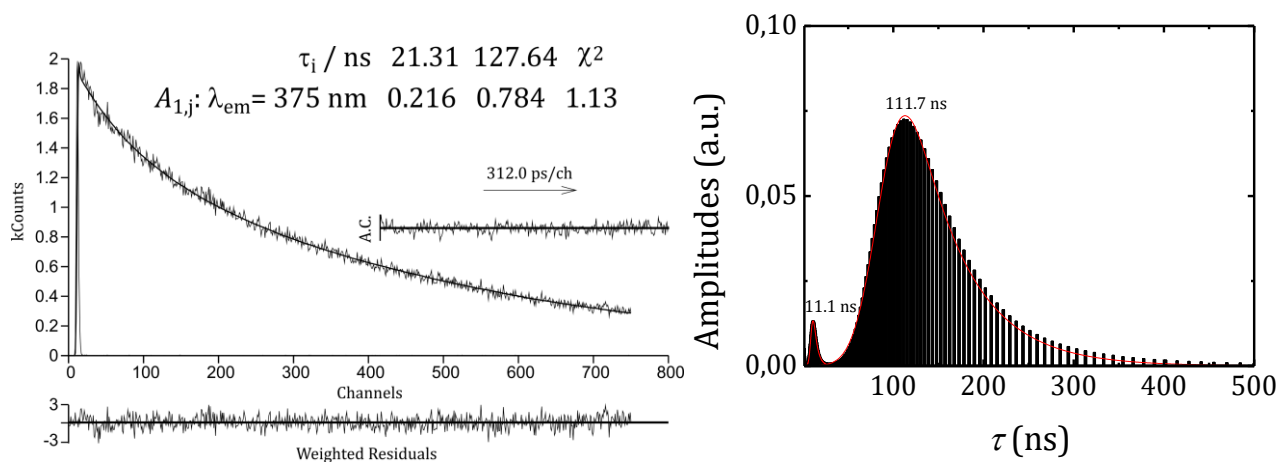


Figure 3.54. Left panel. Independent analysis of the fluorescence decay for the PNIPAMPy(32)182 polymer in DMF at 80°C with excitation at 339 nm and emission at 375 nm. The instrument profile curve is also shown. For a better judgment of the quality of the fits shown as insets are the weighted residuals and the A.C. functions. Right panel. MEM analysis of the fluorescence decay for PNIPAMPy(32)182 in DMF at 80 °C. Probe function contained 200 terms (maximum) over range of 1-500 ns. Fitting range of 1024 channels with 0.312 ns/channel.

The two distributions of decay times obtained indicate that, indeed, at the monomer emission wavelength, two exponentials are sufficient to describe the fluorescence decays of PNIPAMPy(32)182 in DMF in the range of temperature investigated, Figure 3.54.¹⁶⁷

This method only allows the analysis of the monomer decay and because of it, and also because the excimer reversibility is almost absent in this case, it is impossible to detect correctly the excimer lifetime. Although when making the 1st derivative (data not shown) it seems that another component with a value close to the excimer lifetime is present.

In Figure 3.55, the lifetimes, pre-exponential and rate constants obtained from the analysis of the fluorescence decays are shown.

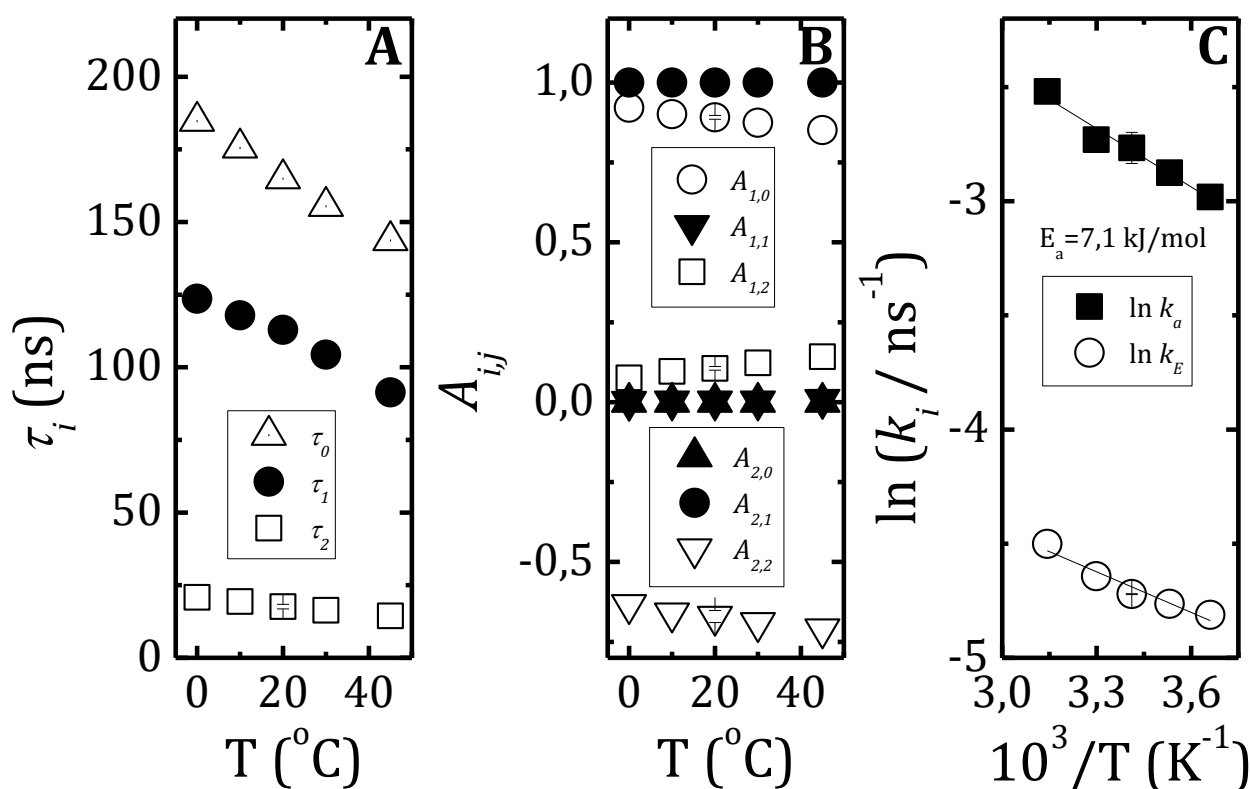


Figure 3.55. (A) Fluorescence decay times (τ_i), (B) pre-exponential factors (A_{ij}): at 375 nm ($A_{1,j}$) and 520 nm ($A_{2,j}$) as a function of the temperature and (C) $\ln k_i$ as a function of the reciprocal of the temperature for PNIPAMPy(32)182 in DMF.

The data here presented show that the steady-state behaviour (I_E/I_M obtained from the fluorescence emission spectra) correctly reproduces the I_E/I_M (Figure 3.56B) obtained from time resolved data (data in Figure 3.55). This similarity of the I_E/I_M obtained from both steady state (SS) and time-resolved (TR) allows once more the validation of the proposed model (Scheme 3.2).

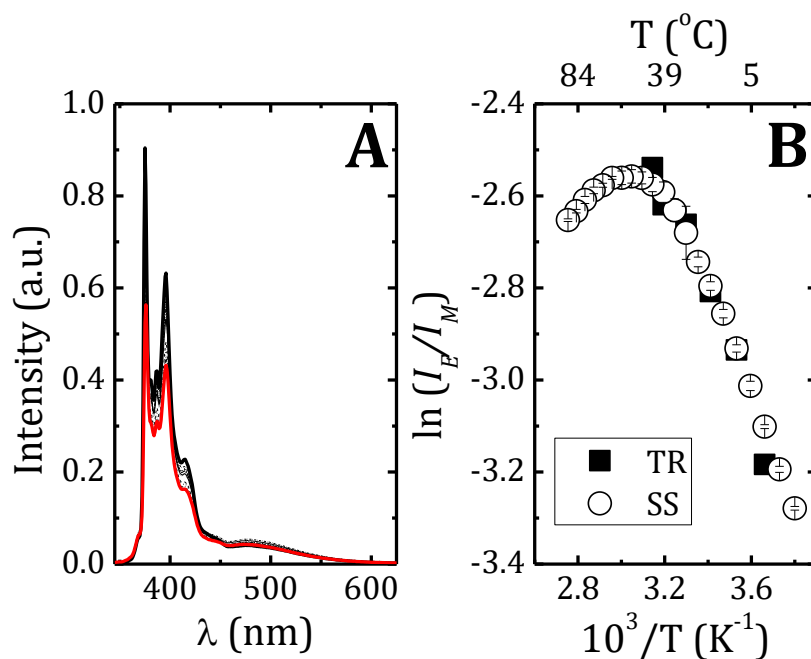


Figure 3.56. (A) Emission spectra ($\lambda_{exc} = 339$ nm) (bold black line and red line represents the emission spectra at and -10 and 90°C , respectively) and (B) plots of $\ln(I_E/I_M)$ vs. $10^3/T$ obtained from Steady State (SS) and TR (see text for details) for the PNIPAMPy(32)182 in DMF. The SS I_E/I_M was taken from Method A, see Section 7.2.6.1.2.1 in Chapter 7.

The dependence of the natural logarithm of the rate constants with the reciprocal of temperature show an Arrhenius behaviour (see Figure 3.55C). In contrast to the PAAMePy polymers, the excimer-to-monomer reversibility begins to be relevant only at temperatures above 50°C (Figure 3.56).

Activation energies obtained from the SS and TR approach are, within the experimental error, identical with values of 8.4 ± 1.6 kJ/mol (Table 3.14). Briefly, this interpretation means that, if the system motions are faster than the solvent response (solvent relaxation), the effective (microscopic) friction coefficient of the solvent will be smaller than the adiabatic (zero-frequency) macroscopic friction coefficient. This situation may occur when the intrinsic barriers are high and consequently the zero-activation energy value of the rate constant (frequency at the top of the barrier) is sufficiently large to compete with solvent relaxation.

By using the kinetic equations derived from Scheme 3.2 and with the data obtained from the fluorescence decays (decay times and pre-exponential coefficients), all the rate constants and the α and β factors could be determined. The equations and formalism relating the rate constants to the decay times and pre-exponential factors can be found in detail in ref. ⁵¹ and in Appendix B.

Table 3.13. Monomer and excimer decay time (τ_M and τ_E , respectively), excimer association, dissociation and decay rate constants (k_a , k_d and k_E , respectively), fractions of *GSD*, *MAGRE* and isolated monomers [$\beta(1-\alpha)$, $(1-$

$\alpha(1-\beta)$ and α , respectively] of PNIPAMPy(32)182 in different solvents recovered by using the data of Table 3.15 in Scheme 3.2.

Solvent	η (mPa.s)	τ_M (ns)	τ_E (ns)	k_a (ns ⁻¹)	k_d (ns ⁻¹)	k_E (ns ⁻¹)	$\beta(1-\alpha)$	A	$(1-\alpha)(1-\beta)$
MeOH	0.5929 ³⁵	324.63	48.27	0.023	0.040	0.021	0.108	0.311	0.581
DMF	0.924 ³⁵	169.42	96.72	0.060	0.008	0.010	0.119	0.776	0.035
Dx	1.3075 ¹¹⁴	218.47	45.10	0.017	0.035	0.022	0.038	0.681	0.281
DMSO	1.991 ³⁵	170.90	67.42	0.030	0.001	0.015	0.046	0.931	0.023

3.3.1.3.1. Intra vs. Intermolecular Interactions

The k_a , k_d and, in special, k_E ($1/\tau_E$) values obtained are not the one typically found for intermolecular interactions so the existence of intermolecular interactions is very improbable for the conditions used.¹⁶⁸

3.3.1.3.2. Monomer That Gives Rise To The Excimer (MAGRE), Isolated Monomers and GSD

For PNIPAMPy(32)182, the fraction of GSD in methanol, $\beta(1-\alpha)$, (0.108) is identical to the found for the PAAMePy polymers [0.080 for PAAMePy(2)77 in methanol, see Table 3.4].⁶⁵ However, in contrast with what happens to the PAAMePy polymers, the MAGRE contribution for PNIPAMPy(32)182 is ~50 times smaller when compared with PAAMePy(2)77 in good solvents.⁶⁵ In DMF, the fraction of isolated monomers (α) is large with a value (0.776) and similar to the theoretical mole fractions (0.737, see Table 3.12) of single-labelled chains relative to all labelled chains, i.e., intrinsically isolated monomers.⁶⁵

Two things may explain the α value dependence with solvents: (1) at the lower viscosity results essentially from singly labelled chain or (2) is, independently of the solvent, and arises from singly and multi labelled chains. (2) is more likely to give a higher contribution, but both (1) and (2) can explain the dependence of α if the increase the solvent viscosity some of the multi labelled chain that were forming excimer (at lower viscosity) could not be able to do so anymore when in the presence of solvents of higher viscosity and then were contributing to the increased parameter α , See Scheme 3.3. In Table 3.14, the comparison of the data obtained for the PNIPAMPy(32)182 polymer is compared with other previously published PNIPAMPy polymers¹³³, a PAAMePy polymer with the most similar labeling degree and with two dipyrenylpropanes.^{44-46,169}

The fact that the free monomer lifetime is much lower can be explained by the fact that there is a much higher polydispersivity and so, more different kinds of free monomers, each one contributing with their lifetime. The fact that is lower must mean that more of the free monomer correspond to multilabelled chains since different kinds of chain backbone do not give so different values [220 ns for Py₂-PNIPAM-6K and 226 ns for PAAMePy(2)133]. The fact that the excimer lifetime is longer can mean that the excimer found in these polymers is parallel sandwich or could mean that there are two (or more) different kind of

Polymers

excimers but that, for some reason (small contribution of one of the excimer or similar lifetime values), cannot be distinguished by TR.

Table 3.14. Viscosity of the solvents (η), activation energies of excimer formation and dissociation (E_a and E_d), enthalpy of excimer formation (ΔH), entropy of excimer formation (ΔS), rate constants of excimer formation (k_a), dissociation (k_d) and decay (k_E), excimer and monomer lifetimes (τ_E and τ_M), and fractions of isolated monomers (α), MAGRE monomers [$X = (1-\alpha)(1-\beta)$] and ground-state dimers [$Y = \beta(1-\alpha)$] for several compounds in different solvents at T= 293 K unless noted.

Compound	Solvent	η (cP)	E_a (kJ.mol ⁻¹)	E_d (kJ.mol ⁻¹)	$-\Delta H$ (kJ.mol ⁻¹)	$-\Delta S$ (J.mol ⁻¹)	k_a (ns ⁻¹)	k_d (μ s ⁻¹)	k_E (μ s ⁻¹)	τ_E (ns)	τ_M (ns)	α	X	Y
			8.6 (10.2) ^a											
PNIPAMPy(32)182	DMF	0.924 ³⁵	7.1 ^b	19.5	10.9±1.6 ^d	6 ^d	0.063	0.7	8.9	113	165	0.947	0.103	0.006
			8.6±1.6 ^c											
Py-PNIPAM-2%¹³³	EtOH	1.200 ³⁵						NA		52, 118	210	0.160	0.070	0.760
Py₂-PNIPAM-6K¹³³					ND			0.0034	3.6	17	60	220		NA
PAAMePy(2)133	Dx	1.3075 ¹¹⁴					0.023	0.007	0.013	76	226	0.43	0.09	0.48
1Py(3)1Py	Heptane	0.4181 ³⁵	12 ⁴⁴	32 ⁴⁴	20 ⁴⁴	14 ⁴⁶	~0.073 ⁴⁶	~0.68 ⁴⁶	6.4 ⁴⁶	156 ⁴⁶	~253 ¹¹⁶			
	Hexadecane	3.454 ¹¹⁵	18.4 ⁴⁶	33.6 ⁴⁶	15.2 ⁴⁶				ND					
	MCH	0.734 ³⁵	20 ⁴⁴	42 ⁴⁴	22 ⁴⁴									
1Py(3)2Py	Mesitylene	0.659 ¹⁷⁰			20.5 ⁴⁴	31	0.128 ¹¹³	1.3 ¹¹³	6.7 ¹¹³	150 ¹¹³	367 ¹¹³		NA	
	Heptane ⁴⁵	0.4181 ³⁵		ND	23	ND	~0.266	~1.25			ND			
	Toluene ¹⁶⁹	0.5859 ³⁵			ND		0.126	0.9	7.2	140	291			

NA - not applicable, ND - not determined. ^a Obtained from the LTL of the Stevens-Ban plot, see Figure 3.56B. The data derived from the Steady State are in brackets. ^b Obtained from the Arrhenius plot, see Figure 3.55C. ^c Obtained from $E_a = \Delta H + E_d$. ^d Obtained from the van't Hoff plot, $\ln k_a/k_d$ vs $1/T$.

3.3.1.3.3. Excimer Formation Rate Constant

The value of k_a is temperature-dependent, increasing with the temperature (from 5.1×10^7 to 8.1×10^7 s⁻¹ from -10 to 90 °C), $\eta_{\text{DMF}} = 0.924$ cP at 20°C.³⁵ At 20°C, the k_a value is of 6.3×10^7 s⁻¹ which is consistent with the value found for intramolecular excimer formation (at 25°C) with 1,n-di(1-pyrenyl)alkanes (n= 3-4) in methycyclohexane¹¹⁶ ($\eta_{\text{MCH}} = 0.670$ cP at 25°C).³⁵

For 1Py(3)1Py literature values in heptane ($\eta = 0.4181$ cP at 20°C)³⁵ range from $k_a(1) = 0.073$, $k_d(1) = 0.00068$ and $k_E(1) = 0.0074$ ns⁻¹ (with $\tau_E(1) = 138$ ns $E_a(1) = 18.4$ kJ/mol)¹¹⁶

For an end-labelled PNIPAM polymer the decays were found to be tetra exponential in the monomer with decay times (depending on the size of the PNIPAM skeleton) of 2, 43-44, 89-124 and 190 ns in acetonitrile and $\tau_E = 54$ -57 ns, leading (from a Birks' modified scheme) to $k_a = 8.1$ -3.9 ns⁻¹ and $k_d = 2.6$ -4.0 μs^{-1} .¹³³

The E_a value is smaller than the activation energy value for the viscous flow in DMF [$E_\eta(\text{DMF}) = 13.2 \pm 0.2$ kJ/mol¹⁴⁵], which means that there is no additional barrier associated to the chain.

3.3.1.3.4. Excimer Dissociation Rate Constant

The values found for the dissociation rate constant k_d in DMF (from 8 to 33 μs^{-1}) are not so different from those obtained for the reciprocal excimer lifetime k_E (from 13 to 20 μs^{-1}).

It should be noted that the values obtained for E_a using the values of k_d were very close to those obtained for E_a without using the values of k_d , see Table 3.14.

3.3.1.3.5. Monomer and Excimer Lifetimes

As can be seen in Figure 3.53B for the PNIPAMPy(32)182 polymer, the decay time associated to the excimer (113 ns) is similar to the one found for a sandwich-like symmetric intramolecular excimer in 1Py(3)1Py (117.5 ns in MCH).^{44,51,112,113,116}

In the presence of only one excimer it would be expected that it should be the most stable conformation, however the value of the decay time goes in favour of the less stable. Although not typical, similar values were found for all Py-PNIPAM-X% but more similarly with Py-PNIPAM-2% in ethanol, a solvent of comparable viscosity to DMF. Nevertheless, the isolated monomer appears with a lifetime value (165 ns) that is not the typical for unquenched pyrene substituted derivatives (smaller than the one obtained with the PAAMePy polymers in methanol, dioxane or water).⁶⁵ Similar values for the fluorescence lifetime were found for a pyrene-lipid in phosphatidylcholine (POPC) vesicles in the absence of oxygen,¹⁷¹ in a pyrene end-capped poly(ethylene oxide) polymer with γ -cyclodextrin,^{103,172-175} in pyrene in a matrix of polystyrene (PS) and poly(methylmethacrylate) (PMMA) at 30 kbar¹⁷⁶ and (in solution) in

the presence of CH_3I ¹⁷⁷ and surfactants¹⁵⁵. However, even smaller values (105 ns) were found for the monomer lifetime of a pyrene randomly labelled PNIPAM with low pyrene content (0.1%) (Py-PNIPAM-0.1%) in 2-butanone that is distinct from the structure of PNIPAMPy(32)182 in the monomer that possess the pyrene unit. In Py-PNIPAM-0.1%, the carbonyl group is linked to an amine that is in turn connected to the 1-butylpyrene¹³³ while in PNIPAMPy(32)182 the carbonyl group is linked to an oxygen that is in turn connected to the 1-methylpyrene. The other differences are that the Py-PNIPAM-0.1% has only 0.12% mol of pyrene units and has a number \bar{M}_n of 104 kDa while here we present a polymer with 0.5% pyrene content and a $\bar{M}_n \approx 2$ kg/mol. In order to compare, we can determine the number of pyrene groups per NIPAM monomer, for Py-PNIPAM-0.1% and PNIPAMPy(32)182 there is 1 pyrene group per 833 and 5 NIPAM monomers, respectively. For Py₂-PNIPAM-25K and Py₂-PNIPAM-45K, only a decay analysis at the monomer was done with values 76 and 174 ns and 58 and 185 ns in acetonitrile, respectively.¹³³

3.3.1.3.6. The Blob Model vs. Sum of Exponentials Model

The experimental fluorescence (monomer and excimer) decays, which in our opinion are essential in a discussion of systems with such complexity, were not presented nor the scale (ps/ch) used but were analysed independently in the monomer and excimer regions, fitted with 4-exponentials in both regions (except for the Py₂-PNIPAM-25K and Py₂-PNIPAM-45K polymers which were analysed with two exponentials) in ref. ¹³³. The monolabelled sample was used as a model compound to determine the natural lifetime of pyrene attached to the PNIPAM chain and fixed in the analysis of the decays of Py₂-PNIPAM-YK and Py-PNIPAM-X%.

It was there reported that all excimer decays showed a pronounced spike at the early times (2 ns) which was attributed to short-lived pyrene species. This was also suggested by Siu and Duhamel, who studied excimer formation kinetics using two models (the “blob model” and the “differential” method “sums of exponentials”), and concluded that the procedure of using sums of exponentials is more general than the “blob model”.¹⁷⁸ Beside they assume that no excimer-to-monomer reversibility exists.

In our case, both independent and global analyses of the decays were obtained. The exponentials terms used were the minimum to give a proper fitting (good χ^2 , autocorrelations function and weighted residuals). Besides that, several scales (time/channel) were used and no evidence of lifetime distribution was found nor the spike reported by Duhamel *et al.*¹³³ The spike observed by Duhamel *et al.*¹³³ is probably due to aggregates that are formed in the presence of water, even if residual. This was also observed for some PAAMePy polymers at acidic pH values and in some PAAMePy in dioxane:water mixtures.⁶⁴ Duhamel's *et al.* observation seems to happen with longer chains.¹³³

We considered that the observation of a bi-exponential decay at the monomer emission to support our view that no evidence for distributions of decay times exist, indeed these values can be easily attributed to the free monomer (comparing for example with the monomer lifetime of 1-methylpyrene in DMF) and the monomer that give rise to the excimer. Besides, the presence of similar values for the decay time of the monomer that gives rise to the excimer (*MAGRE*) in both monomer and excimer decays gives evidence for the non-existence of a distribution of decay times (and therefore of rate constants).

3.3.2. Summary

The photophysical characterization of one PNIPAMPy polymer was performed in organic solvents (of different viscosities) and as a function of temperature. Three methods of analyses of the fluorescence decays were discussed.

In summary, the foregoing results indicate that pyrene excimer formation in the PNIPAMPy(32)182 in DMF is correctly described by a kinetic scheme with 3 species: *MAGRE*, isolated monomer and excimer, where the number of exponential terms is equal to the number of species that are kinetically involved. Therefore, this method of analysis seems favourable to other alternative methods, which do not provide clear physical insights namely the same amount of direct physical parameters (rate constants and fractions of ground-state species).

3.3.3. Supplementary Information

In Figure 3.57 the fluorescence emission spectra of different concentrations solutions of PNIPAMPy(32)182 polymers are shown together with the variation of the excimer-to-monomer ratio as a function of the optical density. From Figure 3.57 it is seen that for the range of concentrations used, there should not exist intermolecular interaction since the excimer-to-monomer ratio is constant for all the $\Delta O.D.$ values. Although this was found to be true until at least 0.4, the solutions used had typically a $\Delta O.D.$ lower than 0.2 at the maximum absorption wavelength.

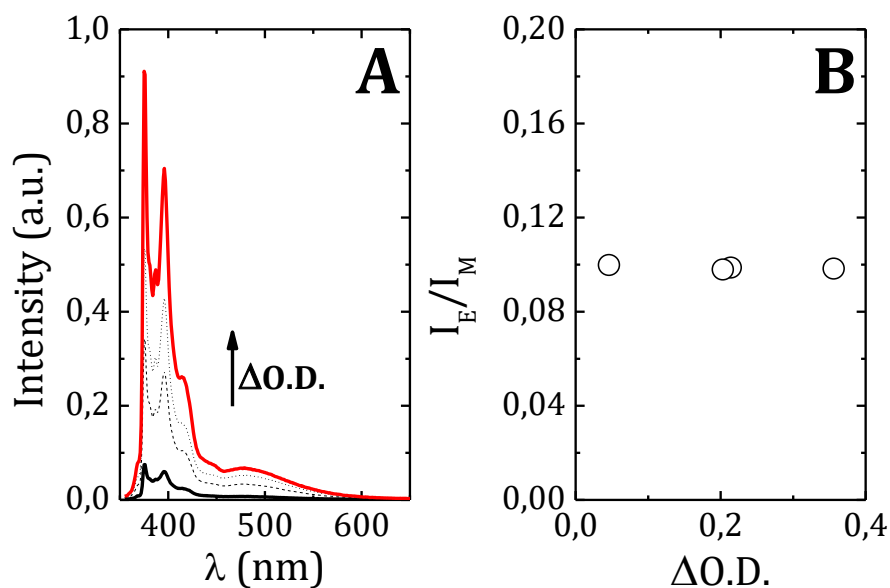


Figure 3.57. (A) Emission spectra and (B) I_E/I_M ratio vs. $\Delta O.D.$ of PNIPAMPy(32)182 in DMF at $\lambda_{exc} = 350$ nm and 293 K.

The analyses of the fluorescence decays was first made with a global analysis (i.e., 375, 480 and 520 nm together) and with no imposed decay times (Figure 3.58) and then with an independent analysis (i.e., at each wavelength of emission separately: 375 and 520 nm) (Figure 3.59) and with no imposed decay times. The procedure for both consisted in analysing firstly with the exponential terms needed to obtain a proper fitting, starting with one and then increasing the number of exponentials. The fitting was considered good when the χ^2 value was found between 0.9 and 1.3 and both weighted residuals and autocorrelation functions were good. For this system, the fitting was good with three, and only three, exponential terms.

Polymers

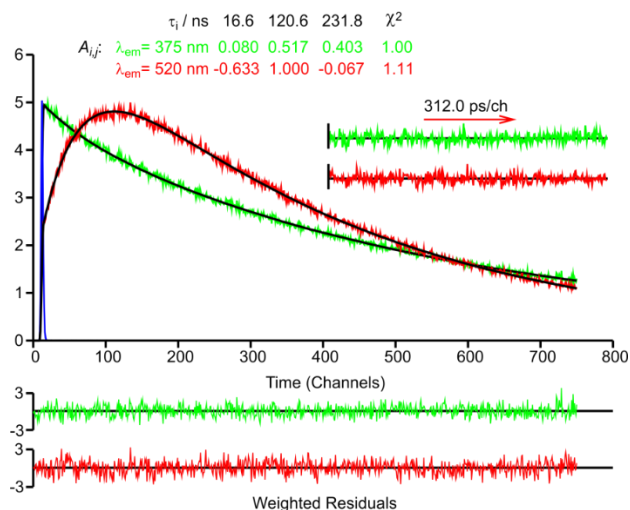


Figure 3.58. Free global analysis of the fluorescence decay of the PNIPAMPy(32)182 polymer in dimethylformamide collected at the monomer and at the excimer emission wavelengths (375 nm and 520 nm, respectively) with excitation at 339 nm and $T = 293$ K. The instrument profile curve is also shown. For a better judgment of the quality of the fits shown as insets are the weighted residuals and the A.C. functions.

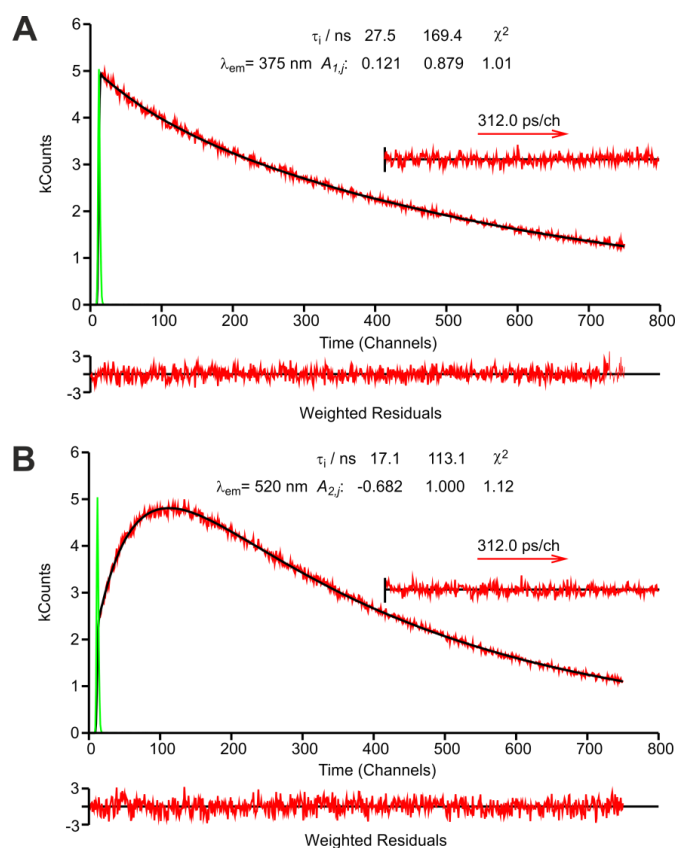


Figure 3.59. Free independent analysis of the fluorescence decay of the PNIPAMPy(32)182 polymer in dimethylformamide collected at (A) the monomer (375 nm) and (B) the excimer emission wavelength (520 nm) with excitation at 339 nm and $T = 293$ K. The instrument profile curve is also shown. For a better judgment of the quality of the fits shown as insets are the weighted residuals and the A.C. functions.

The global and individual analyses of the decays show the following: 1) at both wavelengths the independent analysis of the decays leads to bi-exponential decays with only a common decay time: associated to the *MAGRE*. At the monomer emission decay time (375 nm) the additional decay time mirrors the lifetime of the free monomers whereas at the excimer emission (520 nm) the excimer decay. 2) Due to its low contribution ($a_{1,1} \times \tau_1$) at 375 nm, the decay time attributed to the monomer that gives rise to the excimer (*MAGRE*) becomes best defined at longer emission wavelengths (520 nm) (see Figure 3.59). Because of 1) and 2), the decays collected at the monomer emission were reanalysed fixing the *MAGRE* decay time (with the value obtained from the independent analysis of the decays at the excimer emission wavelength – 520 nm) (Figure 3.59B). The resulting decay analysis (Figure 3.60) shows just a slightly higher value for the χ^2 . This procedure was made for the decays obtained at all temperatures and the $\ln k_M$ (obtained from both freely and fixed analysed decay) values were plotted as a function of the reciprocal of the temperature (Figure 3.61B).

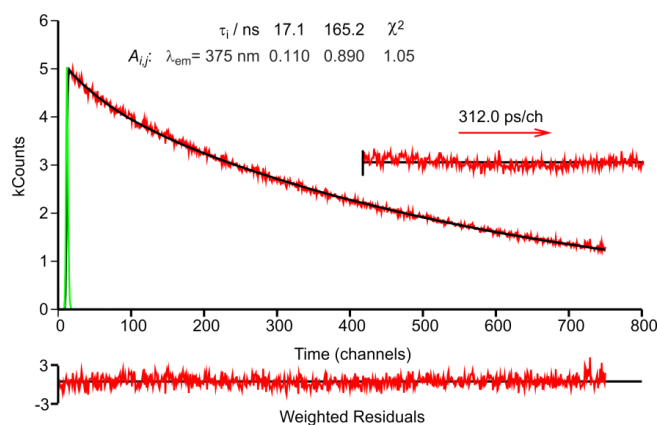


Figure 3.60. Independent analysis (fixing the lifetime of *MAGRE* obtained from Figure 3.59B) of the fluorescence decay of the PNIPAMPy(32)182 polymer in dimethylformamide collected at the monomer (375 nm) emission wavelength with excitation at 339 nm and $T = 293 \text{ K}$. The instrument profile curve is also shown. For a better judgment of the quality of the fits shown as insets are the weighted residuals and the A.C. functions.

The trend of $\ln k_M$ vs $1/T$ showed a better linear dependence with the imposed *MAGRE* decay showing that it is a valid consideration.

Polymers

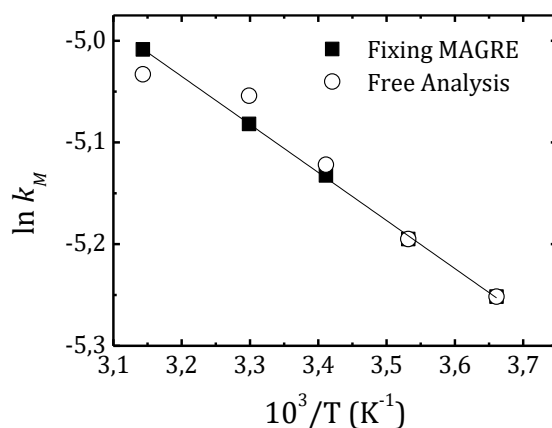


Figure 3.61. Plot of the $\ln k_M$ as a function of the reciprocal of the temperature obtained from the free and fixed independent analysis at the monomer emission wavelength (375 nm) of PNIPAMPy(32)182 in DMF; see text for further details.

The global analysis (with the imposed *MAGRE* decay time) performed at the emission wavelengths of the monomer (375 nm) and excimer (520 nm) gives the same decay times that the previously obtained from independent/individual analysis.

Finally, the values obtained were fixed in the global (simultaneous) analyses since the global analyses with no imposed decay times can give some wrong information by mixing the lifetime and pre-exponential factors when the lifetimes are too similar (see both - freely and fixed - global analyses at 20°C in Figure 3.58 and Figure 3.62, respectively).

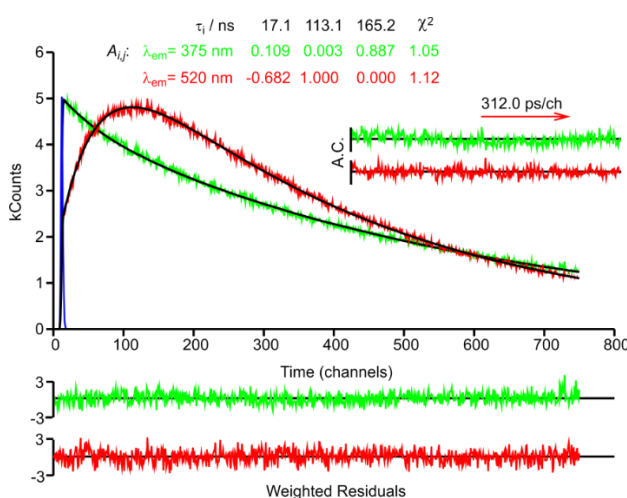


Figure 3.62. Global analysis of the fluorescence decay of the PNIPAMPy(32)182 polymer in dimethylformamide collected at the monomer and at the excimer emission wavelengths (375 nm and 520 nm, respectively) with excitation at 339 nm and $T = 293$ K with imposed decay time values recovered from independent analysis. The instrument profile curve is also shown. For a better judgment of the quality of the fits shown as insets are the weighted residuals and the A.C. functions; see text for further details.

In Figure 3.63, the fraction of all the species involved are shown as a function of the temperature.

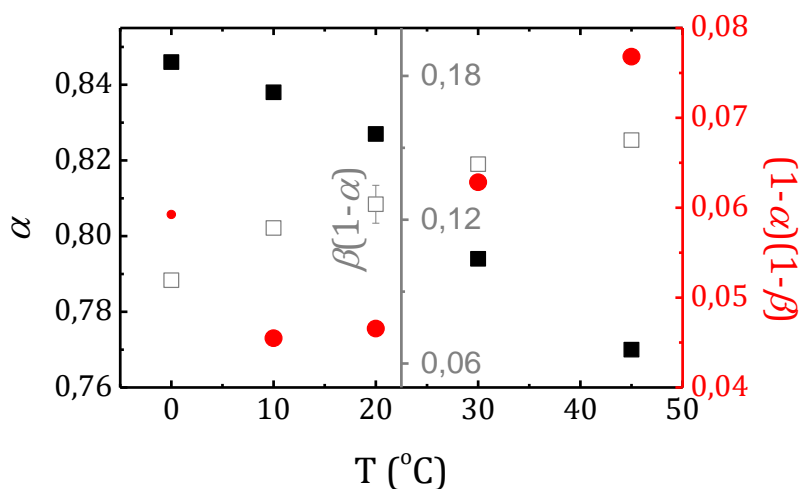


Figure 3.63. Fractions of MAGRE $[(1-\alpha)(1-\beta)]$, isolated monomers (α) and GSD $[\beta(1-\alpha)]$ as a function of the temperature.

As expected, the increase in the temperature leads to a decrease of the fraction of isolated monomers, α , and an increase of the $(1-\alpha)(1-\beta)$ values, corresponding to the fraction of MAGRE. However, the fraction of GSD also increases slightly. This can be explained by three possibilities. (1) The variations on the $[\beta(1-\alpha)]$ values is very small and the error must be considerable, (2) it is possible that, with time, more aggregation is occurring since the decays were measured from -10 to 90°C, and (3) the polymer chain is in a less restricted medium and can rearrange the chains in order to set the pyrene units together, in a more probable conformation, leading to an increase in the GSD value.

One way to remove the first possibility would be to try to remove most of the non- and mono-labelled polymer chains in a way that the values of the other species would be of the same order. To eliminate the second possibility, it would be interesting to make the same experiment but now from 90 to -10°C, but (2) is not very probable, since the polymer seemed to be highly soluble in DMF, changing the solvent could also clarify this point. For the third possibility, maybe by making different decays (at the same temperature) of the same sample (deaerated always before the measurement) with time to see if the chain is rearranging, although this could be also an indication of (2). Maybe by changing the viscosity of solvents some input could be obtained in order to elucidate this strange behaviour.

The extinction coefficient of the parent compound chosen for the PNIPAMPy polymers here investigated (1-pyrenylmethacrylate) was obtained in DMF, Figure 3.64.

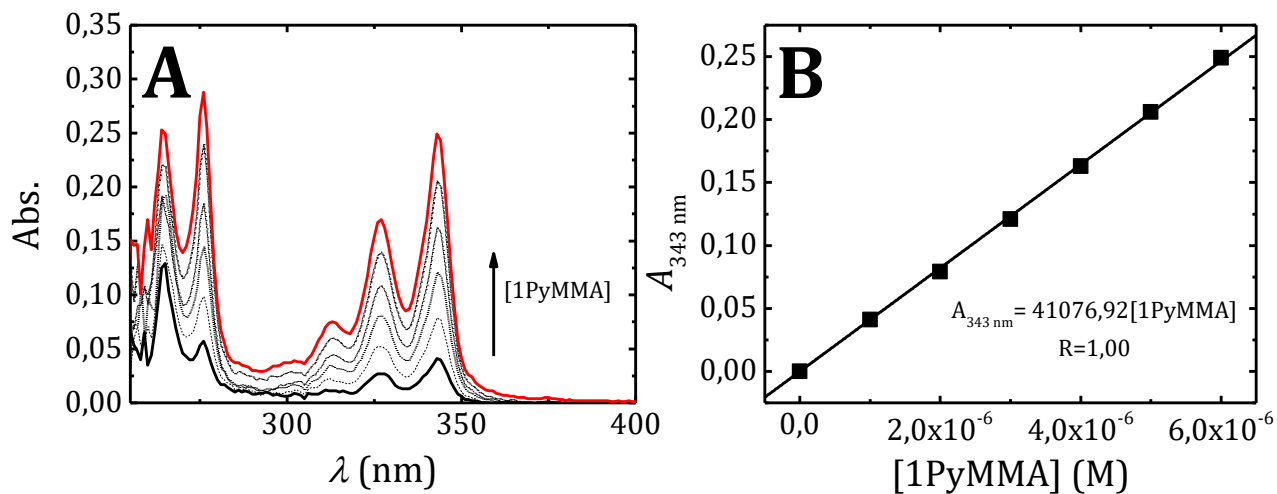


Figure 3.64. Determination of the molar extinction coefficient at 343 nm. (A) Absorption spectra of 1-pyrenylmethacrylate (1PyMMA) in DMF at different concentrations and (B) absorbance at 343 nm as a function of the concentration of 1PyMMA in DMF.

Polymers

Table 3.15. Values taken from the analysis of the fluorescence decays of the PNIPAMPy(32)182 polymer in different solvents. Fluorescence decay times (τ_i), pre-exponential factors ($A_{i,j}$) and chi-squared values (χ^2) recovered from the fitting. The viscosity (η) of the solvents are also presented.

Solvent	η (mPa.s)	τ_2 (ns)	τ_1 (ns)	τ_M (ns)	$A_{1,1}$	$A_{1,2}$	$A_{1,0}$	$A_{2,1}$	$A_{2,2}$	$A_{2,0}$	χ^2 (Mon.)	χ^2 (Exc.)
Dx	1.3075 ¹¹⁴	14.54	114.30	218.47	0.043	0.276	0.681	-0.627	0.908	0.092	0.94	1.35
MeOH	0.5929 ³⁵	12.89	122.16	324.63	0.106	0.583	0.311	-0.583	0.997	0.003	1.33	1.38
DMSO	1.991 ³⁵	27.74	69.05	170.90	0.064	0.005	0.931	-0.495	0.669	0.331	1.02	1.02
DMF	0.924 ³⁵	18.84	107.11	169.42	0.106	0.048	0.846	-0.652	0.916	0.084	1.14	1.02

Table 3.16. Relevant parameters obtained from the steady state (SS) [λ_{\max}^{Abs} , P_A , λ_1 , λ_3 , λ_{\max}^E , I_1/I_3 , I_E/I_M , P_M , P_E and $P_M \cdot P_E$] for PNIPAMPy(55)13 in CH₂Cl₂.

λ_{\max}^{Abs} (nm)	P_A	λ_1 (nm)	λ_3 (nm)	λ_{\max}^E		I_1/I_3					I_E/I_M^d					P_M^e	P_E^f	$P_M \cdot P_E^f$	
				λ_{exc} (nm)		λ_{exc} (nm)					λ_{exc} (nm)								
				315	335	339	315	335	339	345	350	315	335	339	345	350			
344.7±0.1	2.74	375 ^a	387 ^b , 386 ^c	484	482	483	1.76	1.65	1.72	1.76	1.53	1.32	1.40	1.20	1.21	1.66	2.59	2.18	0.41

^a with λ_{exc} = 315, 335, 339, 345 and 350 nm. ^b with λ_{exc} = 315, 339, 345 and 350 nm. ^c with λ_{exc} = 335 nm. ^d I_E/I_M ratios were taken by Method A, C (in brackets) and D (in square brackets). ^e taken with λ_{em} = 375 nm. ^f taken with P_E at λ_{em} = 480 and 520 nm.

Chapter 4

Chemosensors

4.1. Introduction

4.1.1. Chemical Sensors

A chemosensor is a molecule that interacts with an analyte inducing a chemical stimulus which produces a detectable change. It must be constituted by, at least, two components; a chemical receptor capable of recognizing the guest of interest and a transducer or signalling unit which converts that binding event into a measureable physical change. Finally this change will be measured by an appropriate method and converting it to useful information.

Some sensors may include a separator (spacer) which can be, for example, $-(\text{CH}_2)_n$.¹⁷⁹ Depending on the response to this stimulus, they can be classified as electronic, optical, *etc.*, sensors.

In this work, only optical chemosensor in which the physical change is based on absorbance or/and fluorescence emission (covering the UV and visible region of the electromagnetic spectra) will be covered.

In Figure 4.1 it can be seen the illustration of a chemosensor where the detectable change is the enhancement of the fluorescence emission (turn-on chemosensor).

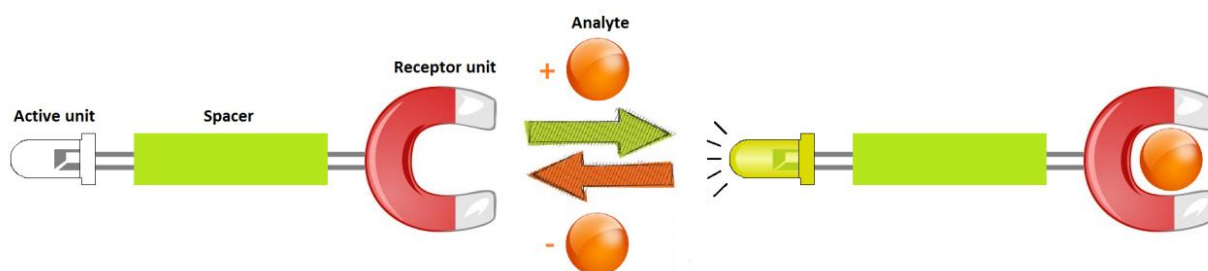


Figure 4.1. Illustration of the operation of a turn-on chemosensor. Adapted from ref. ¹⁸⁰

A great range of selective receptors for cationic species has been prepared and, by coupling those receptors (ionophores) to the adequate fluorophores, powerful chemosensors have been developed. The characteristics of the ionophore in terms of the ligand topology and the number and nature of the complexing atoms must be adequate to the type of cation being studied and can be predicted by the Hard and Soft Acid Bases Theory. The Hard Soft Acids Bases theory states that hard acids bind strongly with hard bases and soft acids bind strongly with soft bases.¹⁸¹

4.1.2. Importance of Fluorescence Probes and Chemosensors

The development of chemosensors has received considerable attention due to their biological and environmental important roles. In this work, the focus will be on cation chemosensors.

Cations play an important role both in the environment as the biological level. Some cations are necessary for the proper functioning of the metabolism but when encountered in excess they are associated with various pathologies. For example, zinc in excess is associated with diseases such as Alzheimer's, epilepsy, Parkinson's, ischemic stroke and infantile diarrhea.¹⁸²

In turn, the accumulation of mercury in the body is responsible for several complications such as prenatal brain damage; serious cognitive and motion disorders; and Minamata disease.^{183,184}

4.1.3. Mechanisms of Transduction

There are several mechanisms that are inherent to chemosensing such as photoinduced–electron transfer (PET), photoinduced charge transfer (PCT), excited state intramolecular proton transfer (ESIPT), Förster resonance energy transfer (FRET) and excimer and exciplex formation. In each class of sensors, distinction is to be made according to the structure of the complexing moiety: chelators, podands (Figure 4.3A), coronands (crown ethers, Figure 4.3B), cryptands, calixarenes.¹⁸⁵

4.1.3.1. Photoinduced Electron Transfer (PET)

When a fluorophore absorbs a photon, an electron is promoted from the highest occupied molecular orbital (HOMO) to the lowest unoccupied molecular orbital (LUMO), which leaves a hole in the former orbital. If the cation receptor is an electron donor (e.g. an amino group) and since the fluorophore can now work as electron acceptor, this hole can be filled via PET from the HOMO of the donor (cation receptor in its free form) to the HOMO of the fluorophore. This new electron inhibits the decay of the previously excited one, and in this way fluorescence is quenched. Cation binding raises the redox potential of the donor, and the HOMO that was involved in the PET process has now a lower energy (stabilization arising from the dative covalent bonding between the donor and the metal ion, which

requires both electrons). As a consequence, PET becomes impossible, and fluorescence intensity is enhanced (chelation induced enhancement of fluorescence - CHEF), Figure 4.2.^{186,187}

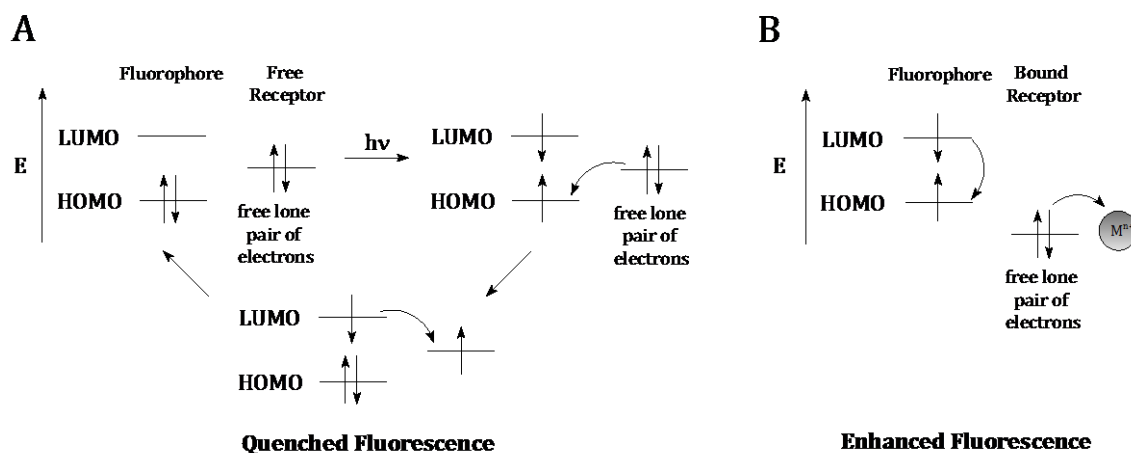


Figure 4.2. Mechanisms for (A) PET and (B) CHEF adapted from ref. ³⁴.

In Figure 4.3 some PET based chemosensors are presented.

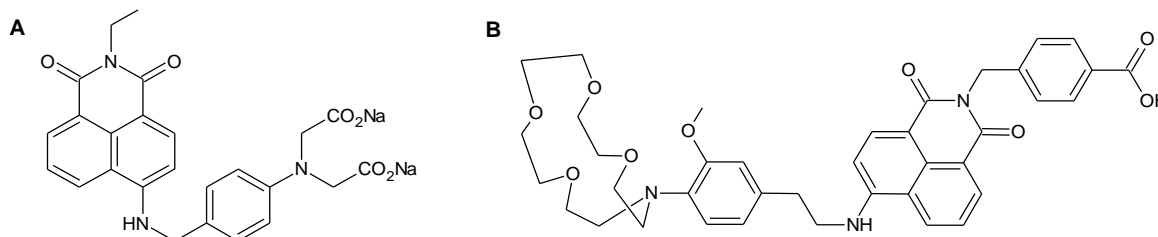


Figure 4.3. Structure of some PET based chemosensors: example of (A) a podand-based^{188,189} and (B) a crown-containing¹⁹⁰ PET sensor.

4.1.3.2. Excited State Intramolecular Proton Transfer (ESIPT)

In the excited state, the acidic or basic properties of a molecule are different from the correspondent ground state; one of the causes is the electronic density redistribution upon light absorption. Molecules that are more acidic or basic in the excited state than in the ground state (photo-acids and photo-bases, respectively) are able to undergo excited state proton transfer upon excitation.

The two excited states forms can reach equilibrium on a very short time scale and, in aqueous solution, this equilibrium can be shifted by changing, for example, the pH.

When the same molecule contains both proton-donor and proton-acceptor groups in a close proximity, the solvent loses influence, since the proton can be transferred directly from the acidic site to the basic site. This process is named excited-state intramolecular proton transfer (ESIPT). The proton donor is commonly a hydroxyl or amino group and the basic proton acceptor should be either a heterocyclic nitrogen or a carbonyl oxygen. These two groups normally form hydrogen bonds in the ground state, and this bond in the excited state facilitates proton transfer.¹⁹¹

The ESIPT process can be recognized in steady-state spectra: the absorbance is generally similar to that of the parent chromophore but the fluorescence is significantly different. ESIPT dyes generally have large Stokes shift and are ideal candidates for use as fluorescence labels to avoid interference from other fluorescent materials present in the sample. An advantage of the large Stokes shift is the almost complete lack of spectral overlap between absorption and emission, which makes ESIPT dyes promising for use in fluorescent sensors.¹⁹¹

Excimer based sensors were already discussed in Section 1.3.2.

4.1.4. Competitiveness Study

Whenever it appears that a ligand is selective to a particular analyte, studies of competitiveness should be complemented. The competitiveness study consist in verifying if the parameter that has undergone changes in the presence of an analyte remains still visible in the presence of other ions, molecules, *etc.* To do this, it is necessary to prepare several samples with different ions (or other molecules) to compete with the analyte for which the ligand is allegedly selective, add the ligand and check if the parameter still changes with the addition of other components.

The studies of competitiveness are made in general according to the application that is intended to give to the sensor. For instance, if it is to in the future apply to the determination of an analyte in a living being, one should make the study of competitiveness with sodium once it exist in great abundance in living organisms.¹⁹²

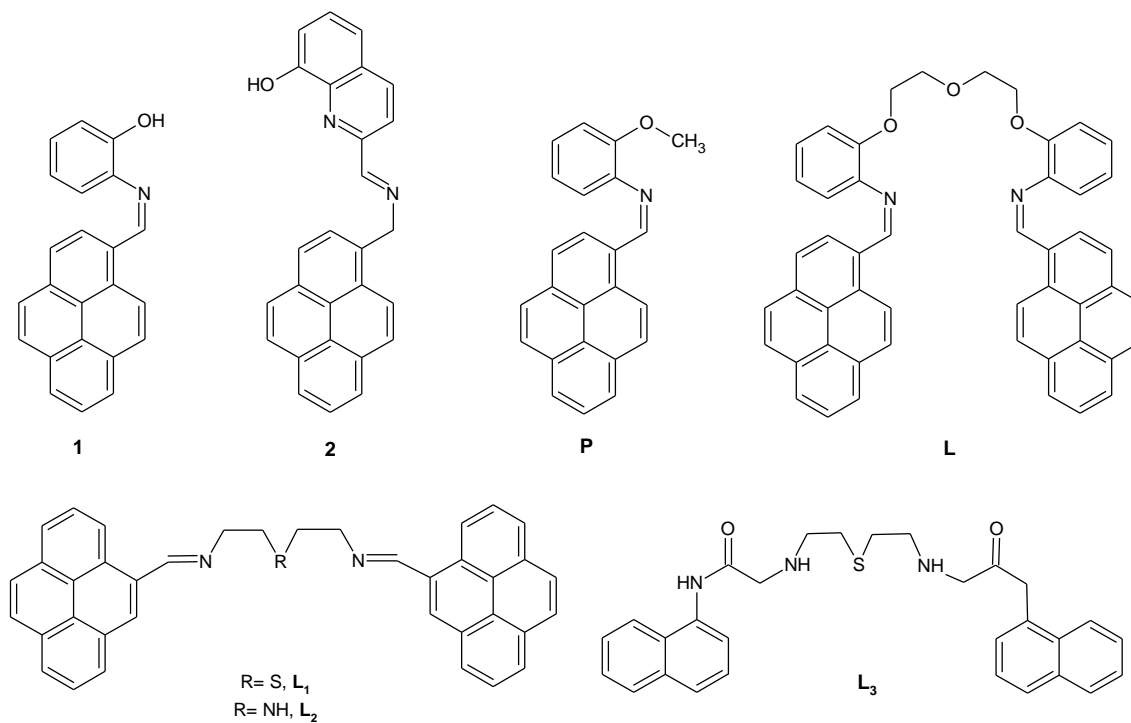
4.2. Synthesis

All the chemosensors found in Scheme 4.1 were synthesized in the group of Prof. Carlos Lodeiro. The synthetic procedure of compounds 1 and 2 can be found in ref. ¹⁹³ and ¹⁹⁴, respectively. The compounds P and L were synthesized by Javier Fernández-Lodeiro and the synthetic method can be found in ref. ¹⁹⁵ whereas the naphthalene-based chemosensor were synthesized by Adrián Fernández-Lodeiro and the synthetic method can be found in ref. ¹⁹⁵.

Chemosensors

The compounds **L**₁ and **L**₂ were synthesized by Daniela Pinheiro, with the collaboration of Cristina Nuñez; see Scheme 7.3 in Chapter 7. Note that compound **P** can be a good parent for both compounds **L** and **1**.

Chemosensors



Scheme 4.1. Chemical structure of compounds 1, 2, P and L, L1, L2 and L3. From Yellow to Pink Using a Fluorimetric and Colorimetric Pyrene Derivative and Mercury (II) ions.

4.2.1. Photophysical Characterization of Compound 1

The absorption, fluorescence emission (and excitation) spectra of **1** were obtained in dichloromethane. The absorption spectra show a characteristic pyrene derivative spectra¹⁹⁵ with a maximum at 426 nm (red shifted compared to the pyrene absorption spectra) and a high extinction coefficient value ($112870 \text{ cm}^{-1}\cdot\text{M}^{-1}$). Moreover, the emission spectra of **1** displays an unresolved and broad emission band centred at *ca.* 500 nm, with low fluorescence likely resulting from a photoinduced electron transfer process from the nitrogen lone pair to the aromatic moiety (intramolecular PET)¹⁹⁶ (Figure 4.4).

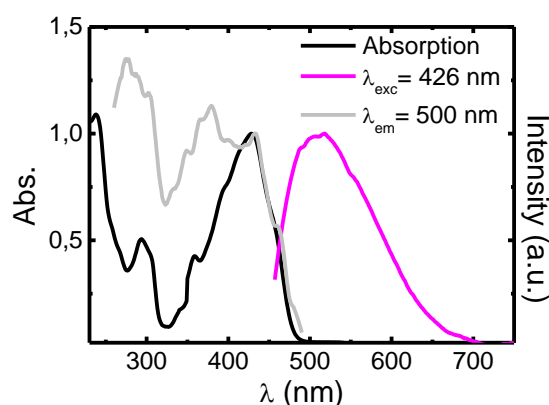


Figure 4.4. Normalized absorption, smoothed emission ($\lambda_{\text{exc}} = 426 \text{ nm}$) and excitation spectra ($\lambda_{\text{em}} = 500 \text{ nm}$) of compound **1** in dichloromethane at 298 K.

4.2.1. Sensorial Ability of Compound 1 Towards H^+ , Zn^{2+} , Cd^{2+} , Cu^{2+} , Ni^{2+} , Pb^{2+} , Fe^{2+} , Hg^{2+} and Al^{3+} Ions

M. Shellaiah et al. explored the photophysical behaviour of compound **1** in CH_3CN after the addition of different metal ions (Li^+ , Ag^+ , K^+ , Na^+ , Cs^+ , Ni^{2+} , Fe^{3+} , Co^{2+} , Zn^{2+} , Cd^{2+} , Pb^{2+} , Ca^{2+} , Cr^{3+} , Mg^{2+} , Cu^{2+} , Mn^{2+} , Hg^{2+} , Fe^{2+} and Ag^{2+}) in H_2O .¹⁹⁷ Compound **1** showed better selectivity towards Cu^{2+} upon treatment with 2.5 equiv. of this metal ion in CH_3CN .¹⁹⁷ Probe **1** illustrated the fluorescence turn-on sensing towards Cu^{2+} via CHEF through excimer (**1-1***) formation. The 2:1 stoichiometry of the sensor complex (**1** + Cu^{2+}) was also calculated from Job plots based on UV-Vis absorption titrations.¹⁹³

In that work,¹⁹³ the solubility of compound **1** in different solvents was tested (see Figure 8.2). In our work, we selected CH_2Cl_2 as the preferential solvent to evaluate the sensorial ability of compound **1** for H^+ , Zn^{2+} , Cd^{2+} , Cu^{2+} , Ni^{2+} , Pb^{2+} , Fe^{2+} , Hg^{2+} and Al^{3+} ions by absorption and fluorescence emission spectroscopy. The results obtained in this solvent (CH_2Cl_2) could be compared with that obtained in CH_3CN ¹⁹⁷ to evaluate the influence of the solvent in the coordination properties.

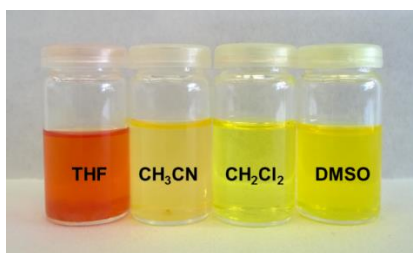


Figure 4.5. Visual colour showed by compound **1** in the different solvents tested (THF, CH₃CN, CH₂Cl₂ and DMSO).

Figure 4.6 shows the absorption and emission spectra of compound **1** upon the addition of H⁺. As can be seen, in the ground state the addition of H⁺ induces to the appearance of a new (orange) coloured band located at *ca.* 545 nm.

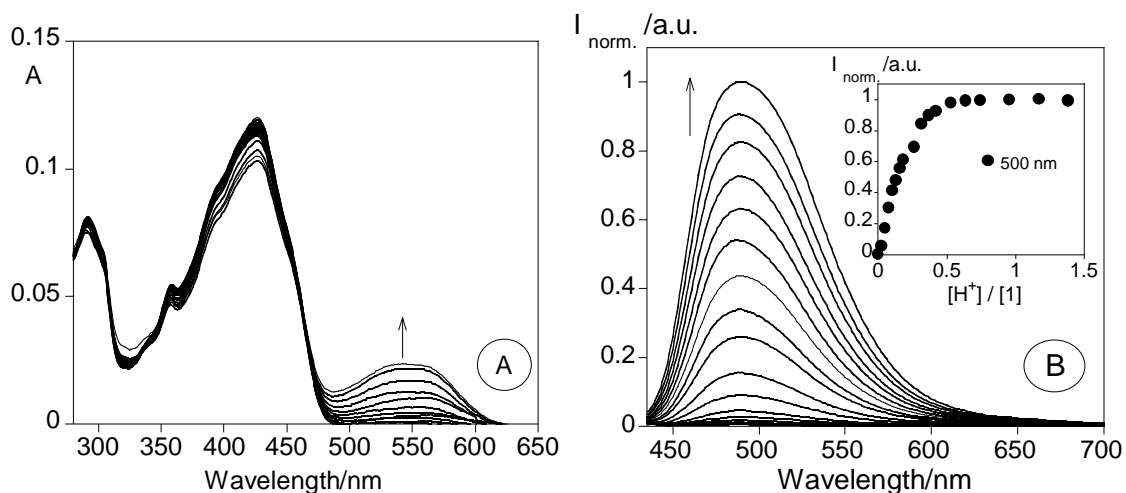


Figure 4.6. Spectrophotometric (A) and spectrofluorometric (B) titrations of compound **1** with the addition of H⁺ in dichloromethane. The inset represents the emission intensity at 500 nm (B) as a function of [H⁺]/[**1**]. ([**1**] = 3.0 × 10⁻⁶ M, λ_{exc.(B)} = 426 nm, T = 298 K).

Moreover, in Figure 4.6 and inset, a blue shift and an enhancement of the emission intensity can be observed.

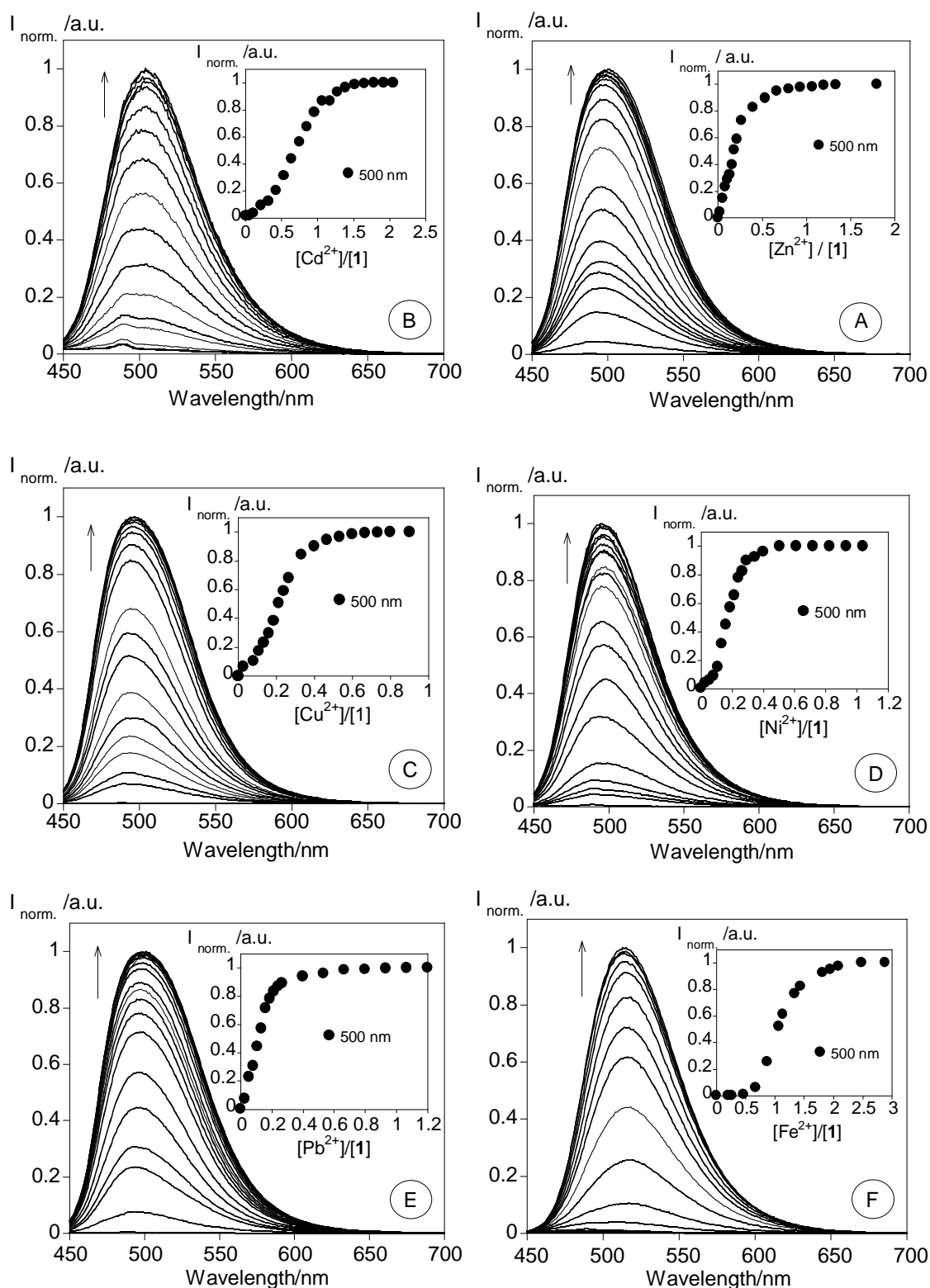


Figure 4.7. Spectrofluorometric titrations of compound 1 with the addition of Zn^{2+} (A), Cd^{2+} (B), Cu^{2+} (C), Ni^{2+} (D), Pb^{2+} (E) and Fe^{2+} (F) in dichloromethane. The inset represents the emission intensity at 500 nm as a function of $[\text{Zn}^{2+}]/[1]$ (A), $[\text{Cd}^{2+}]/[1]$ (B), $[\text{Cu}^{2+}]/[1]$ (C), $[\text{Ni}^{2+}]/[1]$ (D), $[\text{Pb}^{2+}]/[1]$ (E) and $[\text{Fe}^{2+}]/[1]$ (F). ($[1] = 3.0 \times 10^{-6}$ M, $\lambda_{\text{exc.}} = 426$ nm, $T = 298$ K).

The appearance of the long wavelength absorption band clearly indicates the potential of **1** as a colorimetric probe. However, this becomes clearer with the addition of metal ions. Indeed, the addition of one equivalent of transition and post-transition metal ions (Zn^{2+} , Cd^{2+} , Cu^{2+} , Ni^{2+} , Pb^{2+} , Fe^{2+} , Hg^{2+} and Al^{3+}) did not induce spectral changes in the absorption spectra with the sole exception of Hg^{2+} for which a change of colour from yellow to pink was detected. Nevertheless, when the amount of metal ions is increased to 10 equivalents, a colorimetric behaviour is equally visualized with Cu^{2+} and Fe^{2+} (see Picture 4.1A and B).

In which regards the emission behaviour (spectra) of **1**, a blue-shift and an enhancement of the emission spectra (with maximum at 500 nm) was observed upon addition of the aforementioned metal ions (see Figure 4.7). However, probe **1** does not show any spectral changes upon addition of the Al^{3+} metal ion (data not shown). Figure 4.7 shows the emission spectra of compound **1** with the incremental addition of Zn^{2+} , Cd^{2+} , Cu^{2+} , Ni^{2+} , Pb^{2+} and Fe^{2+} metal ions with excitation at 426 nm.

As an example of the colorimetric behaviour observed, Figure 4.8 presents the absorption and emission spectra of compound **1** upon addition of Hg^{2+} .

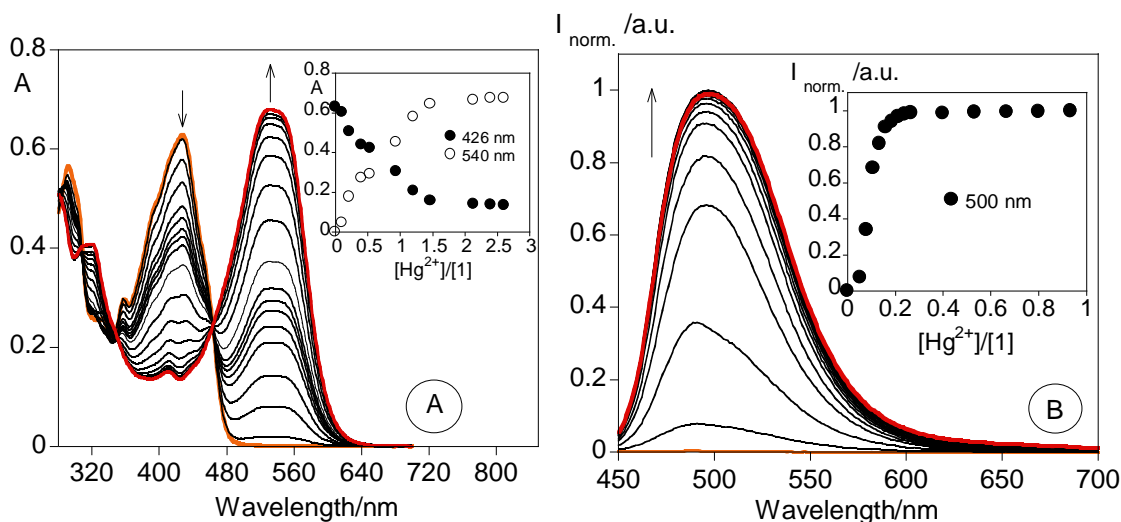


Figure 4.8. Spectrophotometric (A) and spectrofluorometric (B) titrations of compound **1** with the addition of Hg^{2+} in dichloromethane. The inset represents the absorption (A) at 426 and 540 nm; and represents the emission intensity (B) at 500 nm as a function of $[\text{Hg}^{2+}]/[\mathbf{1}]$. ($[\mathbf{1}]_{\text{Abs.}} = 1.20 \times 10^{-5} \text{ M}$, $[\mathbf{1}]_{\text{em.}} = 3.0 \times 10^{-6} \text{ M}$, $\lambda_{\text{exc.}} = 426 \text{ nm}$, $T = 298 \text{ K}$).

As seen with H^+ , the increase of Hg^{2+} ion concentration (in a dichloromethane solution) causes an absorbance decrease at ca. 426 nm and an increase at ca. 540 nm. However, in this case sharp isosbestic points were detected (Figure 4.8A) at 282, 310 and 345 nm and, more evident, at 465 nm. The appearance of the new band and consequently of the observed red shift of the maxima results from the

interaction of these ions (H^+ and Hg^{2+}) with the ligand; in this case, a change from *yellow* to *pink* was visualized. Moreover the reversibility of colour indicates that there is no degradation of **1** under acidic media and in the presence of Hg^{2+} .

Taking into account the heavy metal ion nature of Hg^{2+} , it would be expected a CHEQ effect (Chelation Enhancement of the Quenching) in the emission spectra.¹⁹⁸ However, a CHEF at 500 nm was observed (see Figure 4.7B) similar to that showed for compound **1** with 2.5 equiv. of Cu^{2+} in CH_3CN .¹⁹⁷ In this particular case, the formed complex emission contribution overcomes the heavy metal ion effect, which is usually coupled with non-radiative decay routes, such as the S_1 to T_1 intersystem crossing, which would have the effect of decreasing the fluorescence emission.

As mentioned above, the low fluorescence likely results from a PET process from the nitrogen lone pair to the aromatic moiety. Upon cation binding the redox potential of the donor is raised and the HOMO that was involved in the PET process has now a lower energy (stabilization arising from the covalent bonding between the donor and the metal ion, which requires both electrons). As a consequence, PET becomes impossible, and fluorescence intensity is enhanced.

In order to evaluate the potential of the proposed turn-on fluorescent probe for detecting metal ions, the detectable amount of Zn^{2+} , Cd^{2+} , Cu^{2+} , Ni^{2+} , Hg^{2+} , Pb^{2+} and Fe^{2+} metal ions were explored by a standard addition method in dichloromethane. The analytical results are summarized in Table 4.1. The association constants for metal ion interaction were determined using the HypSpec program¹⁹⁹ and the main results are gathered in Table 4.1. As expected, the highest association constant was obtained for mercury ion with a value of $\log K_{ass.} = 13.11 \pm 0.02$, followed by Cu^{2+} , Zn^{2+} , Pb^{2+} , Ni^{2+} , Cd^{2+} and Fe^{2+} metal ions. A stoichiometry of two ligands per metal ion was postulated.

Table 4.1. Association constants ($K_{ass.}$) and minimal amount of metal ions detectable by fluorescence emission for compound **1** in dichloromethane at 293 K.

Metal ion	Log $K_{ass.}$ (M:L)	Minimum amount detectable (μM)
Zn²⁺	12.52±0.01 (1:2)	1.20
Cd²⁺	9.80±0.01(1:2)	1.54
Cu²⁺	13.00±0.01 (1:2)	2.51
Ni²⁺	10.52±0.01 (1:2)	2.62
Pb²⁺	11.31±0.01 (1:2)	2.00
Fe²⁺	9.59±0.01 (1:2)	13.24
Hg²⁺	13.11±0.02 (1:2)	0.62

Figure 4.9 shows a graphic bar of compound **1** without metal and upon addition of 0.5 equivalents of each metal ion together (picture on top) with the respective colour changes. Similar to the association constants, the strongest interaction was observed with Hg^{2+} and Cu^{2+} metal ions.

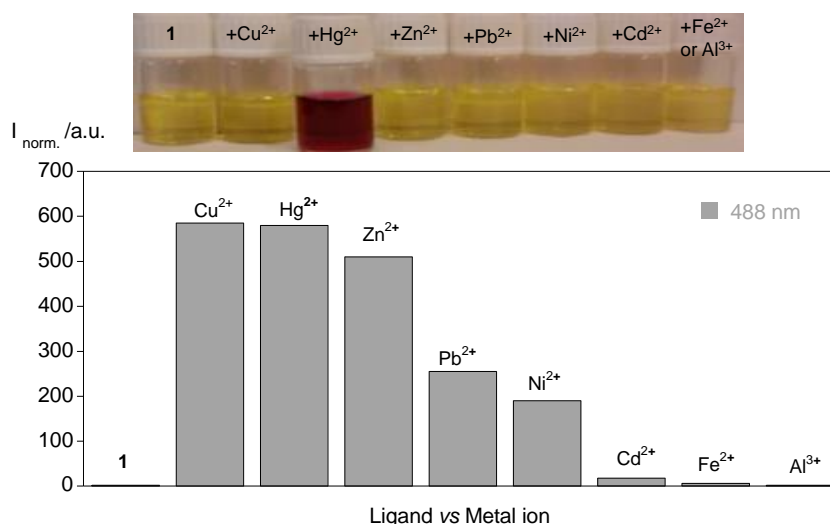


Figure 4.9. From bottom to top. Normalized fluorescence intensity at 488 nm of compound **1** in dichloromethane with 0.5 equivalents of metals (Zn^{2+} , Cd^{2+} , Cu^{2+} , Ni^{2+} , Pb^{2+} , Fe^{2+} , Hg^{2+} and $\text{Al}^{3+} = \text{M}^{n+}$) added in dichloromethane; and picture of these solutions.

Picture 4.1 shows the colorimetric behaviour of system **1** under four different conditions A to D. Condition A shows the colour of the solutions of **1** with the addition of one equivalent of metal ions; condition B with the addition of 10 equivalents; condition C with the initial addition of 10 equivalents and further addition of one equivalent of Hg^{2+} ; condition D with the initial addition of 10 equivalents of metal ions and further addition of three equivalents of proton.

Taking into account the results observed, we might conclude that compound **1** is colorimetric selective for Hg^{2+} ion in low concentrations, up to one equivalent. Moreover a different palette of pink, orange and violets colours can be developed with **1** upon examining the different metal ions and protons as colour modulators.



Picture 4.1. Naked-eye colorimetric behaviour of system **1** in four different conditions A to D. Condition A shows the naked eye colour solutions of **1** with the addition of one equivalent of metal ions; condition B with the addition of ten equivalents; condition C with the initial addition of ten equivalents and further addition of one equivalent of Hg^{2+} ; condition D with the initial addition of ten equivalents of metal ions and further addition of three equivalents of proton.

Compound **1** showed a selective fluorescence response to Cu^{2+} in CH_3CN ¹⁹⁷ but better response in mercury in CH_2Cl_2 . The results obtained in CH_2Cl_2 offered the advantage of using compound **1** as a colorimetric and fluorescence molecular probe for the detection of different metal ions. It was also observed that a small quantity of the different metal ions was necessary to obtain a spectrophotometric and/or spectrofluorometric response in CH_2Cl_2 solution.

4.2.2. Time-Resolved Data

Further knowledge on the photophysical behaviour of **1** comes from time resolved data. The fluorescence decay of compound **1** was obtained in dichloromethane with excitation at 451 nm and with emission at 500 nm, see Figure 4.10.

In the case of the free ligand the decay is single exponential with a decay time of 7 ps. In the presence of mercury, the analysis of the decays leads to a bi-exponential fit. The 3.35 ns species is the dominant absorbing species with a contribution of more than 98% to the total emission. It is worth noting that the 3.35 ns species (found for **1** in the presence of mercury) is much different than the value obtained for the free ligand (7 ps) thus once more confirming that PET is precluded.

Chemosensors

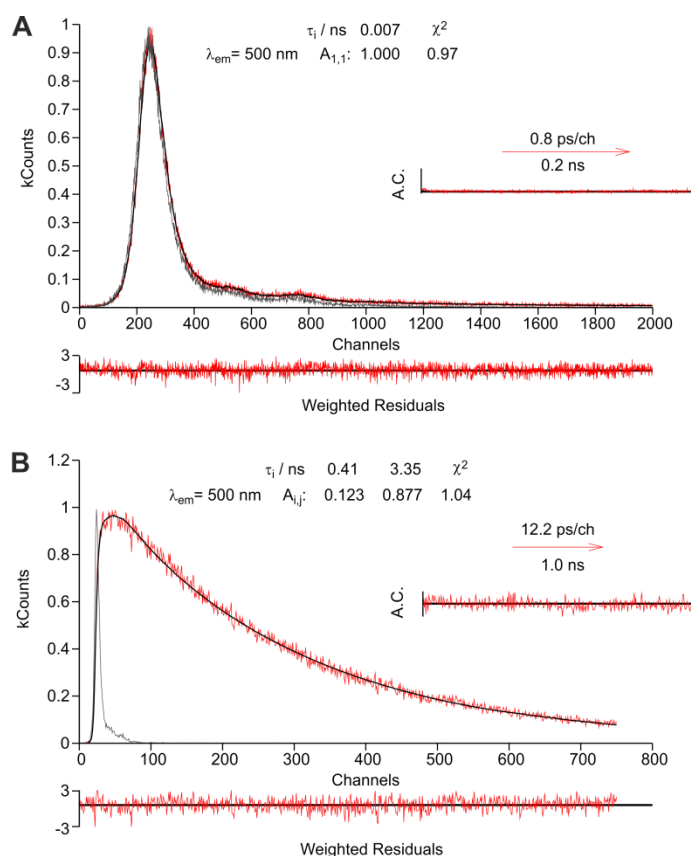


Figure 4.10. Fluorescence decay of compound **1** in dichloromethane (A) metal free and (B) with $[Hg^{2+}]/[1] = 1$ at $T = 293$ K with $\lambda_{exc} = 451$ nm (picoLED) and collected at $\lambda_{em} = 500$ nm. The instrument profile curve, decay times (τ_i), pre-exponential factors ($A_{i,j}$), χ^2 values, weighted residuals, and autocorrelation functions (A.C.) are shown as insets.

4.2.3. Summary

In summary, the Schiff base pyrene derivative (**1**) was successfully synthesized and fully characterized. Probe **1** shows to be colorimetric with a change of colour from yellow to pink for Hg^{2+} metal ion at low concentration (till one equivalent), and fluorimetric with a strong enhancement of the emission intensity with the highest association constant of $\log K_{ass.} = 13.11 \pm 0.02$. Moreover from the starting yellow colour, a different palette of pink, orange and violets colours can be developed with dye **1** when examining different metal ions and protons as colour modulators. The results obtained in CH_2Cl_2 offered the advantage of using compound **1** as a colorimetric and fluorescence molecular probe, while in CH_3CN , only a fluorescence response was showed by probe **1**.

4.2.4. Supporting Information

4.2.4.1.1. Crystallography Data

Yellow crystals of compound **1** suitable for X-ray diffraction were obtained by slow diffusion of diethyl ether into a dichloromethane solution of compound **1** at room temperature. Compound **1** was subjected

to X-ray single crystal analysis, and Figure 4.11 shows the ORTEP view. Summary of the crystallographic data and the structure refinement parameters is reported in Table 4.2.

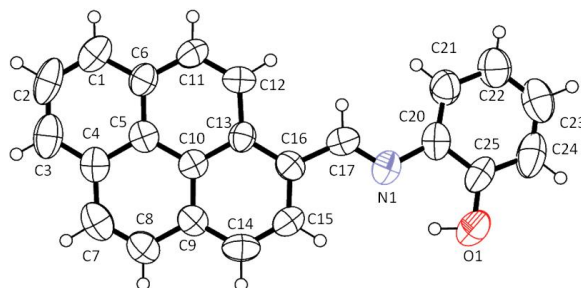


Figure 4.11. Crystal structure of compound **1**. Ellipsoids are shown at the 50% probability level. Selected bond lengths (Å) and angles (°): C(17)-C(16), 1.464(9), N(1)-C(17) 1.279(8), N(1)-C(20) 1.423(9), C(20)-C(25) 1.384(9), C(25)-O(1) 1.358(9), C(25)-C(24) 1.384(11), C(13)-C(16)-C(17) 123.9(7), N(1)-C(17)-C(16) 123.6(8), C(17)-N(1)-C(20) 120.8(7), C(25)-C(20)-N(1) 114.2(8), C(21)-C(20)-N(1) 128.1(7), O(1)-C(25)-C(20) 119.9(8), O(1)-C(25)-C(24) 118.7(8).

The crystal of compound **1** belongs to the monoclinic space group P2(1)/c. As shown in Figure 5, the structure is quite planar where the unique remarkable point shows that the hydroxyl group is pointing out of the molecular plane with an angle of 114.2° [C(25)-C(20)-N(1)]. It is not indicated that there are weak intermolecular π - π stacking interactions in the crystal lattice of compound **1**.

Table 4.2. Crystal data and structure refinement for compound **1**.

	Compound 1
Empirical formula	C ₅₀ H ₃₇ N ₃ O ₂
Formula weight	711.83
Temperature	293(2) K
Wavelength	0.71073 Å
Crystal system	Monoclinic
Space group	P2(1)/c
Unit cell dimensions	a = 12.376(6) Å, α = 90° b = 11.291(5) Å, β = 107.914 (7)° c = 12.249(6) Å, γ = 90°
Volume	1628.6 (13) Å ³
Z	2

Chemosensors

Density (calculated)	1.452g/cm ³
Absorption coefficient	0.089mm ⁻¹
F(000)	748
Crystal size	0.34 x 0.22 x 0.18 mm ³
Theta range for data collection	1.73 to 25.09 ^o
Index ranges	-14 ≤ h ≤ 12, -10 ≤ k ≤ 13, -14 ≤ l ≤ 14
Reflections collected	5359
Independent reflections	2416 [R(int.) = 0.0689]
Completeness to theta =	83.3% (25.09 ^o)
Absorption correction	None
Refinement method	Full-matrix least-squares on F ²
Data / restraints / parameters	2416 / 0 / 234
Goodness-of-fit on F ²	1.115
Final R indices [I>2sigma(I)]	R1 = 0.1294, wR2 = 0.2471
R indices (all data)	R1 = 0.2392, wR2 = 0.2970
Largest diff. peak and hole	0.204 / -0.163e ^Å -3

4.3. Steady-State and Time-Resolved Investigations on Pyrene-Based Chemosensors

4.3.1. Spectrophotometric Studies

Absorption, emission, and excitation spectra of **P** and **L** were obtained in dioxane at 298 K, and the results are presented in Figure 4.12 and Table 4.3.

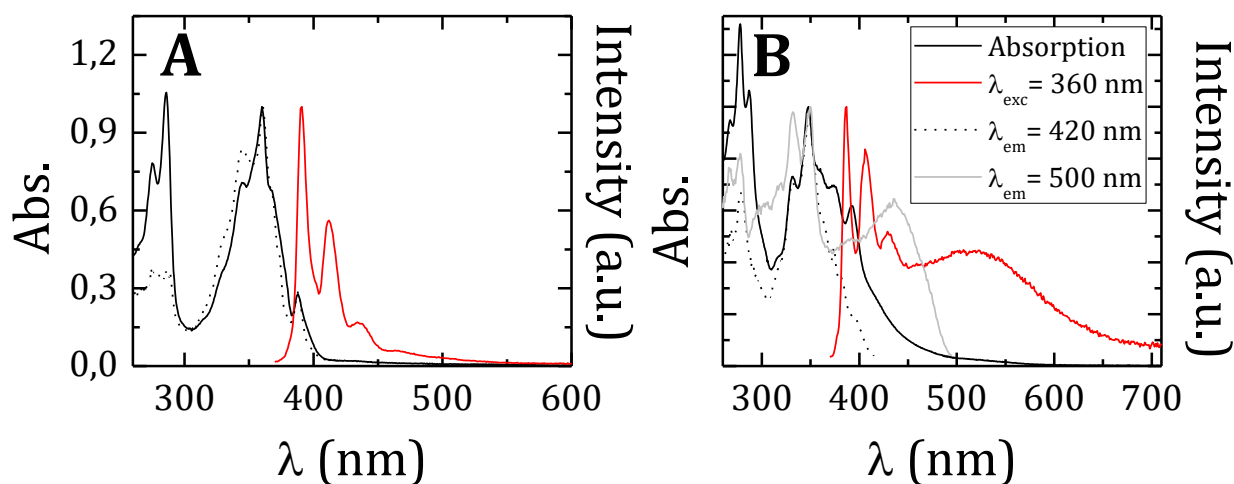


Figure 4.12. Absorption and fluorescence emission and excitation spectra ($\lambda_{em1} = 420$ nm for P and L and $\lambda_{em2} = 500$ nm for L) for (A) P and (B) L in dioxane.

For **P**, both the absorption and emission spectra show a single band, which is attributed to the monomer (absorption and emission) of this compound by comparison with pyrene.³⁸ However, it should be noticed that in contrast with pyrene, where the first electronic transition has a forbidden character, in the case of **P**, the 0,0 transition is now allowed, as can be seen from Figure 4.12A. In the case of compound **L** in dioxane, an absorption band in the 400–500 nm region is now visible together with an emission band with maxima at ~500 nm. Two potential reasons can be appointed to rationalize the origin of this band in **L**: (i) a small amount of water that persists from the synthetic and purification procedure, even if this is dried to exhaustion; (ii) the formation (resulting from the interaction between the two pyrene units in **L**) of an intramolecular dimer. In dioxane, the presence of the 400–500 nm absorption band (seen as a tail) in **L** and its absence in **P** suggests that (ii) mirrors a more realistic situation. Along the text, the reference to this dimer should be viewed as resulting from an intramolecular interaction between the two pyrene units in **L**. In the case of **L**, it is also worth noting that the excitation spectra collected in the monomer emission region mirrors the absorption spectra of the monomer (see Figure 4.13), whereas when collected in the long emission wavelength band (~550 nm), it displays a band in 400–550 nm (Figure 4.12, right panel), which strongly suggests that the great majority of the latter band is originated through a static mechanism (from direct excitation of preformed intramolecular dimers).

Chemosensors

Table 4.3. Absorption, emission and excitation wavelength maxima ($\lambda_{\max}^{abs.}$, $\lambda_{\max}^{em.}$ and $\lambda_{\max}^{exc.}$) and molar extinction coefficients (ϵ) for chemosensors **P** and **L** in dioxane at 298 K. The viscosities of the solvents are also presented.

Compound	Solvent	η (mPa.s ⁻¹)	$\lambda_{\max}^{abs.}$ (nm)	ϵ (cm ⁻¹ .M ⁻¹)	$\lambda_{\max}^{em.}$ (nm)	$\lambda_{\max}^{exc.}$ (nm)
P	Dx	1.3075 ¹¹⁴	361	44 801	392	363 ^{a,b}
	CH ₃ CN	0.345 ³⁵	358		392	
	DMSO	1.991 ³⁵	362			
L	Dx	1.3075 ¹¹⁴	348	55 283	386	362-363

^a and ^b Obtained from the excitation spectra with emission collected at 420 and 500 nm, respectively (see Figure 4.14).

It is worth noting that the I_0/I ratio for the same [metal ion]/[**P**] ratio is 5 times higher with Cu²⁺ than it is with Ag⁺ and Zn²⁺; although further studies with other metals are needed, this suggests a peculiar selectivity of **P** toward Cu²⁺.

Chemosensors

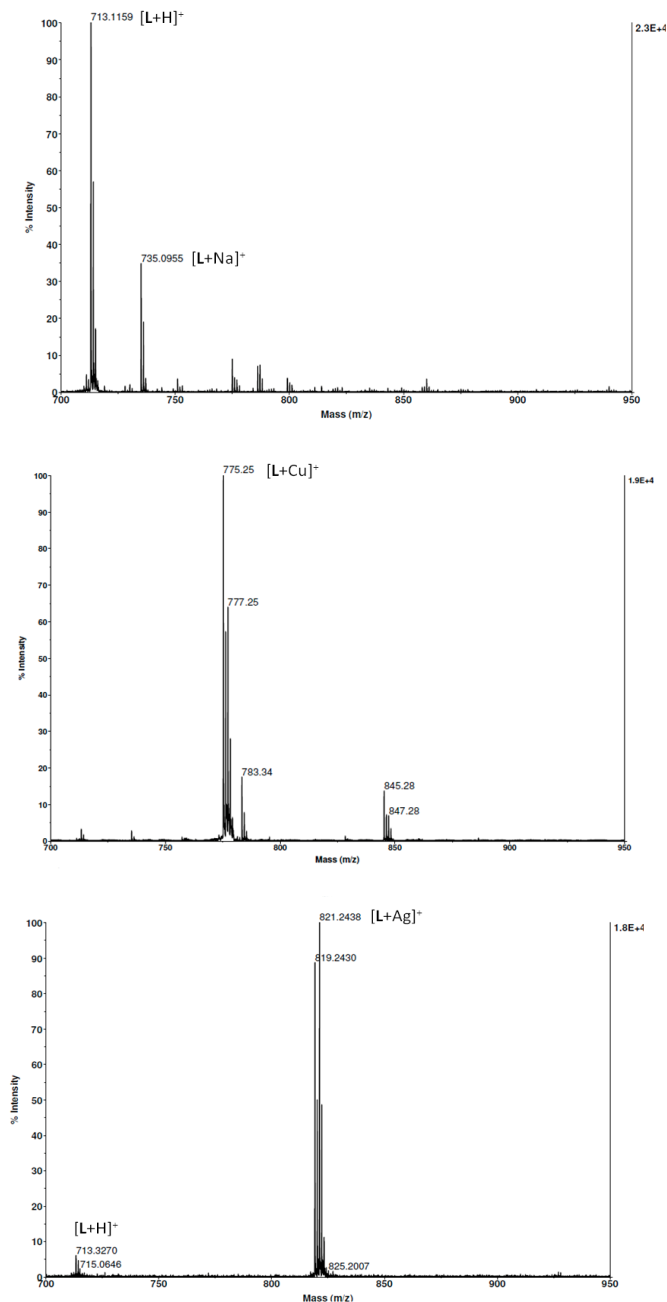


Figure 4.13. From top to bottom, MALDI-TOF-MS spectra of compound L before and after titration with Cu(BF₄)₂ and Ag(BF₄)₂ (1 equiv. of a metal ion). Note that the Na⁺ ion on the top spectrum is from the glassware.

4.3.2. P and L upon the Addition of Water

Upon the addition of water, a new band, in addition to the monomer (390 nm) band, appears for both **P** and **L** with a maximum that varies between 405 and 495 nm; see Figure 4.15.

Chemosensors

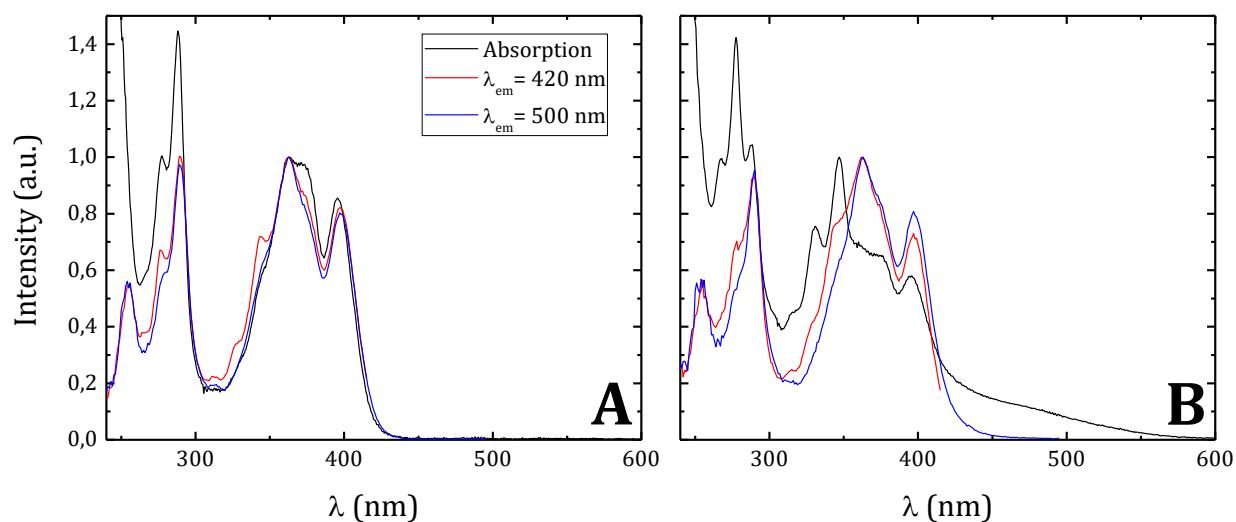


Figure 4.14. Absorption and excitation spectra of compounds P (left panel) and L (right panel) in dioxane. $\lambda_{em}(P) = 420 \text{ nm}$, $\lambda_{em1}(L) = 420 \text{ nm}$, $\lambda_{em2}(L) = 500 \text{ nm}$ and $[P] = [L] = 5 \times 10^{-6} \text{ M}$.

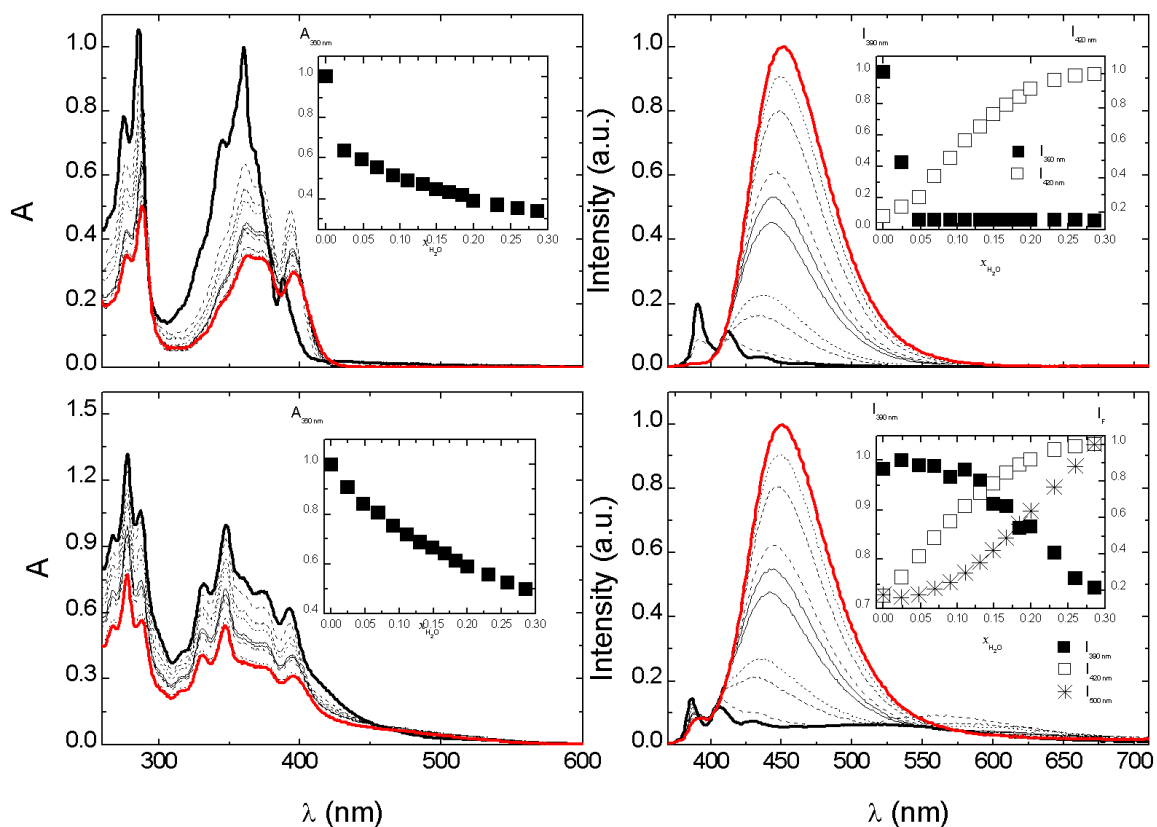


Figure 4.15. Absorption (left panels) and emission (right panels) spectra of P (top panels) and L (bottom panels) in dioxane at room temperature after the addition of water ($\lambda_{exc} = 360 \text{ nm}$ and $[P] = [L] = 5.00 \times 10^{-6} \text{ M}$). The insets show variation with the mole fraction of water of the absorption at 390 nm and the fluorescence intensities at 390 and 420 nm for P and 390, 420, and 500 nm for L. The bold dark line is for $\phi_{H_2O} = 0$, whereas the bold red line is for $\phi_{H_2O} = 0.29$.

By collection of the excitation spectra with emission in this band (i.e., at values in the extremities of this band: 420 and 500 nm), a vibronically resolved band with a maximum at 360 nm is observed for the two compounds (see Figure 4.14 and Figure 4.15). This seems to attest further the identical nature of this band in the two compounds. Moreover, it is worth noticing the fact that with **P** upon collection at 420 and 500 nm, i.e., along this new band that only appears by the addition of water, the excitation spectra match the absorption spectra. The same is, however, not valid for **L**, where although the excitation bands when collected at 420 and 500 nm are identical, a partial departure from full overlap with the absorption spectra is now obtained.

This suggests that in the case of **L** the long emission band is the result of more than one species; i.e., one is identical with that observed with **P** (not absorbing in the ground state, as attested by the left top panel in Figure 4.15), and the additional band (in **L**) is likely to be due to the excimer/dimer, which is also present in the ground state.

As can be seen from Figure 4.15, water strongly influences the absorption and emission spectra of **L**. To exclude the possibility of reaction between **L** and water, an independent experiment was carried out involving the run of the absorption spectra upon the (i) addition of water to **L** and (ii) subsequent removal of water from **L**. A solution of **L** in a dioxane:water mixture ($\phi_{\text{H}_2\text{O}} = 0.80$) was dried with the aim of complete removal of the solvent mixture (water included). The dried compound (in a film form) was again dissolved in dioxane; the two obtained spectra (before and after the removal of water) were found to be identical. In order to have further knowledge on the nature of the emissive species at long emission in both **P** and **L**, the emission wavelength maximum of this emission band was plotted as a function of the water fraction and dielectric constant²⁰⁰ of the media for $T = 293 \text{ K}$; see Figure 4.16. It can be seen that this band red-shifts with an incremental amount of water and that the values are basically identical with the two compounds in the same dioxane:water mixtures. The pronounced red shift of this band with the increase in the dielectric constant of the media strongly suggests the presence of a charged species. Others with similar compounds have associated the shift of this emergent band to an exciplex.²⁰¹ However, further and convincing arguments on the nature of this band come from time-resolved data (see below).

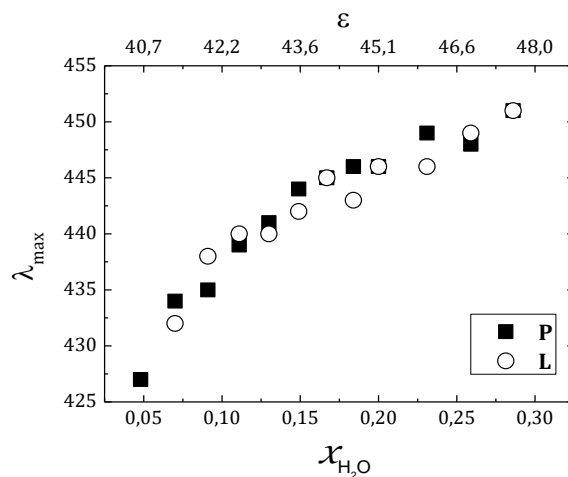


Figure 4.16. Dependence of the wavelength maxima (λ_{max}) with the mole fraction of water ($\phi_{\text{H}_2\text{O}}$) and the dielectric constant (ϵ) taken from the emission spectra of P (closed symbols) and L (open symbols) for $\lambda_{\text{exc}} = 360 \text{ nm}$ and $[\text{P}] = [\text{L}] = 5 \times 10^{-6} \text{ M}$.

4.3.3. Time-Resolved Data

The fluorescence decays for the two compounds (**P** and **L**) were obtained with excitation at 381 nm (monomer absorption band; see Figure 4.12) and were collected at 420 and 500 nm for **P** and 420 and 550 nm for **L**. With both **P** and **L**, the longest emission wavelength was specifically chosen away from its maximum in order to avoid emission contribution from the monomer species. Upon the addition of water to **P**, the fluorescence decays are now bi-exponential (with values ranging from 40 to 70 ps and from 190 to 700 ps), whereas with **L**, these are only properly fit to a tri-exponential decay law; see Figure 4.17. With **P**, the two decay times increase with the addition of water, but clearly the longer decay time increases deeply.

Chemosensors

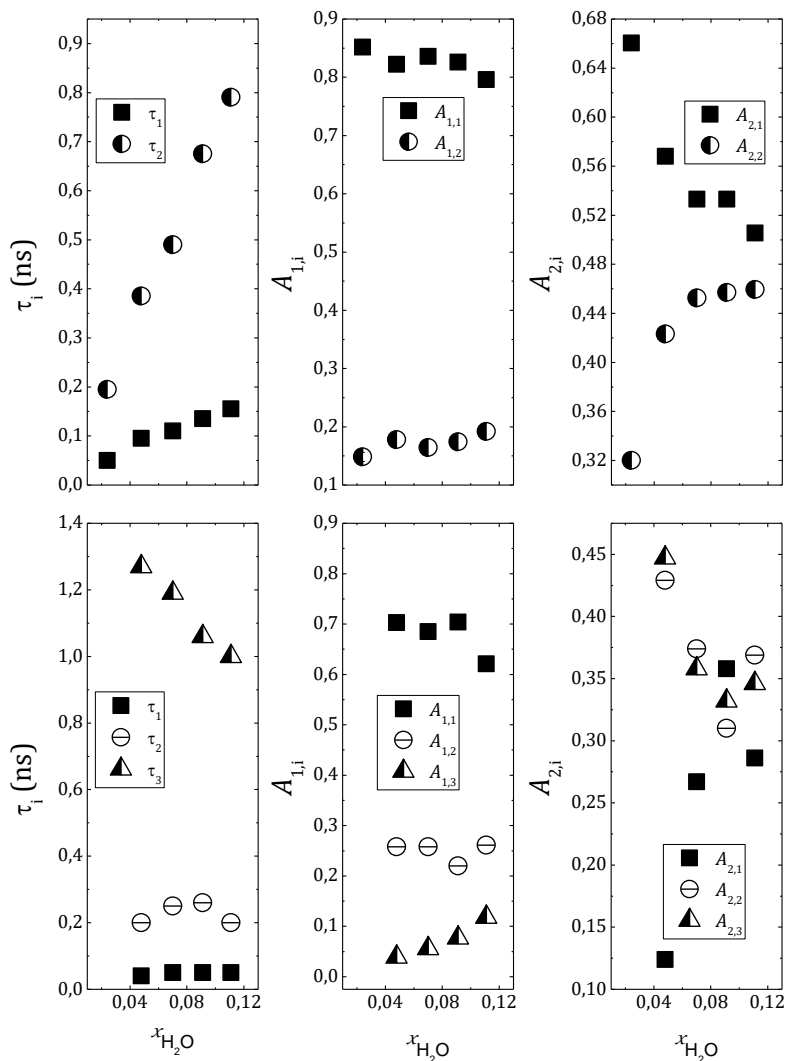


Figure 4.17. From left to right: Dependence of the decay times (τ_i) and pre-exponential factors obtained from the fluorescence decays collected at the monomer emission wavelength (420 nm, $A_{1,i}$) and at 500 nm for P and 550 nm for L ($A_{2,i}$) in dioxane:water mixtures (here expressed in mole fraction of water, ϕ_{H_2O}). P: top panels. L: bottom panels.

Moreover, whereas at the monomer (420 nm) emission wavelength the pre-exponential factors are kept rather constant (ranging from 0.8 to 0.9 and therefore associated with the highly quenched monomer decay time), when collected at 500 nm, the pre-exponential factor associated with the longer component increases at the expense of the shorter component, which indicates the longer component to be associated with the exciplex formed species. Furthermore, the reduced contribution of the longer decay time (pre-exponential factors varying from 0.1 to 0.2) mirrors the fact that the exciplex is also emitting at this emission wavelength. At 500 nm, the pre-exponential factor associated with the exciplex is dominant and increases with the water amount, in agreement with the steady-state spectra. In the case of compound L, we now observed three decay times in which besides the two previously indicated τ_1 and τ_2 , an additional longer decay time (with a value of ~ 1 ns) is present but only with a significant

contribution at longer emission wavelengths. In addition, the absence of a rising component at this emission wavelength gives a clear indication that the majority of this species is already present in the ground state.

4.3.4. Interaction of P and L with Metal Cations

In order to further explore the behaviour of compounds **P** and **L** as potential chemosensors toward Cu^{2+} , Zn^{2+} and Ag^+ , additional studies involving titrations with these metal ions were performed. The addition of incremental amounts of the metal cations to a dioxane solution of **P** leads to a decrease in the absorption maxima with, however, the same shape in the spectra; see Figure 4.18. The same is valid for the emission spectrum, which shows that the decrease of the fluorescence intensity is likely due to a quenching process that involves metal-ligand interaction in the ground state.

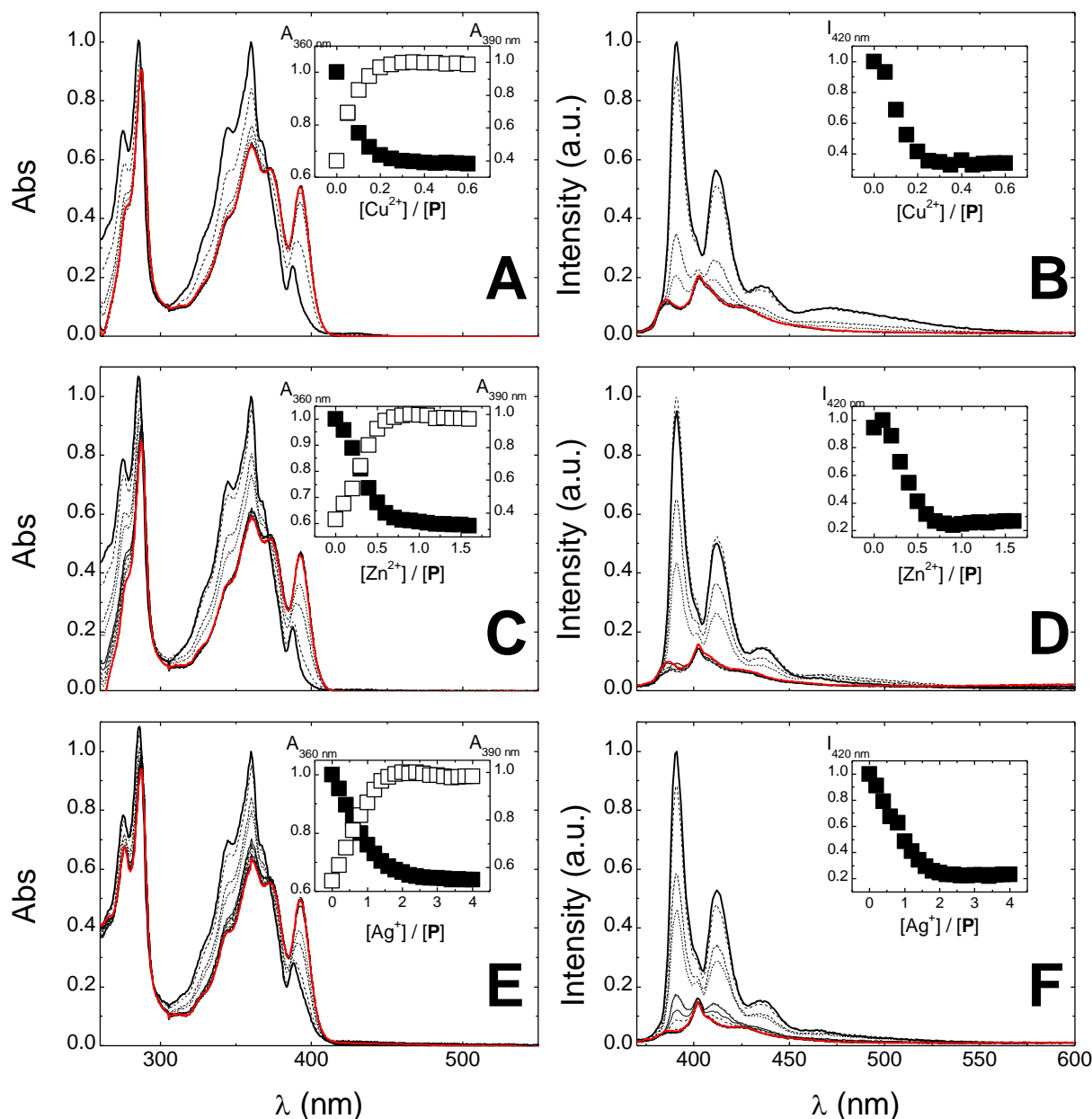


Figure 4.18. Absorption (left panels) and fluorescence emission (right panels) titrations of chemosensor P as a function of the increasing amounts of (A and B) $\text{Cu}(\text{BF}_4)_2$, (C and D) $\text{Zn}(\text{BF}_4)_2$, and (E and F) $\text{Ag}(\text{BF}_4)$ in dioxane. The insets show the absorption at 360 and 390 nm and the fluorescence intensity at 420 nm. $[\text{P}] = 5.00 \times 10^{-6}$ M and $\lambda_{\text{exc}} = 360$ nm. The bold dark line is for $[\text{Cu}^{2+}]/[\text{P}] = [\text{Zn}^{2+}]/[\text{P}] = [\text{Ag}^+]/[\text{P}] = 0$, whereas the bold red line is $[\text{Cu}^{2+}]/[\text{P}] = 0.6$, $[\text{Zn}^{2+}]/[\text{P}] = 1.6$, and $[\text{Ag}^+]/[\text{P}] = 4$, respectively.

It is relevant to point out that in the presence of metal cations, for both **P** and **L**, the emission band of the exciplex is absent. Figure 4.19 depicts the absorption and emission spectra of **L** in dioxane and in the presence of increasing amounts of Cu^{2+} (A and B), Zn^{2+} (C and D), and Ag^+ (E and F). Upon the addition of metal cations, the long wavelength absorption tail becomes well-defined with an isoabsorptive wavelength (425 nm for Cu^{2+} , 430 nm for Zn^{2+} and 410 nm for Ag^+), which indicates a ground-state

equilibrium between the monomer and dimer species. In contrast with this behaviour, in the emission spectra, the intensity of the band collected at the monomer region (390 nm) increases and that for the excimer/dimer decreases upon metal addition with well-defined crossing points in the titration curve (see insets in Figure 4.18). This shows that, upon the addition of the metal cation, the pyrene units in **L** split, and there is an increment of the monomer emission with a decrease of the excimer/dimer emission. The formation of a 1:1 (metal/ligand) stoichiometry after titration of **L** with Cu^{2+} , Zn^{2+} , and Ag^+ was confirmed unambiguously by the Job's plot method.²⁰² The new low energy bands (*ca.* 121 nm red shift) were responsible for the change of colour, perceptible to the naked eye, which is shown in Picture 4.2. In dioxane, the colour of the solution changes from yellow to dark red (Cu^{2+}), intense red orange (Zn^{2+}), and intense gold yellow (Ag^+) after the addition of 1 equiv. of the appropriate metal ion to a solution of **L** in the same solvent. In the case of probe **P**, the colour of the dioxane solution changes from pale yellow to intense yellow (Cu^{2+} and Zn^{2+}) and colourless (Ag^+) after the addition of 1 equiv. of the appropriate metal ion.

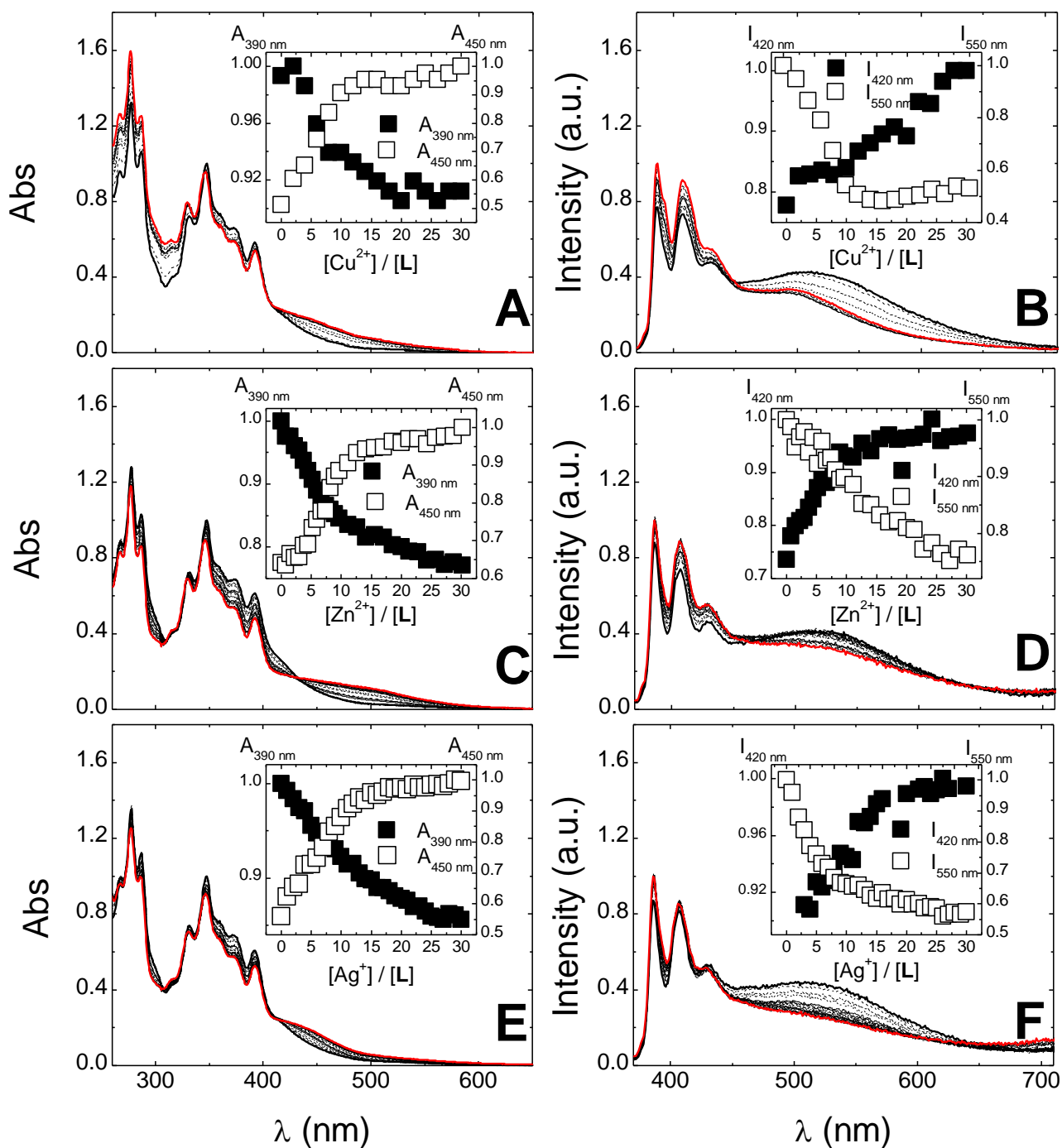
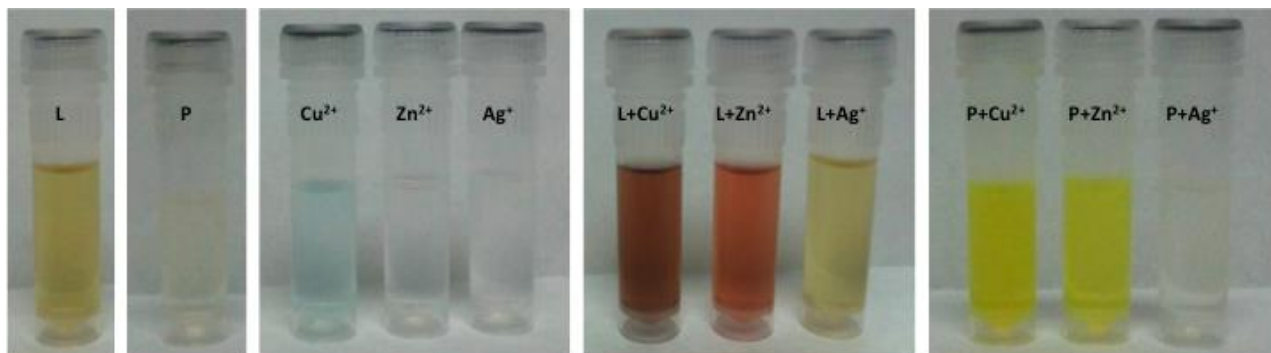


Figure 4.19. Absorption (left panels) and fluorescence emission (right panels) titrations of chemosensor L as a function of the increasing amounts of (A and B) $\text{Cu}(\text{BF}_4)_2$, (C and D) $\text{Zn}(\text{BF}_4)_2$, and (E and F) $\text{Ag}(\text{BF}_4)$ in dioxane. The insets show the absorption at 360 and 390 nm and the fluorescence intensity at 420 nm ($[\text{L}] = 5.00 \times 10^{-6}$ M, and $\lambda_{\text{exc}} = 360$ nm). The bold dark line is for $[\text{Cu}^{2+}]/[\text{L}] = [\text{Zn}^{2+}]/[\text{L}] = [\text{Ag}^+]/[\text{L}] = 0$, whereas the bold red line is for $[\text{Cu}^{2+}]/[\text{L}] = [\text{Zn}^{2+}]/[\text{L}] = [\text{Ag}^+]/[\text{L}] = 30$.

From Picture 4.2, it can be seen that the colours observed in all cases are the result of the metal-to-ligand interaction and not just to the mixture of two (coloured) solutions; e.g., in the case of Cu^{2+} when the

(pale) blue solution of Cu^{2+} is added to the yellow solution of **L**, it should be green with just the result of colour overlap and not dark red, as was obtained. These results suggest the use of **L** for colorimetric detection of the explored metal ions.



Picture 4.2. Colour changes observed after the interaction of **L** (6.80×10^{-4} M) and **P** (1.00×10^{-4} M) with Cu^{2+} (1 eq.), Zn^{2+} (1 eq.), and Ag^+ (1 eq.) in dioxane. Initial colours of **L**, **P** and metallic solutions.

The stability constants for the interaction of **L** with Cu^{2+} , Zn^{2+} , and Ag^+ were calculated using HypSpec software and are summarized in Table 4.4.¹⁹⁹ Taking into account the values obtained, the strongest interaction expected for sensor **L** is with Ag^+ . These values are in agreement with the MALDI-TOF-MS results previously discussed. In the case of **P**, we were unable to obtain with HypSpec the stability constants for the interaction with Ag^+ , Cu^{2+} , and Zn^{2+} .

In this case (**P**), a great number of equivalents of each metal ion were necessary to achieve a plateau (equilibrium). This result suggested **L** as the more favourable system over **P** for interaction with the explored metal ions. This could be due to the fact that a better stabilization of each metal ion was obtained with the bichromophoric system **L**.

Table 4.4. Stability constants for chemosensor **L** in the presence of Cu^{2+} , Zn^{2+} , and Ag^+ in dioxane for an interaction 1:1 (Metal/Ligand).

Interaction (M/L) in dioxane	$\Sigma \log \beta$ (absorption)	$\Sigma \log \beta$ (emission)
Cu^{2+} (1:1)	3.67 ± 0.003	3.10 ± 0.031
Zn^{2+} (1:1)	3.99 ± 0.002	4.08 ± 0.008
Ag^+ (1:1)	10.69 ± 0.002	10.82 ± 0.015

4.3.5. Time-Resolved Data

Time-resolved data provide further and relevant information regarding the excimer-forming processes in the absence and presence of metal cations. In pure dioxane, the results presented so far have shown that the band at 390 nm can be attributed to a monomer emission, i.e., to an excited pyrene with no other pyrene in its vicinity. In the case of **L**, the longer emission wavelength can be attributed to the emission of an excimer/dimer. In order to avoid contribution/"contamination" of the monomer emission in the excimer region (and vice versa), we collected the emission decays in the extremities of each emission band: 420 nm (monomer) and 550 nm (excimer).

It is worth remembering that, from steady-state data, the exciplex emission is absent for **L** in the presence of metal cations. It is also worth noting the extraordinary quenching suffered by the decay times of these pyrene derivatives in comparison with other known and investigated pyrene system derivatives, i.e., from nano-⁶⁵ to picosecond (in our work with **P** and **L**) time regime. This shows that the imine groups are strong quenchers of pyrene fluorescence.

Figure 4.20 depicts the emission decays in dioxane in the absence (A) and presence (B) of Ag⁺. Global analysis of the decays shows that these are again fitted with the sums of three exponentials. It is also worth noting that the decay times are generally kept constant upon the addition of Ag⁺. However, the same does not happen with the pre-exponential factors.

Chemosensors

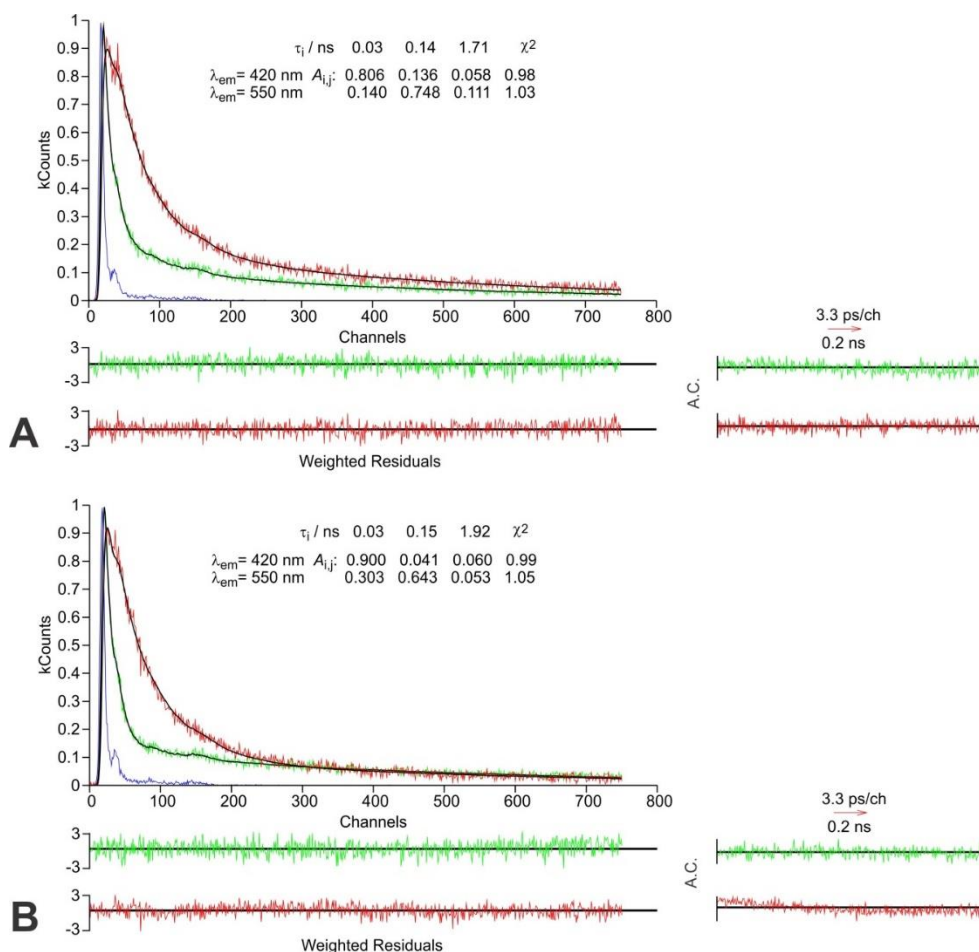


Figure 4.20. Fluorescence decays of L in dioxane ($T=293$ K) at $\lambda_{exc}=381$ nm in (A) absence and (B) presence of Ag^+ (ratio $[Ag^+]/[L]=2:1$). The instrument profile curve, decay times (τ_i), pre-exponential factors ($A_{i,j}$), χ^2 values, weighted residuals, and autocorrelation functions (A.C.) are shown as the insets.

From Figure 4.20, it can be seen that, upon the addition of Ag^+ at $\lambda_{em}=420$ nm, there is basically no change in the pre-exponential value associated with the shorter component (the decay associated with the monomer ~ 30 ps). However, the same is not valid with the $A_{2,1}$ pre-exponential at $\lambda_{em}=550$ nm, where an increase is observed upon the addition of Ag^+ . Indeed, the addition of Ag^+ leads to an increase (basically doubling the values) of the $A_{2,1}$ and $A_{2,3}$ pre-exponential factors, which means that upon complex formation the monomer contribution (at the excimer/dimer emission) increases and the excimer/dimer emission decreases as a result of complexation with the imine moieties and a consequent split of the pyrene chromophores.

In addition, it can also be seen that a substantial decrease occurs, upon the addition of Ag^+ , with the pre-exponential factor associated with the 140–150 ps decay time (related to the decay of the excimer/dimer species) at $\lambda_{em}=420$ nm. This means that the addition of Ag^+ leads to a decrease in the excimer-to-monomer reversibility.

With these facts in mind and also with the previous knowledge in polymer systems bearing pyrene pendant chromophores where the process of dimer formation has been shown to occur with tens of picoseconds,⁶⁴ we propose the following interpretation. The shorter decay component (~ 30 ps) should be attributed to the monomer decay that gives rise to the excimer/dimer. This is the major component at 420 nm with a pre-exponential factor (concentration of the species at time zero) of ~ 0.8 – 0.9 in both the absence and presence of Ag^+ . This short component is kinetically linked to the ~ 0.14 ns component (which is associated with the decay of the instantaneously formed dimer/excimer). This is likely to be kinetically linked to the other species (the other long component with ~ 1.7 – 1.9 ns), which should be associated with the emission of a relaxed dimer.¹⁹⁹ This mirrors the quick rearrangement of the pyrene groups in the (instantaneously formed) dimer to a more stable (dimer) conformation.

4.3.6. Conclusions

In this work, the synthesis and characterization of two new compounds, **P** and **L**, containing pyrene units was undertaken. The investigation of these two chemosensors has shown that these are sensitive to water and metal cations. In the case of water sensing, the two ligands showed a new band that was attributed to an exciplex species and whose contribution increases with the water amount. The interaction of **L** toward Cu^{2+} , Zn^{2+} , Ag^+ , Cd^{2+} and Hg^{2+} metal ions was also explored in the gas phase using MALDI-TOF-MS.

Several metal-ion titrations of **L** with Cu^{2+} , Ag^+ , and Zn^{2+} followed by absorption and emission studies were performed in dioxane. In all cases, the stability constant values suggest a stoichiometry of 1:1 ligand/metal. The strongest interaction expected for sensor **L** was with Ag^+ in all of the solvents tested, with the highest value being observed in the non-coordinative solvent dioxane. Compound **P** was found to be more selective to Cu^{2+} .

Further detailed information could be obtained from time-resolved experiments: (1) Extraordinary quenching is suffered by these pyrene derivatives, mirrored from the decrease from nanoseconds, the usual range of pyrene derivative lifetimes, to picoseconds, which is likely due to the imine groups that are strong quenchers of pyrene fluorescence. (2) Global analysis of the emission decays in dioxane in the absence and presence of Ag^+ shows that the decays are only fitted with the sums of three exponentials, which were associated with the monomer, and the two additional components with the kinetics of a dimer formation.

4.3.7. Supporting Information

In Figure 4.21 and Figure 4.22 the fluorescence excitation spectra of P and L at different emission wavelength with the increase in water proportion are, respectively, shown.

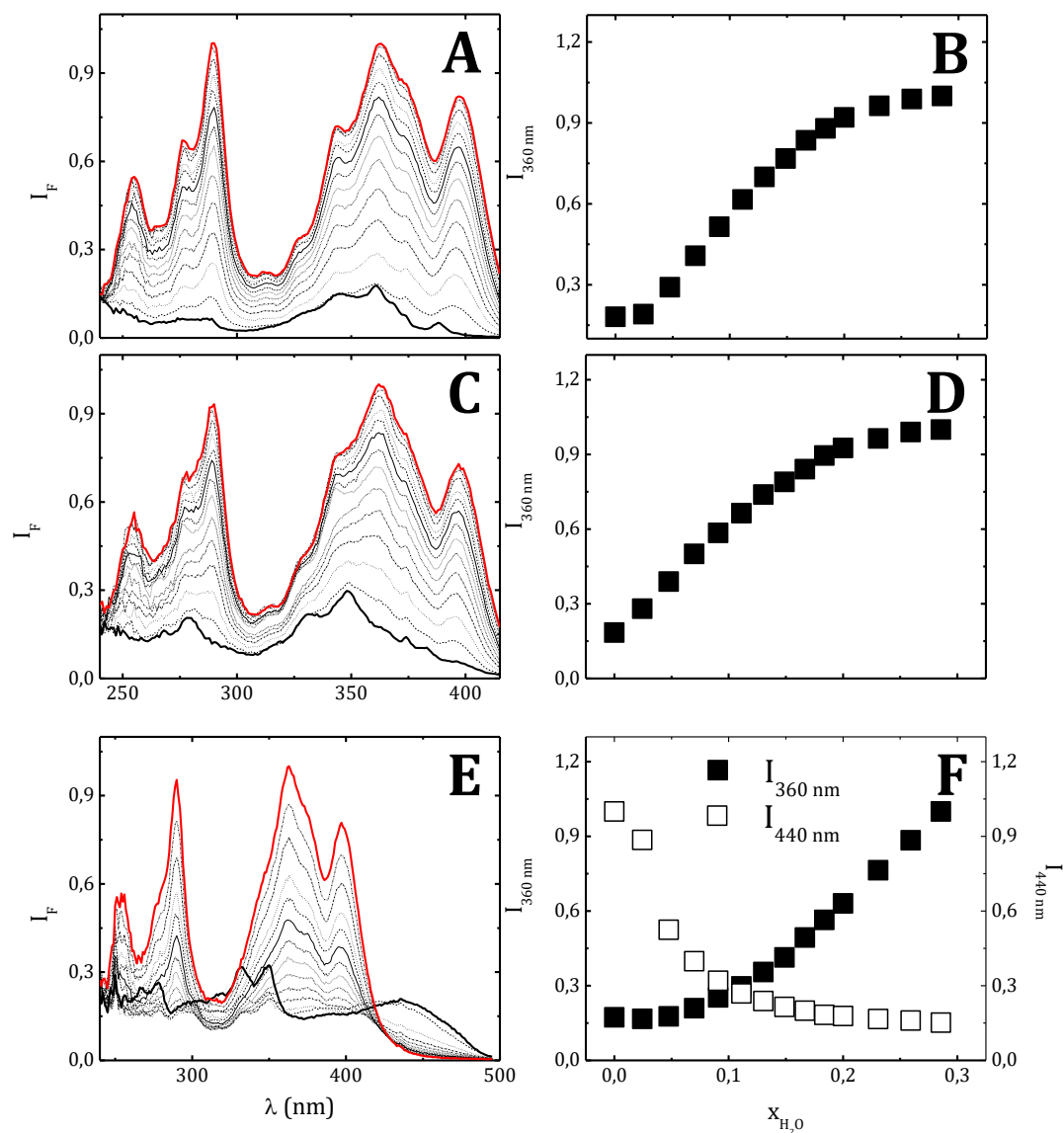


Figure 4.21. Fluorescence excitation titrations of chemosensor (A) P and (C and E) L collected at 420 nm and 500 nm (from top to bottom) as a function of increasing amounts of water in dioxane. (B), (D) and (F) show the fluorescence intensities at 360 nm for excitation spectra collected at 420 nm for P, and the fluorescence intensities at 360 nm and 440 nm for excitation spectra collected at 500 nm for L. ($[P] = [L] = 5.00 \times 10^{-6}$ M, $\lambda_{em}(P) = 420$ nm, $\lambda_{em1}(L) = 420$ nm and $\lambda_{em2}(L) = 500$ nm). The bold dark line is for $x_{H_2O} = 0$ whereas the bold red line is for $x_{H_2O} = 0.29$.

Chemosensors

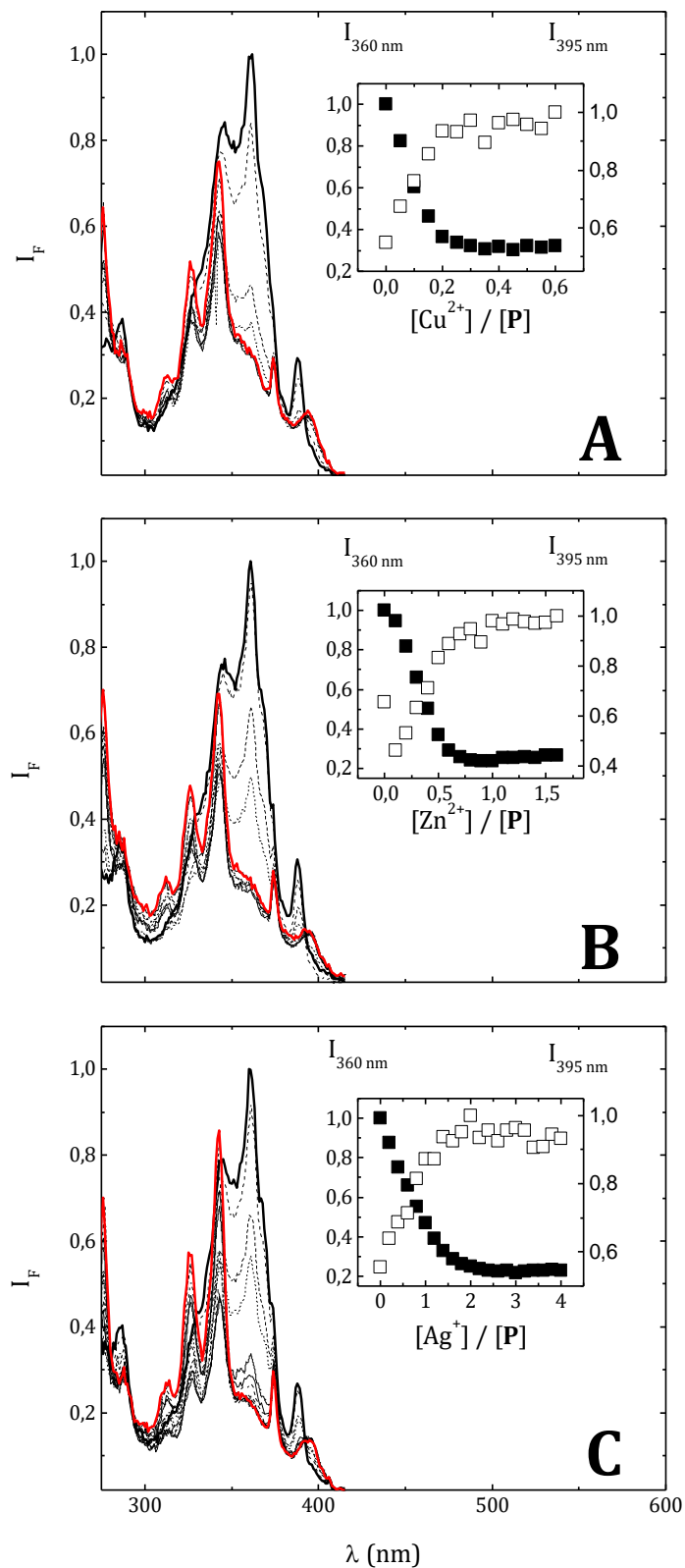


Figure 4.22. Fluorescence excitation titrations of chemosensor P collected at 420 nm as a function of increasing amounts of (A) $Cu(BF_4)_2$, (B) $Zn(BF_4)_2$ and (C) $Ag(BF_4)$ in dioxane. The insets show the fluorescence intensities at 360 and 395 nm, ($[P] = 5.00 \times 10^{-6}$ M, $\lambda_{em1} = 420$ nm). The bold dark line is for $[Cu^{2+}]/[P] = [Zn^{2+}]/[P] = [Ag^+]/[P] = 0$ whereas the bold red line is for $[Cu^{2+}]/[P] = 0.6$, $[Zn^{2+}]/[P] = 1.6$ and $[Ag^+]/[P] = 4$, respectively.

The absorption and emission spectra of L in (black) pure dioxane, (red) in $x_{\text{H}_2\text{O}} = 0.80$ in dioxane and (grey) after the removal of water are presented in Figure 4.23.

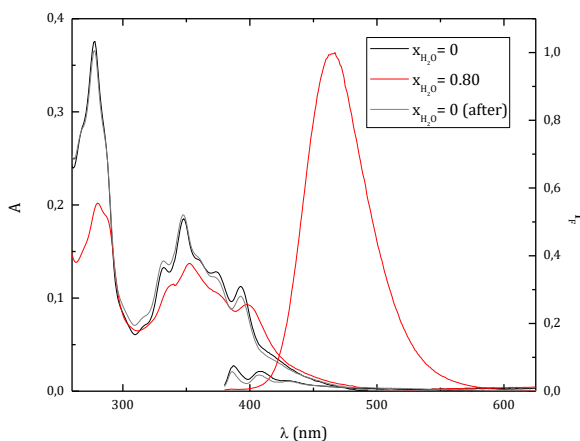


Figure 4.23. Absorption and emission spectra of L: (black) in pure dioxane, (red) in $x_{\text{H}_2\text{O}} = 0.80$ in dioxane and (grey) in pure dioxane after the removal of water from solution (B).

4.4. Photophysical Characterization of Compound 2

absorption spectrum of compound 2 in DMSO solution displays the typical absorption bands of the pyrene moiety between 250-400 nm. A maximum at *ca.* 346 nm with an extinction coefficient of $39810 \text{ M}^{-1} \cdot \text{cm}^{-1}$ was observed (Figure 4.24). It is worth noting that with compound 2, in contrast with the ligand 1 (Section 0), the longest wavelength band (at 426 nm) could not be observed.

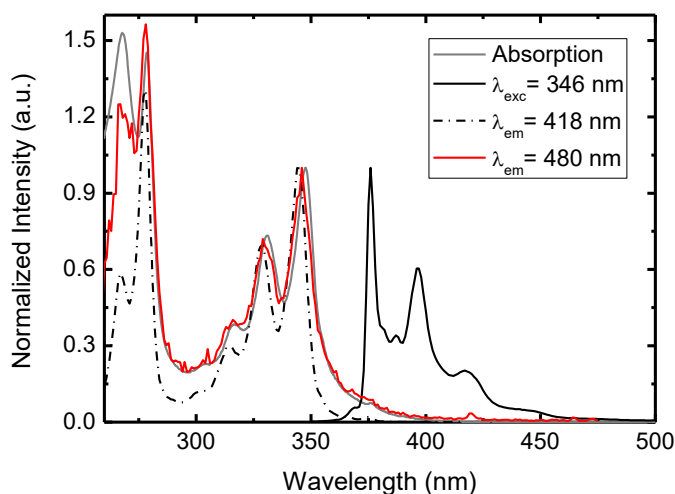


Figure 4.24. Normalized absorption, emission and excitation spectra of a degassed solution of compound 2 in DMSO at 298 K. ($[2] = 3.56 \times 10^{-6} \text{ M}$, $\lambda_{\text{exc}} = 346 \text{ nm}$, $\lambda_{\text{em}} = 418$ and 480 nm).

Upon excitation of compound **2** at 346 nm, the emission spectra display the characteristic emission of the pyrene monomer but with a residual emission that ranges up to 480 nm. By collecting the excitation spectra at 418 nm (monomer emission region) and 480 nm a different spectra is obtained, see Figure 4.24. Very interesting is to note that the excitation spectra obtained at longer emission wavelengths ($\lambda_{em} = 480$ nm) matches the absorption spectra whereas when collected at 418 nm it gives rise to a clearly sharper and better defined “absorption” spectra (characteristic of the pyrene monomer emission). This strongly suggests that the absorption spectra of compound **2** results from the coexistence of two species in the ground state which can be due to intermolecular interaction, a new entity resulting from CT (likely from the imide group or quinoline to the pyrene acceptor group) or the pyrene monomer and of dimer (or exciplex).

It is also worth noting that upon degassing the solution (by bubbling with N_2 or Ar) the fluorescence intensity (from the monomer) is ~ 2 times higher (data not shown).

The spectra in Figure 4.24A were obtained with degassed solutions (30 min. bubbling in a device specially designed for this purpose³⁷ and it can be seen that the emission spectra shows (when excited at $\lambda_{exc} = 346$ nm) the characteristic pyrene monomer emission with vibronic resolution and absence of the excimer/dimer band.

As it is shown in Figure 4.25, the fluorescence decay of compound **2** collected at 418 nm (monomer emission) is single exponential with a decay time of 179 ns. This result shows that when the imine group is not directly connected to pyrene chromophore it leads to an absence of an effective intramolecular quenching effect.

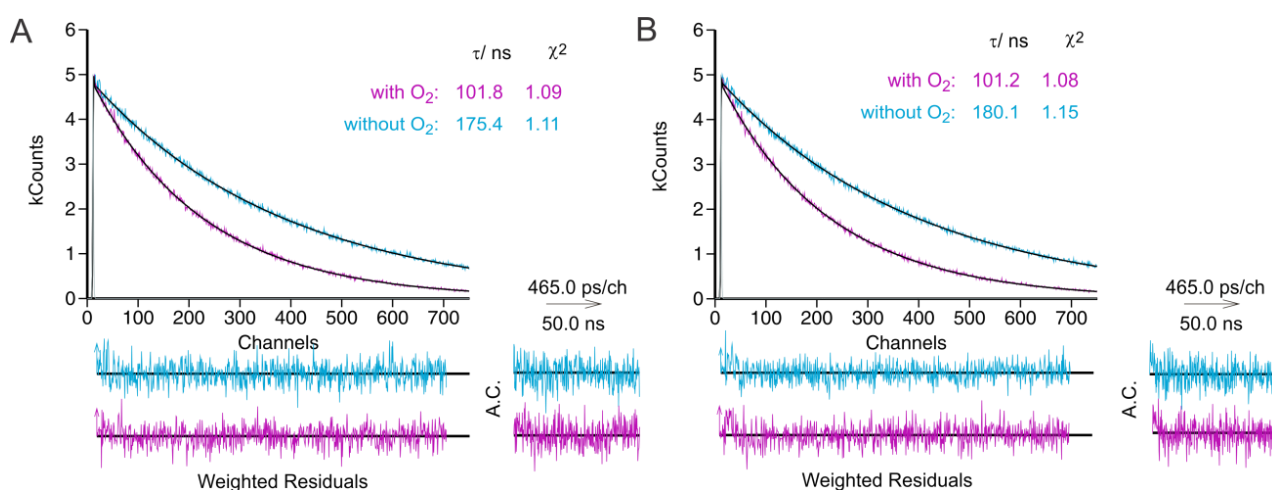


Figure 4.25. Fluorescence decay of compound **2** in DMSO ($T = 293$ K) at $\lambda_{exc} = 339$ nm collected at $\lambda_{em} = 375$ nm (A) without metal added and (B) for $[Zn^{2+}]/[2] = 5$, in the presence (purple) and absence (blue) of oxygen. The

instrument profile curve, decay times (τ_i), pre-exponential factors ($A_{i,j}$), χ^2 values, weighted residuals, and autocorrelation functions (A.C.) are shown as insets.

From Figure 4.25 it can be observed that there is apparently a poor sensitivity to the oxygen quencher (with a rate constant ($k_Q \sim 1.87 \times 10^9 \text{ L mol}^{-1} \text{ s}^{-1}$) of half value of the one found for pyrene in cyclohexane,²⁰³ calculated with Equation 1.9 from Section 1.3.1) and to (the addition of) zinc. This suggests the absence of interaction with the metal Zn^{2+} . The oxygen concentration was taken at atmospheric pressure from ref. ³⁵.

4.4.1. Sensorial Ability of Compound 2 Towards OH^- , Ag^+ , Zn^{2+} , Cd^{2+} , Pb^{2+} , Hg^{2+} , and Al^{3+} Ions

Interaction of compound 2 with the OH^- anion was investigated by spectrophotometric and spectrofluorometric titration. This was made by adding a standard solution of the corresponding tetrabutylammonium hydroxide in DMSO to a solution of compound 2 at room temperature in the same solvent. As it is shown in Figure 4.26A, no significant changes were observed from the spectrophotometric titration. However, a quenching in the emission of compound 2 takes place with the addition of OH^- (see Figure 4.26B). Taking into account that the intermolecular photoinduced proton transfer (PPT) from the hydroxyl group of the molecule is faster than the photo-induced electron transfer (PET) from the amines, the quenching in the emission observed could be due to the deprotonation of the imine nitrogen and the involvement of the free electrons in the PET process with the pyrene unit.

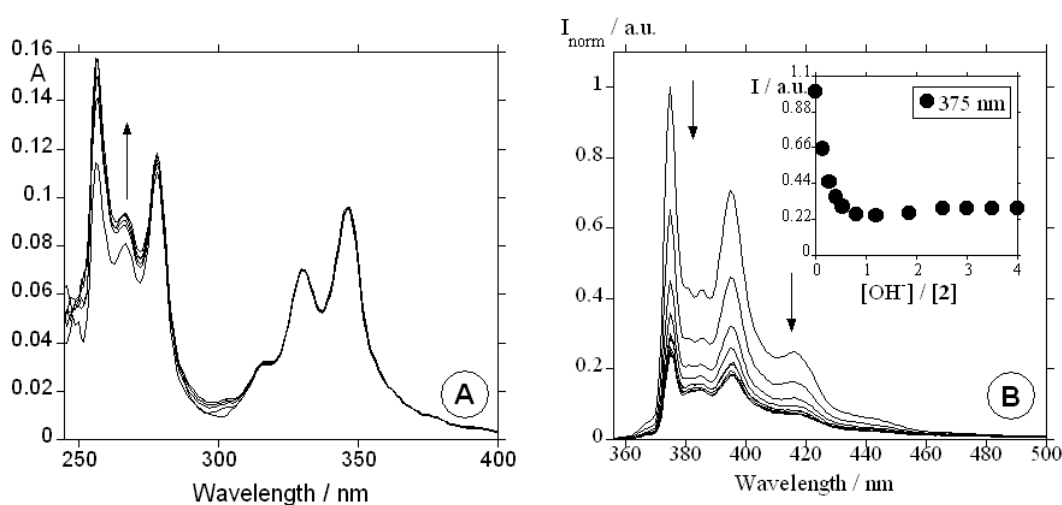


Figure 4.26. Spectrophotometric (A) and spectrofluorometric (B) titrations of compound 2 with the addition of OH^- in DMSO. The inset represents the emission intensity at 375 nm as a function of $[\text{OH}^-]/[\text{2}]$. ($[\text{2}] = 2.50 \times 10^{-6} \text{ M}$, $\lambda_{\text{exc.}} = 346 \text{ nm}$, $T = 298 \text{ K}$).

In order to explore the behaviour of the deprotonated compound **2** as a chemosensor towards Ag^+ , Zn^{2+} , Cd^{2+} , Pb^{2+} , Hg^{2+} and Al^{3+} ions, several metal titrations followed by absorption and emission were performed in DMSO.

Spectrophotometric changes were not observed in any cases (data not shown) but an increase in the fluorescence emission was obtained. As an example, Figure 4.27 shows the emission spectra of the deprotonated compound **2** in the presence of increasing amounts of Zn^{2+} (A) and Cd^{2+} (B). The insets show the normalized fluorescence intensities at 375 nm.

A CHEF effect was observed in all cases (data not shown for Ag^+ , Pb^{2+} , Ag^{2+} and Al^{3+}). This well-known phenomenon is consistent with the involvement of lone pairs of the imine nitrogen atom in the coordination to the metal ion preventing the PET processes whereas the oxygen of the quinoline group is coordinated to the metal preventing the PPT process; thus, complexation results in an enhancement of the fluorescence signal.

As it can be seen in Figure 4.27A, a plateau is reached after the addition of one equivalent of Zn^{2+} , suggesting that one molecule of compound **2** is involved in the coordination to the metal ion.

Additionally the titration of compound **2** with Hg^{2+} , Cd^{2+} , Pb^{2+} and Ag^+ leads to a plateau that is reached after the addition of one metal equivalent, suggesting one unit of compound **2** is coordinated to one metal ion. No changes were observed in the absorption and emission spectra of compound **2** after the addition of Al^{3+} .

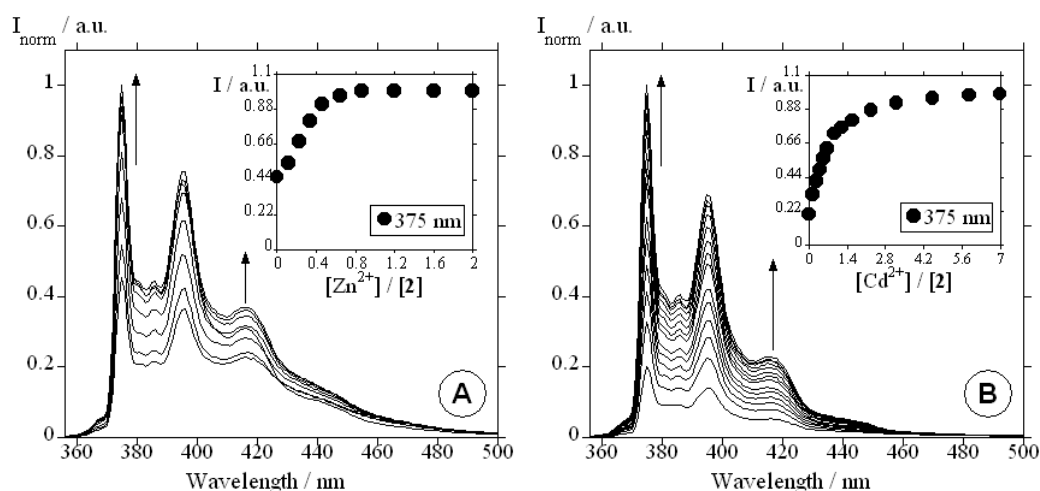


Figure 4.27. Spectrofluorometric titrations of compound **2** with the addition of Zn^{2+} (A) and Cd^{2+} (B) in DMSO. The inset represents the emission intensity at 375 nm as a function of $[\text{Zn}^{2+}]/[\mathbf{2}]$ (A) and $[\text{Cd}^{2+}]/[\mathbf{2}]$ (B) ($[\mathbf{2}] = 2.50 \times 10^{-6} \text{ M}$, $\lambda_{\text{exc.}} = 346 \text{ nm}$, $T = 298 \text{ K}$). Mostrar as restantes titulações tal como para o 1 na Figura 3.

The stability constants for the interaction of compound **2** with the metal ions mentioned above were calculated using HypSpec software and are summarized in Table 4.5.³²

Table 4.5. Association constants calculated by fluorescence emission for compound **2** in DMSO at 293 K.

Metal ion	Log K_{ass} (M:L)
Ag⁺	3.55± 0.01 (1:1)
Zn²⁺	11.52± 0.01 (1:2)
Cd²⁺	5.36± 0.01 (1:1)
Pb²⁺	4.95± 0.01 (1:1)
Hg²⁺	11.48± 0.02 (1:2)

The highest association constant was obtained for zinc and mercury with a value of log K_{ass}= 11.52± 0.01 and 11.48± 0.02, followed by Cd²⁺, Pb²⁺ and Ag⁺ metal ions. A stoichiometry of two ligands per metal ion was postulated for Zn²⁺ and Hg²⁺ and a 1:1 stoichiometry for the remaining metals.

4.4.2. Summary

With the aim of evaluating the role that the distance of the imine bond (C=N) can produce in the photophysical properties of molecular probes containing pyridine units, compound **2** was also studied in DMSO. In that case, after the interaction of compound **2** with Ag⁺, Zn²⁺, Cd²⁺, Pb²⁺ and Hg²⁺, a CHEF effect was observed but the formation of an excimer emission band does not take place. These results points out the importance of the distance of the spacer between the pyrene moiety and the chromophore. The bigger flexibility present in the pyrene unit of compound **2** in respect to compound **1** (Section 0) is crucial to observe the disappearance of the exciplex/excimer observed in **1** pointing out the importance of the structure to observe supramolecular interactions.

4.5. Photophysical Studies of a Naphthalene-Based Emissive Probe for Metal Cations

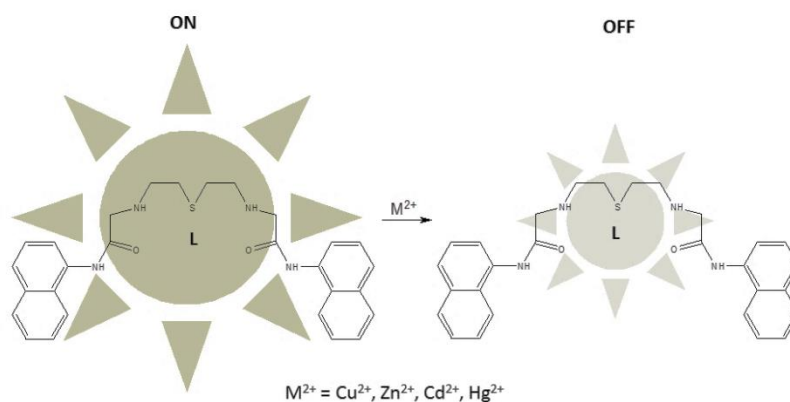


Figure 4.28

An emissive molecular probe bearing two naphthalene units at the extremities was already investigated in the past by us.¹⁷³ The probe interaction with cations (such as Cu^{2+} , Zn^{2+} , Cd^{2+} and Hg^{2+}) and anions (F^- , Cl^- , Br^- , I^- and CN^-) was explored in DMSO where it showed to be remarkably selective for Cu^{2+} and to interact with CN^- and F^- .

Following our ongoing research project in fluorescent materials and emissive compounds and complexes¹⁷³, in this work, the photophysical properties of another symmetric probe **L**, with two naphthalene units in the extreme as well, was described together with its interaction (aiming chemoselectivity) with Cu^{2+} , Zn^{2+} , Cd^{2+} and Hg^{2+} metal ions in acetonitrile.

Molecular probe **L** was found to be soluble in dichloromethane, dimethylsulfoxide, *N,N'*-dimethylformamide, fairly soluble in acetonitrile, ethanol, cyclohexane and dioxane and insoluble in water. In the solid state, **L** presents a brown colour but within the concentrations of ligand in the solvents used, the solution is colourless.

Figure 4.29 shows the (normalized) absorption and fluorescence (excitation and emission) spectra of ligand **L** in acetonitrile. A single band is observed in the absorption which matches (maxima at the same wavelength) with the excitation spectra collected at $\lambda_{em} = 350$ nm. However, the excitation spectrum is broader, clearly mirroring the presence of dimers or higher order aggregates. Very interesting is also to note that the excitation spectra when collected at $\lambda_{em} = 450$ nm, presents an “absorption” band between 300 and 425 nm (Figure 4.29). This is indicative that at longer emission wavelengths the absorption (although with a small molar extinction value) of a dimer is likely to be present. Indeed when exciting

at the tail of the absorption band (330 nm) the obtained emission spectra is different than when excitation at made 290 nm, see Figure 4.29 (right hand panel).

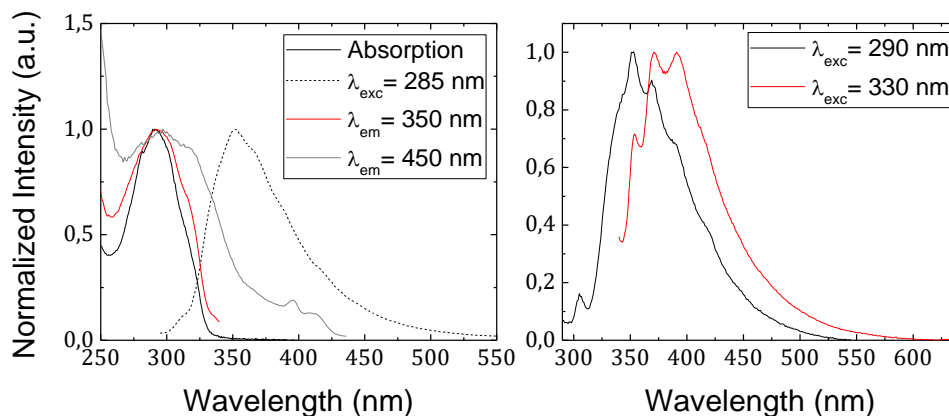


Figure 4.29. From left to right. Normalized absorption, emission ($\lambda_{\text{exc}} = 285$ nm) and excitation spectra ($\lambda_{\text{em}} = 350$ and 450 nm) and normalized emission ($\lambda_{\text{exc}} = 290$ and 330 nm) of L in acetonitrile.

The spectral and photophysical properties of L are summarized in Table 4.6 and include the molar extinction coefficient (ϵ), the fluorescence quantum yield (ϕ_F) and the radiative (k_R) and radiationless (k_{NR}) rate constants in several solvents.

In view of the values in Table 4.6, it can be seen that the ϕ_F value is low, indicating that the fluorescence is not an efficient route for the deactivation of the excited state of L, which is further attested by the small k_F value and high k_{NR} value. This, however, is not limitative to observe the interaction of this fluorescent ligand with metal cations.

Table 4.6. Absorption, emission and excitation wavelength maxima ($\lambda_{\text{max}}^{\text{abs.}}$, $\lambda_{\text{max}}^{\text{em.}}$ and $\lambda_{\text{max}}^{\text{exc.}}$), together with molar extinction coefficient (ϵ), fluorescence quantum yield (ϕ_F), fluorescence lifetime (τ_F), and fluorescence and non-radiative rate constants (k_F and k_{NR}) for the probe L in dichloromethane at T= 293 K.

Solvent	$\lambda_{\text{max}}^{\text{abs.}}$ (nm)	$\lambda_{\text{max}}^{\text{em.}}$ (nm)	$\lambda_{\text{max}}^{\text{exc.}}$ (nm) ^c	$\lambda_{\text{max}}^{\text{exc.}}$ (nm)	$\epsilon_{292 \text{ nm}}$ (M ⁻¹ .cm ⁻¹)	ϕ_F	τ_F (ns)	k_F (ns ⁻¹) ^g	k_{NR} (ns ⁻¹) ^h
CH ₃ CN	290	352 ^a	292	297 ^d	ND		0.08 ^f		ND
CH ₂ Cl ₂	292	352 ^b	296	319 ^e	13081	0.009	0.17 ^f	0.053	5.8
DMSO	295	354 ^b		ND	15040				
							ND		
EtOH	291	351 ^b	292		ND				

^a Obtained from the emission spectra collected at $\lambda_{exc}=285$ nm, see Figure 4.29. ^b Obtained from the emission spectra collected at $\lambda_{exc}=281$ nm. ^c Obtained from the excitation spectra collected at $\lambda_{em}=350$ nm, see Figure 4.29. ^d Obtained from the excitation spectra collected at $\lambda_{em}=450$ nm, see Figure 4.29. ^e Obtained from the excitation spectra collected at $\lambda_{em}=480$ nm. ^f Dominant component (associated to the monomer) of a bi-exponential decay, the other decay time is that of the dimer with 2.63 ns (see text for more details). ^g $k_F = \phi_F / \tau_F$. ^h $k_{NR} = (1 - \phi_F) / \tau_F$. *ND* - not determined.

A more detailed observation shows, however, that the absorption spectrum of **L** is red-shifted and broader when compared with naphthalene itself.³⁵

The presence of a dimer becomes more evident in the fluorescence decay obtained with excitation at 281 nm and collected at 340 nm and 500 nm (data not shown). In this case the global (simultaneous) analysis of the decays at 340 and 500 nm leads bi-exponential decays with the same decay times at and different pre-exponential factors. It is worth mentioning that the pre-exponential factors mirror the concentration at time zero of the associated species: the monomer and the dimer. Since the monomer emits preferentially at shorter wavelengths and the dimer at longer ones, the decay times should therefore be associated with a monomer species (shorter decay component) and dimeric (longer decay component). In addition, the absence of rising components (rise-time) suggests that the dimeric species is not formed in the excited state, but is already present in the ground state.

Upon the addition of the metal ions Cu^{2+} , Zn^{2+} , Cd^{2+} and Hg^{2+} to an acetonitrile solution of **L**, the vibronic progression of the monomer band (Figure 4.29) will change, which is indicative of the formation of a complex involving the metal **M** and the ligand **L** (with its absorption beneath the emission spectra of the monomer).

Indeed, upon addition of different metal cations (**M**), a shift towards lower wavelengths in the absorption spectra likely due to a photoinduced charge transfer (PCT) involving the metal and the ligand, MLCT [with sharp isosbestic points (Figure 4.30 left hand panels) at ~215, ~230, ~250 and ~325 nm and, more evident, at ~290 nm] together with a quenching of the vibronically resolved fluorescence band (maximum at ~352 nm) was observed (Figure 4.30 right hand panels).

Indeed, when a fluorophore contains an electron-donating group (e.g. an amino group) conjugated to an electron-withdrawing group, it undergoes intramolecular charge transfer from the donor to the acceptor upon excitation by light²⁰⁴. The amino group of **L** plays the role of electron donor (within the fluorophore) and interacts with the cation; the latter reduces the electron-donating ability of this group. This results in the stabilization of the HOMO and therefore a higher (HOMO-LUMO energy difference is obtained) leading to a blue shift of the absorption spectrum together with a decrease of the molar absorption coefficient (PCT).

Chemosensors

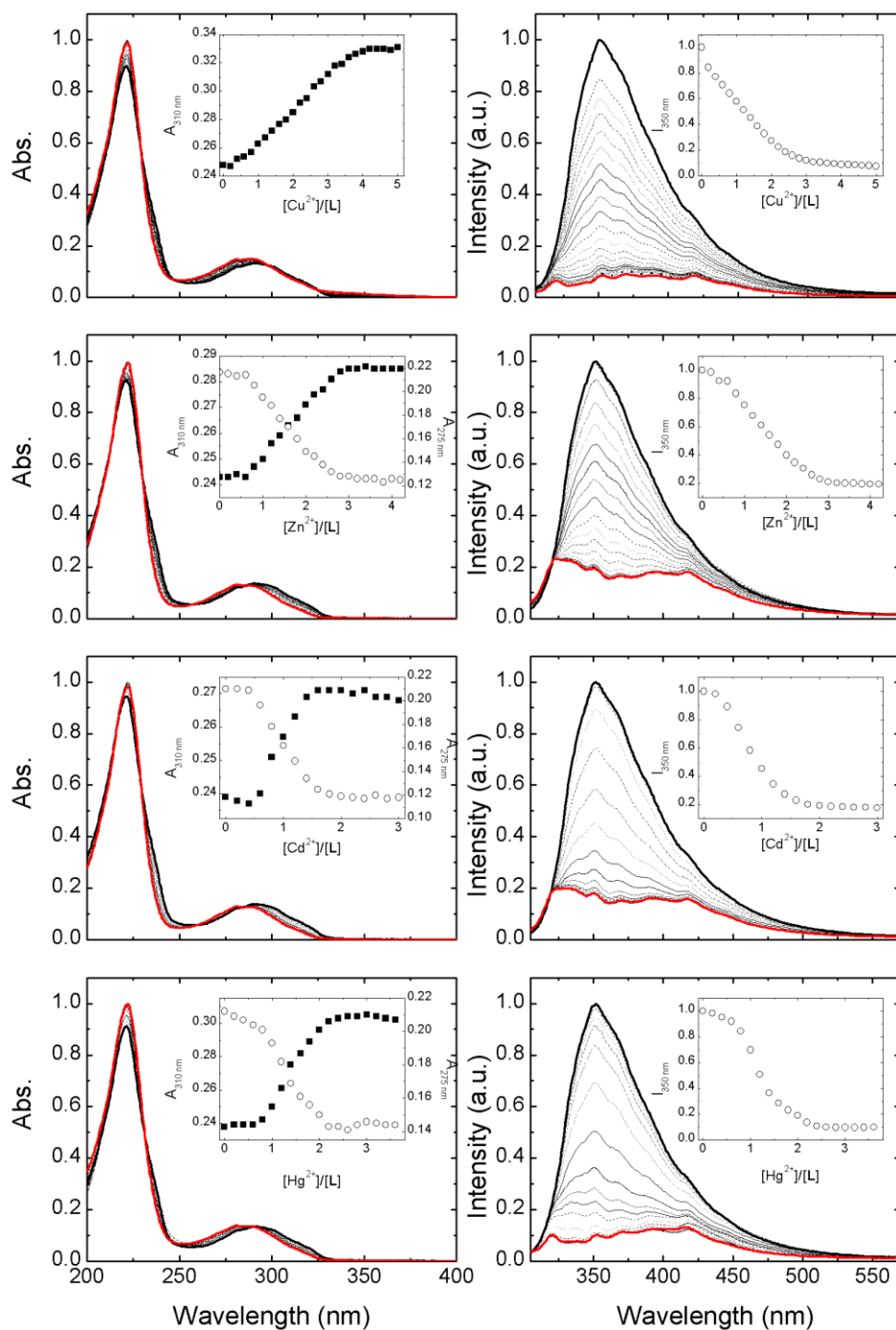


Figure 4.30. From left to right: Absorption and emission ($\lambda_{\text{exc}} = 292 \text{ nm}$) spectra of L in acetonitrile with the addition of Cu^{2+} , Zn^{2+} , Cd^{2+} and Hg^{2+} . Inset from absorption: Representation of the absorption at 275 and 310 nm as a function of $[\text{M}]/[\text{L}]$. Inset from emission: Representation of the fluorescence intensity at 370 nm as a function of $[\text{M}]/[\text{L}]$. The bold black and red lines correspond, respectively to $[\text{M}]/[\text{L}] = 0$ and $[\text{M}]/[\text{L}] = [\text{M}]/[\text{L}]_{\text{max}}$. $[\text{M}]/[\text{L}]_{\text{max}} = 3\text{-}5$. $[\text{L}] = 1 \times 10^{-5} \text{ M}$.

From Figure 4.30 it can also be seen that the change in intensity of the absorption (increase at 275 nm and decrease at 310 nm) and emission (decrease) spectra with the incremental addition of ligand is found non-linear. Again, this is likely a result from the presence of a dimer (resulting from the formation of a complex between the metal and the ligand L).

From Figure 4.30, it is also worth noting that the blue-shift in the absorption spectra upon M addition seems to be independent on the nature of the metal. Moreover, with the addition of the metal M, the ratio of the vibronic bands is changed; this, however, does not show a linear dependence with the incremental addition of M and is likely indicative of the presence/increasing contribution of a dimer resulting from the formation of a complex between the ligand L and the metal M. Indeed, if the quenching effect were only due to an electron or energy transfer from L to M it would induce a decrease of the fluorescence band as a whole; in contrast, an equilibrium $L \leftrightarrow ML$ will promote a gradual change in the absorption (perceptible in Figure 4.31) with a different contribution of L and ML at the excitation wavelength. This would produce a different ratio of the L and ML absorption and emission, which will induce a different vibronic progression of the (total) emission band.

Further and detailed knowledge can be obtained from time-resolved (TR) fluorescence experiments. As mentioned above the fluorescence decays were found to be bi-exponentials. The incremental addition of metal cation leads to non-significant changes on the decay time values. However, the same does not happen with the fractional fluorescence contribution of each species. The fractional contribution (C_i) of each species (when in presence of a bi- or higher order decays) is given by the Equation 2.2 in Section 2.1.1.1.

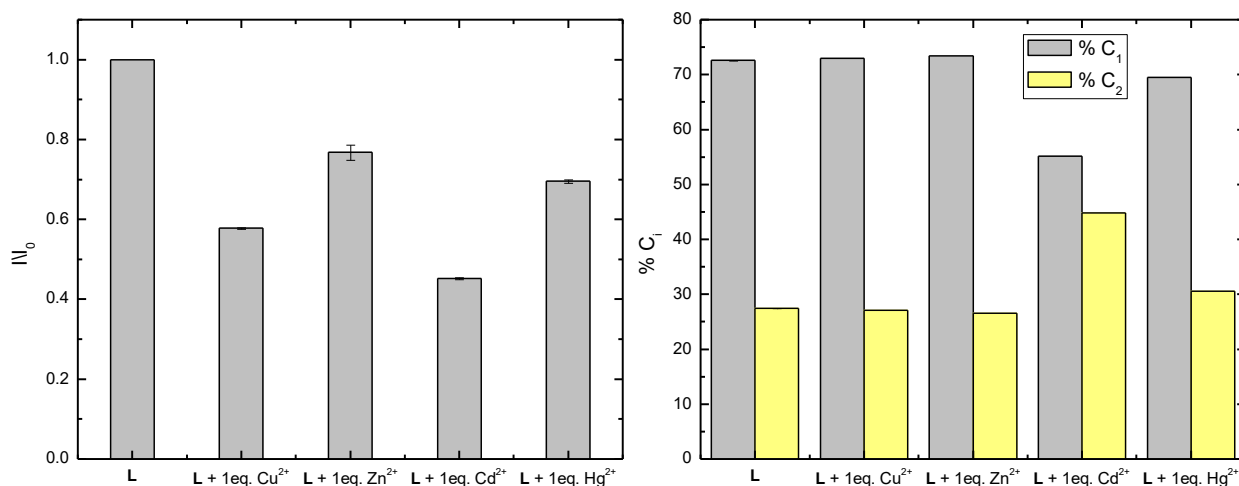


Figure 4.31. I/I_0 ratio (left hand panel) and $\%C_i$ (right hand panel) for free L in acetonitrile and in the presence of 1 equivalent of Cu^{2+} , Zn^{2+} , Cd^{2+} and Hg^{2+} .

From Figure 4.31 it can be seen that although the ratio I/I_0 is lower for the cadmium ion, the decrease is relatively small when compared to the other ions (from a I/I_0 ratio of 0.45 for Cd^{2+} to 0.77 for Zn^{2+}). However, in the case of the fractional contribution of the component 2 (associated to the longer decay time), there is a clear departure of the value of Cd^{2+} with the value of 45% relative to the general constancy found for L alone, Cu^{2+} and Zn^{2+} and Hg^{2+} with a value of $\sim 30\%$. Since the contributions of C_1

and C_2 mirror the ground state contributions of each species if the C_2 species decreases in contribution, the C_1 increases proportionally. Therefore for $L: Cd^{2+}$ the value is now 55% vs. 70% for L alone and interacting with all the other metals.

The stability constants for the interaction of L with Cu^{2+} , Zn^{2+} , Cd^{2+} and Hg^{2+} were calculated using HypSpec software and are summarized in 2.¹⁹⁹ Taking into account these values, the sequence of the strongest interaction expected for L decreases in the follow order: $Hg^{2+} > Cd^{2+} > Zn^{2+} > Cu^{2+}$.

Table 4.7. Stability constants for probe L in the presence of Cu^{2+} , Zn^{2+} , Cd^{2+} and Hg^{2+} in acetonitrile for an interaction 1:1 (Metal/Ligand).

Interaction (M:L)	$\Sigma \log \beta$ (Abs)	$\Sigma \log$ (Emission)
Cu^{2+} (1:1)	$6.12 \pm 8.16 \times 10^{-3}$	$6.34 \pm 1.89 \times 10^{-2}$
Zn^{2+} (1:1)	$6.73 \pm 1.56 \times 10^{-3}$	$6.84 \pm 8.97 \times 10^{-2}$
Cd^{2+} (1:1)	$8.42 \pm 2.74 \times 10^{-3}$	$8.38 \pm 5.74 \times 10^{-2}$
Hg^{2+} (1:1)	$9.94 \pm 1.86 \times 10^{-3}$	$9.97 \pm 5.89 \times 10^{-2}$

4.5.1. Conclusions

The spectral and photophysical characterization of a probe bearing two naphthalene units and its interaction with different metal ions (Zn^{2+} , Cu^{2+} , Cd^{2+} and Hg^{2+}) was undertaken in acetonitrile. In all cases a blue shift in the absorption spectra and a quenching fluorescence emission of the ligand was observed. From TR it is shown that the ligand L show a higher affinity towards the metal ion cadmium in acetonitrile medium. Also probe L apparently was not selective for any of the metal ions studied, the different values of I/I_0 obtained permits to differentiate between Zn^{2+} , Cu^{2+} , Cd^{2+} and Hg^{2+} .

4.6. Photophysical characterization of L_1 and L_2

Molecular probe L_1 and L_2 , were found to be soluble in dichloromethane, acetonitrile and dioxane. In the solid state, L_1 and L_2 presents a pale and gold yellow colour but within the concentrations of the free ligand and in the solvents used, the solutions were colourless.

The absorption, fluorescence emission (and excitation) spectra of both compounds were obtained in dichloromethane. The absorption spectra show a characteristic pyrene derivative spectra¹⁹⁵ (Figure 4.32) with a maximum at *ca.* 360 and 344 nm (red shifted compared to the pyrene absorption spectra) for the compounds L_1 and L_2 , respectively. Moreover, the fluorescence emission spectra of both compounds display two bands, one resolved with maximum at 394 and 395 nm and another unresolved

and broad with maximum at *ca.* 511 and 490 nm for the compounds **L**₁ and **L**₂, respectively. Both compounds have low emission intensities and possess only two resolved vibronics in the monomer band which is also characteristic of pyrene derivatives,¹⁹⁵ see Figure 4.32.

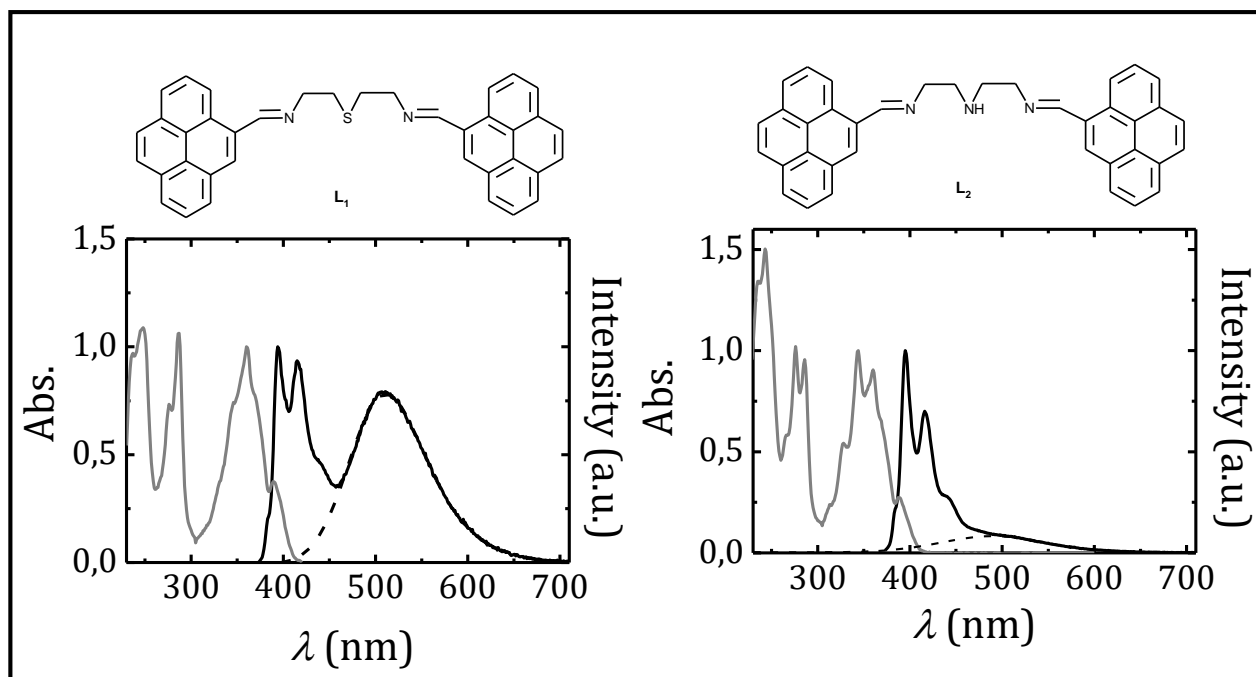


Figure 4.32. Absorption and fluorescence emission spectra ($\lambda_{exc}=360$ nm) of compounds **L**₁ and **L**₂ in dichloromethane.

The absorption spectra of Figure 4.32 shows that there is more vibronic resolution for **L**₂ and that the amount of dimer formed is higher in **L**₁ than **L**₂. Very curious is the fact that, in contrast to other systems, the dimer absorption band is not present at longer absorption wavelengths with the absorption spectra of **L**₁ and **L**₂ in dichloromethane apparently only reflecting the absorption of the monomer species. However, when the excitation spectra is collected at the dimer emission wavelengths (from 510 to 600 nm), a new band, mirroring the absorption of the dimer, can be observed essentially in the absorption region of the monomer with a tail at longer wavelengths for **L**₁ that is absent for **L**₂. This shows a unique behaviour for these systems with an overlap of the monomer and dimer absorption bands.

Moreover, the vibronic resolution of the absorption spectra (as seen by the 0-1 to 0-2 ratio optical densities, a parameter that can be considered similar to the P_A in pyrene polymers) of **L**₂ is different in acetonitrile and dichloromethane (data not shown). From the fact that the dimer absorbs in the region of the monomer this likely indicates that more dimer is present in acetonitrile.

The spectral and photophysical properties of L_1 and L_2 are summarized in Table 4.8 and include the fluorescence quantum yield (ϕ_F), the wavelength maxima (λ_{\max}^{abs} , λ_{\max}^{em} and λ_{\max}^{exc}), the fluorescence lifetimes (τ_1 and τ_2) and the contribution (C_i, λ_{em}) of each specie for the probes L_1 and L_2 in different solvents at $T=293$ K.

In view of the values in Table 4.8, it can be seen that the ϕ_F value is low (~ 0.030) in all solvents investigated, indicating that the fluorescence is not an efficient route for the deactivation of the excited state of both ligands. The low fluorescence quantum yield likely results from a photoinduced electron transfer (PET) from the nitrogen lone pair to the aromatic moiety. This, however, is not limitative to observe the interaction of this with metal cations by fluorescence spectroscopy.

4.6.1. Sensorial Ability of Compound L_1 and L_2 Towards Pb^{2+} , Cu^{2+} , Ag^+ , Zn^{2+} , Hg^{2+} and Cd^{2+} Ions

Upon the addition of the metal ions Cu^{2+} and Pb^{2+} to a dichloromethane solution of ligands, an absorbance decrease at *ca.* 360 nm and increase at *ca.* 460 nm was observed. Some isosbestic points were detected (Figure 4.34) at 388 nm ($L_1 + Pb^{2+}$), 268 and 320 nm ($L_1 + Cu^{2+}$), 253, 288 and 313 nm ($L_2 + Pb^{2+}$) and 240, 254, 266, 289 and 318 nm ($L_2 + Cu^{2+}$). A CHEF at 510 nm was observed (see Figure 4.34 panels B, D, F and H).

Chemosensors

Table 4.8. Absorption, fluorescence emission and excitation wavelength maxima (λ_{\max}^{abs} , λ_{\max}^{em} and λ_{\max}^{exc}), extinction coefficient (ϵ_{λ}), excimer-to-monomer intensities ratio (I_E/I_M), fluorescence quantum yield (ϕ_F), fluorescence lifetime (τ_1 and τ_2), and the contribution (C_i , λ_{em}) of each specie for the probes L₁ and L₂ in different solvents at T= 293 K. The viscosity (η) and polarity index (P.I.) of the solvents are shown as well.

Compound	Solvent	η (mPa.s)	P.I.	λ_{\max}^{abs} (nm)	$\epsilon_{360\text{ nm}}$ (M ⁻¹ .cm ⁻¹)	λ_{\max}^{em} (nm) (λ_{exc})	I_E/I_M (λ_{exc})	ϕ_F
L ₁	CH ₂ Cl ₂	0.449 ³⁵	3.1	243.6, 249.6, 276.8, 287.4, <u>361.8</u> , 370.6, 389.4	35584	<u>394</u> , 415, 511.0±2.2 (339, 360 and 373), 504 (460)	6.4±0.6 (339, 360, 373)	0.039±0.009
				[L ₁]/[Ag ⁺]= 0.25		[L ₁]/[Pb ²⁺]= 1.0	276.4, 286.8, 345.2, <u>361</u> , 389	
L ₁	Dx	1.3075 ¹¹⁴	4.8					0.028
	CH ₃ CN	0.345 ³⁵	5.8					
	DMF	0.924 ³⁵	6.4	276, 286, 345, <u>361</u> , 388		<u>394</u> , 415, 512 (345)	0.77 (345)	
	DMF + 75 μ L H ₂ O			276.5±0.5, 286, 345.0±1.0, <u>360</u> , 388		<u>394</u> , 416, 514		
DMF + 750 μ L H ₂ O			277, 285.5±0.5, <u>359.5</u> ±0.5, 388.5±0.5		<u>401</u> , 418, 517			
L ₂	CH ₂ Cl ₂	0.449 ³⁵	3.1	243, 276, 286, 328, <u>344</u> , 359.5±0.5, 388±1.0	35584	<u>396.0</u> ±0.7, 416.8±0.4, 511.3±1.9 (339, 345, 360 and 373), 545 (460)	1.47±0.14 (339, 360, 373)	0.028
				[L ₂]/[Ag ⁺]= 0.50		[L ₂]/[Pb ²⁺]= 1.0	276, 286, 344, <u>360</u> , 391	

Chemosensors

Compound	Solvent	η (mPa.s)	P.I.	λ_{\max}^{abs} (nm)	$\epsilon_{360 \text{ nm}}$ (M ⁻¹ .cm ⁻¹)	λ_{\max}^{em} (nm) (λ_{exc})	I_E/I_M (λ_{exc})	ϕ_F
L ₂	Dx	1.3075 ¹¹⁴	4.8					0.030±0.003
	CH ₃ CN	0.345 ³⁵	5.8	276, 286, 344, 360, 392		<u>395</u> , 416 (360), ~450 (460)		0.030±0.003
	DMF	0.924 ³⁵	6.4	276, 285.5±0.5, 328, <u>344</u> , 359.5±0.5, 387.5±0.5		375, <u>395</u> , 416, 508 (345)	0.94 (345)	
	DMF + 75 μ L H ₂ O			276, 285, 328, <u>344</u> , 358.5±0.5, 387.5±0.5		376, <u>395</u> , 415, 509		
	DMF + 750 μ L H ₂ O			277, 287, 334.5±0.5, <u>361.5±0.5</u> , 394±1.0		375, <u>396</u> , 443		

^a when exciting at 345 nm, the maximum emission wavelength of the more red-shifted band was not clear. The underlined values correspond to the most intensive peak in the S₀→S₁ and S₁→S₀ transition.

As mentioned before, the low fluorescence quantum yield likely results from a photoinduced electron transfer (PET) from the nitrogen lone pair to the aromatic moiety. Upon cation binding the redox potential of the donor is raised and the HOMO that was involved in the PET process has now a lower energy (stabilization arising from the covalent bonding between the donor and the metal ion, which requires both electrons). As a consequence, PET becomes impossible, and fluorescence intensity is enhanced.

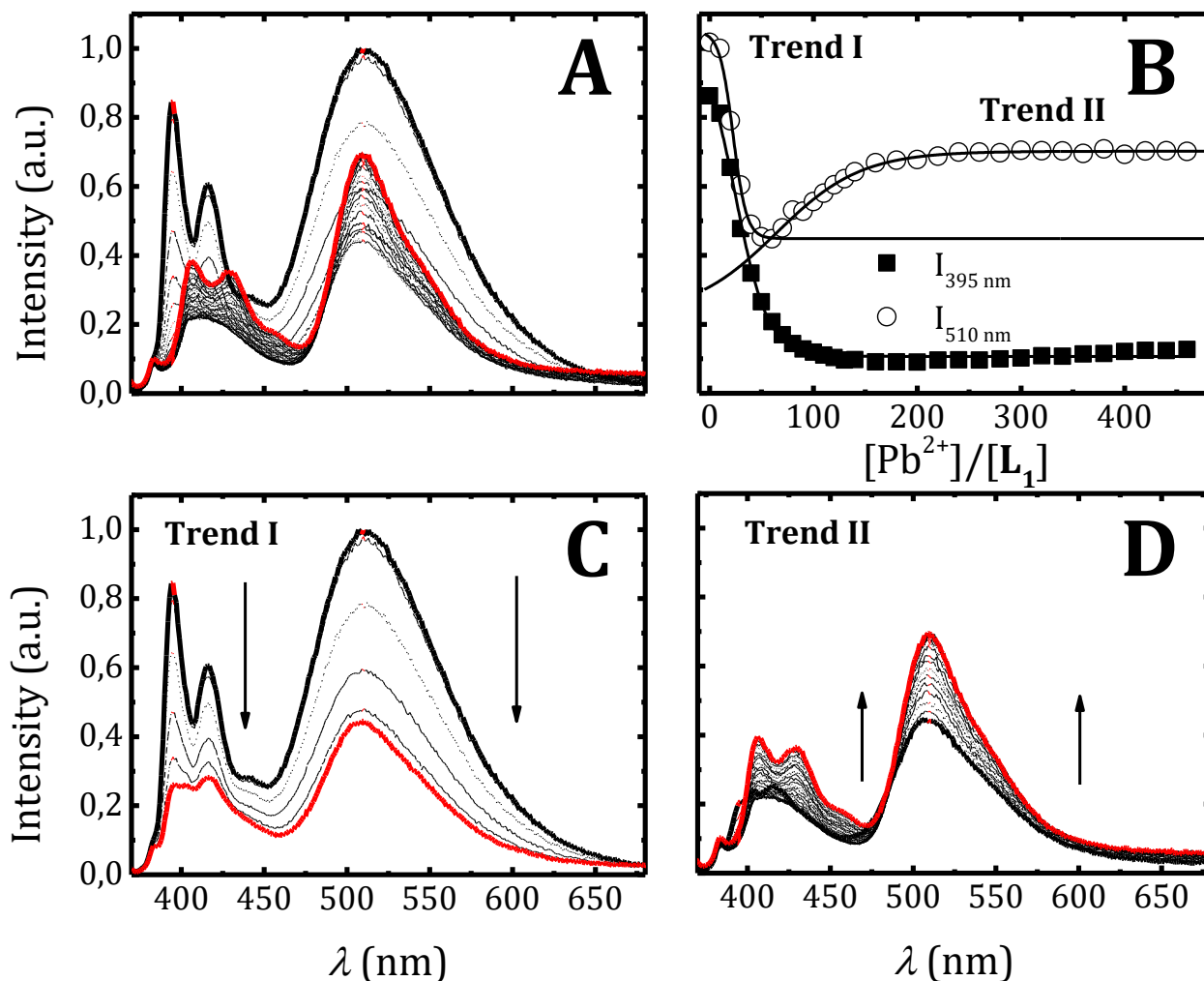


Figure 4.33. (A) (C) and (D) Fluorescence emission spectra ($\lambda_{exc} = 360$ nm) of L₁ in dichloromethane with the addition of Pb²⁺ in dichloromethane. (B) Fluorescence emission intensities taken at 395 and 510 nm.

In order to evaluate the potential of the proposed turn-on fluorescent probe for detecting metal ions, the detectable amount of Ag⁺, Cd²⁺, Cu²⁺, Hg²⁺, Pb²⁺ and Zn²⁺ metal ions were explored by a standard addition method in dichloromethane. The results are summarized in Figure 4.36.

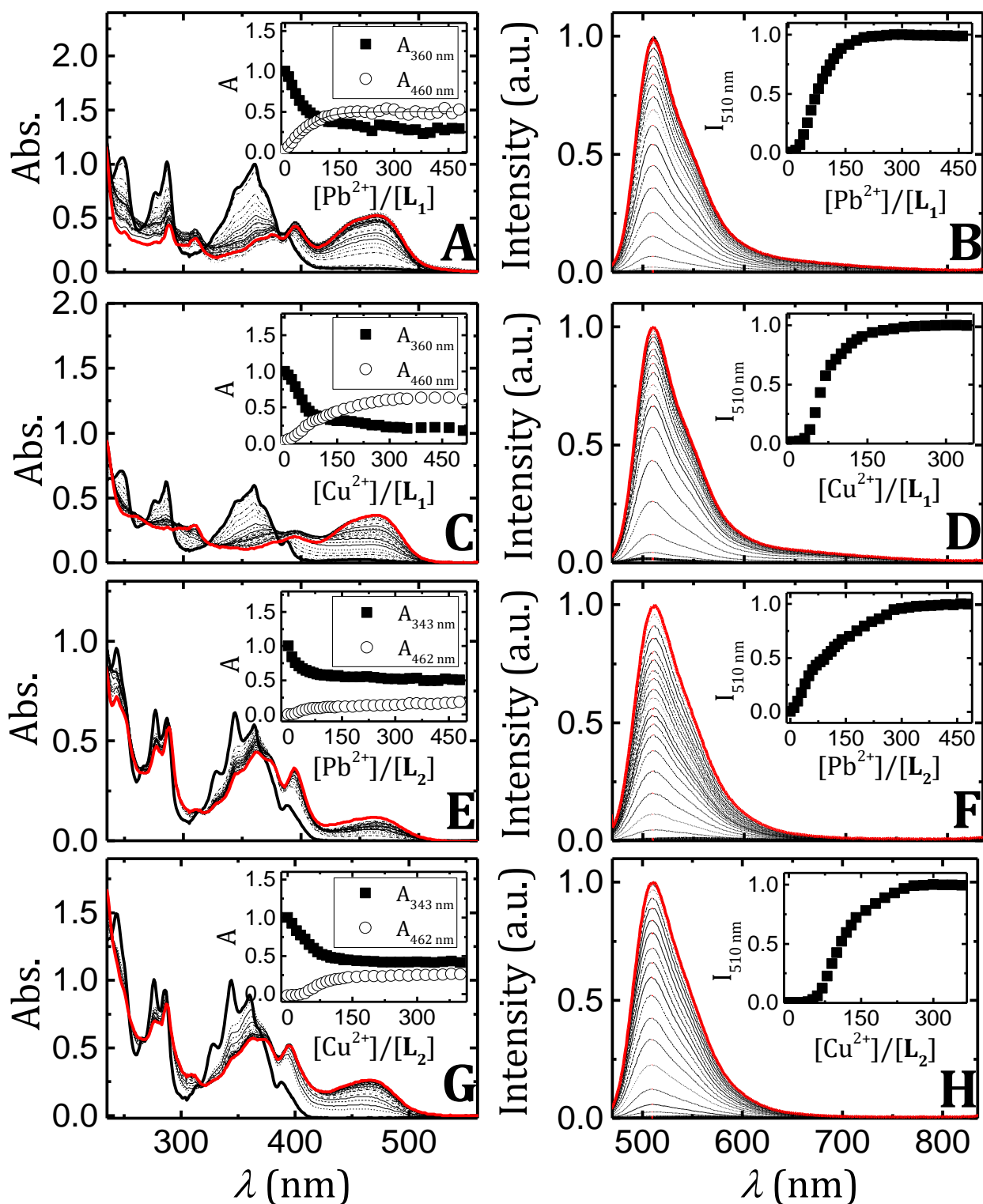


Figure 4.34. Absorption (A, C, E and G) and fluorescence emission spectra (B, D, F and H) ($\lambda_{\text{exc}} = 460 \text{ nm}$, 465 nm for F) of compound L₁ (top panels) and L₂ (bottom panels) in dichloromethane with the addition of Pb²⁺ (A, B, E and F), Cu²⁺ (C, D, G and H) in dichloromethane. The right insets represents the absorbance at 360 and 460 nm for L₁ and 343 and 462 nm for L₂ and the left insets the emission intensity at 510 nm as a function of [Pb²⁺]/[L] (A, B, E and F) and [Cu²⁺]/[L] (C, D, G and H).

The association constants for metal ion interaction were determined using HYPERQUAD software (see Section 7.2.4) and the main results are gathered in Table 4.9. The stoichiometry obtained for L_1 was typically of 1 metal per ligand for both Cu^{2+} and Pb^{2+} and 2:1 for L_2 .

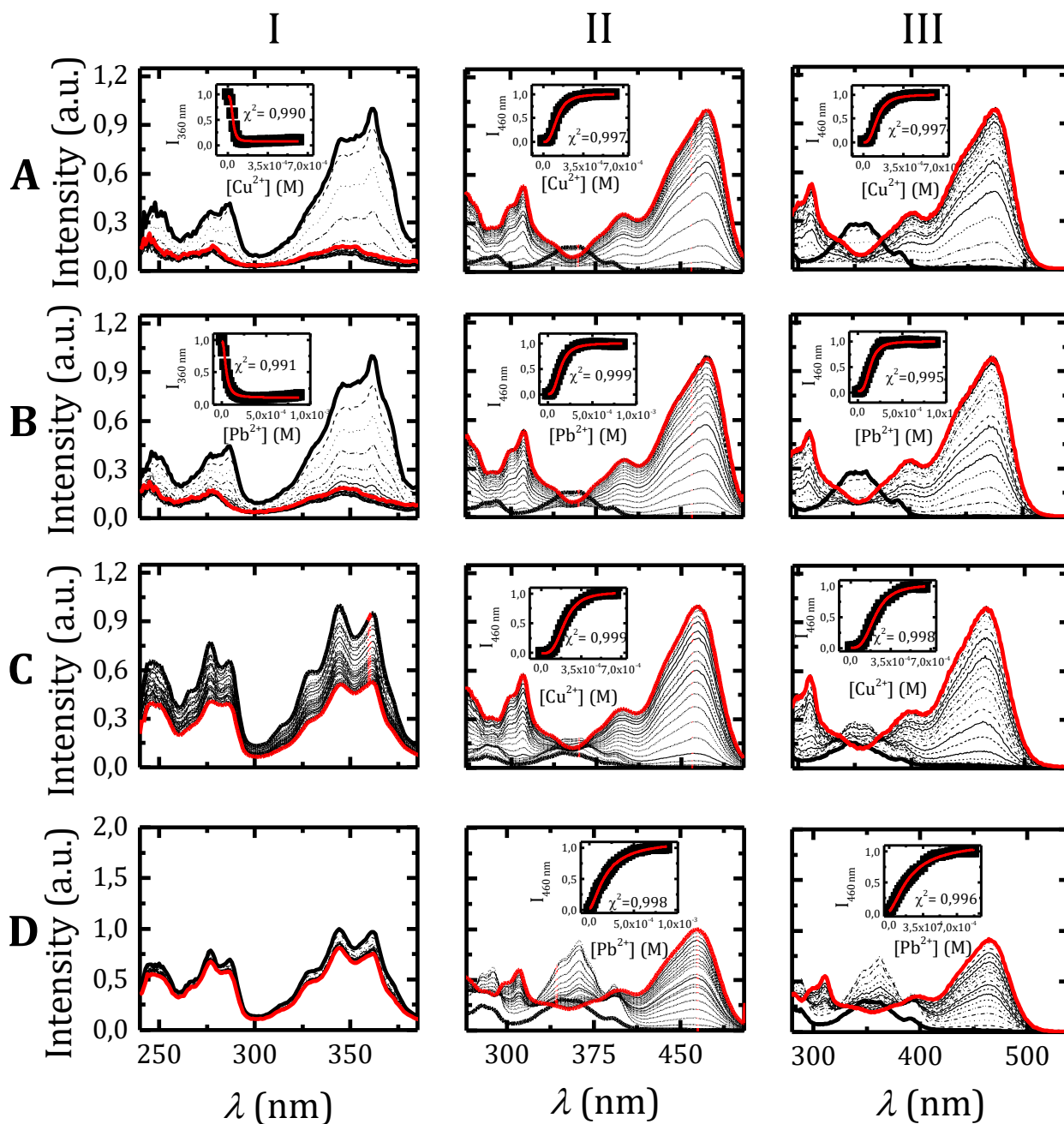


Figure 4.35. Fluorescence excitation spectra with (I) $\lambda_{em}=395$ nm, (II) 510 nm and (III) 580 nm for (A and B) L_1 and (C and D) L_2 in dichloromethane with the addition of (A and C) Cu^{2+} and (B and D) Pb^{2+} in dichloromethane. The insets represent the fluorescence intensity at (I) 360 and (II and III) 460 nm as a function of the concentration of the metal cation.

The fluorescence emission spectra (with $\lambda_{exc}=360$ nm) of L_1 is quenched with the addition of the metal cations until 50 equivalents (~ 23 min), but the width of this band changes after the addition of 30 equivalents of Pb^{2+} (~ 9 min) from 28 to 14 nm using a GaussMod function to fit the longer band (see Equation 7.19), which can be seen by the different shape of the longer band. The explanation found is that there is an initial quenching of the ligand and that, after some time, with the addition of the cation a new band appears in the absorption (at longer wavelengths) that emits in the same region that of the dimer. This seems to indicate that there is a quenching of the ligand concomitant with the appearance of the emission band from the CT species.

Table 4.9. Stability constants for probe L_1 and L_2 in dichloromethane in the presence of Cu^{2+} and Pb^{2+} in dichloromethane.

Ligand	Metal ion	Ionic radii (pm)	Log $\beta \pm \sigma$ (M:L)
L_1	Pb^{2+}	133	4.1 ± 0.02 (1:1) ^a
	Cu^{2+}	87	2.72 ± 0.006 (1:1) ^a
L_2	Pb^{2+}	133	8.3 ± 0.06 (2:1) ^b
	Cu^{2+}	87	7.59 ± 0.008 (2:1) ^a

^{a,b} obtained from the fitting of the absorbance at 460 and 360 nm vs. $[M^{2+}]$, respectively.

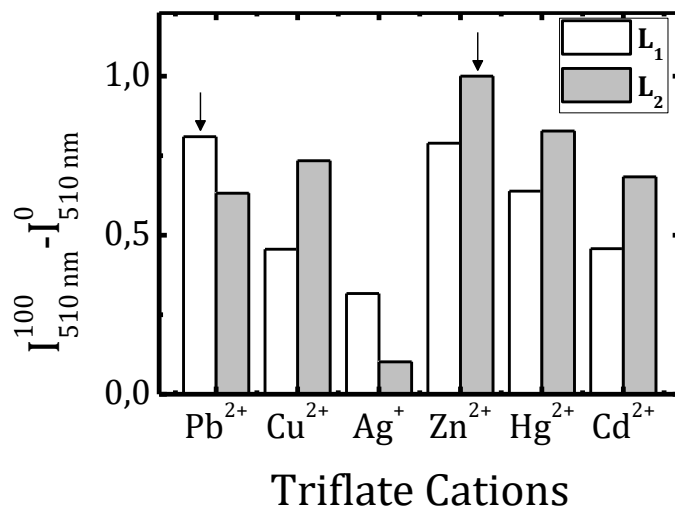


Figure 4.36. Difference of intensities at 510 nm for compound L_1 and L_2 in dichloromethane (obtained from the emission spectra collected at $\lambda_{exc}=460$ nm) between the ligand in the presence of 100 equivalents of metal (Pb^{2+} , Cu^{2+} , Ag^+ , Zn^{2+} , Hg^{2+} and Cd^{2+}) in acetonitrile and the free ligand.

4.6.2. Time-resolved Fluorescence Measurements

The fluorescence decays of L_1 in dichloromethane with excitation at 339 nm and emission at 550 nm in the absence and presence of Pb^{2+} display a monoexponential decay in dichloromethane and a double exponential decay when 1 equivalent of Pb^{2+} is added. Very interesting is to observe that the lifetime in the absence of the metal ion is of 24.78 ns and upon addition of this metal remains basically unchanged. The additional component of 2.54 ns represents less than 2% of the total fluorescence at 550 nm and is likely to be due to a small amount of water associated to the lead salt used (see SI on the effect of the water addition).

The fact that the plateau is reached at hundreds of equivalents of metals is likely to be due to the slow kinetic (Figure 4.34). Although the kinetic seems to be slow, the fluorescence decays were collected right after each addition of metal cation. This was done for several reason: 1) because the fluorescence decay measurements were really slow (because of the very small ϕ_F) and 2) because the interaction with the metals is reversible which means that the time and duration of the measurement will affect the results. For this reason, the decays were measured, for both ligands, in the same conditions.

The time-resolved data of L_1 and L_2 in dichloromethane and upon addition of one equivalent of the metal ion Pb^{2+} is summarized on Table 4.10. The absorption spectra of the solutions used for these measurements are shown in Figure 4.44. From Figure 4.44 and for L_2 it can be observed that upon addition of Pb^{2+} , the absorption spectra changes particularly in the enhancement of the absorption of the red-edge of the spectra and a change of the vibronic mode ratio at the $S_0 \rightarrow S_1$ and $S_0 \rightarrow S_2$ absorption bands.

Observation of Table 4.10 and Figure 4.37, shows that only with a triple exponential fit the decays of L_2 can be properly fit. The decays mirror the contribution of the monomer emission (shorter component of 0.51 ns) and of the dimer emission (associated of the 22.74 ns component). The additional middle lifetime component of 5.37 has an insignificant contribution, particularly at 395 nm, although at 550 nm its contribution for the total emission is now significant. The absence of rising components at 550 nm shows that all the dimer is already formed in the ground-state (likely involving the interaction of the two pyrene groups). Upon addition of Pb^{2+} the three lifetimes increase in absolute value which is an indication of a chelation enhancement of fluorescence. Moreover, the contribution of this additional species (middle lifetime component) at 395 nm is still meaningless although once more at 550 nm it contributes to 29.5% of the total emission. We attribute the nature of this species to a residual contamination with another ion (metal or proton), or to an additional component also associated to the dimer.

Chemosensors

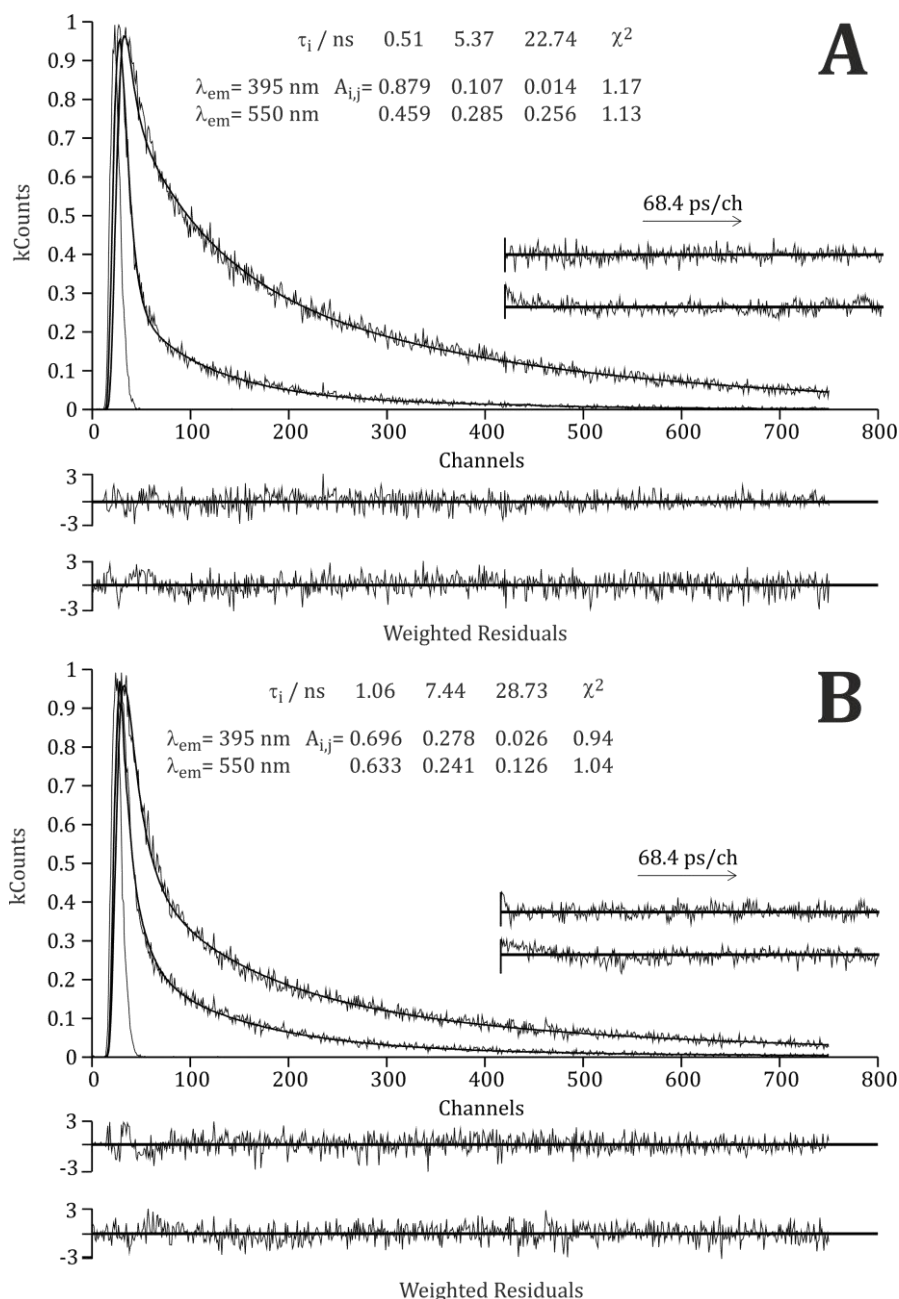


Figure 4.37. Fluorescence decays of L₂ in dichloromethane (T= 293 K) at $\lambda_{exc} = 339$ nm in (A) absence and (B) presence of Pb²⁺ (ratio [Pb²⁺]/[L₂]= 1:1). The instrument profile curve, decay times (τ_i), pre-exponential factors ($A_{i,j}$), χ^2 values, weighted residuals, and autocorrelation functions (A.C.) are shown as the insets.

The effect of water in the photophysical properties of L₁ can be seen in Figure 4.39. In Figure 4.39, the absorption and fluorescence (emission and excitation) in the absence of water and in the presence of a small amount water (50 μ L) and high amount of water (750 μ L) are shown. The observation of the emission spectra shows that the addition of a small amount of water leads to a small increase of the total fluorescence. This suggest that small amounts of water have the ability to disrupt some of the aggregates leading to the presence of more isolated molecules in solution. The addition of water in a higher amount leads now to not only an increase of the total emission but also a change in the I_E/I_M ratio (from 0.80 to

0.40) which suggests that some structural change is occurring with the compound. The absorption spectra obtained under the same conditions decreases gradually with the addition of water. This strongly suggest that water is playing a role (possibly leading to some degree of degradation) on the properties of the compounds. This should be taken into account when interpreting the data in dichloromethane and acetonitrile, although these solvents have been dried to exhaustion.

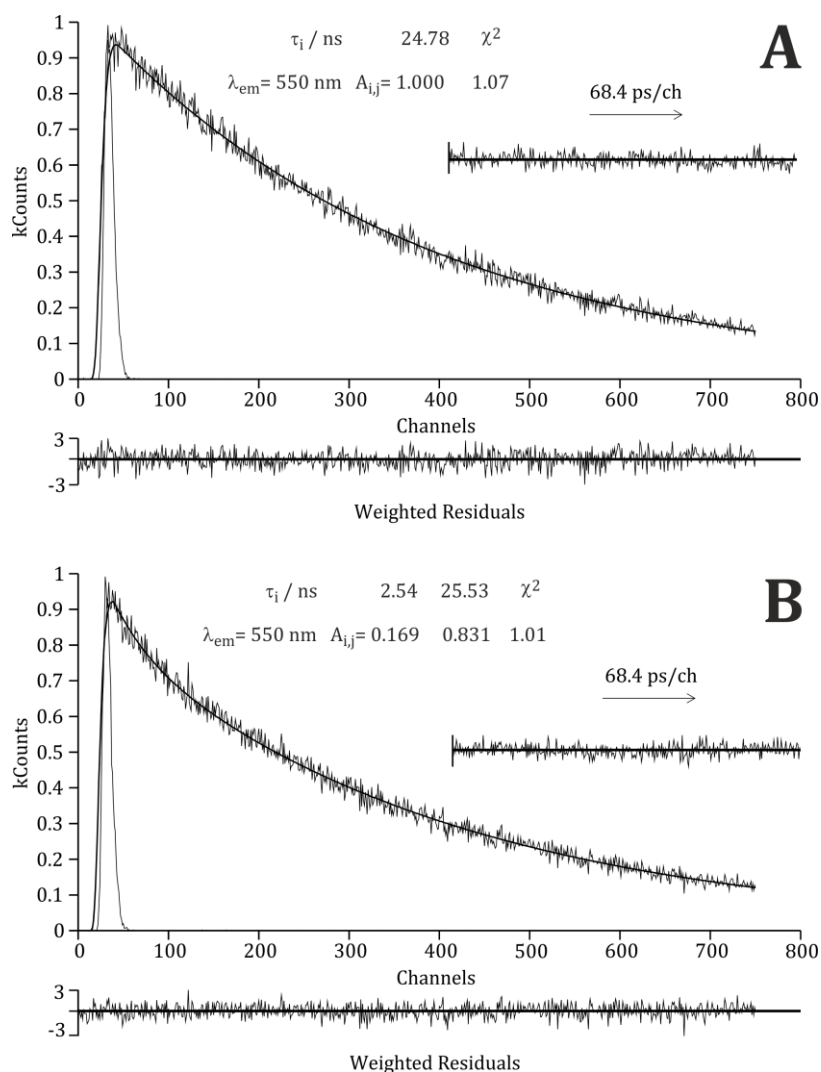


Figure 4.38. Fluorescence decays of L_1 in dichloromethane ($T = 293$ K) at $\lambda_{exc} = 339$ nm in (A) absence and (B) presence of Pb^{2+} (ratio $[Pb^{2+}]/[L_1] = 1:1$). The instrument profile curve, decay times (τ_i), pre-exponential factors ($A_{i,j}$), χ^2 values, weighted residuals, and autocorrelation functions (A.C.) are shown as the insets.

Table 4.10. Fluorescence lifetime (τ_i), pre-exponential decay ($A_{i,j}$) and contribution of each species at the different emission wavelengths ($C_{i,\lambda_{em}}$).

Compounds	τ_1 (ns)	τ_2 (ns)	τ_3 (ns)	$A_{i,1}$	$A_{1,2}$ (λ_{em})	$A_{1,3}$ (λ_{em})	$C_{1,395\text{ nm}}$	$C_{2,395\text{ nm}}$	$C_{3,395\text{ nm}}$
				($\lambda_{em}=395\text{ nm}$) ($\lambda_{em}=550\text{ nm}$)			(%)	(%)	(%)
L₁			24.78	<i>NE</i>		1			100
[L₁]/[Pb²⁺]= 1.0		2.54	25.53	<i>NE</i>					
L₂	0.51	5.37	22.74	0.879	0.107	0.014	33.4	42.8	23.7
				0.459	0.285	0.256	3.1	20.2	76.7
[L₂]/[Pb²⁺]= 1.0	1.06	7.44	28.73	0.696	0.278	0.026	20.8	0.6	78.7
				0.633	0.241	0.126	11.0	29.5	59.5

NE - not existent.

In the case of L₂ the absorption and emission spectra are depicted in Figure 4.39 under the same conditions of the above described L₁, i.e., in the absence of water and with a small and high amount of added water. In contrast to L₁, a small amount of water has basically no influence in the spectral (absorption and fluorescence) of the compound whereas a high addition of water leads to a radical change in the spectra which may be due to the formation of an exciplex¹⁹⁵ (which was not confirmed because the dependence with solvent polarity of this band was not done) or microaggregates.

4.6.1. Multivariate Data Analysis Procedure

The characterization of 2 compounds (L₁ and L₂) in interaction with 6 metal cations each (i.e., 12 samples) is conducted resorting to two well established methods: (i) hierarchical cluster analysis (HCA) for defining the data structure and (ii) principal component analysis (PCA) for data overview and feature selection. HCA is especially suitable for cases in which there is no a priori identification of classes, suggesting a structure of the data based on clusters. These clusters are further detailed and rationalized by PCA with biplot representation.²⁰⁵

The last techniques allow the visualization of the data, and thus direct observation of the most relevant patterns.

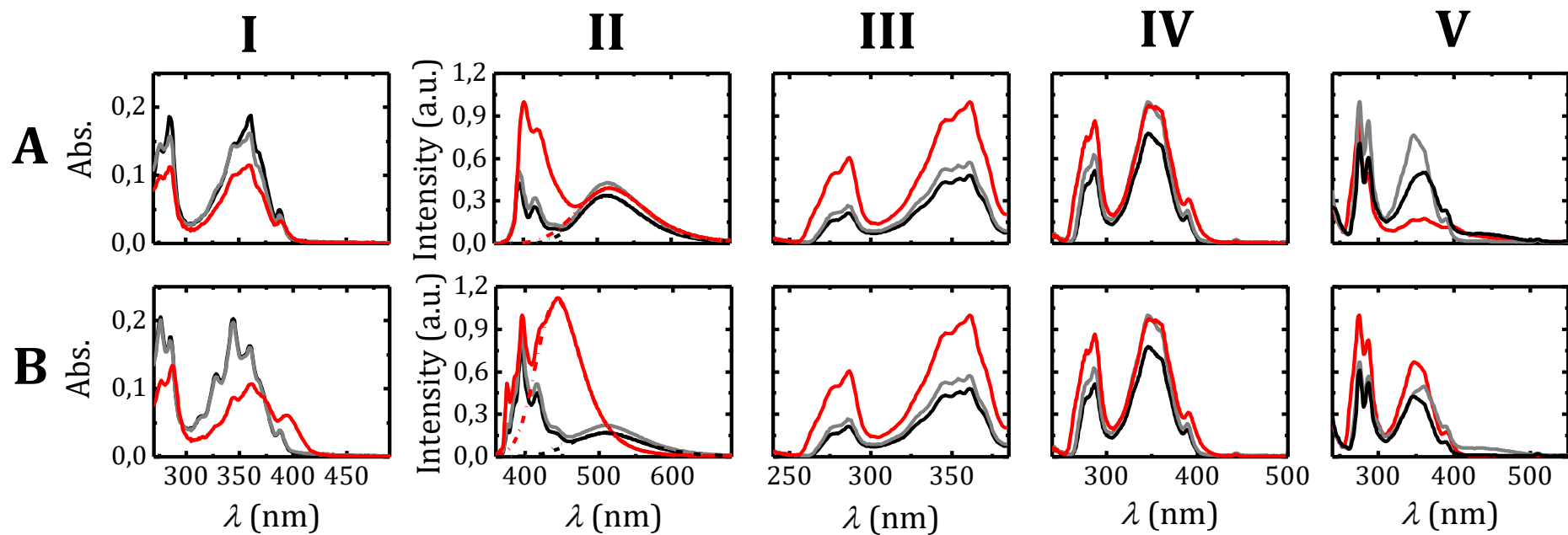


Figure 4.39. (I) Absorption, (II) fluorescence emission spectra ($\lambda_{exc.} = 345$ nm), (III) fluorescence excitation spectra at $\lambda_{em} = 360$ nm, (IV) $\lambda_{em} = 510$ nm and at (V) $\lambda_{em} = 600$ nm of (A) L₁ and (B) L₂ in dimethylformamide with 0, 50 and 750 μ L of water (black, grey and red line, respectively).

The procedure based on HCA and PCA requires a description of the objects, i.e. points in Euclidean space. In this analysis, each compound corresponds to one of these points, being described on the basis of 8 main components related to physicochemical and spectroscopic properties. Specifically, the data set contains information on 12 these samples characterized by 8 observations, including the Ionic Charge (+ or 2+) (Charge), Effective Ionic Radii (Radii), absorbance ratios at 360 nm between the ligand with 100 equivalents of metal (considering the factor of dilution) and the free ligand (A360N), absorbance ratios at 460 nm between the ligand with 100 equivalents of metal (considering the factor of dilution) and the free ligand (A460DF), fluorescence emission intensity ratios at 395 nm (for the fluorescence emission spectra with $\lambda_{exc}= 360$ nm) between the ligand with 100 equivalents of metal (considering the absorbance at 360 nm) and the free ligand (I395N), fluorescence emission intensity ratios at 510 nm (for the fluorescence emission spectra with $\lambda_{exc}= 460$ nm) between the ligand with 100 equivalents of metal (considering the absorbance at 460 nm) and the free ligand (I510N), bandwidth ratios (calculated using a GaussMod function) of the band of the fluorescence emission spectra ($\lambda_{exc}= 360$ nm) present at longer wavelengths between the ligand with 100 equivalents of metal and the free ligand (BandWN) and the area under the fluorescence emission spectra ratios ($\lambda_{exc}= 360$ nm) between the ligand with 100 equivalents of metal and the free ligand (TAEL). The software code were developed using R programming (version 3.0.1).²⁰⁶

4.6.1.1. Hierarchical Cluster Analysis

The main goal of clustering algorithms is to group the data into a number of sensible clusters according to their similarities. In the exploratory data analysis, HCA is used, for which a recent review can be found in ref. ²⁰⁷. The use of hierarchical methods is extremely common, and one of the reasons is that they allow the visualization of the data structure, even in complex cases. The HCA procedure is graphically represented by a dendrogram, which consists of a cluster structure and illustrates the fusions or divisions made at each successive stage of the analysis. It allows inspecting the overall structure of the data, and estimate the number of clusters.

All the compounds are linked based on their similarities or differences. The bigger the distance between two samples, the bigger is the difference between them. The result of the association is the hierarchical structure, in which similar compounds are merged.

4.6.1.2. Principal Component Analysis (PCA)

Principal component analysis (PCA) is one of the simplest and most robust ways of taking high-dimensional data, and using the dependencies between the variables to represent it in a more tractable, lower-dimensional form, respecting structure and preserving variance.^{205,208,209}

By construction, the first principal component is the one which maximizes the variance (reflected by its eigenvalue) when data are projected onto a line, which stands for a direction in the p -space, assuming you have p variables, and the second one is orthogonal to it, and still maximizes the remaining variance. This is the reason why using the first two components should yield the better approximation of the original variables space (considering a matrix X of dim $n \times p$) when it is projected onto a plane. The most influential variables in the system are highlighted, and the most relevant factors may be identified. In order to identify in which set of parameters the variance is the biggest, all parameters are normalized using Equation 4.1 (known as z score).

$$z = \frac{x - \mu}{\sigma} \quad \text{Equation 4.1}$$

In Equation 4.1, z is the normalized value of the raw value x of a parameter, μ is the mean of the set of values from this parameter and σ is the standard deviation from this set.

In the present work, PCA summarizes the information residing in the data corresponding to the physicochemical and spectroscopic data of a specific set of samples, into a form which may be more easily inspected and interpreted. The original multi-dimensional space, defined by those parameters, is contracted into a few descriptive dimensions, which represent the main variation in the data. Each principal component (PC) can be displayed graphically and analyzed separately, and its meaning may often be established on the basis of a few physicochemical and spectroscopic features. Essentially, the procedure is carried out by a linear transformation of the m parameters x_i into a new set, the principal components u_i , Equation 4.2.

$$u_i = w_{i1}x_1 + w_{i2}x_2 + \dots + w_{im}x_m \quad \text{Equation 4.2}$$

In Equation 4.2, $w_{i1} \dots w_{im}$ are the loadings, i.e. the weights of the each parameter in the linear combination.²⁰⁸

Since the first principal components retain most of the variance, several variables can be summarized by a few components and a plot of the first two or three PC s enables the visualization of most of the information contained in the data. PCA requires the solution of an eigenvalue problem, either based on the correlation or variance/covariance matrices of the original variables. In this work, we present results based on the correlation approach. In either case, these components are ranked, and the percentage of explained variance λ_i decreases from the first PC to the second and so on,²⁰⁹ suggesting the criteria for the selection of the most relevant first p principal components. The most common one is Pearson's,²⁰⁹ which can be used in both the variance/covariance and the correlation approaches. The value p is selected as the minimum integer that warrants the agreement with Equation 4.2.

$$\frac{\sum_{i=1}^p \lambda_i}{\sum_{i=1}^m \lambda_i} \geq 0.8$$

Equation 4.3

If the correlation matrix is used, the most common criterion corresponds to retain the p components for which $\lambda_i \geq 1$ although other values have been suggested.²⁰⁹

4.6.2. Results and Discussion

A comprehensive characterization of the compounds is performed to explore the physicochemical profiles and the relations between a set of spectroscopic properties.

The dendrograms presented in Figure 4.40 provides a two dimensional plots of the data structure, indicating the merging compounds and the merging distances. The data possess structure in which four groups of compounds are visible (cutoff distance of 4).

From Figure 4.40B, the group I assembled the compounds that possess a ratio (L + metal/L) of areas under the fluorescence emission spectra with $\lambda_{exc} = 360$ nm (TAEI) between 0.462 and 1.041 and with a ratio fluorescence intensities at 510 nm ($\lambda_{exc} = 460$ nm, I510N) between 3550 and 8357. Group II has the remainings compounds, i.e., the compounds with TAEI between 1.378 and 1.832 or the I510N with values between 16432.01 and 25479.19. Group I.I has the intensities ratio taken at 395 nm ($\lambda_{exc} = 360$ nm, I395N) between 0.562 and 0.593 and group I.II the remainings (between 0.867 and 1.487). Group II.II.I have only a compound that have a TAEI of 1.041 and group II.II.II the compounds with the TAEI parameter with values between 0.462 and 0.812. In group II.II.II.I possess the I510N of 7858 and in group II.II.II.II have the compounds that have I510N with values between 3550 and 4440. In subgroup II.II.II.II.I, a compound with a TAEI of 0.462 while in subgroup II.II.II.II.II, the TAEI have values between 0.622 and 0.771. From group II, two other groups are divided (II.I and II.II). The first has I510N between 4496 and 8357 and the second I510N between 16432.01 and 25479.19. In group II.II only one compound is present with I510N = 4496 and in group II.II.II are the compounds with I510N between 8107 and 8357. Group II.II.II is then divided in other two groups (II.II.II.I and II.II.II.II). In the first the absorbance ratio at 460 nm between ligand with metal and free ligand (A460DF) is almost the double (0.061) of the second (0.037). In groups II.II.I and II.II.II the differences are essentially in both the TAEI and I395N (TAEI 0.713 and 1.643, and I395N 0.985 and 2.498, for I and II, respectively).

Chemosensors

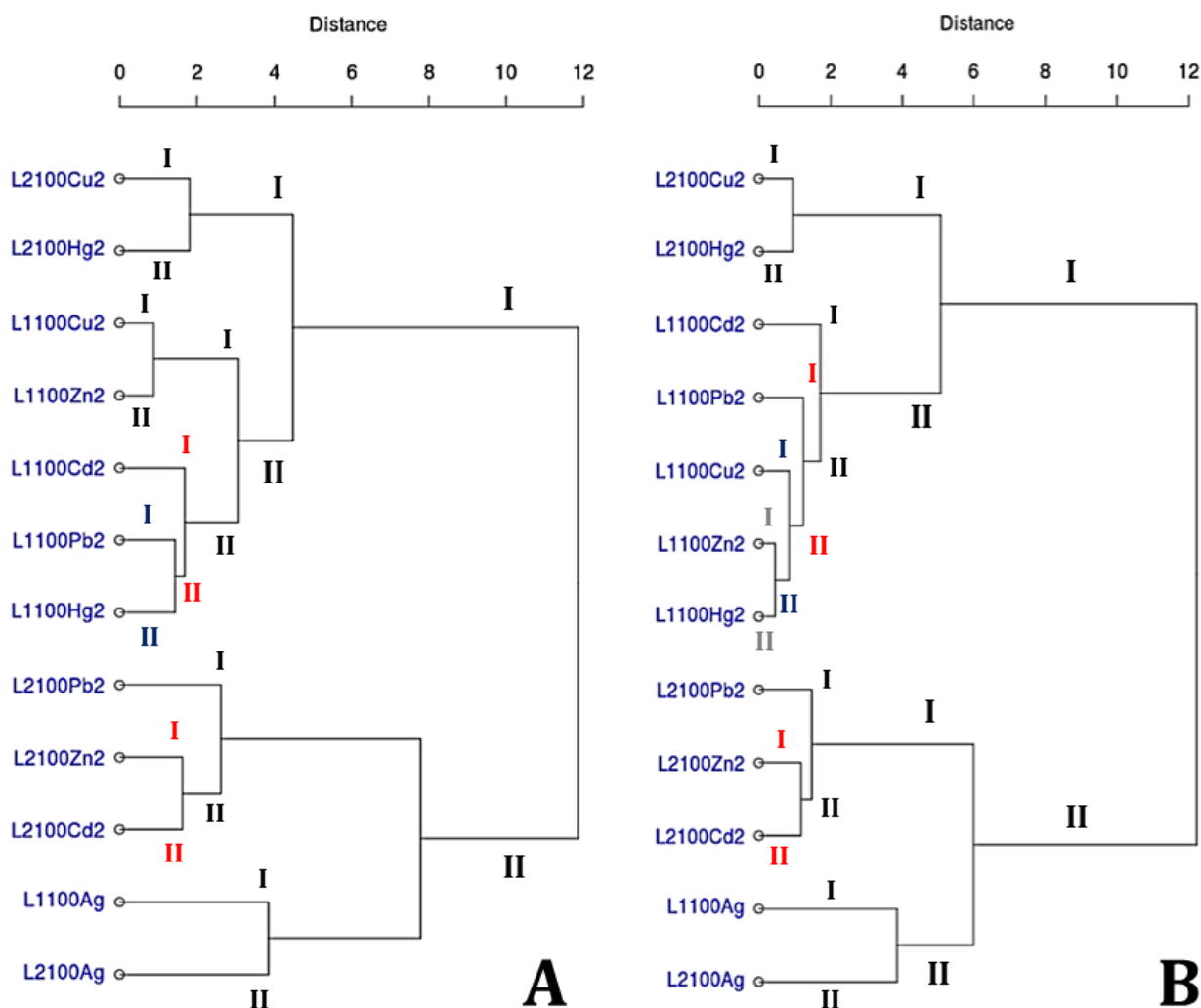


Figure 4.40. Dendrograms constructed resorting to Ward's method with Euclidean distances, using the physicochemical/spectroscopic properties as variables defining each compound: (a) similarity among the compounds using 8 parameters, including charge and radii; (b) similarity among the compounds considering only 6 spectroscopic parameters. After establishing the number of clusters, PCA was then applied on the data set containing only 6 spectroscopic parameters (Figure 4.40B) in order to reveal the relationship between the chemical compounds and the spectroscopic information in the defined groups.

In Figure 4.40A, the dendrogram is, in terms of groups, very similar only differing in the second division of the group I.II. In this case, I.II.I join together the metals with the smallest ionic effective radii (Radii, 73 and 74 pm for copper and zinc, respectively). In group I.II.II are the compound with the interaction of metal cation with the radii parameter between 95 and 119 pm. The last group (group I.II.II) is then divided in two more groups (I.II.II.I and I.II.II.II), which are constituted by the compounds with radii 95 and between 102 and 119, respectively.

From dendrogram in Figure 4.40A, the most similar samples are L_1 with copper and zinc (with $d \sim 1$) while in panel B the most similar samples are L_1 with zinc and mercury. In this last case, all parameters considered are very close (the maximum variance being of 2.6% for the TAEI parameter).

Table 4.11 summarizes the PCA results, using the correlation matrix. It is seen that the first two principal components are able to recover ca. 87% of the data variability, indicating that a graphical representation based on these two components is clearly meaningful.

Table 4.11. PCA results for the first two components using the correlation approach (N= 12).

Principal components	Explained variance (%)	Cumulative explained variance (%)
<i>PC₁</i>	59.9	59.9
<i>PC₂</i>	26.9	86.8

The scree graph of the eigenvalues, presented in Figure 4.41, shows that the first component contains, in fact, the most relevant information for discrimination.

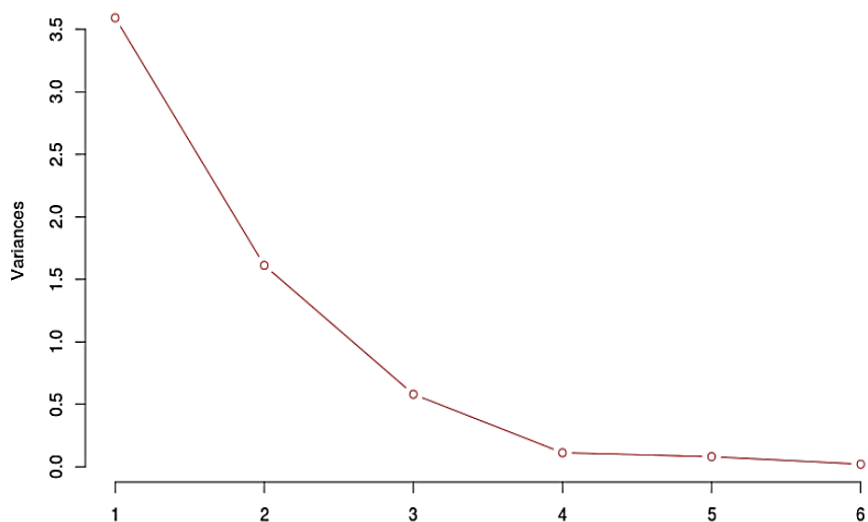


Figure 4.41. Scree plot of eigenvalues for the 6 spectroscopic parameters. Principal components are sorted by decreasing fraction of the total explained variance.

Figure 4.42 displays a composed view of the compounds in a biplot form,²⁰⁵ considering the new orthonormal principal component system. Compounds that are close together correspond to observations that have similar scores on the components displayed in the plot. Moreover, those compounds corresponds to observations that have similar values on the variables. Compounds that are close together have similar spectroscopic profiles. Vectors that point in the same direction correspond

to variables that have similar response profiles, and can be interpreted as having similar meaning in the context set by the data. In other words, a group of vectors pointing in the same direction correspond to a group of compounds having similar spectroscopic profiles.

The representation, in two dimensions, allows the visual discrimination between the compounds. As a preliminary PCA result, the data scores representation is in direct agreement with the results obtained with HCA.

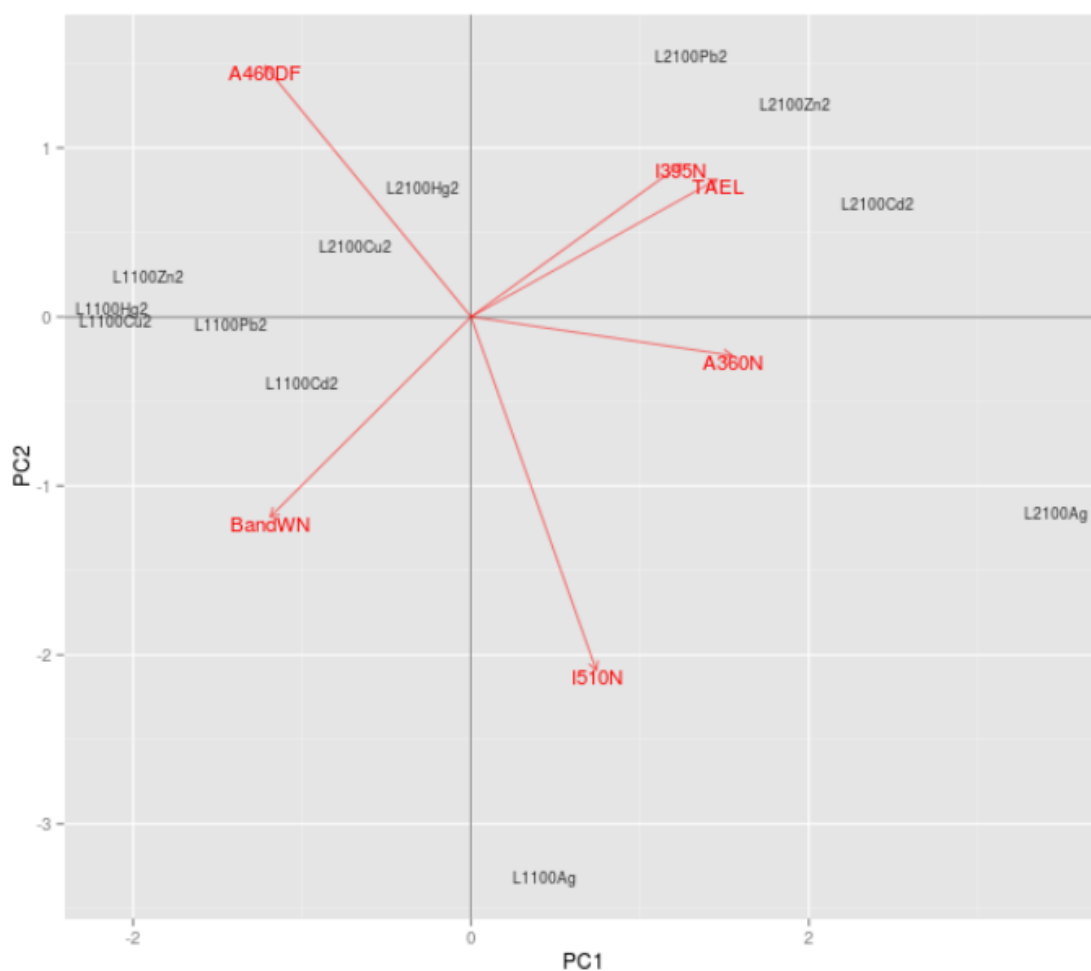


Figure 4.42. Representation of the samples on the first two components, with 87% of information recovery.

In Figure 4.42 the points representing the compounds are discriminated along the first component (PC₁), if one takes into account the lower relevance of the second component. This suggests that there are significant changes in the spectroscopic profile of the compounds included in the groups defined in Figure 4.40.

The first component, retains mainly information over A360N and TAEL (absolute weights of 0.501 and 0.472, respectively). The second component is mostly related with I510N (0.678) and A460DF (0.481). These parameters are connected since I510N is taken with excitation at 460 nm. High values of these parameters suggest an increase of complexation between metal and ligand.

The length of the red vectors in Figure 4.42 approximates the variances of the variables. The longer the vector, the higher is the variance. This Figure also shows a strong relationship between I395N and TAEL and a weak relationship between (i) I510N and three parameters, BandWN, TAEL and I395; (ii) A460N and the same set of parameters, as extracted from the angles between the vectors corresponding to these variables. The correlation between BandWN and A460DF, and the other parameters is negative.

Sample L2100Ag (L_2 compound with 100 equivalents of Ag^+) stands out with the highest A360N, the lowest A460DF and an absence of BandWN. Compound L1100Ag (L_1 compound with 100 equivalents of Ag^+) also stands out, with the highest I510N and a lower value of A460DF.

It is important to note that if an unknown sample would be to study, an addition of one or both ligands would be made to this sample and all parameters collected. Once all data obtained, a new dendrogram would be constructed and some inferences could be taken. If, for instance, the unknown sample get grouped in any group one could considerate the possibility of being one of the sample known in this group and investigate further. However, not fitting in any group give even more information, since this would mean that it is not constituted by the metal studied. Of course, this is more interesting the bigger is the set of samples and parameters, however, also more complex to interpret.

4.6.3. Summary

The photophysical characterization of two bipyrenyl ligands L_1 and L_2 (differing on the central atom of the molecule linking the two pyrene units) was obtained in dichloromethane. The association constants of L_1 and L_2 in dichloromethane with lead (II) and copper (II) were obtained and a stoichiometry of 1:1 and 2:1 was obtained, respectively. The time-resolved data reveal the presence of one (in the absence of metal) or two (in the presence of lead) species in the case of L_1 . For L_2 , only with three components the fluorescence decay could be correctly fitted and this is valid for the situation of absence and presence of metal cation. The addition of Ag^+ , Zn^{2+} , Hg^{2+} and Cd^{2+} was also made and it indicate that, of all the ions added, L_1 and L_2 were more selective to Pb^{2+} and Zn^{2+} , respectively. Furthermore, HCA analysis was made in order to obtain more information about this system.

4.6.4. Supplementary Information

Figure 4.43 show the absorption, fluorescence emission and excitation spectra of both ligands (L_1 and L_2) in DMF.

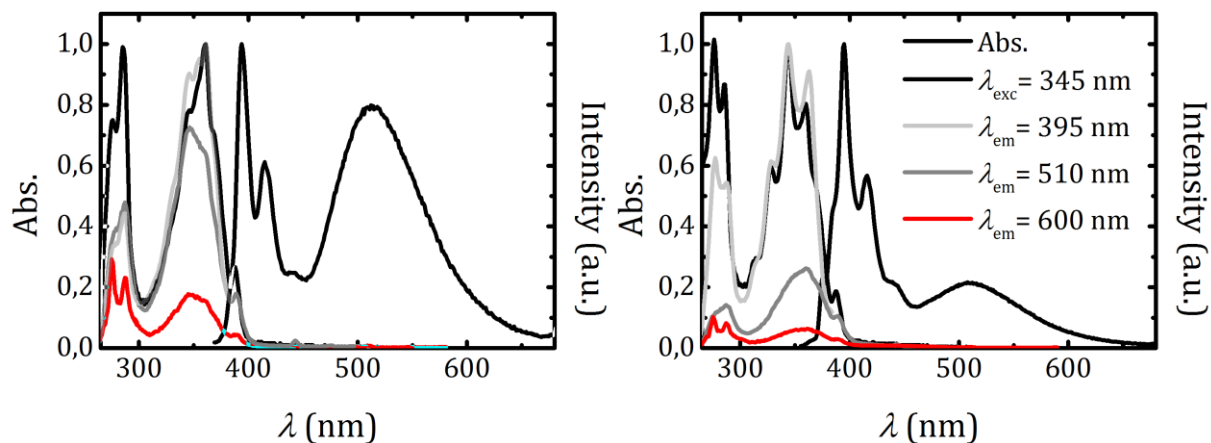


Figure 4.43. Absorption, fluorescence emission ($\lambda_{exc} = 345$ nm) and excitation spectra ($\lambda_{exc} = 395, 510$ and 600 nm) for L_1 and L_2 in DMF. The fluorescence peak at half the excitation wavelength were omitted.

Figure 4.44 show the absorption spectra of both ligands (L_1 and L_2 in dichloromethane) with and without 1 equivalent of lead in dichloromethane.

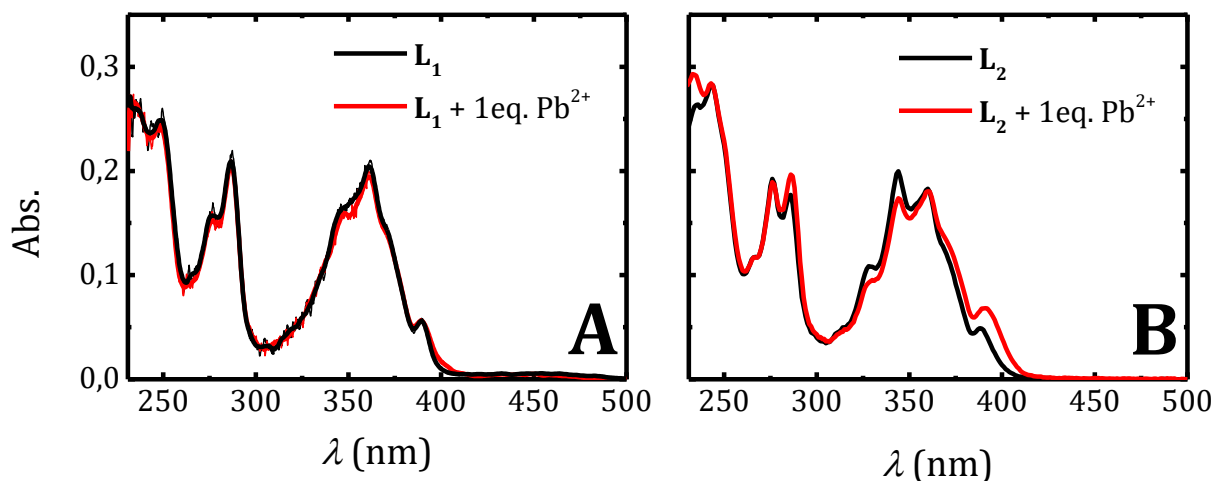


Figure 4.44. Absorption spectra of (A) L_1 and (B) L_2 in dichloromethane without and with 1 equivalent of Pb^{2+} in dichloromethane (black and red lines, respectively). In (A) the absorption spectra were smoothed with 54 points using the Savitzky-Golay method. The original spectra are shown as well.

Figure 4.45 show the absorption, fluorescence emission and excitation spectra of both ligands in dichloromethane with and without 1eq. of lead in dichloromethane.

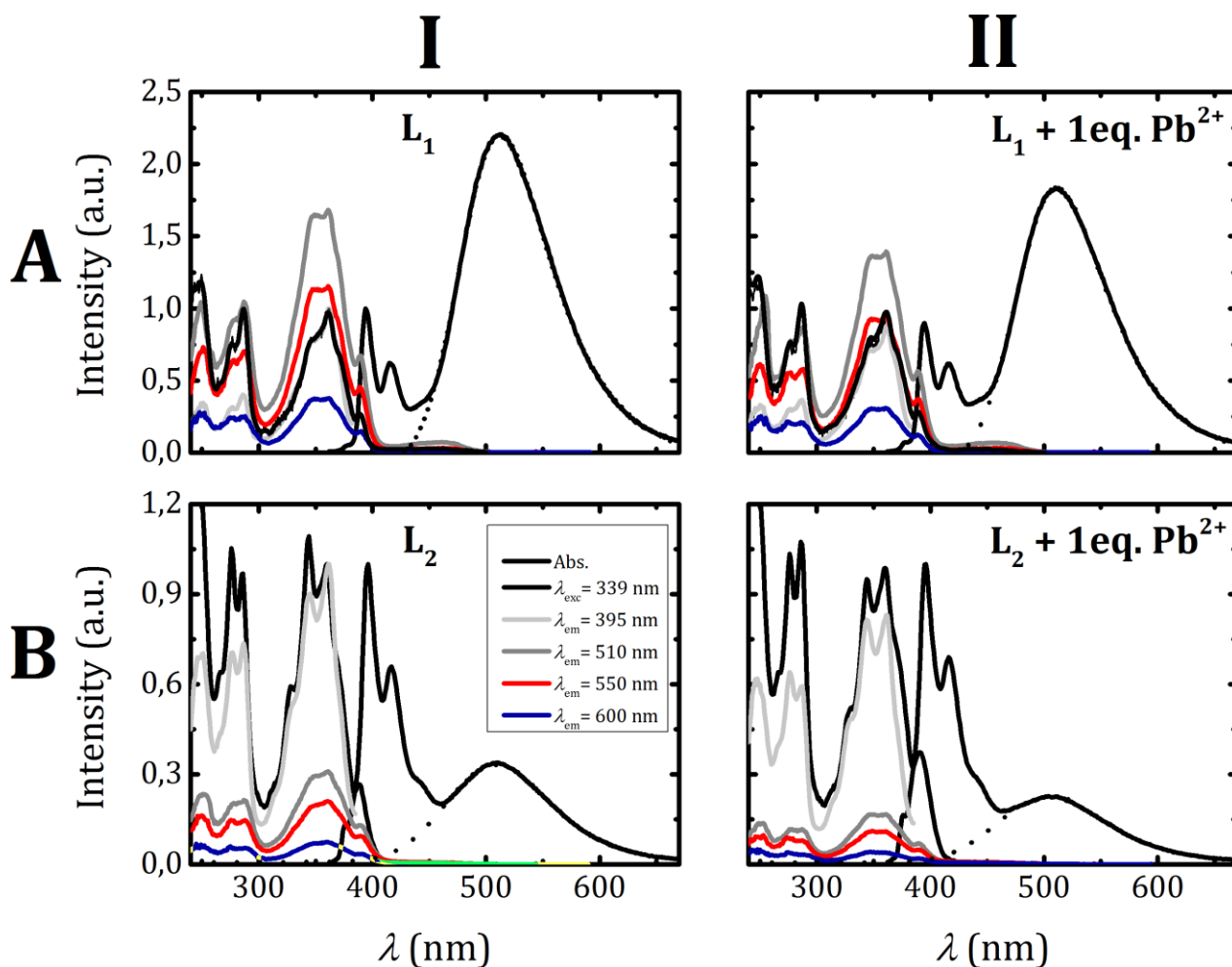
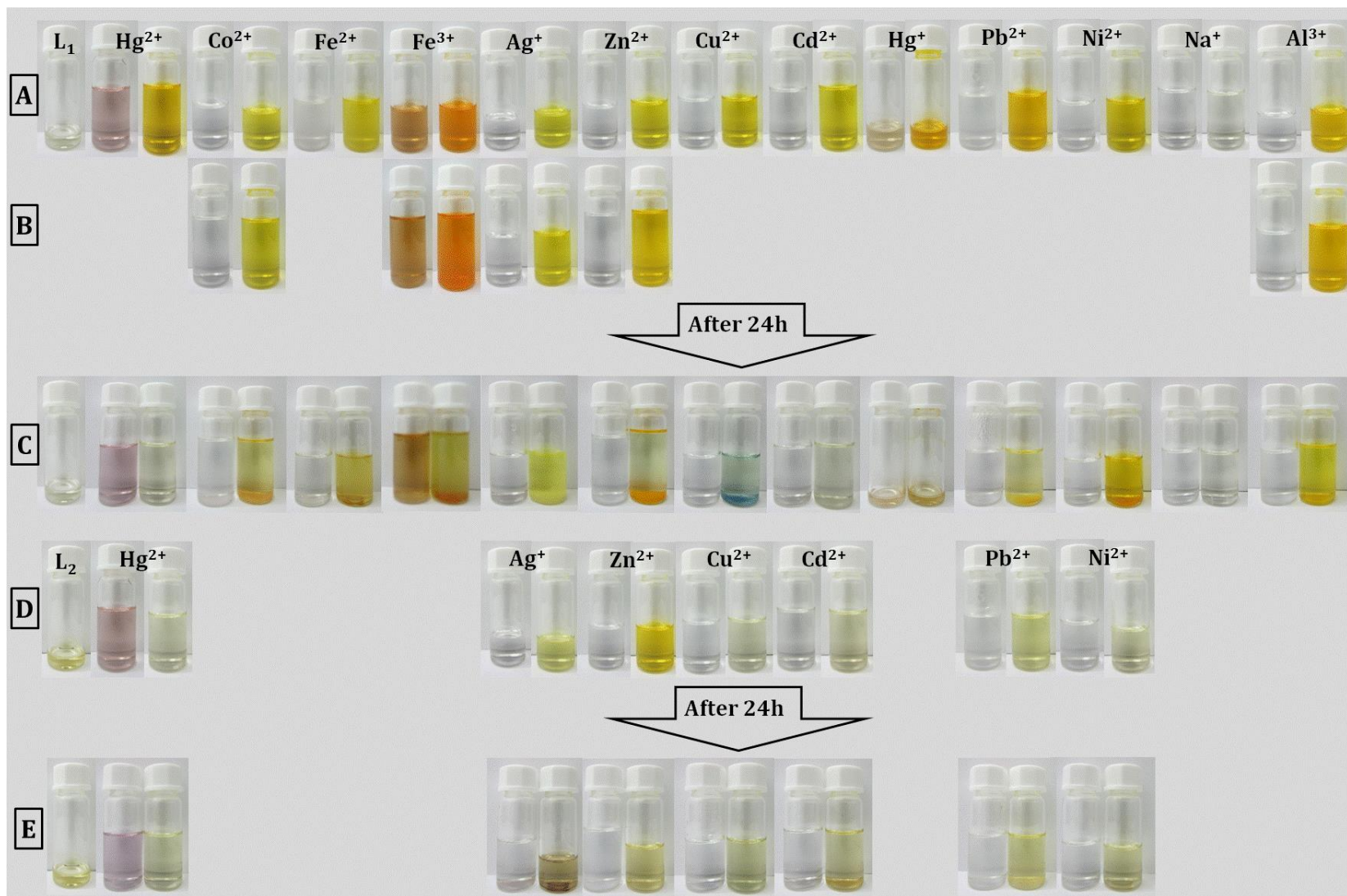


Figure 4.45. Absorption, fluorescence emission ($\lambda_{exc} = 339$ nm) and excitation spectra ($\lambda_{em} = 395, 510, 550$ and 600 nm) of the free L₁ and L₂ in dichloromethane (AI and BI, respectively) and of L₁ and L₂ with 1 equivalent of Pb²⁺ in dichloromethane (AII and BII, respectively). L₁ and L₂ spectra were acquired before the fluorescence decay measurements. After the measurement of the free ligand, the same solution was used for the measurement of the ligand with metal. The absorption spectra of L₁ were smoothed with 54 points using the Savitzky-Golay method. The original spectra are shown as well. The fluorescence peak at half the excitation wavelength were omitted. The longer wavelength band was fitted with GaussMod function.

Picture 4.3 show the naked-eye colourimetric behaviour of both ligands in dichloromethane.



Picture 4.3. Naked-eye colorimetric behaviour of L₁ (A, B and C) and L₂ (D and E) in dichloromethane in three (A to C) and two (D and E) different conditions, respectively. Condition A shows the naked eye colour solutions of L₁ with the addition of one equivalent of metal ions in dichloromethane; condition B with the addition of two equivalents; condition C with one equivalent (for Hg²⁺, Fe²⁺, Cu²⁺, Cd²⁺, Hg⁺, Pb²⁺, Ni²⁺ and Na⁺) and two equivalents (for Co²⁺, Fe³⁺, Ag⁺, Zn²⁺ and Al³⁺) after 24h. Condition D shows the naked eye colour solutions of L₂ with the addition of one equivalent of metal ions in dichloromethane; condition E with one equivalent and after 24h.

Chapter 5

Coumarins

5.1. Introduction

Coumarins consist of fused benzene and α -pyrone rings and comprise a very large class of phenolic substances of natural origin²¹⁰⁻²²¹. For example, they are found in traces amounts in the lavender, strawberries, cherries, apricot and cinnamon. At least 1300 have been identified, mainly as secondary metabolites in green plants^{210-218,221} but also in fungi and bacteria,²¹⁹ with photophysical and photobiological properties which have made them used in various research fields.²²⁰

Coumarins and its derivatives have several applications, some can be used as pesticides, laser dyes, in medicine, perfumes, as photosensitizers and probes.²²²⁻²²⁵ A coumarin derivative of great clinical significance is the highly potent anticoagulant warfarin, see structure in Figure 5.1.^{226,227} As pesticides, the commercial Coumaphos® and Potassan® are well-known, see structure in Figure 5.1.

Coumarin (unsubstituted compound of Figure 5.2) is a pleasant smelling compound and for this reason is found in countless cosmetic products (such as perfumes, eaux de toilette and cologne, deodorants and aftershaves).²²⁸ The well-known deodorant brand Axe®, for instance, use coumarins.

As probes, coumarins have been used for instance, in solvation studies due to their high sensitivity to the polarity of the medium.²²⁹ These coumarins were also employed as laser dyes,²³⁰⁻²³² specially the 7-amino derivatives.²³³

Due to their antioxidant properties they were used as well as food additives in order to keep the quality of aliments and drinks (such as tea and wine) for longer periods.²³⁴⁻²³⁶

Coumarins

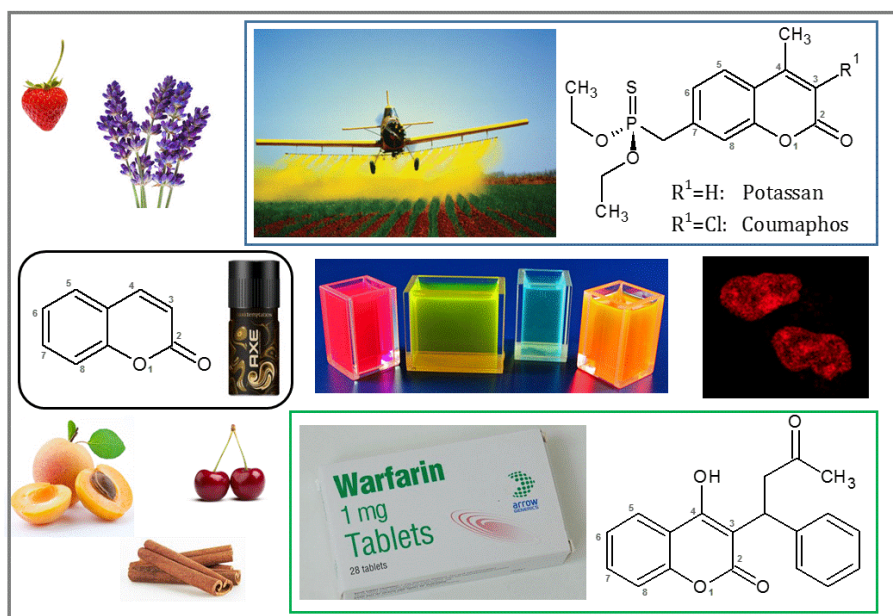


Figure 5.1. Collage illustrating the origin, applications and structures of some coumarins. From left to right and top to bottom. Schwebach, Tina [Photograph; Strawberry].²³⁷ Ray, Vitamin [Photograph; Lavender].²³⁸ Formuzis, Alex [Photograph; Airplane distributing pesticide].²³⁹ Structure of Potassan and Coumaphos. Structure of Coumarin. [Photograph; Axe® Deodorant].²⁴⁰ [Photograph; Laser Dyes].²⁴¹ [Photograph, Fluorescent probes].²⁴² [Photograph; Peach]. [Photograph; Cherries].²⁴³ [Photograph; Warfarin]. Structure of Warfarin. [Photograph; Cinnamon].²⁴⁴

In Figure 5.2 the structure of all the coumarins studied in this chapter are showed.

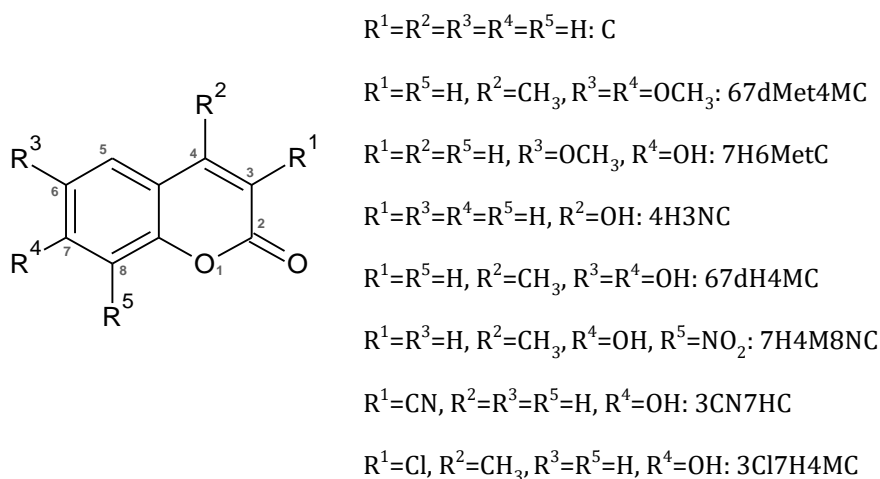


Figure 5.2. Structure of 6,7-dimethoxy-4-methylcoumarin (67dMet4MC), 7-hydroxy-6-methoxycoumarin or Scopoletin (7H6MetC), 4-hydroxy-3-nitrocoumarin (4H3NC), 6,7-dihydroxy-4-methylcoumarin or 4-methylsculetin (67dH4MC), 7-hydroxy-4-methyl-8-nitrocoumarin (7H4M8NC), 3-chloro-7-hydroxy-4-methylcoumarin (3Cl7H4MC) and 3-cyano-7-hydroxycoumarin (3CN7HC).

It is important to note in Figure 5.2 that 67dMet4MC can be used as parent compound for 67dH4MC.

5.2. Absorption, Steady State and Time-Resolved Fluorescence

5.2.1. 6,7-Dimethoxy-4-Methylcoumarin (67dMet4MC)

In Figure 5.3 the absorption spectra of 67dMet4MC in different dioxane:H₂O fractions are presented. The solutions used for the presentation of this absorption spectra were concentrated in order to avoid noise in the spectra, however, the solutions used for the emission spectra were more diluted ($A_{\max} = 0.2-0.3$).

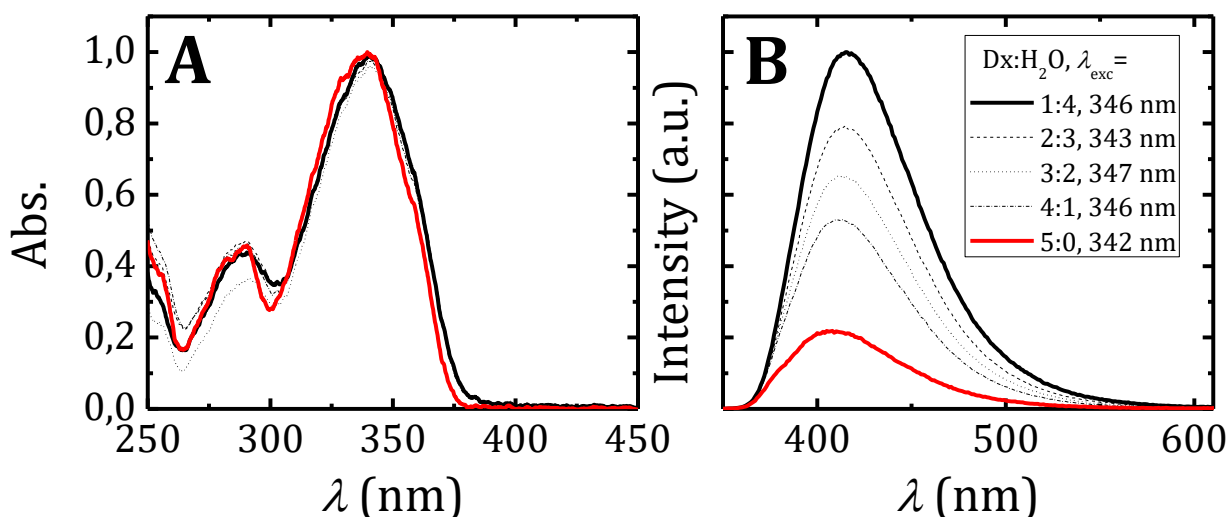


Figure 5.3. (A) Absorption and (B) fluorescence emission spectra of 67dMet4MC in different dioxane:H₂O mixtures (the λ_{exc} chosen was the absorbance maximum of each mixture).

The solutions of 67dMet4MC in the different dx:H₂O solutions present one band in both absorption and fluorescence emission spectra resulting from the absorption/emission of the neutral specie (Figure 5.3A and B). The shape of the band does not change with the water content, however the fluorescence emission maxima does change slightly by shifting to the red region of the visible spectra with the increase in the water percentage (Table 5.1).

In Table 5.1, the fluorescence quantum yields and lifetimes can be found for 67dMet4MC in the dx:H₂O mixtures. From the observation of the rate constant values (Table 5.1), it can be seen that the k_F remains approximately constant whereas the non-radiative constant decrease with the increase in the amount of water (increase in polarity).

Coumarins

Table 5.1. Absorption maxima wavelength ($\lambda_{\max}^{S_0 \rightarrow S_n}$), fluorescence emission maxima wavelength ($\lambda_{\max}^{S_n \rightarrow S_0}$), fluorescence quantum yield (ϕ_F), fluorescence lifetime (τ_F), fluorescence and non-radiative rate constants (k_F and k_{NR} , respectively) for 67dMet4MC in dx:H₂O mixtures.

Dx:H ₂ O/ Solvent	$\lambda_{\max}^{S_0 \rightarrow S_n}$ (nm)	$\lambda_{\max}^{S_n \rightarrow S_0}$ (nm)	$\lambda_{\max}^{S_n \rightarrow S_0}$ (nm) (77K)	ϕ_F	ϕ_F (77K)	ϕ_{Ph}	τ_F (ns)	τ_{Ph} (s)	k_F^c (ns ⁻¹)	k_{NR}^d (ns ⁻¹)
5:0	299.4, 294, <u>341.6</u>	406.3±1.2		0.22±0.25			0.42±0.05		0.19±0.03	2.21±0.27
4:1	229.2, 291, <u>338.8</u>	411±1.4		0.25±0.07			1.67±0.05		0.16±0.04	0.44±0.02
3:2	231.2, 291.3±0.1, <u>344.4</u>	412.7±1.7		0.39±0.08			2.52±0.02		0.16±0.03	0.24±0.03
2:3	299.6, 288.8, <u>339.4</u>	413.7±1.2		0.48±0.12			3.23±0.04		0.15±0.04	0.16±0.04
1:4	299.8, 290.4, <u>340</u>	414.7±0.5		0.51±0.12			3.58±0.06		0.15±0.03	0.13±0.03
0:5 pH~7.2		416		0.58±0.03			3.76		0.15	0.225
(Benzene)	340	405		0.091						
(MCH)	338	405	392	0.096	0.34	0.078	0.20	1.03	0.48	4.5
(EtOH)	341	410	392	0.32	0.26	0.018	2.30	1.33	0.14	0.30
(EtOH:HCl)	341					0.086		1.51		
(EEN)	322					0.35		1.02		

^a and ^b These lifetimes were determined using ns and ps-TCSPC with NanoLED excitation ($\lambda_{exc.} = 339$ nm) or/ and collected at 410 and 400 nm. The solutions were previously degassed and the L38 filter used. ^c $k_F = \phi_F / \tau_F$. ^d $k_{NR} = 1 - \phi_F / \tau_F$. The values in brackets are from ref. ²⁴⁵.

5.2.2. Scopoletin (7H6MetC)

The absorption spectra of Scopoletin (Figure 5.4) in dioxane:water mixtures presented only one band that is attributed to the neutral specie as 67dM4MC (previous Section) and the absorption maxima red-shifted with the increasing fraction of water (Table 5.2).

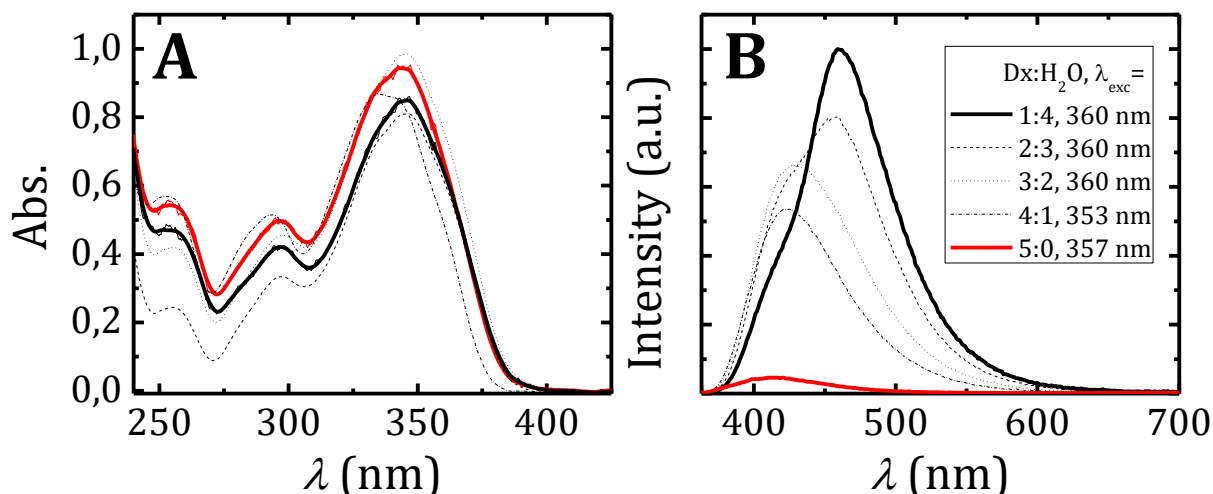


Figure 5.4. (A) Smoothed absorption and (B) fluorescence emission spectra of Scopoletin in different dioxane:H₂O mixtures. The original absorption spectra are also shown. Water at pH \approx 5.5.

The fluorescence emission spectra for the different dioxane:water fractions (Figure 5.4B) present two emission bands with maxima at 424 and 459 nm, due to the neutral and anionic species, respectively. Besides, there is a gradual increase of the anionic emission together with the diminution of the emission of the neutral specie with the increase of the water content.

The absorption spectra presents two bands as a function of the pH, one with maximum at 342 nm, that correspond to the absorption of the neutral specie, and another with maximum at 386 nm corresponding to the anionic form of Scopoletin. The presence of an isoabsorptive point at 354 nm indicates that the anionic specie is formed at the expense of the neutral form in the ground state. Beside the absorption spectra of Scopoletin in water for different pH values (Figure 5.5), allowed the determination of the fundamental state pK_a (see Section 7.2.5.2.2 in Chapter 7). The value obtained was pK_a= 7.4 (8 from ref. ²⁴⁵ and 7.8 from ref. ^{246,247}).

Coumarins

Table 5.2. Absorption maxima wavelength ($\lambda_{\max}^{S_0 \rightarrow S_n}$), fluorescence emission maxima wavelength ($\lambda_{\max}^{S_n \rightarrow S_0}$) and fluorescence quantum yield (ϕ_F) for Scopoletin in dx:H₂O mixtures.

Dx:H ₂ O/ Solvent	$\lambda_{\max}^{S_0 \rightarrow S_n}$ (nm)	$\lambda_{\max}^{S_n \rightarrow S_0}$ (nm)	$\lambda_{\max}^{S_n \rightarrow S_0}$ (nm) (77K)	$\lambda_{\max}^{T_n \rightarrow S_0}$ (nm)	ϕ_F^{Total}	$\phi_F^{N^*,Ap}$	$\phi_F^{A^*,Ap}$	$\phi_F^{N^*}$ b	$\phi_F^{A^*}$	ϕ_F (77 K)	Φ_{Ph}	τ_{Ph} (s)
5:0	253.4, 295, 336, <u>342.3±3.3</u>	416.7±7.4			0.031±0.007	NA		0.22				
4:1	252.6, 294.4, <u>342.8±2.0</u>	424.3±1.7			0.196±0.062	(0.076)	(0.044)	0.25	(0.057)			
3:2	255.2, 299.4, <u>344.8±1.1</u>	426.7±0.9			0.317±0.084	(0.15)	(0.10)	0.39	(0.14)			
2:3	255.6, 294.4, <u>345.7±1.7</u>	457.7±2.1			0.452±0.068	(0.15)	(0.27)	0.48	(0.35)			
1:4	252.2, 294.4, <u>344.7±0.9</u>	458±2.2			0.551±0.095	(0.20)	(0.45)	0.51	(0.63)			
0:5	352 ^a	460 ^a			0.60±0.07	(0.27)	(0.65)	0.58	(~1)			
(MCH)		409	401	490, <u>529</u>	0.16					0.28	0.010	1.8
(EtOH)		420	401	490, <u>530</u>	0.40					0.73	0.0033	0.16
(EtOH:HCl)		420	401	489, <u>529</u>	0.29					0.20	0.013	0.78
(EEN)		453	427	<u>522</u> , 560	0.59					0.17	0.002	1.4

^a The water used to prepare this solution was pH~6.9. ^b Taken from 67dM4MC, Table 5.1. NA - not applicable.

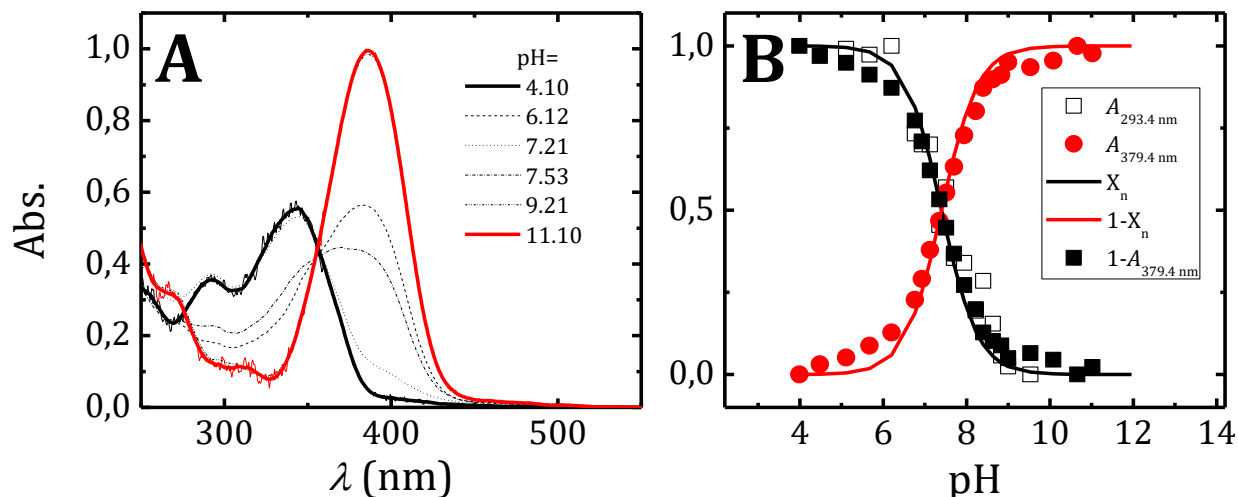


Figure 5.5. (A) Smoothed absorption spectra of Scopoletin and (B) respective titration curve. The original absorption spectra are also shown.

In the same way, using the fluorescence emission spectra (Figure 5.6), the excited state pK_a for the equilibrium between the neutral and anionic species was obtained. The estimated value was $pK_a^* = 0.95$ (1.1 in ref. ²⁴⁵ and 0.74 in ref. ²⁴⁸). Another equilibrium was discussed in ref. ¹⁷⁵, the one between the cationic and neutral specie, but the pK_a was not possible to determined, but its value was assumed to be below $pH = -0.71$ since this cationic specie was seen at this pH.

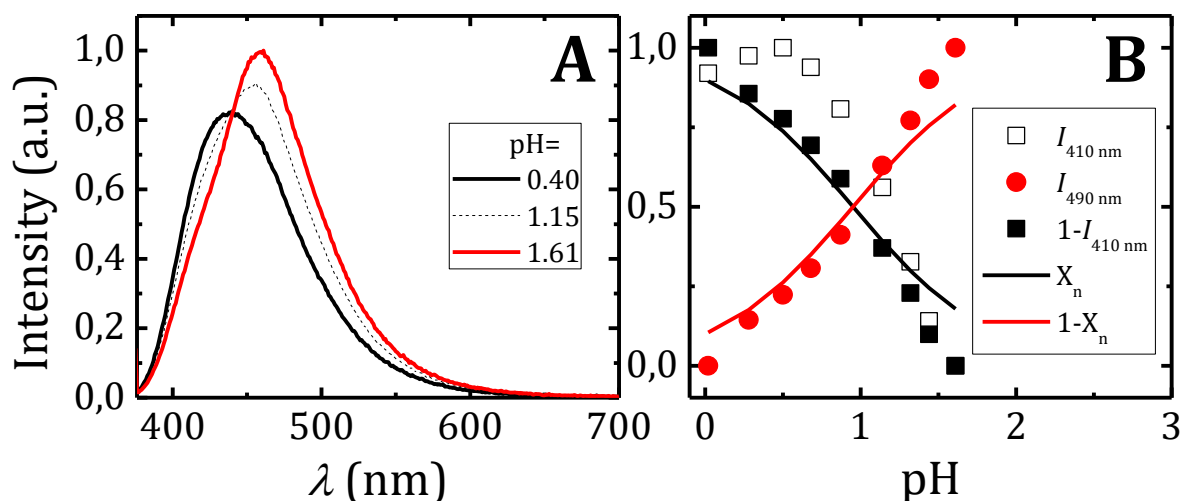


Figure 5.6. (A) Fluorescence emission spectra ($\lambda_{exc} = 373$ nm) of Scopoletin and (B) respective titration curve.

The fluorescence decays of Scopoletin in dx:H₂O collected at $\lambda_{em} = 410$ and 500 nm (and with $\lambda_{exc} = 282$ nm) were fitted properly with a sum of 2 exponential terms (Figure 5.7). However, the

fluorescence decays were also obtained at 380 nm where an additional short component varying between 0.08 and 0.18 ns was found for higher contents of dioxane. This, however, was not further explored.

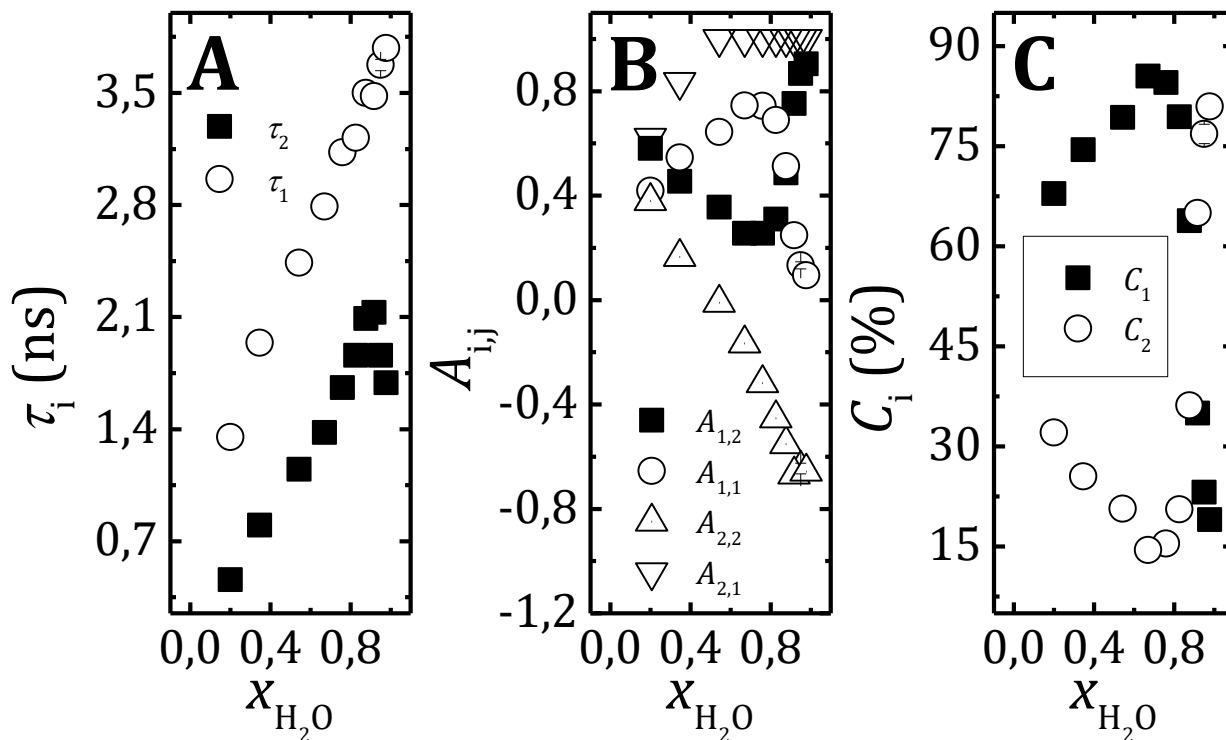


Figure 5.7. (A) Fluorescence decay times, (B) pre-exponential factors and (C) contribution of each species for Scopoletin as a function of the molar fraction of water in dx:H₂O mixtures ($\lambda_{exc}=282$ nm, $\lambda_{em1}=410$ and $\lambda_{em2}=500$ nm).

In this case the pre-exponential do not cancel due to (1) the emission of the neutral form at 500 nm (the emission wavelength used for the TR measurements), see Figure 5.6A for example and (2) the possible presence of another component with negative pre-exponential at this emission wavelength.

In this case and for dx:H₂O mixtures, it is not yet possible to determine the rate constants involved since the components needed (in the analysis of the decays) – the number of species involved – is not clear.

Coumarins

Table 5.3. Fluorescence lifetime (τ_i), pre-exponential factors ($A_{i,j}$), fluorescence and non-radiative rate constants (k_F and k_{NR} , respectively) χ^2 for Scopoletin in dx:H₂O mixtures.

Dx:H ₂ O	τ_1^* (ns)	τ_2^* (ns)	$A_{1,1}^*$	$A_{1,2}^*$	$A_{2,1}^*$	$A_{2,2}^*$	$A_{3,1}^*$	$A_{3,2}^*$	χ^2	k_F (ns ⁻¹)	k_{NR} (ns ⁻¹)
5:0		0.24±0.04		1.000						0.128±0.052	3.696±1.125
4:1	2.84±0.01	1.51±0.08	0.450 ^b (0.380)	0.550 ^b (0.614)			0.815 ^b (0.604)	0.115 ^b (0.306)			
			c	c	c	c	c	c			
3:2	4.35±0.15	2.57±0.06	0.187 (0.119)	0.813 (0.881)	(0.345)	(0.655)	0.850 (0.648)	0.150 (0.352)			
			c	c	c	c	c	c			
2:3	4.98±0.22	2.38±0.16	0.267 (0.072) ^d	0.733 (0.928) ^d	(0.821) ^d	(0.179) ^d	1.00 (1.000) ^d	-0.359 (-0.372) ^d	(1.16) ^d	(1.00) ^d	(1.13) ^d
			c	c	c	c	c	c			
1:4	5.00±0.06	2.18±0.13	0.024 (0.007)	0.976 (0.993)	(1.000)	(-0.335)	1.000 (1.000)	-0.506 (-0.554)			
0:5^a	4.61	1.59	0.016	0.984			1.000	-0.534			

* In this case, a third component was not needed probably due to the experimental limitations of the source (NanoLED). ^a the water used to prepare the mixtures was pH= 6.9. ^b with $\lambda_{exc.}$ = 339 nm and $\lambda_{em.}$ = 400 and 500 nm (13 to 21 ps/ch). ^c with $\lambda_{exc.}$ = 373 nm and $\lambda_{em.}$ = 400, 450 and 530 nm (97.1 ps/ch) ^d with $\lambda_{em.}$ = 380, 450 and 530 nm (183.0 ps/ch). The values in brackets are from ref. ²⁴⁵.

5.2.3. 4-Hydroxy-3-Nitrocoumarin (4H3NC)

In Figure 5.8 the absorption spectra of 4H3NC in different dioxane:H₂O mixtures are shown and the $\lambda_{\max}^{abs.}$ values observed for the different mixtures are indicated in Table 5.4.

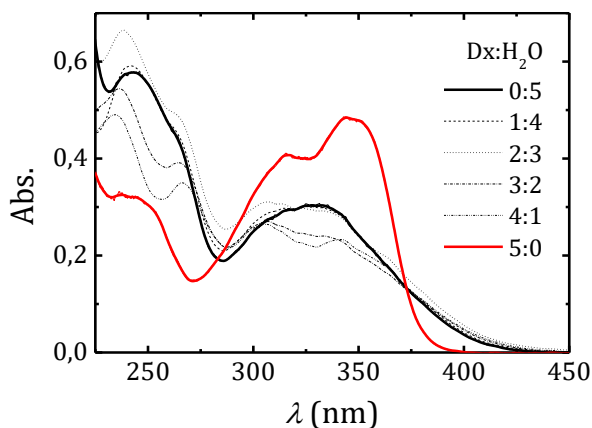


Figure 5.8. Absorption spectra of 4H3NC in different dx:H₂O mixtures. The original absorption spectra are also shown.

Table 5.4. Values of λ_{\max} of 4H3NC in different dx:H₂O mixtures.

Dx:H ₂ O	$\lambda_{\max}^{S_0 \rightarrow S_n}$ (nm)
5:0	236.2, 315.4, <u>344.0</u>
4:1	235.4, 265.6, <u>305.8</u> , 342.4
3:2	236.2, 264.4, <u>306.2</u>
2:3	237.8, 264.0, <u>305.6</u>
1:4	242.8, 264, <u>325.2</u>
0:5	245.6, 264.0, <u>331.4</u>

With this molecule no fluorescence or phosphorescence was detected. The fact that the nitro group quenched the fluorescence emission of the coumarin was expected²⁴⁹, however, phosphorescence signal was anticipated.

5.2.4. 4-methylesculetin (67dH4MC)

The absorption spectra of 67dH4MC (Figure 5.9A) in different dioxane:H₂O solutions possess only one band (due to the neutral specie) with a shift for the red region (Table 5.5) of the spectra with the increase in the water content, as observed with Scopoletin (7H6MetC).

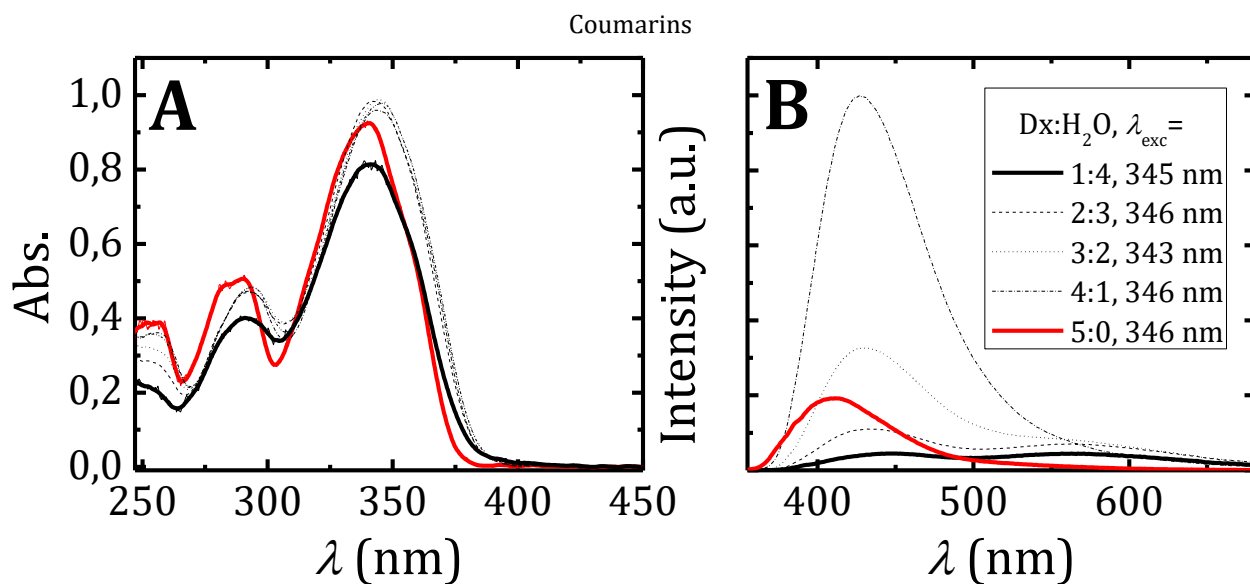


Figure 5.9. (A) Smoothed absorption and (B) fluorescence emission spectra of 67dH4MC in different dx:H₂O mixtures. The original absorption spectra are also shown.

The fluorescence emission spectra of 67dH4MC in dx:H₂O mixtures present one band that shift to the red, with the sole exception of mixtures 2:3 and 1:4 that possess a second band at longer wavelengths (with maxima ~562 nm, Figure 5.9B).

Table 5.5. Absorption maxima wavelength ($\lambda_{\max}^{S_0 \rightarrow S_n}$), fluorescence emission maxima wavelength ($\lambda_{\max}^{S_n \rightarrow S_0}$), fluorescence quantum yield (ϕ_F) for 67dH4MC in dx:H₂O mixtures.

Dx:H ₂ O	$\lambda_{\max}^{S_0 \rightarrow S_n}$ (nm)	$\lambda_{\max}^{S_n \rightarrow S_0}$ (nm)	ϕ_F^{Total}
5:0	339±0.0	412.5±2.5	0.056±0.003
4:1	345.5±0.5	427±0.0	0.265±0.005
3:2	346.5±1.5	429±1.0, 557.5±4.5	0.110±0.011
2:3	345.5±0.5	436.5±0.5, 557±5.0	0.050±0.006
1:4	345±0.0	453.5±3.5, 563±1.0	0.031±0.009
0:5	(420)	(462)	(0.0016)

The values in brackets are from ref. ²⁴⁵.

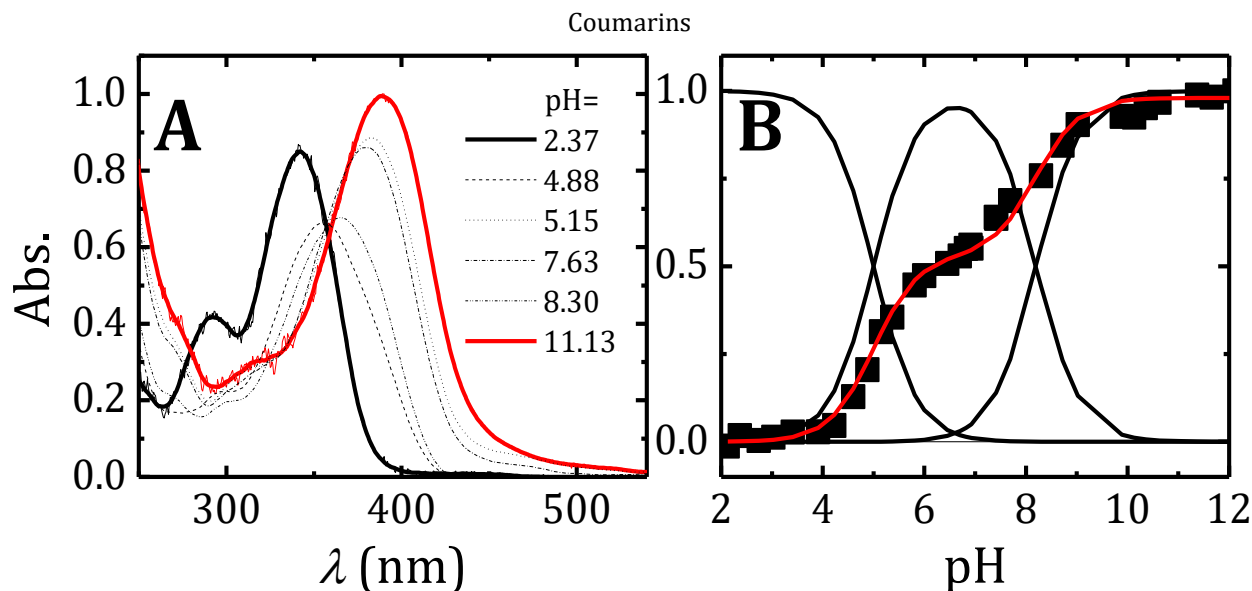


Figure 5.10. (A) Smoothed absorption spectra of 67dH4MC in water at different pH values and (B) respective titration curve for the equilibrium between N (AH), A⁻ and A²⁻. The original absorption spectra are also shown.

The absorption spectra at different pH values (Figure 5.10), reveals the existence of the absorption of three different species. The band with maximum at 340 nm correspond to the neutral form whereas the bands with maximum at 382 and 405 nm correspond to the anionic species, A⁻ and A²⁻, respectively. From the observation of these spectra, two isoabsorptive points were found, one at 359 nm and the other at 373 nm. Since in this case, there are two equilibria, i.e., between N and A⁻ and between A⁻ and A²⁻, there should be two pK_a values. Both fundamental state pK_a values were determined, in this case, a pK_{a₁} = 5 e pK_{a₂} = 8.2 were obtained (Section 7.2.5.2.2 in Chapter 7), respectively (Figure 5.10B). In ref. ¹⁷⁵ a value of 6.5 and 12.5 were obtained.

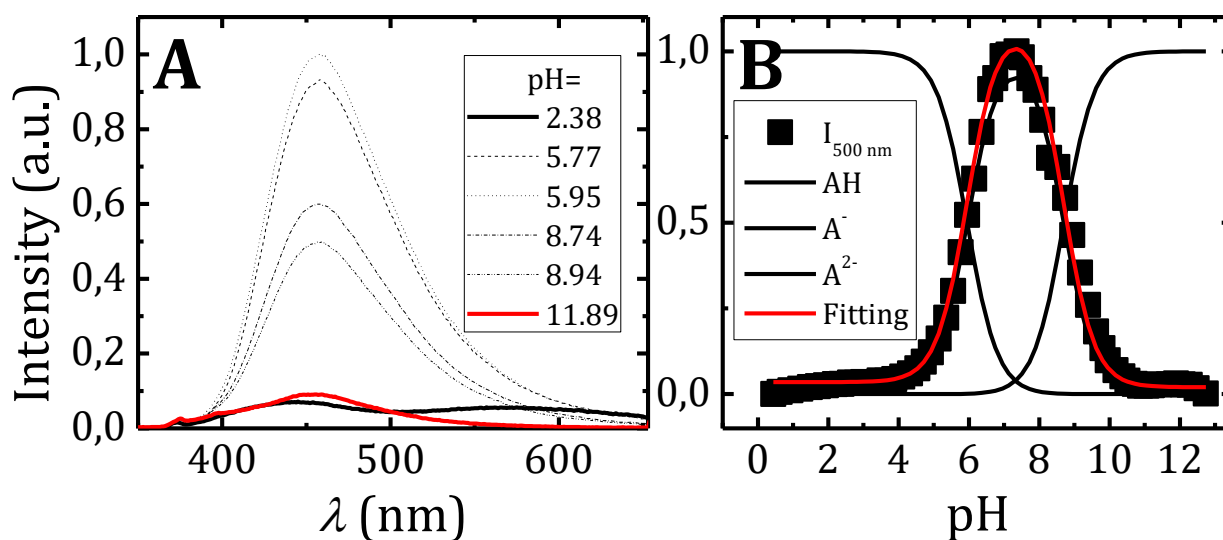
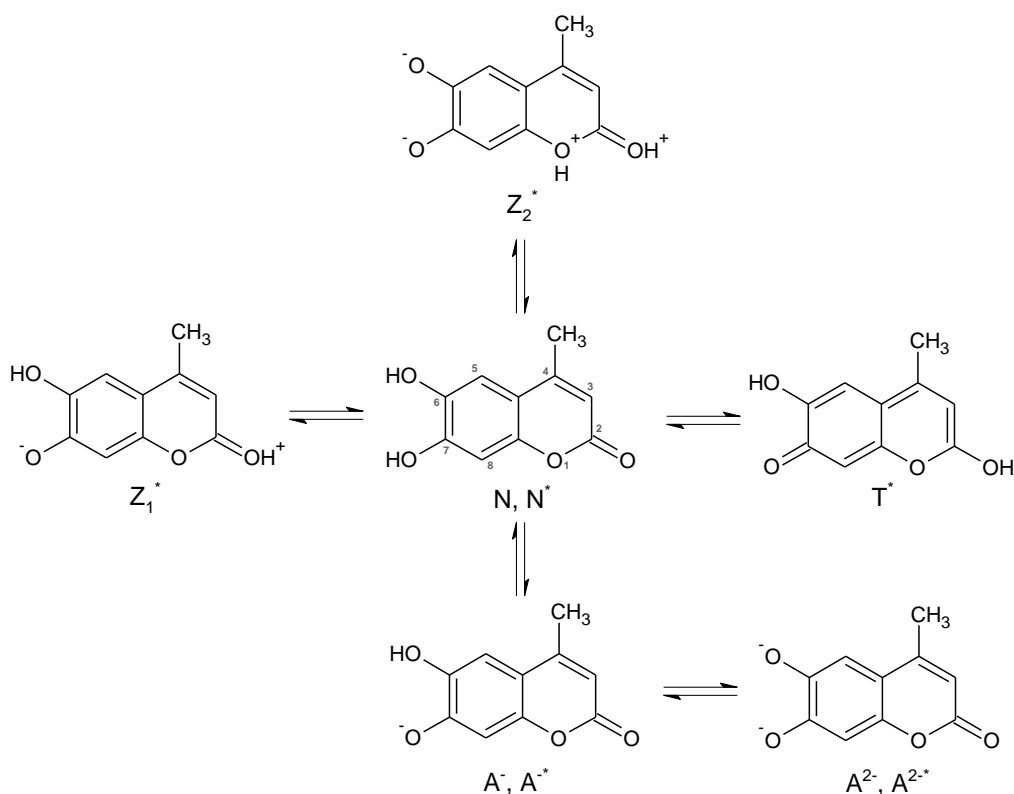


Figure 5.11. (A) Fluorescence emission spectra ($\lambda_{exc} = 330$ nm) of 67dH4MC in water at different pH values and (B) respective titration curve for the equilibrium between AH, A⁻ and A²⁻.

The fluorescence emission spectra presents a single band for $\text{pH} \geq 2.4$ however it was possible to determine the excited state $\text{p}K_{\text{a}}$ ($\text{p}K_{\text{a}}^*$) with the titration curve obtained from the fluorescence intensities at a fixed wavelength (Figure 5.11), the values found were $\text{p}K_{\text{a}1}^* = 5.95$ and $\text{p}K_{\text{a}2}^* = 8.7$. In Figure 5.11B, it is possible to see that between $\text{pH} 0$ and 4 and $\text{pH} 10$ and 12 , the intensities also changes. However, since the variation is not very pronounced, it is assumed to be a pH-dependent specie as a zwitterion or tautomer (Scheme 5.1).



Scheme 5.1. Possible existent species for 67dH4MC.

At $\text{pH} \sim 12$, the fluorescence decay of 4-methylesculetin is monoexponential with a lifetime of 2.2 ns that can be attributed to the anionic specie. However, it is relevant to note that this measurement was not made with a pulse Picker nor a NanoLED. This way, it is possible that this lifetime is longer as expected since the anionic lifetime of 3Cl7H4MC is $\sim 5 \text{ ns}$.²⁵⁰

In $\text{Dx}:\text{H}_2\text{O}$ mixtures, three species seem to exist when the decay collected at 420 nm ($\lambda_{\text{exc.}} = 282 \text{ nm}$, Figure 5.12). The longest lived decay time must be related to the anionic specie once it is just seen from 60% of dioxane and is typically the one with higher values. The neutral specie must be related to the

decay times with intermediary values but the third component was not yet identified. These decays were collected at 380 nm and 500 nm. However, for simplicity, they were not shown.

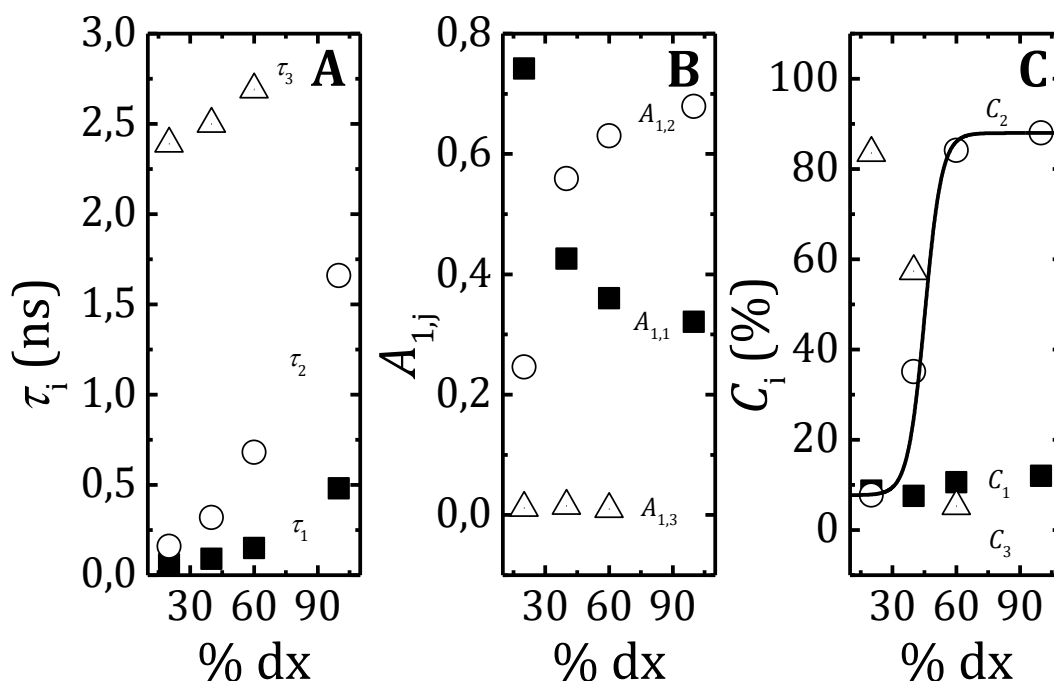


Figure 5.12. (A) Fluorescence decay times, (B) pre-exponential factors and (C) contribution of each specie for 4-methylscutellin as a function of dx percentage in dx:H₂O mixtures ($\lambda_{exc.} = 282$ nm, $\lambda_{em.} = 420$ nm).

Besides, the phosphorescence emission spectra present all the same vibrationally resolved band with only a shift of the phosphorescence emission maxima of the spectra correspondent to the neutral specie (Figure 5.13). In EEN, this band is red shifted and is identified as being the anionic specie phosphorescence emission. The vibronic resolution in EEN is not seen very well due to the low signal, however, the vibronic resolution is clearly seen in ref. ²⁴⁵²⁵¹²⁵¹²⁵¹²⁵⁰²⁴⁹²⁴⁸²⁴⁷²⁴⁶²⁴⁵²⁴⁴²⁴²²⁴²²⁴².

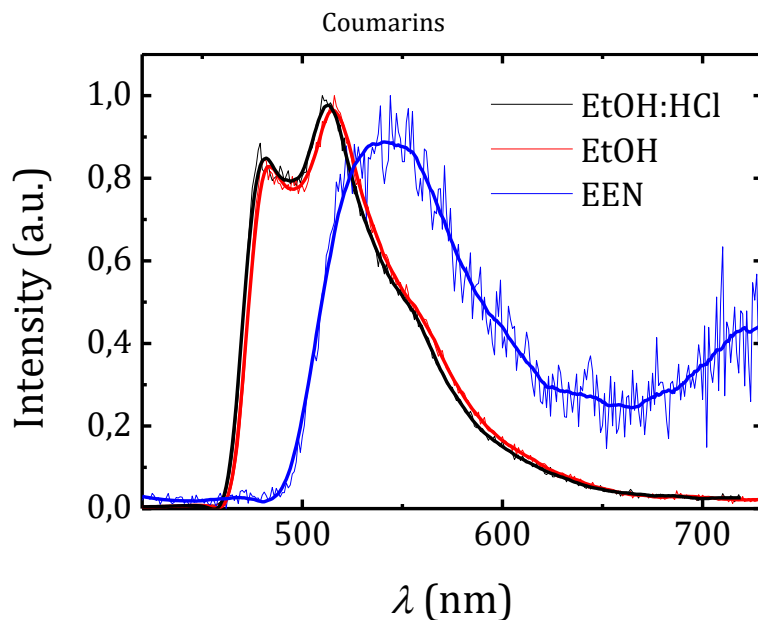


Figure 5.13. Smoothed phosphorescence emission spectra of 67dH4MC in different media. The original spectra are also shown.

The phosphorescence decay of 67dH4MC (Figure 5.14) were also acquired in the same solvents, the phosphorescence lifetime are gathered in Table 5.6.

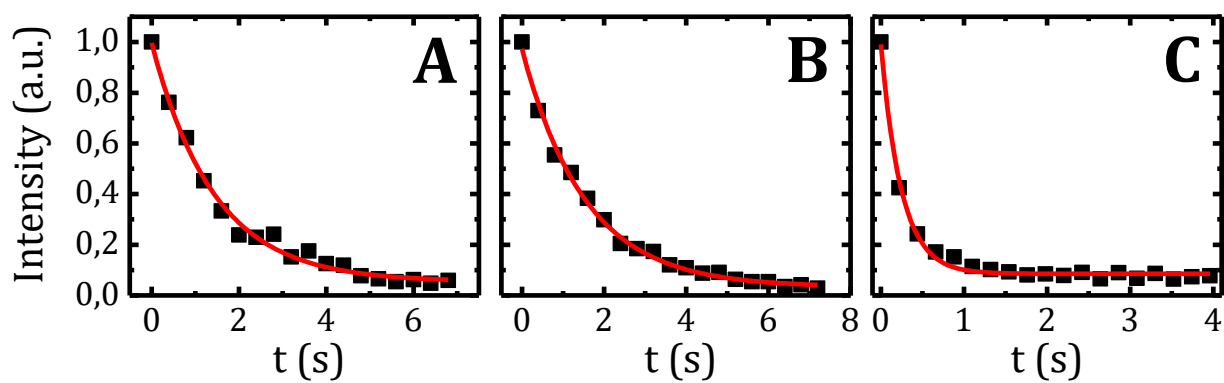


Figure 5.14. Phosphorescence decay of 67dH4MC in (A) ethanol:HCl (9:1) (B) ethanol and (C) ether:ethanol: NH_3 (EEN) (10:9:1) mixture.

The obtained phosphorescence data (Figure 5.13 and Figure 5.14) are listed in Table 5.6.

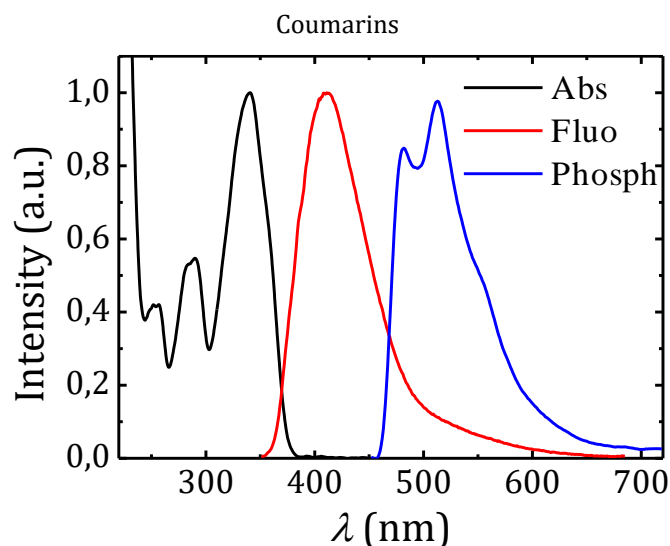


Figure 5.15. Absorption (smoothed), fluorescence and phosphorescence (smoothed) emission spectra (black, red and blue lines, respectively) of 67dH4MC in dioxane, phosphorescence made in ethanol.

Table 5.6. λ_{\max} , ϕ_F , ϕ_{Ph} , τ_{Ph} and k_{Ph} values for 67dH4MC in four different media.

Solvent	$\lambda_{\max}^{S_0 \rightarrow S_n}$ (nm)	$\lambda_{\max}^{S_n \rightarrow S_0}$ (nm)	$\lambda_{\max}^{T_n \rightarrow S_0}$ (nm)	ϕ_F	ϕ_{Ph}	τ_{Ph} (s)	k_{Ph} (s ⁻¹)
MCH	(348)	(417)	(480, 515)	(0.27)	(0.10)	(1.51)	(0.066)
Ethanol	347.5±0.5	(428)	481±0, 515.5±0.5	(0.43)	(0.0018)	1.51±0.03	0.002±0.0
Ethanol:HCl	352±4	(428)	479.5±0.5, 511.5±1.5	(0.066)	(0.13)	1.88±0.45	0.074±0.018
EEN	391±1	(460, 562)	(522, 555)	(0.13)	(0.002)	0.23±0.02	0.009±0.001

The values in brackets are from ref²⁴⁵.

5.2.5. 7-Hydroxy-4-Methyl-8-Nitrocoumarin (7H4M8NC)

The absorption and fluorescence emission spectra of 7H4M8NC in different dioxane:H₂O mixture can be seen in Figure 5.16.

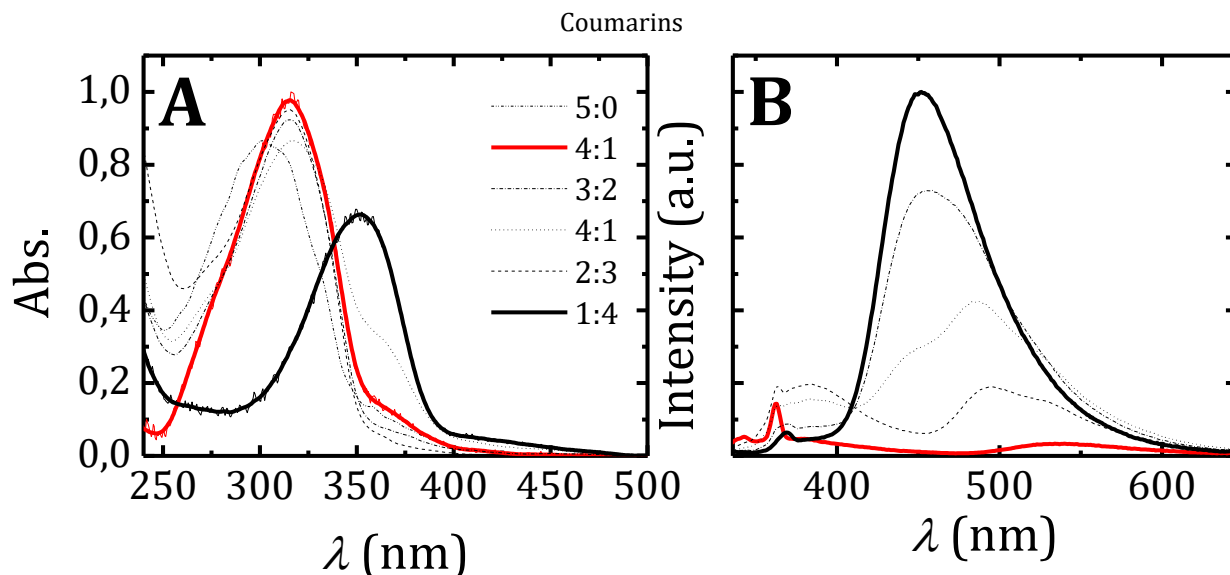


Figure 5.16. (A) Smoothed absorption and (B) fluorescence emission spectra of 7H4M8NC ($\lambda_{exc} = 328$ nm) in different dx:H₂O mixtures. The original absorption spectra are also shown.

The fluorescence decay of 7H4M8NC should be monoexponential however a second term was needed. Besides, the contribution of this longer lifetime is of 50%. One explanation is that, using these experimental conditions, a longer lifetime (~ 7 ns as seen in EtOH, see Table 5.7) could be present but incorrectly measured. This way, in order to try to compensate, a high value of pre-exponential is attributed leading to a high contribution of this second specie. This second component is possibly due to the presence of traces amounts of water.

From the photophysical study of 7H4M8NC in water at different pH values (Figure 5.17), the pK_a was determined, the obtained value was $pK_a = 4.5$.

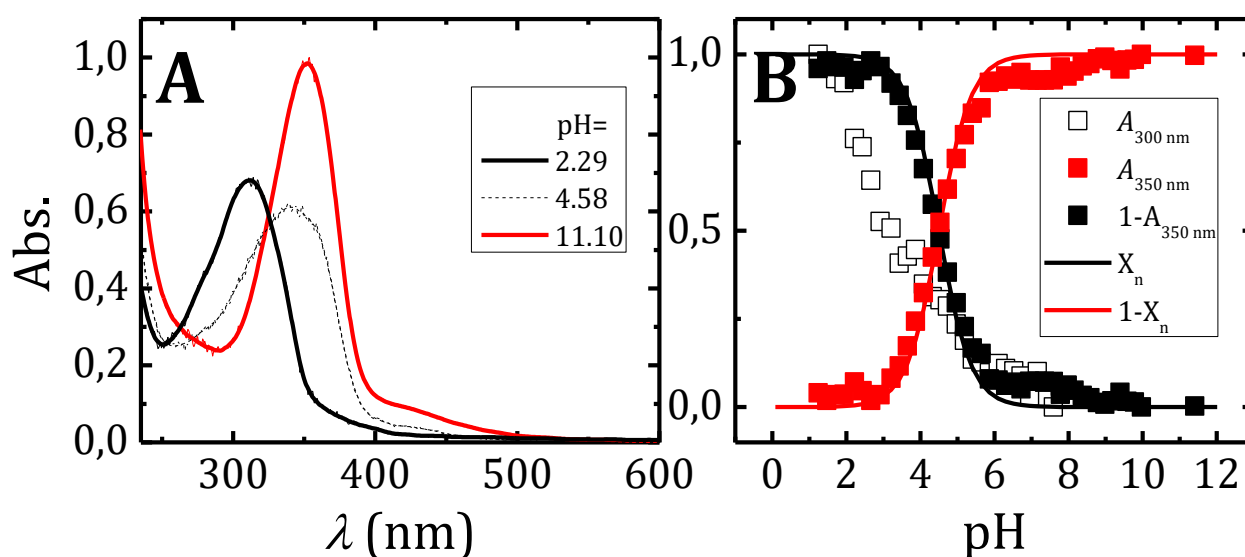
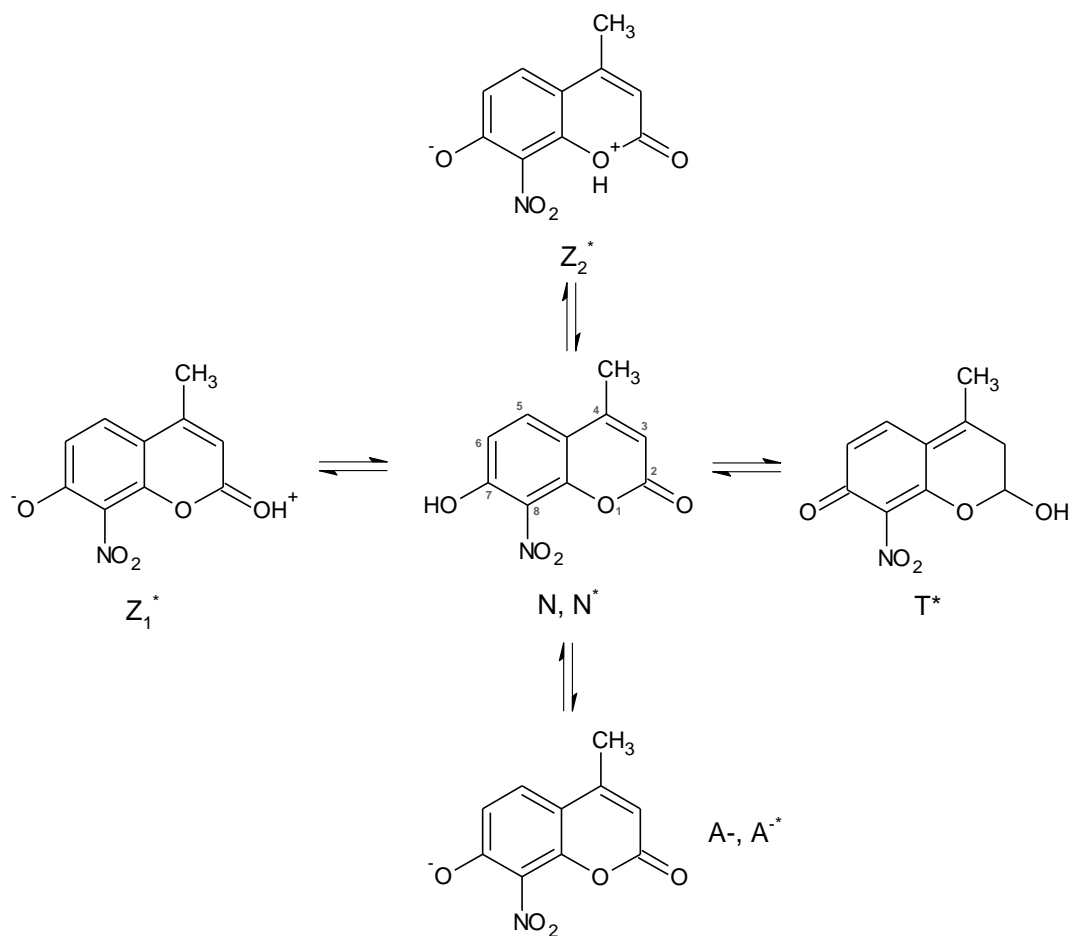


Figure 5.17. (A) Smoothed absorption spectra of 7H4M8NC in water at different pH values and (B) respective titration curve. The original spectra are also shown.

Coumarins



Scheme 5.2. Possible existent species for 7H4M8NC.

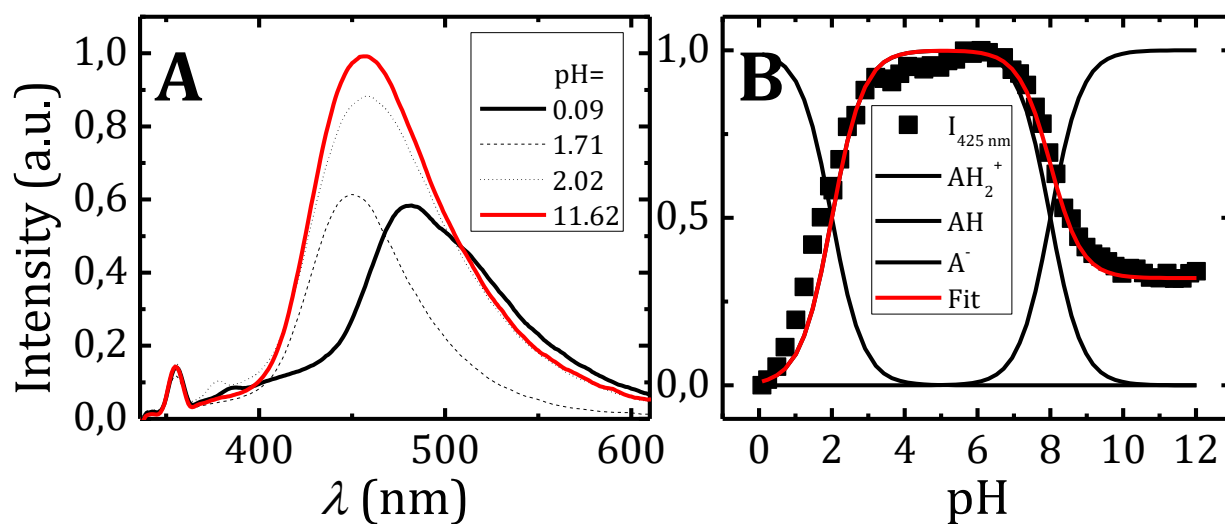


Figure 5.18. (A) Fluorescence emission spectra ($\lambda_{\text{exc}} = 317$ nm) of 7H4M8NC in water at different pH values and (B) respective titration curve.

The excited state pK_a 's were also determined by fluorescence titration curve (Figure 5.18), and the values obtained were of 2 and 8.

The phosphorescence emission spectra of 7H4M8NC in different media can be found in Figure 5.19.

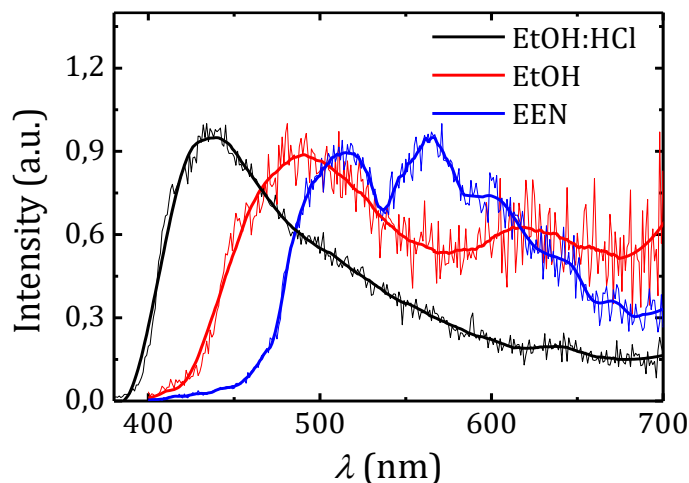


Figure 5.19. Smoothed phosphorescence emission spectra of 7H4M8NC in different media. The original spectra are also shown.

The phosphorescence decays of 7H4M8NC in basic, neutral and acidic media are shown in Figure 5.20.

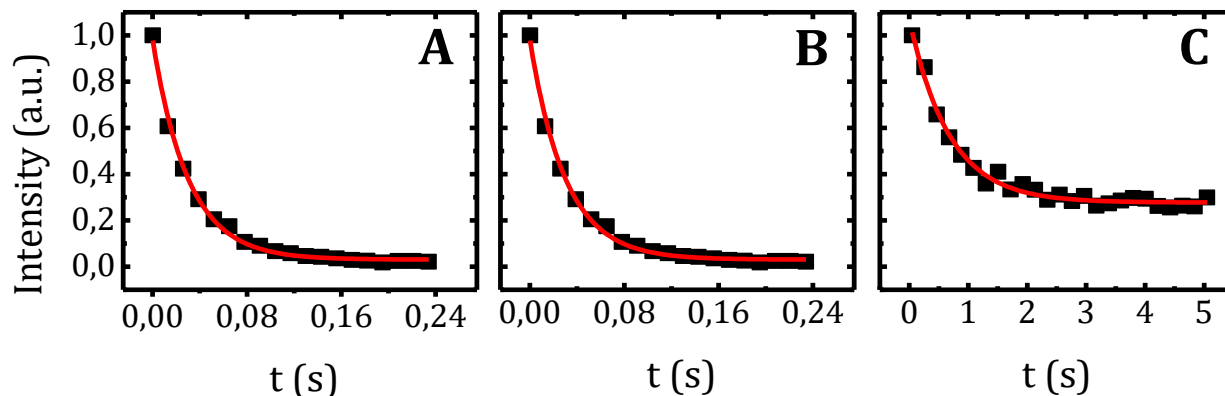


Figure 5.20. Phosphorescence decays of 7H4M8NC in (A) ethanol:HCl (9:1) (B) ethanol and (C) ether:ethanol: NH_3 (10:9:1) mixtures.

The phosphorescence results discussed earlier can be found in Table 5.7.

The fluorescence decay of 7H4M8NC in ethanol (Table 5.7) should be fitted with only one exponential, however an additional term was needed. Its lifetime is similar to the found for anionic species and can be due, this way, to the presence of small amounts of water.

Coumarins

Table 5.7. Values of λ_{\max} , of the absorption, fluorescence and phosphorescence emission spectra, fluorescence and phosphorescence lifetimes (τ_1 and τ_{Ph} , respectively), pre-exponential factors ($A_{i,j}$), chi-squared (χ^2) values of the analysis and contribution (C_i) of each species for 7H4M8NC in different dx:H₂O mixtures.

Dx:H₂O/ Solvent	$\lambda_{\max}^{S_0 \rightarrow S_n}$ (nm)	$\lambda_{\max}^{S_n \rightarrow S_0}$ (nm)	$\lambda_{\max}^{T_n \rightarrow S_0}$ (nm)	τ_1^a (ns)	τ_2^a (ns)	$A_{1,1}^a$	$A_{1,2}^a$	χ^2	C_1 (%)	C_2 (%)	τ_{Ph} (s)
5:0	301	380, <u>540</u>		0.28	2.44	0.897	0.103		50	50	
4:1	316	384, <u>495</u>									
3:2	313	383, <u>487</u>									
2:3	318	388, <u>459</u>									
1:4	<u>315</u> , 357	452									
0:5	350	ND									
EtOH	324		481	1.65	7.41	0.984	0.016		93.2	6.8	0.0007
EtOH:HCl	318		434								0.030
EEN	368		513, <u>571</u>								0.367

^a with $\lambda_{exc.} = 282$ and $\lambda_{em.} = 380$ nm.

5.3. Summary

The photophysical characterization of several hydroxycoumarins (HC) was performed in dioxane:water (dx:H₂O) mixtures and in water as a function of pH. Fluorescence quantum yield were obtained for all the dx:H₂O mixtures and the spectra deconvoluted in order to obtain the quantum yield of the different species present. With the pH titration, both ground and excited states pK_a were obtained. With all HC the excited state was found more acidic than in the ground state.

The phosphorescence emission spectra (and lifetimes) were obtained in acidic, neutral and basic media. Data was obtained from both flash photolysis and time-resolved experiments. However, in the case of the TCSPC data, further interpretation are needed in order to cover the short and long time scales.

From the preliminary results, the kinetic schemes of some coumarins were proposed.

5.4. Supplementary Information

In Table 5.8, all the original values (not averaged as in Table 5.1) are shown.

Table 5.8. Absorption maxima wavelength ($\lambda_{\max}^{S_0 \rightarrow S_n}$), fluorescence emission maxima wavelength ($\lambda_{\max}^{S_n \rightarrow S_0}$), fluorescence quantum yield (ϕ_F), fluorescence lifetime (τ_F), fluorescence and non-radiative rate constants (k_F and k_{NR} , respectively) for 67dMet4MC in dx:H₂O mixtures.

Dx:H₂O	$\lambda_{\max}^{S_n \rightarrow S_0}$ (nm)	ϕ_F	τ_F (ns)	k_F^c (ns ⁻¹)	k_{NR}^d (ns ⁻¹)
	408	0.11	0.48 ^a	0.229	1.85
5:0	406	0.069±0.007	0.41 ^b	0.168	2.27
	(405)	(0.065)	(0.37)	(0.18)	(2.5)
	413	0.26	1.66 ^a	0.157	0.45
4:1	410	0.20±0.048	1.73 ^b	0.116	0.46
	(410)	(0.34)	(1.61)	(0.21)	(0.41)
	415	0.33	2.54 ^a	0.130	0.26
3:2	411	0.36±0.058	2.50 ^b	0.144	0.26
	(412)	(0.51)	(2.51)	(0.20)	(0.20)
	415	0.41	3.27 ^a	0.125	0.18
2:3	412	0.41±0.067	3.17 ^b	0.129	0.19
	(414)	(0.67)	(3.24)	(0.21)	(0.10)
1:4	415	0.51	3.65 ^a	0.140	0.13

Coumarins

Dx:H ₂ O	$\lambda_{\max}^{S_n \rightarrow S_0}$ (nm)	ϕ_F	τ_F (ns)	k_F^c (ns ⁻¹)	k_{NR}^d (ns ⁻¹)
	414	0.42±0.074	3.59 ^b	0.117	0.16
	(415)	(0.69)	(3.50)	(0.20)	(0.089)
0:5	(419)	(0.69)	(3.84)	(0.18)	(0.081)
0:5 pH~7.2	416	0.58±0.033	3.76 ^b	0.154	0.225

The values in brackets are from ref. ²⁴⁵, a and b These lifetimes were determined using ns and ps-TCSPC with NanoLED excitation ($\lambda_{exc.} = 339$ nm) or/ and collected at 410 and 400 nm, respectively. The solutions were previously degassed and the L38 filter used. ^c $k_F = \phi_F / \tau_F$. ^d $k_F = 1 - \phi_F / \tau_F$.

The lifetimes of 67dM4MC are represented as a function of the water mole fraction (for dx:H₂O mixtures) and show to be fit with a Boltzmann-like equation, Figure 5.21.

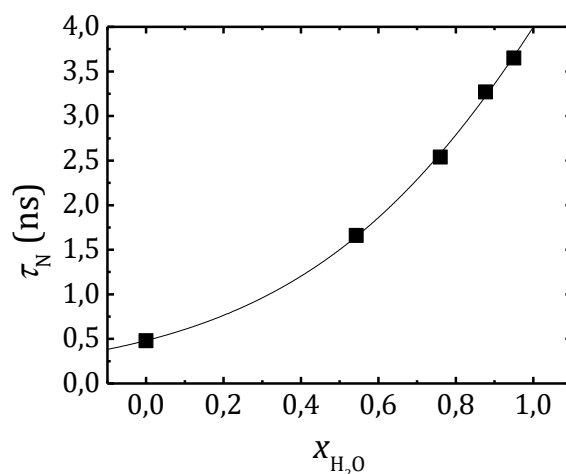


Figure 5.21. Lifetimes of 67dM4MC as a function of the molar fraction of water for dioxane:water mixtures. The data was fitted with a Boltzmann curve with the respective equation:

$$y = 11.761 - 11.736 / [1 + \exp([x - 1.264] / 0.394)]$$

All the original values for Scopoletin, 4-methylesculetin are shown in Table 5.9 and Table 5.10, respectively.

Coumarins

Table 5.9. Absorption maxima wavelength ($\lambda_{\max}^{S_0 \rightarrow S_n}$), fluorescence emission maxima wavelength ($\lambda_{\max}^{S_n \rightarrow S_0}$), fluorescence quantum yield (ϕ_F), fluorescence lifetime (τ) and fluorescence and non-radiative rate constants (k_F and k_{NR} , respectively) for Scopoletin in dx:H₂O mixtures.

Dx:H ₂ O	$\lambda_{\max}^{S_0 \rightarrow S_n}$ (nm)	$\lambda_{\max}^{S_n \rightarrow S_0}$ (nm)	ϕ_F^{Total}	$\phi_F^{N^*,Ap}$	$\phi_F^{A^*,Ap}$	$\phi_F^{A^*}$	τ_1 (ns)	τ_2 (ns)	k_F (ns ⁻¹)	k_{NR} (ns ⁻¹)
	253.4, 295, 336, <u>342.3±3.3</u>	416	0.035							
5:0	340	408	0.021	NA			-	0.28 ^b	0.075	2.571
	(340)	(426)	(0.036)	(0.025)	(0.011)	(0.018)	-	(0.20)	(0.180)	(4.820)
	252.6, 294.4, <u>344.4</u>	425	0.285							
4:1	344 ^a	422 ^a	0.19±0.03 ^a				2.83 ^{a,b}	1.43 ^{a,b}		
	(340)	(426)	(0.12)	(0.076)	(0.044)	(0.057)	(2.85)	(1.59)		
	255.2, 299.4, <u>346.4</u>	428	0.439				4.14 ^c	2.56 ^c		
3:2	344 ^a	426 ^a	0.29±0.06 ^a				4.45 ^{a,b}	2.50 ^{a,b}		
	(344)	(426)	(0.25)	(0.15)	(0.10)	(0.140)	(4.45)	(2.64)		
	255.6, 294.4, <u>348</u>	458	0.567				5.14 ^c	2.55 ^c		
2:3	345 ^a	455 ^a	0.41±0.02 ^a				4.67 ^{a,b}	2.17 ^{a,b}		
	(344)	(460)	(0.42)	(0.15)	(0.27)	(0.350)	(5.14) ^d	(2.42) ^d		
	252.2, 294.4, <u>346</u>	459	0.633				4.99 ^c	2.34 ^c		
1:4	344 ^a	455 ^a	0.46±0.04 ^a				5.08 ^{a,b}	2.02 ^{a,b}		
	(344)	(460)	(0.65)	(0.20)	(0.45)	(0.630)	(4.93)	(2.18)		
0:5 pH≈ 5.5	<u>343</u>						4.32 ^c	1.19 ^c		
0:5^a	352	460	0.60±0.07				4.61 ^b	1.59 ^b		
0:5	(340)	(460)	(0.92)	(0.27)	(0.65)	(~1)	(4.36)	(1.74)		

^a the water used to prepare the mixtures was pH= 6.9. ^b with λ_{exc} = 339 nm and λ_{em} = 400 and 500 nm (13 to 21 ps/ch). ^c with λ_{exc} = 373 nm and λ_{em} = 400, 450 and 530 nm (97.1 ps/ch) ^d with λ_{em} = 380, 450 and 530 nm (183.0 ps/ch). The values in brackets are from ref. ²⁴⁵. NA - not applicable.

Coumarins

Table 5.10. Absorption maxima wavelength ($\lambda_{\max}^{S_0 \rightarrow S_n}$), fluorescence and phosphorescence emission maxima wavelength ($\lambda_{\max}^{S_n \rightarrow S_0}$ and $\lambda_{\max}^{T_n \rightarrow S_0}$, respectively), fluorescence quantum yield (ϕ_F), phosphorescence lifetime and rate constant (τ_{Ph} and k_{Ph} , respectively) for 67dH4MC in dx:H₂O mixtures.

Dx:H ₂ O/ Solvent	$\lambda_{\max}^{S_0 \rightarrow S_n}$ (nm)	$\lambda_{\max}^{S_n \rightarrow S_0}$ (nm)	$\lambda_{\max}^{T_n \rightarrow S_0}$ (nm)	ϕ_F^{Total}	ϕ_F^N	ϕ_F^A	τ_{Ph} (s)	k_{Ph} (s ⁻¹)
5:0	339 (339)	415 (410)		0.058 (0.053)	0.058 (0.053)	*		
4:1	346 (345)	427 (427)		0.260 (0.27)	(0.16)	(0.12)		
3:2	348 (345)	428, 553 (430, 562)		0.099 (0.12)	(0.068)	(0.050)		
2:3	346 (345)	436, 552 (437, 562)		0.044 (0.056)	(0.027)	(0.029)		
1:4	345 (345)	450, 564 (457, 562)		0.022 (0.040)	(0.010)	(0.030)		
0:5	(420)	(462)		(0.0016)	(**)	(0.0016)		
pH= 3.0		(462)						
pH= 4.1		(471)						
pH= 5.5		(460)						
pH= 6.5		(468)						
7.5 ≤ pH ≤ 10.0		(461)						
11.2 ≤ pH ≤ 13.2		(460)						
Ethanol	347 (348)		481, <u>516</u> (481, <u>515</u>)				1.54 (1.48)	0.0012 ^a (0.0012)
Ethanol:HCl	356 (348)		479, <u>510</u> (480, <u>513</u>)				1.43 (2.32)	0.091 ^a (0.056)
EEN	392 (390)		544 (522, <u>555</u>)				0.246 (0.205)	0.008 ^a (0.0098)

*only neutral specie is emitting. **only anionic form is emitting. The values in brackets are from ref. ²⁴⁵.^a Using ϕ_{Ph} of ref. ²⁴⁵.

Chapter 6

Concluding Remarks

The photophysical characteristics of pyrene were used to investigate the properties of poly(acrylic acid) and poly(*N*-isopropyl)acrylamide polymers covalently labelled with this probe. The influence of the polymer backbone size, degree of labelling, position of the probe, nature of the solvent, pH, temperature, and interactions with others amphiphiles, on the observed pyrene photophysics namely on conformation changes and dynamics of the polymer chains were investigated. Steady state and time-resolved techniques were used and the different behaviours displayed by the pyrene chromophore lead to the observation of different behaviours giving rise to different kinetic schemes. From the Birks' kinetic scheme (found for oligomers) to the more complex kinetic scheme with 3-4 species, all these were solved and the obtained rate constants used to discuss and rationalize the polymer behaviour. The simplest behaviour was found for 1Py(10)1Py and some dipyrenylacetamides in pure organic solvents and of dioxane:water mixtures, which were shown to obey to a Birks' kinetic scheme. When pyrene was covalently and randomly linked to the polymer chains (PAAMePy and PNIPAMPy) a more complex behaviour was found, with the presence of both static and dynamic mechanisms for excimer formation, as well as the coexistence of free monomers. Besides, the knowledge acquired in dynamic modelling, when applied to the several pyrene oligomers, may give insightful information, especially that in this case, the full structure can be used, in contrary to the polymers investigated in Section 3.2.2.3.2.3.

The proton transfer and tautomerization reactions in hydroxycoumarins were investigated in water and organic solvents.

It is anticipated that future works in the picosecond range and with an appropriate source may provide additional (relevant) information on the coumarins when done as a function of pH. These experiments might be elucidative later to the assignment of all the decay times in dx:H₂O mixtures. It would be important to excite all the samples at a isosbestic point and also in a way that allows avoiding Raman peaks for the dx:H₂O mixtures.

Concluding Remarks

Future work in the PAAMePy polymers would consist in completing the TR data of the remaining polymers, whereas for PNIPAMPy it would be interesting to obtain, with a new (better) synthesis, these polymers with similar probing degree and size but with low polydispersity in order to compare to the data here presented. Still for the polymers, it would be interesting to compare different oligomers/polymers with the pyrene units labelled in the end and along (in known positions) the polymeric chain.

Chapter 7

Methods and Sample Preparation

7.1. Compounds

7.1.1. Oligomers

The 1Py(3)1Py and 1Py(10)1Py oligomers were purchased from Invitrogen - Molecular Probes and used as received. 1-methylpyrene (acquired from Fluka) and 1-pyrenylmethacrylate (1PyMMA, acquired from Aldrich) was also used as received for its use as parent compound the dipyrenylalkanes (Section 2.2.1) and for the PNIPAMPy polymers (Section 3.3), respectively. The pyrene acetamide based oligomers were a kind gift of prof. António Maçanita and Klass Zachariasse.

7.1.2. Coumarins

All coumarins were purchased from Lancaster and used as received with the sole exception of 7-hydroxy-4-methyl-8-nitrocoumarin that was, when needed, three times recrystallized in dry ethanol.

7.1.3. PAAMePy Polymers

7.1.3.1. Reagents

The polymers poly(acrylic acid) (PAA) with nominal $M_n = 2000 \text{ g.mol}^{-1}$ and $450\,000 \text{ g.mol}^{-1}$ (Aldrich), 1-methylpyrrolidone (1MP, Riedel de Haën), 1,3-dicyclohexylcarbodiimide (1,3DCC, Aldrich), 1-pyrenylmethylamine hydrochloride (1PyCH₂NH·HCl, Aldrich), 1-pyrenylmethylamine (1PyCH₂NH₂, Aldrich), boric acid (H₃BO₃, Panreac), 1,4-dioxane (Dx, Panreac), dichloromethane (CH₂Cl₂, Aldrich), and dimethylformamide (DMF, Aldrich), sodium hydroxide pellets (NaOH, Aldrich), were obtained from commercial sources and used as received. Triethylamine (TEA, Aldrich) was freshly distilled under reduced pressure.

1-Pyrenylmethylamine hydrochloride was neutralized by treatment with 1 M K_2CO_3 , followed by addition of CH_2Cl_2 . After 2h, the organic layer was extracted and dried over anhydrous Na_2SO_4 . The solvent was removed in a rotary evaporator, giving a yellow solid.

A 25% aqueous solution of PAA with nominal molecular weight of 150 000 g/mol (Wako Chemicals, Japan). Before labelling with 1-pyrenylmethylamine, the solution of PAA 150 kg/mol was freeze dried to give solid PAA, which was used in the postmodification step. The polymers were kindly provided by Dr. Dan Anghel.

Spectrum Medical Industries supplied the dialysis membranes with a molecular weight cut-off of 12 000-14 000 g/mol.

Dowex 50W-X8, Na-form, 20–50 mesh cation exchange resin (Fluka) was treated with a solution of 2M HCl overnight to obtain the H-form. After the treatment, the resin was washed several times with distilled deionized water.

7.1.3.2. Synthesis

PAAMePy(2)52, PAAMePy(2)77, PAAMePy(450)53 and PAAMePy(450)87. A mixture of PAA (1.0 g) with $M_n = 2$ or 450 kg.mol⁻¹ and 1-methylpyrrolidone (1MP) was heated for 2h at more than 60 °C and subjected to agitation in an inert atmosphere. A solution of 1-pyrenylmethylamine (1PyCH₂NH₂) in 1-methylpyrrolidone (1MP) was added rapidly, followed by addition of triethylamine (TEA, see amounts in Table 7.1) and freshly distilled solution of 1,3-dicyclohexylcarbodiimide (1,3DCC, see amounts in Table 7.1) in 1MP. Reaction of this mixture was protected from light with aluminum foil and refluxed at 60 °C for 24h under inert atmosphere. After cooling, the solution was neutralized with a concentrated aqueous solution of sodium hydroxide until the modified polymer has precipitated all in the form of a yellow solid. The solid was filtered by suction and washed three times with 1MP (20 mL, previously heated to 60 °C) and three times with methanol (MeOH, 20 mL). The solid was then dissolved in 4 mL deionized water and added to 40 mL of MeOH. After storage in the refrigerator overnight the precipitated result was decanted and dried under reduced pressure. The remaining mixture was allowed to precipitate and the latter procedure repeated once more. An aqueous solution of the purified polymer was passed through the cation exchange column to convert it into its acid form. The solution was then lyophilized and the water removed by sublimation.⁶⁵

All washes and precipitation of the PAAMePy(450)53 polymer were made in ethanol. As to PAAMePy(450)87, after washing with 1MP and MeOH, the solid was dissolved in hot water due to its high viscosity. Two precipitations were made, the last in ethanol.⁶⁵

PAAMePy(2)12, PAAMePy(2)18, PAAMePy(2)24, PAAMePy(2)41, PAAMePy(2)132, PAAMePy(2)133, PAAMePy(450)10, PAAMePy(450)11, PAAMePy(450)77 and PAAMePy(450)517. PAA with $M_n = 2$ or $450 \text{ kg}\cdot\text{mol}^{-1}$ was dissolved in distilled water in a round bottom flask and 1,4-dioxane was added with stirring. Boric acid (see amounts in Table 7.1) and 1-pyrenylmethylamine (see amounts in Table 7.1) were added and the reaction was carried out under reflux for some time (see time in Table 7.1). In the case of the PAAMePy(450)11 polymer, the resulting yellow solution was concentrated under reduced pressure and the product precipitated with dichloromethane. After removal of the solvent by decantation, the product was precipitated twice with dimethylformamide/dichloromethane to give a dark yellow solid which was dried in vacuum at 90°C for 2h. Finally, the solid was ground into a powder, and washed several times with dichloromethane.⁶⁴

PAAMePy(450)11. IR (cm^{-1}): 3484 br, 3429 br, 3233 sh, 2951 sh, 2858 sh, 2281 sh, 2036 w, 1950 w, 1706 m, 1637 m, 1619 sh, 1540 m, 1452 m, 1419 w, 1385 sh, 1255 sh, 1232 sh, 1192 m, 1115 m, 1079 w, 1045 sh, 949 sh, 889 w, 867 w, 847 m, 799 m, 767 sh, 615 m, 546 w, 485 w.

^1H NMR (300 MHz, rt, DMSO- d_6 , TMS): $\delta = 8.49\text{-}8.11$ (series of overlapping multiplet signals, Py), 4.83 (s, $\text{CH}_2\text{-Py}$), 3.5 (vbr, NH), 2.24 (br, CH-chain), 1.75 (br, CH_2 chain), 1.44 (br, CH_2 chain).

^{13}C CP/MAS NMR: δ) 177 (COOH and NHCO), 123 (Py-C), 40 (CH and CH_2).⁶⁴

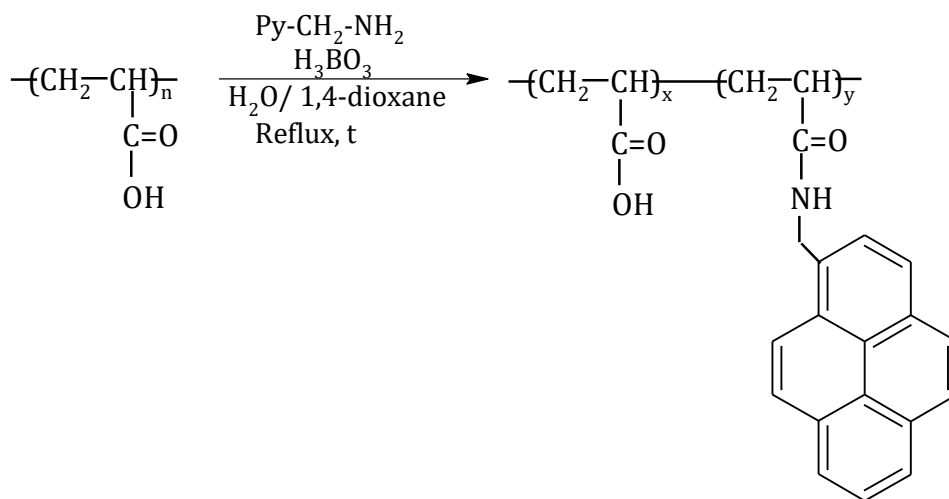


Figure 7.1. Preparation of PAAMePy(2)12, PAAMePy(2)18, PAAMePy(2)24, PAAMePy(2)41, PAAMePy(2)132, PAAMePy(2)133, PAAMePy(450)10, PAAMePy(450)11, PAAMePy(450)77 and PAAMePy(450)517 polymers.

Methods and Sample Preparation

Table 7.1. Synthetic conditions of the different PAA polymers with different pyrene loadings (PAAMePy).

Polymer Ref.	Polymer	PAA (g)	H ₂ O (mL)	Dx (mL)	H ₃ BO ₃ (g, mmol)	1PyCH ₃ NH ₂ (g, mmol)	1MP (mL)	Reflux time (h)	1PyCH ₃ NH ₂ HCl (g, mmol)	TEA (μL, mmol)	1,3DCC (g, mmol)	η (g)
SNG91	PAAMePy(2)12	1.0	5	75	0.100	0.600		~144				
SNG89	PAAMePy(2)18	1.0	5	70	0.068	0.240		~70				
SNG77c	PAAMePy(2)24	1.0	15	40	0.028	0.120	NA	20 (115°C)		NA		
SNG90	PAAMePy(2)41	1.0	5	70	0.015	0.087, 0.380		70 (~115°C)				
	PAAMePy(2)52	1.0			NA				0.287, 1.25	195, 1.41	0.284, 1.77	
	PAAMePy(2)77	1.0		NA		0.096, 0.417 ^a	50	24	NA	65, 47	0.095, 0.459 ^a	
SNG98	PAAMePy(2)132	1.0			0.068	0.240						
SNG92	PAAMePy(2)133	1.0	5	75	0.010	0.040		~48				
SNG101	PAAMePy(450)10	1.0	10	75	0.115	0.354		~24		NA		
SNG96	PAAMePy(450)11	1.0	10	75	0.109, 1.76	0.350, 1.52		15				1.1
	PAAMePy(450)53											
SNG95	PAAMePy(450)77	1.0	10	79	0.016	0.040, 0.170		19		NA		0.6
	PAAMePy(450)87											
SNG97	PAAMePy(450)517	1.0	10	75	0.010, 0.16	0.010, 0.043		19 (115°C)		NA		

^a dissolved in 5 mL of 1-methylpyrrolidone. The value in brackets is the temperature of the bath used.

7.1.3.3. Physical Measurements

The diffusion NMR done for PAAMePy(2)12 was performed with a Bruker Avance III 400 MHz, equipped with a double resonance 5 mm broadband BBFO probe with Z-axis pulse field gradients.

The acquisition parameters used on DOSY experiments were:

Pulse sequence "ledbpg2s" for diffusion measurements using stimulation echo and LED using bipolar gradients pulses,²⁵² a spectral width of 12 ppm, an offset of 4.636 ppm, acquisition time of 1.6 s and diffusion time (big DELTA) of 50 ms. The gradient pulse (little DELTA) was of 4.4 ms and 64 scans per increment. The gradient calibration constant was 5.3500094 G/mm.

The DOSY experiment was run with a linear gradient ramp from 2% to 95%, with 32 increments.

The processing parameters used were:

The data was processed and analysed with Mnova software and using "Bayesian DOSY Transform" method with a resolution factor of 2, 3 repetitions and 128 points in diffusion dimension, to determine the diffusion coefficient constant.

Solution ¹H spectra of PAAMePy(450)11 and PAAMePy(450)517 polymers were acquired using a Bruker CXP 300 spectrometer. ¹³C{¹H} CP/MAS NMR spectra were recorded at 125.72 MHz on a (11.7 T) Bruker Avance 500 spectrometer, with an optimized $\pi/2$ pulse for ¹H of 3.5 μ s, 2 ms contact time, spinning rates of 7-9 kHz, and 4 s recycle delays. Chemical shifts are quoted in parts per million from tetramethylsilane. IR spectra were obtained as KBr pellets using a FTIR Mattson-7000 infrared spectrophotometer.⁶⁴

7.1.3.4. Monte Carlo

This simulation was made considering that the number of particles, volume and temperature remain constant (canonical ensemble or *NVT*). The molecule was described through the coarse-grain model which consists of describing groups of atoms by rigid spheres. In this case, each monomer without pyrene was described as being the particle of type 1 (red in Figure 3.45- snapshot) and each monomer with pyrene as a particle of type 2 (blue in Figure 3.45). To carry out these simulations, it is considered that the molecule moved in a solvent with a constant dielectric permittivity $\epsilon_r = 78.4$, the one from water at the temperature used for both experiment and simulation, $T = 298$ K. To simulate the increase in pH, carried the added polymer and also opposite charge ions in order to keep the system neutral.²⁵³

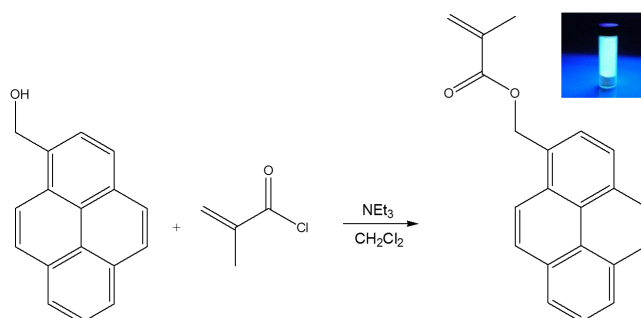
All the Monte Carlo (MC) simulations were performed employing the standard Metropolis algorithm. Three different types of MC trial moves were employed for the polyions (PIs): (i) single segment move, (ii) translation of the entire chain, and (iii) slithering move (see Section 3.2.2.3.1.4 in Chapter 3). The

single-particle trial move was attempted 10 times more often than the other two types of trial moves. The counterions were subjected to translational trial moves only. Each simulation included an equilibration of at least 2×10^5 trial moves per particle followed by a production run of at least 6×10^5 trial moves per particle. Statistical uncertainties were evaluated by dividing the total simulation into subbatches. All the simulations were performed using the simulation package MOLSIM.²⁵³

7.1.4. PNIPAMPy Polymers

7.1.4.1. Preparation of a Polymerizable Pyrene Derivative (1-pyrenylmethyl methacrylate)

To 1-pyrenemethanol (0.501 g, 2.157 mmol) was added dry dichloromethane (17 ml), triethylamine (Et_3N) (0.243 g, 2.372 mmol) and methacryloic chloride (0.251 g, 2.372 mmol) was then slowly added at 0 °C (in an ice bath) under nitrogen. After the mixture was stirred for additional 14h at room temperature, it was poured into the water. The reaction mixture was washed with aqueous sodium bicarbonate (NaHCO_3), water and dried over anhydrous sodium sulphate (Na_2SO_4), followed by evaporation to dryness.²⁵⁴



Scheme 7.1. Synthetic route to prepare 1-pyrenylmethyl methacrylate.

The residue was purified by silica column flash chromatography ($\text{CHCl}_3/\text{hexane} = 1:1$ (v/v)) with the help of a UV lamp (Figure 7.2) to obtain 1-pyrenylmethyl methacrylate as a white yellowish solid (0.238 g, 37 %).



Figure 7.2. Photograph of the purification of 1-pyrenylmethyl methacrylate by silica column flash chromatography.

^1H NMR: (400 MHz, CDCl_3 , TMS standard, 25 °C): δ (ppm) 8.33-8.01 (m, 9H, Pyrene H), 6.15 (s, 1H, alkenyl H), 5.92 (s, 2H, -Ar- CH_2 -), 5.57 (s, 1H, alkenyl H), 1.97 (s, 3H, -alkene- CH_3).

From the ^1H -NMR spectra the modified polymer was found to have, on average, 0.5 mol % of pyrene content. The Py content of 0.5 mol % is lower than the maximum theoretical value of about 1 mol % (based on the quantities of reagents used), see Section 3.3.3 in Chapter 3.

7.1.4.2. Preparation of Polymers with Different Pyrene Loadings

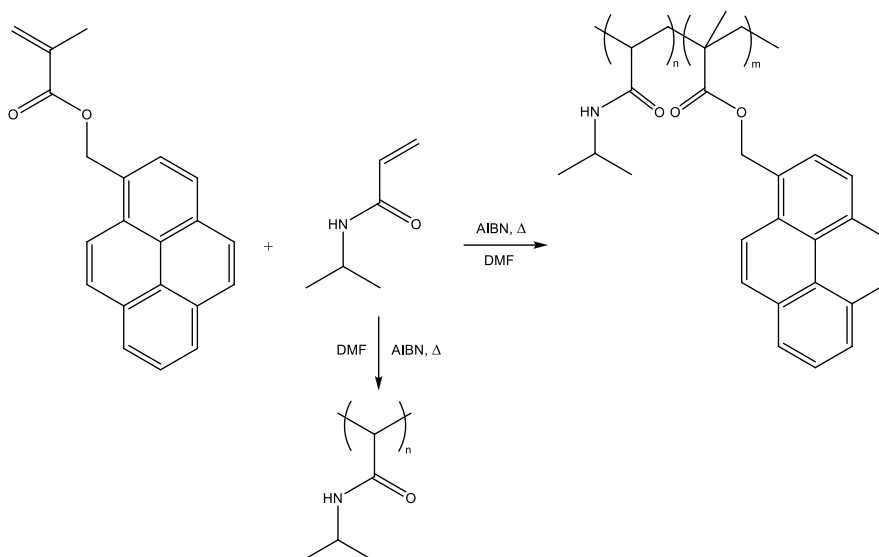
To *N*-isopropylacrylamide (NIPAM), azobisisobutyronitrile (AIBN) and 1-pyrenylmethyl methacrylate (1PyMMA) was added dry dimehtylformamide (DMF) under nitrogen. After the mixture was stirred for additional t hours with Δ temperature (see

Table 7.2), a DMF solution of hydroquinone (HQ) was added to stop the polymerization. DMF was then evaporated, the product dissolved in acetone and the solution poured into an excess of hexane to precipitate. After that, it was vacuum filtered, dissolved again in acetone, precipitated in ether, and once more vacuum filtered and dried.^{254,255}

The *N*-isopropylacrylamide polymers with different loadings of pyrene and with different size chains were prepared using a predetermined amount of NIPAM, AIBN and pyrene monomer (see

Table 7.2). Two temperatures and reaction times were tested to see the influence of these parameters on the size of the polymers obtained.

Methods and Sample Preparation



Scheme 7.2. Synthetic routes to prepare polymers with different pyrene loadings.

Azobisisobutyronitrile, triethylamine from Merck, methacryloic chloride, *N*-isopropylacrylamide from Aldrich, sodium bicarbonate, sodium sulphate, hydroquinone, 1-pyrenemethanol from Aldrich.

The solvents used for the synthesis procedure (acetone, chloroform, dichloromethane, dried DMF, hexane, ether and water) were of analytical grade.

In Figure 7.3, a photograph of the some of the PNIPAMPy polymers synthesized with the same procedure are showed in day light and under UV light.



Figure 7.3. From left to right. Picture of PNIPAMPy with 0%, 1%, 2.5% and 7.5% mol of Py in day light and under UV light (365 nm).

Methods and Sample Preparation

Table 7.2. Information (synthetic conditions and physical properties) from PNIPAM polymers with different pyrene loadings (PNIPAMPy).

Samples*	Expected Pyrene Loadings (%mol)	Pyrene Loading (by ¹ H NMR, %mol) ^a	NIPAM (g) (mmol)	AIBN (mg) (mmol)	1PyMMA (mg) (mmol)	T (°C)	t (h)	V _{DMF} (ml)	HQ (mmol)	Obtained				
										m _{polymer} (g)	η (%)	M _w ^{GPC} (kg/mol)	PDI ^{GPC}	M _w ^{MALDI RD} (kg/mol)
1*	0	0	0.501	5.01	0,	60	24	5	0.031	ND	ND	ND	ND	ND
PNIPAM(M _w)			4.427	0.031	0									
2*	0	0	0.500	5.00	0	60	≥31	5	0.031	0.409	ND	ND	ND	ND
PNIPAM(M _w)			4.419	0.030	0					82				
3	0	0	0.515	5.15	0	80	24	5	0.031	0.424	29.2	8.46	2.0 (64%)	1.2
PNIPAM(29)			4.551	0.031	0					82			1.5 (24%)	1.2
													1.2 (12%)	1.1
4*	0	0	0.502	5.35	0	80	24	5	0.031	0.436	ND	ND	ND	ND
PNIPAM(M _w)			4.433	0.033	0					87				
5*	0.5 (0.50)	NA	0.501	5.10	6.70	80	24	5	0.031	ND	ND	ND	ND	ND
			4.424	0.031	0.022									
6	1.0	0.55	0.300	3.18	8.07	80	24	3	0.022	0.182	31.8	6.09	2.1 (79%)	1.2
PNIPAMPy(32)182			2.651	0.019	0.027					61			1.8 (12%)	1.1
													1.4 (9%)	1.1
7	2.5 (2.49)	3.02	0.502	5.40	33.2	80	24	5	0.031	0.275	74.2	3.35	2.0 (76%)	1.2
PNIPAMPy(74)33			4.436	0.033	0.111					51			1.0 (24%)	1.1
8*	5	NA	0.301	3.44	40.0	80	24	3	0.022	ND	ND	ND	ND	ND
			2.660	0.021	0.133									
9	7.5	7.41	0.301	4.49	60.0	80	24	3	0.022	0.224	55.0	3.65	1.1 (59%)	1.1
PNIPAMPy(55)13			2.660	0.0273	0.200					62			1.1 (41%)	1.1

Methods and Sample Preparation

Samples*	Expected Pyrene Loadings (%mol)	Pyrene Loading (by ¹ H NMR, %mol) ^a	NIPAM (g) (mmol)	AIBN (mg) (mmol)	1PyMMA (mg) (mmol)	T (°C)	t (h)	V _{DMF} (ml)	HQ (mmol)	Obtained					
										m _{polymer} (g)	η (%)	M _w ^{GPC} (kg/mol)	PDI ^{GPC}	M _w ^{MALDI RD} (kg/mol)	PDI ^{MALDI RD}
10*	0	0	0.300	3.21	0	85	3	3	0.022	0.026	9	ND	ND	ND	ND
11	1.0	1.0	2.651	0.020	0	85	3	3	0.022	0.117	38	66.7	3.24	2.0 (74%)	1.2
PNIPAMPy(67)100			0.301	4.00	8.0					0.027				0.348	1.4 (26%)
12	2.5	2.4	0.301	3.39	20.0	85	3	3	0.022	0.348	109 ^a	36.6	6.00	1.1 (76%)	1.2
PNIPAMPy(37)42			2.660	0.021	0.067					1.6 (24%)				1.1	
13*	5.0	19.0 ^a	0.302	3.43	40.03	85	3	3	0.022	0.066	119.8 ^b	3.12*	1.2 (63%)	1.2	
PNIPAMPy(120)			2.668	0.021	0.133					19				1.1 (37%)	1.1
14*	0	0	0.302	3.06	0	65	24	3	0.022	ND	ND	ND	ND	ND	ND
15*	2.5		2.267	0.019	0	65	24	2.5	0.017	ND	ND	ND	ND	ND	ND
PNIPAMPy(M _w)			0.250	2.72	16.6					2.209				0.017	0.055

*Appropriate nomenclature for these polymers will just be given after complete characterization. ^a ¹H NMR shows the presence of <1% of NIPAM. ^b This value is probably due to the presence of impurities.

The effects of time and temperature could not be taken since the polydispersity or/and initial reactant proportions were not the same for all the polymers. However, the yield seems to be higher for highest synthesis duration in contrast with the increased temperature that seems to not affect much.

Table 7.3. Physical properties of some PNIPAM obtained by MALDI-TOF.

Polymer	Loading nominal (% mol)	Loading NMR (% mol)	MALDI linear detection				MALDI reflector detection			
			M_n (g/mol)	M_w (g/mol)	PDI	Obs.	M_n (g/mol)	M_w (g/mol)	PDI	Obs.
3 PNIPAM(29)	0	0	2945 ^a	4310	1.5	~53% ^b	1613 ^a	2015	1.2	64% ^d
			1935	2455	1.3	~39%	1247	1465	1.2	24%
			1331	1515	1.1	~8%	1103	1244	1.1	12%
6 PNIPAMPy(32)182	1.0	0.6	2487 ^a	3218 ^a	1.3 ^a		1706 ^a	2103	1.2	79% ^d
							1599	1814	1.1	12%
							1264	1445	1.1	9%
7 PNIPAMPy(74)33	2.5	3.0					1637 ^a	2041	1.2	76% ^d
							907	1017	1.1	24%
9 PNIPAMPy(55)13	7.5	7.4					992 ^a	1138	1.1	59% ^d
							939	1076	1.1	41%
11 PNIPAMPy(67)100	1.0	1.0 ^c				ND	1694 ^a	2006	1.2	74% ^d
							1110	1351	1.2	26%
12 PNIPAMPy(37)42	2.5	2.4 ^c					944 ^{a,e}	1091	1.2	76% ^{d,f}
							1401	1606	1.1	24%
13* PNIPAMPy(120)	5.0	19.0 ^c					1036	1233	1.2	63% ^d
							943	1076	1.1	37%

^a Several distributions were observed. ^b Estimated on the basis of distribution maxima. ^c ¹H NMR shows the presence of <1% of NIPAM. ^d Estimated on the basis of distribution areas. ^e In this case, the main distribution was calculated as the average of 5 very similar distributions. ^f The area of the main distribution was calculated as the sum of the areas of 5 very similar distributions.

After characterization of some PNIPAMPy by GPC and observation of high PDI (Figure 7.4), another purification procedure, now by GPC, of sample 6 was tried. In order to do that, a normal GPC was done but the sample run was then collected (diluted) in three different fraction (the 1st until 15 mL, the 2nd between 15 and 17 mL and the 3rd from 17 to 19 mL).

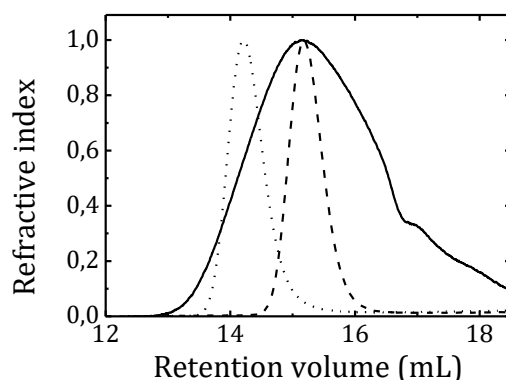


Figure 7.4. Normalized GPC elution traces of sample 16 in dimethylformamide (DMF) at a flow rate of 1.0 ml.min⁻¹. The dotted and dashed lines correspond to the poly(methyl methacrylate) polymers with $M_w = 20.31$ and 50.00 kg/mol, respectively.

After collecting three different fractions, one of them was chosen to be further characterized and compared with the polydisperse PNIPAMPy polymer. The second fraction was chosen and the solvent evaporated since the fraction collected was quite diluted. However, due to the presence of lithium bromide, the absorption spectrum of the fraction collected (and evaporated) had a considerable absorbance in the visible region. For this reason, further purification is needed in order to remove this agent. We tried different approach such as washing the organic layer containing the polymer with water and column chromatography using silica gel as the stationary phase and DMF as the eluent. Neither one of them worked. We consider making dialysis using an appropriate membrane but the volume was low and the accessible membranes not adequate. A possible successful approach could be the chromatography using a C18 silica gel column that allow the use of water as eluent and enabling the elimination of lithium bromide.

7.1.4.3. Physical Measurements

¹H-NMR spectra of the PNIPAMPy were run on a Bruker Avance III 400 operating at 400.15 MHz (¹H). Signal of the deuterated solvent (CDCl₃) was used as an internal reference. The pyrene content (x) of the PNIPAMPy(M_w) $_x$ was calculated through the percentage of pyrene in moles (% mol Py) obtained from ¹H-NMR. The M_w of the polymer was obtained first by MALDI and then GPC. For ¹H-NMR, MALDI and

GPC characterization, deuterated chloroform, tetramethylsilane (TMS), dithranol, sodium tetrafluoroborate (NaBF₄), acetone and dimethylformamide were used.

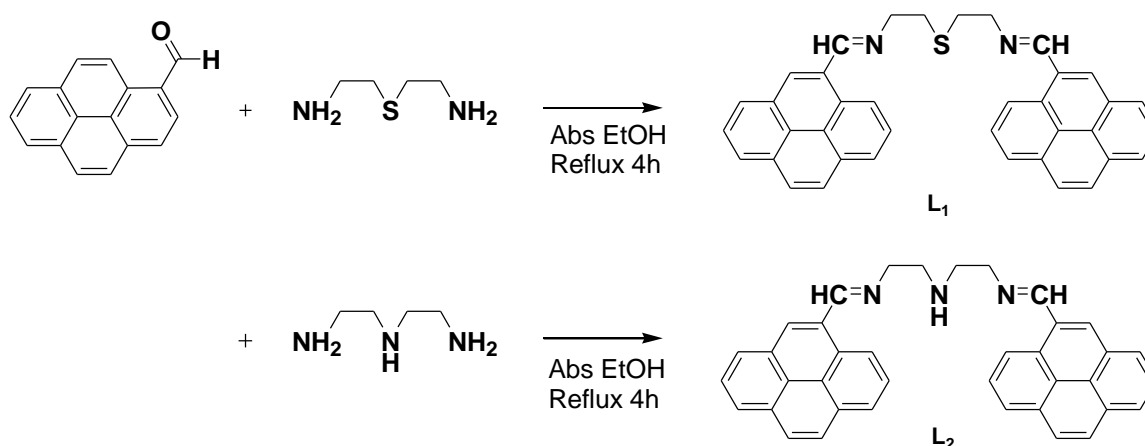
MALDI-TOF MS analyses were performed on a Voyager-DETM PROBiospectrometry Workstation model (Applied Biosystems) and data were analysed with Voyager V5.1 software. Dithranol was employed as the matrix and NaBF₄ was added to improve the ionization. Samples and matrix were dissolved in acetone and the spectra were recorded on the positive linear and reflector modes.

GPC was carried out using high performance size-exclusion chromatography (HPSEC), with refractive index (Knauer K-2301) detection. The column set consisted of a PL 10 mL guard column (50 × 7.5 mm²), followed by two MIXED-B PL columns (300 × 7.5 mm², 10 μL). The HPLC pump was set with a flow rate of 1 mL/min and the analyses were carried out at 60 °C using an Elder CH-150 heater. The eluent was DMF, containing 0.3% of LiBr. Before injection (100 μL), the samples were filtered through a polytetrafluoroethylene (PTFE) membrane with 0.2 μm pore size. The system was calibrated against PMMA standards. The concentration of the samples characterized varied between 3.97 and 11.23 mg/ml.

7.1.5. Chemosensors

7.1.5.1. L₁ and L₂

Compound L₁ and L₂ were synthesized following the reaction pathway shown in Scheme 7.3.



Scheme 7.3. Schematic synthesis procedure for L₁ and L₂.

L₁: Elemental analysis (%) calcd. for C₃₈H₂₈N₂S (544.71 g/mol): C 83.79, H 5.18, N 5.14, S 5.89; found: C 83.42, H 5.51, N 5.24, S 5.57; FT-IR (KBr): $\tilde{\nu}$ = 1625 (N=C), 1453 (C=C) cm⁻¹.

$\eta = 71\%$ (g)

m.p. = 167.0-168.9 °C

L₂: Elemental analysis (%) calcd for C₃₈H₂₉N₃(H₂O)₆ (635.75 g/mol): C 71.79, H 6.50, N 6.61, O 15.10; found: C 72.73, H 6.41, N 10.97; FT-IR (KBr): $\tilde{\nu} = 1624$ (N=C), 1455 (C=C) cm⁻¹.

$\eta = 24.6\%$

m.p. = 109.1-111.7 °C

7.1.6. Surfactants

In order to study the PAAMePy-surfactant interaction (Section 3.2.2.2), several surfactants were used. C₁₂E₄ (Aldrich), C₁₂E₅ 98.0 % (BioChemika), CTAB (Fluka) e SDS 96.0 % (Fluka) were used as received. Their chemical structure are presented in Section 3.2.2.2.1.1.

7.1.7. Metals

The metal cations Ag(BF₄), Ag(CF₃SO₃) Al(NO₃)₃.6H₂O, Cd(CF₃SO₃)₂, Cu(BF₄)₂, Cu(CF₃SO₃)₂, FeCl₂.4H₂O, Hg(CF₃SO₃)₂, Ni(CF₃SO₃)₂, Pb(CF₃SO₃)₂, Zn(BF₄)₂ and Zn(CF₃SO₃)₂ salts and fluoroboric acid (HBF₄) were kindly gifted by Prof. Carlos Lodeiro.

7.1.8. Solvents

For the spectroscopic and photophysical measurements, all the solvents used were of spectroscopic or equivalent grade. When necessary, solvents were purified by the methods described in ref. ²⁵⁶ and/or dried by the methods described in ref. ²⁵⁷. The regeneration of the molecular sieves (3A or 4A types) used was made by leaving them overnight at T= 260 °C.

Water was twice distilled and passed through a Millipore apparatus.

The ideal solvent for the preparation of sample solutions would dissolve all types of compounds, be non-flammable and non-toxic and would be completely transparent at all wavelengths. Table 7.4 lists the solvents used in this work. With volatile organic solvents, such as acetone or dichloromethane, it is advised to use a stoppered cell to eliminate evaporation, which can result very quickly in changes in concentration.

7.1.9. Samples

7.1.9.1. Storage

Depending on the properties of the compounds, they were either kept in the fridge or freezer or just left in desiccators and kept from the light to ensure their good conditions in the time of analysis.

7.1.9.2. Preparation of the PAAMePy Polymer Solutions

The chromophore concentration of the PAAMePy solutions ranged from 1×10^{-5} to 10^{-6} M, $O.D._{max} \leq 0.2$, to guarantee no intermolecular interactions (see lifetime of intermolecular excimer and no variation of I_E/I_M with O.D.). The solutions were, most of the times, deoxygenated by bubbling with N_2 gas (between 15 minutes to 1 hour) and sealed with the proper cuvettes to avoid quenching (particularly of the monomer emission due to its long lifetime). This was further confirmed by the absence of variation of the I_E/I_M ratio with the solution concentration.

Before using the syringe employed to filter the solutions, the ink indicating the volume was removed with acetone in order to not contaminate the solution. Moreover, the solutions were stored in the minimum period of time essential to carry out the experiment in question since they could precipitated due to the low solubility of pyrene (particularly in water). Whenever possible a new solution was then prepared to ensure that it was in good conditions and similar to the others previous studied polymers, see example in Figure 3.57 in Section 3.3.3.

7.1.9.2.1. Organic Solutions

The solutions of the polymers were prepared (in organic solvents) at room temperature except for the polymers where the solubilisation was found to be difficult. In these situations, the solutions were heated to a temperature below the boiling point of the solvent and never higher than 50 °C, on the other hand the sample was also subject to stirring with the assistance of a magnet (with maximum R.P.M) or sonication. However, to avoid any possibility of degradation of the polymer, the use of sonication was ceased and none of the results here presented were obtained from solutions with sonication.

7.1.9.2.1. Dioxane:Water (Dx:H₂O) mixtures

A concentrated solution of PAAMePy in dioxane was prepared since they are more soluble in this solvent than in water. This more concentrated solution was then used to prepare more diluted ones with the desired volume fractions of dioxane.

In the preparation of dioxane:water mixtures, the appearance of bubbles was observed for some volume fractions of dioxane. These bubbles were removed by deoxygenation or through agitation with a Pasteur pipette.

To collect the absorption spectra in these mixtures, blanks with the same fractions of dioxane:water were used and prepared the same day of the study.

7.1.9.2.1. Water (at different pH values)

For the preparation of solutions of PAAMePy in water, various approaches were considered and the more suitable for each polymer was carefully chosen. First, a concentrated stock solution was prepared and from this solution a number of solutions were prepared at different pH values. These solutions were prepared the day before and deoxygenated immediately before running the spectra or decay. With this approach it was not possible to study accurately (and reproducibly) the behavior of the polymers. A deoxygenation uneven, erroneous measurement of volume, pH variation or precipitation (with time) may have been factors which did not allow reproducible results.

Methods and Sample Preparation

Table 7.4. Properties [molecular weight (M_w), boiling (b. p.) and melting points (m. p.), density (d), refractive index (n_D), viscosity (η), dielectric constant (ϵ), T=10% at $\lambda(\text{nm})=**$) of the solvents and mixtures of solvents] used in this work.

Solvent	M_w (g/mol)	b. p. (°C)	m. p. (°C)	Polarity index	d (g/mL)	n_D^a	η^b (mPa.s)	ϵ^c	T=10% at $\lambda(\text{nm})=^d$	Hazard ^e	Ref.
Water	18.015	100.0	0.0	9, 10.2	0.9982	1.332988	1.0019	80.16		None	35,258
Ammonia solution (28% aq.)	17.031										
Acetone	58.08	56.2	-95.0	5.1	0.7899	1.35868	0.303 ^f	20.7 ^f	329	F	35,258
Acetonitrile	41.05	81.8	-44.0	5.8	0.7857	1.34411	0.345 ^f	35.94 ^f	190		35
Cyclohexane	84.16	81.0	7.0	0.2	0.7785	1.42623	0.975	2.023	205	F	35,258
Cyclohexane, methyl-	98.19	101.0	-127.0		0.7694	1.42312	0.734	2.020	207		35
Chloroform	119.38	61.0	-64.0	4.1	1.4832	1.4459	0.58	4.806	245	F/T	
Diethyl ether	74.12	34.0	-116.0	2.8	0.7138	1.35243	0.242	4.335			35,258
1,4-Dioxane	88.11	101.0	12.0	4.8	1.0337	1.42241	1.439 ^g	2.209 ^f	215		35
Dimethylsulfoxide	78.14	189.0	19.0	7.2	1.1014	1.4793	1.991 ^f	46.45 ^f	262	H	35,258
Dimethylformamide	73.09	153.0	-60.0	6.4	0.944	1.43047	0.924	36.71 ^f	270		35
Dichloromethane	84.93	39.6	-95.0	3.1	1.3266	1.42416	0.449 ^g	8.93 ^f	232		35
Ethanol	46.07	78.0	-114.0	5.2	0.7893	1.36143	1.200	24.55	205	F	35,258
Methanol	32.04	65.0	-98.0	5.1	0.7914	1.32840	0.5929	32.66 ^f	205	F	35,258
Decane	142.29	174.15	-29.64	0.3	0.7300	1.41189	0.9284	1.991			35
Decalin (mixture of cis+trans)	138.25	190±1	-125.0		0.896	1.474					117
Dodecane	170.34	216.32	-9.58		0.7487	1.42167	1.508	2.015			35
Hexane	86.18	69.0	-95.0	0	0.6548 ^h	1.37486	0.3126	1.8863	195	F	35,258
Heptane	100.20	98.0	-91.0	0	0.6837	1.38764	0.4181	1.9246	197		35

Methods and Sample Preparation

Solvent	M_w (g/mol)	b. p. (°C)	m. p. (°C)	Polarity index	d (g/mL)	n_D^a	η^b (mPa.s)	ϵ^c	T=10% at λ (nm)= ^d	Hazard ^e	Ref.
Toluene	92.14	111.0	-95.0	2.4	0.8669	1.49693	0.5859	2.379 ^f	285		35

^a Refractive index at 20°C at the average sodium line, unless otherwise noted. ^b Viscosity at 20 °C unless otherwise noted. ^c Dielectric constant at 20°C unless noted. ^d Wavelength at which transmittance of 10-nm path length is 10%. ^e F= flammable; T= toxic; H= health hazard. ^f measured at 25°C. ^g measured at 15°C.

Table 7.5. Organic solvent mixtures used in this work that form clear glasses at 77 K with a low cracking frequency.³⁵

Glass	Proportion	% Crack	Media
Ethanol	-	10	Neutral
EtOH: conc. HCl	9:1	30	Acidic
Et₂O:EtOH:NH₃ (28% aq.)	10:9:1	10	Basic

The next approach consisted on preparing similarly a concentrated stock solution but preparing the solutions the day of analysis and without deoxygenating them. However, even with this procedure the results obtained were not very reliable and reproducible. Then, the subsequent method adopted consisted on giving up making a concentrated stock solution but to prepare just only one solution with ~ 0.1 of absorbance, the pH of this solution was changed and the solution was analysed and so on. This approach was very successful for small polymers with low degree of pyrene labelling as PAAMePy(2)132 and PAAMePy(2)133. However, it was a time consuming process, not resulting for all the polymers. The following approach consisted in filtering the solutions using a syringe and a syringe filter with pore size of $0.45 \mu\text{m}$ with nylon, GHP or polyester membrane; thus even if the polymer solution was not completely solubilized, the filtered solution was free of non-dissolved polymer which greatly contributed to the reducing of the solution scattering. However, the problem was mainly found to be the time for measuring all the prepared solution (at different pH values) in a time inferior to one day, particularly because of the neutral pH range. Thus, a universal buffer was added and then the total (polymer + buffer) solution filtered. With this approach, good results were achieved for all the short chain polymers [PAAMePy(2)]. The solutions of PAAMePy(450) could not be filtered because of the small pore size of the membranes and by using the same procedure for long chain polymers [PAAMePy(450)], the process did not seem to lead to reproducible results. All these seem to indicate that, despite the degree of labelling being similar, these longer polymers were less soluble in water. This can be interpreted by the existence (in terms absolute) of more pyrene units in the long chain polymers. These polymers were left under constant stirring and heating for longer periods, but precipitated then or during the experiment (followed by observation of a lowering of the absorbance). For this reason, it was decided to prepare a stock solution in methanol enough to only require a maximum volume of (methanol) stock solution of $40 \mu\text{L}$ (to a total of 10 ml, i.e., $\leq 0.4\%$) to prepare a solution of (mostly) water with the desired solution with an absorbance at 335 nm (approximately 0.1). Besides this preparation in methanol, the buffer was also added and filtered. In all cases the solution was used on the day of analysis and never stored for repeating the procedure because it seemed to deteriorate with time. For the time-resolved fluorescence studies, additional precautions have to be considered since the possibility of precipitation during the experiment is higher due to the longer acquisition time. Thus, whenever possible the (absorption and emission) spectra were run before and after the decay to verify the existence (or not) of fluctuations in the systems. These results were reproduced using another approach. Instead of preparing a low volume of polymer (typically, 5-10 ml), 25 to 30 ml were prepared and no buffer solution was used. Besides, the PAAMePy(2) were not filtered, but a pH ~ 12 solution was prepared, where it seems that the polymer is more soluble due to the chain elongation allowing a better polymer-solvent interaction. The same was made for the PAAMePy(450) although it was still needed to prepare a stock solution in methanol.

7.1.9.2.2. With Surfactants (at two pH values)

For the aqueous solutions of PAAMePy the pH was measured before the addition of any surfactant. In this study, it was found that the solutions when deoxygenating were forming a high amount of foam, therefore it was chosen to make this study without deoxygenating, probably disrupting the structure of the micelles.

7.1.9.3. Preparation of the Chemosensors Solutions

In chemosensors preparation, the preferred solvents are those that allow a greater number of applications (in biological domains or others), i.e., the selection would start with water, ethanol, methanol, acetonitrile, dichloromethane, DMSO and DMF.

Mostly, the chemosensors were soluble in dichloromethane, DMSO and DMF. To use solvents as acetonitrile or ethanol, sonication was often used except for compounds which could degrade like an imine.

Generally, the solutions were prepared using the smaller possible amount of glassware to avoid contaminations.

Preferably, the extinction coefficient was measured in the solvent chosen for the study and then this parameter was used to determine the concentration of the solution to make the desired titrations. This was made to avoid spending unnecessary compound and possible contaminations (using less material), to use always fresh solutions (prepared in the day of analysis).

All spectroscopic titrations were performed (at 293 K) as follows: (i) a solution of the ligand was prepared by dissolving an appropriate amount of the ligand in the solvent and diluted to the desired concentration (typically 10^{-5} - 10^{-6} M); (ii) titrations were carried out by the addition of microliter amounts of standard solutions of the ions dissolved preferably in the same solvents (with concentrations around $[M]=10^{-4}$ - 10^{-3} M); (iii) 3 ml of the solution was placed to a 1 cm quartz cuvette. To acquire the fluorescence spectra relatively fast (yet with sufficient resolution), an integration time of 0.1 s was used and in order to homogenize the solution manual agitation was performed after each addition of metal and before running the absorption or emission spectrum.

In terms of choosing the solvent, the coordination should be also weighted. Less coordinative solvents should be preferred. Besides this, care must be taken using DMSO which absorbs easily water and is in solid state at $T < 19^{\circ}\text{C}$ and with dichloromethane which evaporate really fast at room temperature.

In order to choose the counter-ion of the salt it is always best to start with triflate, if the metal is not soluble in the chosen solvent it should be tried tetrafluoroborate and after that perchlorate. The others

should be avoided. The triflates are big in comparison to the metal ions and, for this reason, should not compete with the metal ion.

Table 7.6. Solubility of the several metals used.

Metals	Soluble	Fairly soluble	Slightly soluble	Insoluble	Ref.
	H ₂ O				
Cu(OTf)₂	MeOH, EtOH, DMF, MeCN, formamide, i-PrCN and acetone				259
Cu(BF₄).nH₂O	H ₂ O	Alcohols			260
	Dx				
Zn(OTf)₂	H ₂ O, MeCN		MeOH	CH ₂ Cl ₂	261
Zn(BF₄).nH₂O	H ₂ O, EtOH				262
	Dx				
Hg(OTf)₂	H ₂ O, MeCN	CH ₃ NO ₂ and		hexane, ether,	263
		CH ₂ Cl ₂		and toluene	
Hg(BF₄).nH₂O	Dx				
Cd(OTf)₂	MeCN				
	EtOH				
Cd(BF₄).nH₂O	H ₂ O, Alcohols, Dx				

Table 7.7. Counter-ions of metal salts.

NO₃⁻	Nitrates	
ClO₄⁻	Perchlorates	
BF₄⁻	Tetrafluoroborates	Choosing metal salts
Cl-, I-, Br- and F-	Halides	OTf- > BF₄⁻ > ClO₄⁻ > remaining counter-ions
OTf-	Triflates	

7.1.9.4. Preparation of an Universal Buffer

To prepare 50 ml of this buffer, NaOH (1 M) was prepared. 0.177 g of boric acid was dissolved in 5 ml of NaOH (1 M) and 0.177 g of boric acid, 17 ml NaOH (1 M), 0.005 moles of citric acid (1.0507 g) and 0.005 moles of phosphoric acid (0.34 ml) were added.

7.1.10. Cleaning Process

The glassware was cleaned right away covering completely the materials with chromosulphuric acid or nitric acid (65%) for at least 24h. After this procedure, they were rinsed with water and dried in an oven (except volumetric glassware) or with acetone and/or dichloromethane and further dried with hair drier (when the glassware needed to be used immediately).

The quartz cuvettes were cleaned with nitric acid (65%) for 24h maximum to avoid future scattering problems²⁶⁴ or sulphuric acid (98%) for few seconds, then rinsed with water and acetone and/or dichloromethane and dried.

The chromosulphuric (red), nitric, chloridric and sulphuric acids (colourless) were, generally, reused and just discarded in the moment they changed colour (usually turning to green, yellow, brown and brown, respectively).

Generally, the materials (in particular the cuvettes) were also rinsed with the solvent to be used and absorption and emission spectra were collected to assure that the materials were well cleaned. When the absorption or/and emission spectra showed traces of impurities, the cleaning procedure was repeated.

To cover volumetric and Pasteur pipettes with chromosulphuric acid, a tall test tube was used hold by the assistance of a holder and a claw.

In some cases, particularly with some chemosensors, the acidity of the material or rests of Cr^{3+} were critical. To remove H^+ ions, to the material was poured an aqueous solution (1 M) of NaOH and an aqueous solution (1 M) of ethylene diamine tetraacetic acid disodium salt dehydrate (EDTA), both for 1h. To remove Cr^{3+} , only EDTA was needed. The glassware was rinsed with water, acetone and dichloromethane and dried. Besides, sometimes, to assure that nothing was in the glassware, the compound was put inside to complex with whatever ion was inside and then was passed by the solvent used for the future experiment.

7.1.10.1. Preparation of Chromosulphuric Acid

70 g of sodium dichromate dehydrate ($\text{Na}_2\text{Cr}_2\text{O}_7 \cdot 2\text{H}_2\text{O}$) were dissolved in 70 ml of distilled water. 1L of H_2SO_4 was placed in a separating funnel and allowed to drop in an aqueous solution of $\text{Na}_2\text{Cr}_2\text{O}_7 \cdot 2\text{H}_2\text{O}$ with stirring on an ice bath because the reaction is exothermic.

7.1.10.2. Preparation of EDTA

To prepare EDTA solution, a water solution at pH 8 was first prepared. EDTA was dissolved in this water with vigorous stirring (and heated when necessary) and if the solubilisation was not achieved, additional NaOH (in pellets) were added.

7.2. Techniques

7.2.1. pH Measurements

The measured pH values were obtained with a Crison micropH 2000 and adjustments of the hydrogen ion concentration of the solutions were made with microvolumes of concentrated HCl (or HClO₄) and NaOH solutions. The pH was accepted after having at least three similar values. When pH titrations were made for PAAMePy polymers, it was started from basic pH value due to the higher solubility and stability of the polymer solution.

7.2.2. Temperature

For temperature dependent experiments, one or two devices were used depending on the temperature range of the study. Below 20 °C, a refrigerated circulator bath (with ethanol) Julabo F30-C or Grant TC-120 was used additionally to an assembled temperature controller OMEGA or TOHO in the sample holder. For temperatures above room temperature, only the temperature controller was used. This controller is placed directly in the sample holder and seemed to be enough to control the temperatures for $T \geq 20$ °C.

7.2.3. Deoxygenation

To remove oxygen from the sample solutions, two methods were used in this work. One consists on using quartz cuvettes properly modified,³⁷ the other consists solely on using a pipette whose bubbling nitrogen inside an unmodified cubic quartz cuvette sealed with Parafilm®. This last method showed not to be enough for all compounds (for example, PAAMePy) so it was only rarely used for compounds with relatively small lifetimes. Usually, the polymer solutions were degassed under a steady stream of nitrogen for, at least, 30 min with a special cuvette elsewhere described³⁷ whereas with the other compounds solutions, these were left bubbling for approximately 15 minutes. Deoxygenation for 30 minutes showed to not be enough for more viscous solvent as DMF, so these samples were left for 1h.

The small tube inside the cuvette is where the nitrogen enters and it was seen that depending on the position of the cuvette more or less scatter was found in the decay. This could be due to surface scratches and/or fingerprints but it could be also due to the occasional bubbling of the cuvette while measuring the decay. For that reason, another cuvette with a shorter tube was made. The slit was covered with tape

in order to avoid reflections from inside the apparatus which could be in the origin of scatter in the fluorescence decays.

7.2.4. Binding Constant Determination

In order to calculate the association constants, the HYPERQUAD software was used. To do that the titration data corrected for the absorption and fluorescence emission (Equation 7.1 and Equation 7.2, respectively) is uploaded to the software as a .txt file together with the information of the ligand and metal concentration, aliquot added ($V_{\text{metal added}}$), volume of the ligand (V_{ligand}), *etc.*

$$A_{\text{corr.}} = \frac{A \times V_{\text{metal added}}}{V_{\text{ligand}}} \quad \text{Equation 7.1}$$

$$I_{\text{corr.}} = \frac{I}{1 - 10^{-A_{\text{corr.}}^{\lambda_{\text{exc}}}}} \quad \text{Equation 7.2}$$

Where $A_{\text{corr.}}$ is the absorbance corrected considering the dilution factor, A is the absorbance, $I_{\text{corr.}}$ is the fluorescence emission intensity corrected considering the corrected absorbance at the excitation wavelength ($A_{\text{corr.}}^{\lambda_{\text{exc}}}$) and I is the fluorescence emission intensity.

7.2.5. UV-Vis Absorption

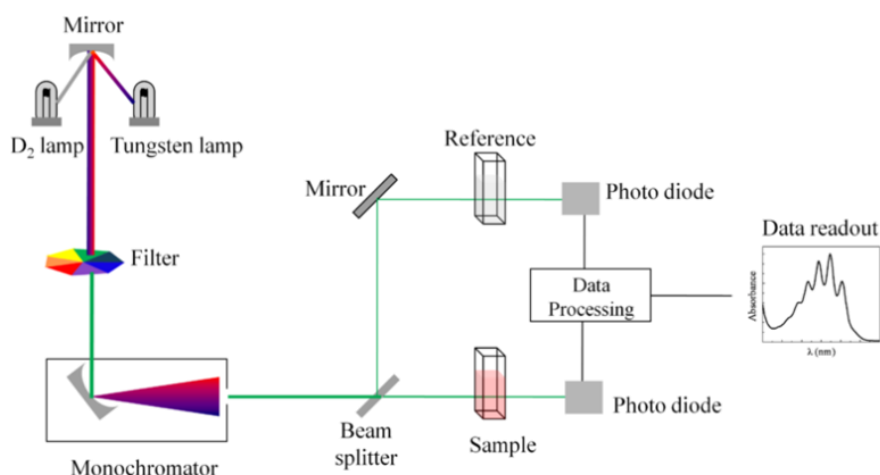


Figure 7.5. Schematic representation of a conventional double-beam spectrophotometer from.

The radiation beam generated from the lamp is filtered and by passing by a monochromator is divided in two. One of the beams passes through the sample while the other through the reference in order to subtract the solvent and cuvette material (usually quartz) absorption from the sample. In a single beam, this subtraction has to be made separately, i.e., by making both absorption spectra of the sample and

reference and manually by making subtracting one another. To avoid possible photodecomposition, the spectra are generally traced from longer to shorter wavelengths (i.e., from lower to higher energies). The absorption measurements can be made at a single wavelength or by making a scan over a range of wavelengths. If the range of wavelengths chosen represents the range where a certain molecule absorbs, the spectrum obtained correspond to the absorption spectrum of this molecule.

The material used to make absorption spectra of solutions is generally quartz since glass and plastic absorbs more (see Figure 7.6). In this case, to obtain the absorption spectra, plastic or glass could be used since it is subtracted in the reference and much cheaper. Glass and quartz offer the advantage of allowing the use of all solvents, while plastic doesn't. On the other hand, a plastic cuvette could be thrown away while a glass and quartz cuvettes need to be clean and reutilized.

Usually absorption cuvettes are faded in the two faces where the beam is not passing, but since in this work fluorescence was always made after absorption, the cuvettes used were the one for fluorescence (quartz with all faces clear).

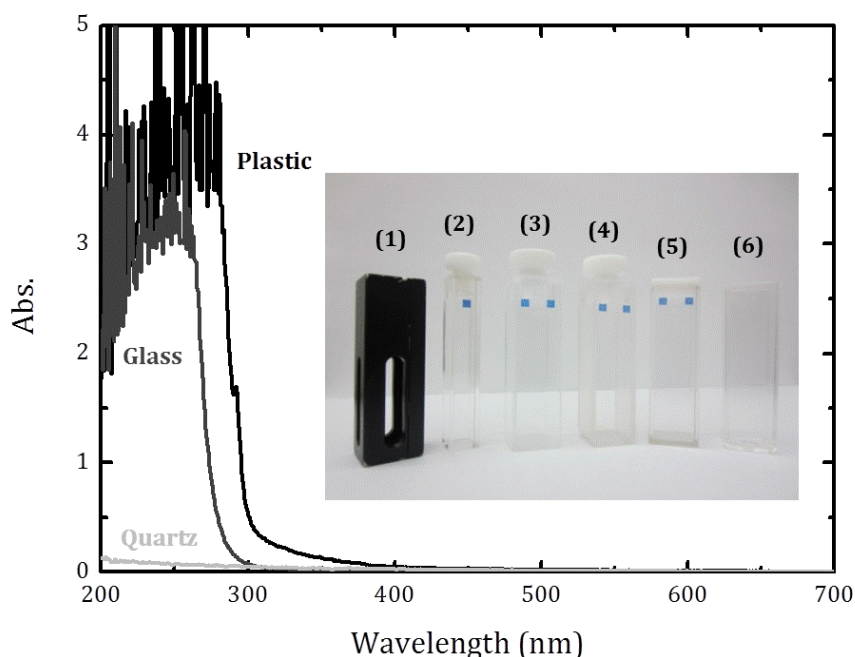


Figure 7.6. (A) Absorption spectra of plastic, glass and quartz cuvettes and (B) photos of the cuvettes used in this work. (1) holder for (2), (2) quartz cuvette with path length of 5 mm with stopper, (3) 10 mm ($V \geq 3$ mL) with stopper, (4) glass cuvette of 10 mm ($V \geq 3$ mL) with stopper, (5) open-topped cubic quartz cuvette of 10 mm ($V \geq 3$ mL) with stopper, (6) open-topped polystyrene (PS) cuvette of 10 mm ($V \geq 3$ mL) without stopper.

There are several kinds of cuvettes depending of the application needed, besides the material; different shapes, sizes, covers and/or opening of cuvettes exist. In Figure 7.6 some cuvettes are showed.

Shimadzu UV-2101 and 2450 (the spectrophotometers most used in this work) are double-beam spectrophotometers which have two types of source lamps: D2 (deuterium) and W1 (halogen) lamps. The D2 and W1 lamps are used for ultraviolet region (190 nm - radiation source switching wavelength) and visible/near-infrared region (radiation source switching wavelength- 900 nm), respectively. The radiation source switching wavelength can be arbitrarily specified in the range between 282 and 393 nm. Besides these equipments, a Cary UV-Vis-NIR 5000 was also used in this work.



Picture 7.1. Photo of Shimadzu UV-2101.

7.2.5.1. Molar extinction coefficients

The molar extinction coefficients (ϵ) were obtained from the slope of the plot of the absorbance (at a given wavelength) versus the concentration; this was made using at least 5 solutions of different concentrations, see Figure 3.64 in Section 3.3.3.

7.2.5.2. Spectrophotometric titrations

7.2.5.2.1. P_A Parameter Determination

The P_A parameter was used typically for the pyrene oligomers and polymers and is defined as the peak-to-valley absorbance ratio in the first vibronic $S_2 \leftarrow S_0$ transition.⁶⁵

In some cases, the total variation of this parameter in, e.g., a pH range, was investigated. To obtain the difference between the maximum and minimum value was calculated, Equation 7.3.

$$\Delta P_A = P_A^{\max} - P_A^{\min} \quad \text{Equation 7.3}$$

The same was necessary, for the maximum absorption wavelength (λ_{Abs}^{\max}), P_M , P_E , $P_M - P_E$ (Section 7.2.6.1.2.3) and I_E/I_M (Section 7.2.6.1.2.3) parameters.

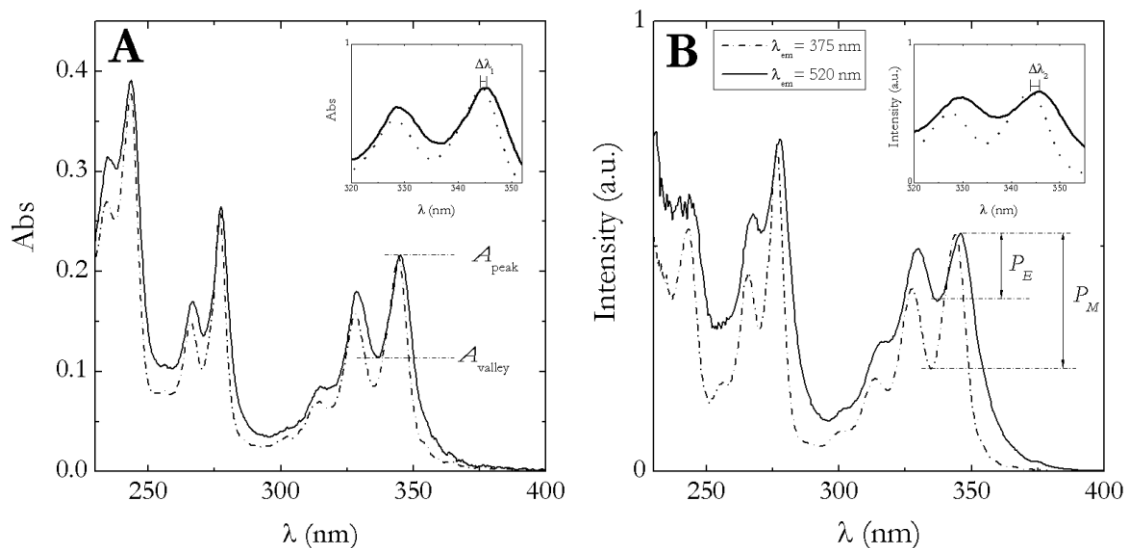


Figure 7.7. (A) Absorption and (B) normalized excitation spectra collected at the monomer ($\lambda_{em}=375$ nm) and excimer ($\lambda_{em}=520$ nm) of Pyrene in dioxane; $[Py]=8 \times 10^{-4}$ M. The definitions of P_A , P_M , P_E , $\Delta\lambda_1$ e $\Delta\lambda_2$ are illustrated as insets.

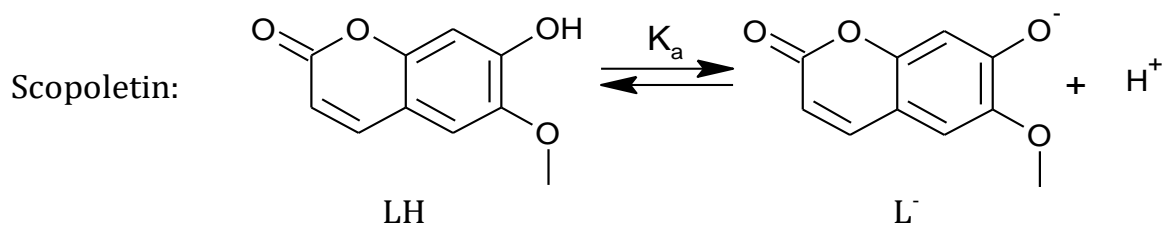
7.2.5.2.2. pK_a Determination

The plot of P_A , λ_{max}^{Abs} , $P_M - P_E$, P_M and P_E as a function of pH shows, in some cases, a clear inflexion which was fitted to a sigmoidal Boltzmann-like equation with Equation 7.4.⁶⁵

$$P_A, \lambda_{max}^{Abs}, P_M, P_E, P_M - P_E = A_0 + \frac{A_1 - A_0}{1 + e^{\frac{pH - pK_a}{dpH}}} \quad \text{Equation 7.4}$$

This fitting allowed the estimation of the pK_a of the PAAMePy polymers.

The pK_a of the coumarins (Chapter 5) was determined by first normalizing the absorbance values between 0 and 1. For instance, for 7H6MC (Scopoletin) that only shows the equilibrium (at the pH range investigated) between neutral and anionic form the K_a is given by Equation 7.5, Scheme 7.4.



Scheme 7.4. Scheme of the acid-base equilibrium of Scopoletin.

$$K_a = \frac{[L^-][H^+]}{[LH]} \Leftrightarrow [LH] = \frac{[L^-][H^+]}{K_a} \quad \text{Equation 7.5}$$

$$x_L = \frac{[L^-]}{[LH] + [L^-]} \quad \text{Equation 7.6}$$

$$x_{LH} = \frac{[LH]}{[LH] + [L^-]} \quad \text{Equation 7.7}$$

$$x_{LH} + x_L = 1 \quad \text{Equation 7.8}$$

By merging Equation 7.5 to Equation 7.6 one obtain Equation 7.9 and Equation 7.10.

$$\begin{aligned} X_{LH} &= \frac{[LH]}{[LH] + [L^-]} = \frac{\frac{[L^-][H^+]}{K_a}}{\frac{[L^-][H^+]}{K_a} + [L^-]} = \frac{\frac{[L^-][H^+]}{K_a}}{\frac{[L^-][H^+] + [L^-]K_a}{K_a}} = \\ &= \frac{[L^-][H^+]K_a}{K_a([L^-][H^+] + [L^-]K_a)} = \frac{[L^-][H^+]}{[L^-]([H^+] + K_a)} = \frac{[H^+]}{[H^+] + K_a} = \frac{10^{-pH}}{10^{-pH} + K_a} \end{aligned} \quad \text{Equation 7.9}$$

Since the values were normalized, X_L is simply given by $1 - X_{LH}$. To obtain the K_a for this simple case (equilibrium between two species), it is only needed to choose the best K_a value (by iteration) to fit Equation 7.9 and Equation 7.10 to the experimental (normalized) data.

$$\begin{aligned} X_L &= \frac{[L^-]}{[LH] + [L^-]} = \frac{[L^-]}{\frac{[L^-][H^+]}{K_a} + [L^-]} = \frac{[L^-]}{\frac{[L^-][H^+] + [L^-]K_a}{K_a}} \\ &= \frac{[L^-]K_a}{[L^-][H^+] + [L^-]K_a} = \frac{[L^-]K_a}{[L^-]([H^+] + K_a)} = \frac{K_a}{[H^+] + K_a} = \frac{K_a}{10^{-pH} + K_a} \end{aligned} \quad \text{Equation 7.10}$$

When in the presence of a diprotic acid, such as the 4-methylesculetin, 2 equilibria are present: $LH_2 \rightleftharpoons LH + H$ and $LH \rightleftharpoons L + H$ and the K_a 's are the given with Equation 7.12 to Equation 7.14.

$$x_{LH_2} + x_{LH} + x_L = 1 \quad \text{Equation 7.11}$$

$$x_{LH_2} = \frac{[LH_2]}{[LH_2] + [LH] + [L^-]} = \frac{[H^+]^2}{[H^+]^2 + K_{a_1}[H^+] + K_{a_1}K_{a_2}} \quad \text{Equation 7.12}$$

$$x_{LH} = \frac{[LH]}{[LH_2] + [LH] + [L^-]} = \frac{K_{a_1}[H^+]}{[H^+]^2 + K_{a_1}[H^+] + K_{a_1}K_{a_2}} \quad \text{Equation 7.13}$$

$$x_L = \frac{[L]}{[LH_2] + [LH] + [L^-]} = \frac{K_{a_1}K_{a_2}}{[H^+]^2 + K_{a_1}[H^+] + K_{a_1}K_{a_2}} \quad \text{Equation 7.14}$$

7.2.6. Fluorescence

7.2.6.1. Steady-State Fluorescence

In this work, the fluorescence emission and excitation spectra were obtained with two different spectrofluorometre models: Fluorolog 3-22 and Fluoromax 4. However, the two equipments way of operating is identical and will be resumed briefly in the next paragraph.

The light source (a xenon lamp of 150 W or 450 W) emits a continuous and constant flow of photons to allow the measurement of the fluorescence emission by the detector, since the emission of fluorescence is very fast ($\sim 10^{-9}$ s). The beam of radiation is divided in two beams which work together to decrease the noise created from radiant power fluctuations. The upper beam is passed through the sample while the lower beam is passed through an attenuator and adjusted to try and match the fluorescent power given from the sample. Before reaching the sample, the upper beam of light is filtered by an excitation spectrometer (monochromator, filter and mirrors) that allows a single wavelength of radiation reach the sample. In the sample compartment, the sample responds to the incoming radiation. The resulting radiation is filtered by an emission spectrometer that feeds the signal to a photomultiplier detector (PMT). The PMT is at 90° of the excitation source to reduce the stray light from the beam. The radiation from the fluorescence of the sample and the lower attenuated beam are detected by separate transducers and converted to an electrical signal that is interpreted by a computer system.

On one hand, a fluorescence emission spectrum is produced by fixing the excitation wavelength (at the desired $\lambda_{exc.}$) and stepping the emission spectrometer through a wavelength region, and recording the variation in intensity as a function of the wavelength. On the other hand, an excitation spectrum is obtained by varying the excitation wavelengths and fixing the emission wavelength (at the desired $\lambda_{em.}$).

The schematic representation of a typical fluorometre and photographs of the models used are presented in Figure 7.8.

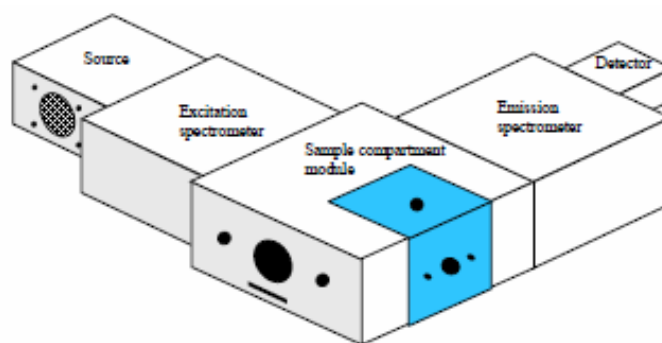


Figure 7.8. Schematic representation of a fluorometre with one detector.²⁶⁵

In Fluorolog 3-22, it is possible to adapt another source of excitation and/or detector. This can be made by assembling, another detector such as for the infrared (IR) region. In relation to the source, it was often used a pulsed lamp to make emission and excitation phosphorescence spectra. To do that the source can be substituted or present in the same housing.

The phosphorescent lifetimes could be measured in Fluorolog 3-22 by changing the source since the decay times are typically 10^{-3} s.

The fluorescence spectra were recorded with a Horiba-Jobin-Ivon SPEX Fluorolog 3-22 or Fluoromax 4 spectrometers and were corrected for the instrumental response. The modular spectrofluorometre Horiba-Jobin-Ivon SPEX Fluorolog 3-22 has double grating excitation and emission monochromators. The bandpass for excitation and emission is 0–15 nm and the wavelength accuracy is of ± 0.5 nm. The excitation source consists in an ozone-free 450 W Xenon lamp and the emission detector is an Hamamatsu R928 Photomultiplier (200–900 nm range), cooled with a Products for Research thermoelectric refrigerated chamber (model PC177CE005), or a Hamamatsu R5509-42 (900–1400 nm range), cooled to 193 K in a liquid nitrogen chamber (Products for Research model PC176TSCE-005), and a photodiode as the reference detector. The Fluoromax has single grating excitation and emission monochromators.

The slits, integration time, excitation and emission wavelengths were chosen in accordance to the molecule properties in question and the condition of the lamp. For example, for PAAMePy using Fluoromax-4, the excitation and emission monochromators were set at 0.3 mm, giving a spectral bandwidth of 1.275 nm. The data interval was 0.5 nm and the integration time was 0.5 seconds.



Picture 7.2. From left to right. Pictures of the Horiba-Jobin-Yvon SPEX Fluorolog 3-22 and Fluoromox-4 spectrofluorimetres used in these work.

7.2.6.1.1. Fluorescence Quantum Yield (Φ_F) Determination

The fluorescence quantum yield was obtained with a chosen reference depending on the absorption spectrum and emission intensity of the molecule. Between the references used in this work are quinine sulphate in $[H_2SO_4]=0.5\text{ M}$ or in $[H_2SO_4]=0.05\text{ M}$ ($\Phi_F=0.55$ and 0.53 , respectively)³⁵ and α_i ($i=3$) in ethanol ($\Phi_F=0.054$).

The fluorescence quantum yield of a compound can be obtained preparing, at least, two solutions: one (i) of the compound which quantum yield needs to be determined and the other (ii) of the standard with the same absorption at one wavelength (at least). This/these wavelength(s) will be used to excite both samples to obtain the fluorescence emission spectra. These spectra will be then integrated and used in Equation 2.4. The fluorescence quantum yields were measured with deaerated solutions and typically with at least 2 different references.

$$\phi_F^T = \phi_F^{ref.} \cdot \frac{I_F^{cp.} \cdot n_{cp.}^2}{I_F^{ref.} \cdot n_{ref.}^2} = \phi_F^{ref.} \cdot \frac{\int I_{cp.}(\lambda) d\lambda \cdot n_{cp.}^2}{\int I_{ref.}(\lambda) d\lambda \cdot n_{ref.}^2} \quad \text{Equation 7.15}$$

Where ϕ_F^T is the total quantum yield (when in presence of more than one species), I_F is the integrated fluorescence emission intensity (*i.e.* the area of the fluorescence emission spectra, $\int I(\lambda) d\lambda$), n is the refractive index of the solvent where the compounds are dissolved and the subscripts *ref.*, *cp.* and *F* refers to reference, compound and fluorescence, respectively.

For some compounds, such as the bichromophoric oligomers, PAAMePy, PNIPAMPy or some coumarins that possess more than one species in the excited state, the calculation of the fluorescence quantum yields was determined using references. For instance, the fluorescence quantum yield of the excimer (ϕ_F^E) is given by the Equation 2.5.

$$\phi_F^E = \frac{\phi_{F,ap.}^E}{1 - \frac{\phi_{F,ap.}^M}{\phi_F^M}} \quad \text{Equation 7.16}$$

In Equation 7.16, $\phi_{F,ap.}^E$ and $\phi_{F,ap.}^M$ are the apparent fluorescence quantum yields of the excimer and monomer, respectively and where (ϕ_F^M) is the monomer fluorescence quantum yield of the reference compound (preferably, the same compound with only a pyrene unit) where $\phi_F^M + \phi_F^E = \phi_F^T$.

7.2.6.1.2. Spectrofluorimetric Titrations

7.2.6.1.2.1. I_E/I_M Determination

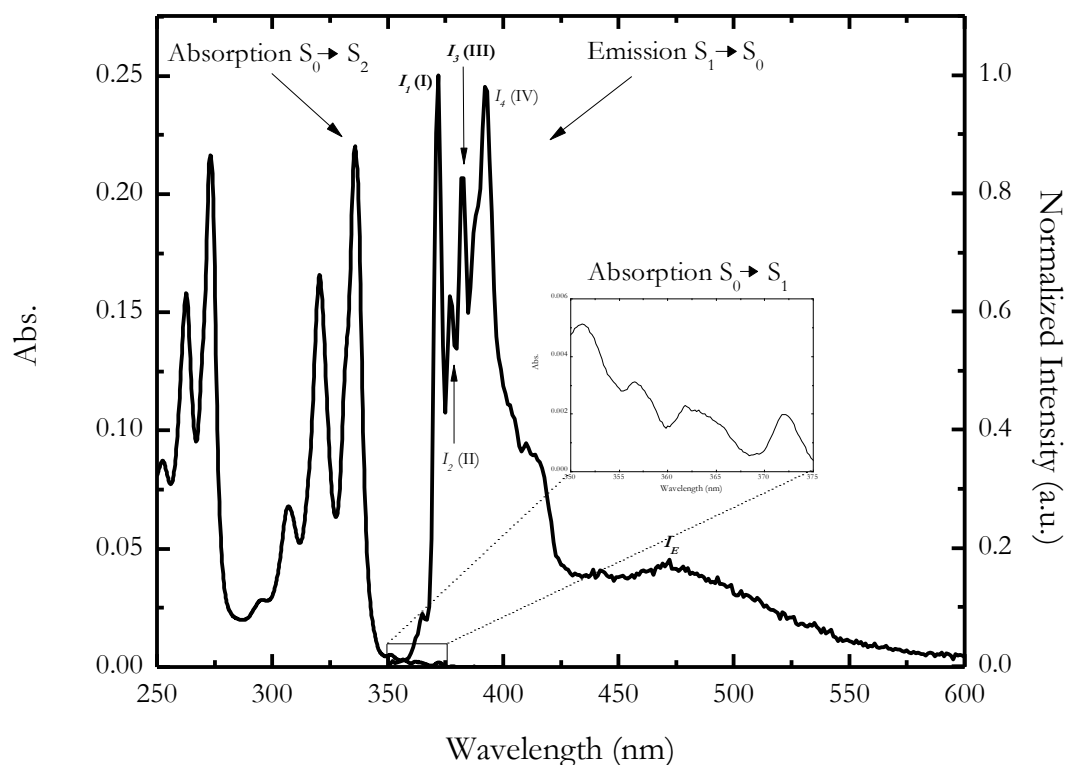


Figure 7.9. Normalized emission spectra of Pyrene in dioxane; [Py]= 8×10^{-4} M, $\lambda_{exc.} = 316$ nm. Illustrations of I_1 , I_2 , I_3 , I_4 and I_E .

There are different manners for obtaining the monomer and excimer intensity ratio. One is to take the maximum intensity on the desired band or the intensities at a fixed wavelength (in the monomer – 376 nm for example- and excimer – 480 nm for example- emission, respectively) and another is to integrate these bands. The determination of the integrated ratio band implies to obtain the emission of the monomer (at concentrations where there is no excimer for intermolecular excimer or of a parent –

similar compound without the possibility to form excimer), normalize both (compound and parent) spectra and subtract the parent spectra from the compound to obtain both isolated emission of the monomer and excimer (and calculate the areas) for the compound. Another way, is to fit directly the excimer band with a curve such as Gauss (Equation 7.17), Bigaussian (Equation 7.18) or GaussMod (Equation 7.19), subtract the total spectra to the fitting of the excimer band and integrate both areas (subtraction and fitting of the excimer band). In order to do that, the xx axis must be first converted from wavelength to frequency (Equation 1.1). However, in this work this procedure was not made because the fitting were quite good in wavelengths.

$$I_F = I_{F_0} + \left(A / w \times \sqrt{\pi/2} \right) \times e^{-2((v-v_c)/w)^2} \quad \text{Equation 7.17}$$

$$I_F = I_{F_0} + H \exp \left[-0.5 \left(\frac{v-v_c}{w_1} \right)^2 \right] \quad (v < v_c) \quad \text{Equation 7.18}$$

$$I_F = I_{F_0} + H \exp \left[-0.5 \left(\frac{v-v_c}{w_2} \right)^2 \right] \quad (v \geq v_c)$$

$$\text{double } z = (v - v_c) / w - w / t_0$$

$$I_F = I_{F_0} + A / t_0 \times \exp \left[\left(0.5 \times (w / t_0)^2 - (v - v_c) / t_0 \right) \times \frac{1}{\sqrt{\pi}} \int_{-\infty}^z \frac{1}{\sqrt{2\pi}} \exp \left(-\frac{y^2}{2} \right) dy \right] \quad \text{Equation 7.19}$$

$$y = I_{F_0} + (f_1 \times f_2)(v); f_1(v) = \frac{A}{t_0} \exp \left(-\frac{v}{t_0} \right); f_2(v) = \frac{1}{\sqrt{2\pi}w} \exp -\frac{(v - v_c)^2}{2w}$$

Where I_{F_0} is the offset (in Equation 7.17 and Equation 7.19) and base (in Equation 7.18), A the area (in Equation 7.17) and the amplitude (in Equation 7.19), w the width, v_c is the center (in frequency units preferably), H the height, w_1 and w_2 are the widths from the left and the right side of the Bigaussian curve and t_0 is an unknown.

In this work, all these methods were compared.

7.2.6.1.2.2. I_1/I_3 Determination

I_1/I_3 is given by the ratio of intensities of vibronic bands I and III , respectively. In some circumstances, the I_2 was not visible which could lead to make the I_1/I_4 ratio instead. As can be seen in Figure 3.11 in Chapter 3, I_3 is around 380 nm, so even when I_2 was not visible, the I_3 was always considered to be the peak around 380 nm and, for that, it has always been correctly taken.

7.2.6.1.2.3. $P_M \cdot P_E$ Determination

In this work, P_M and P_E were obtained from the excitation spectra collected at 375 nm and 520 nm, respectively, but others emission wavelengths from the monomer and excimer bands could have been used. $P_M \cdot P_E$ consists on calculating the differences between P_M and P_E .

Beside these parameters, the normalized intensity of the excimer can be plotted in function on the normalized monomer intensity.

As can be seen, the P_M-P_E is easier to read and interpret and also quicker to represent than the normalized intensities. In this work, P_M-P_E was represented instead of the normalized intensities.

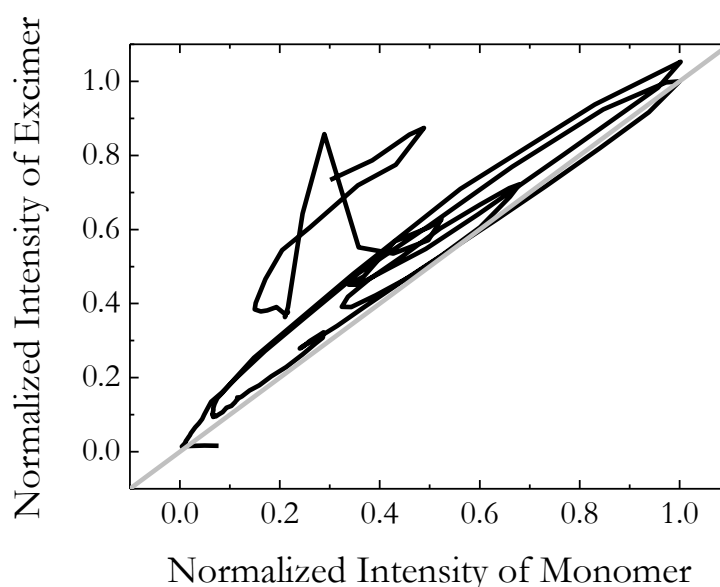


Figure 7.10. Representation of the normalized intensity of the excimer ($\lambda_{em}= 520$ nm) vs. the normalized intensity of the monomer ($\lambda_{em}= 375$ nm) of a PAAMePy in methanol, at 293 K.

7.2.6.2. Time-Resolved Fluorescence

The method employed is known as time-correlated single photon counting (TCSPC), and is based on the repetitive and precise time registration of single photons of, in this case, a fluorescence signal. The reference for the timing is the corresponding excitation pulse. If the probability of registering more than one photon per cycle being is low, the histogram of photon arrivals per time must give the correct lifetimes. This can (and should) be achieved attenuating the light level at the sample if necessary.

The light pulses are directed to the sample cuvette, a filter is used to attenuate the light levels to meet the precondition of single photon statistics at the detector. Upon excitation, the fluorescent sample will emit radiation at a longer wavelength than that of the excitation. An optical cut-off filter can be used to filter the fluorescent signal from scattered excitation. Then it is directed to the photon detector, again possibly via some appropriate collection optics (e.g. lens). The electrical signal obtained from the detector is fed to a pre-amplifier and then to the TCSPC electronics. The laser driver also provides the electric sync necessary for the photon arrival time measurement, Figure 7.12.

Time-resolved (TR) measurements were just made when an appropriate standard for the time scale and excitation wavelength was measured and showed to be mono exponential with good autocorrelation function, chi square and residues.

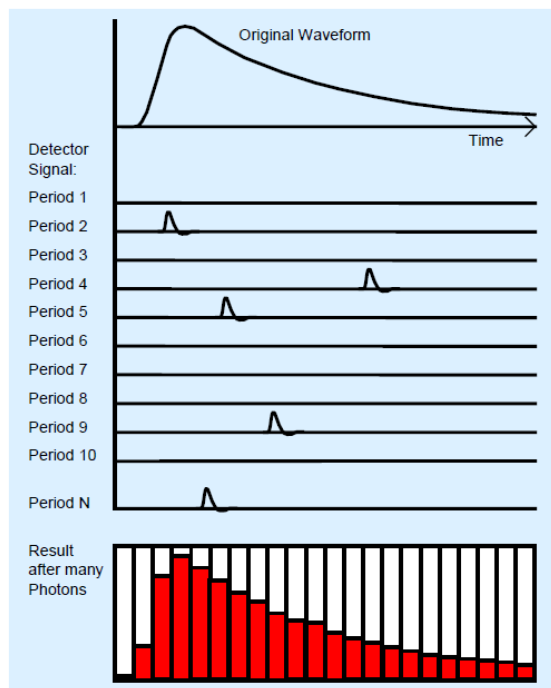


Figure 7.11. The TCSPC measurement principle. Fluorescence lifetime histogram: exponential decay.

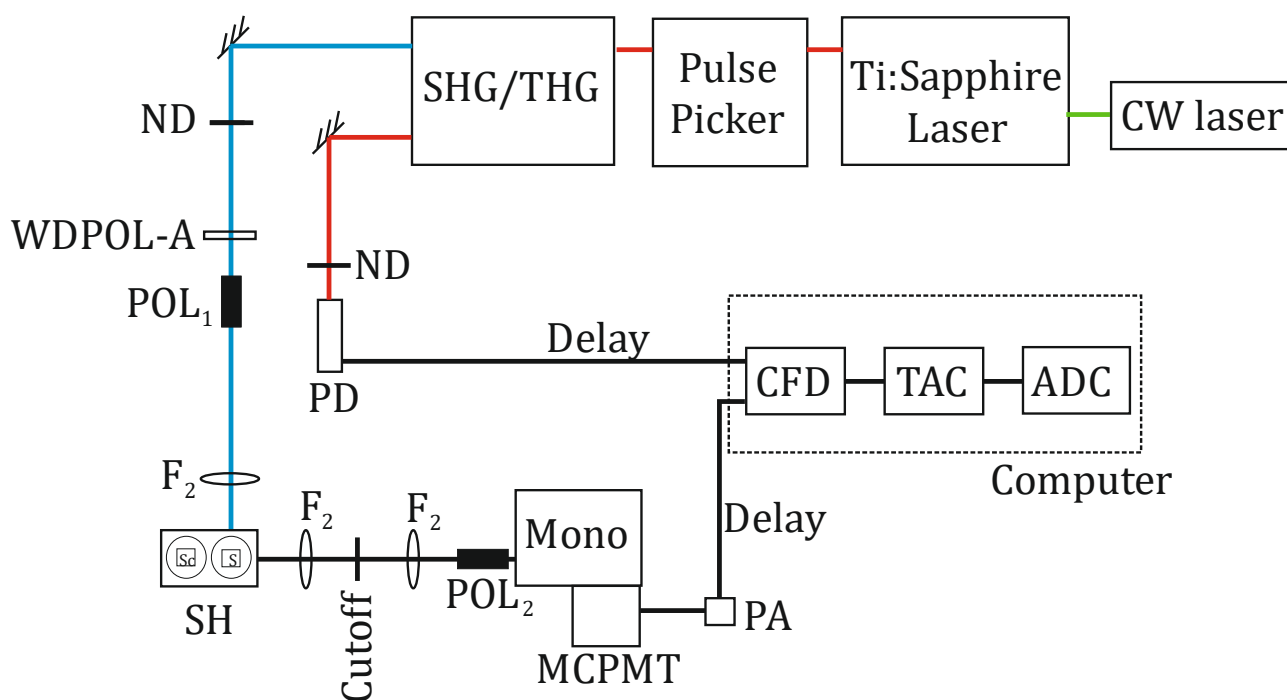


Figure 7.12. Time correlated single photon counting experimental setup: SHG/THG, second and third harmonic generator; ND, neutral density filter; WDPOL-A, depolariser; POL₁, vertically aligned polariser; POL₂, polariser at magic angle; F₂, lenses; PD, photodiode; Mono, monochromator; MCPMT, microchannel plate photomultiplier; PA, pre-amplifier; CFD, constant fraction discriminators; TAC, time-to-pulse height converter; ADC, analog-to-digital signal converter; S, sample; Sc, scatter. Adapted from ref. ³¹.

TR showed to be difficult to obtain because of the long acquisition time and scatter (particularly for PAAMePy polymers), or/and because of the low fluorescence quantum yield (chemosensors **P** and **L**) or fluorescence at the collected emission wavelength (as 520 nm for PAAMePy polymers).

It had to be made a compromise to obtain enough counts to such complex systems and with the time of acquisition would be enough to overrule precipitation, presence of oxygen, *etc.* Typically 5000 counts for each wavelength show to be enough for PAAMePy polymers.

To avoid scattering effects of these samples, the sample were previously filtered, appropriate cuvettes were slightly changed to remove oxygen, the shiny part of the slits were covered with tape to avoid reflections, the external light was minimized covering all equipment with black rags (for ns-TCSPC).

The emission for Py derivatives was monitored at 375, 480 and 520 nm using a cut-off filter at 360 nm (L38). The fluorescence decays and the instrumental response function (IRF) were collected using 1024 channels using different time scale ratio (from 52.1 to 342 ps/ch), until typically $2-5 \times 10^3$ counts at the maximum were reached. A Ludox solution was used at the excitation wavelength to obtain the instrumental response function which was convoluted with the desired theoretical function for the decay analysis. The full width at half-maximum (FWHM) of the IRF was about 0.98 ns and was highly

reproducible with identical system parameters. The fluorescence decays were analysed using the modulating functions method implemented (SAND program) of G. Striker.^{266,267}

To eliminate the light quantity of dispersed light filters (L38 or GG400) were often used after the sample holder and before the emission monochromator.

7.2.6.2.1. With Nanosecond Time Resolution

Fluorescence decays with nanosecond time-resolution were measured using a home-built Time-Correlated Single Photon Counting (TCSPC) apparatus,^{37,268} with an Horiba-JI-IBH NanoLED as excitation source, ($\lambda_{exc.} = 282, 311, 339, 373$ or 450 nm). Briefly, the apparatus consists of Jobin-Ivon H20 excitation and emission monochromators, a Philips XP2020Q photomultiplier, and a time-to-amplitude converter (2145), Multichannel Analyser (AccuSpec) and START and STOP discriminators (2126) from Canberra instruments. Alternate measurements, controlled by Decays software (Biodinâmica-Portugal) of the pulse profile and the sample emission were performed. A more detailed description of the equipment with drawings of the different components as well as decays of typical aromatic hydrocarbons (including pyrene) can be found in detail in ref. ³⁷.



Figure 7.13. Picture of the ns-TCSPC apparatus used in this work.

Time-resolved (TR) fluorescence measurements were performed using a home-built picosecond TCSPC apparatus elsewhere described²⁶⁹ except that as excitation source, a Horiba-JI-IBH NanoLED, $\lambda_{exc} = 339$ nm, was used. The full width at half-maximum (FWHM) of the IRF was about 0.98 ns and was highly reproducible with identical system parameters.

7.2.6.2.2. With Picosecond Time Resolution

Fluorescence decays with picosecond time-resolution were measured using a home-built TCSPC apparatus. The excitation source consists in either a picosecond Spectra Physics mode-lock Tsunami® Laser /Ti:Sapphire) Model 3950 (repetition rate about 82 MHz, tuning range 700-1000 nm), pumped by a Millennia® Pro-10s, frequency-doubled continuous wave (CW), diode-pumped, solid-state laser ($\lambda_{em}= 532$ nm) or the previously referred NanoLED. In the case of the use of the laser, a harmonic generator model GWU-23PS (Spectra Physics) is used to produce the second and third harmonic from the Ti:Sapphire laser exciting beam frequency output. The samples were measured with excitation at 395 nm and the horizontally polarized output beam from the GWU (second harmonic) was first passed through a ThorLabs depolarizer (WDPOL-A) and after by a Glan-Thompson polarizer (Newport 10GT04) with vertical polarization.

7.2.6.2.3. Fluorescence Decay Analysis

Sandbox is the software system used for analysis of TR fluorescence experiments for the discrete sum of exponentials (Section 2.1.1). The analysis makes uses of the improved modulating functions method (requiring no initial guess) which is then refined using a nonlinear least-squares analysis. The Quality of the fit is evaluated by the χ^2 value, weighted residuals, and autocorrelation function. The sandbox includes a facility to correct for possible scatter light.

When using the MEM method (Section 3.3) the lifetime windows contained 200 discrete, exponentially spaced cells from 1 to 500 ns.

7.2.7. Phosphorescence

Phosphorescence experiments were performed with a quartz NMR-like (EPR) tube. Due to the smaller l , an absorbance of ~ 0.3 (checked with a 1 cm length cuvette) was used in contrast to the ~ 0.1 used in fluorescence experiments. This tube was put inside a Dewar (fixed to the equipment with an appropriate holder) filled up with liquid nitrogen. During the experiment, the liquid nitrogen level was checked.

7.2.7.1. Steady-State and Time-resolved Phosphorescence

Phosphorescence measurements were recorded with a Horiba-Jobin-Ivon SPEX Fluorolog 3-2.2 spectrometer equipped with a 1934 D Phosphorimeter unit and a 150 W pulsed Xenon lamp. The phosphorescence spectra were corrected for the wavelength response of the system. The slits, integration time, excitation and emission wavelengths were defined according to the system under investigation.

7.3. Theoretical studies

7.3.1. Molecular Dynamics

Molecular dynamics (MD) studies were performed resorting to the Gromacs package, version 4.5.5^{270,271} employing the GROMOS 53a6 force field.²⁷² In order to inspect the behaviour of an oligomer with the structural properties of the PAAMePy polymer. The structures were drawn and equilibrated in Avogadro and their topologies generated by the automated force field topology builder (ATB) server.²⁷³

Four systems (oligomers with 8 monomers) with pyrene units in different positions were considered, with pyrene units at positions 2 and 7, 3 and 6, 4 and 5 and 7 and 8. In each case, the solute molecules were enclosed in a cubic box, of appropriate size with the necessary water molecules. The solvent was considered explicitly using the SPC216 water model. All the calculations were carried out in the NPT ensemble and under periodic boundary conditions, at a temperature of 298 K and a pressure of 1.0 bar coupled, respectively, to v-rescale and Berendsen external baths. A standard time step of 2 fs was used for both equilibration and production runs. Nonbonded interactions were computed on the basis of a neighbour list, updated every 10 steps. The long range electrostatic interactions were computed using the particle mesh Ewald method.²⁷⁴ For the Lennard-Jones energies, a cut-off of 1.2 nm was applied. Each system was firstly subjected to an energy minimization step and then to a production run of 100 ns using the LINCS algorithm.²⁷⁰ The first 40 ns were considered sufficient to achieve equilibration. MD trajectories were visualized, and configuration images extracted using the VMD 1.9 software.²⁷⁵

The conformation of each oligomer in water was analysed resorting to a geometric cluster analysis. The goal is to identify similar structures sampled during the MD simulation and evaluate their prevalence. The analysis was performed using a clustering algorithm²⁷⁶ which is based on the mutual root-mean-square deviations (RMSD) between all conformations sampled during the production run, being each cluster mutually exclusive. The cut-off considered was 0.4 nm.

Chapter 8

References

- (1) Rohatgi-Mukherjee, K. K. *Fundamentals of Photochemistry*; New Age International Limited, 1978.
- (2) Bozzelli, J. W.; Kemp, M. A Fluorescence Lecture Demonstration. *Test. Demonstr.* **1982**, 59 (9), 787–788.
- (3) Cristopher Jobson. Underwater Experiments: Astounding Photographs of Jellyfish by Alexander Semenov | Colossal <http://www.thisiscolossal.com/2012/01/underwater-experiments-astounding-photographs-of-jellyfish-by-alexander-semenov/> (accessed Sep 16, 2015).
- (4) Mushroom lights up the night in Brazil: Researcher finds bioluminescent fungus not seen since 1840 <http://phys.org/news/2011-07-mushroom-night-brazil-bioluminescent-fungus.html> (accessed Sep 16, 2015).
- (5) How to Make Your Own Homemade Glow Sticks «Science Experiments <http://science.wonderhowto.com/how-to/make-your-own-homemade-glow-sticks-0146580/> (accessed Sep 17, 2015).
- (6) Firefly.org | Firefly & Lightning Bug Facts, Pictures, Information About Firefly Insect Disappearance <http://www.firefly.org/> (accessed Sep 17, 2015).
- (7) bioluminescence - Reef Central Online Community <http://www.reefcentral.com/forums/showthread.php?t=1517269> (accessed Sep 17, 2015).
- (8) The Cookiecutter Shark | Deep Dwelling Sharks <http://2012.extrememarine.org.uk/deepdwellers/dogfish-sharks/the-cookiecutter-shark/index.html> (accessed Sep 17, 2015).
- (9) UV Black Fluorescent Tube Currency Detector Machine EURO , 220V - 230V 50Hz <http://www.counterfeit-moneydetector.com/sale-1867821-uv-black-fluorescent-tube-currency-detector-machine-euro-220v-230v-50hz.html> (accessed Sep 17, 2015).
- (10) Creatures of the deep - Sea Stoke MagazineSea Stoke Magazine <http://seastoke.com/issue/issue-one/article/creatures-of-the-deep/> (accessed Sep 17, 2015).
- (11) Kim, E. Fujifilm FinePix x100 Sample Photos Live! <http://erickimphotography.com/blog/2011/02/10/fujifilm-finepix-x100-sample-photos-live/> (accessed Sep 17, 2015).
- (12) Photoluminescent EXIT 30cm <http://www.phosphorescentpaint.co.uk/photoluminescent-exit-sign/276-photoluminescent-exit-sign.html> (accessed Sep 17, 2015).

References

- (13) Refractive surgery and Excimer laser | Instituto Oftalmológico Amigó <http://www.ioamigo.com/en/service/refractive-surgery-excimer-laser/> (accessed Sep 17, 2015).
- (14) Challenges in Creating Artificial Photosynthesis - HowStuffWorks <http://science.howstuffworks.com/environmental/green-tech/energy-production/artificial-photosynthesis3.htm> (accessed Sep 17, 2015).
- (15) Imagining their world: Images and ESL Students | Karen's Comments <http://www.coetail.com/kjwilson/2013/09/25/imagining-their-world-images-and-esl-students/> (accessed Sep 17, 2015).
- (16) Optical brightener - Wikipedia, the free encyclopedia https://en.wikipedia.org/wiki/Optical_brightener (accessed Sep 17, 2015).
- (17) Solar Technology | SEIA <http://www.seia.org/policy/solar-technology> (accessed Sep 17, 2015).
- (18) Samsung UA32D4003 32" Multi-System LED TV 110 220 240 volts pal ntsc <http://www.220-electronics.com/samsung-ua32d4003-32-multi-system-led-tv.html> (accessed Sep 17, 2015).
- (19) California Startup, Tribogenics, Develops Smart Phone Sized Portable X-ray Machines | BespokeTC Blog <http://bespoketc.com/blog/?p=4196> (accessed Sep 17, 2015).
- (20) Schott, H. Densities, Refractive Indices, and Molar Refractions of the System Water-Dioxane at 25° C. *J. Chem. Eng. Data* **1961**, 6 (1), 19–20.
- (21) The electromagnetic spectrum | imagcwp journal on WordPress.com <https://imagcwp.wordpress.com/2013/01/30/the-electromagnetic-spectrum/> (accessed Sep 17, 2015).
- (22) Electromagnetic Spectrum <http://www2.lbl.gov/MicroWorlds/ALSTool/EMSpec/EMSpec2.html> (accessed Sep 17, 2015).
- (23) antenna - http://www.wpclipart.com/telephone/antenna_tower/antenna.png.html http://www.wpclipart.com/telephone/antenna_tower/antenna.png.html (accessed Sep 17, 2015).
- (24) Amana RCS10TS 1000 Watt Microwave with Touchpad Controls <http://www.globeequipment.com/Commercial-Kitchen-Equipment/Cooking-Equipment/Microwave-Ovens/Rcs10ts> (accessed Sep 17, 2015).
- (25) Pentagon Equipment Disrupting Phone System. *Boca Rat. News* **1998**.
- (26) Bulb light PNG image, free picture download <http://pngimg.com/img/objects/bulb> (accessed Sep 17, 2015).
- (27) - X-Ray Recycling Services - <http://www.boscodigital.com/x-ray-recycling/> (accessed Sep 17, 2015).
- (28) CAUTION - RADIOACTIVE MATERIALS - Incom Direct - Incom Direct <http://incomdirect.com/caution-radioactive-materials/> (accessed Sep 17, 2015).
- (29) Reflection, Transmission and Absorption – Definitions and Measurements <http://www.azooptics.com/Article.aspx?ArticleID=767> (accessed Feb 18, 2016).
- (30) Turro, N. J. *Modern Molecular Photochemistry*; University Science Books: Sausalito, California, 1991.

References

- (31) Seixas de Melo, J. S.; Pina, J.; Dias, F. B.; Maçanita, A. L. Experimental Techniques for Excited State Characterisation. In *Applied Photochemistry*; Evans, R. C., Douglas, P., Burrows, H. D., Eds.; Springer, 2013; pp 533–585.
- (32) “Conjugation” The Key to Color of Organic Molecules <http://www.textiletuts.com/color-organic-molecules-conjugation/> (accessed Dec 10, 2015).
- (33) NPTEL :: Biotechnology - Bioanalytical Techniques and Bioinformatics <http://nptel.ac.in/courses/102103044/5> (accessed Sep 17, 2015).
- (34) Valeur, B. *Molecular Fluorescence. Principles and Applications*; Willey-VCR: Weinheim, 2002.
- (35) Montalti, M.; Credi, A.; Prodi, L.; Gandolfi, M. T. *Handbook of Photochemistry*; Taylor and Francis, 2006.
- (36) Wardle, B. *Principles and Applications of Photochemistry*; Wiley, 2009.
- (37) Seixas de Melo, J. S. The Influence of Oxygen on the Lifetime of Luminescent Probes. A Simple Device for Degassing Solutions for Fluorescence Measurements . *Chem . Educ.* **2005**, *10*, 29–35.
- (38) Birks, J. B. *Photophysics of Aromatic Molecules*; Wiley: London, 1970.
- (39) Birks, J. B. The Spectroscopy of the Pi-Electronic States of Aromatic Hydrocarbons. In *Organic Molecular Photophysics*; Birks, J. B., McGlynn, S. P., Eds.; Wiley: Bristol, 1973; Vol. 1, pp 1–55.
- (40) Birks, J. B. Excimers. *Reports Prog. Phys.* **1975**, *38* (8), 903–974.
- (41) Birks, J. B.; Christophorou, L. G. Resonance Interactions of Fluorescent Organic Molecules in Solution. *Nature* **1962**, *4849*, 33.
- (42) Sinnokrot, M. O.; Sherrill, C. D. Substituent Effects in Pi-Pi Interactions: Sandwich and T-Shaped Configurations. *J. Am. Chem. Soc.* **2004**, *126* (24), 7690–7697.
- (43) Gonzalez, C.; Lim, E. C. Quantum Chemistry Study of the van Der Waals Dimers of Benzene, Naphthalene, and Anthracene: Crossed (D-2d) and Parallel-Displaced (C-2h) Dimers of Very Similar Energies in the Linear Polyacenes. *J. Phys. Chem. A* **2000**, *104* (13), 2953–2957.
- (44) Zachariasse, K. A.; Busse, R.; Duvneek, G.; Kuhnle, W. Intramolecular Monomer and Excimer Fluorescence with Dipyrenylpropanes - Double-Exponential Versus Triple-Exponential Decays. *J. Photochem.* **1985**, *28* (2), 237–253.
- (45) Tsuchida, A.; Ikawa, T.; Tomie, T.; Yamamoto, M. Intramolecular Pyrene Excimer Formation of 1,3-Dipyrenylpropanes with Full and Partial Ring Overlaps. *J. Phys. Chem.* **1995**, *99* (20), 8196–8199.
- (46) Zachariasse, K. A.; Duvneek, G.; Kuhnle, W.; Leinhos, U.; Reynders, P. Multicomponent Fluorescence Decay Analysis in Intramolecular Excimer Formation with Dipyrenylalkanes. In *Photophysical Processes in Organized Molecular Systems*; Honda, K., Ed.; Elsevier: Amsterdam, 1991; pp 83–100.
- (47) Zachariasse, K. A.; Duvneek, G.; Busse, R. Intramolecular Excimer Formation with 1,3-Di(1-Pyrenyl)Propane - Decay Parameters and Influence of Viscosity. *J. Am. Chem. Soc.* **1984**, *106* (4), 1045–1051.
- (48) Vandendriessche, J.; Palmans, P.; Toppet, S.; Boens, N.; Schryver, F. C.; Masuhara, H. Configurational and Conformational Aspects in the Excimer Formation in Bis(carbazoles). *J.*

References

- Am. Chem. Soc.* **1984**, *106* (26), 8057–8064.
- (49) Mahrt, J.; Willig, F.; Storck, W.; Weiss, D.; Kietzmann, R.; Schwarzburg, K.; Tufts, B.; Trosken, B. Luminescence and Configurations of Perylene Dimers in a Langmuir-Blodgett Film. *J. Phys. Chem.* **1994**, *98* (7), 1888–1894.
- (50) Akimoto, S.; Ohmori, A.; Yamazaki, I. Dimer Formation and Excitation Relaxation of Perylene in Langmuir-Blodgett Films. *J. Phys. Chem. B* **1997**, *101* (19), 3753–3758.
- (51) Seixas de Melo, J. S.; Costa, T.; de Castro, C. S.; Maçanita, A. L. Photophysics of Fluorescently Labeled Oligomers and Polymers. In *Photochemistry*; Albini, A., Ed.; The Royal Society of Chemistry, 2013; Vol. 40.
- (52) Podeszwa, R.; Szalewicz, K. Physical Origins of Interactions in Dimers of Polycyclic Aromatic Hydrocarbons. *Phys. Chem. Chem. Phys.* **2008**, *10* (19), 2735–2746.
- (53) Rampazzo, E.; Bonacchi, S.; Montalti, M.; Prodi, L.; Zaccheroni, N. Self-Organizing Core-Shell Nanostructures: Spontaneous Accumulation of Dye in the Core of Doped Silica Nanoparticles. *J. Am. Chem. Soc.* **2007**, *129*, 14251.
- (54) Sotero, P.; Arce, R. Surface and Adsorbates Effects on the Photochemistry and Photophysics of Adsorbed Perylene on Unactivated Silica Gel and Alumina. *J. Photochem. Photobiol. A Chem.* **2004**, *167*, 191.
- (55) Gago, S.; Costa, T.; Seixas de Melo, J.; Gonçalves, I. S.; Pillinger, M. Preparation and Photophysical Characterisation of Zn-Al Layered Double Hydroxides Intercalated by Anionic Pyrene Derivatives. *J. Mater. Chem.* **2008**, *18* (8), 894–904.
- (56) Hashimoto, S.; Uehara, K.; Sogawa, K.; Takadad, M.; Fukumurad, H. Application of Time- and Space-Resolved Fluorescence Spectroscopy to the Distribution of Guest Species into Micrometer-Sized Zeolite Crystals. *Phys. Chem. Chem. Phys.* **2006**, *8*, 1458.
- (57) Cheng, K. A. W. Y.; Schepp, N. P.; Cozens, F. L. Resolution of Ultrafast Pyrene Excimer Emission Rise Times in Zeolites X and Y. *Photochem. Photobiol.* **2006**, *82* (1), 132.
- (58) Cheng, K. A. W. Y.; Schepp, N. P.; Cozens, F. L. Ultrafast Dynamics of Pyrene Excimer Formation in Y Zeolites. *J. Phys. Chem. A* **2004**, *108* (35), 7132.
- (59) Seixas de Melo, J.; Costa, T.; Oliveira, N.; Schillén, K. Fluorescence Studies on the Interaction between Pyrene-Labelled Poly(acrylic Acid) and Cyclodextrins. *Polym. Int.* **2007**, *56* (7), 882–899.
- (60) Costa, T.; Seixas de Melo, J. The Effect of Gamma-Cyclodextrin Addition in the Self-Assembly Behavior of Pyrene Labeled Poly(acrylic) Acid with Different Chain Sizes. *J. Polym. Sci. Part A-Polymer Chem.* **2008**, *46* (4), 1402–1415.
- (61) Branco, T. J. F.; Ferreira, L. F. V.; Rego, A. M. B.; Oliveira, A. S.; Da Silva, J. P. Pyrene-p-Tert-Butylcalixarenes Inclusion Complexes Formation: A Surface Photochemistry Study. *Photochem. Photobiol. Sci.* **2006**, *5*, 1068.
- (62) Shiraishi, Y.; Ishizumi, K.; Nishimura, G.; Hirai, T. Effects of Metal Cation Coordination on Fluorescence Properties of a Diethylenetriamine Bearing Two End Pyrene Fragments. *J. Phys. Chem. B* **2007**, *111*, 8812.
- (63) Seixas de Melo, J.; Costa, T.; Miguel, M. D.; Lindman, B.; Schillén, K. Time-Resolved and Steady-State Fluorescence Studies of Hydrophobically Modified Water-Soluble Polymers. *J. Phys. Chem. B* **2003**, *107* (46), 12605–12621.

References

- (64) Costa, T.; de Melo, J. S. S.; Castro, C. S.; Gago, S.; Pillinger, M.; Goncalves, I. S. Picosecond Dynamics of Dimer Formation in a Pyrene Labeled Polymer. *J. Phys. Chem. B* **2010**, *114* (39), 12439–12447.
- (65) Seixas de Melo, J.; Costa, T.; Francisco, A.; Macanita, A. L.; Gago, S.; Goncalves, I. S. Dynamics of Short as Compared with Long Poly(acrylic Acid) Chains Hydrophobically Modified with Pyrene, as Followed by Fluorescence Techniques. *Phys. Chem. Chem. Phys.* **2007**, *9* (11), 1370–1385.
- (66) Winnik, F. M. Photophysics of Preassociated Pyrenes in Aqueous Polymer-Solutions and in Other Organized Media. *Chem. Rev.* **1993**, *93* (2), 587–614.
- (67) Stevens, B. Evidence for the Photoassociation of Aromatic Hydrocarbons in Fluid Media. *Nature* **1961**, *25* (4804), 725.
- (68) Maçanita, A. L.; Horta, A.; Pierola, I. F. Photophysics of Siloxanes - Influence of Preformed Dimers and Transition from Low-Temperature to High-Temperature Behavior of Dimeric and Polymeric Methylphenylsiloxane. *Macromolecules* **1994**, *27* (4), 958–963.
- (69) Zachariasse, K. A. Kinetics and Thermodynamics of Excimer Formation. Excited State Equilibria. *Trends Photochem. Photobiol.* **1994**, *3*, 211–227.
- (70) Stevens, B.; Ban, M. I. SPECTROPHOTOMETRIC DETERMINATION OF ENTHALPIES + ENTROPIES OF PHOTOASSOCIATION FOR DISSOLVED AROMATIC HYDROCARBONS. *Trans. Faraday Soc.* **1964**, *60* (5019), 1515–1523.
- (71) Ortiz, G. G.; Pacheco-Moisés, F.; El Hafidi, M.; Jiménez-Delgado, A.; Macías-Islas, M. A.; Rosales Corral, S. A.; Célis de la Rosa, A.; Sánchez-González, V. J.; Arias-Merino, E. D.; E., V.-B. I. Detection of Membrane Fluidity in Submitochondrial Particles of Platelets and Erythrocyte Membranes from Mexican Patients with Alzheimer Disease by Intramolecular Excimer Formation of 1,3 Dipyrenylpropane. *Dis. Markers* **2007**, *24* (3), 151–156.
- (72) Glushko, V.; Thaler, M. S. R.; Karp, C. D. Pyrene Fluorescence Fine Structure as a Polarity Probe of Hydrophobic Regions: Behavior in Model Solvents. *Arch. Biochem. Biophys.* **1981**, *210* (1), 33–42.
- (73) Dong, D. C.; Winnik, M. A. THE Py SCALE OF SOLVENT POLARITIES. SOLVENT EFFECTS ON THE VIBRONIC FINE STRUCTURE OF PYRENE FLUORESCENCE and EMPIRICAL CORRELATIONS WITH ET and Y VALUES. *Photochem. Photobiol.* **1982**, *35* (1), 17–21.
- (74) Reichardt, C. Solvatochromic Dyes as Solvent Polarity Indicators. *Chem. Rev.* **1994**, *94* (8), 2319–2358.
- (75) Kidd, J. Observations on Naphthalene, a Peculiar Substance Resembling a Concrete Essential Oil, Which Is Produced during the Decomposition of Coal Tar, by Exposure to a Red Heat. *Philos. Trans.* **1821**, *111*, 209–221.
- (76) Erlenmeyer, E. Studien Über Die S. G. Aromatischen Säuren. *Ann. der Chemie und Pharm.* **1866**, *137* (3), 327–359.
- (77) Olson, R. ; Oró, J.; Zlatkis, A. Organic Compounds in meteorites—II Aromatic Hydrocarbons. *Geochim. Cosmochim. Acta* **1967**, *31* (10), 1935–1948.
- (78) Berlman, I. B. *Handbook of Fluorescence Spectra of Aromatic Molecules*; Academic Press: N.Y., 1971.
- (79) Bamberger, E.; Philip, M. No Title. *Justus Liebigs Ann. Chem.* **1887**, *240*, 147–192.

References

- (80) Gräbe, C. No Title. *Justus Liebigs Ann. Chem.* **1871**, 158, 285–299.
- (81) Goldschmiedt, G. No Title. *Justus Liebigs Ann. Chem.* **1907**, 351, 218–232.
- (82) Figueira-Duarte, T. M.; Müllen, K. No Title. *Chem. Rev.* **2011**, 111, 7260–7314.
- (83) Hansen, H. K.; Riverol, C.; Acree, W. E. Solubilities of Anthracene, Fluoranthene and Pyrene in Organic Solvents: Comparison of Calculated Values Using UNIFAC and Modified UNIFAC (Dortmund) Models with Experimental Data and Values Using the Mobile Order Theory. *Can. J. Chem. Eng.* **2000**, 78 (6), 1168–1174.
- (84) Delouis, J. F.; Delaire, J. A.; Ivanoff, N. Pyrene Fluorescence Quenching and Triplet-State Formation in the Presence of DABCO (1,4-Diazabicyclo[2-2-2]octane): A Laser Photolysis Study. *Chem. Phys. Lett.* **1979**, 61 (2), 343–346.
- (85) Bains, G.; Patel, A. B.; Narayanaswami, V. Pyrene: A Probe to Study Protein Conformation and Conformational Changes. *Molecules* **2011**, 16 (9), 7909–7935.
- (86) Lehrer, S. Pyrene Excimer Fluorescence as a Probe of Protein Conformational Change. In *Proteins: Structure, Function, and Engineering*; Biswas, B. B., Roy, S., Eds.; Springer US, 1995; Vol. 24, pp 115–132.
- (87) Uglea, C. V.; Negulescu, I. I. *Synthesis and Characterization of Oligomers*; CRC Press, 1991.
- (88) Schryver, F. C.; Collart, P.; Vandendriessche, J.; Goedeweck, R.; Swinnen, A.; van der Auweraer, M. Intramolecular Excimer Formation in Bichromophoric Molecules Linked by a Short Flexible Chain. *Acc. Chem. Res.* **1987**, 20 (5), 159–166.
- (89) Zachariasse, K. A.; Macanita, A. L.; Kuhnle, W. Chain Length Dependence of Intramolecular Excimer Formation with 1,n-bis(1-Pyrenylcarboxy)alkanes for n=1-16, 22, and 32. *J. Phys. Chem. B* **1999**, 103 (43), 9356–9365.
- (90) Bernardo, M. A.; Alves, S.; Pina, F.; De Melo, J. S.; Albelda, M. T.; Garcia-Espana, E.; Llinares, J. M.; Soriano, C.; Luis, S. V. Polyamine Linear Chains Bearing Two Identical Terminal Aromatic Units. Evidence for a Photo Induced Bending Movement. *Supramol. Chem.* **2001**, 13 (3), 435–445.
- (91) Zachariasse, K. A.; Duvencek, G.; Kuhnle, W.; Reynders, P.; Striker, G. The Kinetic-Parameters for Intramolecular Excimer Formation from the Meso and Racemic Diastereoisomers of 2,4-Di(2-Pyrenyl) Pentane - Evidence for Rapid Conformer Interconversion. *Chem. Phys. Lett.* **1987**, 133 (5), 390–398.
- (92) Chandross, E. A.; Dempster, C. J. Intramolecular Excimer Formation and Fluorescence Quenching in Dinaphthylalkanes. *J. Am. Chem. Soc.* **1970**, 92 (12), 3586–3593.
- (93) Zachariasse, K. A.; Kuhnle, W.; Weller, A. Intramolecular Excimer Formation with Non-Planar Molecules: 1,3-Dibiphenylpropane. Kinetic and Thermodynamic Results. *Chem. Phys. Lett.* **1978**, 59 (3), 375–380.
- (94) Eaton, D. F.; Smart, B. E. Are Fluorocarbon Chains Stiffer than Hydrocarbon Chains? Dynamics of End-to-End Cyclization in a C₈F₁₆ Segment Monitored by Fluorescence. *J. Am. Chem. Soc.* **1990**, 112 (7), 2821–2823.
- (95) Declercq, D.; Delbeke, P.; Deschryver, F. C.; Vanmeervelt, L.; Miller, R. D. Ground-State and Excited-State Interaction in Di-1-Pyrenyl-Substituted Oligosilanes. *J. Am. Chem. Soc.* **1993**, 115 (13), 5702–5708.
- (96) Viriot, M. L.; Bouchy, M.; Donner, M.; Andre, J. C. Kinetics of Partly Diffusion Controlled

References

- Reactions. 12. Intramolecular Excimers as Fluorescent Probes of the Microviscosity of Living Cells. *Photobiochem. Photobiol.* **1983**, *5* (5), 293–306.
- (97) Ramírez-Iñiguez, A. L.; Ortiz, G. G.; El Hafidi, M.; Rincón-Sánchez, A. R.; Macías-Rodríguez, E.; Pacheco-Moisés, F. P. Accute Treatment of Constant Darkness Increases the Efficiency of ATP Synthase in Rat Liver Mitochondria. *Ann. Hepatol.* **2009**, *8* (4), 371–376.
- (98) Hirayama, F. Intramolecular Excimer Formation. I. Diphenyl and Triphenyl Alkanes. *J. Chem. Phys.* **1965**, *42* (9), 3163–3171.
- (99) Klopffer, W. Excimer and Monomer Fluorescence of 1,3-Biscarbazolyl Propane. *Chem. Phys. Lett.* **1969**, *4* (4), 193–194.
- (100) Kanaya, T.; Goshiki, K.; Yamamoto, M.; Nishijima, Y. INTRAMOLECULAR END-TO-END EXCIMER FORMATION OF BIS(1-PYRENYLMETHOXY)CARBONYL)ALKANES - A STUDY OF END-TO-END COLLISIONAL FREQUENCY ON A CHAIN MOLECULE. *J. Am. Chem. Soc.* **1982**, *104* (13), 3580–3587.
- (101) Reynders, P.; Kuhnle, W.; Zachariasse, K. A. Ground-State Dimers in Excimer-Forming Bichromophoric Molecules - Nmr and Single-Photon-Counting Data .2. Racemic and Meso Dipyrenylpentanes and Dipyrenylalkanes. *J. Phys. Chem.* **1990**, *94* (10), 4073–4082.
- (102) Benniston, A. C.; Harriman, A.; Lawrie, D. J.; Rostron, S. A. A Closely-Coupled Pyrene Dimer Having Unusually Intense Fluorescence. *European J. Org. Chem.* **2004**, *2004*, 2272–2276.
- (103) Maçanita, A. L.; Zachariasse, K. A. Viscosity Dependence of Intramolecular Excimer Formation with 1,5-Bis(1-Pyrenylcarboxy)pentane in Alkane Solvents as a Function of Temperature. *J. Phys. Chem. A* **2011**, *115* (15), 3183–3195.
- (104) Birley, A. W. *Polymer Science Dictionary*. Mark S. M. Alger, Elsevier Applied Science, London, 1989. Pp. Xii + 531, Price £98.00. ISBN 1-85 166-220-0. *Polym. Int.* **1991**, *24* (2), 127.
- (105) Lakowicz, J. R. *Principles of Fluorescence Spectroscopy*, 3rd ed.; Springer Science: New York, 2006.
- (106) Yadav, A.; Kurur, N. D.; Pandey, S. Intramolecular Excimer Formation Dynamics of 1,3-Bis-(1-Pyrenyl)propane within 1-Butyl-3-Methylimidazolium Hexafluorophosphate and Its Polyethylene Glycol Mixtures. *J. Phys. Chem. B* **2015**, *119* (42), 13367–13378.
- (107) Birks, J. B.; Dyson, D. J.; Munro, I. H. 'Excimer' Fluorescence. II. Lifetime Studies of Pyrene Solutions. *Proc. R. Soc. London. Ser. A. Math. Phys. Sci.* **1963**, *275* (1363), 575–588.
- (108) Duvencek, G. KINETISCHE UNTERSUCHUNGEN AN DIARYLALKANEN, 1986.
- (109) Rice, S. a.; Butler, P. R.; Pilling, M. J.; Baird, J. K. A Solution of the Debye–Smoluchowski Equation for the Rate of Reaction of Ions in Dilute Solution. *J. Chem. Phys.* **1979**, *70* (9), 4001.
- (110) Costa, T.; Seixas de Melo, J.; Burrows, H. D. Fluorescence Behavior of a Pyrene-End-Capped Poly(ethylene Oxide) in Organic Solvents and in Dioxane-Water Mixtures. *J. Phys. Chem. B* **2009**, *113*, 618–626.
- (111) Vasilescu, M.; Almgren, M.; Angelescu, D. On the Intramolecular Excimer Formation of 1,10-Bis(1-Pyrene)Decane in Organized Media. *J. Fluoresc.* **2000**, *10* (4), 339–346.
- (112) Zachariasse, K. A.; Striker, G. Three and Only Three Excited-State Species (One Monomer and Two Excimers) in 1,3-di(1-Pyrenyl)propane. *Chem. Phys. Lett.* **1988**, *145* (3), 251–254.
- (113) Zachariasse, K. A.; Duvencek, G.; Kuhnle, W. Double-Exponential Decay in Intramolecular

References

- Excimer Formation - 1,3-Di(2-Pyrenyl)Propane. *Chem. Phys. Lett.* **1985**, *113* (4), 337–343.
- (114) Geddes, J. A. The Fluidity of Dioxane-Water Mixtures. *J. Am. Chem. Soc.* **1933**, *55* (12), 4832–4837.
- (115) Hardy, R. C. Viscosity of N-Hexadecane. *J. Res. Natl. Bur. Stand. (1934)*. **1958**, *61* (5), 433–436.
- (116) Zachariasse, K. A.; Kuhnle, W.; Leinhos, U.; Reynders, P.; Striker, G. Time-Resolved Monomer and Excimer Fluorescence of 1,3-Di(1-Pyrenyl)Propane at Different Temperatures - No Evidence for Distributions from Picosecond Laser Experiments with Nanosecond Time Resolution. *J. Phys. Chem.* **1991**, *95* (14), 5476–5488.
- (117) Decahydronaphthalene, mixture of cis + trans, reagent grade, 98% | C₁₀H₁₈ | Sigma-Aldrich <http://www.sigmaaldrich.com/catalog/product/sial/d251?lang=pt®ion=PT> (accessed Sep 29, 2015).
- (118) G., P. O.; Baner, A. L. *Plastic Packaging: Interactions with Food and Pharmaceuticals*, 2nd ed.; Wiley-VCH, 2008.
- (119) *Modern Superabsorbent Polymer Technology*; John Wiley & Sons, 1997.
- (120) Chung, J. E.; Yokoyama, M.; Yamato, M.; Aoyagi, T.; Sakurai, Y.; Okano, T. Thermo-Responsive Drug Delivery from Polymeric Micelles Constructed Using Block Copolymers of poly(N-Isopropylacrylamide) and Poly(butylmethacrylate). *J. Control. Release* **1999**, *62* (1–2), 115–127.
- (121) Yan, H.; Tsujii, K. Potential Application of poly(N-Isopropylacrylamide) Gel Containing Polymeric Micelles to Drug Delivery Systems. *Colloids Surf B Biointerfaces* **2005**, *46* (3), 142–146.
- (122) Titow, W. V. *PVC Technology*; Springer, 1984.
- (123) Miller-Chou, B. A.; Koenig, J. L. A Review of Polymer Dissolution. *Prog. Polym. Sci.* **2003**, *28*, 1223–1270.
- (124) Cooper, W. J.; Krasicky, P. D.; Rodriguez, F. Effects of Molecular Weight and Plasticization on Dissolution Rates of Thin Polymer Films. *Polymer (Guildf)*. **1985**, *26* (7), 1069–1072.
- (125) Daniels, F.; Alberty, R. A. *Physical Chemistry*; Wiley, 1975.
- (126) Hansen, E. F.; Derrick, M. R.; Schilling, M. R.; Garcia, R. THE EFFECTS OF SOLUTION APPLICATION ON SOME MECHANICAL AND PHYSICAL PROPERTIES OF THERMOPLASTIC AMORPHOUS POLYMERS USED IN CONSERVATION: Poly(vinyl Acetate)s. *J. Am. Inst. Conserv.* **1991**, *30* (2 (8)), 203–213.
- (127) Holmberg, K.; Jonsson, B.; Kronberg, B.; Lindman, B. *Surfactants and Polymers in Aqueous Solutions*, 2 nd.; John Willey & Sons: West Sussex, 2003.
- (128) Evans, D. F.; Wennerström, H. *The Colloidal Domain: Where Physics, Chemistry, Biology, and Technology Meet*; Willey-VCH: New York, 1999.
- (129) Morita, H.; Doi, M. Mesoscale Simulation of Line-Edge Structures Based on Polymer Chains in Development and Rinse Processes. *J. Micro/Nanolithography, MEMS, MOEMS* **2010**, *9* (4), 41213–41217.
- (130) He, G.; Yan, N.; Yang, J.; Wang, H.; Ding, L.; Yin, S.; Fang, Y. Pyrene-Containing Conjugated Polymer-Based Fluorescent Films for Highly Sensitive and Selective Sensing of TNT in Aqueous Medium. *Macromolecules* **2011**, *44* (12), 4759–4766.

References

- (131) Kalyanasundaram, K.; Thomas, J. K. Environmental Effects on Vibronic Band Intensities in Pyrene Monomer Fluorescence and Their Application in Studies of Micellar Systems. *J. Am. Chem. Soc.* **1977**, *99* (7), 2039–2044.
- (132) Zhao, C.; Wu, D.; Lian, X.; Zhang, Y.; Song, X.; Zhao, H. Amphiphilic Asymmetric Comb Copolymer with Pendant Pyrene Groups and PNIPAM Side Chains: Synthesis, Photophysical Properties, and Self-Assembly. *J. Phys. Chem. B* **2010**, *114* (19), 6300–6308.
- (133) Yip, J.; Duhamel, J.; Qiu, X. P.; Winnik, F. M. Long-Range Polymer Chain Dynamics of Pyrene-Labeled Poly(N-Isopropylacrylamide)s Studied by Fluorescence. *Macromolecules* **2011**, *44* (13), 5363–5372.
- (134) Duan, Q.; Miura, Y.; Narumi, A.; Shen, X.; Sato, S.-I.; Satoh, T.; Kakuchi, T. Synthesis and Thermo-responsive Property of End-Functionalized poly(N-Isopropylacrylamide) with Pyrenyl Group. *J. Polym. Sci. Part A Polym. Chem.* **2006**, *44* (3), 1117–1124.
- (135) Zhang, Z.; Zheng, P.; Cai, D.; An, X.; Shen, W. Interaction of Ionic Surfactants with a Hydrophobic Modified Thermosensitive Polymer. *J. Dispers. Sci. Technol.* **2013**, *35* (5), 695–705.
- (136) Niskanen, J.; Wu, C.; Ostrowski, M.; Fuller, G. G.; Tenhu, H.; Hietala, S. Interfacial and Fluorescence Studies on Stereoblock Poly(N-Isopropylacryl Amide)s. *Langmuir* **2012**, *28* (41), 14792–14798.
- (137) Swaminathan, R.; Periasamy, N. Analysis of Fluorescence Decay by the Maximum Entropy Method: Influence of Noise and Analysis Parameters on the Width of the Distribution of Lifetimes. *Proc. Indian Acad. Sci. - Chem. Sci.* **1996**, *108* (1), 39–49.
- (138) Swaminathan, R.; Periasamy, N. Analysis of Fluorescence Decay by the Maximum Entropy Method: Influence of Noise and Analysis Parameters on the Width of the Distribution of Lifetimes. *Proc. Indian Acad. Sci. - Chem. Sci.* **1996**, *108* (1), 39–49.
- (139) Duhamel, J.; Yekta, A.; Winnik, M. A.; Jao, T. C.; Mishra, M. K.; Rubin, I. D. A Blob Model to Study Polymer Chain Dynamics in Solution. *J. Phys. Chem.* **1993**, *97* (51), 13708–13712.
- (140) Costa, T.; Seixas de Melo, J. S.; Miguel, M. G.; Lindman, B.; Schillén, K. Complex Formation between a Fluorescently-Labeled Polyelectrolyte and a Triblock Copolymer. *J. Phys. Chem. B* **2009**, *113*, 6205–6214.
- (141) Fulmer, G. R.; Miller, A. J. M.; Sherden, N. H.; Gottlieb, H. E.; Nudelman, A.; Stoltz, B. M.; Bercaw, J. E.; Goldberg, K. I. NMR Chemical Shifts of Trace Impurities: Common Laboratory Solvents, Organics, and Gases in Deuterated Solvents Relevant to the Organometallic Chemist. *Organometallics* **2010**, *29* (9), 2176–2179.
- (142) Plawski, J. L. *Transport Phenomena Fundamentals, Third Edition*, 3rd Editio.; CRC Press.
- (143) Sachs, L.; Reynarowych, Z. *Applied Statistics - A Handbook of Techniques*, 2nd ed.; 1984.
- (144) Costa, T.; Melo, J. S. S. de. *Photophysics of Macromolecular Pyrene-Containing Systems*, University of Coimbra, 2008, Vol. PhD.
- (145) Hickey, K.; Waghorne, W. E. Viscosities and Volumes of Dilute Solutions of Formamide in Water + Acetonitrile and for Formamide and N,N-Dimethylformamide in Methanol + Acetonitrile Mixed Solvents: Viscosity B-Coefficients, Activation Free Energies for Viscous Flow, and Partial Molar. *J. Chem. Eng. Data* **2001**, *46* (4), 851–857.
- (146) Macanita, A. L.; Magalhaes, J.; Dias, A.; Teles, H.; Iglesias, E. Dipole-Dipole Interactions between the Terminal Groups of 1,n-Diarenecarboxy Alkanes, N= 1, 2, ..., 6. *J. Chem. Soc.*

References

- Faraday Trans.* **1990**, 86 (24), 4011–4016.
- (147) Ian Griffiths – Surfactant systems <https://people.maths.ox.ac.uk/griffit4/multilayer.html> (accessed Sep 21, 2015).
- (148) Vicki Caligur 3.3, 14., B. 2008. Detergents and Solubilization Reagents. *Biofiles* **2008**, 3 (3).
- (149) Patel, T.; Ghosh, G.; Aswal, V.; Bahadur, P. Micellization of Sodium Dodecyl Sulfate and Polyoxyethylene Dodecyl Ethers in Solution. *Colloid Polym. Sci.* **2009**, 287 (10), 1175–1181.
- (150) Daful, A. G.; Baulin, V. A.; Avalos, J. B.; Mackie, A. D. Accurate Critical Micelle Concentrations from a Microscopic Surfactant Model. *J. Phys. Chem. B* **2011**, 115 (13), 3434–3443.
- (151) Shinzawa-Itoh, K.; Ueda, H.; Yoshikawa, S.; Aoyama, H.; Yamashita, E.; Tsukihara, T. Effects of Ethyleneglycol Chain Length of Dodecyl Polyethyleneglycol Monoether on the Crystallization of Bovine Heart Cytochrome c Oxidase. *J. Mol. Biol.* **1995**, 246 (5), 572–575.
- (152) Vautier-Giongo, C.; and Barney L. Bales*. Estimate of the Ionization Degree of Ionic Micelles Based on Krafft Temperature Measurements. *J. Phys. Chem. B* **2003**, 107 (23), 5398–5403.
- (153) Basu Ray, G.; Chakraborty, I.; Moulik, S. P. Pyrene Absorption Can Be a Convenient Method for Probing Critical Micellar Concentration (Cmc) and Indexing Micellar Polarity. *J. Colloid Interface Sci.* **2006**, 294 (1), 248–254.
- (154) Majhi, P. R.; Mukherjee, K.; Moulik, S. P.; Sen, S.; Sahu, N. P. Solution Properties of a Saponin (Acaciaside) in the Presence of Triton X-100 and Igepal. *Langmuir* **1999**, 15 (20), 6624–6630.
- (155) Turro, N. J.; Kuo, P. L. PYRENE EXCIMER FORMATION IN MICELLES OF NONIONIC DETERGENTS AND OF WATER-SOLUBLE POLYMERS. *Langmuir* **1986**, 2 (4), 438–442.
- (156) Aguiar, J.; Carpena, P.; Molina-Bolívar, J. A.; Carnero Ruiz, C. On the Determination of the Critical Micelle Concentration by the Pyrene 1:3 Ratio Method. *J. Colloid Interface Sci.* **2003**, 258 (1), 116–122.
- (157) Turro, N. J.; Kuo, P. L. Fluorescence Probes for Aqueous Solutions of Nonionic Micelles. *Langmuir* **1985**, 1 (1), 170–172.
- (158) Lindman, B.; Karlström, G. Polymer-Surfactant Systems. In *The Structure, Dynamics and Equilibrium Properties of Colloidal Systems*; Bloor, D. M., Wyn-Jones, E., Eds.; Springer Netherlands, 1990; Vol. 324, pp 131–147.
- (159) Myers, D. *Surfactant Science and Technology*, 3rd Editio.; WILEY, 2005.
- (160) Lee, J. W.; Kim, S. Y.; Kim, S. S.; Lee, Y. M.; Lee, K. H.; Kim, S. J. Synthesis and Characteristics of Interpenetrating Polymer Network Hydrogel Composed of Chitosan and Poly(acrylic Acid). *J. Appl. Polym. Sci.* **1999**, 73 (1), 113–120.
- (161) Binder, K.; Heerman, D. W. Monte Carlo Simulation in Statistical Physics An Introduction, Springer Series in Solid-State. In *Sciences 80*; Springer-Verlag: Germany, 1988.
- (162) Allen, M. P.; Tildesley, D. J. *Computer Simulation of Liquids*; Oxford Science Publications: New York, 1996.
- (163) Attig, N.; Binder, K.; Grubmuller, H.; K., K. (John von N. I. for C. *Monte Carlo Simulation of Polymers: Coarse-Grained Models Computational Soft Matter: From Synthetic Polymers to Proteins*; NIC Series: Julich, 2004.

References

- (164) Martinho, J. M. G.; Farinha, J. P.; Berberansantos, M. N.; Duhamel, J.; Winnik, M. A. Test of a Model for Reversible Excimer Kinetics - Pyrene in Cyclohexanol. *J. Chem. Phys.* **1992**, *96* (11), 8143–8149.
- (165) Mortimer, R. G. *Physical Chemistry*, 3rd Editio.; Elsevier: Canada, 2008.
- (166) Miyazawa, K.; Winnik, F. M. Solution Properties of Hydrophobically-Modified Phosphorylcholine-Based Polymers in Water and in the Presence of Surfactants. *J. Phys. Chem. B* **2003**, *107* (38), 10677–10682.
- (167) Dias, F. B.; Lima, J. C.; Pierola, I. F.; Horta, A.; Macanita, A. L. Internal Dynamics of Poly(methylphenylsiloxane) Chains as Revealed by Picosecond Time Resolved Fluorescence. *J. Phys. Chem. A* **2001**, *105* (45), 10286–10295.
- (168) Turro, N. J.; Arora, K. S. PYRENE AS A PHOTOPHYSICAL PROBE FOR INTERMOLECULAR INTERACTIONS OF WATER-SOLUBLE POLYMERS IN DILUTE-SOLUTIONS. *Polymer (Guildf)*. **1986**, *27* (5), 783–796.
- (169) Reynders, P.; Dreeskamp, H.; Kuhnle, W.; Zachariasse, K. A. Conformer Analysis and Intramolecular Excimer Formation with the Meso and Racemic Diastereoisomers of 2,4-Di(2-Pyrenyl)Pentane - Comparison of Nmr and Single-Photon-Counting Data. *J. Phys. Chem.* **1987**, *91* (15), 3982–3992.
- (170) Kelly, F. J.; Stokes, R. H. Diffusion Coefficients and Densities for the Systems Carbon Tetrachloride +m-Xylene and Carbon Tetrachloride + Mesitylene at 25[degree]. *Trans. Faraday Soc.* **1959**, *55* (0), 388–390.
- (171) Chong, P. L.; Thompson, T. E. Oxygen Quenching of Pyrene-Lipid Fluorescence in Phosphatidylcholine Vesicles. A Probe for Membrane Organization. *Biophys. J.* **1985**, *47* (5), 613–621.
- (172) Halder, B.; Mallick, A.; Chattopadhyay, N. Photophysics of Pyrene-End-Capped Poly(ethyleneoxide) in Aqueous Micellar Environments. *J. Mol. Liq.* **2004**, *115* (2-3), 113–120.
- (173) Fernandes, L.; Boucher, M.; Fernández-Lodeiro, J.; Oliveira, E.; Nuñez, C.; Santos, H. M.; Capelo, J. L.; Faza, O. N.; Bértolo, E.; Lodeiro, C. Exploiting Anionic and Cationic Interactions with a New Emissive Imine-Based β -Naphthol Molecular Probe. *Inorg. Chem. Commun.* **2009**, *12* (9), 905–912.
- (174) Cabral, C.; Seixas de Melo, J. A Comprehensive Investigation of the Solution Photophysics and Acid-Base Reactions of Substituted Hydroxycoumarins, Universidade de Coimbra: Coimbra, 2009, Vol. Master.
- (175) Seixas de Melo, J.; Macanita, A. Fotofísica Molecular de Cumarinas E Tiofenos, Instituto Superior Técnico: Lisboa, 1996, Vol. Doutor.
- (176) Kim, J. J.; Beardslee, R. A.; Phillips, D. T.; Offen, H. W. Fluorescence Lifetimes of Pyrene Monomer and Excimer at High Pressures. *J. Chem. Phys.* **1969**, *51* (6), 2761–2762.
- (177) Martinho, J. M. G.; Reis e Sousa, A. T.; Oliveira Torres, M. E.; Fedorov, A. Fluorescence Quenching of Pyrene Monomer and Excimer by CH₃I. *Chem. Phys.* **2001**, *264* (1), 111–121.
- (178) Siu, H.; Duhamel, J. Comparison of the Association Level of a Pyrene-Labeled Associative Polymer Obtained from an Analysis Based on Two Different Models. *J. Phys. Chem. B* **2005**, *109* (5), 1770–1780.
- (179) Kim, T. W.; Park, J.; Hong, J.-I. Zn²⁺ Fluorescent Chemosensors and the Influence of Their

References

- Spacer Length on Tuning Zn²⁺ Selectivity. *J. Chem. Soc. Perkin Trans. 2* **2002**, No. 5, 923–927.
- (180) Prodi, L.; Bolletta, F.; Montalti, M.; Zaccheroni, N. Luminescent Chemosensors for Transition Metal Ions. *Coord. Chem. Rev.* **2000**, *205* (1), 59–83.
- (181) Pearson, R. G. Hard and Soft Acids and Bases. *J. Am. Chem. Soc.* **1963**, *85* (22), 3533–3539.
- (182) Choi, J. Y.; Kim, D.; Yoon, J. A Highly Selective “turn-On” Fluorescent Chemosensor Based on Hydroxy Pyrene–hydrazone Derivative for Zn²⁺. *Dye. Pigment.* **2013**, *96* (1), 176–179.
- (183) Martínez, R.; Espinosa, A.; Tárraga, A.; Molina, P. A New Bis(pyrenyl)azadiene-Based Probe for the Colorimetric and Fluorescent Sensing of Cu(II) and Hg(II). *Tetrahedron* **2010**, *66* (21), 3662–3667.
- (184) Vedamalai, M.; Wu, S.-P. A BODIPY-Based Colorimetric and Fluorometric Chemosensor for Hg(ii) Ions and Its Application to Living Cell Imaging. *Org. Biomol. Chem.* **2012**, *10* (28), 5410–5416.
- (185) New Trends in Fluorescence Spectroscopy Applications to Chemical and Life Sciences. *Springer Series on Fluorescence Methods and Applications*. Valeur, B. Springer Berlin Heidelberg 2001.
- (186) Valeur, B.; Leray, I. Design Principles of Fluorescent Molecular Sensors for Cation Recognition. *Coord. Chem. Rev.* **2000**, *205* (1), 3–40.
- (187) Minkin, V. I.; Dubonosov, A. D.; Bren, V. A.; Tsukanov, A. V. Chemosensors with Crown Ether-Based Receptors. *ARKIVOC* **2008**, (iv), 90–102.
- (188) Gunnlaugsson, T.; Lee, T. C.; Parkesh, R. A Highly Selective and Sensitive Fluorescent PET (Photoinduced Electron Transfer) Chemosensor for Zn(ii). *Org. Biomol. Chem.* **2003**, *1* (19), 3265–3267.
- (189) Swinburne, A. N.; Steed, J. W. Podands. In *Supramolecular Chemistry*; John Wiley & Sons, Ltd, 2012.
- (190) He, H.; Mortellaro, M. A.; Leiner, M. J. P.; Young, S. T.; Fraatz, R. J.; Tusa, J. K. A Fluorescent Chemosensor for Sodium Based on Photoinduced Electron Transfer. *Anal. Chem.* **2002**, *75* (3), 549–555.
- (191) Wu, J.; Liu, W.; Ge, J.; Zhang, H.; Wang, P. New Sensing Mechanisms for Design of Fluorescent Chemosensors Emerging in Recent Years. *Chem Soc Rev* **2011**, *40* (7), 3483–3495.
- (192) House, J. E. *Inorganic Chemistry*; Elsevier, 2008.
- (193) Pinheiro, D.; de Castro, C. S.; Seixas de Melo, J. S.; Oliveira, E.; Nuñez, C.; Fernández-Lodeiro, A.; Capelo, J. L.; Lodeiro, C. From Yellow to Pink Using a Fluorimetric and Colorimetric Pyrene Derivative and Mercury (II) Ions. *Dye. Pigment.* **2014**, *110* (0), 152–158.
- (194) Fernández-Lodeiro, J.; Nuñez, C.; Capelo, J. L.; Lodeiro, C. 2-((Pyren-1-Ylmethylamino)methyl)quinolin-8-Ol. *Molbank* **2010**, *2010* (4), M698.
- (195) Fernandez-Lodeiro, J.; Nunez, C.; de Castro, C. S.; Bertolo, E.; Seixas de Melo, J. S.; Capelo, J. L.; Lodeiro, C. Steady-State and Time-Resolved Investigations on Pyrene-Based Chemosensors. *Inorg. Chem.* **2013**, *52* (1), 121–129.
- (196) Niko, Y.; Kawauchi, S.; Otsu, S.; Tokumaru, K.; Konishi, G. Fluorescence Enhancement of Pyrene Chromophores Induced by Alkyl Groups through Σ – π Conjugation: Systematic

References

- Synthesis of Primary, Secondary, and Tertiary Alkylated Pyrenes at the 1, 3, 6, and 8 Positions and Their Photophysical Properties. *J. Org. Chem.* **2013**, *78* (7), 3196–3207.
- (197) Shellaiah, M.; Wu, Y.-H.; Singh, A.; Ramakrishnam Raju, M. V; Lin, H.-C. Novel Pyrene- and Anthracene-Based Schiff Base Derivatives as Cu²⁺ and Fe³⁺ Fluorescence Turn-on Sensors and for Aggregation Induced Emissions. *J. Mater. Chem. A* **2013**, *1* (4), 1310–1318.
- (198) Fluorescent Chemosensors for Ion and Molecule Recognition, Copyright, 1993 Advisory Board, Foreword. In *Fluorescent Chemosensors for Ion and Molecule Recognition*; Comstock, M. J., Ed.; American Chemical Society, 1993; Vol. 538, pp i – vi.
- (199) Gans, P.; Sabatini, A.; Vacca, A. Investigation of Equilibria in Solution. Determination of Equilibrium Constants with the HYPERQUAD Suite of Programs. *Talanta* **1996**, *43* (10), 1739–1753.
- (200) Åkerlöf, G.; Short, O. A. The Dielectric Constant of Dioxane—Water Mixtures between 0 and 80°. *J. Am. Chem. Soc.* **1936**, *58* (7), 1241–1243.
- (201) Bichenkova, E. V; Sardarian, A. R.; Wilton, A. N.; Bonnet, P.; Bryce, R. A.; Douglas, K. T. Exciplex Fluorescence Emission from Simple Organic Intramolecular Constructs in Non-Polar and Highly Polar Media as Model Systems for DNA-Assembled Exciplex Detectors. *Org. Biomol. Chem.* **2006**, *4* (2), 367–378.
- (202) MacCarthy, P. Simplified Experimental Route for Obtaining Job's Curves. *Anal. Chem.* **1978**, *50* (14), 2165.
- (203) Geiger, M. W.; Turro, N. J. PYRENE FLUORESCENCE LIFETIME AS A PROBE FOR OXYGEN PENETRATION OF MICELLES. *Photochem. Photobiol.* **1975**, *22* (6), 273–276.
- (204) Pina, F.; Lima, J. C.; Lodeiro, C.; Seixas de Melo, J.; Díaz, P.; Albelda, M. T.; García-España, E. Long Range Electron Transfer Quenching in Polyamine Chains Bearing a Terminal Naphthalene Unit. *J. Phys. Chem. A* **2002**, *106* (35), 8207–8212.
- (205) GABRIEL, K. R. The Biplot Graphic Display of Matrices with Application to Principal Component Analysis. *Biometrika* **1971**, *58* (3), 453–467.
- (206) Venables, W. N.; Smith, D. M. *An Introduction to R, Notes on R: A Programming Environment for Data Analysis and Graphics, Version 3.0.1*; 2013.
- (207) Almeida, J. A. S.; Barbosa, L. M. S.; Pais, A. A. C. C.; Formosinho, S. J. Improving Hierarchical Cluster Analysis: A New Method with Outlier Detection and Automatic Clustering. *Chemom. Intell. Lab. Syst.* **2007**, *87* (2), 208–217.
- (208) Joliffe, I. T. *Principal Component Analysis*, 2nd editio.; Springer: New York, 2002.
- (209) Cova, T. F.; Pereira, J. L.; Pais, A. A. Is Standard Multivariate Analysis Sufficient in Clinical and Epidemiological Studies? *J. Biomed. Inform.* **2013**, *46* (1), 75–86.
- (210) Ana Maria Silván, *; Maria José Abad; Paulina Bermejo; Monica Sollhuber, †; and Angel Villar. Antiinflammatory Activity of Coumarins from Santolina Oblongifolia. *J. Nat. Prod.* **1996**, *59* (12), 1183–1185.
- (211) Chihiro Ito, †; Masataka Itoigawa *, ‡; Shinya Katsuno, †; Mitsuo Omura, §.; Harukuni Tokuda, ⊥; Hoyoku Nishino, ⊥; and Hiroshi Furukawa†. Chemical Constituents of Clausena Excavata: Isolation and Structure Elucidation of Novel Furanone-Coumarins with Inhibitory Effects for Tumor-Promotion1. *J. Nat. Prod.* **2000**, *63* (9), 1218–1224.
- (212) Roberto Carrizo F., †; Marta E. Sosa, ‡; Laura S. Favier, †; Fabricio Penna, §.; Eduardo

References

- Guerreiro, †; Oscar S. Giordano, †; and Carlos E. Tonn*, †. Growth-Inhibitory Activities of Benzofuran and Chromene Derivatives toward *Tenebrio Molitor*. *J. Nat. Prod.* **1998**, *61* (10), 1209–1211.
- (213) Christoph Steinbeck *, †; Volker Spitzer, ‡; Moacir Starosta, ‡; and Gilsane von Poser‡. Identification of Two Chromenes from *Calea Serrata* by Semiautomatic Structure Elucidation. *J. Nat. Prod.* **1997**, *60* (6), 627–628.
- (214) Neil Comey; Ingrid Hook; Helen Sheridan, *; and John Walsh; James, P. Isolation of (S)-(-)-2,3-Dihydro-2,6-Dimethyl-4H-Benzopyran-4-One from Roots of *Leontopodium Alpinum*. *J. Nat. Prod.* **1997**, *60* (2), 148–149.
- (215) Tawnya C. McKee; Richard W. Fuller; Conni D. Covington, †; John H. Cardellina II; Robert J. Gulakowski; Benjamin L. Krepps; James B. McMahon; and Michael R. Boyd*. New Pyranocoumarins Isolated from *Calophyllum Lanigerum* and *Calophyllum Teysmannii*. *J. Nat. Prod.* **1996**, *59* (8), 754–758.
- (216) M. Carmen Zafra-Polo, †; M. Carmen González, †; José R. Tormo, †; Ernesto Estornell, ‡; and Diego Cortes*, †. Polyalthidin: New Prenylated Benzopyran Inhibitor of the Mammalian Mitochondrial Respiratory Chain. *J. Nat. Prod.* **1996**, *59* (10), 913–916.
- (217) Tawnya C. McKee; Conni D. Covington, †; Richard W. Fuller; Heidi R. Bokesch, ‡; Sherry Young, †; John H. Cardellina II; Marian R. Kadushin, §.; D. Doel Soejarto, ⊥; Peter F. Stevens, ‖; Gordon M. Cragg, Δ.; et al. Pyranocoumarins from Tropical Species of the Genus *Calophyllum*: A Chemotaxonomic Study of Extracts in the National Cancer Institute Collection. *J. Nat. Prod.* **1998**, *61* (10), 1252–1256.
- (218) Pengsuparp, T.; Serit, M.; Hughes, S. H.; Soejarto, D. D.; and John M. Pezzuto*. Specific Inhibition of Human Immunodeficiency Virus Type 1 Reverse Transcriptase Mediated by Soulattrolide, a Coumarin Isolated from the Latex of *Calophyllum Teysmannii*. *J. Nat. Prod.* **1996**, *59* (9), 839–842.
- (219) Jurd, L.; King, A. D.; Mihara, K. Antimicrobial Properties of Umbelliferone Derivatives. *Phytochemistry* **1971**, *10* (12), 2965–2970.
- (220) Murray, R. D. H. Coumarins. *Nat. Prod. Rep.* **1989**, *6* (6), 591–624.
- (221) H. N. Nigg *, ‡; J. O. Strandberg, ‡; R. C. Beier, §.; H. D. Petersen, ‖; and J. M. Harrison⊥. Furanocoumarins in Florida Celery Varieties Increased by Fungicide Treatment. *J. Agric. Food Chem.* **1997**, *45* (4), 1430–1436.
- (222) Coleman*, R. S.; and Mihaela L. Madaras. Synthesis of a Novel Coumarin C-Riboside as a Photophysical Probe of Oligonucleotide Dynamics. *J. Org. Chem.* **1998**, *63* (16), 5700–5703.
- (223) Lee-Chiang Lo, *; Yuan-Chang Liao; Chi-Hsien Kuo; and Chao-Tsen Chen*. A Novel Coumarin-Type Derivatizing Reagent of Alcohols: Application in the CD Exciton Chirality Method for Microscale Structural Determination†. *Org. Lett.* **2000**, *2* (5), 683–685.
- (224) Miriam Hirshberg *, §.; Kim Henrick §, ‖; Lesley Lloyd Haire, §.; Nishi Vasisht, §.; Martin Brune, ⊥; John E. T. Corrie, ⊥; and Martin R. Webb⊥. Crystal Structure of Phosphate Binding Protein Labeled with a Coumarin Fluorophore, a Probe for Inorganic Phosphate,. *Biochemistry* **1998**, *37* (29), 10381–10385.
- (225) M.-L. Horng; J. A. Gardecki; and M. Maroncelli*. Rotational Dynamics of Coumarin 153: Time-Dependent Friction, Dielectric Friction, and Other Nonhydrodynamic Effects. *J. Phys. Chem. A* **1997**, *101* (6), 1030–1047.

References

- (226) Landefeld, C. S.; Beyth, R. J. Anticoagulant-Related Bleeding: Clinical Epidemiology, Prediction, and Prevention. *Am. J. Med.* **2015**, *95* (3), 315–328.
- (227) Bell, R. G.; Stark, P. Inhibition of Prothrombin Synthesis and Epoxidation of Vitamin K1 by Anticoagulants in Vitro. *Biochem. Biophys. Res. Commun.* **1976**, *72* (2), 619–625.
- (228) de Groot, A. C. Fragrances. In *Handbook of Occupational Dermatology*; Kanerva, L., Elsner, P., Wahlberg, J. E., Maybach, H. I., Eds.; Berlin, 2000; pp 497–508.
- (229) Arindam Chowdhury; Sarah A. Locknar; Lavanya L. Premvardhan; and Linda A. Peteanu*. Effects of Matrix Temperature and Rigidity on the Electronic Properties of Solvatochromic Molecules: Electroabsorption of Coumarin 153. *J. Phys. Chem. A* **1999**, *103* (48), 9614–9625.
- (230) Yatsuhashi*, T.; and Nobuaki Nakashima. Hot Molecule as an Intermediate in Multiphoton Reaction: Two-Photon Decarbonylation of Coumarin. *J. Phys. Chem. A* **2000**, *104* (6), 1095–1099.
- (231) Brian A. Pryor; Phillip M. Palmer; Peter M. Andrews; Mitchell B. Berger; and Michael R. Topp*. Spectroscopy of Jet-Cooled Water Complexes with Coumarin 151: Observation of Vibronically Induced Conformational Barrier Crossing. *J. Phys. Chem. A* **1998**, *102* (19), 3284–3292.
- (232) McCarthy, P. K.; Blanchard, G. J. AM1 Study of the Electronic Structure of Coumarins. *J. Phys. Chem.* **1993**, *97* (47), 12205–12209.
- (233) T. Gustavsson, *; L. Cassara; V. Gulbinas, †; G. Gurzadyan, ‡; J.-C. Mialocq; S. Pommeret; M. Sorgius; and P. van der Meulen§. Femtosecond Spectroscopic Study of Relaxation Processes of Three Amino-Substituted Coumarin Dyes in Methanol and Dimethyl Sulfoxide. *J. Phys. Chem. A* **1998**, *102* (23), 4229–4245.
- (234) André Fougerousse; Emmanuel Gonzalez; and Raymond Brouillard*. A Convenient Method for Synthesizing 2-Aryl-3-Hydroxy-4-Oxo-4H-1-Benzopyrans or Flavonols. *J. Org. Chem.* **2000**, *65* (2), 583–586.
- (235) Chang, S.; and Robert H. Grubbs*. A Highly Efficient and Practical Synthesis of Chromene Derivatives Using Ring-Closing Olefin Metathesis. *J. Org. Chem.* **1998**, *63* (3), 864–866.
- (236) Mario Foti *, ‡ †; Mario Piattelli, ‡; Maria Tiziana Baratta, §.; and Giuseppe Ruberto*, §. Flavonoids, Coumarins, and Cinnamic Acids as Antioxidants in a Micellar System. Structure–Activity Relationship. *J. Agric. Food Chem.* **1996**, *44* (2), 497–501.
- (237) NC Seasonal Sensation – Strawberry Recipes | WakeMed Voices <http://wakemedvoices.org/2011/04/nc-seasonal-sensation-%E2%80%93-strawberry-recipes/> (accessed Feb 16, 2016).
- (238) DIY Lavender Sachets For Your Bed or Drawers. <http://www.how2girl.com/diy-lavender-satchels-for-your-bed-or-drawers/> (accessed Feb 16, 2016).
- (239) ADD, ADHD and Autism Causation: Could it be Chlorinated Hydrocarbon Pesticides - Salem-News.Com <http://www.salem-news.com/articles/june032010/add-adhd-pl.php> (accessed Feb 16, 2016).
- (240) AXE Philippines - Anarchy <http://www.axephilippines.com/anarchy> (accessed Feb 16, 2016).
- (241) Dye Lasers & Accessories: Pulsed Dye Lasers, CW (Continuous Wave), Laser Dyes from Radiant Dyes Laser <http://www.warsash.com.au/products/lasers/DYE-LASERS.php> (accessed Feb 16, 2016).

References

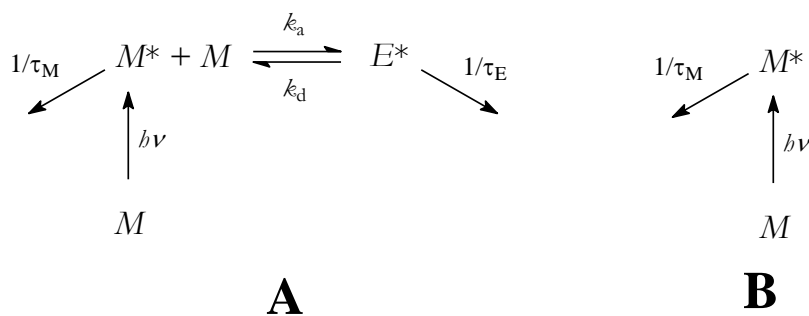
- (242) Narayanaswamy, N.; Kumar, M.; Das, S.; Sharma, R.; Samanta, P. K.; Pati, S. K.; Dhar, S. K.; Kundu, T. K.; Govindaraju, T. A Thiazole Coumarin (TC) Turn-On Fluorescence Probe for AT-Base Pair Detection and Multipurpose Applications in Different Biological Systems. *Sci. Rep.* **2014**, *4*.
- (243) Leaning Rock Cherries Ltd - Jobs <http://leaningrockcherries.webs.com/jobs.htm> (accessed Feb 16, 2016).
- (244) What Exactly is Cinnamon? (with pictures) <http://www.wisegeek.org/what-exactly-is-cinnamon.htm> (accessed Feb 16, 2016).
- (245) Pina, J.; Seixas de Melo, J. Fotofísica E Fotoquímica de Pironas, Cumarinas E Seus Derivados Fotocrômicos, Universidade de Coimbra: Coimbra, 2000, Vol. Licenciatu.
- (246) Yakatan, G. J.; Juneau, R. J.; Schulman, S. G. Phototautomerism in the Lowest Excited Singlet State of 4-Methylumbelliferone. *Anal. Chem.* **1972**, *44* (6), 1044–1046.
- (247) Vladimír, V. Fluorescence of Some Simple Umbelliferone Derivatives. *Collect. Czechoslovak Chem. Commun.* **1979**, *44* (2), 508–518.
- (248) Schulman, S. G.; Rosenberg, L. S. Tautomerization Kinetics of 7-Hydroxy-4-Methylcoumarin in the Lowest Excited Singlet State. *J. Phys. Chem.* **1979**, *83* (4), 447–451.
- (249) Tasuku Ueno †, ‡; Yasuteru Urano †, §; Hirotatsu Kojima †, ‡; and Tetsuo Nagano* †, ‡. Mechanism-Based Molecular Design of Highly Selective Fluorescence Probes for Nitritative Stress. *J. Am. Chem. Soc.* **2006**, *128* (33), 10640–10641.
- (250) de Melo, J. S. S.; Cabral, C.; Lima, J. C.; Maçanita, A. L. Characterization of the Singlet and Triplet Excited States of 3-Chloro-4-Methylumbelliferone. *J. Phys. Chem. A* **2011**, *115* (30), 8392–8398.
- (251) Fernandes, P. A Fotofísica de Hidroxicumarinas E Seus Tioderivados, Universidade de Coimbra: Coimbra, 1999, Vol. Licenciatu.
- (252) Wu, D. H.; Chen, A. D.; Johnson, C. S. An Improved Diffusion-Ordered Spectroscopy Experiment Incorporating Bipolar-Gradient Pulses. *J. Magn. Reson. Ser. A* **1995**, *115* (2), 260–264.
- (253) Linse, P. Molsim. 4.0.0 ed. Lund University, Sweden 2004.
- (254) Amemori, S.; Kokado, K.; Sada, K. Polymer Phase-Transition Behavior Driven by a Charge-Transfer Interaction. *Angew. Chemie Int. Ed.* **2013**, *52* (15), 4174–4178.
- (255) Hashidzume, A.; Zheng, Y.; Takashima, Y.; Yamaguchi, H.; Harada, A. Macroscopic Self-Assembly Based on Molecular Recognition: Effect of Linkage between Aromatics and the Polyacrylamide Gel Scaffold, Amide versus Ester. *Macromolecules* **2013**, *46* (5), 1939–1947.
- (256) Armarego, W. L. E.; Chai, C. L. L. *Purification of Laboratory Chemicals*, 5th Editio.; Elsevier Science, 2003.
- (257) Williams, D. B. G.; Lawton, M. Drying of Organic Solvents: Quantitative Evaluation of the Efficiency of Several Desiccants. *J. Org. Chem.* **2010**, *75* (24), 8351–8354.
- (258) Owen, T. *Fundamentals of UV-Visible Spectroscopy A Primer*; Hewlett-Packard, 1996.
- (259) Gupta, M. K. Copper(II) Trifluoromethanesulfonate [1]. *Synlett* **2005**, *6*, 1044–1045.
- (260) Yadav, J. S.; Reddy, B. V. S.; Shankar, K. S.; Premalatha, K. Copper(II) Tetrafluoroborate as Mild and Versatile Catalyst for the Rapid Synthesis of B -Acetamido Ketones and Ketoesters

References

- via a Three Component Reaction. *Org. Commun.* **1** (4), 76–83.
- (261) Ham, P. Zinc Trifluoromethanesulfonate. In *Encyclopedia of Reagents for Organic Synthesis*; John Wiley & Sons, Ltd, 2001.
- (262) Ranu, B. C. Zinc Tetrafluoroborate. In *Encyclopedia of Reagents for Organic Synthesis*; John Wiley & Sons, Ltd, 2001.
- (263) Nishizawa, M. Mercury(II) Trifluoromethanesulfonate. In *Encyclopedia of Reagents for Organic Synthesis*; John Wiley & Sons, Ltd, 2001.
- (264) *Fluoromax-4 & Fluoromax-4P with USB*; HORIBA, 2009.
- (265) Inc., J. Y. Fluorolog®-3. **2002**.
- (266) Striker, G. Effective Implementation of Modulation Functions. In *Deconvolution and Reconvolution of Analytical Signals*; Bouchy, M., Ed.; University Press: Nancy, 1982.
- (267) Striker, G.; Subramaniam, V.; Seidel, C. A. M.; Volkmer, A. Photochromicity and Fluorescence Lifetimes of Green Fluorescent Protein. *J. Phys. Chem. B* **1999**, *103* (40), 8612–8617.
- (268) Seixas de Melo, J.; Fernandes, P. F. No Title. *J. Mol. Struct.* **2001**, *565*, 69–78.
- (269) Pina, J.; Seixas de Melo, J.; Burrows, H. D.; Macanita, A. L.; Galbrecht, F.; Bunnagel, T.; Scherf, U. Alternating Binaphthyl-Thiophene Copolymers: Synthesis, Spectroscopy, and Photophysics and Their Relevance to the Question of Energy Migration versus Conformational Relaxation. *Macromolecules* **2009**, *42* (5), 1710–1719.
- (270) Hess, B.; Kutzner, C.; van der Spoel, D.; Lindahl, E. GROMACS 4: Algorithms for Highly Efficient, Load-Balanced, and Scalable Molecular Simulation. *J. Chem. Theory Comput.* **2008**, *4* (3), 435–447.
- (271) van der Spoel, D.; van Maaren, P. J.; Caleman, C. GROMACS Molecule & Liquid Database. *Bioinformatics* **2012**, *28* (5), 752–753.
- (272) Schuler, L. D.; Daura, X.; van Gunsteren, W. F. An Improved GROMOS96 Force Field for Aliphatic Hydrocarbons in the Condensed Phase. *J. Comput. Chem.* **2001**, *22* (11), 1205–1218.
- (273) Malde, A. K.; Zuo, L.; Breeze, M.; Stroet, M.; Poger, D.; Nair, P. C.; Oostenbrink, C.; Mark, A. E. An Automated Force Field Topology Builder (ATB) and Repository: Version 1.0. *J. Chem. Theory Comput.* **2011**, *7*, 4026–4037.
- (274) Essmann, U.; Perera, L.; Berkowitz, M. L.; Darden, T.; Lee, H.; Pedersen, L. G. A Smooth Particle Mesh Ewald Method. *J. Chem. Phys.* **1995**, *103* (19), 8577–8593.
- (275) Humphrey, W.; Dalke, A.; Schulten, K. VMD: Visual Molecular Dynamics. *J Mol Graph* **1996**, *14* (1), 27–28,33–38.
- (276) Daura, X.; Gademann, K.; Jaun, B.; Seebach, D.; van Gunsteren, W. F.; Mark, A. E. Peptide Folding: When Simulation Meets Experiment. *Angew. Chemie Int. Ed.* **1999**, *38* (1-2), 236–240.
- (277) Seixas de Melo, J.; Maçanita, A. L. Three Interconverting Excited Species: Experimental Study and Solution of the General Photokinetic Triangle by Time-Resolved Fluorescence. *Chem. Phys. Lett.* **1993**, *204* (5,6), 556.

Appendices

Appendix A. Solution of the Birks' Kinetic Scheme



Scheme A.1. Classic Birks' kinetic scheme for (A) one monomer and one excimer (e.g. 1Py(10)1Py in heptane) and (B) one monomer (e.g. 1-methylpyrene in heptane at low concentrations).

$$I_F^{M^*} = k_F^M [M^*] \quad \text{Equation A.1}$$

$$I_F^{E^*} = k_F^E [E^*] \quad \text{Equation A.2}$$

From Equation A.1 and Equation A.2, one can obtain the differential equations for both monomer and excimer. The time-evolution of the monomer and excimer intensities in Scheme A.1 can be obtained by two differential equations, Equation A.3 and Equation A.4.

$$\frac{d}{dt}[M^*] = - \underbrace{\left(k_a + \frac{1}{\tau_M} \right)}_{k_X} [M^*] + k_d [E^*] + I_a \quad \text{Equation A.3}$$

$$\frac{d}{dt}[E^*] = - \underbrace{\left(k_d + \frac{1}{\tau_E} \right)}_{k_Y} [E^*] + k_a [M^*] \quad \text{Equation A.4}$$

Under photostationary conditions, $\frac{d}{dt}[M^*] = \frac{d}{dt}[E^*] = 0$

$$0 = -\underbrace{\left(k_d + \frac{1}{\tau_E}\right)}_{k_Y} [E^*] + k_a [M^*] \Leftrightarrow 0 = -k_Y [E^*] + k_a [M^*] \Leftrightarrow$$

Equation A.5

$$\Leftrightarrow k_Y [E^*] = k_a [M^*] \Leftrightarrow [E^*] = \frac{k_a [M^*]}{k_Y}$$

$$\frac{I_F^{E^*}}{I_F^{M^*}} = \frac{k_F^E [E^*]}{k_F^M [M^*]} = \frac{k_F^E}{k_F^M} \times \frac{k_a [M^*]}{k_Y [M^*]} = \frac{k_F^E}{k_F^M} \times \frac{k_a}{k_d + 1/\tau_E}$$

Equation A.6

For the reference compound (B) in Scheme A.1:

$$\frac{d}{dt} [M^*] = I_a - \frac{1}{\tau_M} [M^*]$$

Equation A.7

$$0 = I_a - \frac{1}{\tau_M} [M^*] \Leftrightarrow [M^*] = I_a \tau_M$$

Equation A.8

$$\frac{I_M^0}{I_M} = \frac{k_F^{M^0}}{k_F^M} \times \frac{[M_0^*]}{[M^*]} = \frac{k_F^{M^0}}{k_F^M} \times \frac{I_a \tau_M}{\frac{k_d [E^*] + I_a}{k_a + 1/\tau_M}} = \frac{I_a \tau_M (k_a + 1/\tau_M)}{k_d [E^*] + I_a}$$

Equation A.9

The time-concentration dependence equations of the monomer and excimer are given by Equation A.10 and Equation A.11.

$$[M^*](t) = a_{1,1} e^{-\lambda_1 t} + a_{1,2} e^{-\lambda_2 t} = a_{1,1} e^{-t/\tau_1} + a_{1,2} e^{-t/\tau_2} = \frac{I_M}{k_F^M}(t)$$

Equation A.10

$$[E^*](t) = a_{2,1} e^{-\lambda_1 t} + a_{2,2} e^{-\lambda_2 t} = a_{2,1} e^{-t/\tau_1} + a_{2,2} e^{-t/\tau_2} = \frac{I_E(t)}{k_F^E}$$

Equation A.11

Where a_{1i} and a_{2i} are the pre-exponential factors associated with the decay times τ_i ($i = 1, 2$) at the monomer and excimer emission wavelengths, respectively. The derivation of Equation A.10 and Equation A.11 leads to, respectively, Equation A.12 and Equation A.13.

$$\frac{d}{dt}[M^*](t) = -\lambda_1 a_{1,1} e^{-\lambda_1 t} - \lambda_2 a_{1,2} e^{-\lambda_2 t} \quad \text{Equation A.12}$$

$$\frac{d}{dt}[E^*](t) = -\lambda_1 a_{2,1} e^{-\lambda_1 t} - \lambda_2 a_{2,2} e^{-\lambda_2 t} \quad \text{Equation A.13}$$

Consequently, the substitution of Equation A.10 and Equation A.11 into Equation A.3 and Equation A.4 leads to Equation A.14 and Equation A.15.

$$\begin{aligned} \frac{d}{dt}[M^*](t) &= -k_X (a_{1,1} e^{-\lambda_1 t} + a_{1,2} e^{-\lambda_2 t}) + k_d (a_{2,1} e^{-\lambda_1 t} + a_{2,2} e^{-\lambda_2 t}) = \\ &= -k_X a_{1,1} e^{-\lambda_1 t} - k_X a_{1,2} e^{-\lambda_2 t} + k_d a_{2,1} e^{-\lambda_1 t} + k_d a_{2,2} e^{-\lambda_2 t} = \\ &= (k_d a_{2,1} - k_X a_{1,1}) e^{-\lambda_1 t} + (k_d a_{2,2} - k_X a_{1,2}) e^{-\lambda_2 t} \end{aligned} \quad \text{Equation A.14}$$

$$\begin{aligned} \frac{d}{dt}[E^*](t) &= -k_Y (a_{2,1} e^{-\lambda_1 t} + a_{2,2} e^{-\lambda_2 t}) + k_a (a_{1,1} e^{-\lambda_1 t} + a_{1,2} e^{-\lambda_2 t}) = \\ &= -k_Y a_{2,1} e^{-\lambda_1 t} - k_Y a_{2,2} e^{-\lambda_2 t} + k_a a_{1,1} e^{-\lambda_1 t} + k_a a_{1,2} e^{-\lambda_2 t} = \\ &= (k_a a_{1,1} - k_Y a_{2,1}) e^{-\lambda_1 t} + (k_a a_{1,2} - k_Y a_{2,2}) e^{-\lambda_2 t} \end{aligned} \quad \text{Equation A.15}$$

By substituting the Equation A.12 and Equation A.13 to the left part of Equation A.14 and Equation A.15, a simple mathematical manipulation leads to Equation A.16 and Equation A.17, respectively.

$$\begin{aligned} -\lambda_1 a_{1,1} e^{-\lambda_1 t} - \lambda_2 a_{1,2} e^{-\lambda_2 t} &= -k_X (a_{1,1} e^{-\lambda_1 t} + a_{1,2} e^{-\lambda_2 t}) + k_d (a_{2,1} e^{-\lambda_1 t} + a_{2,2} e^{-\lambda_2 t}) \Leftrightarrow \\ -\lambda_1 a_{1,1} e^{-\lambda_1 t} - \lambda_2 a_{1,2} e^{-\lambda_2 t} &= -k_X a_{1,1} e^{-\lambda_1 t} - k_X a_{1,2} e^{-\lambda_2 t} + k_d a_{2,1} e^{-\lambda_1 t} + k_d a_{2,2} e^{-\lambda_2 t} \Leftrightarrow \\ (k_X - \lambda_1) a_{1,1} e^{-\lambda_1 t} + (k_X - \lambda_2) a_{1,2} e^{-\lambda_2 t} &= k_d a_{2,1} e^{-\lambda_1 t} + k_d a_{2,2} e^{-\lambda_2 t} \end{aligned} \quad \text{Equation A.16}$$

$$\begin{aligned} -\lambda_1 a_{2,1} e^{-\lambda_1 t} - \lambda_2 a_{2,2} e^{-\lambda_2 t} &= -k_Y (a_{2,1} e^{-\lambda_1 t} + a_{2,2} e^{-\lambda_2 t}) + k_a (a_{1,1} e^{-\lambda_1 t} + a_{1,2} e^{-\lambda_2 t}) \Leftrightarrow \\ -\lambda_1 a_{2,1} e^{-\lambda_1 t} - \lambda_2 a_{2,2} e^{-\lambda_2 t} &= -k_Y a_{2,1} e^{-\lambda_1 t} - k_Y a_{2,2} e^{-\lambda_2 t} + k_a a_{1,1} e^{-\lambda_1 t} + k_a a_{1,2} e^{-\lambda_2 t} \Leftrightarrow \\ (k_Y - \lambda_1) a_{2,1} e^{-\lambda_1 t} + (k_Y - \lambda_2) a_{2,2} e^{-\lambda_2 t} &= k_a a_{1,1} e^{-\lambda_1 t} + k_a a_{1,2} e^{-\lambda_2 t} \end{aligned} \quad \text{Equation A.17}$$

In Scheme A.1, the boundary conditions are that at the moment of excitation ($t=0$) the monomer concentration is $[M_0^*]$ and the excimer concentration is zero. These statements can be translated by Equation A.18 and Equation A.19, respectively.

$$a_{11} + a_{12} = [M_0^*] = 1$$

Equation A.18

$$a_{21} + a_{22} = 0$$

Equation A.19

Considering the boundary conditions, the manipulation of Equation A.16 and Equation A.17 lead to the equations that translate the pre-exponential factors at the monomer and excimer emission wavelengths, Equation A.20.

$$\begin{aligned}
 & \left\{ \begin{array}{l} (k_X - \lambda_1) a_{1,1} e^{-\lambda_1 t} = k_d a_{2,1} e^{-\lambda_1 t} \\ (k_X - \lambda_2) a_{1,2} e^{-\lambda_2 t} = k_d a_{2,2} e^{-\lambda_2 t} \\ (k_Y - \lambda_1) a_{2,1} e^{-\lambda_1 t} = k_d a_{1,1} e^{-\lambda_1 t} \\ (k_Y - \lambda_2) a_{2,2} e^{-\lambda_2 t} = k_d a_{1,2} e^{-\lambda_2 t} \\ a_{1,1} + a_{1,2} = 1 \\ a_{2,1} + a_{2,2} = 0 \end{array} \right. \Leftrightarrow \left\{ \begin{array}{l} a_{1,1} = \frac{k_d a_{2,1}}{(k_X - \lambda_1)} \\ a_{1,2} = \frac{k_d a_{2,2}}{(k_X - \lambda_2)} \\ a_{2,1} = \frac{k_d a_{1,1}}{(k_Y - \lambda_1)} \\ a_{2,2} = \frac{k_d a_{1,2}}{(k_Y - \lambda_2)} \\ a_{1,1} + a_{1,2} = 1 \\ a_{2,1} = -a_{2,2} \end{array} \right. \Leftrightarrow \left\{ \begin{array}{l} \dots \\ \dots \\ \dots \\ \dots \\ \frac{k_d a_{2,1}}{(k_X - \lambda_1)} + \frac{k_d a_{2,2}}{(k_X - \lambda_2)} = 1 \\ \dots \end{array} \right. \\
 \\
 & \Leftrightarrow \left\{ \begin{array}{l} \dots \\ \dots \\ \dots \\ \dots \\ k_d \left(\frac{a_{2,1}}{(k_X - \lambda_1)} + \frac{a_{2,2}}{(k_X - \lambda_2)} \right) = 1 \\ \dots \end{array} \right. \Leftrightarrow \left\{ \begin{array}{l} \dots \\ \dots \\ \dots \\ \dots \\ \frac{a_{2,1}}{(k_X - \lambda_1)} + \frac{a_{2,2}}{(k_X - \lambda_2)} = \frac{1}{k_d} \\ \dots \end{array} \right. \\
 \\
 & \Leftrightarrow \left\{ \begin{array}{l} \dots \\ \dots \\ \dots \\ \dots \\ \frac{a_{2,1}}{(k_X - \lambda_1) \times (k_X - \lambda_2)} + \frac{a_{2,2}}{(k_X - \lambda_2) \times (k_X - \lambda_1)} = \frac{1}{k_d} \\ \dots \end{array} \right. \Leftrightarrow \left\{ \begin{array}{l} \dots \\ \dots \\ \dots \\ \dots \\ \frac{a_{2,1} (k_X - \lambda_2) + a_{2,2} (k_X - \lambda_1)}{(k_X - \lambda_1) (k_X - \lambda_2)} = \frac{1}{k_d} \\ \dots \end{array} \right. \\
 \\
 & \Leftrightarrow \left\{ \begin{array}{l} \dots \\ \dots \\ \dots \\ \dots \\ a_{2,1} k_X - a_{2,1} \lambda_2 + a_{2,2} k_X - a_{2,2} \lambda_1 = \frac{(k_X - \lambda_1) (k_X - \lambda_2)}{k_d} \\ a_{2,1} = -a_{2,2} \end{array} \right.
 \end{aligned}$$

$$A = \frac{a_{1,2}}{a_{1,1}} = \frac{\frac{(k_X - \lambda_1)}{(\lambda_1 - \lambda_2)}}{-\frac{(k_X - \lambda_2)}{(\lambda_1 - \lambda_2)}} = -\frac{(k_X - \lambda_1)}{(k_X - \lambda_2)} = \frac{(\lambda_1 - k_X)}{(k_X - \lambda_2)} \quad \text{Equation A.21}$$

Equation A.3 and Equation A.4 can be rewritten as Equation A.22.

$$\frac{d}{dt} \begin{bmatrix} M^* \\ E^* \end{bmatrix} = \begin{bmatrix} -k_X & k_d \\ k_a & -k_Y \end{bmatrix} \begin{bmatrix} M^* \\ E^* \end{bmatrix} \quad \text{Equation A.22}$$

The eigenvalues λ_1 and λ_2 are obtained by the resolution of the second-order determinant of the matrix given by Equation A.22.³⁸

$$\begin{aligned} \begin{vmatrix} -k_X + \lambda & k_d \\ k_a & -k_Y + \lambda \end{vmatrix} = 0 &\Leftrightarrow (-k_X + \lambda)(-k_Y + \lambda) - k_a k_d = 0 \Leftrightarrow \\ \Leftrightarrow k_X k_Y - \lambda k_X - \lambda k_Y + \lambda^2 - k_a k_d = 0 &\Leftrightarrow 1\lambda^2 + \underbrace{(-k_X - k_Y)}_b \lambda + \underbrace{(k_X k_Y - k_a k_d)}_c = 0 \\ x = \frac{-b \pm \sqrt{b^2 - 4ac}}{2a} & \\ \lambda = \frac{-(-k_X - k_Y) \pm \sqrt{(-k_X - k_Y)^2 - 4(1)(k_X k_Y - k_a k_d)}}{2(1)} &\Leftrightarrow \\ \Leftrightarrow \lambda = \frac{(k_X + k_Y) \pm \sqrt{(-k_X)^2 + 2(-k_X)(-k_Y) + (-k_Y)^2 - 4k_X k_Y + 4k_a k_d}}{2} &\Leftrightarrow \\ \Leftrightarrow \lambda = \frac{(k_X + k_Y) \pm \sqrt{k_X^2 - 2k_X k_Y + k_Y^2 + 4k_a k_d}}{2} &\Leftrightarrow \\ \Leftrightarrow \lambda_{1,2} = \frac{(k_X + k_Y) \pm \sqrt{(k_X - k_Y)^2 + 4k_a k_d}}{2} & \end{aligned} \quad \text{Equation A.23}$$

From Equation A.21 and Equation A.23, the association (k_a), dissociation (k_d) and consecutively, excimer decay (k_E) rate constants in Scheme A.1 can be obtained.

Appendices

$$A = \frac{a_{1,2}}{a_{1,1}} = \frac{(\lambda_1 - k_X)}{(k_X - \lambda_2)} \Leftrightarrow A(k_X - \lambda_2) = (\lambda_1 - k_X) \Leftrightarrow Ak_X - A\lambda_2 = \lambda_1 - k_X \Leftrightarrow$$

$$\Leftrightarrow k_X(A+1) = \lambda_1 + A\lambda_2 \Leftrightarrow k_X = \frac{(\lambda_1 + A\lambda_2)}{(A+1)}, k_X = k_a + \frac{1}{\tau_M} \Leftrightarrow k_a = \frac{(\lambda_1 + A\lambda_2)}{(A+1)} - \frac{1}{\tau_M}$$

Equation A.24

$$\lambda_1 + \lambda_2 = \frac{(k_X + k_Y) + \sqrt{(k_X - k_Y)^2 + 4k_a k_d}}{2} + \frac{(k_X + k_Y) - \sqrt{(k_X - k_Y)^2 + 4k_a k_d}}{2} \Leftrightarrow$$

$$\lambda_1 + \lambda_2 = \frac{(k_X + k_Y)}{2} + \frac{\sqrt{(k_X - k_Y)^2 + 4k_a k_d}}{2} + \frac{(k_X + k_Y)}{2} - \frac{\sqrt{(k_X - k_Y)^2 + 4k_a k_d}}{2} \Leftrightarrow$$

$$\Leftrightarrow \lambda_1 + \lambda_2 = -\frac{\cancel{2}(k_X + k_Y)}{\cancel{2}} \Leftrightarrow \lambda_1 + \lambda_2 = k_X + k_Y$$

$$k_Y = \lambda_1 + \lambda_2 - k_X, k_Y = k_d + \frac{1}{\tau_E} \Leftrightarrow k_d = k_Y - \frac{1}{\tau_E} = \lambda_1 + \lambda_2 - k_X - \frac{1}{\tau_E}$$

Equation A.25

Where $k_X = k_a + k_M$, $k_M (=1/\tau_M)$ is obtained from the fluorescence decay time of the parent compound and k_a is determined by Equation A.24.

$$\lambda_1 \times \lambda_2 = \frac{(k_X + k_Y) + \sqrt{(k_X - k_Y)^2 + 4k_a k_d}}{2} \times \frac{(k_X + k_Y) - \sqrt{(k_X - k_Y)^2 + 4k_a k_d}}{2} \Leftrightarrow$$

$$\lambda_1 \times \lambda_2 = \frac{(k_X + k_Y)}{2} \times \frac{(k_X + k_Y)}{2} + \frac{\sqrt{(k_X - k_Y)^2 + 4k_a k_d}}{2} \times \frac{(k_X + k_Y)}{2} - \frac{(k_X + k_Y)}{2} \times \frac{\sqrt{(k_X - k_Y)^2 + 4k_a k_d}}{2} \Leftrightarrow$$

$$\lambda_1 \times \lambda_2 = \frac{(k_X + k_Y)^2}{4} - \frac{(\sqrt{(k_X - k_Y)^2 + 4k_a k_d})^2}{4} = \frac{(k_X + k_Y)^2}{4} - \frac{(k_X - k_Y)^2 + 4k_a k_d}{4}$$

$$= \frac{k_X^2 + 2k_X k_Y + k_Y^2 - k_X^2 + 2k_X k_Y - k_Y^2}{4} + k_a k_d = k_X k_Y + k_a k_d \Leftrightarrow k_Y = \frac{\lambda_1 \times \lambda_2 - k_a k_d}{k_X}$$

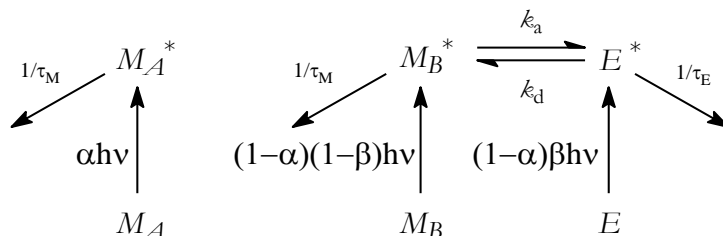
Equation A.26

With Equation A.26, it is now possible to determine k_E with Equation A.27.

$$k_E = k_Y - k_d$$

Equation A.27

Appendix B. Solution of a Kinetic Scheme Involving Two Monomers and One Excimer



Scheme B.1. Kinetic scheme for a system involving two monomers and one excimer (e.g. PAAMePy in methanol).

Under the transient approach (instantaneous formation of the excited species), the differential equations ruling the time dependence concentration of the three excited species are, according to Scheme B.1 given by Equation B.1, Equation B.2 and Equation B.3.^{63,277}

$$\frac{d}{dt}[M_A^*](t) = -k_0[M_A^*] = -k_M[M_A^*] \quad \text{Equation B.1}$$

$$\frac{d}{dt}[M_B^*](t) = -\underbrace{(k_a + 1/\tau_M)}_{k_X}[M_B^*] + k_d[E^*] \quad \text{Equation B.2}$$

$$\frac{d}{dt}[E^*](t) = -\underbrace{(k_d + 1/\tau_E)}_{k_Y}[E^*] + k_a[M_B^*] \quad \text{Equation B.3}$$

Where $[M_A^*]$, $[M_B^*]$ and $[E^*]$ are the concentration of M_A , M_B and E in the excited state.

In Scheme B.1, k_a and k_d are the rate constants of excimer formation and dissociation, respectively, α , $(1-\alpha)\beta$ and $(1-\alpha)(1-\beta)$ are the fractions of light absorbed, respectively, by the free monomers (M_A), the MAGRE monomers (M_B) and the *GSD* (E). From Scheme B.1, the excited state concentration time dependence of each species (M_A , M_B and E) is given by Equation B.4, Equation B.5 and Equation B.6, respectively.

Appendices

$$\left[M_{A}^{*} \right](t) = a_0 e^{-\lambda_0 t} \quad \text{Equation B.4}$$

$$\left[M_{B}^{*} \right](t) = a_{1,1} e^{-\lambda_1 t} + a_{1,2} e^{-\lambda_2 t} \quad \text{Equation B.5}$$

$$\left[E^{*} \right](t) = a_{2,1} e^{-\lambda_1 t} + a_{2,2} e^{-\lambda_2 t} \quad \text{Equation B.6}$$

By derivating Equation B.4, Equation B.5 and Equation B.6, one obtain Equation B.7 to Equation B.9, respectively.

$$\frac{d}{dt} \left[M_{A}^{*} \right](t) = -\lambda_0 a_0 e^{-\lambda_0 t} \quad \text{Equation B.7}$$

$$\frac{d}{dt} \left[M_{B}^{*} \right](t) = -\lambda_1 a_{1,1} e^{-\lambda_1 t} - \lambda_2 a_{1,2} e^{-\lambda_2 t} \quad \text{Equation B.8}$$

$$\frac{d}{dt} \left[E^{*} \right](t) = -\lambda_1 a_{2,1} e^{-\lambda_1 t} - \lambda_2 a_{2,2} e^{-\lambda_2 t} \quad \text{Equation B.9}$$

The fluorescence decays follow sums of exponential laws described by Equation B.10 and Equation B.11.

$$I_M(t) = I_{375nm}(t) = a_{10} e^{-t/\tau_0} + a_{11} e^{-t/\tau_1} + a_{12} e^{-t/\tau_2} \quad \text{Equation B.10}$$

$$I_E(t) = I_{520nm}(t) = a_{21} e^{-t/\tau_1} + a_{22} e^{-t/\tau_2} \quad \text{Equation B.11}$$

By using Equation B.1 to Equation B.3 and by equalling to Equation B.7 to Equation B.9, respectively, one obtain Equation B.12 to Equation B.14.

$$-\lambda_0 a_0 e^{-\lambda_0 t} = -\frac{1}{\tau_M} a_0 e^{-\lambda_0 t} \Leftrightarrow -\lambda_0 = -\frac{1}{\tau_M} \quad \text{Equation B.12}$$

$$\begin{aligned} -\lambda_1 a_{1,1} e^{-\lambda_1 t} - \lambda_2 a_{1,2} e^{-\lambda_2 t} &= -k_X (a_{1,1} e^{-\lambda_1 t} + a_{1,2} e^{-\lambda_2 t}) + k_d (a_{2,1} e^{-\lambda_1 t} + a_{2,2} e^{-\lambda_2 t}) \Leftrightarrow \\ -\lambda_1 a_{1,1} e^{-\lambda_1 t} - \lambda_2 a_{1,2} e^{-\lambda_2 t} &= -k_X a_{1,1} e^{-\lambda_1 t} - k_X a_{1,2} e^{-\lambda_2 t} + k_d a_{2,1} e^{-\lambda_1 t} + k_d a_{2,2} e^{-\lambda_2 t} \Leftrightarrow \end{aligned} \quad \text{Equation B.13}$$

$$\begin{aligned} (k_X - \lambda_1) a_{1,1} e^{-\lambda_1 t} + (k_X - \lambda_2) a_{1,2} e^{-\lambda_2 t} &= k_d a_{2,1} e^{-\lambda_1 t} + k_d a_{2,2} e^{-\lambda_2 t} \\ -\lambda_1 a_{2,1} e^{-\lambda_1 t} - \lambda_2 a_{2,2} e^{-\lambda_2 t} &= -k_Y (a_{2,1} e^{-\lambda_1 t} + a_{2,2} e^{-\lambda_2 t}) + k_a (a_{1,1} e^{-\lambda_1 t} + a_{1,2} e^{-\lambda_2 t}) \Leftrightarrow \\ -\lambda_1 a_{2,1} e^{-\lambda_1 t} - \lambda_2 a_{2,2} e^{-\lambda_2 t} &= -k_Y a_{2,1} e^{-\lambda_1 t} - k_Y a_{2,2} e^{-\lambda_2 t} + k_a a_{1,1} e^{-\lambda_1 t} + k_a a_{1,2} e^{-\lambda_2 t} \Leftrightarrow \\ (k_Y - \lambda_1) a_{2,1} e^{-\lambda_1 t} + (k_Y - \lambda_2) a_{2,2} e^{-\lambda_2 t} &= k_a a_{1,1} e^{-\lambda_1 t} + k_a a_{1,2} e^{-\lambda_2 t} \end{aligned} \quad \text{Equation B.14}$$

Equation B.1 and Equation B.2 can be rewritten in a matrix form, Equation B.15.

$$\frac{d}{dt} \begin{bmatrix} M_B^* \\ E^* \end{bmatrix} = \begin{bmatrix} -k_X & k_d \\ k_a & -k_Y \end{bmatrix} \begin{bmatrix} M_B^* \\ E^* \end{bmatrix} \quad \text{Equation B.15}$$

$$\begin{vmatrix} -k_X + \lambda & k_d \\ k_a & -k_Y + \lambda \end{vmatrix} = 0 \quad \text{Equation B.16}$$

$$\lambda_{1,2} = \frac{(k_X + k_Y) \pm \sqrt{(k_X - k_Y)^2 + 4k_a k_d}}{2} \quad \text{Equation B.17}$$

$$\lambda_0 = 1/\tau_0 = k_0 \quad \text{Equation B.18}$$

For more details in the steps to obtain Equation B.17 from Equation B.16, please see Appendix A. The sum and the product of the lambda values (λ_1 and λ_2) are given by Equation B.19 and Equation B.20.

$$\lambda_1 + \lambda_2 = k_X + k_Y \quad \text{Equation B.19}$$

$$\lambda_1 \times \lambda_2 = k_X k_Y + k_a k_d \quad \text{Equation B.20}$$

In Scheme B.1, the boundary conditions are given by Equation B.21 to Equation B.23.

$$\sum_{j=0}^2 a_{i,j} = 1 \quad (i=1) \quad \text{Equation B.21}$$

$$\sum_{j=1}^2 a_{i,j} = (1-\alpha)(1-\beta) \quad (i=1) \quad \text{Equation B.22}$$

$$\sum_{j=1}^2 a_{i,j} = \beta(1-\alpha) \quad (i=2) \quad \text{Equation B.23}$$

Considering the boundary conditions, the manipulation of Equation B.13 and Equation B.14 lead to the equations that translate the pre-exponential factors at the monomer and excimer emission wavelengths.

$$\left\{ \begin{array}{l} \lambda_0 = k_0 \\ \lambda_1 + \lambda_2 = k_X + k_Y \\ \lambda_1 \times \lambda_2 = k_X k_Y + k_a k_d \\ (k_X - \lambda_1) a_{1,1} e^{-\lambda_1 t} = k_d a_{2,1} e^{-\lambda_1 t} \\ (k_X - \lambda_2) a_{1,2} e^{-\lambda_2 t} = k_d a_{2,2} e^{-\lambda_2 t} \\ (k_Y - \lambda_1) a_{2,1} e^{-\lambda_1 t} = k_a a_{1,1} e^{-\lambda_1 t} \\ (k_Y - \lambda_2) a_{2,2} e^{-\lambda_2 t} = k_a a_{1,2} e^{-\lambda_2 t} \\ \sum_{j=0}^2 a_{i,j} = 1 \quad (i=1) \\ \sum_{j=1}^2 a_{i,j} = (1-\alpha)(1-\beta) \quad (i=1) \\ \sum_{j=1}^2 a_{i,j} = \beta(1-\alpha) \quad (i=2) \end{array} \right\} \Leftrightarrow \left\{ \begin{array}{l} \lambda_0 = k_0 \\ a_{1,1} = \frac{k_d a_{2,1}}{(k_X - \lambda_1)} \\ a_{1,2} = \frac{k_d a_{2,2}}{(k_X - \lambda_2)} \\ a_{2,1} = \frac{k_a a_{1,1}}{(k_Y - \lambda_1)} \\ a_{2,2} = \frac{k_a a_{1,2}}{(k_Y - \lambda_2)} \\ a_{1,0} + a_{1,1} + a_{1,2} = 1 \\ a_{1,1} + a_{1,2} = 1 - \alpha - \beta + \alpha\beta \\ a_{2,1} + a_{2,2} = \beta(1-\alpha) \end{array} \right\} \Leftrightarrow$$

$$\Leftrightarrow \left\{ \begin{array}{l} a_{1,1} = \frac{k_d a_{2,1}}{(k_X - \lambda_1)} \\ a_{1,2} = \frac{k_d a_{2,2}}{(k_X - \lambda_2)} \\ a_{2,1} = \frac{k_a a_{1,1}}{(k_Y - \lambda_1)} \\ a_{2,2} = \frac{k_a a_{1,2}}{(k_Y - \lambda_2)} \\ a_{1,0} = 1 - a_{1,1} + a_{1,2} = \lambda - \lambda + \alpha + \beta - \alpha\beta \\ a_{1,1} + a_{1,2} = (1-\alpha)(1-\beta) \\ a_{2,1} + a_{2,2} = \beta(1-\alpha) \end{array} \right\} \Leftrightarrow \left\{ \begin{array}{l} a_{1,1} = \frac{k_d a_{2,1}}{(k_X - \lambda_1)} \\ a_{1,2} = \frac{k_d a_{2,2}}{(k_X - \lambda_2)} \\ \frac{k_a a_{1,1}}{(k_Y - \lambda_1)} + \frac{k_a a_{1,2}}{(k_Y - \lambda_2)} = \beta(1-\alpha) \\ a_{1,1} + a_{1,2} = (1-\alpha)(1-\beta) \end{array} \right\} \Leftrightarrow$$

Equation B.24

$$\Leftrightarrow \left\{ \begin{array}{l} a_{1,1} = \frac{k_d a_{2,1}}{(k_X - \lambda_1)} \\ a_{1,2} = \frac{k_d a_{2,2}}{(k_X - \lambda_2)} \\ \frac{k_a a_{1,1}}{(k_Y - \lambda_1)} + \frac{k_a a_{1,2}}{(k_Y - \lambda_2)} = \beta(1-\alpha) \\ a_{1,2} = (1-\alpha)(1-\beta) - a_{1,1} \end{array} \right\} \Leftrightarrow \left\{ \begin{array}{l} a_{1,1} = \frac{k_d a_{2,1}}{(k_X - \lambda_1)} \\ a_{1,2} = \frac{k_d a_{2,2}}{(k_X - \lambda_2)} \\ \frac{k_a a_{1,1}}{(k_Y - \lambda_1)} + \frac{k_a [(1-\alpha)(1-\beta) - a_{1,1}]}{(k_Y - \lambda_2)} = \beta(1-\alpha) \\ a_{1,2} = (1-\alpha)(1-\beta) - a_{1,1} \end{array} \right\}$$

$$R_A = \frac{A\lambda_2 + \lambda_1}{A+1} - k_M \quad \text{Equation B.25}$$

$$R'_A = \frac{A\lambda_1 + \lambda_2}{A+1} - k_M \quad \text{Equation B.26}$$

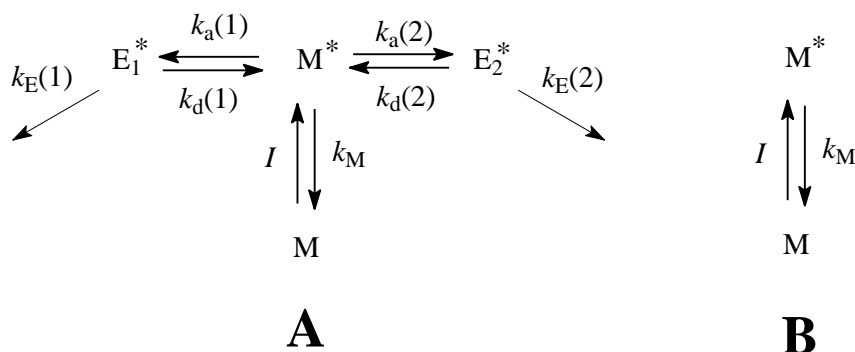
$$R'_B = \frac{B\lambda_1 + \lambda_2}{B+1} - k_M \quad \text{Equation B.27}$$

$$k_a = \frac{\frac{\lambda_1\lambda_2}{k_M} - R'_A - k_M}{\frac{k_E - R'_A - k_E + k_M}{k_M} - \frac{R'_A}{R'_A}} \quad \text{Equation B.28}$$

$$k_d = \frac{(R'_A - k_E + k_M)(R'_B - k_a)}{R'_B} \quad \text{Equation B.29}$$

$$\beta = \frac{k_a - R_A}{k_a - R_A + k_d} \quad \text{Equation B.30}$$

Appendix C. Solution of a Kinetic Scheme Involving One Monomer and Two Conformationally Different Excimers [e.g. 1Py(3)1Py]



Scheme C.1. Classic Birks' kinetic scheme for (A) one monomer and two conformationally different excimers (e.g. 1Py(3)1Py in heptane) and (B) one monomer (e.g. 1-methylpyrene in heptane at low concentrations).

$$I_F^{M^*}(t) = k_F^M [M^*](t) \quad \text{Equation C.1}$$

$$I_F^{E^*}(t) = f_1(\lambda) k_F^{E_1} [E_1^*](t) + f_2(\lambda) k_F^{E_2} [E_2^*](t) \quad \text{Equation C.2}$$

$$[M^*](t) = a_{1,1} e^{-\lambda_1 t} + a_{1,2} e^{-\lambda_2 t} + a_{1,3} e^{-\lambda_3 t} + I_0 = a_{1,1} e^{-\lambda_1 t} + a_{1,2} e^{-\lambda_2 t} + a_{1,3} e^{-\lambda_3 t} + b\nu \quad \text{Equation C.3}$$

$$[E_1^*](t) = a_{2,1} e^{-\lambda_2 t} + a_{2,2} e^{-\lambda_2 t} + a_{2,3} e^{-\lambda_3 t} \quad \text{Equation C.4}$$

$$[E_2^*](t) = a_{3,1} e^{-\lambda_2 t} + a_{3,2} e^{-\lambda_2 t} + a_{3,3} e^{-\lambda_3 t} \quad \text{Equation C.5}$$

Where M^* , E_1^* and E_2^* are the monomer in the excited state and the two conformationally different excimers.

Equation C.3 to Equation C.5 can be written in the matrix form, see Equation C.6.

$$\begin{bmatrix} M^* \\ E_1^* \\ E_2^* \end{bmatrix} = \begin{bmatrix} a_{1,1} & a_{1,2} & a_{1,3} \\ a_{2,1} & a_{2,2} & a_{2,3} \\ a_{3,1} & a_{3,2} & a_{3,3} \end{bmatrix} \cdot \begin{bmatrix} e^{-\lambda_1 t} \\ e^{-\lambda_2 t} \\ e^{-\lambda_3 t} \end{bmatrix} \quad \text{Equation C.6}$$

Where the eigenvalues λ_i are the reciprocal decay times of the shorter ($\lambda_3=1/\tau_3$), the intermediate ($\lambda_2=1/\tau_2$) and the longer ($\lambda_1=1/\tau_1$) decay times.

The derivation of Equation C.3 to Equation C.5 leads to Equation C.7 to Equation C.9.

$$\frac{d}{dt}[M^*] = -\lambda_1 a_{1,1} e^{-\lambda_1 t} - \lambda_2 a_{1,2} e^{-\lambda_2 t} - \lambda_3 a_{1,3} e^{-\lambda_3 t} \quad \text{Equation C.7}$$

$$\frac{d}{dt}[E_1^*] = -\lambda_1 a_{2,1} e^{-\lambda_1 t} - \lambda_2 a_{2,2} e^{-\lambda_2 t} - \lambda_3 a_{2,3} e^{-\lambda_3 t} \quad \text{Equation C.8}$$

$$\frac{d}{dt}[E_2^*] = -\lambda_1 a_{3,1} e^{-\lambda_1 t} - \lambda_2 a_{3,2} e^{-\lambda_2 t} - \lambda_3 a_{3,3} e^{-\lambda_3 t} \quad \text{Equation C.9}$$

Under the transient approach (instantaneous formation of the excited species), the differential equations ruling the time dependence concentration of the three excited species are, according to Scheme C.1, given by Equation C.10 to Equation C.12.

$$\frac{d}{dt}[M^*] = -\underbrace{\left(k_{a1} + k_{a2} + \frac{1}{\tau_M} \right)}_{k_X} [M^*] + k_{d1} [E_1^*] + k_{d2} [E_2^*] \quad \text{Equation C.10}$$

$$\frac{d}{dt}[E_1^*] = +k_{a1} [M^*] - \underbrace{\left(k_{d1} + \frac{1}{\tau_{E1}} \right)}_{k_Y} [E_1^*] + 0 [E_2^*] \quad \text{Equation C.11}$$

$$\frac{d}{dt}[E_2^*] = +k_{a2} [M^*] + 0 [E_1^*] - \underbrace{\left(k_{d2} + \frac{1}{\tau_{E2}} \right)}_{k_Z} [E_2^*] \quad \text{Equation C.12}$$

By joining Equation C.7 to Equation C.9 with Equation C.10 to Equation C.12, respectively one can obtain Equation C.16.⁴⁶

Appendices

$$\begin{aligned}
 & -\lambda_1 a_{1,1} e^{-\lambda_1 t} - \lambda_2 a_{1,2} e^{-\lambda_2 t} - \lambda_3 a_{1,3} e^{-\lambda_3 t} = -k_X \left(a_{1,1} e^{-\lambda_1 t} + a_{1,2} e^{-\lambda_2 t} + a_{1,3} e^{-\lambda_3 t} \right) + \\
 & k_{d1} \left(a_{2,1} e^{-\lambda_1 t} + a_{2,2} e^{-\lambda_2 t} + a_{2,3} e^{-\lambda_3 t} \right) + k_{d2} \left(a_{3,1} e^{-\lambda_1 t} + a_{3,2} e^{-\lambda_2 t} + a_{3,3} e^{-\lambda_3 t} \right) \Leftrightarrow \\
 & -\lambda_1 a_{1,1} e^{-\lambda_1 t} - \lambda_2 a_{1,2} e^{-\lambda_2 t} - \lambda_3 a_{1,3} e^{-\lambda_3 t} = -k_X a_{1,1} e^{-\lambda_1 t} - k_X a_{1,2} e^{-\lambda_2 t} - k_X a_{1,3} e^{-\lambda_3 t} + \\
 & + k_{d1} a_{2,1} e^{-\lambda_1 t} + k_{d1} a_{2,2} e^{-\lambda_2 t} + k_{d1} a_{2,3} e^{-\lambda_3 t} + k_{d2} a_{3,1} e^{-\lambda_1 t} + k_{d2} a_{3,2} e^{-\lambda_2 t} + k_{d2} a_{3,3} e^{-\lambda_3 t} \\
 & \Leftrightarrow (k_X - \lambda_1) a_{1,1} e^{-\lambda_1 t} + (k_X - \lambda_2) a_{1,2} e^{-\lambda_2 t} + (k_X - \lambda_3) a_{1,3} e^{-\lambda_3 t} = \\
 & = (k_{d1} a_{2,1} + k_{d2} a_{3,1}) e^{-\lambda_1 t} + (k_{d1} a_{2,2} + k_{d2} a_{3,2}) e^{-\lambda_2 t} + (k_{d1} a_{2,3} + k_{d2} a_{3,3}) e^{-\lambda_3 t}
 \end{aligned}$$

Equation C.13

$$\begin{aligned}
 & -\lambda_1 a_{2,1} e^{-\lambda_1 t} - \lambda_2 a_{2,2} e^{-\lambda_2 t} - \lambda_3 a_{2,3} e^{-\lambda_3 t} = -k_Y \left(a_{2,1} e^{-\lambda_1 t} + a_{2,2} e^{-\lambda_2 t} + a_{2,3} e^{-\lambda_3 t} \right) + \\
 & + k_{a1} \left(a_{1,1} e^{-\lambda_1 t} + a_{1,2} e^{-\lambda_2 t} + a_{1,3} e^{-\lambda_3 t} \right) \Leftrightarrow -\lambda_1 a_{2,1} e^{-\lambda_1 t} - \lambda_2 a_{2,2} e^{-\lambda_2 t} - \lambda_3 a_{2,3} e^{-\lambda_3 t} = \\
 & = -k_Y a_{2,1} e^{-\lambda_1 t} - k_Y a_{2,2} e^{-\lambda_2 t} - k_Y a_{2,3} e^{-\lambda_3 t} + k_{a1} a_{1,1} e^{-\lambda_1 t} + k_{a1} a_{1,2} e^{-\lambda_2 t} + k_{a1} a_{1,3} e^{-\lambda_3 t} \Leftrightarrow \\
 & \Leftrightarrow (k_Y - \lambda_1) a_{2,1} e^{-\lambda_1 t} + (k_Y - \lambda_2) a_{2,2} e^{-\lambda_2 t} + (k_Y - \lambda_3) a_{2,3} e^{-\lambda_3 t} = k_{a1} a_{1,1} e^{-\lambda_1 t} + k_{a1} a_{1,2} e^{-\lambda_2 t} + \\
 & + k_{a1} a_{1,3} e^{-\lambda_3 t}
 \end{aligned}$$

Equation C.14

$$\begin{aligned}
 & -\lambda_1 a_{3,1} e^{-\lambda_1 t} - \lambda_2 a_{3,2} e^{-\lambda_2 t} - \lambda_3 a_{3,3} e^{-\lambda_3 t} = -k_Z \left(a_{3,1} e^{-\lambda_1 t} + a_{3,2} e^{-\lambda_2 t} + a_{3,3} e^{-\lambda_3 t} \right) + \\
 & + k_{a2} \left(a_{1,1} e^{-\lambda_1 t} + a_{1,2} e^{-\lambda_2 t} + a_{1,3} e^{-\lambda_3 t} \right) \Leftrightarrow -\lambda_1 a_{3,1} e^{-\lambda_1 t} - \lambda_2 a_{3,2} e^{-\lambda_2 t} - \lambda_3 a_{3,3} e^{-\lambda_3 t} = \\
 & = -k_Z a_{3,1} e^{-\lambda_1 t} - k_Z a_{3,2} e^{-\lambda_2 t} - k_Z a_{3,3} e^{-\lambda_3 t} + k_{a2} a_{1,1} e^{-\lambda_1 t} + k_{a2} a_{1,2} e^{-\lambda_2 t} + k_{a2} a_{1,3} e^{-\lambda_3 t} \Leftrightarrow \\
 & (k_Z - \lambda_1) a_{3,1} e^{-\lambda_1 t} + (k_Z - \lambda_2) a_{3,2} e^{-\lambda_2 t} + (k_Z - \lambda_3) a_{3,3} e^{-\lambda_3 t} = k_{a2} a_{1,1} e^{-\lambda_1 t} + k_{a2} a_{1,2} e^{-\lambda_2 t} + \\
 & + k_{a2} a_{1,3} e^{-\lambda_3 t}
 \end{aligned}$$

Equation C.15

Appendices

$$\left(\begin{array}{l}
 (k_X - \lambda_1) a_{1,1} e^{-\lambda_1 t} = (k_{d1} a_{2,1} + k_{d2} a_{3,1}) e^{-\lambda_1 t} \\
 (k_X - \lambda_2) a_{1,2} e^{-\lambda_2 t} = (k_{d1} a_{2,2} + k_{d2} a_{3,2}) e^{-\lambda_2 t} \\
 (k_X - \lambda_3) a_{1,3} e^{-\lambda_3 t} = (k_{d1} a_{2,3} + k_{d2} a_{3,3}) e^{-\lambda_3 t} \\
 (k_Y - \lambda_1) a_{2,1} e^{-\lambda_1 t} = k_{a1} a_{1,1} e^{-\lambda_1 t} \\
 (k_Y - \lambda_2) a_{2,2} e^{-\lambda_2 t} = k_{a1} a_{1,2} e^{-\lambda_2 t} \\
 (k_Y - \lambda_3) a_{2,3} e^{-\lambda_3 t} = k_{a1} a_{1,3} e^{-\lambda_3 t} \\
 (k_Z - \lambda_1) a_{3,1} e^{-\lambda_1 t} = k_{a2} a_{1,1} e^{-\lambda_1 t} \\
 (k_Z - \lambda_2) a_{3,2} e^{-\lambda_2 t} = k_{a2} a_{1,2} e^{-\lambda_2 t} \\
 (k_Z - \lambda_3) a_{3,3} e^{-\lambda_3 t} = k_{a2} a_{1,3} e^{-\lambda_3 t} \\
 a_{1,1} + a_{1,2} + a_{1,3} = 1 \\
 a_{2,1} + a_{2,2} + a_{2,3} = 0 \\
 a_{3,1} + a_{3,2} + a_{3,3} = 0
 \end{array} \right) \Leftrightarrow \left(\begin{array}{l}
 a_{1,1} = \frac{k_{d1} a_{2,1} + k_{d2} a_{3,1}}{(k_X - \lambda_1)} \\
 a_{1,2} = \frac{k_{d1} a_{2,2} + k_{d2} a_{3,2}}{(k_X - \lambda_2)} \\
 a_{1,3} = \frac{k_{d1} a_{2,3} + k_{d2} a_{3,3}}{(k_X - \lambda_3)} \\
 a_{2,1} = \frac{k_{a1} a_{1,1}}{(k_Y - \lambda_1)} \\
 a_{2,2} = \frac{k_{a1} a_{1,2}}{(k_Y - \lambda_2)} \\
 a_{2,3} = \frac{k_{a1} a_{1,3}}{(k_Y - \lambda_3)} \\
 a_{3,1} = \frac{k_{a2} a_{1,1}}{(k_Z - \lambda_1)} \\
 a_{3,2} = \frac{k_{a2} a_{1,2}}{(k_Z - \lambda_2)} \\
 a_{3,3} = \frac{k_{a2} a_{1,3}}{(k_Z - \lambda_3)} \\
 a_{1,1} + a_{1,2} + a_{1,3} = 1 \\
 a_{2,1} + a_{2,2} + a_{2,3} = 0 \\
 a_{3,1} + a_{3,2} + a_{3,3} = 0
 \end{array} \right) \quad \text{Equation C.16}$$

The eigenvalues λ_1 , λ_2 and λ_3 are obtained by the resolution of the third-order determinant (Equation C.17) of the coefficient matrix of Equation C.10 to Equation C.12.

Appendices

$$\begin{aligned}
 & \begin{vmatrix} \lambda - k_X & k_{d1} & k_{d2} \\ k_{a1} & \lambda - k_Y & 0 \\ k_{a2} & 0 & \lambda - k_Z \end{vmatrix} = 0 \Leftrightarrow (\lambda - k_X) \begin{vmatrix} \lambda - k_Y & 0 \\ 0 & \lambda - k_Z \end{vmatrix} - k_{d1} \begin{vmatrix} k_{a1} & 0 \\ k_{a2} & \lambda - k_Z \end{vmatrix} + \\
 & + k_{d2} \begin{vmatrix} k_{a1} & \lambda - k_Y \\ k_{a2} & 0 \end{vmatrix} = 0 \Leftrightarrow (\lambda - k_X) [(\lambda - k_Y)(\lambda - k_Z) - 0] - k_{d1} [k_{a1}(\lambda - k_Z) - 0] + \\
 & + k_{d2} [0 - k_{a2}(\lambda - k_Y)] = 0 \Leftrightarrow (\lambda - k_X) (\lambda^2 - \lambda k_Z - \lambda k_Y + k_Y k_Z) - k_{d1} (k_{a1} \lambda - k_{a1} k_Z) + \\
 & - k_{d2} k_{a2} (\lambda - k_Y) = 0 \Leftrightarrow \lambda^3 - \lambda^2 k_Z - \lambda^2 k_Y + \lambda k_Y k_Z - \lambda^2 k_X + \lambda k_Z k_X + \lambda k_Y k_X - k_X k_Y k_Z + \\
 & - k_{d1} k_{a1} \lambda + k_{d1} k_{a1} k_Z - k_{d2} k_{a2} \lambda + k_{d2} k_{a2} k_Y = 0 \Leftrightarrow \lambda^3 - \underbrace{(k_X + k_Y + k_Z)}_p \lambda^2 + \\
 & \underbrace{(k_Z k_X + k_Y k_X + k_Y k_Z - k_{d1} k_{a1} - k_{d2} k_{a2})}_q \lambda - \underbrace{k_X k_Y k_Z + k_{d1} k_{a1} k_Z + k_{d2} k_{a2} k_Y}_r = 0
 \end{aligned}
 \end{aligned}$$

Equation C.17

The three components must provide at least 8 equations. The equations have 3 decay times and 9 pre-exponential coefficients, but for matrix inversion 2 additional parameters (s1 and s2 are needed), if no monomer emission exists at the emission wavelengths of rows 3 and 4. This yields at least 10 unknowns and 12 equations. The matrix of rate constant $[k_{i,j}]$ is then evaluated from Equation C.18.

$$k_{i,j} = \begin{bmatrix} -k_X & k_d 1 & k_d 2 \\ k_a 1 & -k_Y & 0 \\ k_a 2 & 0 & -k_Z \end{bmatrix} = [A_{i,j}] \times [-\lambda_{i,j}] \times [A_{i,j}]^{-1}$$

Equation C.18

Where the experimental “matrix of fluorescence intensities” read as Equation C.19.

$$[A_{i,j}] = [s_{i,j}] \times [a_{i,j}] = \begin{bmatrix} 1 & 0 & 0 \\ 0 & s_1 & s_1 \times s_3 \\ 0 & s_2 \times s_4 & s_2 \end{bmatrix} \cdot \begin{bmatrix} a_{2,2} & a_{2,3} & a_{2,4} \\ a_{3,2} & a_{3,3} & a_{3,4} \\ a_{4,2} & a_{4,3} & a_{4,4} \end{bmatrix}$$

Equation C.19

Equation C.19 was solved with the MatLab program presented in Appendix D.

Appendix D. MatLab Program for the Kinetics Involving One Monomer and Two Conformationally Different Excimers [e.g. 1Py(3)1Py]

```
function q=Pysergiorun(s)
global lamb amp1 amp2 amp2c q k val a f
```

```
%Data
```

```
ka1=s(1);
```

```
ka2=s(2);
```

```
kd1=s(3);
```

```
kd2=s(4);
```

```
beta=s(5);
```

```
%beta=0.00000001;
```

```
gama=s(6);
```

```
%gama=0.00000001;
```

```
kM=0.004096;
```

```
kE1=s(7);
```

```
kE2=s(8);
```

```
%kE1=0.01667;
```

```
%kE2=0.006019;
```

```
X=kM+ka1+ka2;
```

```
Y=kE1+kd1;
```

```
Z=kE2+kd2;
```

```
%Matrix of rate constants
```

```
k(1,1)=-X;
```

```
k(1,2)=kd1;
```

```
k(1,3)=kd2;
```

```
k(2,1)=ka1;
```

```
k(2,2)=-Y;
```

```
k(2,3)=0;
```

```
k(3,1)=ka2;
```

```
k(3,2)=0;
```

```
k(3,3)=-Z;
```

%calculating lambdas and amplitudes

%b is the initial concentrations vector

```
b=[1-beta;beta*gama;beta*(1-gama)];
```

```
[vec,val]=eig(k);
```

```
c=inv(vec)*b;
```

```
c0=[c(1) 0 0;0 c(2) 0;0 0 c(3)];
```

```
a=vec*c0;
```

%Ordering lambdas and amplitudes

```
[norma,idx]=sort([val(1,1);val(2,2);val(3,3)],'ascend');
```

```
val(1,1)=norma(1);
```

```
val(2,2)=norma(2);
```

```
val(3,3)=norma(3);
```

```
aidx=[a(1,idx(1)) a(1,idx(2)) a(1,idx(3));a(2,idx(1)) a(2,idx(2)) a(2,idx(3));a(3,idx(1)) a(3,idx(2))
a(3,idx(3))];
```

%calculating fractions of preformed excimers 1 and 2

```
pfe1=beta*gama;
```

```
pfe2=beta*(1-gama);
```

%errors

%calculating errors in lambdas

```
q1=val(1,1)+lamb(1);
```

```
q2=val(2,2)+lamb(2);
```

```
q3=val(3,3)+lamb(3);
```

%calculating errors in monomer amplitudes

```
q4=aidx(1,1)/(1-beta)-amp1(1);
```

```
q5=aidx(1,2)/(1-beta)-amp1(2);
```

```
q6=aidx(1,3)/(1-beta)-amp1(3);
```

%calculating errors in excimer amplitudes

%f is the fraction IE1/IE2 at the emission wavelength

%in this version-3, f is given IN POSITION M3

%calculating sum of amps in the excimer

```
amp2c(1)=aidx(2,1)*f+aidx(3,1);
```

```
amp2c(2)=aidx(2,2)*f+aidx(3,2);
```

```
amp2c(3)=aidx(2,3)*f+aidx(3,3);
```

%normalizing and calculating excimer amplitude errors.

%see Reading order of ampi(j)

```
q7=amp2c(1)/(amp2c(2)+amp2c(3))-amp2(1);
```

```
q8=amp2c(2)/(amp2c(2)+amp2c(3))-amp2(2);
```

```
q9=amp2c(3)/(amp2c(2)+amp2c(3))-amp2(3);
```

%global error

```
q=q1^2/lamb(1)+q2^2/lamb(2)+q3^2/lamb(3)+q4^2/amp1(1)+q5^2/amp1(2)+q6^2/amp1(3)+q7^2/abs(amp2(1))+q8^2/abs(amp2(2))+q9^2/abs(amp2(3));
```

```
%q=q1^2/lamb(1)+q2^2/lamb(2)+q3^2/lamb(3)+q4^2/amp1(1)+q5^2/amp1(2)+q6^2/amp1(3)+q6^2/amp1(3);
```

```
if aidx(1,2)<0
```

```
    q=100;
```

```
end
```

```
if amp2c(2)<0
```

```
    q=100;
```

```
end
```

```
if ka2<0
```

```
    q=100;
```

```
end
```

```
if kd1<0
```

```
    q=100;
```

```
end
```

```
if kd2<0
```

```
    q=100;
```

```
end
```

```
if kE2<0
```

Appendices

```
q=100;  
end  
if beta<=0  
    q=100;  
end  
if gama<=0  
    q=100;  
end  
if beta>=1  
    q=100;  
end  
if gama>=1  
    q=100;  
end
```

Appendix E. Octave Program

```
clear
%lambda=2.31
lambda=0.36
naa=28
nbase=100000
acum(1:naa-1)=0
for k=2:naa
    fact=factorial(k);
    p=exp(-lambda)*lambda^k/fact
    nchains=fix(nbase*p)
    for ic=1:nchains
x=fix(rand(k,1)*naa+1);
        x=sort(x);
        icode=1;
        while icode<k
            if x(icode)==x(icode+1)
                x(icode+1)=fix(rand(1,1)*naa+1);
                icode;
                x=sort(x);
                icode=1;
            else
                icode=icode+1;
            end
        end
    end
for icode=1:k-1
    if x(icode)==x(icode+1)
        sprintf('ERRO')
    end
end
end
```

```
for i=1:k-1
    dist=x(i+1)-x(i);
    acum(dist)=acum(dist)+1;
end
end
end
acum;
total=sum(acum);
acum=acum./total
```

Appendices

Appendices